Experimental, computational and analytical studies of slug flow

Philip David Manfield

August, 2000

Department of Chemical Engineering & Chemical Technology

Imperial College of Science, Technology & Medicine

London SW7 2BY

A thesis submitted in partial fulfilment of the requirements for the degree of *Doctor of Philosophy of the University of London* and for the Diploma of Membership of Imperial College

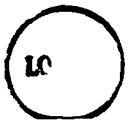

Abstract

This thesis describes an experimental and theoretical investigation into steady-state gas-liquid pipeline flow, with particular reference to slug flow.

The relevant literature is reviewed and the predictive methods pertaining to slug flow are summarised. Published work relating to slug flow in undulating pipes, slug tracking modelling and computational fluid dynamics (CFD) modelling of slug flow is discussed.

Data are presented from three extended campaigns of experiments on air-water flow in a 77.92 mm diameter pipe. The pipe was configured differently in each campaign. In the first, the pipe was 36 m long, straight and inclined downwards at 1.5°. In the second campaign, the pipe was inclined downwards at 1.5° for 14 m and then inclined upwards at 1.5° for 22 m (a "V"-section). Finally, in the third campaign, the pipe was inclined upwards at 1.5° for 14 m and then downwards at 1.5° for 22 m (a "Λ"-section). Results were obtained for the multiphase flow pattern, the liquid holdup, the pressure gradient, slug frequency and slug length distributions. The data are compared with predictive methods from the literature.

Development of a one-dimensional slug modelling scheme is described. The model solves a one-dimensional mass and momentum balance to describe the liquid distribution in the slug tail region: this is used as a basis to "track" the propagation of slugs along a pipe. Key features of the model are its treatment of slugs and waves as "objects" and its use of lookup-tables to significantly increase computation efficiency compared with earlier schemes. Predictions from the model are compared with data from the experiments.

Simulation of a single, isolated liquid slug using a three-dimensional Computational Fluid Dynamics (CFD) scheme is described. Three models of varying complexity are developed: a simulation of the tail of an "infinitely long" slug, a model of a short slug whose front is represented by a solid barrier and a simulation of a slug front as a gas-liquid interface. Results for the translational velocity of the slug tail and the shear stress distribution along the pipe walls are presented.

Detailed summaries of the experiments and CFD simulations are listed in the Appendices. The raw experimental data and CFD input files are provided on compact disc.

Acknowledgements

Firstly and above all, I must express my sincere thanks to Chris Lawrence whose insight, unclouded reasoning and peerless capacity for supporting and guiding his students have been the cause of much envy from many of my less fortunate friends. Similarly, I would like to thank Geoff Hewitt, whose enthusiasm for his subject is unrivalled and often dangerously contagious.

In the Multiphase Flow group I would like to thank my colleagues and friends for their companionship, advice and support. In particular I must express my gratitude to Colin Hale, without whose friendship and help with everything from manhandling steel pipework in the snow, to working with embryonic slug tracking schemes and helping to demystify the vagaries of Visual Basic, I am not certain that this work would ever have been completed.

Within the Chemical Engineering Department, I would like especially to thank Elios Jorisi for all his help with modifying and running the WASP rig and latterly Dan Parsons for filling Elios' steel-toecapped shoes. Thanks are also due to Dick Wood and Margaret Okanlawon for dealing so ably with my numerous computing problems, Bob King and Ken Gurney in the mechanical workshop, Malcolm Dix and the electronics team, Anna Basu, Alcina Mendes-Tatsis and countless others.

Extra curriculum, these three years have been considerably enlivened by the antics of my friends in the College Canoe Club and the IC Symphony Orchestra and I convey my thanks to both groups for welcoming me into their ranks.

This project was funded by the EPSRC and the WASP consortium, without whose support the work would not have been possible. I also extend my thanks to Shell International for their help in funding this work, and for their patience.

I am indebted to Barry Azzopardi at the University of Nottingham for inspiring my original interest in multiphase flow and also for his proposal of the "two-particle problem" that was to lead directly to this work at Imperial College.

Finally, I offer my unqualified thanks to my parents, my family and, of course, to Gaynor.

Table of contents

List of Figures

Chapter 1: Introduction

The simultaneous flow of two or more phases in a pipe is termed multiphase flow. Multiphase flow systems are of great industrial significance and are found commonly in the chemical, process, nuclear, hydrocarbon and food industries. The subject has received widespread research attention, particularly over the past five decades.

Large-scale applications of multiphase flow are found in petroleum recovery. In a multiphase hydrocarbon pipeline, up to four phases (oil, gas, water and solid particles of sand, wax or hydrate) may be present. Such pipelines are increasingly commonplace: current trends in the offshore oil industry are to produce hydrocarbons from small "satellite wells" linked by multiphase flow lines to a central processing unit, which may be on- or offshore. Advances in reservoir and drilling engineering have allowed economical production from smaller reservoirs, in deeper water, further from the central "hub". Increasingly, a thorough understanding of multiphase flows is necessary for economical design and operation of new and existing multiphase pipelines, and the processing facilities which they supply.

In gas-liquid flow, the types of distribution of the gas-liquid interface are termed *flow regimes* or *flow patterns*. A number of classifications are commonly used to describe gas-liquid flow patterns. Idealised illustrations of the main horizontal flow patterns are shown in Figure 1.1. It should be noted that differentiation between the various flow patterns is somewhat subjective; often a flow will exhibit properties of more than one flow pattern simultaneously.

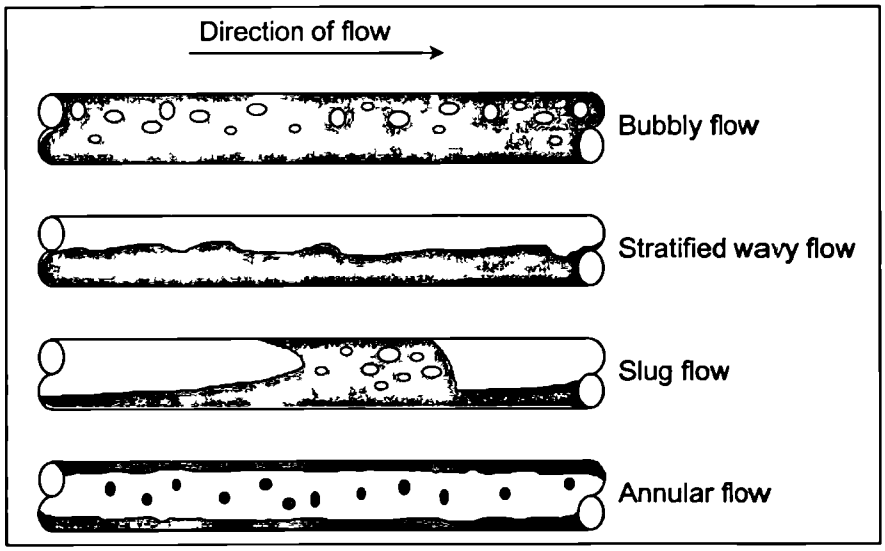

Figure 1.1. The main horizontal flow patterns

When the gas superficial velocity is low relative to the liquid flow rate, the gas tends to disperse into bubbles within a continuous liquid phase, and the flow pattern is said to be **bubbly flow**. Due to buoyancy effects, the concentration of gas bubbles is greater at the top of the pipe. At lower liquid velocities, **stratified flow** occurs; the liquid flows along the bottom of the pipe with the gas phase flowing above. This flow pattern is commonly encountered in downhill sections of pipeline. At low gas velocities the interface is usually **smooth**, however ripples and larger waves are formed as the gas velocity is increased, leading to **stratified wavy** flow. When the waves on the interface grow to bridge the pipe, **intermittent flow** can occur, in which periods of stratified flow are separated by zones where the liquid phase is continuous. At low velocities, there is no gas entrainment in the liquid zones and this regime is often referred to as **elongated bubble flow** or **plug flow**. At higher velocities (more commonly encountered in hydrocarbon recovery), gas bubbles are entrained at the fronts of the liquid zones and released at their tails, with a dispersion of gas bubbles occurring in the liquid zone. This latter regime of flow is usually termed **slug flow** with the liquid-continuous zones referred to as **slugs**. Slug flow is very common in oil-gas hydrocarbon pipelines. At high gas velocities with low proportions of liquid, for example in "wet gas" lines, **annular flow** predominates. This flow pattern is characterised by a liquid film which completely wets the pipe wall as a liquid "annulus", with entrained liquid droplets carried along in the gas "core". The liquid film is thicker at the bottom of the pipe due to gravity.

Prediction of the flow pattern that will be encountered in a particular pipeline is an important prerequisite to the calculation of the pressure gradient and liquid holdup which will occur in the system. The multiphase flow pattern also has important implications for the mechanical design of a pipeline and its supports, the formation and deposition of waxes and hydrates in the pipeline, and the corrosion rate of the pipe wall.

A number of predictive methods for pressure drop and liquid holdup exist which do not require knowledge of the flow pattern (some are discussed in Chapter 2), but in general these do not perform well. The more recent phenomenological models which have been developed for specific flow patterns offer better performance albeit over limited, and not easily predictable, ranges of conditions.

A *flow pattern map* is used to identify which flow pattern is likely to occur for a particular combination of phase velocities. A common example is the map of Mandhane *et al.* (1974) which is shown in Figure 1.2.

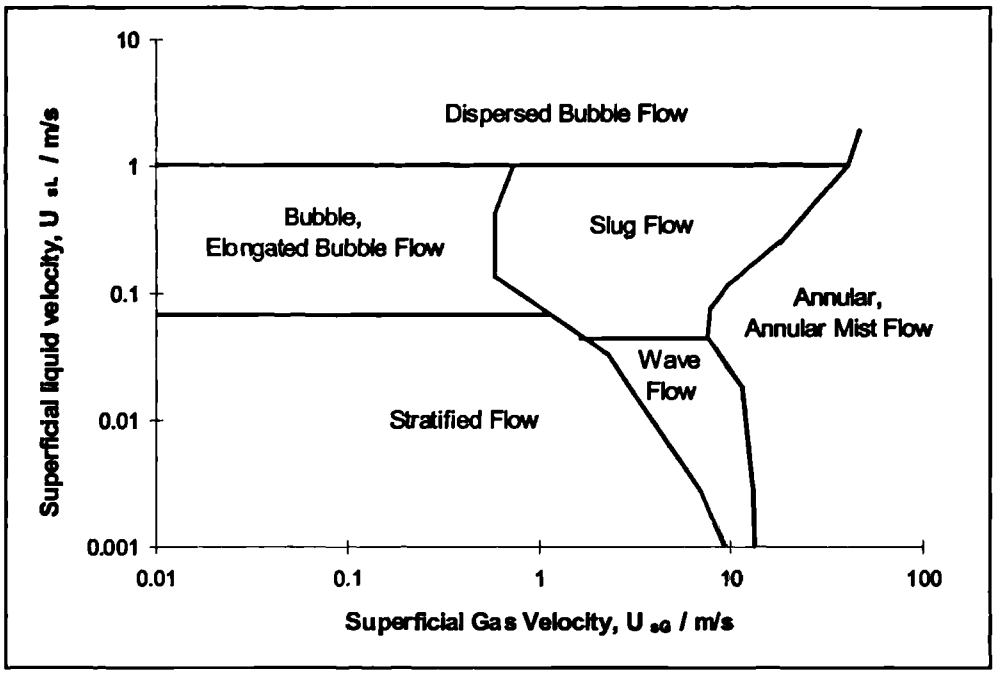

Figure 1.2. Horizontal flow pattern map of Mandhane *et al.* (1974)
[for flow of air and water at atmospheric pressure in an horizontal pipe]

The unsteady-state, intermittent flow pattern known as *slug flow* is of particular interest to the hydrocarbon recovery industry since it may have significant implications for the pressure drop, heat transfer and corrosion occurring in pipelines, and the mechanical design of separation equipment.

Slug flow is a highly complex, chaotic, three-dimensional multiphase flow pattern whose behaviour is extremely difficult to predict. Since the 1950s, many correlations have been presented to forecast such parameters as the pressure drop across an "average" slug and the distribution of slug lengths likely to be encountered in a system (see Hetsroni, 1982). More recently, phenomenological models such as that of Taitel and Barnea (1990) have been developed to predict slug properties. Such models are usually one-dimensional but because of this major simplification, several closure relationships are still required for parameters such as the wall and interfacial shear stresses and the translational velocity of the slug tail.

Simplified phenomenological models have formed the basis of several "slug tracking schemes" in which the progression of individual slugs through a pipeline system is modelled in order to predict conditions some distance downstream of a point at which the flow parameters are known with relative confidence. A number of commercial software programs have been developed around the slug tracking concept. Whilst highly simplified, and computationally intensive, these represent a significant improvement on classical methods of predicting slug flow using correlations. However, there is considerable scope for their improvement, in terms of both their physical models and their computational algorithms. These issues are addressed, to some degree, in Chapter 7 of the present work.

A great deal of experimental and modelling work has been focused on idealised multiphase flow systems. In many analyses, pipes are assumed to be perfectly horizontal or uniformly inclined. However, such systems are rarely encountered in the case of hydrocarbon transport. Neither land nor sub-sea terrain is perfectly level over any appreciable distance, and pipelines must of necessity undergo changes of inclination along their length. The effects of such "hilly terrain" on multiphase flow have received relatively little attention.

In what follows, Chapter 2 summarises the prominent literature pertaining to slug flow in horizontal and "hilly terrain" pipelines. Models for steady-state slug flow are discussed, together with the relationships required for their closure. A review of the available slug tracking schemes is given, in which their key features, advantages and limitations are highlighted.

The subsequent four chapters describe the experimental work which was conducted during this project. In Chapter 3, the Imperial College WASP facility (a 78 mm diameter, 36 m long experimental flow-loop rig) which was used for the investigations is described. Chapters 4, 5 and 6 describe three distinct "campaigns" of experiments in which the WASP facility was arranged to allow investigation of flow in a $-1.5°$ "downhill" section, a $\mp 1.5°$ "V"-section and a $\pm 1.5°$ "Λ"-section, respectively. Several hundred experiments were performed in which "steady-state" data for flow pattern, liquid holdup, pressure gradient, slug frequency, slug length and slug translational velocity were obtained. Data were also collected to allow analysis of the progression of slugs and waves along the test facility, which are compared later with results from a slug tracking model.

In Chapter 7, the development of a one-dimensional slug tracking model is described. Key features of the model are its use of object oriented programming and lookup-tables to significantly increase computation efficiency compared with earlier schemes. This allows a greater level of detail to be included in the model for a given computational effort. A study is presented of the feasibility of modelling the "initiation" of slug flow as a random distribution of short slugs. Predictions from the model are compared with data from the experimental campaigns.

Whilst valuable insights into slug flow behaviour have been obtained from experimental techniques and one-dimensional modelling, a better qualitative understanding of slug flow phenomena is needed to improve the accuracy of slug flow prediction. Chapter 8 of the current work describes calculations performed using three-dimensional CFD modelling as a means to this end. Following a brief review of published work in this area, results from a number of "numerical experiments", conducted using the commercial CFD software CFX4.3 from AEA Technology, are presented. In this work, the behaviour of a single, isolated slug is studied.

Conclusions and recommendations for future work are presented in Chapter 9.

Blank page.

Chapter 2: Literature survey

The key literature published in the field of slug flow research is described in this Chapter, as a basis for the work described later in this thesis. This review is restricted to "steady-state" slug flow (where the pressure and inlet superficial phase velocities are not varied with time). A thorough review of "transient" slug flow was presented by King (1998), who also produced a large body of experimental and analytical work on the subject.

Slug flow is a highly intermittent phenomenon. Thus, modelling of the flow using a classical time-averaging approach, in which the structure of the flow is ignored, is highly limiting. Despite this, correlations based on this approach are commonly used, although more elaborate predictive methods are becoming more prevalent. In slug flow, the space-time succession of stratified regions (*i.e.*, elongated bubbles) and aerated liquid slugs requires closure models for both the separated and dispersed flow fields. It is thus apparent that the irregular nature of the flow poses a distinctive closure problem, whether for empirical or phenomenological modelling.

In Section 2.1, a number of the "flow pattern unspecific" methods for the prediction of pressure drop and liquid holdup are described. These simple, traditional methods for the prediction of multiphase flow are still widely used within industry and are tested against the experimental data collected in the present work, in Chapters 4, 5 and 6.

More detailed "flow pattern specific" methods for slug flow are discussed in Section 2.2. Particular attention is given to "unit-cell" slug flow models, and some of the more notable models are described in detail. The relationships required for closure of the models are summarised in Section 2.3.

Experimental and analytical work pertaining to slug flow in inclined and "hilly" systems is outlined in Section 2.4. Much of this work is associated with the development of "slug tracking" schemes, which are discussed further in Section 2.5.

Chapter 8 of this thesis is concerned with the simulation of slug flow using Computational Fluid Dynamics (CFD). Literature associated with work in this field is briefly reviewed in Section 8.3 of that Chapter.

2.1. *Models not taking account of flow patterns*

The traditional approach to predicting multiphase flow parameters has been to fit correlations to large sets of experimental data. The relationships thus obtained are not easily extended to conditions which are physically very different from the original experimental systems. Correlations obtained in this way have been used as closure for simplified phenomenological models.

The simplest methods of two-phase flow prediction are the homogenous models, where the properties of a gas/liquid mixture are calculated and the flow is treated in a manner analogous to that for single phase flow. An early example of a homogenous model was that by McAdams *et al.* (1942) which used values of the mixture density and viscosity to calculate the two-phase pressure gradient using single phase friction correlations.

An alternative approach is the use of separated flow methods, where the flow of each phase is considered independently and then a procedure is applied to arrive at the result for the two-phase mixture. The most famous example is undoubtedly the work by Lockhart & Martinelli (1949) who proposed a graphical correlation for the prediction of pressure drop and liquid holdup. The correlation was later curve-fitted by Chisholm (1967).

In the present work, only a very limited treatment is given of the use of flow pattern-unspecific methods. For more detail, the reader should consult the authoritative work by Hetsroni (1982).

2.1.1. *Liquid holdup*

A number of empirical correlations for liquid volume fraction, or "holdup" are available which are independent of flow pattern. Many of these are adaptations of the "homogeneous flow" case, in which gas and liquid are assumed to have equal velocities, so that a homogenous liquid holdup may be calculated by geometric consideration of the relative proportion of each phase in the pipe cross-sectional area:

$$\varepsilon_{LH} = \frac{U_{sL}}{U_{sL} + U_{sG}} \qquad [2.1]$$

where ε_{LH} is the time-averaged liquid holdup and U_{sL} and U_{sG} are the average liquid and gas superficial velocities, respectively. The sum of the superficial velocities of all the phases

present in the system is conventionally referred to as the *total superficial velocity* or the *mixture velocity*, U_{Mix}. Thus, for two-phase flow:

$$U_{Mix} = U_{sL} + U_{sG} \qquad [2.2]$$

The two-phase "slip ratio", S, is defined as

$$S = \frac{u_G}{u_L} \qquad [2.3]$$

where u_G and u_L are the actual mean velocities of the phases [$u_L = U_{sL}/\varepsilon_L$ and $u_G = U_{sG}/(1-\varepsilon_L)$].

The liquid holdup is then given exactly by

$$\varepsilon_L = \frac{U_{sL}S}{U_{sL}S + U_{sG}} \qquad [2.4]$$

and many correlations for ε_L are phrased in terms of S.

Chisholm (1972) published a simple algebraic correlation:

$$S = \sqrt{1 + x_G\left(\frac{\rho_L}{\rho_G} - 1\right)} \qquad [2.5]$$

where x_G, the inlet quality, is defined as the fractional mass flow rate of the gas phase at the pipe inlet and ρ_L and ρ_G are respectively the densities of the liquid and gas phases. Thus,

$$x_G = \frac{\rho_G U_{sG}}{\rho_G U_{sG} + \rho_L U_{sL}} \qquad [2.6]$$

Premoli *et al.* (1970) produced a considerably more complicated correlation based on analysis of a large data bank:

$$S = 1 + E_1\left(\frac{j}{1 + jE_2} - jE_2\right)^{\frac{1}{2}} \quad \text{for} \quad \frac{1}{1 + jE_2} > E_2$$
$$S = 1 \quad \text{otherwise} \qquad [2.7]$$

where:

$$j = \frac{U_{sG}}{U_{sL}} \qquad [2.8]$$

$$E_1 = 1.578 Re^{-0.19} \left(\frac{\rho_L}{\rho_G} \right)^{0.22} \quad [2.9]$$

and

$$E_2 = 0.273 \, We \, Re^{-0.51} \left(\frac{\rho_L}{\rho_G} \right)^{-0.08} \quad [2.10]$$

The Weber number, We is defined as

$$We = \frac{(\dot{m}_L + \dot{m}_G)^2 D}{\sigma \rho_L} \quad [2.11]$$

where $\dot{m}_L$ and $\dot{m}_G$ are the mass fluxes of liquid and gas respectively, D is the pipe diameter, and σ is the liquid surface tension.

The Reynolds number, Re, is defined by

$$Re = \frac{(\dot{m}_L + \dot{m}_G) D}{\mu_L} \quad [2.12]$$

where μ_L is the liquid dynamic viscosity.

Many other correlations for liquid holdup are available, these were reviewed by Hetsroni (1982).

2.1.2. Pressure gradient

Prediction of pressure gradient in multiphase flow is one of the most important areas of research, since this parameter above all others is required for the design of piping systems. Many correlations and models have been proposed for the calculation of pressure gradient.

Pan (1996) presented a comprehensive review of pressure drop prediction methods. For reasons of brevity, only the methods applied in this thesis are described in this Chapter, and the reader is directed to Pan (1996) or Hetsroni (1982) for more detailed information.

The correlation by Friedel (1979) was based on a large bank of experimental data. The calculation procedure results in a value for a two-phase modifier, ϕ:

$$\phi = E + \frac{3.24\,F\,H}{Fr^{0.045}\,We_{Mix}^{0.035}} \qquad [2.13]$$

Here,

$$E = (1 - x_G)^2 + x_G^2 \frac{\rho_L f_{GO}}{\rho_G f_{LO}} \qquad [2.14]$$

$$F = x_G^{0.78}(1 - x_G)^{0.24} \qquad [2.15]$$

$$H = \left(\frac{\rho_L}{\rho_G}\right)^{0.91}\left(\frac{\mu_G}{\mu_L}\right)^{0.19}\left(1 - \frac{\mu_G}{\mu_L}\right)^{0.7} \qquad [2.16]$$

where x_G is the inlet quality and f_{LO} and f_{GO} are the friction factors calculated from the gas and liquid Reynolds numbers respectively:

$$Re_{xO} = \frac{(\dot{m}_G + \dot{m}_L)D}{\mu_x} \qquad [2.17]$$

so that

$$\begin{aligned} f_{xO} &= \frac{16}{Re_{xO}} && \text{for } Re_{xO} < 2000 \\ f_{xO} &= 0.079\,Re_{xO}^{-0.25} && \text{for } Re_{xO} \geq 2000 \end{aligned} \qquad [2.18]$$

where the subscript x refers to either the gas or liquid phase. The definition of the Froude number, Fr, used is

$$Fr = \frac{U_{Mix}^2}{gD} \qquad [2.19]$$

and the mixture Weber number, We_{Mix} is given by

$$We_{Mix} = \frac{(\dot{m}_G + \dot{m}_L)^2 D}{\sigma \rho_M} \qquad [2.20]$$

where ρ_M is the mixture density, defined as

$$\rho_M = (1 - \varepsilon_L)\rho_G + \varepsilon_L \rho_L \qquad [2.21]$$

Finally, the mixture pressure gradient is calculated from

$$\left(\frac{dP}{dz}\right)_{Mix} = \phi\left(\frac{dP}{dz}\right)_{LO} \quad [2.22]$$

where

$$\left(\frac{dP}{dz}\right)_{LO} = \frac{2f_{LO}(\dot{m}_G + \dot{m}_L)^2}{\rho_L D} \quad [2.23]$$

2.2. *Flow pattern-specific methods for slug flow*

Most recent predictive methods are flow pattern specific, *i.e.* they take into account the spatial distribution of the liquid and gas within the pipe. Of these, a limited number incorporate a crude method of determining the flow pattern from the value of a parameter based on the phase velocities. The pressure drop correlation of Beggs & Brill (1973), used widely in the hydrocarbon industry, uses this method and is described in this section. The "unit cell" models which are applied specifically to slug flow are described below, in Section 2.2.1.

Beggs & Brill (1973) developed flow pattern-specific correlations for the liquid holdup, ε_L and the two-phase friction factor, f_{TP}, which they used to calculate the pressure gradient.

The "no slip" Reynolds number, Re_{NS}, is given by

$$Re_{NS} = \frac{(\rho_G U_{sG} + \rho_L U_{sL})D}{\mu_L \varepsilon_{LH} + \mu_G(1 - \varepsilon_{LH})} \quad [2.24]$$

The liquid velocity number, N_{LV}, is calculated from

$$N_{LV} = U_{sL}\left(\frac{\rho_L}{g\sigma}\right)^{0.25} \quad [2.25]$$

A parameter X is defined, which is used to obtain two further parameters L_1 and L_2.

$$X = \ln(\varepsilon_{LH}) \quad [2.26]$$

$$L_1 = \exp\left(-4.62 - 3.757X - 0.481X^2 - 0.0207X^3\right) \quad [2.27]$$

$$L_2 = \exp\left(1.061 - 4.602X - 1.609X^2 - 0.179X^3 + 0.000635X^5\right) \quad [2.28]$$

The flow pattern is then determined according to the value of the Froude number, as shown in Table 2.1.

Froude number	Flow pattern
$Fr < L_1$	Segregated
$Fr \geq L_1$ and $Fr < L_2$	Intermittent
$Fr \geq L_1$ and $Fr > L_2$	Distributed

Table 2.1: Flow pattern determination in the Beggs & Brill (1973) correlation

The liquid holdup for a horizontal pipe, ε_{L0} is then calculated from the homogeneous liquid holdup and the Froude number. If the pipe is inclined (*i.e.*, if $\beta \neq 0$) then an additional parameter, C, is also required, as shown in Table 2.2

Flow pattern	ε_{L0}	C (if $\beta > 0$)	C (if $\beta < 0$)
Segregated	$\frac{0.98\varepsilon_{LH}^{0.4846}}{Fr^{0.0868}}$	$(1-\varepsilon_{LH})\ln\left(\frac{0.11N_{LV}^{3.539}}{\varepsilon_{LH}^{3.768}Fr^{1.614}}\right)$	$(1-\varepsilon_{LH})\ln\left(\frac{4.7N_{LV}^{0.1244}}{\varepsilon_{LH}^{0.3692}Fr^{0.5056}}\right)$
Intermittent	$\frac{0.845\varepsilon_{LH}^{0.5351}}{Fr^{0.0173}}$	$(1-\varepsilon_{LH})\ln\left(\frac{2.96\varepsilon_{LH}^{0.305}Fr^{0.0978}}{N_{LV}^{0.4473}}\right)$	
Distributed	$\frac{1.065\varepsilon_{LH}^{0.5824}}{Fr^{0.0609}}$	0	

Table 2.2: Calculation of parameters in Beggs & Brill (1973) model

The liquid holdup at any pipe inclination, $\varepsilon_{L\beta}$ is then calculated:

$$\varepsilon_{L\beta} = \varepsilon_{L0}\left(1 + C\left(\sin 1.8\beta - \frac{\sin^3(1.8\beta)}{3}\right)\right) \quad [2.29]$$

where β is the pipe inclination from the horizontal, in radians. The two-phase density, ρ_{TP}, is defined as

$$\rho_{TP} = \rho_L\varepsilon_{L\beta} + \rho_G(1-\varepsilon_{L\beta}) \quad [2.30]$$

The two-phase friction factor, f_{TP} is then calculated:

$$\frac{f_{TP}}{f_{NS}} = \exp(S) \quad [2.31]$$

Here, f_{NS} is the no-slip friction factor, obtained from

$$f_{NS} = \left(2\log_{10}\left(\frac{Re_{NS}}{4.5223\log_{10} Re_{NS} - 3.8215} \right) \right)^{-2} \quad [2.32]$$

and S is a liquid holdup parameter:

$$S = \frac{\ln y}{-0.0523 + 3.182\ln y - 0.8725(\ln y)^2 + 0.01853(\ln y)^4} \quad [2.33]$$

where

$$y = \frac{\varepsilon_{LH}}{\varepsilon_{L\beta}^{\ 2}} \quad [2.34]$$

Finally, the pressure gradient is calculated:

$$\frac{dP}{dz} = \frac{g\sin\beta\left(\rho_L\varepsilon_{L\beta} + \rho_G(1-\varepsilon_{L\beta}) + \left(\frac{f_{TP}(\dot{m}_G + \dot{m}_L)U_{Mix}}{2D} \right) \right)}{1 - \left(\frac{(\rho_L\varepsilon_{L\beta} + \rho_G(1-\varepsilon_{L\beta}))U_{Mix}U_{sG}}{P} \right)} \quad [2.35]$$

where P is the absolute pressure.

2.2.1. Unit-cell slug flow models

In the "slug unit" concept, an "average slug" and its associated Taylor bubble are modelled, such that the flow is then assumed to consist of a number of identical slug units. The growth, shrinkage, generation and disappearance of slugs as they propagate along the pipe are not considered; these phenomena are the subject of more recent slug tracking models, discussed later in Section 2.5.

An idealised representation of a slug unit is shown in Figure 2.1.

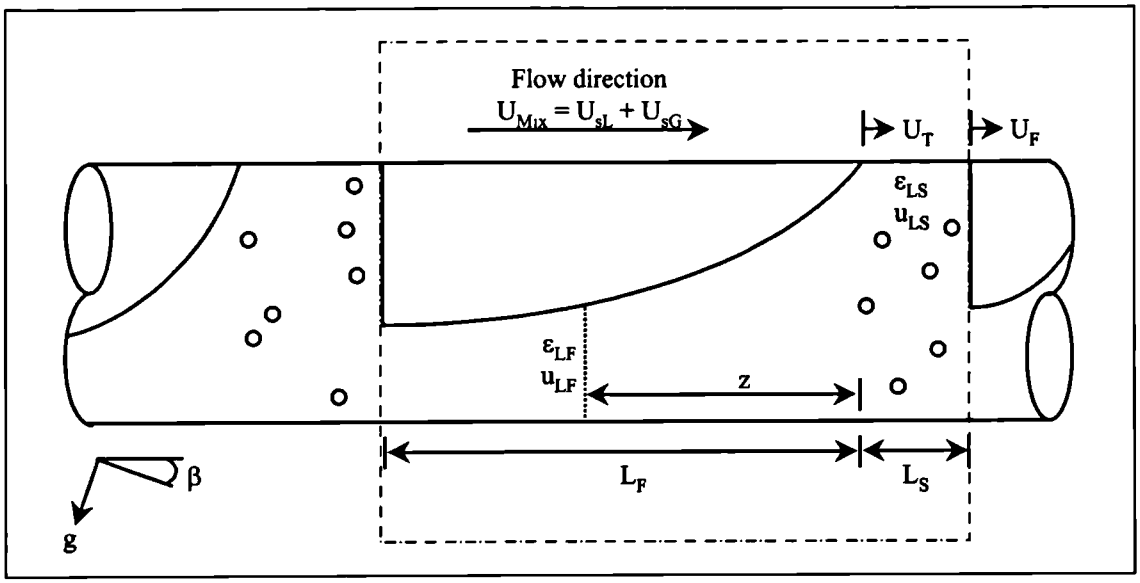

Figure 2.1: An idealised slug unit

The first true "unit cell" model of slug flow, was proposed by Kordyban (1961), who modelled the liquid slug as "skating" over a slow-moving liquid film of uniform thickness. However, a more seminal model was proposed by Dukler & Hubbard (1975), who were the first workers to treat the flow in the film region, and the process of liquid pickup at the slug front in a mechanistic fashion. Their approach was subsequently used and adapted by, amongst others, Nicholson *et al.* (1978), Stanislav *et al.* (1986), Taitel & Barnea (1990a) and Bendiksen *et al.* (1996). Similar models have been proposed for flow in vertical pipes by Fernandes *et al.* (1983), Orell & Rembrand (1986), Sylvester (1987) and Barnea (1990).

Major reviews of work in the field of slug flow were produced by Taitel & Barnea (1990b) and Fabre & Liné (1992), to which the reader is directed for further information. A more recent review of the "state of the art" in slug flow prediction was presented by Grenier *et al.* (1997). King (1998) summarised the key features of the major slug unit models found in the literature at that time.

King (1998) concluded that, since the thickness and velocity of the liquid film at the front of a slug govern the rate at which liquid enters the slug front, the basis of any effective model for developing and/or transient slug flow (*i.e.*, a slug tracking model) must be a realistic model of the film region. At the tail of the slug body, the process of liquid "shedding" occurs in a complex, three-dimensional fashion. This is the subject of a detailed study using Computational Fluid Dynamics (CFD), presented in Chapter 8 of the present work. Liquid flows around the periphery of the pipe, progressively draining into the liquid film towards the

bottom of the tube. The distribution of liquid as it leaves the slug body depends on the slug translational velocity: at low velocities, the "bubble nose" does not tend to protrude into the slug body so that the liquid is predominantly in the lower region of the pipe. However, at higher translational velocities, the nose of the gas bubble protrudes a considerable distance into the slug body, with liquid distributed around its periphery. These effects are explored further in Section 8.4.1 of Chapter 8.

Taitel & Barnea (1990b) presented three slug flow models with varying levels of complexity. The most complex used a solution of the one-dimensional liquid drainage equations in the slug tail region to provide information about the height and velocity of the liquid in the film and calculate a detailed film profile extending from the tail of a slug. This procedure has been used in the present work as a basis for the slug tracking model presented in Chapter 7, and so the stages of the solution procedure are described in detail below:

Step 1

Initially, several auxiliary parameters are calculated. The tail velocity of the slug, U_T is estimated (using, for example, one of the closure relationships described in Section 2.3.3). The liquid holdup in the slug body, ε_{LS} is also calculated (*e.g.*, using a correlation described in Section 2.3.2). In their solution, Taitel & Barnea used their own relationship for the slug translational velocity and the model of Barnea & Brauner (1985) for ε_{LS}. However, the authors noted that a different choice of closure relationships could easily be made, which may give improved predictions when applying the model. The "no slip" assumption is made for flow within the slug body, *i.e.*, the flow is assumed to be homogenous, so that

$$u_{GS} = U_{Mix} = u_{LS} \qquad [2.36]$$

where u_{GS} and u_{LS} are respectively the velocities of the gas and liquid phases inside the slug body.

Step 2

In Taitel & Barnea's analysis, it is assumed that the liquid leaving the upstream end of the slug body forms an unaerated, stratified layer at the bottom of the pipe which develops in the upstream direction, until it is "picked up" by the next slug upstream. The depth of the liquid layer *immediately* upstream of the slug body, used as the initial condition for solution of the differential equation for the film profile, is calculated by assuming that the liquid holdup in the slug body, ε_{LS} and the liquid holdup in the stratified zone immediately upstream of the

slug, ε_{LF} have the same value. Instantaneous separation of the gas and liquid phases is assumed. The calculation is done in two steps, first by solving for γ (the angle subtended by the chord of the liquid interface from the pipe centre, as shown in Figure 2.2) and then calculating the liquid film height, h_{LF}.

$$\varepsilon_{LF} = \frac{1}{2\pi}(\gamma - \sin\gamma) \qquad [2.37]$$

$$h_{LF} = \frac{D}{2}\left(1 - \cos\frac{\gamma}{2}\right) \qquad [2.38]$$

However, if this results in a film thickness greater than that for *critical* flow in the stratified layer, the *critical film thickness* is calculated from the appropriate volumetric liquid shedding rate at the slug tail, and this value is used instead. The critical film thickness is that below which, for a given liquid flow rate, interfacial waves cannot propagate in the upstream direction relative to the slug tail. This is calculated as the value of h_{LF} which satisfies the following equation:

$$(\rho_L - \rho_G)g\cos\beta - \rho_L(U_T - u_{LF})\frac{(U_T - u_{LS})\varepsilon_{LS}}{\varepsilon_{LF}^2}\frac{d\varepsilon_{LF}}{dh_{LF}} - \rho_G(U_T - u_{GF})\frac{(U_T - u_{GS})(1-\varepsilon_{LS})}{(1-\varepsilon_{LF})^2}\frac{d\varepsilon_{LF}}{dh_{LF}} = 0 \qquad [2.39]$$

where, if the flow is assumed to be stratified,

$$\frac{d\varepsilon_{LF}}{dh_{LF}} = \frac{4}{\pi D}\sqrt{1 - \left(2\frac{h_{LF}}{D} - 1\right)^2} \qquad [2.40]$$

which follows from the geometrical discussion below.

Step 3

One-dimensional mass and momentum balances result in the following expression for the profile behind the slug:

$$\frac{-dh_{LF}}{dz} = \frac{\frac{\tau_L S_L}{A_L} - \frac{\tau_G S_G}{A_G} - \tau_I S_I\left(\frac{1}{A_L} + \frac{1}{A_G}\right) + (\rho_L - \rho_G)g\sin\beta}{(\rho_L - \rho_G)g\cos\beta - \rho_L(U_T - u_{LF})\frac{(U_T - u_{LS})\varepsilon_{LSi}}{\varepsilon_{LF}^2}\frac{d\varepsilon_{LF}}{dh_{LF}} - \rho_G(U_T - u_{GF})\frac{(U_T - u_{GS})(1-\varepsilon_{LS})}{(1-\varepsilon_{LF})^2}\frac{d\varepsilon_{LF}}{dh_{LF}}} \qquad [2.41]$$

where h_{LF} is the liquid film height and ε_{LF} is the liquid film holdup a distance z upstream from the rear of the slug body (as shown in Figure 2.1), τ_L is the liquid wall shear stress, τ_G is the gas wall shear stress, τ_I is the interfacial shear stress, S_L is the length of the wetted perimeter of the liquid region, S_G is the length of the perimeter of the gas region, S_I is the length of the chordal gas-liquid interface, A_L and A_G are the cross-sectional areas of the liquid and gas regions respectively, ρ_G is the gas density and g is the acceleration due to gravity. To obtain the solution of the film profile equation, numerical integration is started from the lower of the two liquid heights calculated from Equations [2.38] and [2.39]. In their analysis, to obtain the pressure difference between the ends of a slug unit, Taitel & Barnea proposed that the integration should be continued until a volume balance between the liquid entering the pipe and the liquid in the slug unit was satisfied:

$$U_{sL} = u_{LS}\varepsilon_{LS} + U_T(1-\varepsilon_{LS})\frac{L_F}{L_U} - \frac{U_T}{L_U}\int_0^{L_F}(1-\varepsilon_{LF})dz \qquad [2.42]$$

where L_U is the length of the slug unit, equal to $(L_S + L_F)$. In this analysis, knowledge of the slug body length L_S is required in order to calculate L_U. This may be obtained either from a correlation for slug length, or from a slug frequency prediction. Appropriate closure relationships are discussed in Section 2.3.

In the slug tracking scheme presented in Chapter 7 of this thesis, the lengths L_S and L_F are not known *a priori* and so the tail profile equation is integrated for a (generally, large) specified distance upstream, or until the liquid film height falls below a specified minimum value. The information is then stored and used to compile "lookup tables" of data which describe a number of different slug tail profiles covering the range needed for the calculation.

In the Taitel & Barnea (1990b) analysis, the gas-liquid interface in the film region is assumed to be flat across the cross section of the pipe. This is a very poor approximation in the region immediately upstream of the slug body, but is more valid further from the slug body. This matter is discussed further in Chapter 8 of the present work. The flat interface approximation leads to several useful geometric relationships, as shown in Figure 2.2:

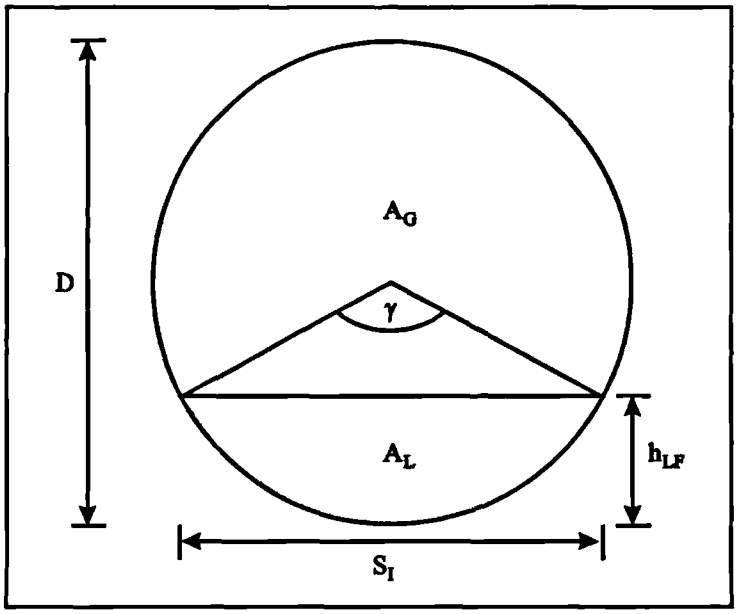

Figure 2.2: Geometry of a flat interface

In the pipe cross-section shown in Figure 2, γ is the angle subtended by the (flat) gas-liquid interface at the pipe axis. Then, the depth of liquid is

$$h_{LF} = \frac{D}{2}\left(1-\cos\frac{\gamma}{2}\right) \qquad [2.43]$$

and the liquid and gas perimeter lengths are respectively

$$S_L = \frac{\gamma D}{2} \qquad [2.44]$$

and

$$S_G = \left(\pi - \frac{\gamma}{2}\right)D \qquad [2.45]$$

The interface length is

$$S_I = D\sin\frac{\gamma}{2} \qquad [2.46]$$

and the liquid film holdup is given by

$$\varepsilon_{LF} = \frac{\gamma - \sin\gamma}{2\pi} \qquad [2.47]$$

so that the cross-sectional areas of the gas and liquid regions are respectively

$$A_G = A(1-\varepsilon_{LF}) \qquad [2.48]$$

and

$$A_L = A\varepsilon_{LF} \qquad [2.49]$$

Cook & Behnia (1997) derived a similar equation to [2.41] but using a slightly different approach, whereby the pressure gradient in each phase was treated separately. They presented experimental data showing that the expression by Taitel & Barnea (1990) tended to overpredict the thickness of the liquid film in the slug tail region.

The above analysis by Taitel & Barnea (1990) does not take account of aeration effects in the liquid film, so that the liquid holdup in the film fraction is always taken to be unity.

Aeration effects *were* included in a later mechanistic model by Bendiksen *et al.* (1996), in which the following expression is solved numerically:

$$-(1-\varepsilon_{LF})\rho_L\left(\frac{\dot{V}_{LF}}{\tilde{h}_F}\right)^2\frac{d\tilde{h}_F}{dz} = -\varepsilon_{LF}\frac{\tau_G S_G}{A} + (1-\varepsilon_{LF})\frac{\tau_{LF}S_L}{A} - \frac{\tau_I S_I}{A} - g\varepsilon_{LF}(1-\varepsilon_{LF})\sin\beta(\rho_S+\rho_G) \qquad [2.50]$$

King (1998) identified errors in the derivation of Equation [2.50] in the original paper by Bendiksen *et al.* (1996). The corrected equation was presented by King, and is the version stated in the present work. In this expression, $\tilde{h}_F$ is the dimensionless height of the aerated liquid film,

$$\tilde{h}_F = \phi\varepsilon_{LF} \qquad [2.51]$$

where ϕ is the holdup of the liquid film, such that for a completely unaerated film, ϕ would be equal to unity.

The slug body density, ρ_S, is given by

$$\rho_S = \rho_L\varepsilon_{LS} + \rho_G(1-\varepsilon_{LS}) \qquad [2.52]$$

The solution of Equation [2.50] is performed simultaneously with a liquid mass balance [2.53] and a volume balance [2.54] over the front of the slug:

$$(U_F - u_{LF})\phi\varepsilon_{LF} = (U_F - u_{LS})\varepsilon_{LS} \qquad [2.53]$$

$$U_{Mix} = u_{GF}(1-\varepsilon_{LF}) + u_{LF}\,\phi\,\varepsilon_{LF} + u_{GFF}\,\varepsilon_{LF}(1-\phi) \quad [2.54]$$

Here, u_{GFF} is the velocity of gas bubbles in the aerated liquid film. Additional information is required to calculate the aeration of the film region: this is beyond the scope of this thesis but was discussed by Bendiksen *et al.* (1996) and King (1998).

2.3. Closure relationships

The simplified models used in the Taitel & Barnea (1990b) model described above require knowledge of a number of variables before they may be used. In the case of the 1-D solution of the slug tail profile Equation [2.41], the unknown variables are: the wall and interfacial shear stresses τ_L, τ_G and τ_I, the slug body liquid holdup ε_{LS} and the translational velocity of the slug tail, U_T. In addition, if the mass balance Equation [2.42] is to be solved, the slug body length, L_S must also be known. In this Section, a number of auxiliary closure relationships are described which may be used to obtain these data.

2.3.1. Shear stresses

Taitel & Barnea (1990b) used classical single-phase flow correlations ~~are used~~ to obtain the gas and liquid wall shear stresses. The gas phase wall shear stress is given by:

$$\tau_G = \frac{\rho_G u_{GF} f_G |u_{GF}|}{2} \quad [2.55]$$

with the friction factor, f_G, given by the Blasius relationship

$$f_G = 0.046 |Re_G|^{-0.2} \quad [2.56]$$

where

$$Re_G = \frac{4 u_{GF} \rho_L A_G}{\mu_G (S_G + S_I)} \quad [2.57]$$

A similar method is used for the calculation of liquid shear stress:

$$\tau_L = \frac{\rho_L u_{LF} f_L |u_{LF}|}{2} \quad [2.58]$$

with

$$f_L = \frac{16}{Re_L} \qquad Re_L \le 4000$$
$$f_L = 0.046|Re_L|^{-0.2} \qquad Re_L > 4000 \qquad [2.59]$$

where

$$Re_L = \frac{4u_{LF}\rho_L A_L}{\mu_L S_L} \qquad [2.60]$$

A number of expressions for f_L (and similarly, f_G) have been proposed, which are applicable to different ranges of the Reynolds number. In slug flow, at the fluid velocities commonly encountered (*e.g.*, $U_{sG} \le 25$ m/s, $U_{sL} \le 1.5$ m/s) the Reynolds numbers are generally sufficiently low that the Blasius relationship may be used. However, where the Reynolds number is very high, a more appropriate equation should be used, for example the expression by Nikuradse (see Schlichting, 1969):

$$\frac{1}{\sqrt{f}} = 4\log_{10}\left(Re\sqrt{f}\right) - 0.4 \qquad [2.61]$$

A wide range of correlations exist for interfacial friction factor, f_I. These were reviewed by Khor *et al.* (1997). Taitel & Barnea (1990b) used the correlation of Andritsos & Hanratty (1987):

$$f_I = f_G \qquad U_{sG} \le U_{AH}$$
$$f_I = f_G\left(1 + 15\left(\frac{U_{sG}}{U_{AH}} - 1\right)\sqrt{\frac{h_{LF}}{D}}\right) \qquad U_{sG} > U_{AH} \qquad [2.62]$$

where $U_{AH} \approx 5$ m s^{-1} is the critical velocity for waves to affect the shear stress on the interface. For consistency, this correlation was retained in applying the Taitel & Barnea (1990b) model in the present work.

The interfacial shear stress is then given by

$$\tau_I = \frac{\rho_G f_I (u_{GF} - u_{LF})|u_{GF} - u_{LF}|}{2} \qquad [2.63]$$

2.3.2. Liquid holdup in the slug body

The gas-liquid interface which forms the slug front normally moves at a high velocity relative to the shallow liquid film ahead of the slug. As the slug "picks up" the liquid film, a process occurs which is analogous to "jetting" of liquid into a stationary slug body. This effect is considered in detail as part of a CFD study presented in Chapter 8 of this thesis, where, in particular, the effects on the velocity profile inside the slug body, and hence the translational velocity of the slug tail, are discussed.

Gas bubbles are normally entrained into the slug body during this "jetting" process. The gas bubbles are then transported through the slug body and are "shed" at the tail. The mechanisms involved are complex. Photographic studies (Davies, 1992) have shown the presence of a large "recirculation zone" of liquid and gas at the front of the slug body, in which large entrained gas bubbles are observed; these break up to form smaller bubbles which move through the slug body towards the tail. During the shedding processes at the slug tail, a portion of the entrained gas passes into the liquid film region behind the slug and the remainder passes into the continuous bubble phase (*i.e.* the Taylor bubble) region. Commonly, unit-cell and slug-tracking models include the simplifying assumptions of instantaneous, perfect dispersion of gas throughout the entire slug body, and instantaneous, perfect separation of the gas and liquid phases at the tail. Thus, a single value of ε_{LS} applies throughout the slug body, and the liquid film is assumed to be completely unaerated.

The liquid holdup in the slug body is an important parameter for the design of multiphase pipelines and their associated separation equipment. It is also required for closure in a number of 1-D slug flow models. In unit-cell slug flow models, all slugs are assumed to be identical and thus a single value of ε_{LS} is applicable to the entire flow system, so that a predictive correlation is generally used. In slug tracking models, where each slug is considered to be unique, a more mechanistic treatment of the gas entrainment processes which occur at the slug front is required. This approach was pursued in the present work, and is described in Chapter 7.

The extensively-used correlation by Gregory *et al.* (1978) was obtained from measurements of liquid holdup, using electrical capacitance probes, in air-water and air-oil flow in horizontal pipes with diameters of 2.58 cm and 5.12 cm. The correlation gives slug body holdup as a function of the mixture velocity only:

$$\varepsilon_{LS} = \frac{1}{1+\left(\frac{U_{Mix}}{8.66}\right)^{1.39}} \qquad [2.64]$$

A more complex correlation for ε_{LS} was proposed by Ferschneider (1983), based on data measured using the Boussens flow loop facility in France, which comprised a 15.24 cm diameter, 120 m long test-section. The data were obtained using natural gas and a light hydrocarbon oil at elevated pressure of between 10 and 50 bar. Ferschneider's correlation took account of the surface tension of the fluids:

$$\varepsilon_{LS} = \frac{1}{\left(1+\left(\frac{U_{Mix}}{\sqrt{((\rho_L-\rho_G)/\rho_l)gD}}\right)^2 \Big/ \left(\frac{\alpha}{Bo^{\beta}}\right)^2\right)^2} \qquad [2.65]$$

where α and β are constants, whose values were not revealed in the paper. The Bond number, Bo, is defined as:

$$Bo = \frac{(\rho_L-\rho_G)gD^2}{\sigma} \qquad [2.66]$$

In a later paper, Paglianti *et al.* (1993) wrote the correlation by Ferschneider (1983) in the form:

$$\varepsilon_{LS} = \frac{1}{\left(1+\frac{Fr^2\ Bo^{0.2}}{625}\right)^2} \qquad [2.67]$$

thereby implying values for α and β of 25 and 0.1 respectively. Their definition of the Froude number was the square root of that used by Beggs & Brill (1973) given in Equation [2.19].

Barnea & Brauner (1985) suggested that the concentration of gas bubbles in the slug body is the maximum that can be supported by the turbulent flow of the liquid. They extended the relationship proposed by Taitel & Dukler (1976) for the prediction of the transition from bubbly flow to slug flow to include this notion, and thereby obtained a prediction for the liquid holdup in the slug body.

Recently, Gomez *et al.* (2000) developed a correlation for slug body holdup for upwardly-inclined flow:

$$\varepsilon_{LS} = \exp\left(-0.45\beta + 2.48\times10^{-6}\,Re_S\right) \qquad [2.68]$$

where β is the angle of upward inclination in radians and Re_S is the slug Reynolds number,

$$Re_S = \frac{\rho_L U_{Mix} D}{\mu_L} \qquad [2.69]$$

A number of workers have presented expressions for slug body holdup based on gas and liquid mass and/or volumetric balances over the slug body. Andreussi & Bendiksen (1989) considered the volumetric flows of gas into the slug front, and out of the slug at the front and the tail. Based on this, King (1998) derived an expression for the slug body void fraction (*i.e.*, the gas holdup) by balancing the flow of gas into and out of the slug body. The derivation was based on the assumptions of no slip within the slug body and no aeration of the liquid film at either end of the slug. King's (1998) expression was:

$$\left(1-\varepsilon_{LS}\right) = \frac{C_1\left(U_F - u_{LS}\right) - C_1 u'_{MF}}{\left(U_T - u_{GS}\right) + C_2 u_{G_0} + C_1\left(U_F - u_{LS}\right)} \qquad [2.70]$$

where C_1 and C_2 are empirical constants (whose values were not given) in Andreussi & Bendiksen's (1989) analysis of the slug *front*. u'_{MF} is a minimum value of the relative velocity ($U_F - u_{LS}$) below which no gas entrainment occurs, and u_{Go} is the velocity of a gas bubble entering a horizontal tube filled with a stagnant liquid, classically given by

$$u_{G_0} = 0.54\sqrt{gD} \qquad [2.71]$$

Nydal & Andreussi (1991) determined the volumetric rate of gas entrainment into the slug front experimentally, by injecting liquid into the bottom of a pipe containing a stratified flow, to cause the formation of a slug. They inferred the gas entrainment rate, $\dot{V}_{GF}$ from a mass balance, and proposed a correlation based on the relative velocity of the slug front and the liquid film, and the length of the chordal gas-liquid interface at the front of the slug (which was assumed to be flat).

$$\dot{V}_{GF} = A\left(0.076\frac{S_1}{D}\left(U_F - u_{LF}\right) - U_{NA}\right) \qquad [2.72]$$

where A is the cross-sectional area of the pipe and U_{NA}=0.15 m/s is the critical relative velocity for gas entrainment to occur. Nydal & Andreussi (1991) based their expression on data obtained using air and water, and subsequently repeated the experiments with different fluids: air/oil, helium/water and Freon/water. They found that higher gas density resulted in a greater rate of gas entrainment. They also reported that when oil was used as the liquid phase, the rate of gas entrainment was slightly higher than for water. This is likely to be due to the lower surface tension of the oil.

By considering a volumetric balance of the gas flow across the slug front,

$$\dot{V}_{GF} = A\varepsilon_{GF}(U_F - u_{GF}) = A\varepsilon_{GS}(U_F - u_{GS}) \qquad [2.73]$$

and substituting into Equation [2.72], ε_{LS} is obtained explicitly:

$$\varepsilon_{LS} = 1 - \frac{0.076\frac{S_I}{D}(U_F - u_{LF}) - U_{NA}}{U_F - u_{GS}} \qquad [2.74]$$

Manolis (1995) proposed a correlation, similar in form to that of Nydal and Andreussi (1991) but regressed from data obtained from the Imperial College WASP facility:

$$\frac{\dot{V}_{GF}}{A} = 0.14576\frac{S_I}{D}((U_F - u_{LF}) - U_{Man}) \qquad [2.75]$$

The value U_{Man}=2.1265 m/s corresponds to the relative velocity ($U_F - u_{LF}$) below which no gas entrainment occurred. This is equivalent to the term u'_{MF} in Andreussi & Bendiksen's (1989) analysis (Equation [2.70]), and U_{NA} in Equation [2.72]. Manolis' original expression was presented in a dimensionally inconsistent form, but has been corrected here.

The Manolis (1995) expression may be rearranged and substituted as above, to give

$$\varepsilon_{LS} = 1 - \frac{0.14576\frac{S_I}{D}[(U_F - u_{LF}) - U_{Man}]}{U_F - U_{Mix}} \qquad [2.76]$$

Aeration of the liquid film in the slug tail has not been widely studied. The relevant works were reviewed by King (1998) who commented on their applicability as closure relationships for slug flow models which included this effect, such as that by Bendiksen (1996).

2.3.3. Slug translational velocity

A liquid slug moves along a pipe at a translational velocity U_T (as shown in Figure 2.1) which is usually greater than the sum of the superficial velocities of the gas and liquid phases, U_{Mix}. This occurs due to the processes of liquid pickup at the slug front, and shedding at the tail.

The translational velocity U_T is traditionally expressed in terms of the C-ratio, defined by Dukler & Hubbard (1975) as

$$C = \frac{U_T}{U_{Mix}} - 1 \qquad [2.77]$$

In their analysis, Dukler & Hubbard (1975) assumed a universal velocity profile in the slug body and developed an expression for the C-ratio,

$$C = 0.021 \ln(Re_S) + 0.022 \qquad [2.78]$$

where Re_S is the slug Reynolds number, defined in Equation [2.69]. Dukler & Hubbard stated that their relationship is valid for the range $3\times10^4 \le Re_S \le 4\times10^5$.

Moalem Maron *et al.* (1982) obtained a value of $C = 1/7 = 0.143$. This was derived from a treatment of the boundary layer development within the slug body, for slug flow between flat plates. They proposed that this would change to the (more commonly accepted value) of 0.2 for flow in a circular pipe. This analysis was subsequently improved by Dukler *et al.* (1985), to include the effect of entrained gas bubbles in the slug body and the resulting asymmetry of the boundary layers. Their expression for horizontal flow was:

$$\frac{U_T}{U_{Mix}} = \frac{(2n+1)(n+1)}{2n^2} \approx 1.22 \qquad [2.79]$$

where n = 7, corresponding to a $\frac{1}{7}^{th}$ power law for the velocity profile.

Ruder *et al.* (1989) considered the case of stagnant liquid draining from the end of a horizontal pipe, so that the propagation of the "slug tail" was analogous to the velocity of the nose of the air bubble. The original analysis of this case was described by Benjamin (1968), who stated that the bubble propagation "drift velocity" was given by $0.542\sqrt{gD}$. Ruder *et al.* (1989) extended Benjamin's analysis and proposed an expression for the C-ratio:

$$C = \frac{0.542\sqrt{gD}}{U_{Mix}} \qquad [2.80]$$

Bendiksen (1984) observed that at high superficial velocities in horizontal slug flow, the nose of the Benjamin bubble does not remain at the top of the pipe but begins to protrude into the slug body and moves closer to the axial centreline of the pipe. He proposed that the Benjamin-type drift velocity was only applicable to slug flow at low velocities, and proposed a relationship which took the Froude number of the mixture into account:

$$\begin{aligned} U_T &= U_{Mix} + 0.542\sqrt{gD} && Fr < 3.5 \\ U_T &= 1.2\,U_{Mix} && Fr \geq 3.5 \end{aligned} \qquad [2.81]$$

Equation [2.81] is *not continuous* and leads to a discontinuity when Fr = 3.5. Here, the Froude number is the square root of Equation [2.19], *i.e.*,

$$Fr = \frac{U_{Mix}}{\sqrt{g\,D}} \qquad [2.82]$$

Davies (1992) and Manolis (1995) conducted experiments at Imperial College to study the translational velocity of a slug tail, for the case of an unaearated liquid slug. In their experiments, gas was injected at a predetermined rate into one end of a pipe which was initially full of liquid. This resulted in the growth of a long gas bubble which "pushed out" liquid from the other end of the pipe. The bubble front velocity, equivalent to the slug tail translational velocity U_T, was measured using electrical conductivity probes spaced a known distance apart. Manolis (1995) correlated these data and obtained an expression in the same form as that of Bendiksen (1984):

$$\begin{aligned} U_T &= 1.033\,U_{Mix} + 0.477\sqrt{gD} && Fr < 2.86 \\ U_T &= 1.216\,U_{Mix} && Fr \geq 2.86 \end{aligned} \qquad [2.83]$$

Again, Manolis' expression has been adjusted to make it dimensionally consistent.

King *et al.* (1997) compared the experimental data of Davies (1992) and Manolis (1995) with the predictions of five correlations. Their comparisons are shown in Figure 2.3, in which the Froude number is defined by Equation [2.82].

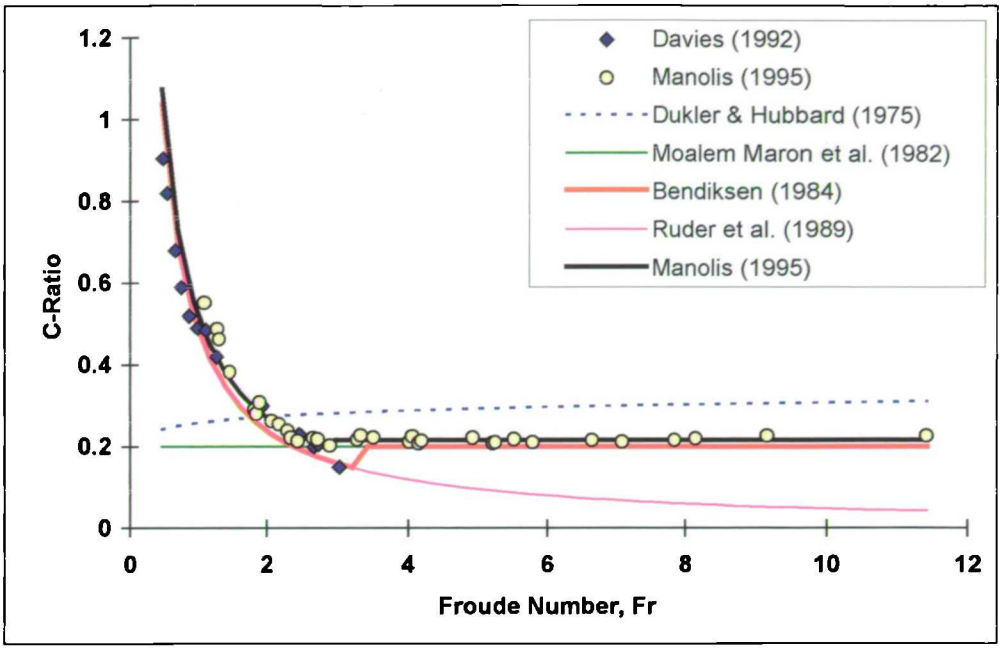

Figure 2.3: Performance of C-Ratio correlations (after King *et al.*, 1997)

The relationships by Dukler & Hubbard (1975) and Moalem Maron *et al.* (1982) do not fit the experimental data at all well. The model by Ruder *et al.* (1989) shows good agreement with the data at low value of the Froude number but significantly underpredicts the C-Ratio at higher mixture velocities. The expressions by Bendiksen (1984) and Manolis (1995) perform much better, with the correlation by Manolis (1995) inevitably providing the better fit to his own data.

The tail of an unaerated slug was modelled using three-dimensional CFD techniques by Pan (1996). This approach is described further in Chapter 8 of the present work.

A common limitation of the correlations by Bendiksen (1984) and Manolis (1995), the experimental data shown in Figure 2.3 and the CFD simulations performed by Pan (1996) and those described in Chapter 8 of this thesis, is that the effects of gas entrainment in the slug body are not considered. This is currently the subject of an experimental investigation at Imperial College by Hale (2000), who has performed similar experiments to those by Davies (1992) and Manolis (1995) but using an aerated liquid mixture instead of a single-phase liquid. The results of these "gassy pushout" experiments show a small ~~but significant~~ effect of gas content on the value of C; since the data have only recently been analysed, no effect of gas content on C was taken into account in the present work. However, the effect is not very significant.

A number of authors have produced expressions for the "wake effect" where the translational velocity of a short slug is significantly higher than that of a long slug with the equivalent mixture velocity, due to the effect of the "recirculation zone" at the front of the slug body on the velocity profile near the tail of the slug.

This effect was first observed in vertical plug and slug flow by Moissis & Griffith (1962). They reported a correlation for the translational velocity U_T of a slug tail in terms of the length of the slug:

$$U_T = U_{T,\infty}\left(1 + 8\exp\left(-1.06\frac{L_S}{D}\right)\right) \qquad [2.84]$$

where $U_{T,\infty}$ is the translational velocity of a long, stable slug at the same mixture velocity.

Barnea & Taitel (1993) proposed an expression of similar form for horizontal flow:

$$U_T = U_{T,\infty}\left(1 + \beta\exp\left(-\psi\frac{L_S}{L_{S,stable}}\right)\right) \qquad [2.85]$$

where β and ψ are empirical constants whose values are 5.5 and 0.6 respectively. The stable slug length, $L_{S,stable}$ was stated to be between 10 and 15 pipe diameters.

Recently, Fagundes Netto and co-workers conducted experimental investigations of the "wake effect" in horizontal flow (Fagundes Netto *et al.*, 1998; Fagundes Netto *et al.*, 1999b). They studied air-water flow at atmospheric pressure in a PVC tube, 53 mm in diameter and 90 m long. Two groups of five electrical capacitance probes, each spaced at a distance of 1 meter, were placed 65 m apart in the test-section and used to obtain liquid holdup/time data, from which slug translational velocity data were obtained. They "launched" pairs of long gas bubbles of known lengths, separated by an unaerated liquid slug of predetermined length, into a pipe full of flowing liquid.

The length of the "leading bubble" ahead of the slug being studied, was specified to be either 20 or 40 times the pipe diameter. Fagundes Netto *et al.* (1998) fitted a single curve through their data, as shown in Figure 2.4.

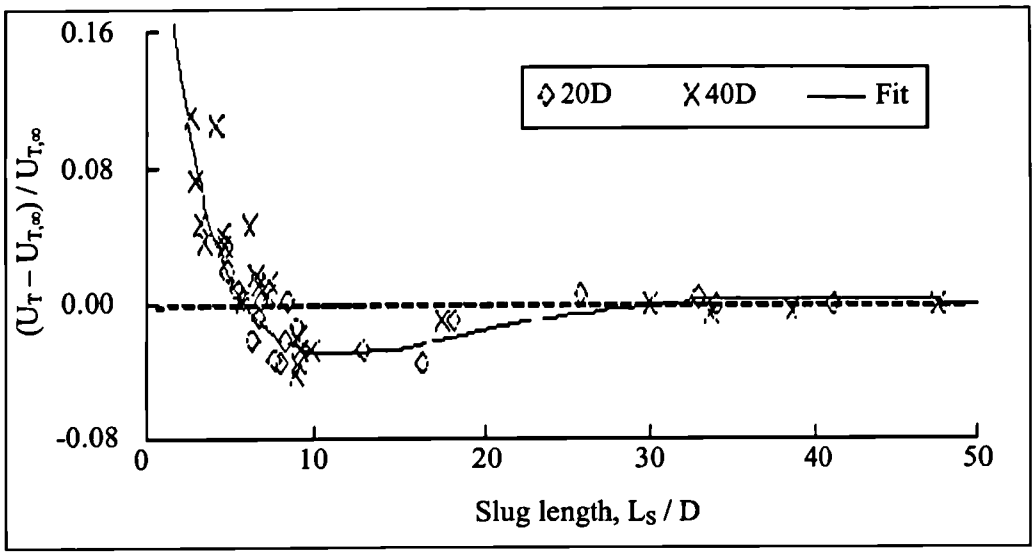

Figure 2.4: Experimental data for the "wake effect" (after Fagundes Netto *et al.*, 1998)

In a subsequent work, Fagundes Netto *et al.* (1999b) presented a considerably larger data set, using leading bubble lengths of 25 and 45 pipe diameters. The range of slug lengths studied was from zero to 50 times the pipe diameter, with mixture velocities of between 1.3 and 2.0 m/s. In each experiment, the length of the "trailing bubble" was 30D. The data are plotted in Figure 2.5.

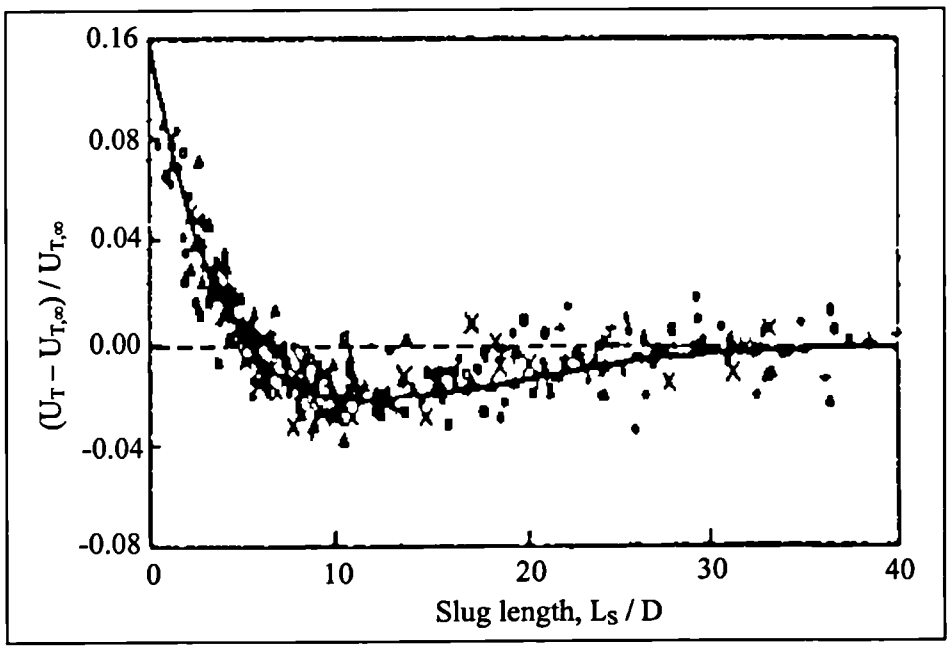

Figure 2.5: Expanded data set for wake effect experiments (after Fagundes Netto *et al.*, 1999b)

Fagundes Netto *et al.* (1999b) correlated U_T as a function of L_S and fitted a single equation to their scattered data,

$$\frac{U_T}{U_{T,\infty}} = 1 + C_1\left(1 - \frac{L_S}{L_C}\right)\exp\left(\frac{-kL_S}{D}\right) \qquad [2.86]$$

where $U_{T,\infty}$ is the translational velocity of a long, stable slug; C_1 and k are empirical constants with values 0.12 and 0.16 respectively, and L_C is a "critical length" of 5.4D. The authors did not mention any observable effect of varying the length of the leading bubble.

In a related study by Fagundes Netto *et al.* (1999a), the shape of the nose and tail of the film region in slug flow was investigated. They observed two different shapes for the slug front interface, which corresponded to the slug and plug flow regimes as defined by Bendiksen (1984). The slug front shapes which they reported were recently modelled using a three-dimensional CFD simulation by Ejedawe & Hughes (1999) in collaboration with the present author.

More recently, Cook & Behnia (2000) presented an alternative equation,

$$\frac{U_T}{U_{T,\infty}} = 1.0 + 0.56\exp\left(\frac{-0.46L_S}{D}\right) \qquad [2.87]$$

which they regressed from their own experimental data, measured at mixture velocities of less than 2.5 m/s. They used air and water for the investigation, conducted using an acrylic tube of length 16 m and diameter 50 mm. They reported no influence of the mixture velocity on the expression for U_T, and made no mention of the effect of the length of the leading bubble ahead of the slug under investigation.

The correlations by Fagundes Netto *et al.* (1999b) and Cook & Behnia (2000) are plotted in Figure 2.6.

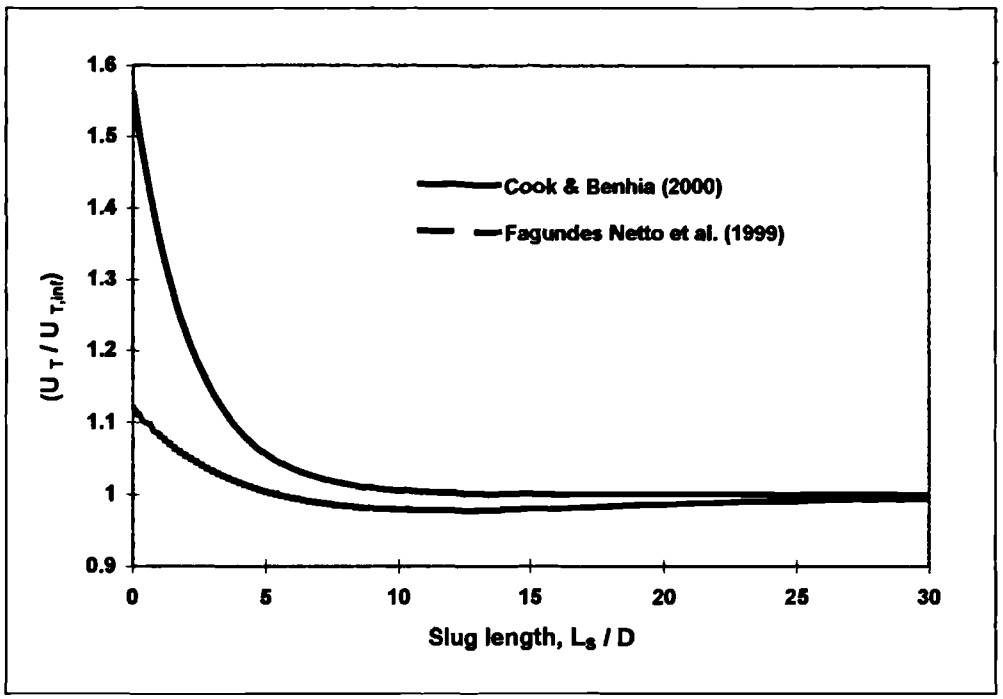

Figure 2.6: Wake effect correlations

The two correlations give significantly different predictions. The expression by Fagundes Netto *et al.* (1999b) suggests that the ratio $(U_T/U_{T,\infty})$ falls *below unity* when the slug length is greater than the "critical length", L_C. This phenomenon was based on their experimental observations, but was not reported by Cook & Behnia (2000), who did not include the effect in their correlation.

The influence of the "wake effect" when applied to a slug tracking scheme is discussed later in Chapter 7 of this thesis. In Chapter 8, a CFD study is presented, in which the wake effect is investigated computationally.

2.3.4. Slug frequency

Whilst not required for closure of the model presented in Chapter 7 of this thesis, calculation of the slug frequency anticipated in a slug flow is an important design parameter. It is also required as input by many "unit cell" models in order to calculate the number of slug units in a given length of pipe, and thus the total pressure drop. Furthermore, the experimental data presented in Chapters 4, 5 and 6 of the present work are compared with predictions from several slug frequency correlations and thus a brief description of these methods is given here, for completeness.

King (1998) reported that slug frequency is one of the "least reliably modelled parameters" of slug flow, due to the random nature of slug generation in a pipeline.

Slug frequency, φ, is defined as the average number of slug units passing a fixed point in the system, per unit time (Gregory & Scott, 1969). When this is plotted as a function of the total superficial velocity, U_{Mix}, the curve typically exhibits a minimum. Many authors have reported slug frequency data and many correlations have been proposed. Several of these are given below:

Gregory & Scott (1969) published a correlation based on a CO_2/water system in a 19 mm diameter horizontal pipe:

$$\varphi = \varphi_0 \left(\frac{U_{sL}}{gD} \left(\frac{U_{GS}^2}{U_{Mix}} + U_{Mix} \right) \right)^{1.2} \qquad [2.88]$$

where $\varphi_0 = 0.0226$ Hz and $U_{GS} = 4.444$ m/s.

Heywood & Richardson (1979) determined the Power Spectral Density (PSD) function of liquid holdup/time traces for air/water flow in a 42 mm diameter pipe. The mean slug frequency was taken to be the frequency at which the maximum power value was obtained from the PSD function. They proposed a correlation given by:

$$\varphi = \varphi_0 \left(\varepsilon_L \left(\frac{L_{HR}}{D} + Fr \right) \right)^{1.02} \qquad [2.89]$$

where Fr is defined by Equation [2.19], $\varphi_0 = 0.434$ Hz and $L_{HR} = 2.02$ m.

Tronconi (1990) studied the formation of slugs from their "precursor" waves which form in the inlet region of a pipe. He assumed that one half of these waves develop into slugs, and obtained the following expression:

$$\varphi = \varphi_0 \frac{u_G}{u_L} \frac{\rho_G}{\rho_L} \qquad [2.90]$$

where φ_0 is 0.61 Hz. Since φ is given in terms of the *actual* phase velocities, a value for the liquid holdup is required in order to use *superficial* velocity measurements.

Manolis *et al.* (1995a) performed experiments using the WASP facility at Imperial College and collected slug frequency data over a range of pressures. Their methodology, similar to that of Gregory & Scott (1969) was based on the definition of a modified Froude number,

$$Fr_{Mod} = \frac{U_{sL}}{gD}\left(\frac{U_{Mix,min}^2 + U_{Mix}^2}{U_{Mix}}\right) \qquad [2.91]$$

where $U_{Mix,min}$ is the value of U_{Mix} at the point where the frequency curve is at a minimum, taken by Manolis *et al.* to be 5 m/s irrespective of pressure. They proposed a correlation for slug frequency as:

$$\varphi = \varphi_0 Fr_{mod}^{1.8} \qquad [2.92]$$

where $\varphi_0 = 0.0037$ Hz.

A more comprehensive review of published correlations and semi-mechanistic models for slug frequency was given by Manolis (1995).

2.3.5. Slug length

Slug length, more so than other parameters of slug flow, has been treated as a statistical variable. This is arguably because both the mean and maximum slug length are important for design consideration. Here, two correlations for the *mean* slug length are considered.

Norris (1982) based a correlation solely on the effect of pipe diameter,

$$\ln\left(\frac{L_s}{0.3048}\right) = -2.099 + 4.859\sqrt{\ln\left(\frac{D}{0.0254}\right)} \qquad [2.93]$$

where L_s is the mean slug length and D is the pipe diameter, both in meters.

An improvement to this correlation was proposed by Scott *et al.* (1986) who attempted to account for two mechanisms of slug growth, namely liquid pickup at the slug front and gas expansion within the slug body:

$$\ln\left(\frac{L_s}{0.3048}\right) = -25.4144 + 28.4948\left[\ln\left(\frac{D}{0.0254}\right)\right]^{0.1} \qquad [2.94]$$

A review of slug length prediction using probability density functions was given by King (1998).

In his study of slug flow in a horizontal pipe using the WASP facility at Imperial College, Manolis (1995) found no obvious trend of slug length with either the gas or liquid superficial velocities. He reported an average slug length of around 20 diameters for liquid superficial velocities in the range 0.5 m/s < U_{sL} < 1.07 m/s, and he did not observe a significantly lower average slug length at lower liquid flows. King (1998) also reported slug flow data from the WASP facility with a horizontal test-section, using air and water at 0 and 5 bar(g). His data exhibited an average slug length of 17 diameters.

Nicholson *et al.* (1978) suggested a range of 12-30 diameters for stable slug flow, whilst the model of Dukler *et al.* (1985) gave a minimum stable length of 8 diameters, with the suggestion that most stable slugs are double this length as they are formed by the merging of two "nearly stable" slugs. The present work (see Chapter 7 of this thesis) suggests that this "merging" is unlikely. However, when the leading slug of a pair "dies", the trailing slug rapidly picks up the liquid volume, achieving the same result.

Burke & Kashou (1995) reviewed the available methods for slug length prediction as part of a more general consideration of the prediction of slug volume. They compared the slug length prediction from the slug flow simulation code OLGA® (see Section 2.5.1) with measured data and found that OLGA was able to reproduce the maximum slug length, which is the value required for the design of slug catcher facilities.

2.4. Slug flow in inclined and "hilly terrain" pipes

Many experimental studies of slug flow have been performed using idealised, horizontal systems. A large body of work also considers the case of "near-horizontal" slug flow, *i.e.* in slightly inclined pipes. This is concerned predominantly with flow in upwardly-inclined pipes; comparatively little work has been published on slug flow in downwardly-inclined pipes. A thorough review of this work is beyond the scope of this Chapter, and reviews of experimental studies of slug flow in inclined pipes may be found in Beggs & Brill (1973) (who also reported correlations for liquid holdup and pressure gradient in such systems) and in Taitel & Barnea (1990b) and Fabre & Liné (1992).

In this Section, a number of recent papers concerned with slug flow in inclined pipes are described and then a more thorough review of work in "hilly terrain" systems is presented.

2.4.1. Inclined flow

The flow pattern transition boundaries are strongly affected by pipe inclination, in particular the stratified/slug flow transition. In upwardly-inclined pipes, the region of the flow pattern map in which slug flow is encountered becomes greatly enlarged with respect to the horizontal case. For downward inclined pipes, slugging is suppressed and stratified flow prevails over wider regions (Kokal & Stanislav, 1989a; Yang *et al.*, 1996). Therefore, where one or more changes of inclination occurs in a pipeline, *i.e.* in so-called "hilly terrain" pipes, these observations imply that slugs grow or decay in sections of pipe with different inclinations. This is discussed further in Sections 2.4.2 and 2.5, below.

Slug flow in upwardly-inclined pipes was studied by Stanislav *et al.* (1986) and by Kokal & Stanislav (1989a, 1989b) who developed a unit-cell model for slug flow which included inclination effects. A key result was that the time-averaged liquid holdup decreased as the pipe inclination was increased.

A correction for the drift velocity term in the slug translational velocity expressions was proposed for inclined flow by Bendiksen (1984), who suggested

$$u_D = 0.35 \sin\beta \sqrt{gD} + 0.542 \cos\beta \sqrt{gD} \qquad [2.95]$$

In their model, Kokal & Stanislav (1989b) used only the second term to calculate u_D, and used the value 0.2 for the C-ratio.

Studies of downwardly-inclined slug flow were conducted at the University of Tulsa (Yang *et al.*, 1996). It was reported that the liquid holdup in the slug body was not affected by the pipe inclination angle. Yang *et al.* (1996) correlated slug translational velocity by:

$$U_T = 1.192\, U_{Mix} + (0.542 \cos\beta + 0.35 \sin\beta)\sqrt{gD} \qquad [2.96]$$

which is similar to the correlations for horizontal flow described in Section 2.3.3. Yang *et al.* (1996) reported that slug length followed a log-normal distribution, as in the case of horizontal flow. They proposed the following (dimensionally inconsistent) relationship:

$$\frac{L_{S,Mean}}{D} = \exp\left(\mu + 0.5000\sigma^2\right)$$
$$\frac{L_{S,0.1\%}}{D} = \exp\left(\mu + 3.0902\sigma^2\right) \qquad [2.97]$$

where $L_{S,Mean}$ and $L_{S,0.1\%}$ are respectively the mean and "one-in-a thousand" slug lengths. Here,

$$\mu = 2.0172U_{sG}^{0.243}e^{-0.01396U_{sG}}\left(1 - 0.00476U_{sL}\right)\left(\cos\beta - 0.0879\sin\beta\right) \qquad [2.98]$$

and

$$\sigma = \left(0.7269 - 0.009008U_{sG}\right)\left(1 - 0.05314U_{sL}\right)\left(\cos\beta - 1.7155\sin\beta\right) \qquad [2.99]$$

where the superficial velocities U_{sG} and U_{sL} are in units of ft/s (1 ft/s = 0.3048 m/s)

Yang *et al.* also reported a correlation for slug frequency in downwardly-inclined flow, similar in form to that of Gregory & Scott (1969):

$$\varphi = 0.02301\left(\frac{U_{sL}}{gD\left(\left[9.9476/U_{Mix}\right] + U_{Mix}\right)}\right)^{1.4844} \qquad [2.100]$$

where U_{sL} and U_{Mix} are in units of ft/s, g is 32.174 ft/s^2 and D is in ft.

Recently, Taitel *et al.* (2000) considered the simplified (Case 3) version of the slug tail solution by Taitel & Barnea (1990b) in downhill flow, and stated that solutions do not exist for a range of low liquid and gas velocities, which would normally result in stratified flow. These cases can occur if the film velocity u_{LF} is faster than the mixture velocity U_{Mix}. However, in a "hilly terrain" system, slugs may be generated in an uphill section of pipe and persist over a "peak" into a downwardly-inclined section where they propagate some distance downstream until they dissipate to form stratified flow. In their analysis, Taitel *et al.* (2000) assumed that, for downward flow, the C-ratio would be the same as for upwardly-inclined flow and the drift velocity would be zero. This assumption would seem, at best, to be a major simplification, and is currently the subject of work in progress at Imperial College (Ujang, 2000).

Woods *et al.* (2000) examined the effect of small downward inclinations on the formation of slugs. They conducted air/water experiments at atmospheric pressure in a 3 inch (78 mm) diameter pipe of length 23 m, at inclinations of –0.2°, –0.5° and –0.8°. They described the

non-linear mechanisms for the growth of short waves (with wavelength < 0.1 m) into slugs, which occurs at low gas velocities. At higher gas velocities they reported that, at the transition to slug flow, the large amplitude "stratified wavy" interfacial waves which are commonly seen in horizontal and upwardly-inclined slug flow, are damped in downwardly-inclined flow. Woods *et al.* (2000) performed photographic studies of slug initiation and concluded that the slug initiation occurs by the growth, through a localised Kelvin-Helmholtz instability, of a small, short wavelength wave positioned on the crest of a larger, long wavelength wave. This phenomenon is the subject of an exhaustive work by Hale (2000).

2.4.2. Flow in "hilly terrain"

The subject of multiphase flow in horizontal and slightly inclined pipes has received enormous attention from the oil transportation industry. Published correlations and phenomenological models are available for straight pipes at various inclinations, to predict various features of the flow patterns required for the design and operation of a hydrocarbon pipeline. However, comparatively little work has been done on the effects of one or more *changes* of inclination part-way along a flowline.

In their introduction to multiphase production, Hill *et al.* (1998) stated that the prediction of flow parameters, in particular pressure drop, is complicated by irregular terrain. Slug formation and decay at high and low points in a hilly-terrain system must be considered, and it is necessary to "track" slugs along a hilly-terrain system to evaluate which flow regimes exist at different points along a pipeline, since the flow in such systems is greatly influenced by what has happened upstream.

In addition to "transient" slugs caused by changes of pipeline operating conditions, and the hydrodynamic slug formation which occurs when waves at the stratified gas-liquid interface grow to reach the top of the pipe, as described in analyses such as that by Taitel & Dukler (1976), Hill *et al.* (1998) stated that at low flow velocities, liquid collects at low points in a hilly-terrain pipeline system. This liquid is periodically "blown out" when the gas pressure behind the liquid blockage balances the hydrostatic liquid head, causing a surging flow as the liquid accumulation "unloads". Hill *et al.* (1998) also accounted for the generation of so-called 'dip slugs' at higher gas velocities with the explanation that as liquid accumulates in a dip, the area available for gas flow is restricted. This results in an increase in gas velocity,

which causes slug growth by the well-documented Kelvin-Helmholtz type instability as described by Taitel & Dukler (1976).

Hill *et al.* (1996) reported test-line and full scale (up to 20 inch diameter) results from a hilly terrain multiphase pipeline in Colombia. They stated that the key issues in such systems are the prediction of pressure drop and characterisation of slug flow. Prediction of pressure drop is important in ensuring that there is enough pressure difference available to obtain the required production rates from reservoir to process. Slug characteristics are important in ensuring that the downstream process can satisfactorily accommodate liquid slugs arriving from the pipeline.

Hill *et al.* (1996) used gamma densitometry techniques to observe flow patterns in their investigation. They reported that for a moderate mixture velocity, an uphill portion of a pipeline could be in slug flow, while a downstream portion of the same pipeline could be in stratified flow; this may be predicted by the various flow pattern maps available. The complication with hilly terrain systems is that slugs arriving at the top of an incline may persist into the downhill section. The distance which the slugs travel downhill is determined by the gas and liquid flow rates.

The phenomenon of slug propagation over a "peak" in a pipeline not only influences whether slugs arrive at the end of a pipeline, and their size, but also has a considerable effect on the pressure drop through a system. Hill *et al.* (1996) stated that for uphill flow, significant gravitational pressure loss occurs across each slug, but that if slug flow persists downhill, this pressure loss is "recovered". However, if the slugs decay rapidly to stratified flow at the top of an incline, only the gas head is recovered in the downhill section. Hill *et al.* (1996) noted that, at that time, pressure drop models did not take account of the fact that slug flow may persist part-way along a downhill section of pipeline before decaying to stratified flow. They proposed a "Decaying Slug Model" which included this effect and which performed better than other slug flow models, predicting their measured field data to within ± 20%. This model was based on the concept of a 'rate of slug growth', whose dimensions were length of slug growth per unit length of pipe passed by the slug front. This value may be negative for the case of slug decay, and may be used to calculate a "survival distance" for a slug in a downhill section of pipeline. The model is described in greater detail by Barrett *et al.* (1998).

Zheng (1991, 1992) reported that the propagation of slugs from upstream flow, over a "peak" into downhill flow was also observed by Rothe & Crowley (1986). They found an unexpected region of slug flow in the downhill portion of their test section after a peak; this could not be reproduced if there was no slug flow in the preceding uphill section of pipe.

Hill *et al.* (1996) presented a procedure for tracking average-length and the largest ("one-in-a-thousand") slugs through a hilly-terrain pipeline, as a basis for slugcatcher design. They also reported test rig studies with three dips and two peaks in a single line, inclined at ±22.5°. The phenomenon of "flow stalling" was observed, in which liquid accumulated in a number of dips simultaneously. This resulted in a large increase in back pressure in the line, as the gas pressure built up to unload more than one dip at once.

Fairhurst & Barrett (1997) reported field data from a wet gas hilly terrain pipeline to illustrate the limitations of modelling methods which do not take into account the phenomena associated with dips and peaks in a pipeline. They also described results from a two- and three-phase experimental test facility, consisting of 6 inch diameter transparent piping arranged as a "dip" with a 21 m long -1° downhill section, followed by a 46 m uphill section at +1.3°. Tests were performed with air-water and air-oil-water mixtures. A series of tests was also performed in which a measured volume of water or oil was poured into the dip and the air flow was then switched on. This was conducted for a series of gas flow rates until the liquid was "blown out" of the pipeline, and the mean holdup downstream of the dip was measured. Fairhurst & Barrett (1997) compared the results of these tests with simulations using a commercial pipeline simulator, PLAC, and concluded that PLAC's predictions were reasonable at low gas flows, but substantially under-predicted the liquid holdup as the gas flow rate was increased.

Molyneux & Tait (1997) also reported studies with the PLAC simulator, in which the effects of changes in gas flow rate ("up-gas transients") were investigated. They also performed tests using a 3 inch diameter test facility, with a 13 m long, ± 5° dip. Tests were performed at pressures up to 10 bar(g) and a transparent test-section was used to observe flow effects at the dip. They concluded that, while PLAC is able to accurately simulate slugging due to transient changes of flow rate, the code does not accurately model individual terrain-induced ("dip") slugs and so provides a poor prediction of the pressure surges resulting from loading and unloading of the dip.

Wood (1991) carried out experiments with a 2 inch (50 mm) diameter test pipe arranged as a 25 m long, -1.75° downhill section followed by 26 m of +1° upwardly-inclined pipe. He used air and water at atmospheric pressure, and his procedure was to partially fill the dip with a measured volume of water, and observe the effect of different air velocities on the liquid behaviour at the dip, and in particular on the formation of slugs at the dip. Six distinct effects were observed at different gas flow rates:

- Static accumulation, where the liquid was unaffected by the gas flow.
- Ripples on the surface of the accumulated liquid.
- Wavy flow, where waves moved a short distance along the uphill section of pipe, but no liquid was removed from the dip.
- Slug formation and collapse: slugs formed at the dip, but collapsed before reaching the end of the uphill section, and the liquid drained back to the dip, so that no liquid reached the end of the pipe.
- Liquid removal by slugs, where slug flow persisted to the end of the pipe, with counter-current liquid flow between slugs where the liquid shed at the slug tail ran back upstream towards the dip.
- Total liquid removal, where all liquid was "blown" out of the dip.

Wood (1991) reported that the "critical gas velocity" at which all liquid was removed from the dip with no counter-current liquid flow, occurred at a superficial gas velocity of 7.7 m/s at atmospheric pressure. He presented an analysis for the calculation of critical gas velocity, using the one-dimensional momentum balance equations developed by Taitel & Dukler (1976). An analysis was also given for the maximum stable liquid accumulation in a pipeline dip, based on consideration of the liquid pickup and shedding rates at the front and tail of a slug, respectively.

In their report of slug formation, based on observation of a hydraulic jump in a horizontal pipe, Petritsch & Mewes (1998) mentioned that similar effects may occur at a pipeline dip, where the liquid level may reach the top of the pipe and initiate slugging. However, their hydraulic jump analysis was restricted to a horizontal geometry.

The work at Tulsa University by Zheng (1991), also described in the subsequent publications by Zheng *et al.* (1992, 1993), presented results from hilly terrain flow tests using air and

kerosene in a 420 m long, 3 inch (75 mm) diameter test section. The experimental data were used to develop a one-dimensional slug tracking model, which is described in Section 2.5.

Recent experimental work by Manabe *et al.* (1999) extended the work by Wood (1991). Investigations were conducted in 20 mm tubes inclined at $\mp 3°, \mp 5°$ and $\mp 7°$, using air/water and air/glycerine as the test fluids. The experimental procedure proposed by Wood (1991) was used without modification. Manabe *et al.* (1999) proposed an experimental correlation for the onset of slugging in a V-section, derived from a modification of the Wallis parameter which is widely used for the prediction of flooding in vertical systems (Wallis, 1961). Their criterion for the onset of slugging was

$$J_G^{**} = -2.81 Q_L + 3.35 \qquad [2.101]$$

where Q_L is the volume of static liquid accumulated in the V-section and J_G^{**} is a modified version of the flooding parameter by Wallis (1969), given by

$$J_G^{**} = \frac{|J_G|}{\sqrt{gD\cos\beta \dfrac{(\rho_L - \rho_G)}{\rho_L} \dfrac{1}{f_D(Bo)^4}}} \qquad [2.102]$$

where J_G is the gas mass flux in kg m^{-2} s^{-1} and the parameter $f_D(Bo)^4$ is an experimental function of the Bond number, which was stated by Manabe *et al.* (1999) only for the case where the pipe inclination β is $\mp 3°$, as

$$\frac{1}{f_D(Bo)^4} = -227 \times 10^{-6} Bo^2 + 2.34 \times 10^{-3} Bo + 0.880 \qquad [2.103]$$

The authors suggested that this function differs when the inclination of the V-section is changed, but did not elaborate. Furthermore, it should be noted that Equation [2.101] is not dimensionally consistent and that the accumulated liquid volume, Q_L is a function of the pipe diameter and inclination, and the liquid flow into the dip. Thus, this criterion is not readily applicable to situations other than that for which it was derived.

2.5. Slug tracking models

Slug tracking models are distinguished from "unit cell" models (discussed in Section 2.2.1) in that they consider each slug individually, and model the propagation of a number of discrete slugs along a pipeline. This technique has significant advantages over the unit cell approach

as the slug length distribution arising from a particular pipeline configuration may be obtained without recourse to statistical correlations. Slug tracking schemes have received considerable interest in recent years. However, they are computationally intensive since a pipeline may contain many hundreds of slugs, each of which requires a unique solution to the modelling equations at each timestep during a transient simulation. As a result, highly simplified physical models have been implemented in the published slug tracking schemes.

Generally, slug tracking models are used to generate statistical data about slug flow at a particular set of conditions. Since slug flow is stochastic, the variables required for the design and operation of hydrocarbon production facilities are usually the *mean* and *maximum* slug lengths and frequencies which are likely to be encountered. Occasionally, slug tracking models are used to reproduce resolved measurements on individual slugs, or small groups of slugs, taken from field or experimental data.

King (1998) reported that discrete slug flow models were first formulated to predict pigging, the operation of "sweeping" accumulated liquid from a pipe using a "pig" (commonly, a neoprene sphere). This is performed in "wet gas" pipelines in particular, in order to maintain the liquid holdup in the pipe at a level below which hydrodynamic slugging will occur. Pigging models, such as that by Minami & Shoham (1993), were therefore developed to predict the behaviour and size of the large liquid slugs which are swept ahead of the "pig".

Scott *et al.* (1987) considered slug growth in long pipelines. They classified slug growth into two distinct types - developing slug growth and long term slug growth. The former occurs where the rate of liquid pickup at the slug front is greater than the shedding rate in the tail, whilst the latter occurs due to gas expansion within the slug body, which increases the mixture velocity and hence the volumetric gas entrainment rate at the slug front. Scott *et al.* (1987) wrote the following expression for developing slug growth:

$$\frac{dL_S}{dt} = \frac{\varepsilon_{LF}}{\varepsilon_{LS}}(U_F - u_{LF}) - (U_T - u_{LS}) \qquad [2.104]$$

where the slug front velocity, U_F is obtained from a liquid volume balance at the slug front:

$$U_F = \frac{u_{LF}\,\varepsilon_{LF} - u_{LS}\,\varepsilon_{LS}}{\varepsilon_{LF} - \varepsilon_{LS}} \qquad [2.105]$$

For the translational velocity at the slug tail, Scott *et al.* (1987) used the expression:

$$U_T = 1.2\,u_{LS} + \sqrt{g\left(h_{LS} - h_{LF}\right)} \qquad [2.106]$$

where h_{LS} and h_{LF} are the equivalent liquid height in the slug body (calculated from the slug body holdup, ε_{LS}) and the height of liquid in the film region ahead of the slug front, respectively. Scott *et al.* (1987) calculated the slug body liquid holdup using the correlation by Gregory *et al.* (1978). They assumed a flat film profile in the slug tail, whose uniform height was determined by a momentum balance between the wall shear stress in the liquid phase, and the interfacial shear stress. The "no slip" assumption was made for the slug body, and the wall shear stress in the gas bubble region was not included in the analysis.

Bendiksen & Espedal (1992) published a model similar to that of Scott *et al.* (1987) as part of their study of the transition from stratified to slug flow. They calculated the slug front velocity using Equation [2.105] and used the method of Bendiksen (1984) to obtain the translational velocity at the tail.

Woods & Hanratty (1996) included slip within the slug body in their analysis. they reported that slip occurred at mixture velocities greater than 7 m/s, and modelled this in the form

$$\begin{aligned} S &= 1 && U_{Mix} < 7\,ms^{-1} \\ S &= 1.5 && U_{Mix} \geq 7\,ms^{-1} \end{aligned} \qquad [2.107]$$

where S, the slip ratio, is defined for the slug body as

$$S = \frac{u_{GS}}{u_{LS}} \qquad [2.108]$$

Woods & Hanratty (1996) derived an expression for the volumetric liquid shedding rate at the slug tail,

$$\dot{V}_{LT} = A\,\varepsilon_{LS}\left(U_T - \frac{U_{Mix}}{\varepsilon_{GS}(s-1)+1}\right) \qquad [2.109]$$

They did not treat the film region analytically, but instead used experimental measurements of film height and slug body holdup. They assumed the gas velocity was equal to that of the Taylor bubble (*i.e.*, the translational velocity of the slug tail) and performed a momentum balance, using the interfacial friction factor correlation of Andritsos & Hanratty (1987), in order to calculate the liquid film velocity.

Barnea & Taitel (1993) used the slug tracking approach to model the development of slugs at the entrance of a pipeline. They simulated the propagation of a large number of slugs, whose lengths were initially prescribed by a normal distribution. Some distance along the pipe, the simulated results showed that a slug length distribution of the form observed by Brill *et al.* (1981) was produced. Barnea & Taitel's (1993) model considered the *slugs only*, so that the film region between slugs was assumed to be "dry". Since no mass balance could thus be performed to calculate the slug front velocity, this was assumed to be equal to the translational velocity of the tail of the next slug downstream. In their analysis, they included an expression for the "wake effect", which is described above in Section 2.3.3.

The propagation of short slugs near to the pipe entrance was the subject of a recent work by Cook & Behnia (2000). They conducted air/water experiments in order to obtain an experimental correlation for the translational velocity of the slug tail, described in Section 2.3.3, above. This correlation was then employed in a model of horizontal slug flow; they assumed an initial normal distribution of slug lengths at the pipe inlet and then calculated the evolution of individual slugs along the pipe. Gas entrainment effects were neglected and thus the liquid holdup in each slug was assumed to be unity. The film region between slugs was not ignored, as in the earlier model by Barnea & Taitel (1993), but the region was assumed to be flat and stationary, so that the film height could be calculated by a simple mass balance. Simulations were performed for mixture velocities of 1.2, 2.5 and 3.5 m/s, which corresponded to the experimental conditions used to derive the correlation for the slug tail velocity. Experimental and computed results for the slug length distribution were reported at a distance of 11m from the pipe inlet. In the simulations, 1000 inlet slugs were "launched", with the mean inlet slug length ranging from 2D to 6D. Cook & Behnia (2000) reported good agreement between their experimental results and the predictions of the model, and also stated that the effect of varying the initial slug length distribution was insignificant. This is contrary to results obtained in the present work, which are presented in Chapter 7 of this thesis. The reason for this discrepancy is probably the assumption of a flat film in Cook & Behnia's (2000) model.

Effects due to the gradual expansion of gas bubbles in a pipeline were first included in a slug flow model by Gilchrist & Wong (1991) and Wong & Gilchrist (1993), who adapted a dynamic model of slugging in vertical pipeline risers to the case of horizontal, hydrodynamic slug flow. Their solution scheme is discussed in a review by King (1998).

Nydal & Banerjee (1995 and 1996) considered the effects of pressure from the outset during the development of their slug tracking model, rather than including them as an addition to an existing kinematic model. Their simplifying assumptions were that there was no gas entrainment in the slug body, and that the liquid film thickness between each slug was constant for any pipe section. They also neglected the pressure drop within the film region. King (1998) describes the derivation of their model in detail.

Nydal & Banerjee (1995 and 1996) used an object-oriented algorithm, in which each slug or bubble in was treated discretely, and in sequence. They recommended that a small time step (of approximately 0.01 s) should be used in the solution. Their algorithm consisted of four steps:

1. Calculate the pressure in the film region for each bubble in the pipe, in turn.
2. For each liquid slug, calculate the liquid velocity u_{LS}. The liquid film holdup and velocity are then obtained.
3. Calculate the velocities of the "borders" of the slug, *i.e.* the front and tail translational velocities.
4. Advance the slug front and tail positions by a distance equivalent to the product of the appropriate velocity and the timestep.

In order to calculate the evolution of the slug length distribution along a pipe, Nydal & Banerjee (1995, 1996) used an expression for the wake effect of the same form used by Barnea & Taitel (1993). This resulted in a log-normal slug length distribution, some distance from the pipe inlet.

Larsen *et al.* (1997) reported results from a dynamic slug tracking scheme which included gas compressibility effects. They developed an object-oriented algorithm to track slugs in two- and three-phase systems. Larsen *et al.*(1997) used the simplifying assumptions of no gas entrainment in the slug body (*i.e.* ε_{LS} equal to unity) and uniform film height in the stratified regions, and did not consider the effect of wave propagation. The model was found to predict the propagation of long slugs in a flexible riser with reasonable accuracy, compared with experimental data obtained by the authors from the SINTEF multiphase flow laboratory.

The effect of gas compressibility on a slug tracking model was also discussed by Taitel & Barnea (1998a). They modelled flow in a horizontal pipe and, as in their earlier (1990a)

model, used the correlation of Gregory *et al.* (1978) for the liquid holdup in the slug body. The liquid film between slugs was assumed to be of uniform thickness, and was calculated using a quasi-equilibrium force balance. The slug front velocity was calculated from a mass balance over the slug front, and the tail velocity from the expression

$$U_T = 1.2U_{Mix} + 0.54\sqrt{gD} \qquad [2.110]$$

As an approximation, Taitel & Barnea (1998a) calculated pressure and density using a force balance, and neglecting accelerational pressure losses. The pressure at each slug was determined at the centre of the slug. Thus, if slug (i+1) is immediately upstream of slug i then the pressure at slug (i+1) is calculated as the pressure at slug i, plus half the frictional and gravitational pressure loss across slug i, plus the pressure drop across the intervening film, plus half the pressure drop across slug (i+1).

At each time step, the pressures at each slug are calculated and used to update the values of the gas density and hence slug body density. The front and tail velocities of each slug are thence updated, and the positions of each slug front and tail are adjusted accordingly.

To eliminate errors in the liquid mass balance caused by the use of a uniform film thickness for each slug unit, Taitel & Barnea (1998a) adjusted the liquid film holdup for each film at each timestep, using a slug unit mass balance:

$$\frac{d\left(L_{F,i}\varepsilon_{LF,i}\right)}{dt} + \frac{d\left(L_{S,i}\varepsilon_{LS,i}\right)}{dt} = (U_{F,i} - U_{Mix,i})\varepsilon_{LS,i} - (U_{F,i+1} - u_{LF,i})\varepsilon_{LF,i} \qquad [2.111]$$

where the subscripts i and (i+1) refer to a neighbouring pair of slugs, with slug i downstream of slug i+1. Since the pressure (and hence the gas density) varies along the pipeline, the total superficial velocity U_{Mix} is no longer constant for each slug.

Taitel & Barnea's (1998a) results showed that the inclusion of gas compressibility caused an increase in the slug unit length, but had only a minor effect on the growth of the slug body as the slug moved downstream.

Slug tracking models were first applied to "hilly terrain" systems by Zheng (1991), and in a subsequent work by Zheng *et al.* (1993). The main features of the model were that it assumed a constant liquid film thickness between slugs, and was based on a "source-sink" concept. In this, elbows (dips or peaks) in the pipeline were allowed to accumulate liquid (*i.e.* act as

liquid "sinks") which would later be released from the elbow. For example, a dip was taken to act as a liquid sink after a slug had passed, so that the sink accumulated liquid shed by the slug tail. This liquid was then added to the next slug to arrive at the dip, resulting in the instantaneous growth of that slug. Zheng (1991) imposed the constraint that a "sink" at a dip may only have a limited capacity, and that when the sink was full, all the liquid was discharged to form a new slug. In this way, his model included the formation of new slugs at the dip as well as the growth of existing ones.

At a peak occurring at the top of an incline, a similar treatment by Zheng (1991) designated the peak as a sink when a slug was present, or as a source when a stratified film existed. In this way, a slug would dissipate as the liquid was removed into the sink, unless the slug was of sufficient length that the sink capacity was reached. In such a case, the slug would be reduced in length, but would persist into the downhill section after the peak. The full sink would then release liquid as a stratified film layer after the passage of the slug. Slugs which persisted over a peak into the downhill pipeline section were assumed to remain a constant length until the next change of pipeline inclination; the effects of slug dissipation in downhill flow were not considered.

The concept developed by Zheng (1991) has more recently been extended by Taitel & Barnea (1998b, 1999) who applied their recent slug tracking model (Taitel & Barnea, 1998a) to hilly terrain systems. Their analysis was much more general than that by Zheng and co-workers, and included effects of gas compressibility. However, the model was simplified using the slug body holdup correlation of Gregory *et al.* (1978) and was restricted to the use of a uniform film thickness between slugs. Taitel & Barnea (1999) stated that "the complication lies primarily in the programming scheme", due to the large number of possible interactions which may occur between slugs and films of different velocities and thicknesses. They did not, however, include the effects of interfacial wave propagation in their model, which is shown in later Chapters of the present work to complicate matters still further!

Taitel & Barnea's (1998b, 1999) treatment of top and bottom elbows between pipe sections of different inclination differed slightly to that of Zheng (1991). They proposed that a slug was unaffected by passage over a top elbow (*i.e.*, a "peak" at the top of a Λ-section) but that the film behind it should flow *downhill* on *both sides* of the elbow. This produces upstream film flow in the rising limb of the Λ-section and, since a uniform film thickness is used between slugs, results in the creation of a "dry zone" at the elbow itself, as shown in Figure 2.7.

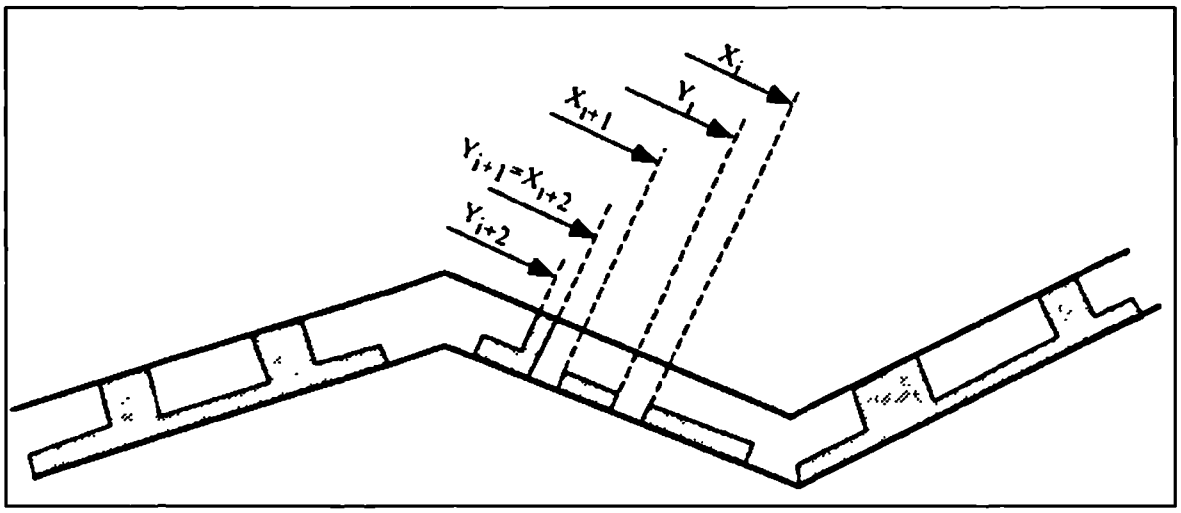

Figure 2.7: Generation of a "dry zone" at a top elbow (*ex.* Taitel & Barnea, 1999)

In their algorithm, Taitel & Barnea (1998b, 1999) treated this dry zone as a special "slug" with zero liquid holdup, but whose front and tail velocities were equal to the velocities of the films on the down- and upstream sides, respectively. This approach was also used to model the dry zones which could result when slugs dissipated in a downwardly-inclined section of pipe if the leading film moved faster than the trailing one.

The approach used to model a bottom elbow (*i.e.*, a "dip" in a V-section) was more akin to the source/sink concept proposed by Zheng (1991). The liquid films in both limbs of a V-section were allowed to flow downhill towards the elbow and accumulate there. Once the accumulated volume could support a new slug, then a slug was "generated" from the dip and moved off downstream. The "critical length" of the "dip slugs" generated in this manner is therefore required for closure of the model, however the relationship used by Taitel & Barnea (1998b, 1999) was not described. In the case where a slug arrived at the bottom elbow before a new slug was generated, all the liquid accumulated in the dip was "swept out" by the existing slug, which instantaneously grew in length as it entered the uphill leg of the V-section.

2.5.1. Commercial simulators for slug flow

Several companies have developed commercial simulation software for multiphase flow, primarily to predict transient slug flow arising from changes in the operating conditions of a pipeline. Three codes are in widespread use within the hydrocarbon industry, OLGA®, PLAC® and TACITE®: of these, only OLGA currently includes a slug tracking scheme.

A brief description of the three codes is given in this Section. A more thorough review, which includes a discussion of the equations used in the models, was presented by King (1998).

OLGA®

OLGA, developed by IFE, Norway, is based around a two-fluid model which additionally includes a liquid droplet field, to allow the modelling of annular flow. The six equations solved (Bendiksen *et al.*, 1991) are for continuity of mass in the droplet field, the annular gas core and the liquid film region, continuity of momentum in the liquid film and the annular core (in which the momentum terms for the droplet field and the gas core are combined), and a total energy balance. The code includes a slug tracking scheme, although slug frequency in the pipe must be specified, which introduces a large degree of uncertainty (King, 1998). Many comparisons of OLGA with field data are available in the literature (*e.g.*, Hustvedt, 1993).

PLAC®

PLAC (Pipeline Analysis Code) was developed by AEA Technology from the TRAC® program (Transient Reactor Analysis Code), which was originally designed to predict fluid flow in loss of coolant accidents in nuclear reactor engineering. PLAC is based on a two-fluid model. The set of six equations solves relationships for the continuity of mass and momentum in each phase, and also energy balances for the gas phase and the gas-liquid mixture. An interfacial coefficient in the equations incorporates some effects of flow pattern. The slug flow model included in PLAC is a development of a pigging model, based on the drag force acting on a solid sphere. No slug tracking procedure is included in the code.

TACITE®

TACITE (Pauchon *et al.*, 1993, 1996) was developed at IFP, France. It is based on a drift flux model in which the mean velocity of the gas is represented as the product of a distribution parameter (C_0) and the total superficial velocity, plus a mean drift velocity which takes account of the relative velocity between the gas and the liquid phases. There are four equations: two for continuity of mass for each of the two phases and one each for conservation of momentum and energy in the two-phase mixture field. Flow pattern is incorporated using a scalar variable, which is zero for dispersed flows and unity for separated flows. Additional closure laws are then used depending on the flow pattern. For slug flow, a

standard expression for slug translational velocity is used (see Section 2.3.3), with slug body holdup given by the model of Andreussi & Bendiksen (1989).

2.5.2. Slug capturing using the two-fluid model

The commercial codes described above generally operate with large nodal size (ranging typically from several meters to several tens or even hundreds of meters). However, recent work by Issa & Woodburn (1998) (see also Hewitt, 1997) has shown that the two-fluid model is capable of capturing many of the principal features of slug flows, including slug initiation, development and propagation. To achieve this, it is necessary to decrease the node size by several orders of magnitude below those used commonly in the commercial simulators. The computation becomes relatively insensitive to node size when this falls below about 25mm (0.3 pipe diameters). Though these results are interesting, this approach has some limitations:

1. The number of nodes required is probably impracticable in the context of an industrial-scale pipeline (although the continuing increase in computing power may eventually overcome this).

2. Although the two-fluid approach does not rely on empirical closure laws to describe certain features of slug flow, it is heavily dependent on the proper selection of empirical relationships for wall and interfacial friction in order to correctly predict the distribution of the phases. This presents some difficulties.

3. The phenomena involved are significantly multi-dimensional and cannot be represented in detail in a one-dimensional framework without recourse to additional closure relationships.

In the present work, two alternative approaches have been pursued. Firstly, an efficient slug tracking methodology has been developed which treats slugs and waves as "objects" whose behaviour is estimated. This model is based on a two-fluid model of the slug tail region, which is solved in the present work over a grid of small (1mm) nodes. Secondly, work has been done towards the computational fluid dynamics (CFD) prediction of the three-dimensional behaviour of slugs. This information can be used, together with experimental data, to formulate empirical relationships which may be used to incorporate multidimensional effects in the slug tracking model.

Chapter 3: Experimental method

The experimental methods applied in this work are described in this Chapter. The aim is to describe the apparatus and techniques in a level of detail that would allow the experiments to be reproduced. All the experiments undertaken for the present work were performed on the high-pressure WASP facility in the Department of Chemical Engineering and Chemical Technology at Imperial College.

In what follows, the basic design of the rig and its control system are described in Section 3.1, the instrumentation and data-acquisition apparatus are summarised in Section 3.2 and the procedure used for the experiments is discussed in Section 3.3.

3.1. The high-pressure WASP facility

The WASP (Water, Air, Sand, Petroleum) Facility is illustrated in Figure 3.1.

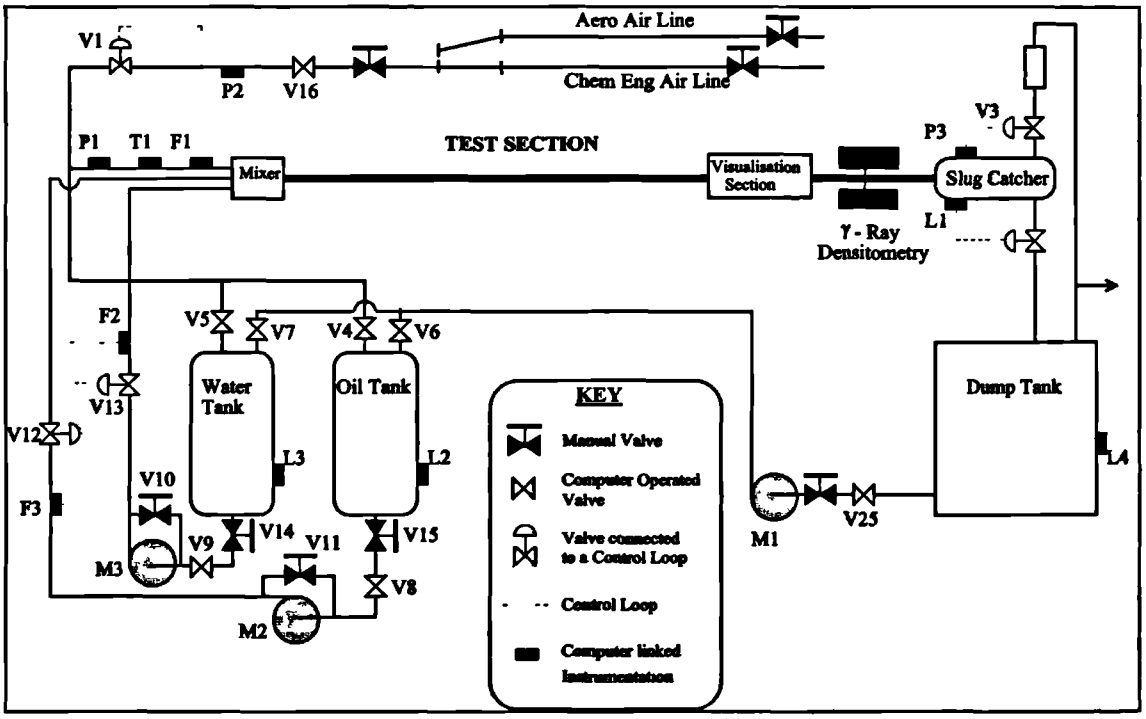

Figure 3.1: The WASP facility

The rig test-section consists of a 3-inch nominal-bore (77.92 mm internal diameter) stainless-steel pipe, approximately 37 m long. It can be aligned horizontally, or inclined slightly (+2 °

to -2 °) from the horizontal. Furthermore, by insertion of a flexible link between two of the steel pipe sections, it is possible to position the test-section to include a change of inclination at a selected position along its length. Such an arrangement was used to configure the test-section as a "V" or "Λ" shape for the "dip" and "peak" experimental campaigns, respectively, as described in Sections 3.3.2 and 3.3.3.

The test pipe is made up of four pipe sections between 6 and 7 meters in length, one 4.8 meter section and a number of smaller "make-up" pipe sections which allow accurate control of the distances between the various instruments. The steel pipe sections are fitted with welded flanges built in accordance with ANSI 600. Most flanges are built to a "tongue-and-groove" specification which ensures continuity of the pipe bore. Other flanges are of the raised-face design. Instrumentation may be located between the flanged joints of consecutive pipe sections. This is discussed in greater detail in Section 3.2. For the present work, two sections of pipe made from acrylic resin (Perspex®) were used; one in the "visualisation section" to allow video recording of the flow, the other in the dual-energy gamma densitometer apparatus described in Section 3.2.1.

3.1.1. Operation of the facility

The facility operates in a "blowdown" mode whereby high pressure air from the supply tanks flows through the test-section and is released to atmosphere through a pressure control valve. The flow of the liquid phases is driven in a similar manner: the head space above the liquid phase in each of the 5 m^3 oil and water tanks is pre-pressurised with air, to an initial pressure of 24 bar, considerably above that at which the experiments are to be conducted. Liquid is then "blown down" through the test section. At liquid superficial velocities greater than 0.2 m/s, pumps M2 and/or M3 (for the oil and/or water phases respectively) are used in addition, to boost the flow rates and to prevent large changes in liquid flow occurring during the course of an experimental run.

The high-pressure air is supplied at a pressure of 24 bar(g) from the 65 m^3 tanks located in the adjacent Aeronautics Department at Imperial College. The compressor which supplies these tanks is kept running during the experiments but, for high flow rates and/or high pressure operation, the tank pressure falls during the test. An alternative mode of operation uses lower-pressure air taken from the Chemical Engineering Department compressed air supply, at approximately 6 bar(g). In this case the high pressure air supply would be disconnected for

safety reasons. The experiments described in the current work used only the high-pressure supply.

A constant (mass) flow rate of air during an experiment is ensured by the use of a critical flow valve in the air inlet line, which eliminates any variation in flow rates due to changes in downstream pressure, which could subsequently affect the flow. For air, critical flow is achieved if the ratio of the upstream to downstream pressures exceeds a value of 1.894 (Manolis *et al.*, 1995b). In the experiments performed for this thesis, the test-section pressure was always lower than 7 bar(g) and the air supply pressure was always greater than 18 bar(g) so that critical flow was always assured.

The air flow rate is measured using a corner-tapping orifice plate (F1) conforming to BS1042. A variety of orifice dimensions may be used according to the air flow rates and/or pressures to be studied. For the experiments in this study, 15mm, 20mm, 25mm and 30mm orifices were used in order to study as wide a range of flow rates as possible.

The experiments described in this thesis were conducted using air and water only. The liquid phase used was water (density: 1000 kg/m^3, viscosity: 1.0 mPas at 23.5 °C, surface tension 0.037 N/m). It should be noted that the measured surface tension of the WASP rig water is significantly below the typical value for pure water (0.072 N/m). This is almost certainly due to slight contamination of the water by the oil. However, the water is analysed regularly and the measured surface tension has remained constant to within ± 0.001 N/m.

Water flow measurement is accomplished using a DANFOSS magnetic flowmeter (F2). This functions by the principal of electromagnetic induction; the water flow is passed through a magnetic field, inducing an electric current which is proportional to the volumetric water flow rate.

Gas and liquid phases are fed to the inlet of the test-section in such a manner that parallel flow of the phases is established before they come into contact. The inlet phase distributor (see Figure 3.2) incorporates a flat plate fixed horizontally between the phase inlets, to ensure the initial separation.

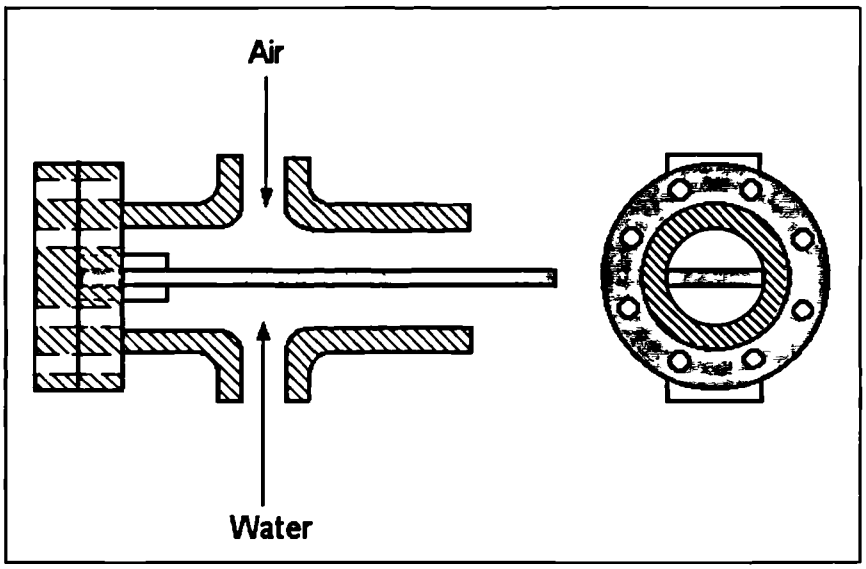

Figure 3.2: The test-section inlet section for two-phase gas-liquid flow

This inlet arrangement has been used on the WASP facility since it was found (Davies, 1992) that non-parallel introduction of the phases can have a significant effect on various flow parameters and in particular on the slug frequency in the system.

The "slug-catcher", situated at the outlet of the test-section, is a baffled gas-liquid separator. From this vessel, air is discharged to atmosphere through a control valve (V3) and silencer, and the two liquid phases are led through a level-control valve (V2) to a "dump tank" at atmospheric pressure. This arrangement of "separation under pressure" avoids large pressure oscillations which would otherwise be induced (as in some other multiphase flow facilities) if a throttle valve was used at the end of the pipe to reduce the pressure of the multiphase flow prior to separation.

If two immiscible liquid phases are used in the experiments, they are allowed to separate under gravity in the dump tank, usually overnight. Once separation has occurred they are then returned to their respective feed tanks by the transfer pump (M1). However, for the present work, only water was used so this separation stage was not required.

Many modifications have been made since the WASP rig's initial construction. The development of the facility is charted in the theses of the author's predecessors: Davies (1992), Hall (1992), Srichai (1994), Manolis (1995), Pan (1996), Roberts (1996), Kurban (1997), Machado (1997), Khor (1998), King (1998), Shaha (1999), Badie (2000), Hale (2000) and Odozi (2000).

3.1.2. The WASP Facility computer control system

Control of the WASP Facility is largely by a computer control system, although a small number of valves are manually controlled for safety reasons. These are the air inlet valves from the high- and low-pressure supplies, sited upstream of V16, and the valve in the liquid transfer line, sited upstream of the transfer pump, M1. All other valves and cocks are operated remotely from the rig control room.

The control computer displays information from the various level, pressure, flow and temperature transducers sited around the rig. The valve positions, shown as a percentage of full-range for the control valves or as a simple on/off state, are also shown for the remotely-operable valves on the facility. Communication between the control computer and the instruments and control valves on the WASP facility is via an ANDS4400 control system.

Two modes of control are possible, "manual" control and automatic control. In "manual" mode, the operator enters values for the valve positions directly into the control computer. All valves may be controlled in this manner, and this mode of operation is predominantly used when the facility is operated at near atmospheric pressure. In addition, up to five feedback control loops may be closed so that the valve positions are adjusted automatically and continually by the computer in order to meet a desired, predetermined "setpoint" value. Currently, feedback control allows automatic control of air flow rate (using a loop linking V1 to F1), water flow rate (V13 to F2), oil flow rate (V12 to F3), slug catcher level (V2 to L1) and slug catcher exit pressure (V3 to P3).

The feedback control algorithm in the computer software implements three-term PID (Proportional, Integral, Derivative) control for the five loops. The transfer function of the algorithm is given by

$$G_c(s) = K_c\left(1+\frac{1}{\tau_I s}+\tau_D s\right) \qquad [3.1]$$

where K_c is the controller gain, τ_I is the integral time constant and τ_D is the derivative time constant. Values of these parameters were set for the WASP rig control loops to allow control over a broad range of pressures and flow rates. However this may impose limitations when operating in a particular range of conditions. King (1998) discusses the limitations of this control scheme when applied to transient multiphase flows.

For the experiments conducted at atmospheric pressure, all control loops were left open and "manual" control of all flow rates was used. For the experiments performed at elevated pressure, the slug catcher level and slug catcher exit pressure loops were closed to allow automatic control of the test-section pressure. However, the positions of the flow rate control valves were still set "manually".

3.2. WASP rig instrumentation and data acquisition

A number of different instruments are available for use on the WASP facility to measure both "gross flow" characteristics such as pressures and inlet flow rates, and "local" data such as liquid holdup at various points along the test section. The instrumentation used for the present work is summarised in Table 3.1.

Measured Parameter	**Range**	**Error in measurement**	**Instrument**
Superficial gas velocity, U_{sG}	0.5 - 28 m/s	± 0.5 %	15, 20, 25, 30 mm orifices, used in accordance with BS1042 (1982)
Superficial liquid velocity, U_{sL} (oil and water)	0 - 0.05 m/s	± 0.5 %	Lowflow flowmeter (Mass3000 MassFlo)
Water superficial velocity, U_{sW}	0.03 - 0.75 m/s	< 1 %	Danfoss 381 MagFlo electromagnetic flowmeter
Liquid holdup (oil and/or water), ε_L	0 - 1	± 5 % of full scale	Gamma densitometer
Liquid holdup (water only), ε_L	0 - 1	± 1.5 % (± 1 mm in measured liquid height)	Conductivity probes
Pressure difference, ΔP	±10 kPa	± 0.1 %	Rosemount differential pressure transducer
Inlet pressure	0 - 50 kPa	± 0.05 kPa	RDP pressure transducer
Exit pressure	0 - 50 kPa	± 0.1 % of full scale	Rosemount static pressure transducer
Test-section temperature		± 1°C	Mineral insulated (Type K) thermocouple

Table 3.1: WASP facility instrumentation

Besides the measurement errors, experiments are subject to setpoint errors where the flow rates or exit pressure may drift. These errors are shown in Table 3.2.

Measured Parameter	Drift from setpoint value during experiment
Water flow rate	± 5%
Air flow rate	± 5%
Test-section exit pressure	± 200 mbar (at 5 bar(g))

Table 3.2: Setpoint errors

However, *actual* flows and pressures are continually recorded during the experiments. Data acquisition is performed using three personal computers, sampling at different frequencies. Gross flow parameters, namely superficial phase velocities, static and differential pressure measurements are sampled by the low-speed data acquisition system at 10 Hz, then averaged over a period of approximately 2.6 seconds and written to file. Voltage signals from the conductivity probes are sampled using the high-speed data acquisition system, which samples up to 10 channels simultaneously at 500 Hz and then writes the data to file, in binary format from which the voltage signal can be reconstructed. The gamma densitometer system uses its own dedicated control and data-acquisition system, which samples the liquid holdup measurement at a frequency of 25 Hz and writes the information to file.

In addition to the instrumentation described in Table 3.1, video images of the flow in the visualisation section (positioned upstream of the gamma densitometer, approximately 35m from the test-section inlet) were recorded at 24 frames / second using an SVHS-format video camera. Data from the flow and pressure transducers, and the differential pressure (DP) transducer were superimposed onto the video recording of the visualisation section using a personal computer with a video input/output card.

3.2.1. Gamma densitometry

The technique of gamma densitometry relies on the attenuation of a beam of gamma photons by different materials or phases in a mixture. This is readily applied to the study of multiphase flows and the method has been widely used to monitor the contents of a flowing pipe. Recently the technique has formed the basis of commercial instrumentation for measurement of volumetric flow rates in multiphase pipelines (Hewitt *et al.*, 1997).

When a perfectly collimated photon beam with initial intensity I_0 is passed through a material of thickness x, its intensity is reduced to

$$I = I_0 e^{-\gamma x} \qquad [3.2]$$

where γ is the linear absorption coefficient of the material. γ is related to the material's density, ρ: the ratio is the mass absorption coefficient of the material, μ:

$$\gamma = \rho\mu \qquad [3.3]$$

Pan (1996) fitted equations to the mass absorption coefficients for air, water and oil, as a function of the energy of the gamma photon beam. He showed that, for a two-phase mixture, the liquid phase fraction ε_L is given by

$$\varepsilon_L = \frac{\ln I - \ln I_G}{\ln I_L - \ln I_G} \qquad [3.4]$$

where I is the measured photon intensity, I_G is the measured photon intensity for a gas-filled pipe and I_L is the measured photon intensity for a liquid-filled pipe. The two latter values are obtained by calibration tests where the test-section is completely filled with gas or liquid.

To measure phase fractions of N phases, (N-1) collimated photon-beams are required. Thus, a single energy gamma ray source is sufficient to measure two phase gas-liquid flow. However, for three phase (gas-liquid-liquid) flow, two photon beams are required: this is achieved in the WASP facility by using a single gamma-ray source which emits photons with two different energies.

The gamma densitometer used in the present work was designed by Pan (1996). Evaluation of its performance when used for two-phase flow measurement is described fully by Pan *et al.* (1994). Recently, two additional gamma densitometer systems have been designed and constructed for future use on the WASP facility (Mareuge, 2000), however these were not used for the work described in this thesis.

The main components of the apparatus are a gamma-ray source, an electronic detection system, a positioning ("stepper motor") system and an electronic control and data-acquisition system. A diagram of the WASP gamma densitometer system is shown in Figure 3.3.

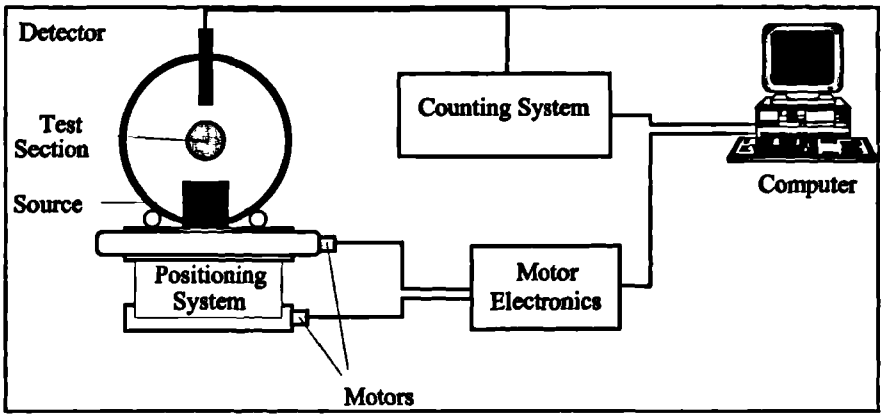

Figure 3.3: WASP facility gamma densitometer system

Selection of the gamma source (Pan *et al.*, 1994) was on the basis of its size, photon intensity and half-life. The source should be small enough to be considered as a point source so that the emitted photons, once collimated, form a narrow, high intensity beam. The half-life should be long so as to give a stable gamma-ray intensity. The source used for the present work was a 20 mCi ^{133}Ba source, with a half-life of approximately 10.7 years, emitting photons with various energies. Two peaks in the photon intensity *vs.* energy curve for this source occur at 31 keV and 81 keV. These energies were used in the experiments.

At the point where the gamma beam passes through the test-section, acrylic pipe is used instead of stainless-steel to avoid excessive absorption and scattering of the gamma photons by the pipe walls. A short (0.4 m) section of transparent acrylic (Perspex®) pipe is thus used, held in place with an arrangement of flanges and butyl rubber gaskets. The inner diameter of the acrylic pipe is slightly smaller than the stainless-steel test-section (76.2 mm *versus* 77.92 mm). The change in diameter, and the use of flanged joints with gaskets instead of the "tongue and groove" flanges used elsewhere in the test-section, causes a small disturbance to the flow as it enters and leaves the acrylic section.

The source is mounted in a lead container / collimator, with an aperture of diameter 4mm and length 14mm. For the experiments described in this thesis, the gamma source was positioned underneath the test-section so that the photon beam passed vertically upwards across the diametrical chord of the pipe. The beam was positioned to a tolerance of ± 0.25mm by detecting the position of the inner pipe walls using successive photon counts taken over several minutes. The apparatus was then operated in "continuous" mode, whereby the gamma photon count was sampled at a frequency of 25 Hz to give a continuous reading of the holdup at the pipe centre.

In an alternative mode of operation, the gamma beam and detector may be traversed across the pipe cross-section to give holdup readings at fifteen chordal positions. This is useful for systems where the curvature of the interface is significant, such as in stratifying/annular flow (Badie, 2000). However, for the present work, this mode was used only in the procedure to calibrate the densitometer apparatus, performed at the start of every experimental campaign.

The system for detecting, amplifying and counting the gamma photons and recording the data consists of five components, manufactured by EG&G Ltd. These are:

- **Photon detector**: Na-I photomultiplier tube and pre-amplifyer.
- **Amplifier**: Delay line amplifier
- **Two Single-Channel Analysers (SCAs)**: each SCA distils the output signal for one of the two photon energies (31 keV and 81 keV)
- **Dual-counter / timer**: Counts the number of scintillations per unit time from each of the SCA signals
- **Data acquisition computer**: a 33 MHz Naga 486 DX personal computer runs a purpose-written application to acquire and log the data from the dual-counter / timer. This PC also controls the stepper motors in the gamma-beam positioning system.

The interrelationship between the components is shown in Figure 3.4.

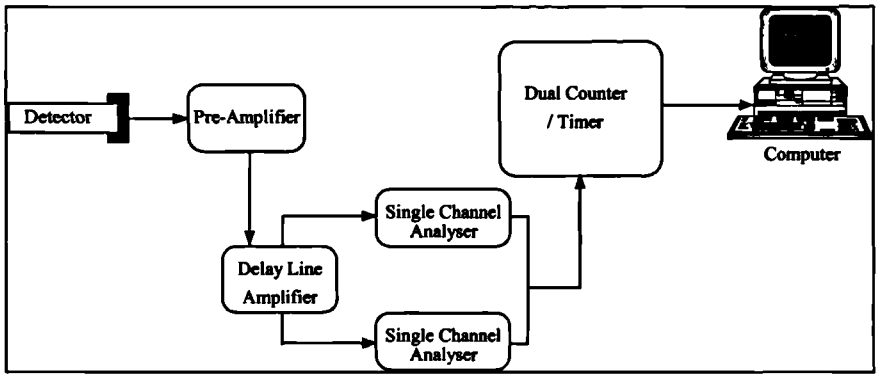

Figure 3.4: Components of the gamma photon detection and counting system

Pan (1996) demonstrated that the error in two-phase liquid holdup measurement was considerably less than ±1% of full scale, for a ten-second counting time. For three-phase (air-oil-water) measurement, the corresponding error is approximately ±3% of full scale (Pan & Hewitt, 1996). However, at a sampling frequency of 25 Hz, the error in the measured liquid

holdup for two-phase flow is approximately ±5% of full scale. This is due to the random nature of photon emission from the source, so that the error varies inversely with the square root of the total photon count, and hence the counting time.

3.2.2. Liquid holdup measurement using conductivity (impedance) probes

In addition to the gamma densitometer sited near the end of the WASP test-section, a number of conductivity probes may be located at points along the test section in order to provide continuous measurements of the liquid height in the pipe.

The conductivity probes on the WASP facility are of various designs, a twin-probe design developed by Manolis (1995), a five-pair probe designed by Srichai (1994) and a single-pair probe designed by Hale (2000). Essentially, all consist of one or more pairs of thin conducting wires, mounted in parallel a small distance apart, vertically across the cross-section of the WASP test-section, perpendicular to the direction of flow. Previous researchers on the WASP facility have used 99.99% pure platinum wire of 0.5 mm diameter. For the third campaign of experiments in the present work, one of the two pairs of wires in the Manolis (1995) probe section was replaced with AISI 316 (Fe/Cr18/Ni10/Mo3) stainless steel, after exploratory bench-top tests confirmed that the performance of a stainless-steel probe was virtually indistinguishable from that of a platinum probe. This is readily apparent in Figure 3.8 below.

In a basic DC mode of operation, if a steady voltage is applied to one wire, the voltage measured in the other wire depends on the conductance of the medium between the wires. However, to eliminate polarisation effects, a high-frequency (10 kHz) AC supply is used. If a very high AC frequency is used then capacitance effects become significant. For frequencies of the order used in the present work, the operation of the probes is essentially the same as for the idealised DC case.

Brown *et al.* (1978) stated that for this "conductance" mode of operation, the conductance G_E of the liquid is given by

$$G_E = \frac{\gamma}{\varepsilon} C_E \qquad [3.5]$$

where γ is the electrical conductivity of the liquid, ε is its dielectric constant and C_E is its capacitance. The implicit assumption is that the gas phase is a perfect electrical insulator. Brown *et al.* (1978) showed that

$$C_E = \frac{\pi \varepsilon h_L}{\ln\left(\frac{d}{r}\right)} \qquad [3.6]$$

where h_L is the liquid height, d is the separation of the wires and r their diameter. Thus, the conductance of the liquid is proportional to the liquid height.

The designs of Hale (2000) and Srichai (1994) are illustrated in Figure 3.5.

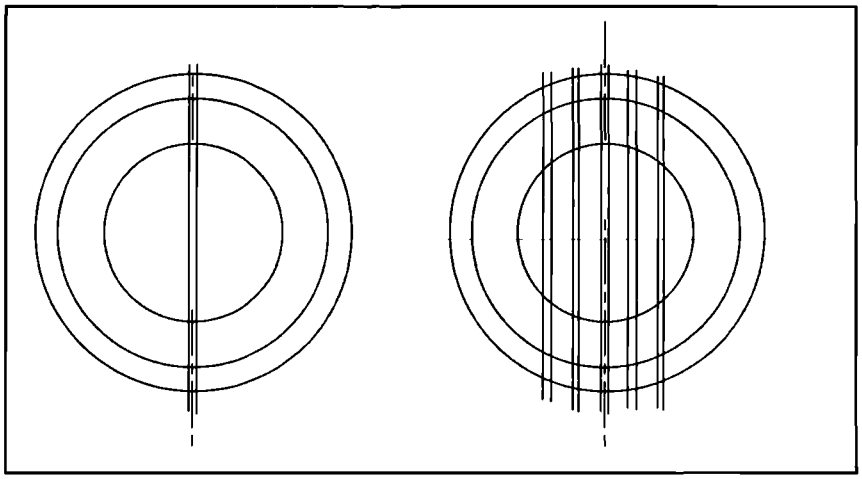

Figure 3.5: Single- and Five-Pair Conductivity Probe Designs

The three designs of probe used on the WASP rig differ only in the way in which the wires are mounted in, and insulated from, the steel test-section. The designs by Hale (1997) and Srichai (1994) use acrylic rings, between which the wires are glued, mounted between steel flanges. These "probe units" have axial dimensions of approximately 94 mm between the outer flange faces.

The design by Manolis (1995) is shown in Figure 3.6. It is based on a much longer section of pipe, consisting of a 1 meter length of stainless-steel pipe in which two single-pair probes are mounted 600 mm apart. Insulation from the steel pipe wall is achieved using a combination of ceramic, PTFE and silicone rubber components.

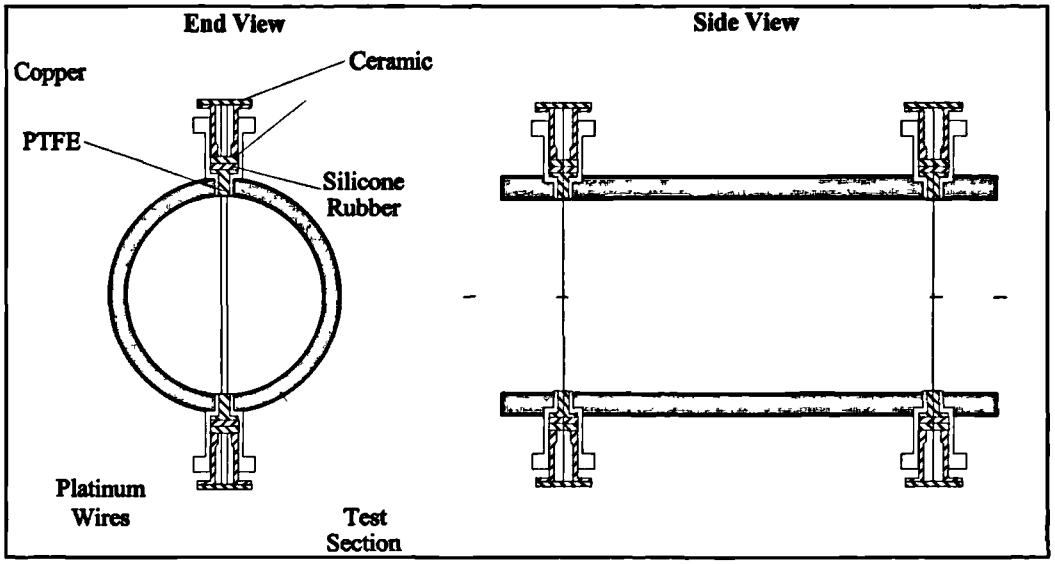

Figure 3.6: Conductivity probe design by Manolis (1995)

Prior to each of the campaigns of experimental work described in this thesis, the probes by Hale and Srichai were removed from the WASP facility for calibration. Transparent acrylic plates were fitted to the ends of the probe casings so that they could be filled with water, the liquid level measured to ± 0.5 mm using a ruler and the output voltage recorded on the data-acquisition computer. An average voltage signal (± 0.001 V) was recorded over a period of 2 minutes for each water level. The graph of h_L *vs.* output voltage was then obtained, and a third-order polynomial curve fitted to it to allow subsequent analysis. A sample calibration curve is shown in Figure 3.7. The dimensionless liquid height, (h_L / D) is plotted against the output voltage from the probe. The liquid holdup can be calculated from (h_L / D) if the liquid interface is assumed to be flat.

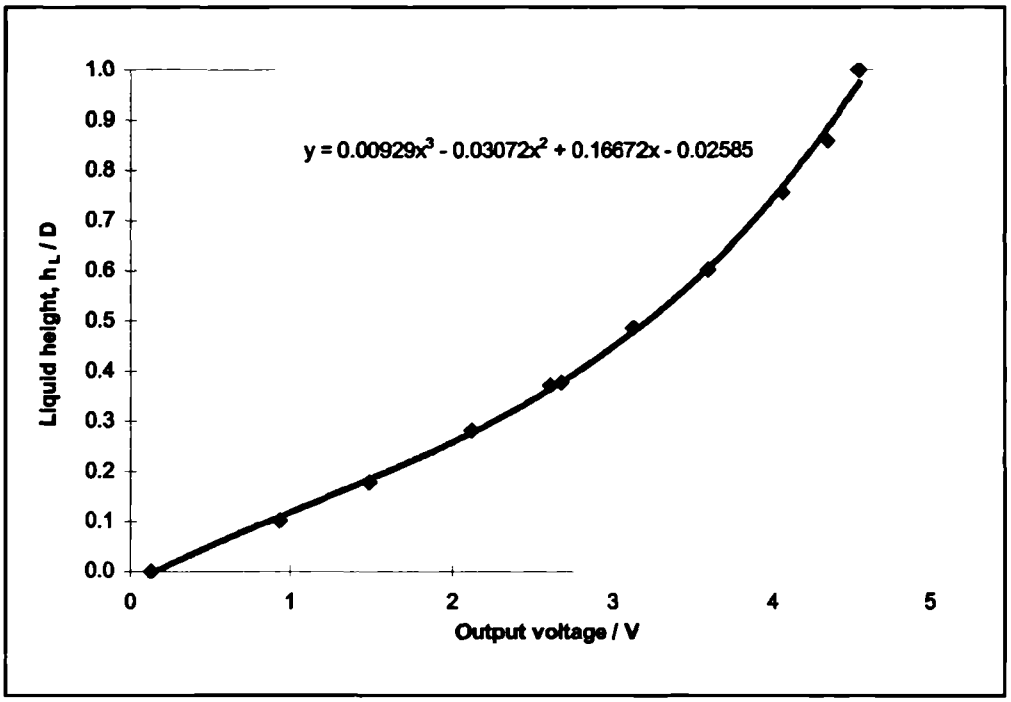

Figure 3.7. Sample bench-top conductivity probe calibration curve produced for the probes by Hale (2000)

The pair of probes designed by Manolis (1995) cannot easily be calibrated in this manner as the section of pipe containing the probes is too large, so a previous calibration of these probes was used for the first two campaigns of experiments described in this thesis.

The probes were originally calibrated *in situ* by Manolis (1995) by comparison against the gamma densitometer. This was achieved by gradually draining the test section of liquid from an initial full state, and halting the draining at a number of intervals. At each interval, the test-section was left to settle for fifteen minutes and then a three-minute reading was taken of the output voltage from the conductivity probes and the corresponding liquid holdup measured by the gamma densitometer. The calibration data are given in Manolis (1995). These were used for the first two experimental campaigns in the present work.

Prior to the final campaign of experiments described in this thesis, the Manolis conductivity probe section was removed from the WASP facility for maintenance and off-line recalibration. The upstream pair of wires were replaced with AISI 316 stainless steel. The downstream platinum wires were left unchanged although their tension was adjusted to produce a more linear relationship between the measured voltage and the liquid holdup in the pipe. In a similar manner to that used with the smaller probe sections by Srichai and Hale, the one-meter pipe section was sealed between transparent acrylic flanges and filled with water

taken from the WASP facility. The pipe section was fixed horizontally during this procedure (verified with a spirit level to a tolerance of (± 0.057°)). The liquid level, visible through the acrylic flanges, was measured using a ruler to an accuracy of ± 0.5mm, and the corresponding output voltage was recorded. Care was taken to ensure that no air bubbles remained attached to the probe wires during this procedure. This was achieved by tapping the pipe section with a hammer before each measurement was taken. The calibration data are shown in Figure 3.8.

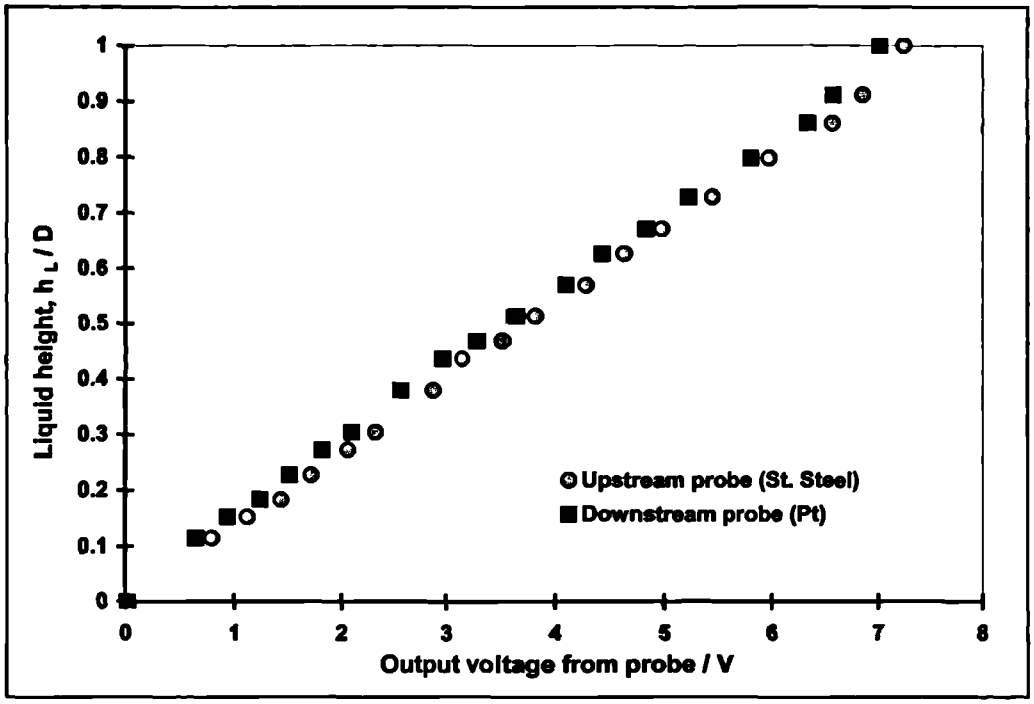

Figure 3.8: Off-line calibration data for Manolis probe section

Equations were fitted to these data for later use in the analysis of experimental results. A fourth-order polynomial expression was found to give an acceptable fit. For the upstream (stainless steel wire) probe this was

$$\frac{h_L}{D} = 0.000166v^4 - 0.00124v^3 - 0.00168v^2 + 0.156v \qquad [3.7]$$

where v is the output voltage from the probe. The regression coefficient for this equation was found to be $R^2 = 0.99934$.

For the downstream (platinum wire) probe the corresponding equation was found to be

$$\frac{h_L}{D} = 0.000236v^4 - 0.00311v^3 + 0.01251v^2 + 0.11894v \qquad [3.8]$$

with a regression coefficient of $R^2 = 0.99915$.

Unlike the gamma technique, the conductivity probes cannot be used with a non-aqueous liquid phase, since they require a significant difference between the electrical conductivities of the gas and liquid phases in order to function. Even for the case of oil-water liquid-liquid flow, it has been found (Odozi, 2000) that the probes do not operate well: it is thought that this is due to the oil phase "coating" the probe wires. Furthermore, the probes intrude into the test-section and so cause an inevitable, albeit minor, disturbance to the flow. However, the conductivity probe technique has two major advantages over gamma densitometry: the probes are very simple and thus cheap to manufacture, and the frequency response is effectively instantaneous, allowing a considerably higher sampling frequency (500 Hz) than that possible with the gamma densitometer (25 Hz).

The conductivity probes form part of an electronic circuit which also includes a power supply, drive and control electronics and a personal computer for data acquisition and recording. Srichai (1994) and Manolis (1995) have described the construction of these components in detail.

3.3. Experimental method

Three extended "campaigns" of experiments were conducted on the WASP facility for the current work, with the test-section arranged as a straight pipe inclined at $-1.5°$, a $\mp 1.5°$ "V"-section and a $\pm 1.5°$ "Λ"-section, respectively.

For all experiments, the WASP facility instrumentation was configured similarly, as discussed in Section 3.2, although the locations of the instruments in the test-section differed slightly for the three campaigns. The configurations for the three campaigns are shown in Figure 3.9, Figure 3.10 and Figure 3.11, respectively.

Experimental runs were grouped according to air flow rate. A particular air flow was selected and a series of runs was performed with successively increasing water superficial velocities. During the course of each experimental run, the air and water superficial velocities were kept as stable as possible, by occasional adjustment of the water and air control valve positions. However, slight variations in the phase velocities were unavoidable (as shown in Table 3.2). Generally, experiments were conducted in groups of between two and five, depending on the

volume of liquid and the pressure in the water feed tank, and the flow rates required. Between each group of experiments, the test-section was "blown" clear of liquid using high-velocity air. With the air and water inlet valves closed so that there was no fluid flow in the test-section, the zero-offset in the pressure gradient measurement was sampled for approximately 60 seconds using the low-speed data acquisition system.

For each experimental run, a similar procedure was followed. The flow control valves and pressure and level control loops (for experiments at elevated pressure) were adjusted to give the required flow rates pressure in the test-section. Data acquisition was not started immediately, to allow time for the transition between the old and new "steady states". For experiments in the slug flow regime, approximately 90 seconds was deemed sufficient for this: if a slug is assumed to travel at 1.2 times the total superficial velocity then even for a low-velocity experiment where U_{Mix}= 3 m/s, the time taken for a slug to pass completely along the 36 m test-section is only 10 seconds. For experiments conducted at high liquid flow rates (*e.g.*, greater than 0.5 m/s) where the air flow rate was also high (*e.g.*. greater than 7 m/s), a shorter "transition period" of 60 seconds was used, due to the correspondingly shorter time taken for the passage of "transient" slugs along the pipe. For each experiment in the stratified smooth and stratified wavy regimes, a two-minute transition period was used to allow for the slower translational velocity of interfacial waves.

After a "steady" flow had been established, data acquisition was started. For the first Campaign, this was performed for a five-minute period for each experiment. For the second and third Campaigns, three-minute sampling periods were used, since the first Campaign had shown that this was a sufficient length of time in which to observe the flow phenomena. The shorter experiments also required less adjustment of flow rates during the course of the run, and allowed a greater number of experiments to be conducted per day during each Campaign.

3.3.1. Campaign 1: downflow experiments (October 1997)

A campaign of experiments was conducted in late 1997 on the Imperial College WASP facility, using air and water at atmospheric pressure and at 5 bar(g), with the rig test-section inclined downwards at an angle of -1.5° to the horizontal. A schematic diagram showing positions of the conductivity probes and other instrumentation in the WASP test-section is shown in Figure 3.9.

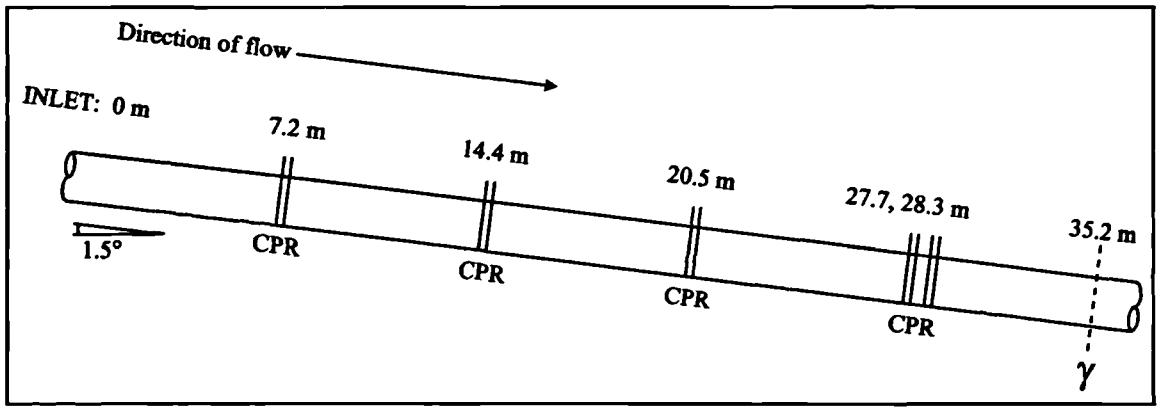

Figure 3.9: Relative positions of conductivity probes (CPR) and gamma densitometer for Campaign 1 (*not to scale*)

A large range of flow rates was studied, with data points spaced fairly coarsely, so that the various flow pattern transitions could be located on a flow pattern map. A summary of the experiments performed in this Campaign is given in Table 3.3.

Pressure / bar(g)	0	5
Data points	100	55
Fluids	Air/Water	Air/Water
Air superficial velocity range, U_{sG} / m/s	1.5 - 25	1 - 9
Water superficial velocity range, U_{sL} / m/s	0.02 - 1.0	0.1 - 1.0

Table 3.3. Summary of Campaign 1 experiments

Water was chosen for the liquid phase so that electrical conductivity probes could be used to measure liquid holdup at several points along the test-section. The gamma densitometer close to the end of the test-section was also used. The use of oil (with or without water) would restrict the holdup measurement to the gamma densitometer only.

The distance between the tappings for the differential pressure (DP) transducer used to measure pressure gradient was 2.54 m, with the downstream-most tapping sited 0.220 m from the flange on the slug catcher vessel.

3.3.2. Campaign 2: "V"-section experiments (February 1998)

The second campaign of experiments was conducted on the WASP facility in early 1998. The test section was arranged as a ∓1.5° "V"-section, with a 1-m long, smooth bore high-pressure flexible hose used to link the up- and downhill sections of the pipeline.

As with the first campaign, a large range of flow rates was investigated, to construct a flow pattern map, using air and water as the test fluid. The range of experimental conditions is summarised in Table 3.4:

Pressure / bar(g)	0	5
Data points	260	210
Fluids	Air/Water	Air/Water
Air superficial velocity range, U_{sG} / m/s	1.5 - 25	1 – 9
Water superficial velocity range, U_{sL} / m/s	0.02 – 0.7	0.1 – 0.7

Table 3.4. Summary of Campaign 2 experiments

A schematic diagram showing positions of the conductivity probes and other instrumentation in the WASP test-section is shown in Figure 3.10.

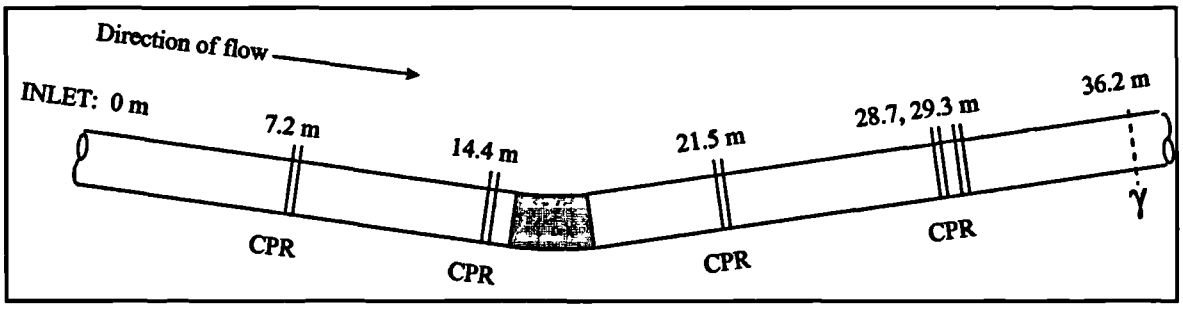

Figure 3.10. Relative positions of conductivity probes and gamma densitometer for Campaign 2 (*not to scale*)

As in Campaign 1, the liquid holdup was measured using the conductivity probes at several points along the test-section, with the gamma densitometer near to the end of the test pipe. The tappings for pressure-gradient measurement using the DP cell were situated 1.86 m apart, with the downstream-most tapping a distance of 0.12 m from the slug-catcher flange.

3.3.3. Campaign 3: "Λ"-section experiments (October 1999)

The third and final campaign of experiments was conducted on the WASP facility in late 1999. The test section was arranged as a ±1.5° "Λ"-section. As in campaign 2, the high-pressure flexible hose was used to link the up- and downhill sections of the pipeline.

As with the first two campaigns, a large region of the flow pattern map was investigated, using air and water as the test fluids, as summarised in Table 3.5

Pressure / bar(g)	0	5
Data points	105	115
Fluids	Air/Water	Air/Water
Air velocity range, U_{sG} / m/s	1.5 – 25	1 - 9
Water velocity range, U_{sL} / m/s	0.02 – 1.0	0.1 - 1.0

Table 3.5. Summary of Campaign 3 experiments

A schematic diagram showing positions of the conductivity probes and other instrumentation in the WASP test-section is shown in Figure 3.11.

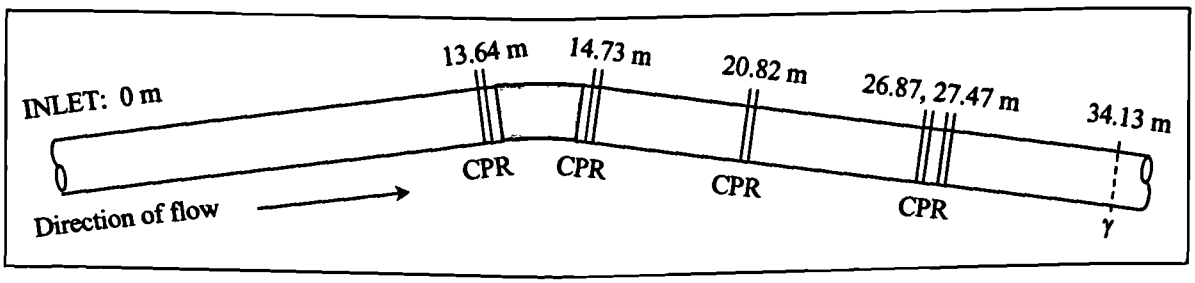

Figure 3.11. Relative positions of conductivity probes and gamma densitometer for Campaign 3 (*not to scale*)

3.3.4. Slug exit velocity experiments

In addition to the three Campaigns described above, a very brief series of experiments was conducted to study the effects which occurred when a liquid slug left the test-section to enter the slug catcher. It has been suggested (King, 1999) that as a slug leaves the end of a pipe, it undergoes rapid acceleration: this phenomenon is predicted by commercial slug-tracking software. To investigate this, the fluid flow at the front and back of several slugs was

observed using a high-speed digital video camera, aimed at the visualisation section. The other instrumentation used for these experiments was for flow- and pressure-measurement only. From the high-speed photographs, the front- and tail-velocities of the slugs were calculated as the slug entered the slug catcher. The results from this series of experiments are presented in Appendix 4. No acceleration of the slugs was observed as they left the pipe, and this investigation was not pursued any further.

Blank page.

Chapter 4: Studies of slug flow in a -1.5 ° downwardly-inclined pipe

In this Chapter, experimental data for two-phase air-water flow in a –1.5° pipe are presented, which were collected in Campaign 1 of the present work. The configuration of the WASP facility for this investigation is described in Section 3.3.1 in Chapter 3. A diagram showing the layout of the test-section for the experimental Campaign is presented in Figure 4.1, in which the positions of the conductivity probes, shown as CPR, and the gamma densitometer, shown as γ, are indicated.

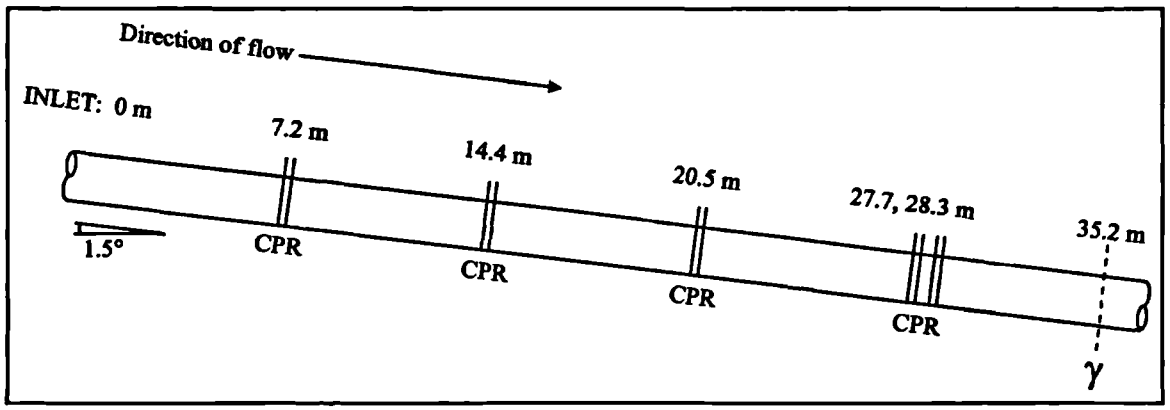

Figure 4.1: Configuration of WASP facility test-section for Campaign 1 (*not to scale)*

Data were collected for steady-state flow at zero and five bar(g) exit pressure. The actual pressures could differ slightly from the set values; actual values were recorded and are included in the CD-ROM data files given at the end of this thesis. Observations of pressure drop, flow pattern, slug frequency, slug length and liquid holdup were made at different points along the test-section. The experimental results are presented in Section 4.1. A comparison of the data with some published predictive models and correlations (which were described previously in Chapter 2) is given in Section 4.2.

4.1. Experimental results

In this section, results from the campaign of experiments are presented. The detailed experimental matrix used for the campaign is included in Appendix 2, in which a unique run number is assigned to each experiment, and the experimental parameters are listed for each case. The original data files recorded for each experiment are included on CD-ROM number CD01, appended to this thesis.

4.1.1. Flow pattern

The results were used to construct flow pattern maps, with flow pattern identification carried out at the transparent visualisation section near the end of the test-section, located immediately upstream of the gamma densitometer, *i.e.*, approximately 35 m from the pipe inlet.

The maps for 0 and 5 bar(g) are shown in Figure 4.2 and Figure 4.3 respectively. The abbreviations for flow patterns used in the legends are described in Table 4.1.

Abbreviation	Flow pattern
str. sm.	Stratified smooth flow
str. wa.	Stratified wavy flow
sw / slug	Transition between stratified wavy and slug flow; some interfacial waves completely block the pipe but no true "slugs" are observed
slug	Slug flow
slug / ann.	Transition between slug and annular flow; the liquid film region between slugs is observed to form an annular layer around the pipe wall
ann.	Annular flow
str. wa. / ann.	Transition between stratified wavy and annular flow

Table 4.1: Explanation of abbreviations used in flow pattern maps

Important features of the maps are the transition boundaries which delineate the various flow regimes. The transition between the stratified and slug flow regime is of most interest. In Figure 4.4, the stratified/slug transition boundaries determined in the present work for a downwardly-inclined pipe are compared with earlier results for a horizontal test-section, measured on the WASP facility by Manolis (1995).

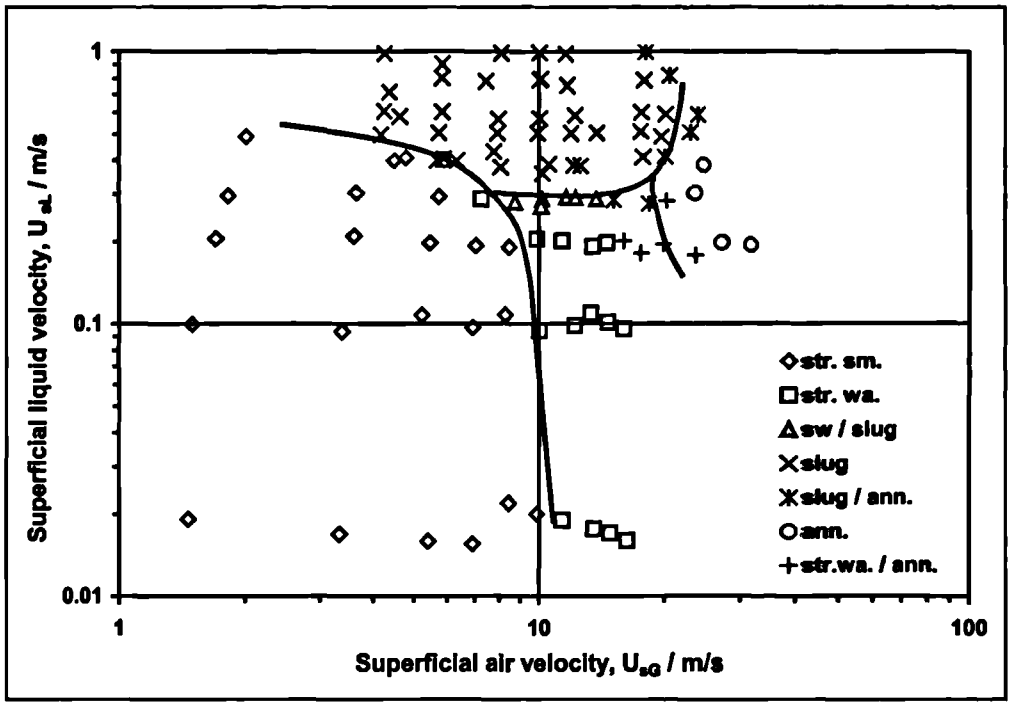

Figure 4.2: Flow patterns measured at 35 m from the test-section inlet, 0 bar(g)

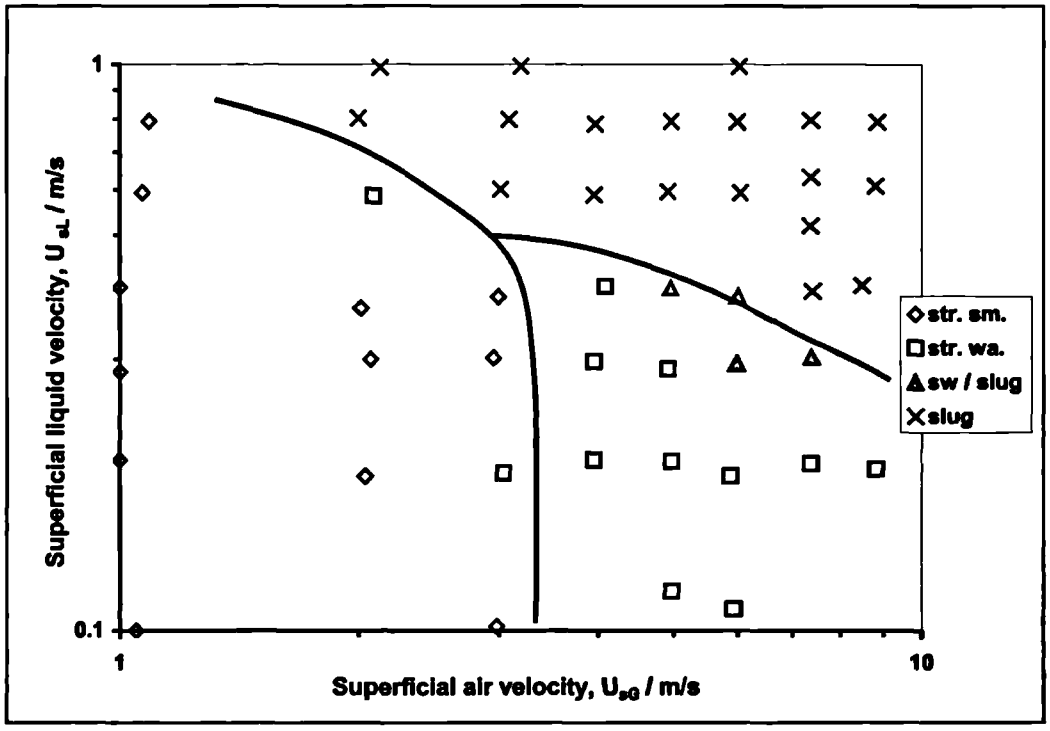

Figure 4.3: Flow patterns measured at 35 m from the test-section inlet, 5 bar(g)

The results from the present work show a considerable decrease in the size of the slug flow regime compared to the corresponding maps for a straight pipe. In Figure 4.4 it is apparent

that the stratified/slug transition occurs at higher superficial liquid velocity for the case of downwardly-inclined flow.

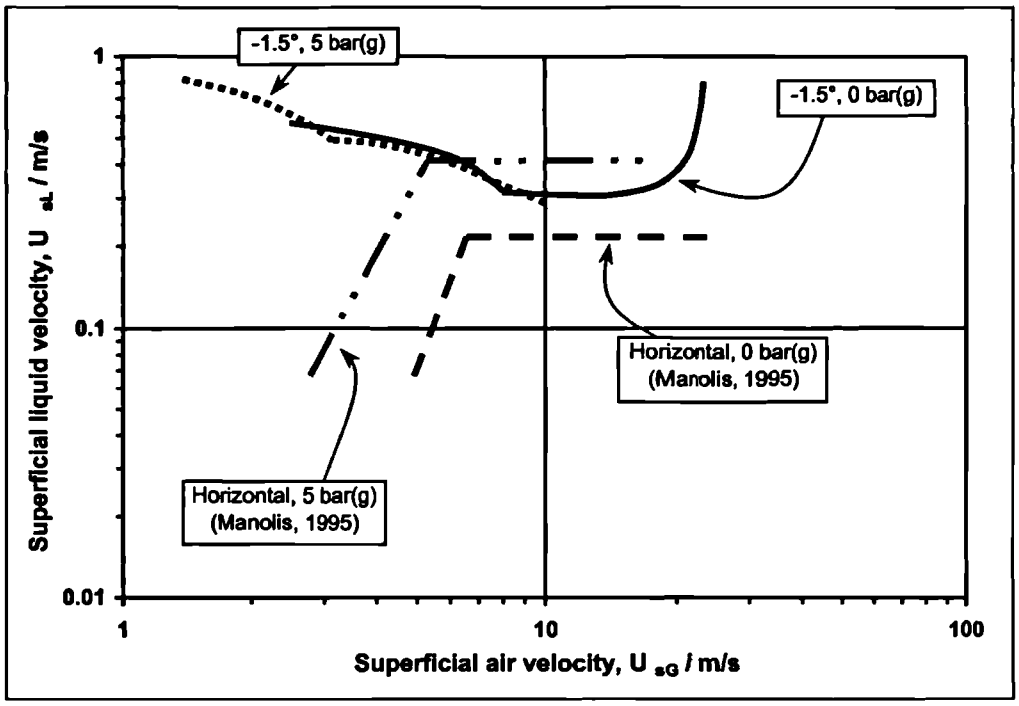

Figure 4.4: Stratified / slug transition boundaries for downwardly-inclined and horizontal air-water flow at 0 and 5 bar(g)s

Manolis (1995) reported a significant effect of pressure on the stratified/slug flow transition boundary in horizontal flow. However, this was not observed in the present study on an inclined pipe.

4.1.2. Liquid holdup

Liquid holdup was measured near to the end of the test-section, using a gamma densitometer. Time-averaged holdup data, calculated as the arithmetic mean of all the holdup samples recorded during the first 180 seconds of each experimental run, are plotted in Figure 4.5. The data are plotted against the quality, x_G, defined as the mass fraction of gas at the pipe inlet:

$$x_G = \frac{\rho_G U_{sG}}{\rho_L U_{sL} + \rho_G U_{sG}} \qquad [4.1]$$

Conventionally, many correlations for average holdup are in terms of the flow quality (see Section 2.1.1 in Chapter 2).

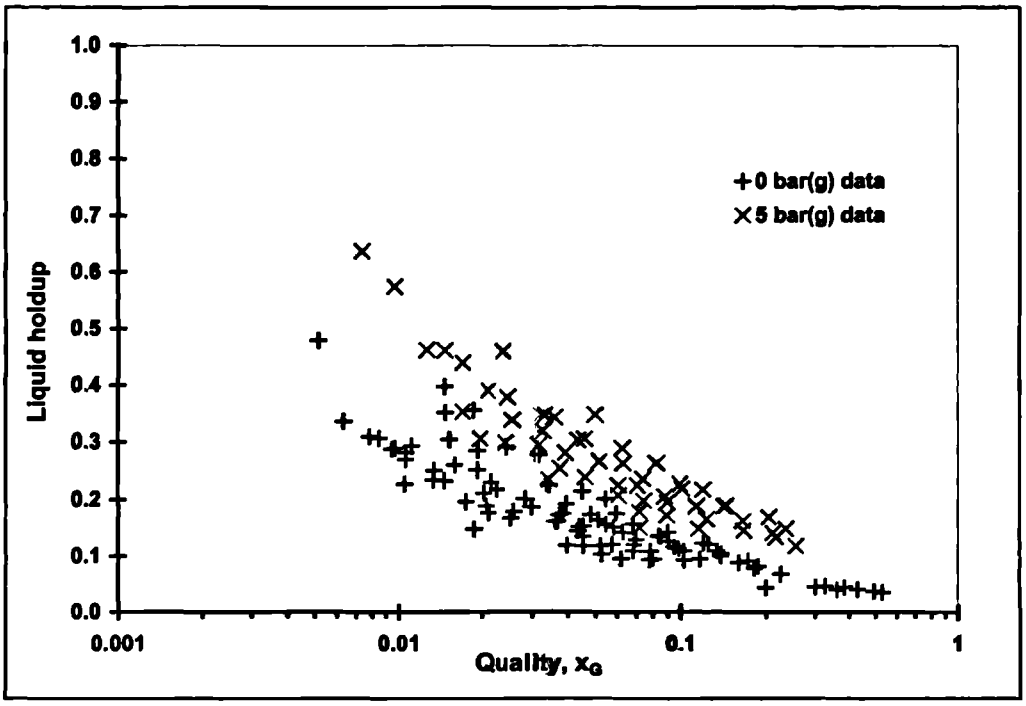

Figure 4.5: Liquid holdup data measured at 35 m from the pipe inlet

These data are compared with predictive correlations in Section 4.2.1.

4.1.3. Slug translational velocity

A brief study of a limited subset of the experimental results was made to investigate the relationship between slug length and tail velocity. The result that the slug tail velocity increases as the length of the liquid slug decreases has recently been demonstrated (Fagundes Netto *et al.*, 1998). This phenomenon has important implications for the modelling of several features of slug flow, notably the "death" of short slugs and the growth of waves into slugs (Hale, 2000). This is discussed further in later Chapters.

The pair of conductivity probes, situated approximately 28 m from the test-section inlet and spaced 0.6 m apart, were used to determine slug tail velocity and slug length for 21 experimental slug-flow runs. Figure 4.6 shows a sample output from the probes (dimensionless liquid height is offset by unity for the probe at 28.3 m).

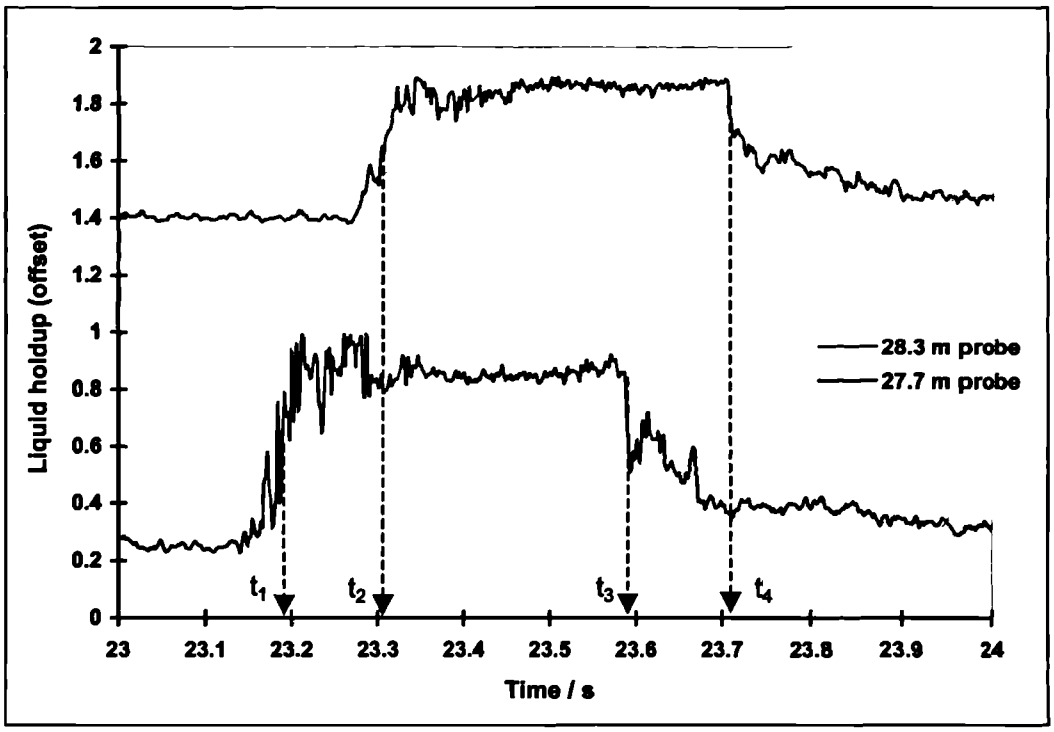

Figure 4.6: Sample output from the conductivity probes at 27.7 m and 28.3 m, showing the passage of a slug

By comparing the arrival times of the front and tail of each slug, front and tail velocities could be calculated. The mean of these was then used to calculate the slug length, using the assumption that the average velocity remained constant between the two probes.

The arrival times of a slug at the first and second probes are denoted by t_1 and t_2 respectively, and t_3 and t_4 are the times at which it leaves the first and second probes respectively. The times $t_1 - t_4$ were obtained for each slug by inspection of the liquid holdup-time traces. The slug front arrival times (t_1 and t_2) were obtained when the liquid holdup at the probe was mid-way between the value in the film at the front of the slug, and the slug body. The slug tail departure times (t_3 and t_4) were more easily obtained when the rear of the slug body passed each probe. This is clearly shown in Figure 4.6. If Δl is the distance between the probes, then the slug front velocity, U_F is given by

$$U_F = \frac{\Delta l}{t_2 - t_1} \qquad [4.2]$$

and the tail velocity, U_T, by

$$U_T = \frac{\Delta l}{t_4 - t_3} \qquad [4.3]$$

so that an average velocity may be used to calculate L_S, the slug length:

$$L_S = \frac{U_P + U_T}{2} \times \frac{(t_3 - t_1) + (t_4 - t_2)}{2} \qquad [4.4]$$

The data are plotted in Figure 4.7 in dimensionless form. The data set consists of 116 slugs, taken from 21 experimental runs. The runs were chosen so that they were regularly spaced across the slug flow regions of the 0 and 5 bar(g) flow pattern maps, and so that the entire range of mixture velocities was represented at both pressures. For each experimental run used, slug lengths and velocities were calculated during a 30-second period, one minute after the start of the run.

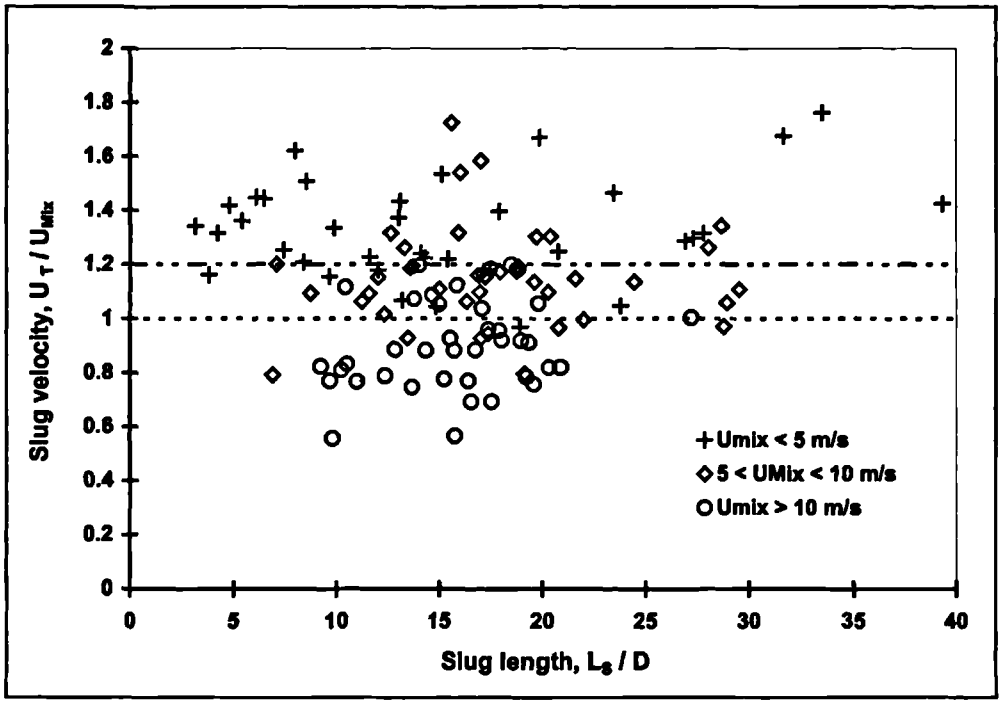

Figure 4.7: Dimensionless slug tail velocity *vs.* dimensionless slug length for a subset of 116 slugs taken from 21 experimental runs

The data are very scattered, due in part to the noise in the conductivity probe signals. Generally the dimensionless slug translational velocity was found to decrease as the mixture velocity increased: this is summarised in Table 4.2. No significant upward trend is discernible for the U_T data as L_S tends to zero, as has been indicated experimentally (*e.g.* Fagundes Netto *et al.*, 1998) and computationally (discussed in Chapter 8 of the present work) for unaerated slugs.

U_{Mix} / m/s	Number of data points	Mean (U_T / U_{Mix})	Std. deviation
$U_{Mix} < 5$	36	1.33	0.183
$5 \leq U_{Mix} < 10$	40	1.15	0.186
$U_{Mix} \geq 10$	40	0.91	0.168

Table 4.2: Variation of dimensionless slug translational velocity for a subset of 116 experimental runs

4.1.4. Slug length

The slug length data obtained from the analysis described in Section 4.1.3 are plotted as a slug length distribution in Figure 4.8.

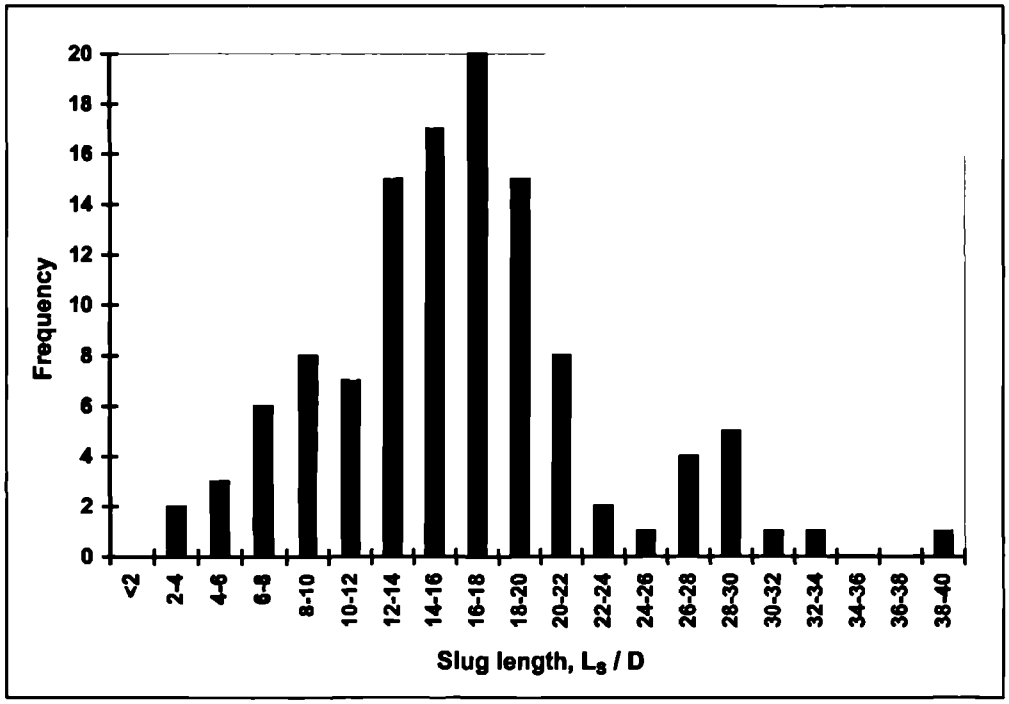

Figure 4.8: Distribution of dimensionless slug lengths for a subset of 116 experimental runs

The mean slug length is 16.32 pipe diameters, with a standard deviation of 6.48.

4.1.5. Slug frequency

The output from the gamma densitometer was used to derive slug frequency data for the runs exhibiting slug flow at the end of the uphill portion of the test section. A typical slug flow trace is given in Figure 4.9.

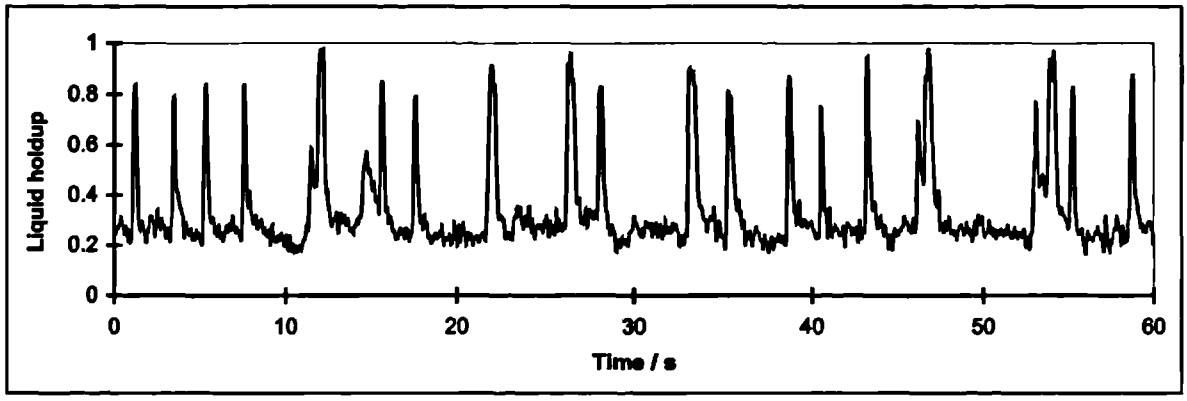

Figure 4.9: Liquid holdup-time trace from the gamma densitometer
U_{sL} = 0.71 m/s, U_{sG} = 4.39 m/s, P = 0 bar(g)

Slug frequency was obtained simply by counting the slug peaks in a measured time period of 180 seconds. Data were obtained for the experiments at 0 bar(g) and 5 bar(g). The expected error is ± 2 counts over 180 seconds or approximately 0.01 Hz.

The plots of slug frequency against superficial gas velocity, shown in Figure 4.10 and Figure 4.11, do not exhibit a characteristic minimum slug frequency occurring at a particular value of U_{sG}. This trend was reported by Manolis (1995) for horizontal slug flow and is also predicted by many correlations for slug frequency (see Section 4.2.4).

The data measured at atmospheric pressure (Figure 4.10) exhibit slightly more scatter than those measured at 5 bar(g) (Figure 4.11). In general, the slug frequencies increase with gas and liquid superficial velocity and also increase with the system pressure.

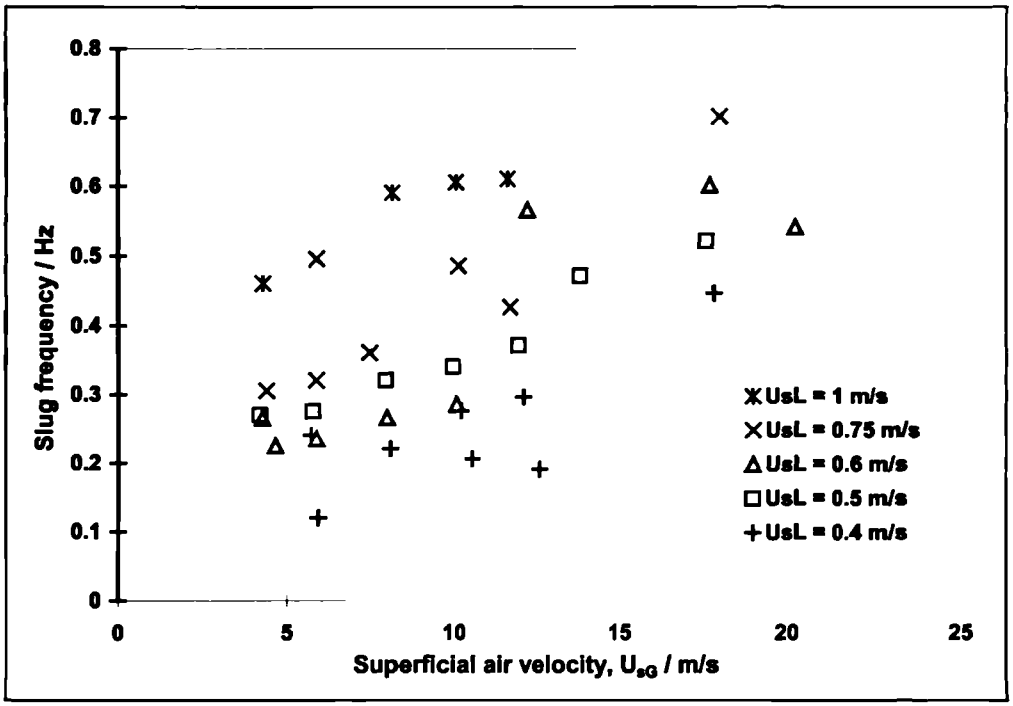

Figure 4.10: Slug frequency at 35.2 m from the inlet, 0 bar(g) runs

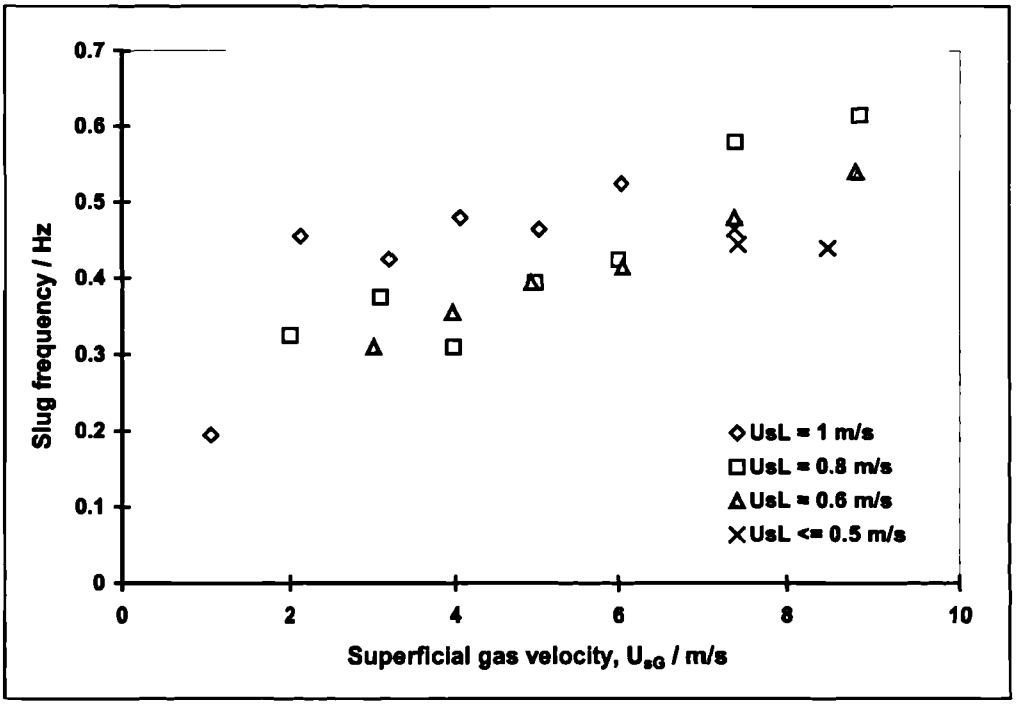

Figure 4.11: Slug frequency at 35.2 m from the inlet, 5 bar(g) runs

4.1.6. Pressure gradient

The pressure gradient was measured using a differential pressure transducer with the two tappings located close to the end of the test-section, upstream of the visualisation section, spaced 2.54 m apart. The pressure gradient was sampled at 10 Hz, and an average of 22 samples was written to an output file every 2.2 seconds. These values are then further averaged over each 180 s experiment, to obtain a time-averaged pressure gradient. It has been demonstrated (Hale, 2000) that the pressure gradient measurement is subject to an offset value which may "drift" during the course of a series of experiments. Therefore, after approximately every third experimental run, the test-section was emptied of liquid and the pressure gradient measurement was sampled with the test-section containing only still air at atmospheric pressure. This offset value was then subtracted from the pressure gradient data measured for the preceding three experiments.

Figure 4.12 shows the pressure gradient data measured for the experiments conducted at atmospheric pressure. The data are grouped according to air flow rates. There are some unusual features in Figure 4.12 where *positive* pressure gradient, *i.e.* a gain in pressure with distance, occurred; for example where $U_{sL} = 0.2$ m/s and $U_{sG} \leq 8$ m/s. In two-phase flow in a pipe, the pressure gradient is normally considered as consisting of three components – namely accelerational, gravitational and frictional. In the present study, the accelerational term is negligible. In the downwardly-inclined pipe studied here, the gravitational pressure gradient is positive and the frictional term is negative. In a fully-developed open-channel type stratified flow (*i.e.* without any gas flow) the two terms are in balance and the net pressure gradient is zero. In the presence of a co-current gas flow, one would expect the pressure gradient to become negative. In slug flow, the net pressure gradient could (in principle) be positive though the frictional term is much higher and the net pressure gradient would normally be negative. The (small) positive pressure gradients observed in the present work are mainly in stratified flow and are likely to have arisen due to errors in the measurement (including the drift effect measured above). The pressure drop measurement system is primarily designed for the higher pressure drops encountered in slug flow. Accurate measurement of pressure gradient in stratified flow presents particular challenges (Shaha, 1999) and is not a prime aim of the present study.

For a system pressure of 5 bar(g), the pressure gradients are all negative, even at low flow rate (see Figure 4.13). This is because (at the higher gas densities) the frictional term is increased and the pressure gradient measurements become more consistent.

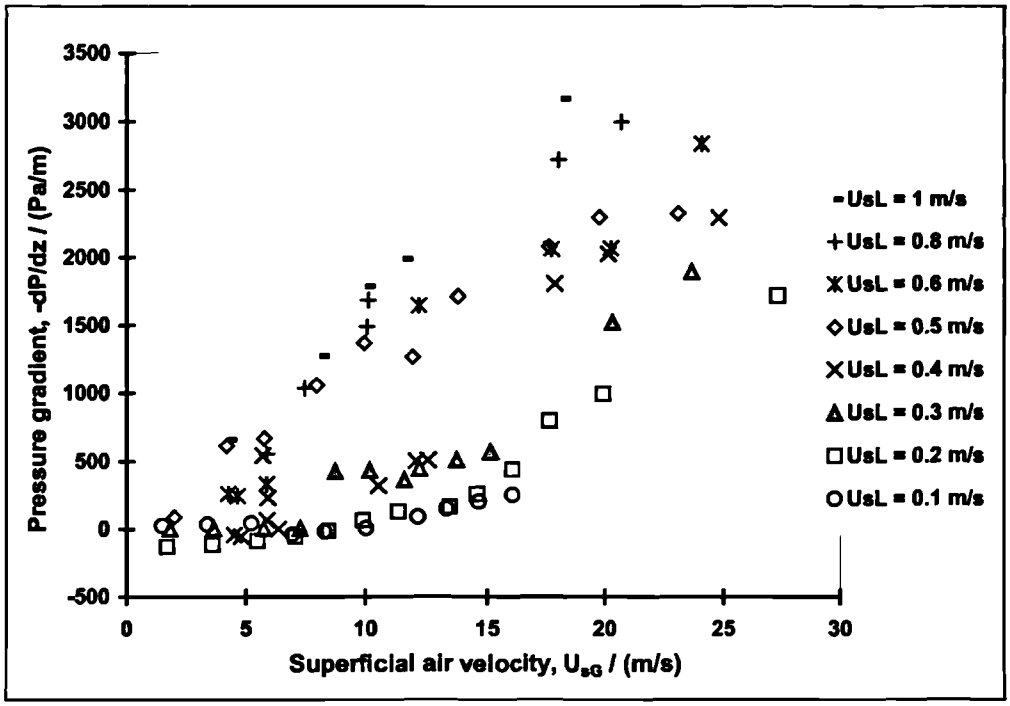

Figure 4.12: Pressure gradient data measured in –1.5° downflow, 0 bar(g) runs

Figure 4.13 shows the same information obtained from the experiments at 5 bar(g). The data are slightly more scattered for the 5 bar(g) data than those measured at atmospheric pressure, with less clearly apparent trends.

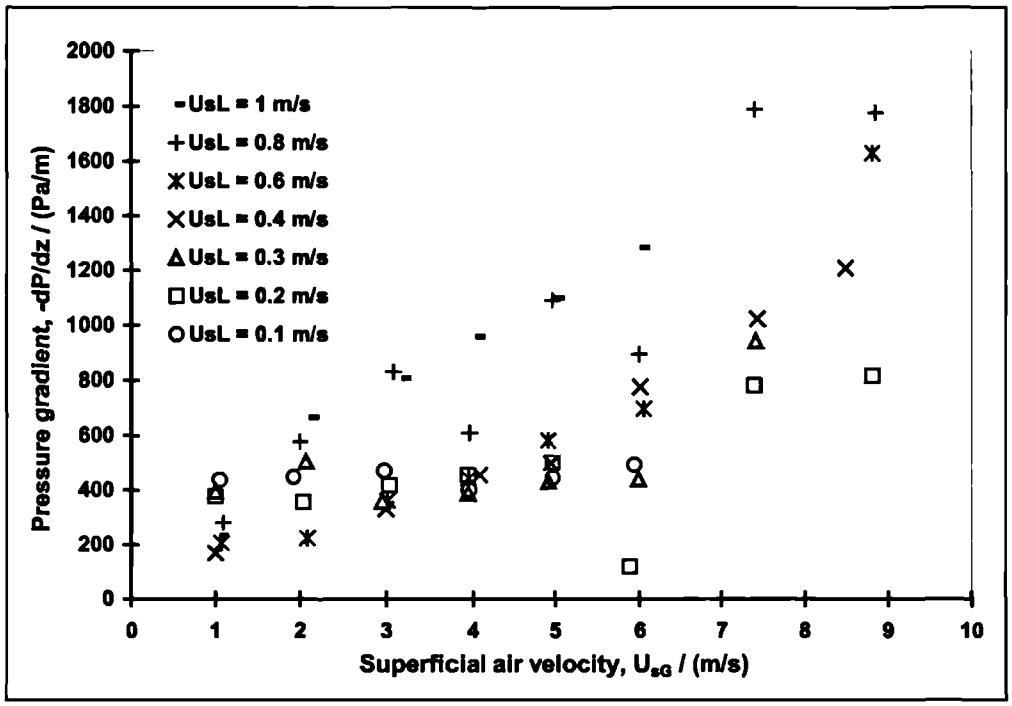

Figure 4.13: Pressure gradient data measured in –1.5° downflow, 5 bar(g) runs

Overall, the data show reasonably consistent increases in pressure gradient with both superficial air and water velocities and a significant increase with system pressure.

4.2. Comparison of experimental data with predictive methods

In this section, comparison is made between the experimental data measured for the –1.5° inclined test-section with several predictive correlations and/or phenomenological models from the published literature. Details of the methods used in this section have been presented in Chapter 2.

4.2.1. Liquid holdup

Figure 4.14 and Figure 4.15 show the liquid holdup data measured in these experiments plotted against the predictions from the correlations of Chisholm (1972) and Premoli *et al.* (1970) respectively. The comparisons are plotted as the logarithm of the ratio (R) of the predicted to the experimental value; this gives an indication of the proportionate error. For $\log_{10}(R) = 0.25$, the predicted value is the measured value × 1.78 and for $\log_{10}(R) = -0.25$, the predicted value is the measured value ÷ 1.78. The large errors seen are typical of those encountered in comparing two-phase data with empirical correlations.

Both correlations perform better at elevated pressure.

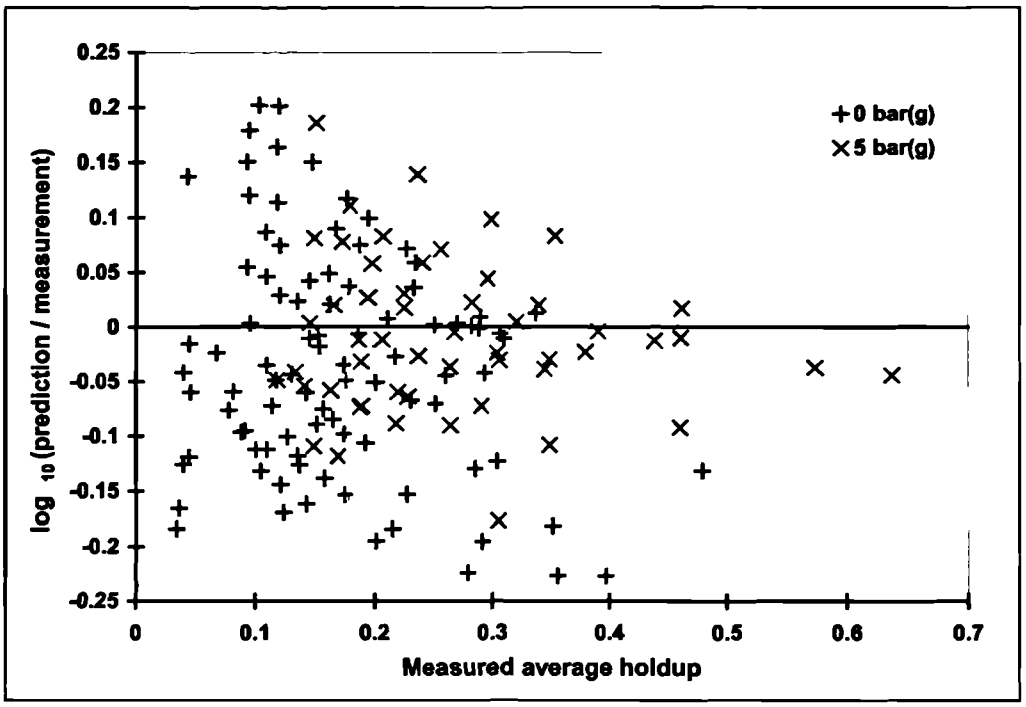

Figure 4.14: Measured liquid holdup data compared with predictions by the Chisholm (1972) correlation; 0 and 5 bar(g), -1.5° downwardly-inclined flow

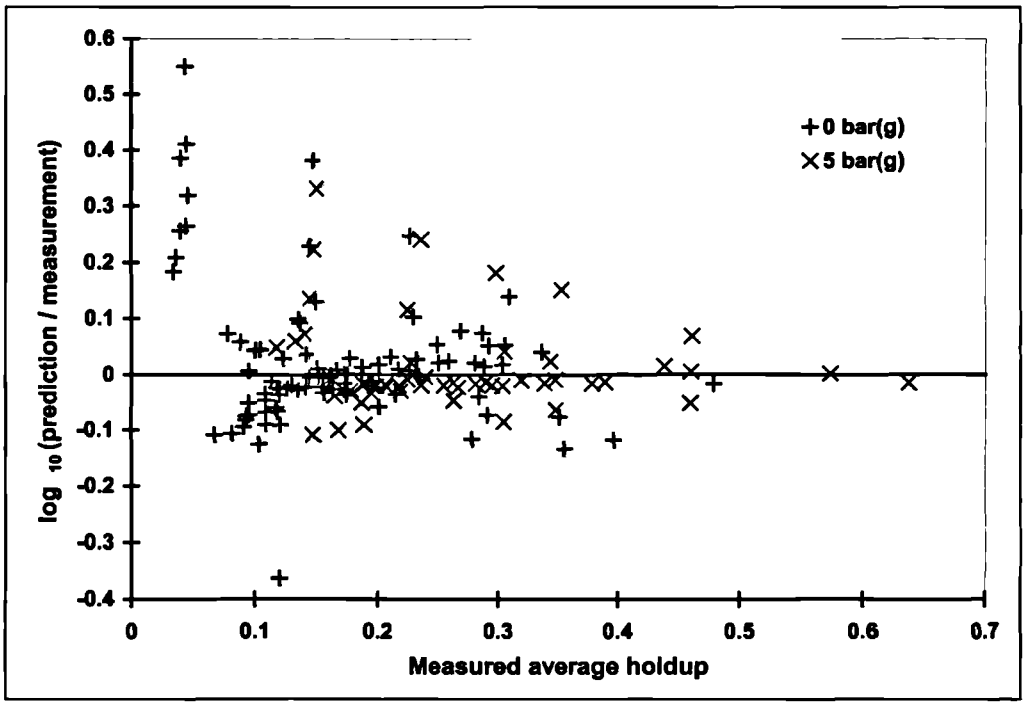

Figure 4.15: Measured liquid holdup data compared with predictions by the Premoli *et al.* (1970) correlation; 0 and 5 bar(g), -1.5° downwardly-inclined flow

In the present work, the relative error in a prediction, E_R is defined as

$$E_R = \frac{P - M}{M} \qquad [4.5]$$

where P and M are the predicted and measured values, respectively. In Appendix 1, a summary is given of the statistical treatment of relative error which has been used, which allows the relative performance of the correlations to be compared using the mean, standard deviation and root mean square relative errors, as shown in Table 4.3:

		Chisholm (1972)	Premoli *et al.* (1970)
0 bar(g) (92 points)	Mean relative error	-0.051	0.116
	Std. deviation	0.232	0.440
	Root mean square	0.236	0.452
5 bar(g) (53 points)	Mean relative error	-0.007	0.049
	Std. deviation	0.164	0.247
	Root mean square	0.163	0.250

Table 4.3: Relative error in liquid holdup correlations for 450 holdup measurements

It is clear that the Chisholm (1972) correlation performs better, with the Premoli *et al.* (1970) expression tending to over-predict the liquid holdup when it is low. However, at high liquid holdups, the Premoli *et al.* correlation performs well.

4.2.2. Slug length

The mean slug length obtained in these experiments is compared with other published values in Table 4.4.

		Slug length, (L_S/D)
(-1.5° downflow)	Experimental result	16.32
	Yang *et al.* (1996) *(correlation)*	20.9†
(Horizontal flow)	King (1998) *(experiment)*	17
	Manolis (1995) *(experiment)*	20
	Nicholson *et al.* (1978) *(correlation)*	12-30
	Dukler *et al.* (1985) *(correlation)*	16
	Norris (1982) *(correlation)*	82.4
	Scott *et al.* (1986) *(correlation)*	118.3

Table 4.4: Comparison of slug length data

The experimental result from this series of experiments is comparable with previous measurements in horizontal slug flow by Manolis (1995) and King (1998), obtained from the WASP facility at Imperial College. The correlations by Nicholson *et al.* (1978) and Dukler *et al.* (1985), also for horizontal slug flow, both agree closely with the present work.

The correlations of Norris (1982) and Scott *et al.* (1986) suggest slug lengths four to seven times greater than those observed in the WASP facility. It is likely that this is because the correlations were regressed using data from long, large-diameter oil pipelines, with considerably greater length/diameter ratio than the WASP facility test-section, so that the authors were assured of fully developed slug flow. Furthermore, the field data may have included the effect of terrain-induced slugging.

The expression by Yang *et al.* (1996) is the only correlation in Table 4.6 based on the superficial velocities of the phases, and the only one intended specifically for use with inclined pipes. A graph showing the slug length prediction by Yang *et al.* (1996) is shown in Figure 4.16.

† In the Yang *et al.* (1996) correlation, the slug length varies with superficial velocity. The value given here is the mean of the values calculated for the velocities used in the present experiments.

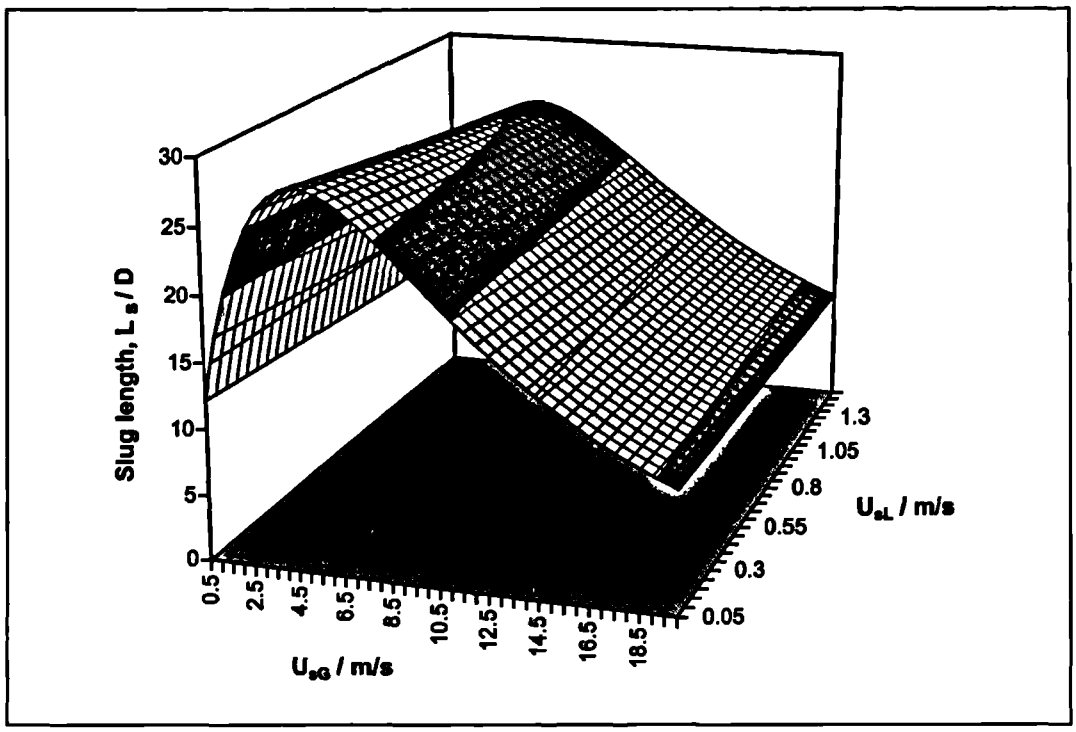

Figure 4.16: Slug length prediction by Yang *et al.* (1996) for –1.5 ° downflow

The correlation by Yang *et al.* (1996) predicts that slug length increases monotonically as the superficial liquid velocity decreases. The authors did not specify ranges of U_{sL} and U_{sG} for which their correlation was valid, even though for downwardly-inclined pipes, slug flow does not exist in a large region of the flow pattern map. This is demonstrated in the results from the present work, shown in Section 4.1.1, above. The expression by Yang *et al.* (1996) predicts a maximum slug length of about 27D for –1.5° downflow, occurring as U_{sL} tends to zero and with a superficial gas velocity of about 4.5 m/s.

The experimental slug length data are compared with the values predicted by the Yang *et al.* (1996) correlation in Figure 4.17:

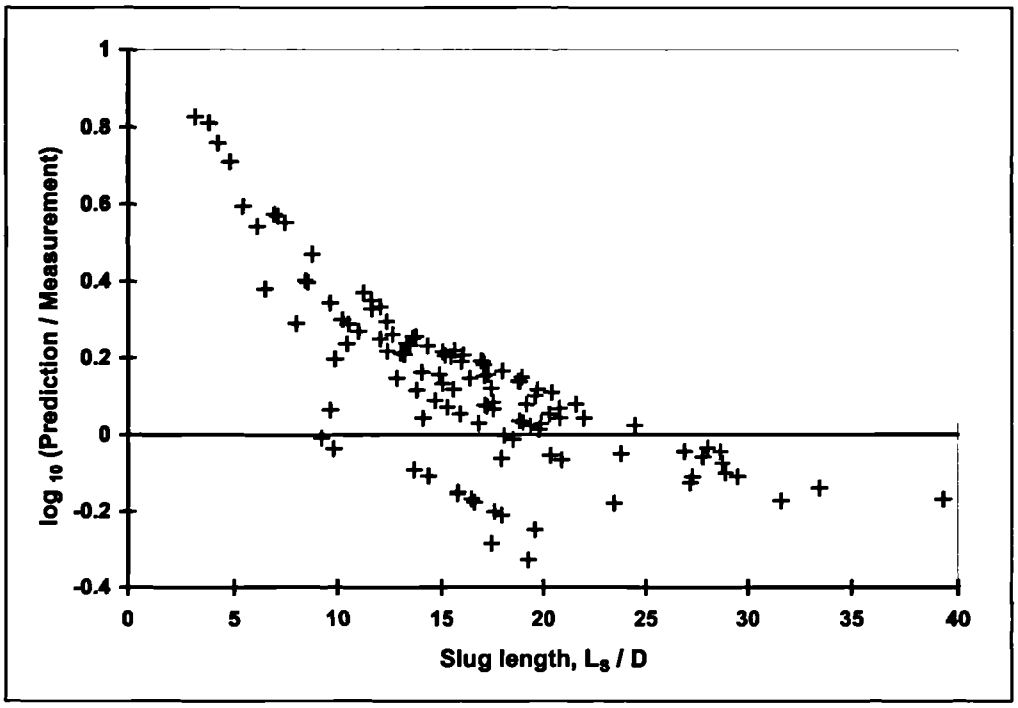

Figure 4.17: Experimental slug length data compared with the Yang *et al.* (1996) correlation, -1.5° downflow

The Yang *et al.* (1996) expression does not successfully predict the data. This is confirmed by the relative error summary in Table 4.5, which uses the definitions presented in Appendix 1 of this thesis.

No. of data points	116
Mean relative error in predictions	0.578
Std. deviation	1.083
Root mean square relative error	1.223

Table 4.5: Relative error in predictions by the Yang *et al.* (1996) correlation

4.2.3. Slug translational velocity

In Figure 4.18, the slug translational velocity data presented in Section 4.1.3 are plotted against the Froude number, using the definition

$$Fr = \frac{U_{Mix}}{\sqrt{gD}} \qquad [4.6]$$

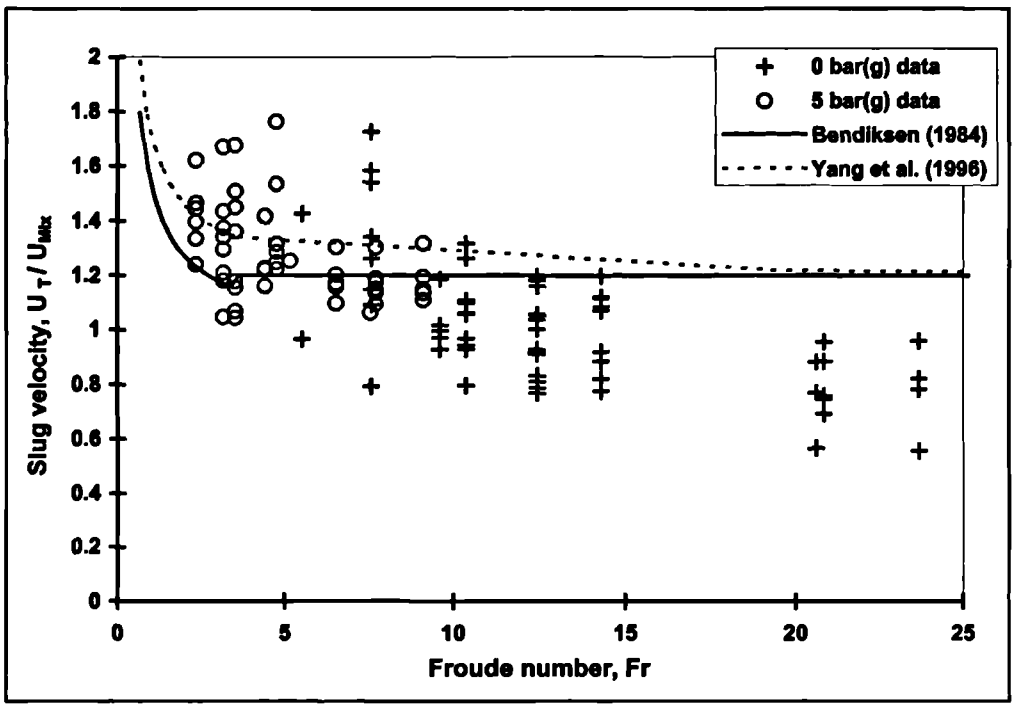

Figure 4.18: Variation of measured slug tail velociy with Froude number (-1.5° downflow, air-water, 0 and 5 bar(g))

Although the data are scattered, they exhibit the characteristic increase in slug translational velocity at low mixture velocities which was reported by Bendiksen (1984) and observed by Manolis (1995). It should be noted that the Bendiksen relationship, plotted in Figure 4.18, was presented for the prediction of *horizontal* slug flow, although the present data (and the correlation by Yang *et al.*, 1996) are plotted in Figure 4.18 for –1.5° downflow.

The experimental data do not tend to the accepted value of U_T/U_{Mix} = 1.2 at high Froude number. Although the asymptote is masked by the scatter in the data, the ratio for the present data set appears to be approximately 0.8, suggesting a negative value of the C-ratio for downhill flow.

In Table 4.6, comparison is made between the experimental data and predictions using the correlations of Bendicksen (1984), and Yang *et al.* (1996), using the definition of relative error given in Appendix 1.

	Bendiksen (1984)	Yang et al. (1996)
Mean relative error in predictions	0.125	0.186
Std. deviation	0.273	0.257
Root mean square relative error	0.299	0.317

Table 4.6: Relative error in predictions from slug tail velocity correlations for 116 data points, -1.5° downflow

The performance of these correlations is similar; both overpredict tail velocity on average, and they have errors of similar magnitude. The Yang *et al.* (1996) expression performs slightly worse, despite its nominal inclusion of the effect of pipe inclination.

The fact that the slug translational velocity is *less* than the total superficial velocity (at high superficial velocities, *i.e.* Froude numbers) is interesting and should be investigated further. A possible explanation might be gravitational acceleration of the film between the slugs.

4.2.4. Slug frequency

The slug frequency data obtained from inspection of the liquid holdup-time traces from the gamma densitometer, reported in Section 4.1.2, are compared with several slug frequency correlations in Table 4.7. The statistical treatment of relative error is described in Appendix 1.

	Relative error in predictions	Gregory & Scott (1969)	Heywood & Richardson (1979)	Tronconi (1990)	Manolis *et al.* (1995)	Yang *et al.* (1996)
0 bar(g) (34 points)	Mean	-0.041	-0.722	-0.936	-0.558	-0.935
	Standard Deviation	0.188	0.177	0.045	0.249	0.053
	Root mean square	0.190	0.742	0.937	0.610	0.937
5 bar(g) (22 points)	Mean	-0.126	-0.443	-0.918	-0.804	-0.808
	Standard Deviation	0.516	0.617	0.048	0.093	0.271
	Root mean square	0.520	0.748	0.919	0.809	0.850

Table 4.7: Relative error in some slug frequency correlations (measured slug frequencies from γ-densitometer traces, 0 and 5 bar(g))

All the correlations underpredict slug frequency at both pressures. Of the methods tested, the Gregory & Scott (1969) correlation performs best: the other expressions are, in comparison, poor. The correlation by Yang *et al.* (1996) is among the worst, despite its development specifically for slug flow in downwardly-inclined pipes. The Gregory & Scott (1969) correlation performs significantly better at atmospheric pressure than it does at 5 bar(g). This is the opposite of the trend reported by King (1998) for horizontal slug flow. King (1998) also found that most of the slug frequency correlations tended to overpredict his slug frequency data for horizontal flow, which is contrary to the results of the present work.

In Figure 4.19 and Figure 4.20 the slug frequency data obtained from the experiments at 0 and 5 bar(g) respectively are compared with the predictions of the Gregory & Scott (1969) correlation. In general, the correlation correctly predicts the trends that frequency increases with gas and liquid superficial velocity. However, due to the reduced size of the slug flow regime in downwardly-inclined flow, slug flow was not observed at low liquid flow rates and thus no comparison can be made with the correlation at superficial liquid velocity of less than about 4 m/s.

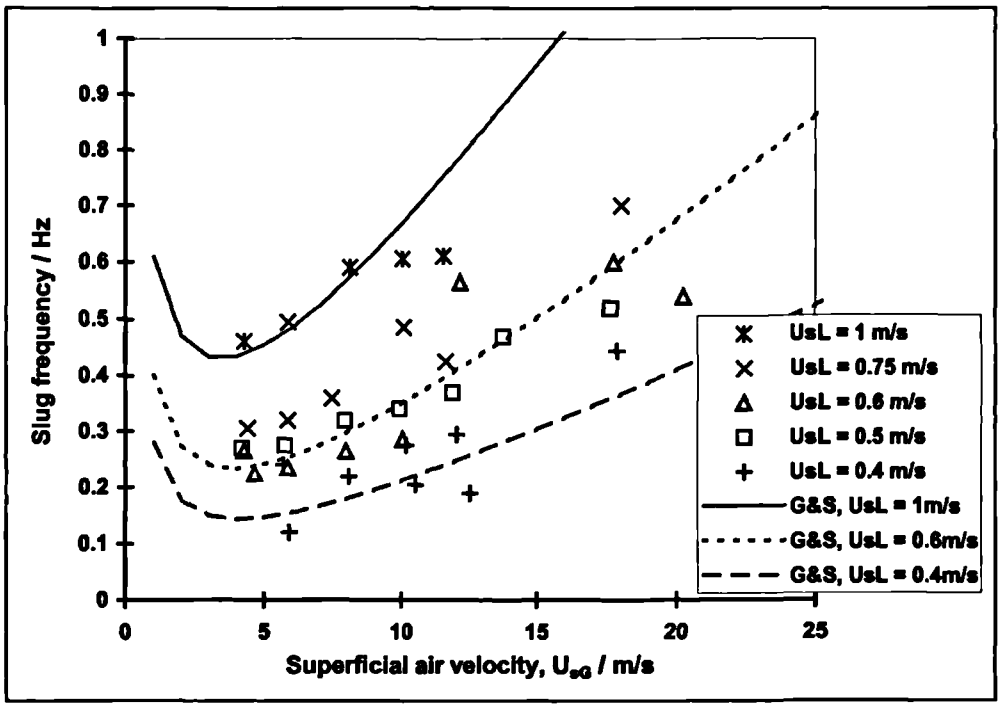

Figure 4.19: Measured slug frequency data compared with Gregory & Scott (1969) correlation (0 bar(g), -1.5° downflow)

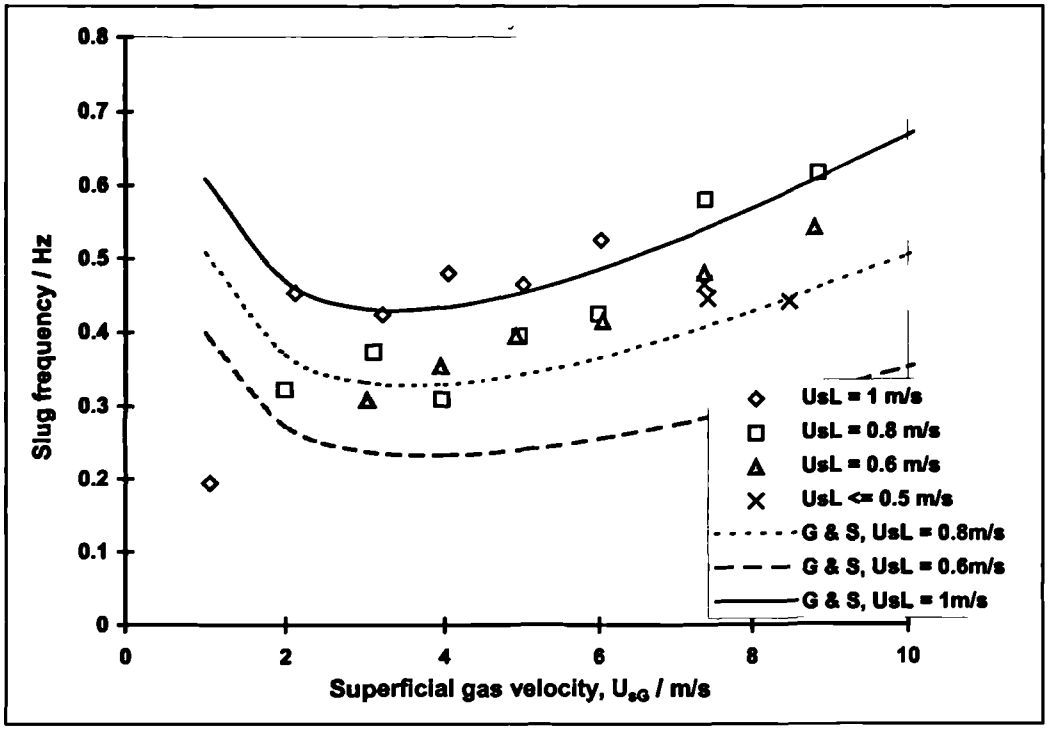

Figure 4.20: Measured slug frequency data compared with Gregory & Scott (1969) correlation (5 bar(g), -1.5° downflow)

4.2.5. Pressure gradient

Predictions of pressure gradient by several methods are compared with the experimental results in Table 4.8. The relative error in a prediction and the statistical treatment of error presented in the table are defined in Appendix 1. In each case, N is the number of datapoints compared.

	Relative Error in predictions	Beggs & Brill (1973)	Friedel (1979)	Taitel & Barnea (1990)
0 bar(g)	N	89	89	59
	Mean relative error	-0.334	0.027	-0.322
	Std. deviation	1.723	4.064	0.217
	Root mean square relative error	1.745	4.041	0.387
5 bar(g)	N	52	52	26
	Mean relative error	-0.577	-0.315	-0.576
	Std. deviation	0.287	0.444	0.113
	Root mean square relative error	0.643	0.541	0.587

Table 4.8: Comparison of relative error in pressure gradient predictions

For the experiments at atmospheric pressure, the phenomenological model of Taitel & Barnea (1990) gives a considerably better prediction of the experimental data, although ~~it does not perform as well as the Beggs & Brill (1973) correlation~~ there is little difference between the methods at higher pressure. At both pressures, the predictions tend to be lower than the experimental results, with the exception of the Friedel (1979) correlation which slightly overpredicts the data measured at atmospheric pressure. Results from the Taitel & Barnea model are given for a smaller subset of the data than the other methods. This is because the solution of the equation for the slug tail film profile is not robust for all mixture velocities at all pipe inclinations. Only those mixture velocities which resulted in a converged solution are considered in the error results presented in Table 4.8.

In general, the relative errors are worse at atmospheric pressure than at 5 bar(g). This reflects the increased scatter of the 0 bar(g) data.

To illustrate the shape of the trends predicted by the methods in Table 4.8, the performance of the Beggs & Brill (1973) and Freidel (1990) correlations, and the Taitel & Barnea (1990) model, is illustrated for a restricted range of liquid flow rates at atmospheric pressure in Figure 4.21, Figure 4.22 and Figure 4.23, respectively.

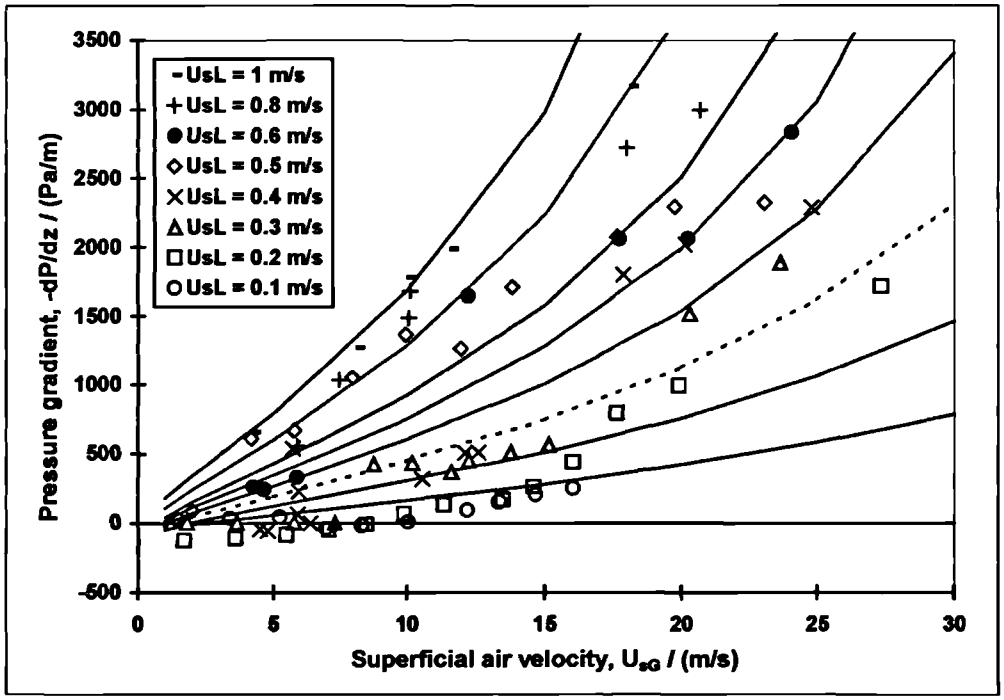

Figure 4.21: Pressure gradient measured at 0 bar(g) compared with prediction by Beggs & Brill (1973)

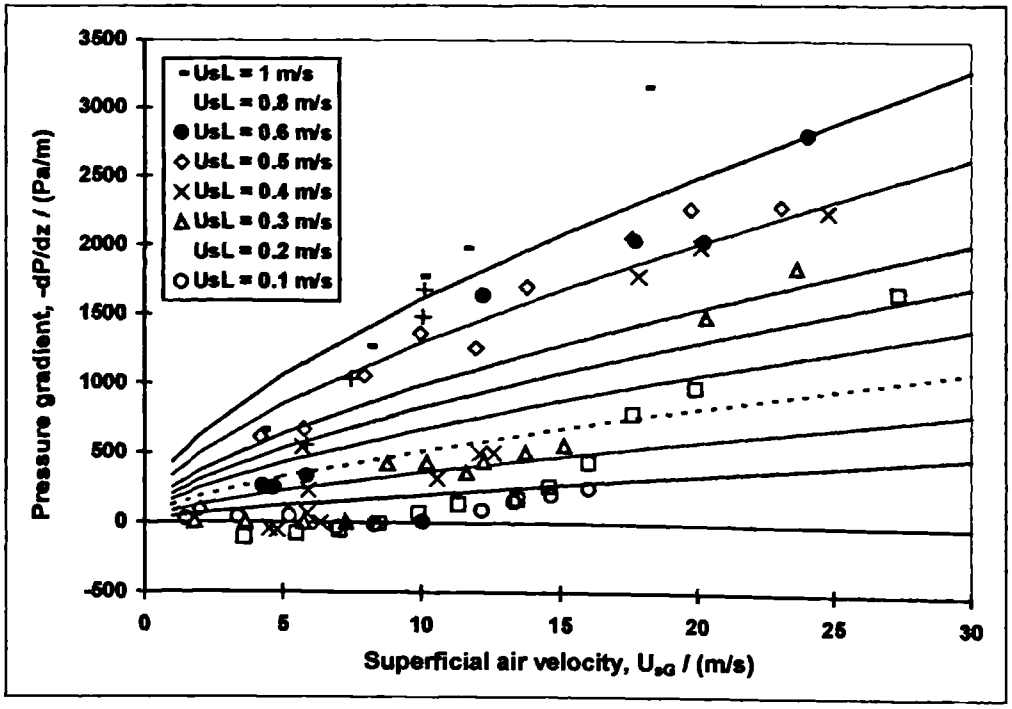

Figure 4.22: Pressure gradient measured at 0 bar(g) compared with prediction by Friedel (1979)

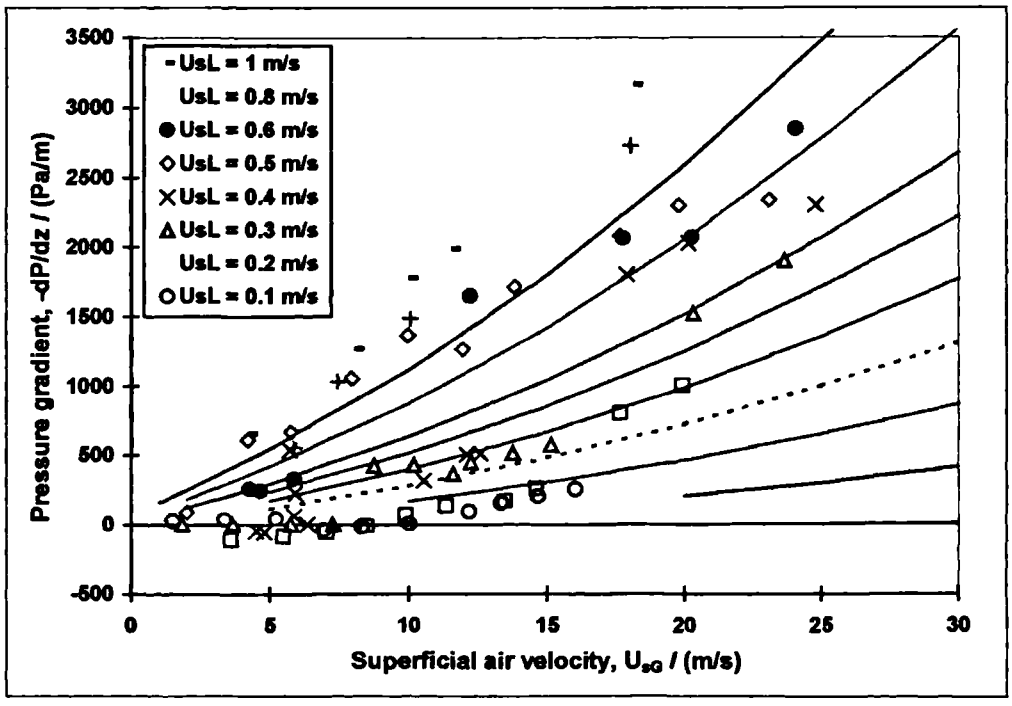

Figure 4.23: Pressure gradient measured at 0 bar(g) compared with prediction by Taitel & Barnea (1990)

The Beggs & Brill correlation (Figure 4.21) and the Taitel & Barnea model (Figure 4.23) show similar trends to those exhibited by the experimental data. However, the Friedel correlation (Figure 4.22) shows a different trend. Of the three methods, only the Beggs & Brill (1973) correlation predicts the pressure recovery (*i.e.*, the positive pressure gradient) which was observed at low gas and liquid flows.

In Figure 4.24, Figure 4.25 and Figure 4.26, the performance of the Beggs & Brill (1973) and Freidel (1990) correlations, and the Taitel & Barnea (1990) model respectively are compared with the experimental data measured at 5 bar(g).

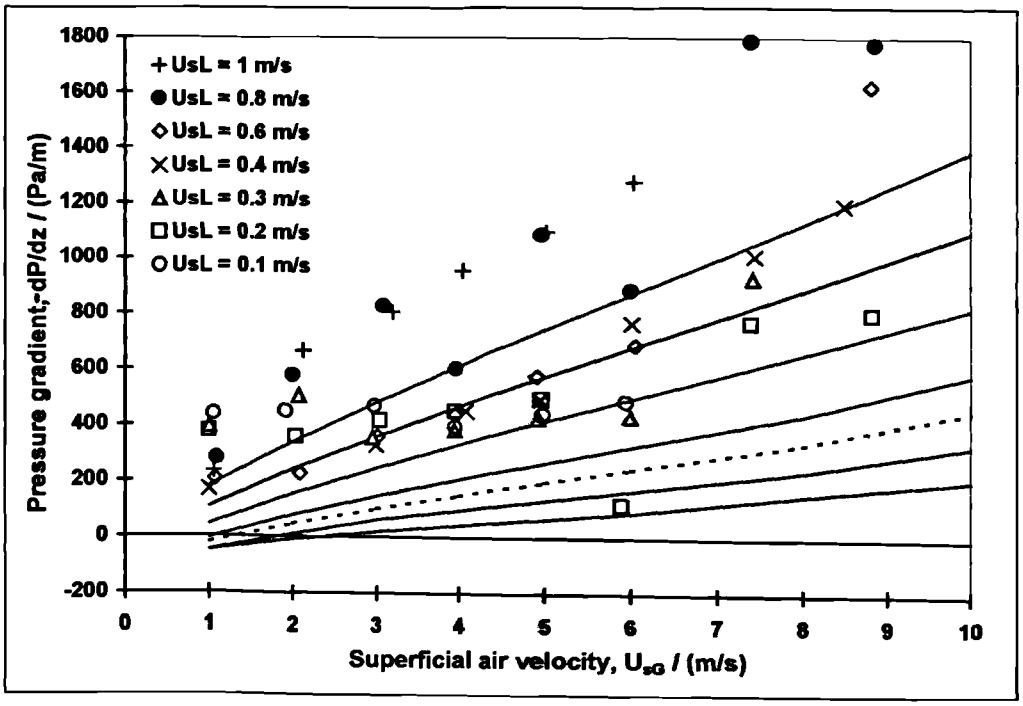

Figure 4.24: Pressure gradient measured at 5 bar(g) compared with prediction by Beggs & Brill (1973)

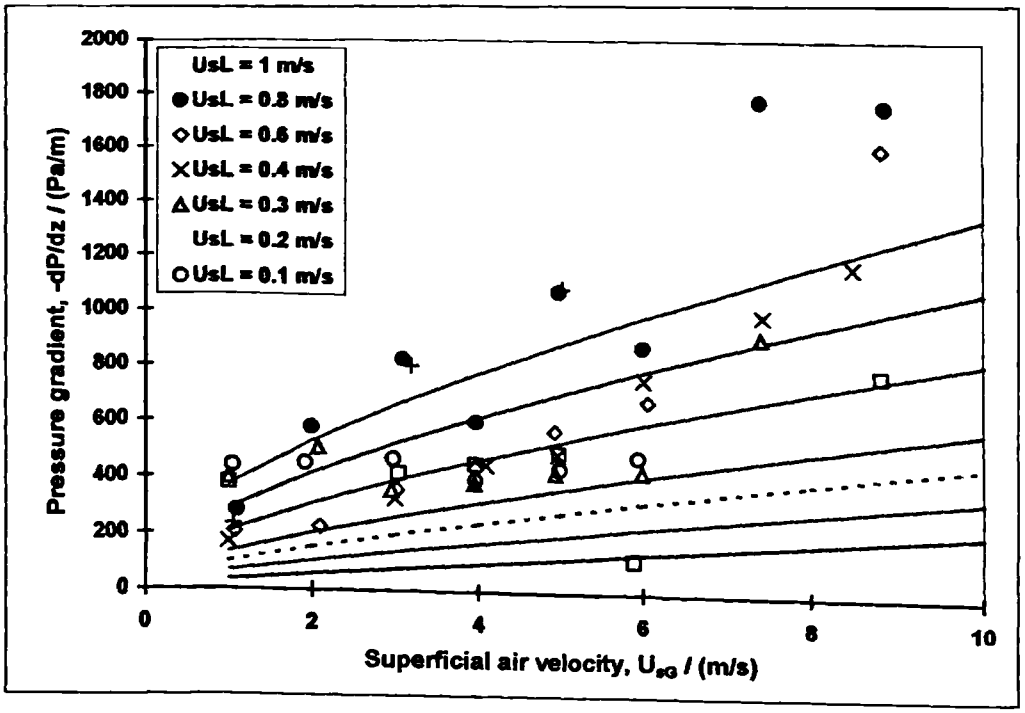

Figure 4.25: Pressure gradient measured at 5 bar(g) compared with prediction by Friedel (1979)

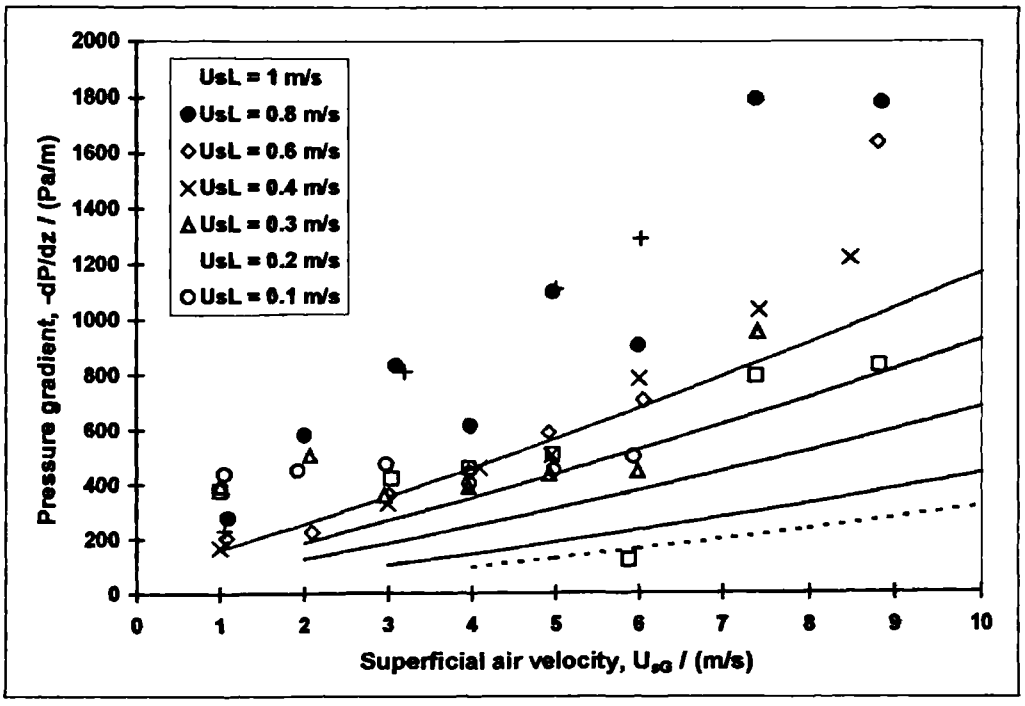

Figure 4.26: Pressure gradient measured at 5 bar(g) compared with prediction by Taitel & Barnea (1990)

At 5 bar(g) the trend predicted by the Beggs & Brill (1973) correlation is similar to that of the Friedel (1979) relationship. As at atmospheric pressure, the Beggs & Brill (1973) method predicts a range of flow rates for which pressure recovery occurs, however this was not observed in the experiments.

4.3. Summary

A large set of data has been presented in this Chapter for two-phase flow in a -1.5° downwardly-inclined test-section, for air-water flow at 0 and 5 bar(g).

Measurements were made of superficial gas and liquid velocities, liquid holdup at five points along the test-section and pressure gradient. The holdup measurements were analysed to obtain estimates of slug length, slug frequency and slug tail velocity. Some general trends were observable, despite the scatter of the data.

In downhill flow, it was found that the size of the slug flow regime was smaller than for horizontal flow, with the stratified/slug transition occurring at significantly higher liquid superficial velocity.

The measured data were compared against several correlations from the literature. Generally, correlations for slug parameters and pressure drop did not predict the experimental data particularly well. It is likely that this is due to the significant difference between horizontal two-phase flow, for which predictive correlations are usually derived, and the downward inclination of the test-section studied in the present work. However, correlations for slug frequency and slug length by Yang *et al.* (1996), which were proposed for the prediction of slug flow in downwardly-inclined pipes, performed at least as badly as earlier methods which were produced for use with horizontal flow.

The slug length and tail velocity data included only a small number of very short slugs which were insufficient to obtain a trend for the change in slug translational velocity with slug length (as seen by Fagundes Netto *et al.*, 1998). However, the increase in the slug translational velocity at low values of the superficial mixture velocity was observed. Generally, poor agreement was seen between the experimental data and the correlations of Bendiksen (1984) and Manolis (1995) at high values of the Froude number, with slug translational velocities considerably *less* than the total superficial velocity. From a

consideration of the liquid mass balance over the slug body, this means that "volume" is picked up at the slug tail – either via liquid flow *into* the tail, or by entrainment of gas at the tail which passes into and through the slug.

Chapter 5: Experimental studies of terrain effects in slug flow I: Flow in a pipeline with a dip

In this Chapter, experimental data for two-phase air-water flow are presented for the "V-section" configuration of the WASP facility shown in Figure 5.1 (see Section 3.3.2 for further details). The schematic diagram in Figure 5.1 shows the relative positions of the conductivity probes (shown as CPR) and the gamma densitometer (shown as γ) in the WASP test-section.

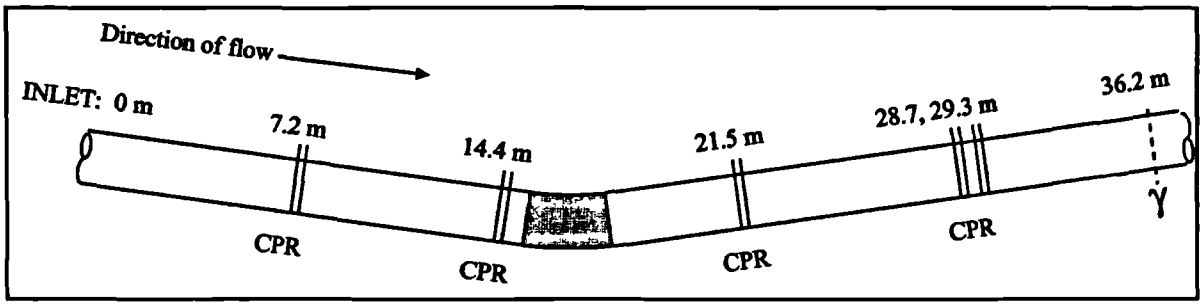

Figure 5.1: Relative positions of conductivity probes and gamma densitometer for Campaign 2 (*not to scale*)

In this work, data were collected for steady-state flows at near-atmospheric and five bar(g) exit pressures; observations of pressure drop, flow pattern, slug frequency, slug length and liquid holdup were made at different points along the test-section. The experimental results are presented in Section 5.1. A comparison of the data with some published predictive models and correlations (which were described previously in Chapter 2) is given in Section 5.2.

5.1. Experimental results

In this section, results from the campaign of experiments are presented. The detailed experimental matrix used for the campaign is included in Appendix 2, in which a unique run number is assigned to each experiment, and the experimental parameters are listed for each case. The original data files recorded for each experiment are included on CD-ROM number CD02, appended to this thesis.

5.1.1. Flow pattern

The results were used to construct flow pattern maps, with flow pattern identification carried out at the transparent visualisation section near the end of the uphill part of the test-section.

The maps for 0 and 5 bar(g) are shown in Figure 5.2 and Figure 5.3 respectively. The abbreviations for flow patterns used in the legends are described in Table 5.1.

Abbreviation	Flow pattern
str. sm.	Stratified smooth flow
str. wa.	Stratified wavy flow
sw / slug	Transition between stratified wavy and slug flow; some interfacial waves completely block the pipe
slug	Slug flow
slug / ann.	Transition between slug and annular flow; the liquid film region between slugs is observed to form an annular layer around the pipe wall
str. wa. / ann.	Transition between stratified wavy and annular flow
bubbly	Bubbly flow
ebf	Elongated bubble flow consisting of long, regular Taylor bubbles separated by short slugs of liquid with very high liquid holdup

Table 5.1: Explanation of abbreviations used in flow pattern maps

Both maps show a considerable increase in the region of slug flow compared to the corresponding maps for a straight horizontal pipe, such as those by King (1998).

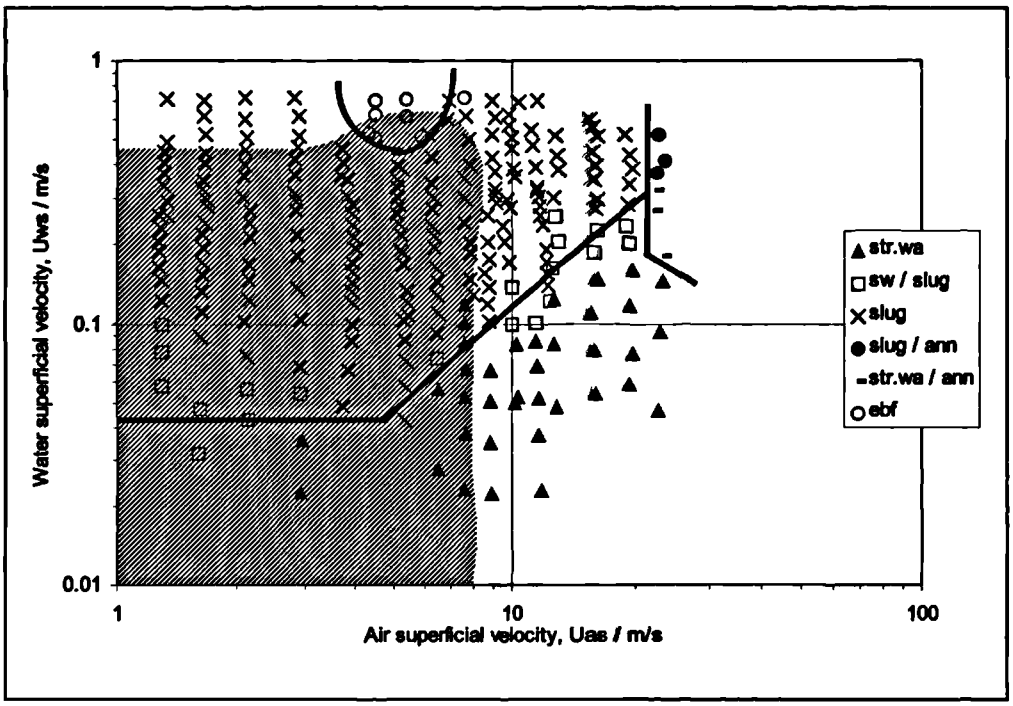

Figure 5.2: Flow patterns measured at 35 m from the test-section inlet, 0 bar(g)

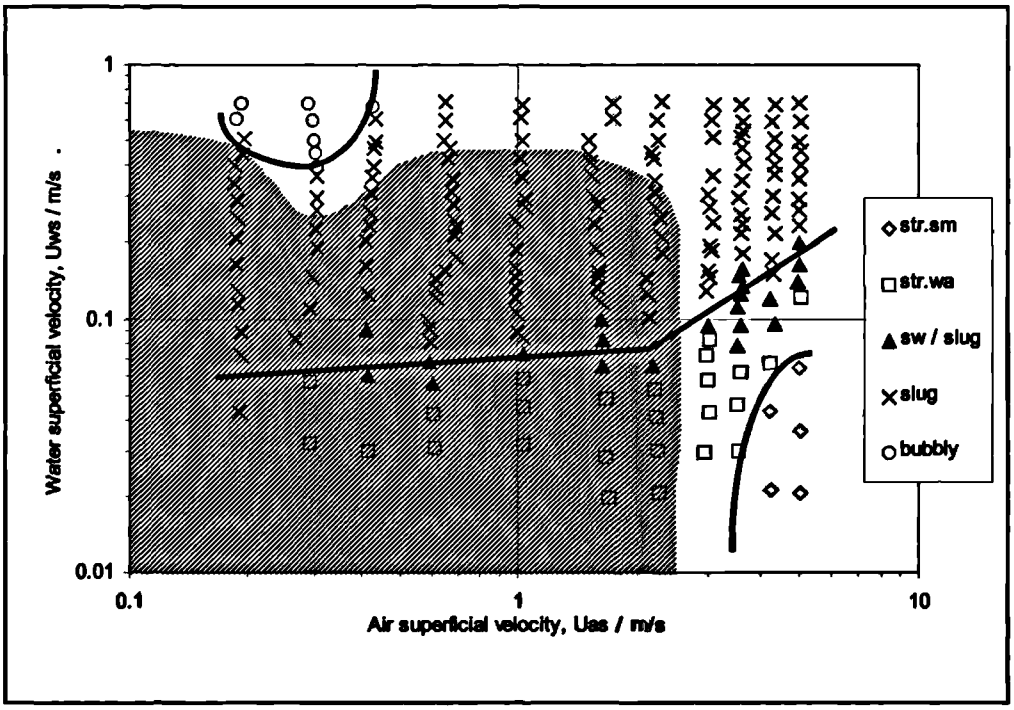

Figure 5.3: Flow patterns measured at 35 m from the test-section inlet, 5 bar(g)

The shaded areas in Figures 5.2 and 5.3 indicate the region in which counter-current film flow was observed in the pipe. This was seen where slug flow or stratified-wavy flow was present

in the uphill part of the test section. After a slug or wave had moved (downstream) past the visualisation section, it was observed that the stratified liquid film at its tail decelerated under gravity, stopped, then flowed "upstream".

This occurs in a large region of the flow pattern map studied, except where the superficial gas velocity is high so that interfacial shear prevents reversal of the film, or where superficial liquid velocity is high, so that the slug frequency is very high and there is insufficient time for film reversal to occur. An analysis of this phenomenon is considered later, in Section 5.2.1.

At medium flow rates, the velocity profile (as seen by observing the motion of small gas bubbles in the liquid film) appeared to be an "S"-shape, as depicted in Figure 5.4.

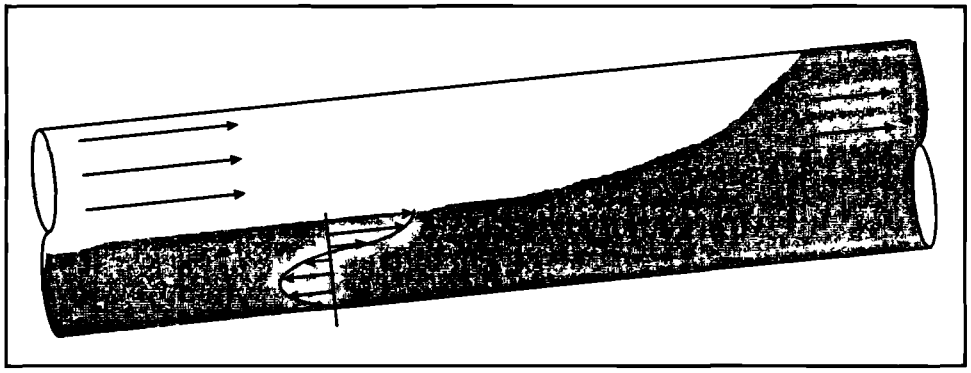

Figure 5.4: Velocity profile observed in liquid film in uphill slug flow

The liquid at the top of the film, near to the gas-liquid interface, was observed to travel downstream with the shearing action of the downstream gas flow. Lower down in the liquid film, the liquid appeared to flow upstream under the action of gravity. It was not clear whether the net liquid flow in the film was in the up- or downstream direction (although, overall, of course, the flow of liquid is *downstream*, the liquid being carried by the slugs).

At atmospheric pressure, the critical superficial gas velocity above which no counter-current flow was observed was approximately 8 m/s. This is in close agreement with the value of 7.7 m/s observed by Wood (1991). For the experiments performed at 5 bar(g), Figure 5.3 shows that the critical gas velocity is found to be about 2.4 m/s.

The flow patterns at different points along the test section were determined by inspection of the liquid holdup / time traces from the conductivity probes. Of most interest were the flow patterns observed at the probes either side of the "dip", *i.e.* those at 14.3 m and 21.4 m from

the inlet. Four flow pattern combinations were observed, as summarised in Table 5.2 with the corresponding conductance probe traces shown in Figures 5.5 – 5.8. In the Figures, the holdup traces are offset by unity for successive probes along the test-section.

Flow pattern upstream of dip	Flow pattern downstream of dip	Trace illustrated in Figure...
Steady	Steady	Figure 5.5
Steady	Dip Slugging	Figure 5.6
Steady	Random Slugging	Figure 5.7
Intermittent	Random Slugging	Figure 5.8

Table 5.2: Flow pattern combinations observed around the dip

The flow patterns referred to in Table 5.2 are defined as follows:

1. *Steady.* Here, the holdup shows only small flutuations with time. It is not possible to discriminate from the holdup traces alone between stratified and annular flow but one may deduce from the visualisation results (shown in Figures 5.2 and 5.3 for the end of the upwardly-inclined leg of the "V"-section, and in Figures 4.2 and 4.3 for downwards-flow) that the "steady" flow observations correspond to stratified and stratified-wavy flow.

2. *Dip slugging.* Here, slug flow with very regular frequency and slug length is observed. This is caused by periodic liquid accumulation and "unloading" of liquid at the dip.

3. *Intermittent.* Here, the flow is showing intermittent features characteristic of incipient slug flow.

4. *Random slugging.* Here the flow is normal slug flow with irregular slug formation.

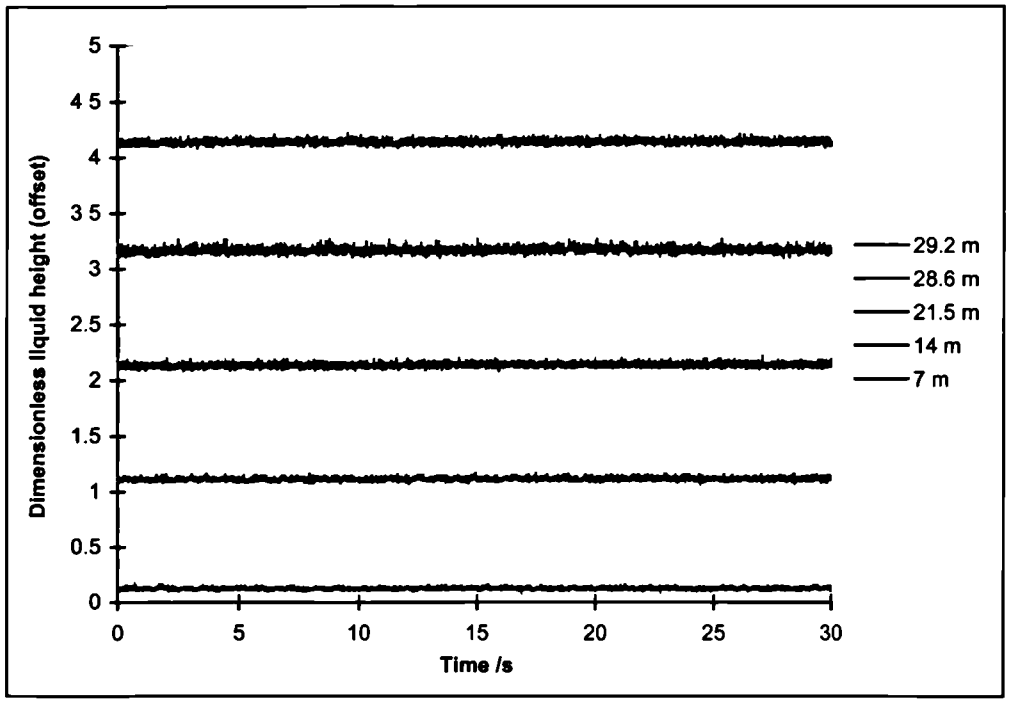

Figure 5.5: "Steady" flow either side of the dip

(U_{sG} = 5.0 m/s, U_{sL} = 0.02 m/s , P = 5 bar(g))

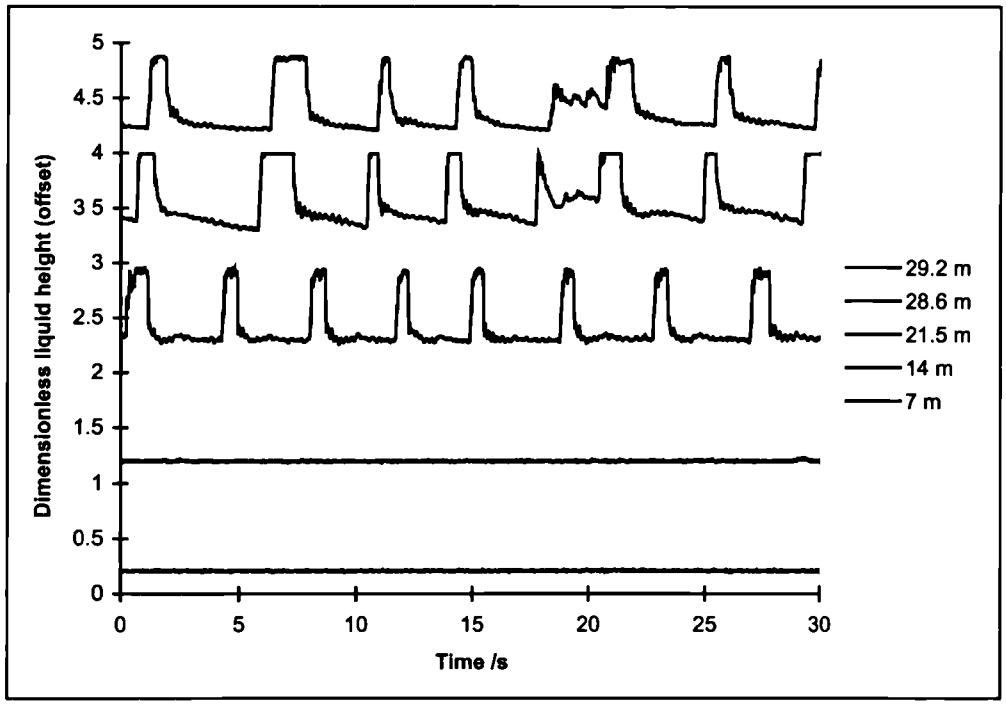

Figure 5.6: "Steady" flow upstream of the dip with "dip slugging" downstream

(U_{sG} = 6.0 m/s, U_{sL} = 0.09 m/s , P = 5 bar(g))

"Steady-dip slugging" traces, such as shown in Figure 5.6 are observed for low gas flow rates at low to medium liquid flows. This classification is characterised by stratified smooth flow in the downhill portion of the "V"-section, with very regular slug flow occurring at the probe located 21.5 m from the inlet, immediately downstream of the "dip". Further downstream, the trace is more irregular and more akin to hydrodynamic slugging, with some random variation in slug frequency and length. It appears as though the short, regular slugs created by "dip slugging" may grow, shrink or merge as they progress downstream, so that the slug flow becomes increasingly chaotic.

At higher gas and liquid flow rates, but not sufficiently high to cause slugging in the downhill leg of the "V"-section, random slugging occurs in the uphill leg as exemplified by the result shown in Figure 5.7. The holdup trace from the probe at 21.5 m from the inlet, downstream of the dip, does not exhibit regular behaviour characteristic of dip slugging (compare Figure 5.6).

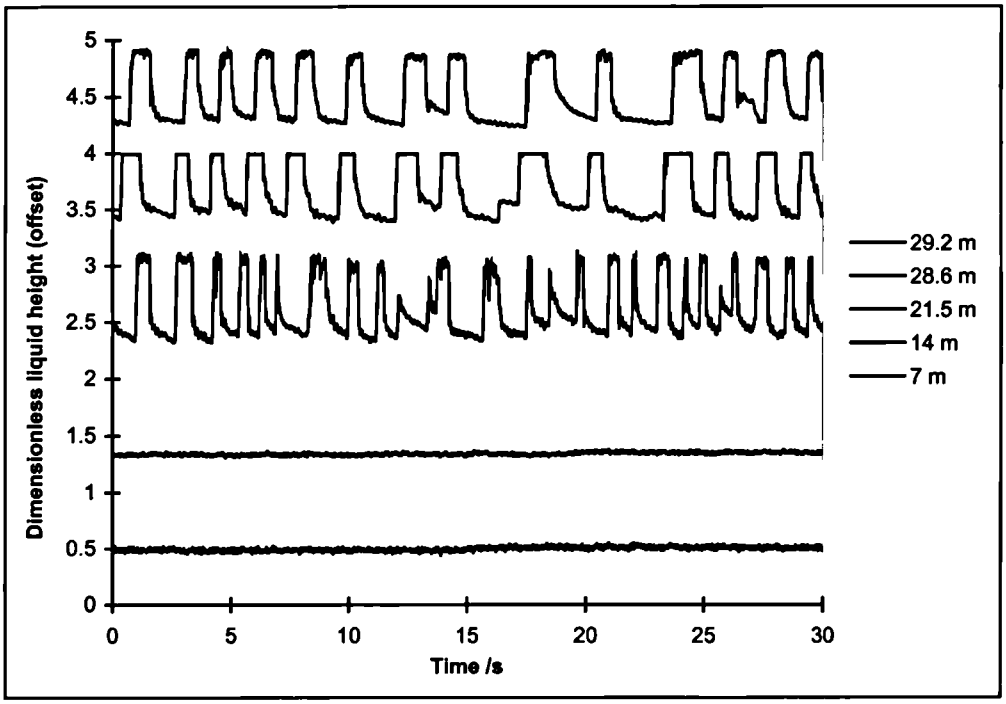

Figure 5.7: "Steady" flow upstream of the dip with "random slugging" downstream (U_{sG} = 0.65 m/s, U_{sL} = 0.5 m/s , P = 5 bar(g))

At the highest gas flow rates, intermittent flow is observed in the upstream leg of the "V"-section with random slugging in the downstream (upflow) leg, as exemplified in the traces shown in Figure 5.8. For most of the experiments performed in this regime, the gas flow rates were above the maximum critical value for flow reversal in the uphill section of the "V", so

that liquid will only flow into the dip from the upstream side. It may be hypothesised that if liquid accumulation in the dip by drainage from the downstream leg is absent, slug formation at the dip itself due to "unloading" of accumulated liquid is presumably less important than the hydrodynamic slug formation processes occurring upstream. It may be surmised that slugs and/or waves are formed in the downhill leg and travel through the dip without being greatly affected by it. There is some evidence for this as indicated by the arrows connecting features in Figure 5.8. These features move at a velocity that would be expected for slugs in this flow: the mixture velocity is 4.3 m/s, thus the slug translational velocity $U_T \approx 4.6$ m/s.

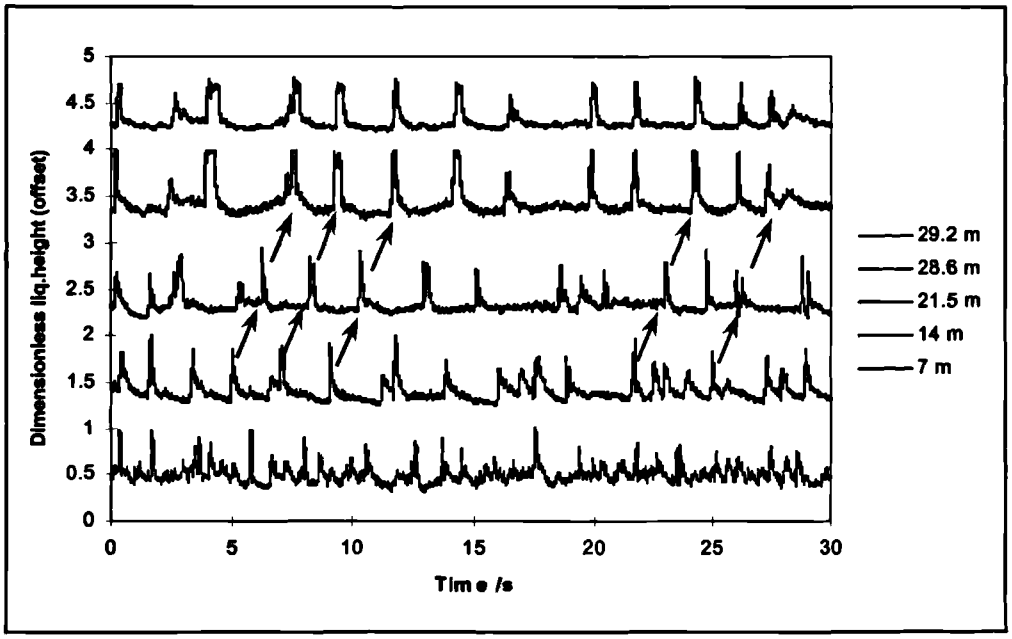

Figure 5.8: "Intermittent" flow upstream of the dip with "random slugging" downstream (U_{sG} = 3.6 m/s, U_{sL} = 0.7 m/s , P = 5 bar(g))

Experimental runs at 0 and 5 bar(g) are grouped according to the four characterisations defined above and plotted as flow pattern maps in Figure 5.9 and Figure 5.10 respectively.

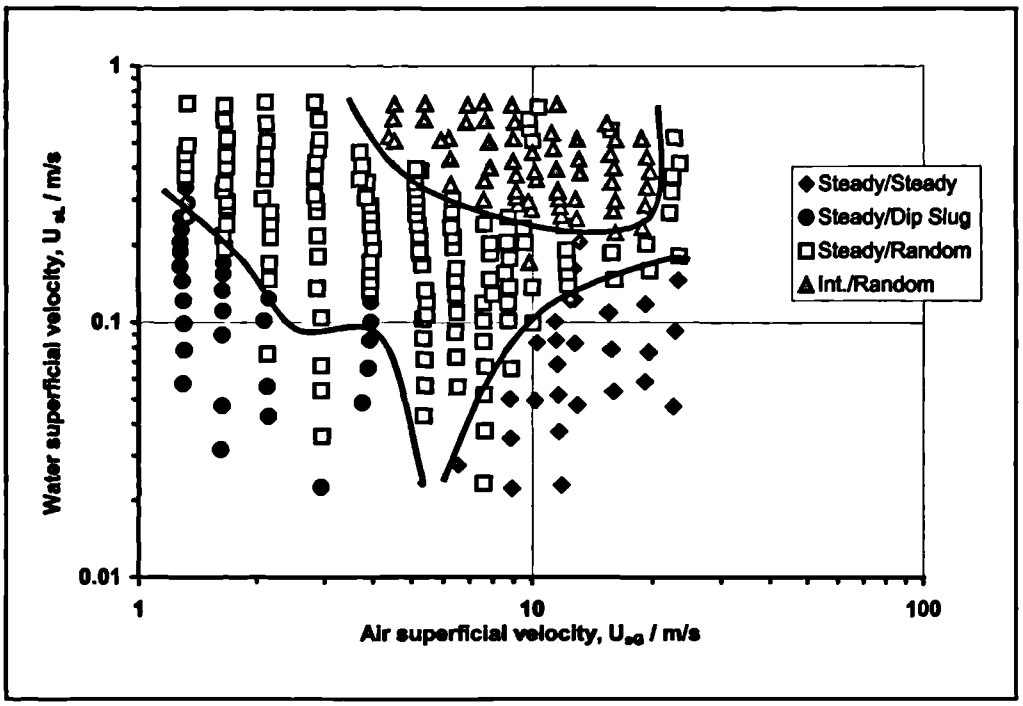

Figure 5.9: Flow regimes either side of the "dip", 0 bar(g)

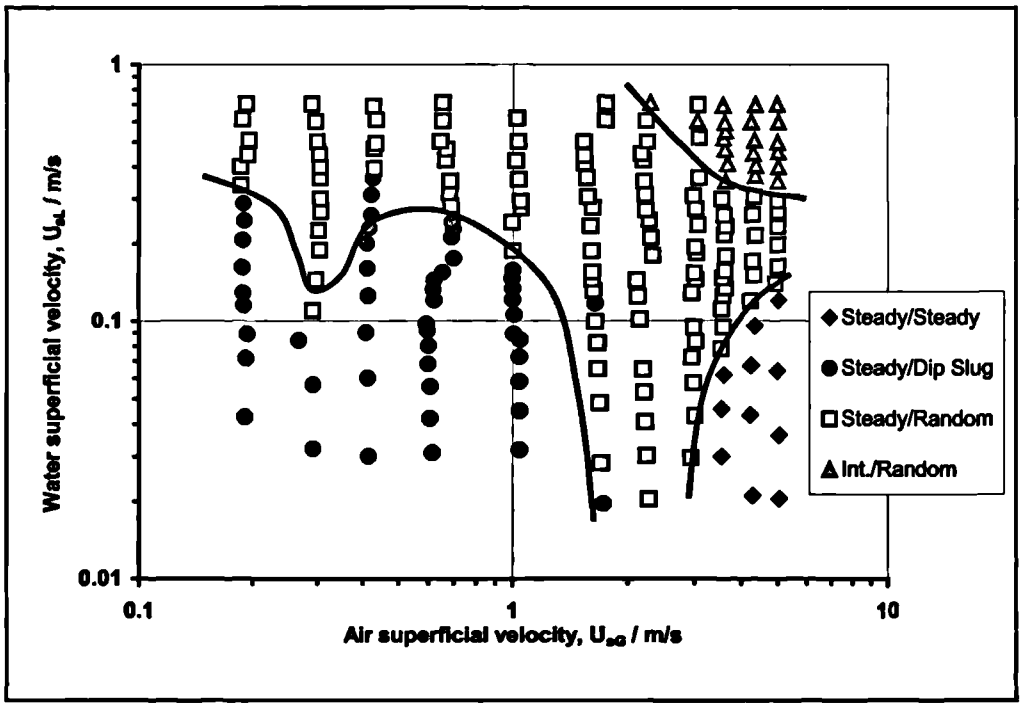

Figure 5.10: Flow regimes either side of the "dip", 5 bar(g)

Note that there is only a loose correlation between the flow patterns at the dip, shown in Figure 5.9 and Figure 5.10, and those near the pipe exit shown in Figure 5.2 and Figure 5.3. However, there appears to be reasonable correlation between the regions of dip slugging and reverse flow for the 5 bar experiments, shown in Figure 5.10 and Figure 5.3 respectively.

This correlation is not as apparent for the 0 bar results, shown respectively in Figure 5.9 and Figure 5.2.

5.1.2. Liquid holdup

Liquid holdup was measured near to the end of the test-section, using a gamma densitometer. Time-averaged holdup data, calculated as the arithmetic mean of all the holdup samples recorded during each 180-second experimental run, are plotted in Figure 5.11. The data are plotted against inlet quality (defined as the mass fraction of gas at the pipe inlet) since this parameter is often used in correlations for liquid holdup. It is interesting to note that the results are grouped quite well in separate lines for the respective pressures when plotted in this way.

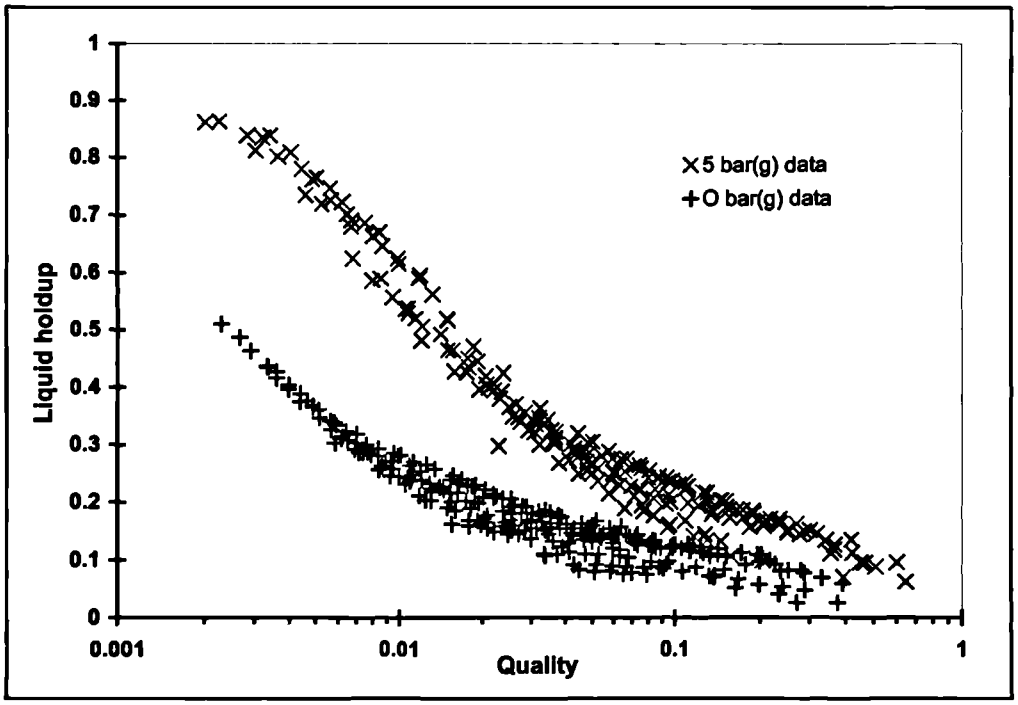

Figure 5.11: Liquid holdup data measured at 36.2 m from the pipe inlet

These data are compared with predictive correlations in Section 5.2.2.

5.1.3. Slug tail velocity: the "wake effect"

As in the first and third Campaigns, a limited subset of the experimental results was studied to investigate the relationship between slug length and tail velocity. The pair of conductivity

probes, situated approximately 29 m from the test-section inlet and spaced 0.6 m apart, was used to determine slug tail velocity and slug length, in the uphill leg of the "V"-section, for approximately 40 experimental slug-flow runs. The calculation procedure was described in Section 4.1.3 in Chapter 4.

The experimental results are plotted in Figure 5.12 in dimensionless form. The data set consists of 233 slugs, taken from 37 experimental runs. The runs were chosen so that they were regularly spaced across the slug flow regions of the 0 and 5 bar(g) flow pattern maps, and so that the entire range of mixture velocities was represented at both pressures. For each experimental run used, slug lengths and velocities were calculated for a 30-second period, one minute after the start of the run.

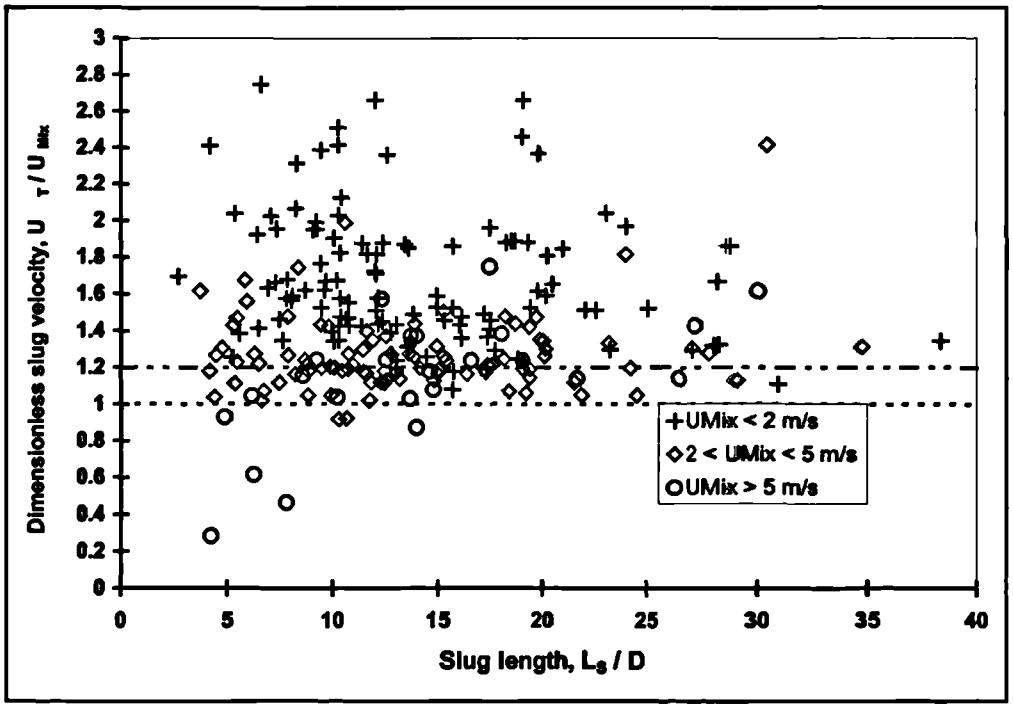

Figure 5.12: Dimensionless slug tail velocity *vs.* dimensionless slug length for a subset of 37 experimental runs

The data shown in Figure 5.12 are grouped according to ranges of mixture velocity. They show the expected trend with mixture velocity (discussed further in Section 5.2.4 and shown in Figure 5.35, below). This shows high values of (U_T/U_{Mix}) for low mixture velocity (where the gravitational motion of the slug tail is significant) and values less than unity at high values of the mixture velocity (where gas may "break through" the slugs). However, for each range of velocity, there is no clear effect of slug length. Such a length effect has been observed by Fagundes Netto *et al.* (1998, 1999a, 1999b) and is predicted in the CFD studies carried out in

the present work (see Chapter 8). However, because of the effect of mixture velocity on slug tail translational velocity and the fact that slug length was a *dependant* variable in the present experiments (as distinct to those of Fagundes Netto *et al.* where slug length was controlled), the effect may be obscured in the data shown in Figure 5.12.

5.1.4. Slug length

The slug length data obtained from the analysis described in Section 5.1.4 are plotted as a slug length distribution in Figure 5.13.

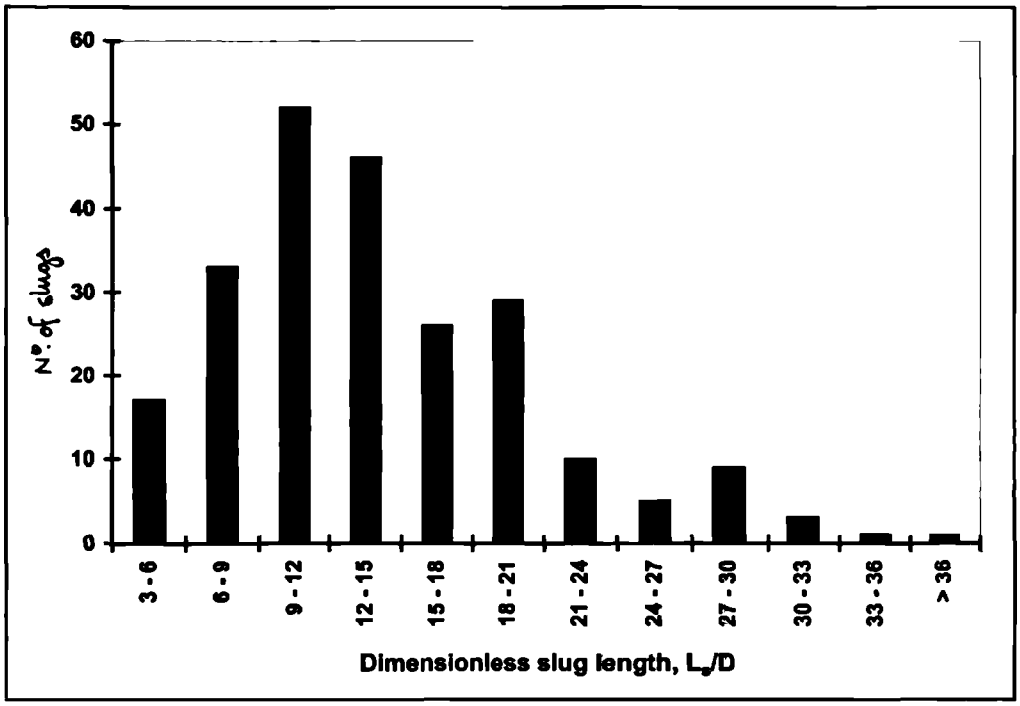

Figure 5.13: Distribution of dimensionless slug lengths for a subset of 37 experimental runs

The mean slug length is 13.9 pipe diameters, with a standard deviation of 6.4.

5.1.5. Slug frequency

Two methods were used to obtain slug frequency data. As in the first Campaign, results were obtained by inspection of the liquid holdup-time traces from the gamma densitometer. Additionally, the data recorded from the conductivity probes were analysed to find the dominant frequency in the power spectral density (PSD) spectrum.

Inspection of the gamma densitometer holdup-time traces

The output from the gamma densitometer was used to derive slug frequency data for the runs exhibiting slug flow at the end of the uphill portion of the test section. The procedure was the same as that used in the first Campaign of experiments, which was described in Section 4.1.5 in Chapter 4.

The plots of slug frequency against superficial gas velocity, shown in Figures 5.14 – 5.17, exhibit a characteristic "tick" shape with a discernible minimum. Manolis (1995) reported that the minimum frequency occurred at an air velocity of approximately 5 m/s for horizontal flow. However, the results from these experiments suggest that for flow in the uphill portion of a "V"-section, the minimum is at a lower value of U_{sG}, approximately 3 m/s for the atmospheric pressure runs, and between 1 and 2 m/s (depending on the water superficial velocity) for the runs at 5 bar(g).

The data measured at atmospheric pressure (Figure 5.14 and Figure 5.15) exhibit considerably more scatter than those measured at 5 bar(g) (Figure 5.16 and Figure 5.17). For the 5 bar(g) data in particular, the "tick" shapes are clearly apparent if the data are plotted according to narrow ranges of superficial liquid velocity. In general, the slug frequencies increase with liquid superficial velocity and also increase with the system pressure.

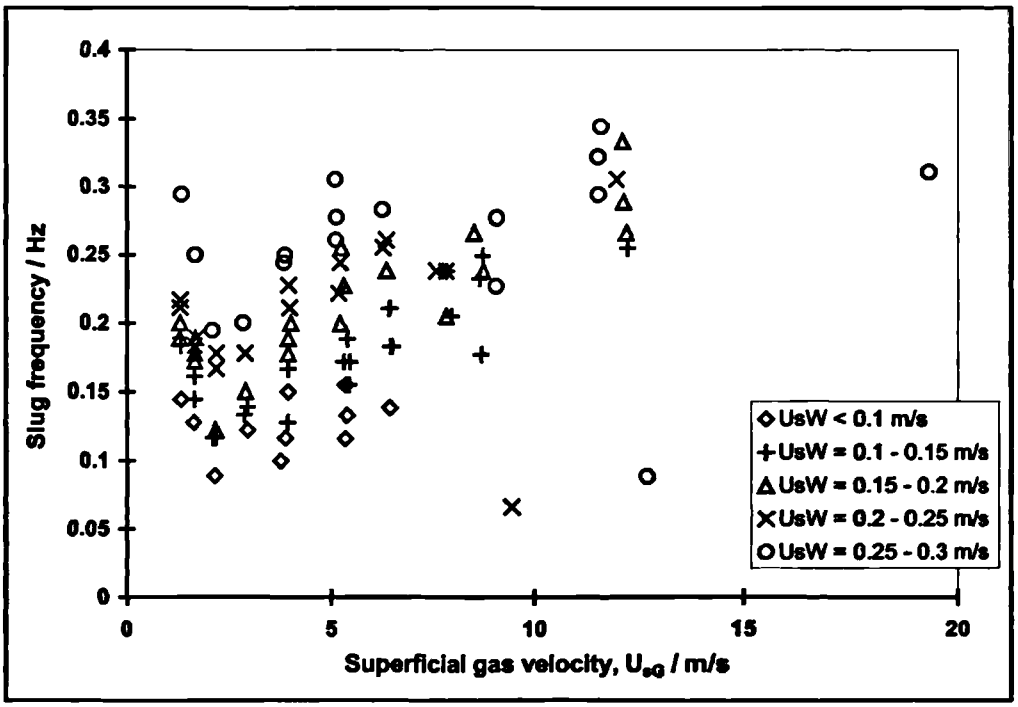

Figure 5.14: Slug frequencies (from inspection of the gamma densitometer traces) at 36.2 m from the inlet, 0 bar(g) runs, 0 m/s < U_{sL} < 0.3 m/s

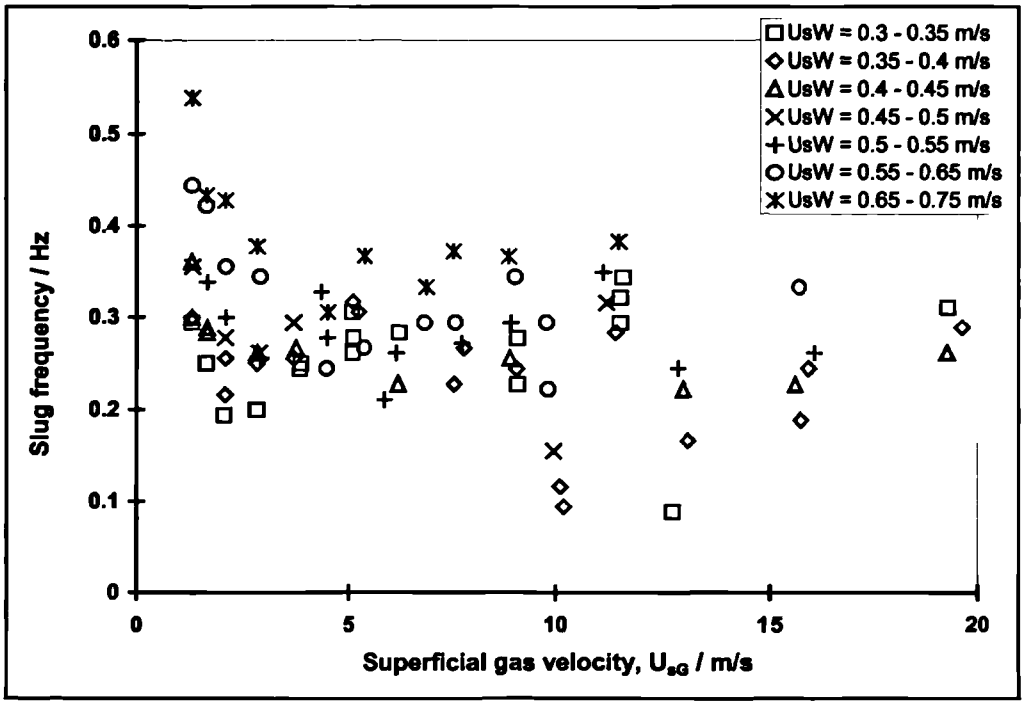

Figure 5.15: Slug frequencies (from inspection of the gamma densitometer traces) at 36.2 m from the inlet, 0 bar(g) runs, 0.3 m/s < U_{sL} < 0.75 m/s

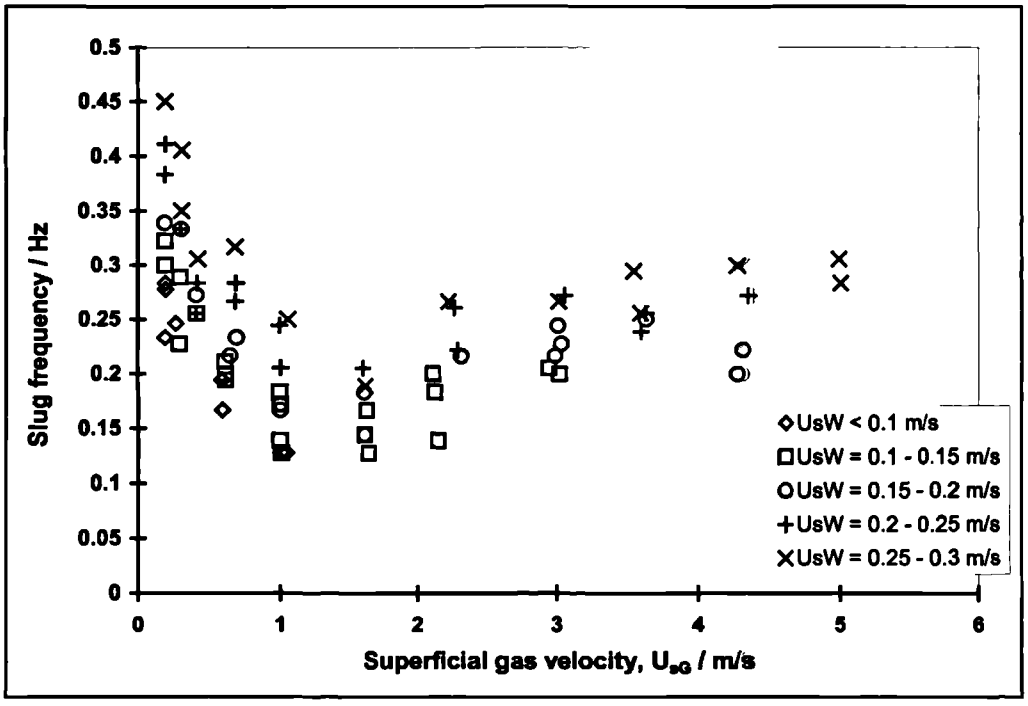

Figure 5.16: Slug frequencies (from inspection of the gamma densitometer traces) at 36.2 m from the inlet, 5 bar(g) runs, 0 m/s < U_{sL} < 0.3 m/s

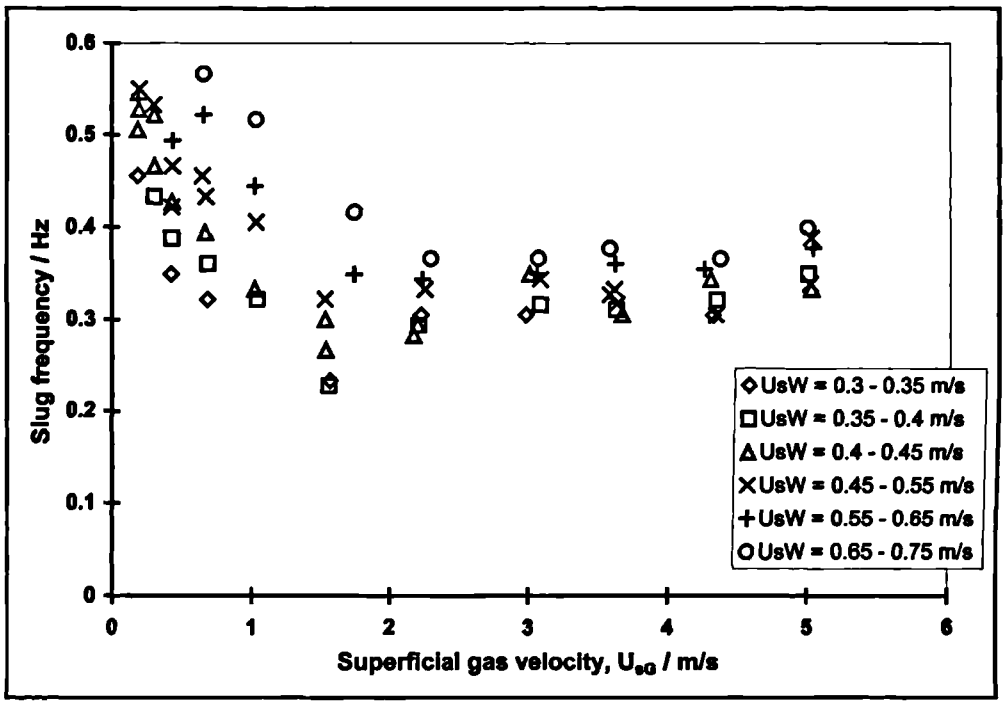

Figure 5.17: Slug frequencies (from inspection of the gamma densitometer traces) at 36.2 m from the inlet, 5 bar(g) runs, 0.3 m/s < U_{sL} < 0.75 m/s

Power spectral density analysis of the conductivity probe signals

Obtaining slug frequency data by inspection of holdup-time traces is tedious and time-consuming, and this is not a practical method for analysis of the multi-channel data from the conductivity probes situated along the pipeline. Instead, average slug frequencies were obtained from these data using power spectral density (PSD) analysis of the normalised holdup-time traces.

The PSD data were obtained using a commercial scientific data analysis software package, DATS_Plus v.2 (Prosig, 1994), running on an IBM PS/2 personal computer.

The slug frequency is taken as the point on the power spectrum with the highest power value. Holdup/time traces with regular slugging, *e.g.* "dip slugging" traces (such as the middle trace in Figure 5.6), produce power spectra such as Figure 5.18, which has an obvious maximum:

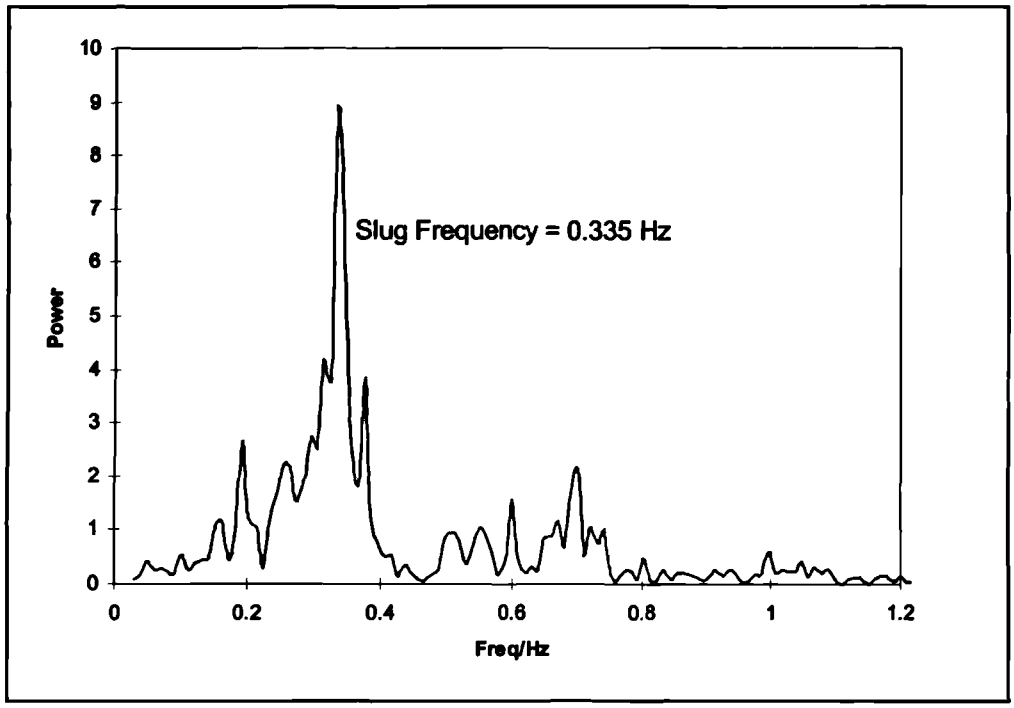

Figure 5.18: Power spectrum from a holdup-time trace with regular slugging

However, the power spectra resulting from PSD analysis of holdup-time traces from experiments exhibiting irregular ("random") slugging (such as Figure 5.8) are considerably more ambiguous. Figure 5.19 shows a typical power spectrum, which has many local maxima with similar power values; automatic selection of the highest power may not necessarily yield the true average slug frequency.

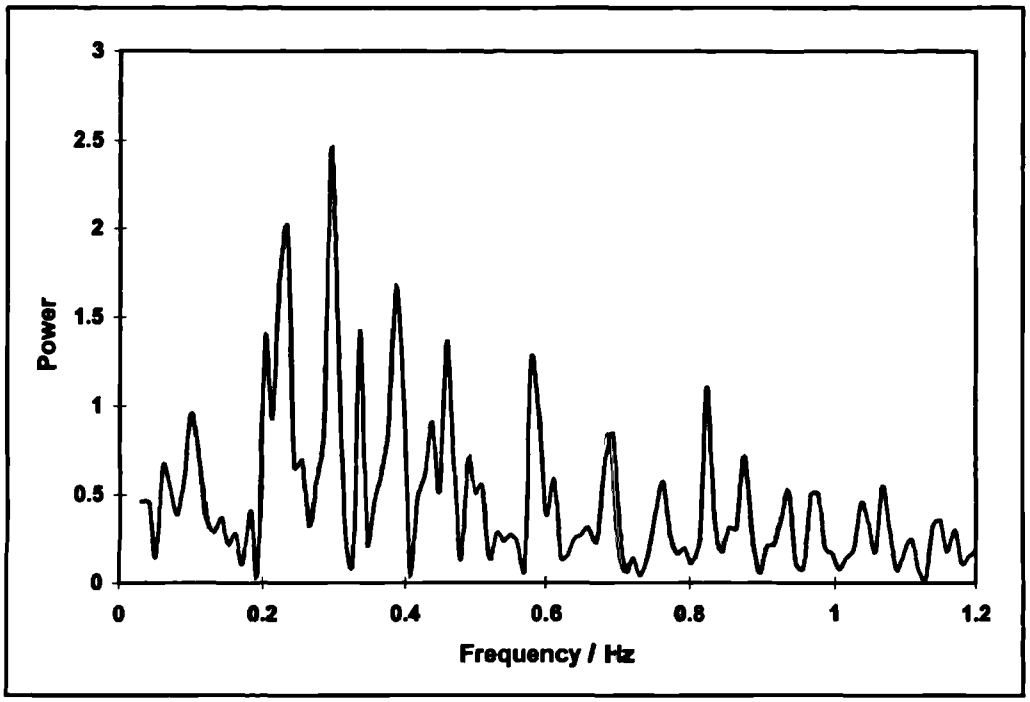

Figure 5.19: Power spectrum from a holdup-time trace with irregular slugging

Due to this ambiguity, it is suggested that the slug frequency data obtained from the PSD analysis of conductivity probe traces are not as reliable as those from the inspection of gamma densitometer data. This must be borne in mind when the slug frequency data are compared with predictive correlations in Section 5.2.5.

Slug frequency data are grouped according to gas flow rate and plotted for the 21.5 m conductivity probe in Figure 5.20 and Figure 5.21, for 0 and 5 bar(g) pressure respectively. Figure 5.22 and Figure 5.23 show the slug frequencies for the same experiments, measured at the conductivity probe 28.7 m from the test-section inlet. The four diagrams show only the results for runs with "steady" flow in the downwardly-inclined part of the test section and slug flow in the uphill leg. Thus, only runs characterised as "steady-dip slugging" or "steady-random slugging" are plotted. The "intermittent-random" experiments at high flow rates are omitted due to the unacceptable amount of noise in the holdup-time traces: this can result in highly ambiguous power spectra, from which it is often impossible to determine the dominant slug frequency with an acceptable degree of accuracy.

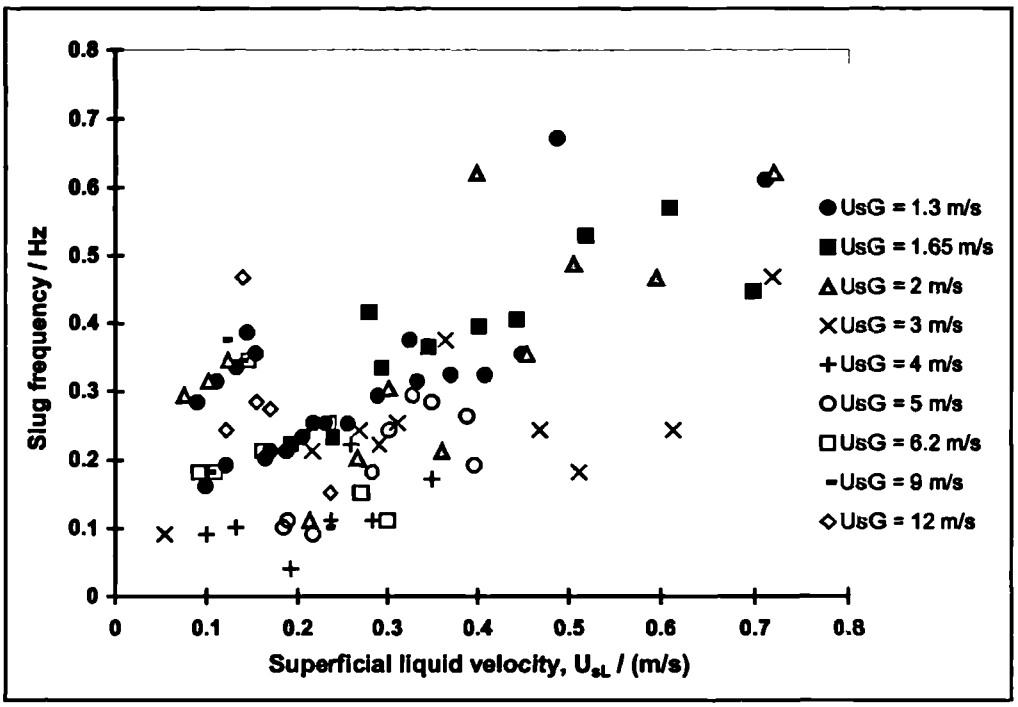

Figure 5.20: Slug frequencies for all experiments with stratified flow upstream of the dip; probe at 21.5 m from the inlet, 0 bar(g)

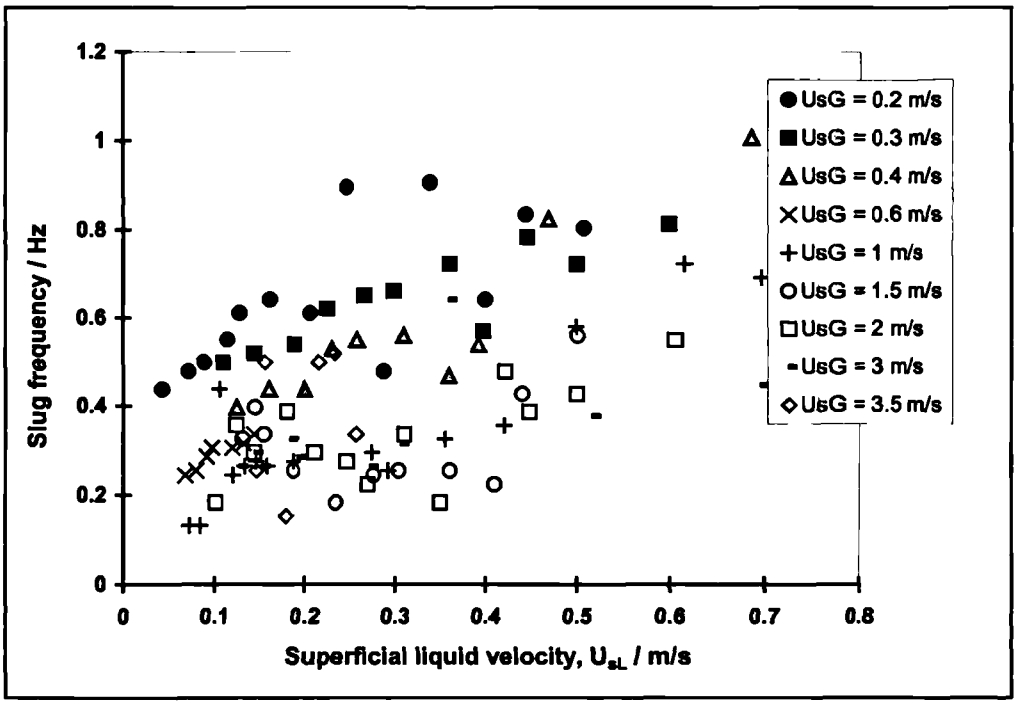

Figure 5.21: Slug frequencies for all experiments with stratified flow upstream of the dip; probe at 21.5 m from the inlet, 5 bar(g)

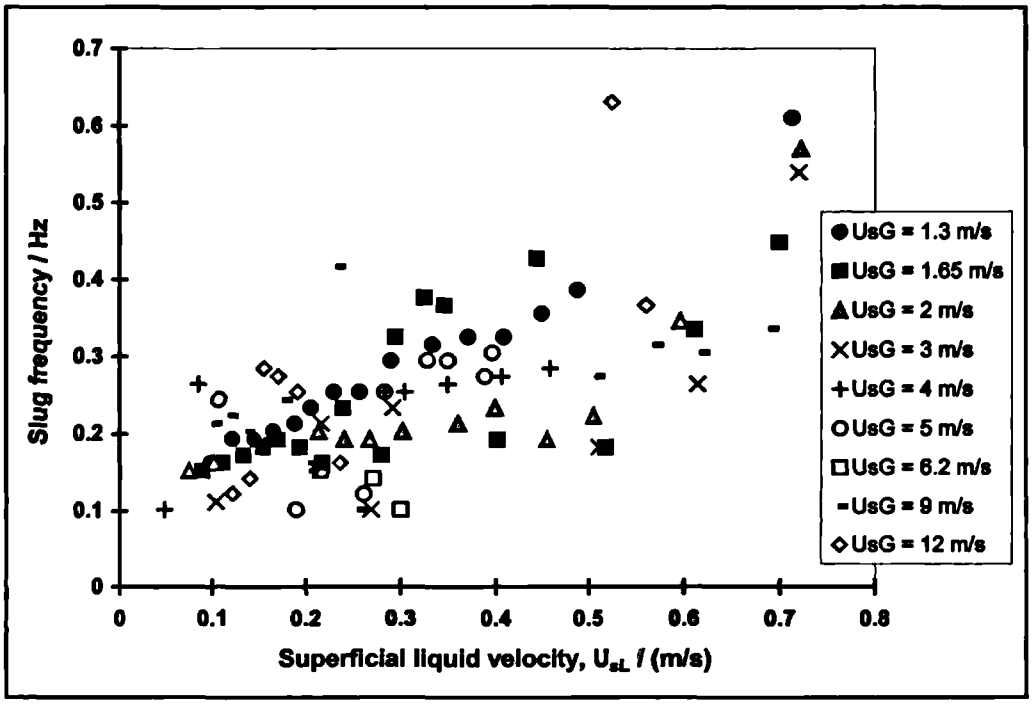

Figure 5.22: Slug frequencies for all experiments with stratified flow upstream of the dip; probe at 28.7 m from the inlet, 0 bar(g)

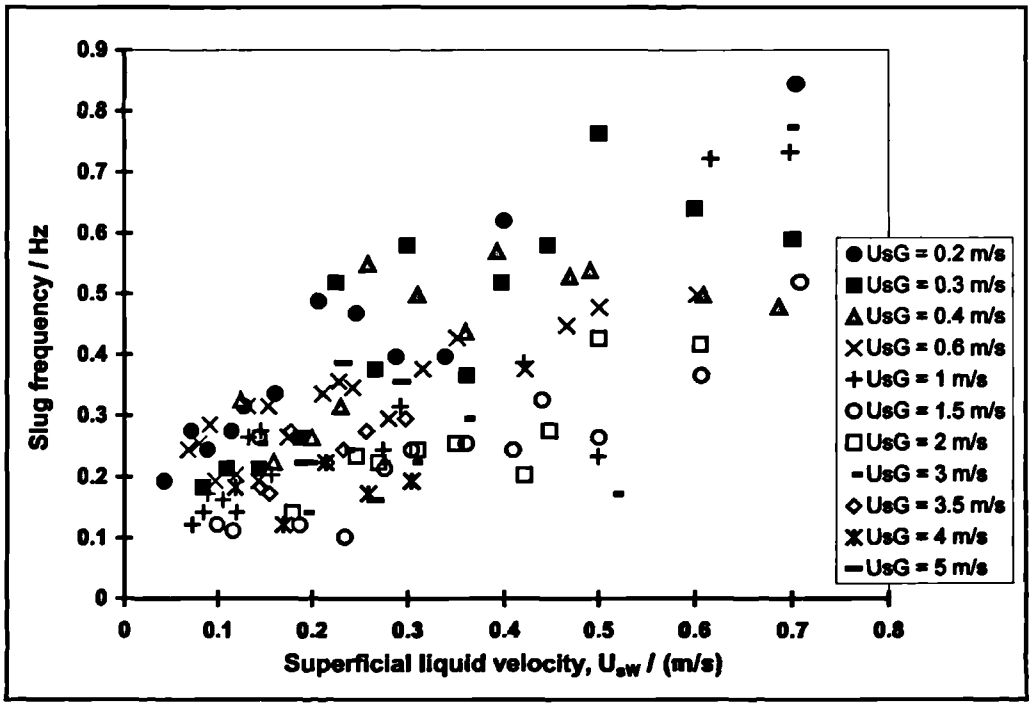

Figure 5.23: Slug frequencies for all experiments with stratified flow upstream of the dip; probe at 28.7 m from the inlet, 5 bar(g)

It is hard to identify general trends clearly, but there is an apparent rise in frequency with superficial liquid velocity and with pressure. The frequencies measured at 28.7 m are lower than those at 21.5 m, indicating significant development of the flow due to slug death. There appears to be a fall in slug frequency with increasing superficial gas velocity, though this may be due to systematic errors in the analysis procedure, where short or frothy slugs do not contribute significantly to the frequency spectrum.

These data may be further subdivided according to the flow patterns observed either side of the "dip". In Figure 5.24 and Figure 5.25, experiments in which the results were characterised as "steady-dip slugging" are plotted for 0 and 5 bar(g) respectively, with slug frequencies measured at the probe located 21.5 m from the test-section inlet.

In Figure 5.26 and Figure 5.27, data from the same experimental runs are plotted for 0 and 5 bar(g) respectively, with slug frequency measurement using the probe 28.7 m from the test-section inlet.

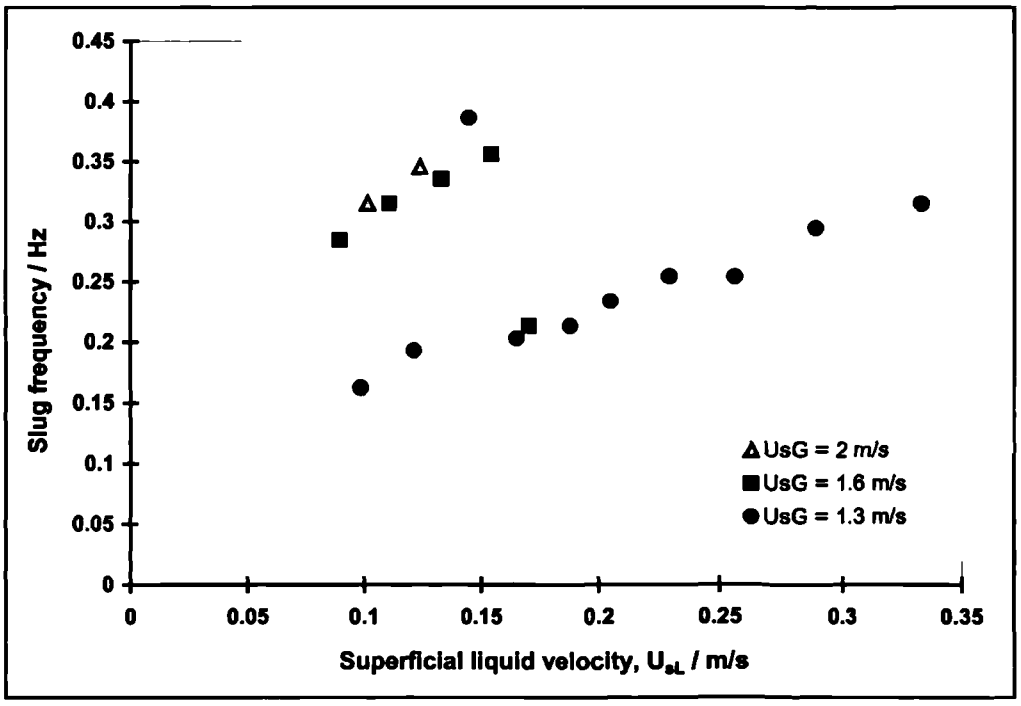

Figure 5.24: Slug frequencies for "steady-dip slugging" experiments; probe at 21.5 m from the inlet, 0 bar(g)

The dip slugging data exhibit less scatter, especially for the data at atmospheric pressure. This reflects the efficiency of the power spectrum analysis for truly periodic data. For the more random time sequences of the intermittent slug traces, a time domain autocorrelation

procedure is expected to produce significantly better results, and this is recommended for future work.

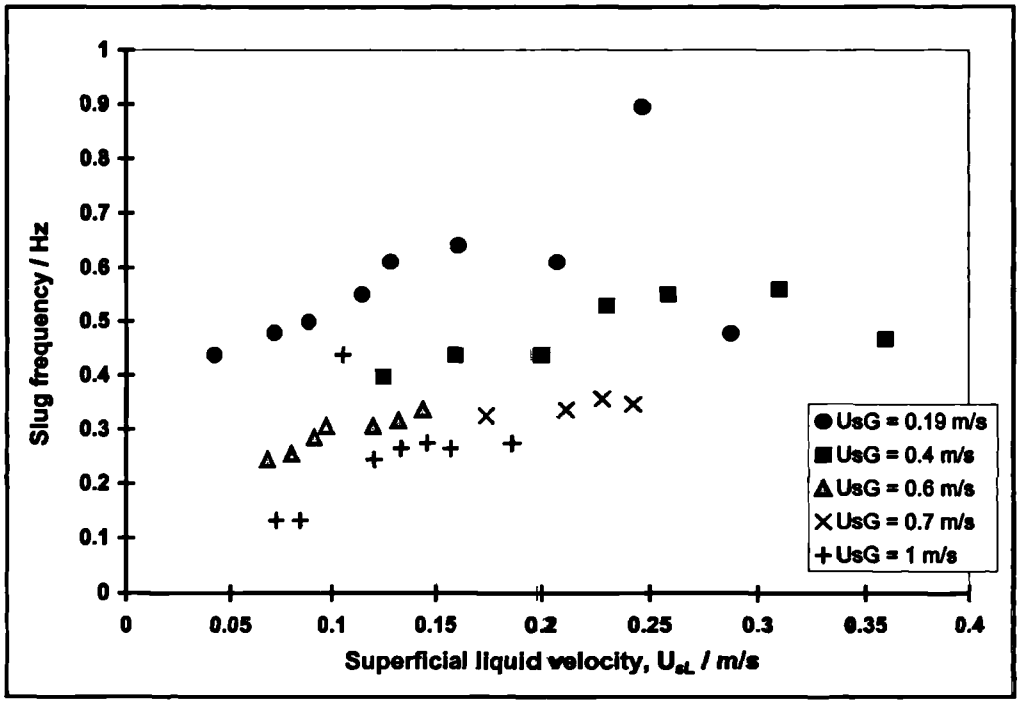

Figure 5.25: Slug frequencies for "steady-dip slugging" experiments; probe at 21.5 m from the inlet, 5 bar(g)

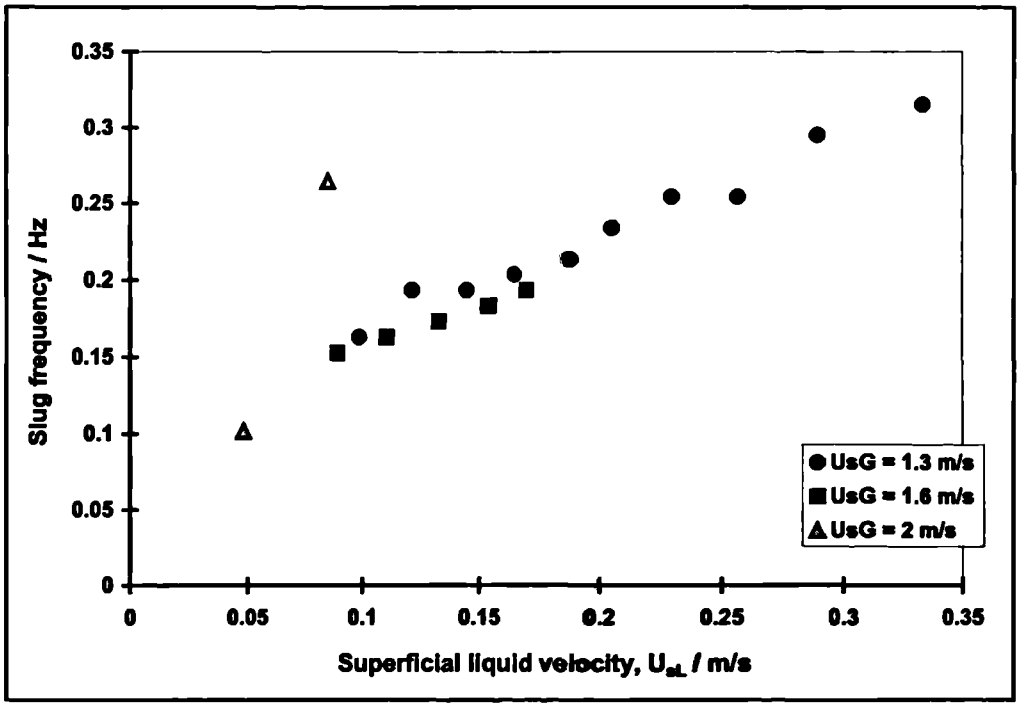

Figure 5.26: Slug frequencies for "steady-dip slugging" experiments; probe at 28.7 m from the inlet, 0 bar(g)

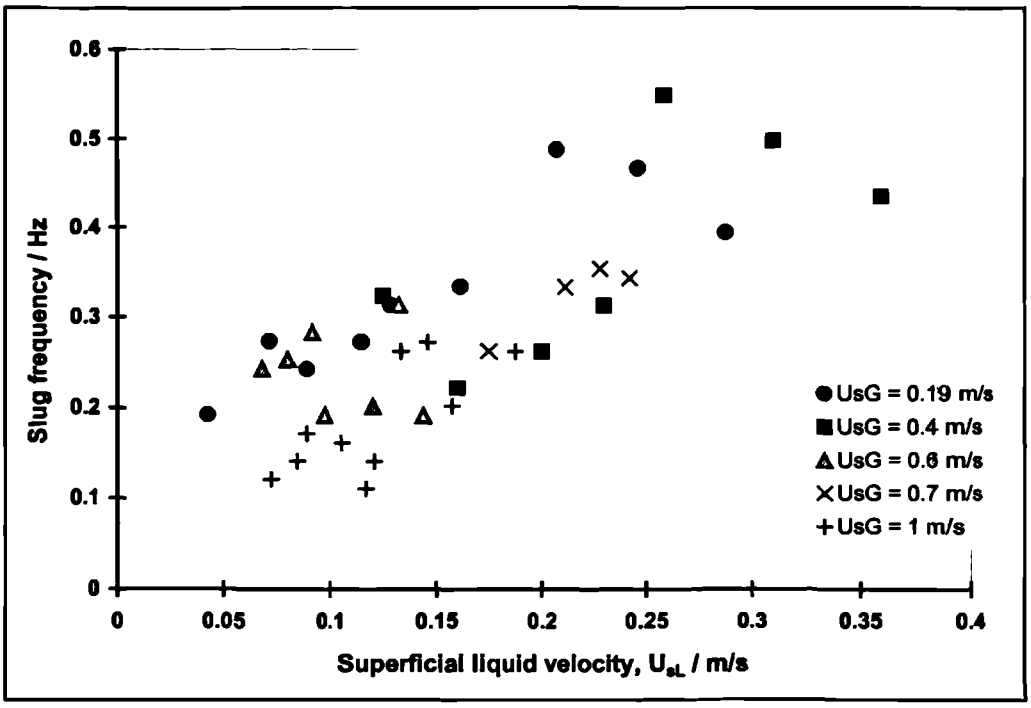

Figure 5.27: Slug frequencies for "steady-dip slugging" experiments; probe at 28.7 m from the inlet, 5 bar(g)

5.1.6. Pressure gradient

The pressure gradient was measured using a differential pressure transducer with tappings located close to the end of the test-section, just upstream of the visualisation section, spaced 1.8 m apart. The pressure gradient was sampled at 10 Hz, and an average of 30 samples was written to an output file every 3 seconds. These values are then further averaged over each 180 s experiment, to obtain a time-averaged pressure gradient. It has been demonstrated (Hale, 2000) that the pressure gradient measurement is subject to an offset value which may "drift" during the course of a series of experiments. Therefore, after approximately every fifth experimental run, the test-section was emptied of liquid and the pressure gradient measurement was sampled with the test-section containing only still air at atmospheric pressure. This offset value was then subtracted from the pressure gradient data measured for the preceding five experiments.

Figures 5.28 and 5.29 show the pressure gradient data measured for the experiments conducted at atmospheric pressure. The data are grouped according to air flow rates. There are some unusual features in Figure 5.28 where very low pressure gradient occurred; for example with a superficial air velocity of 5 m/s. These are attributed to anomalies in the drift correction.

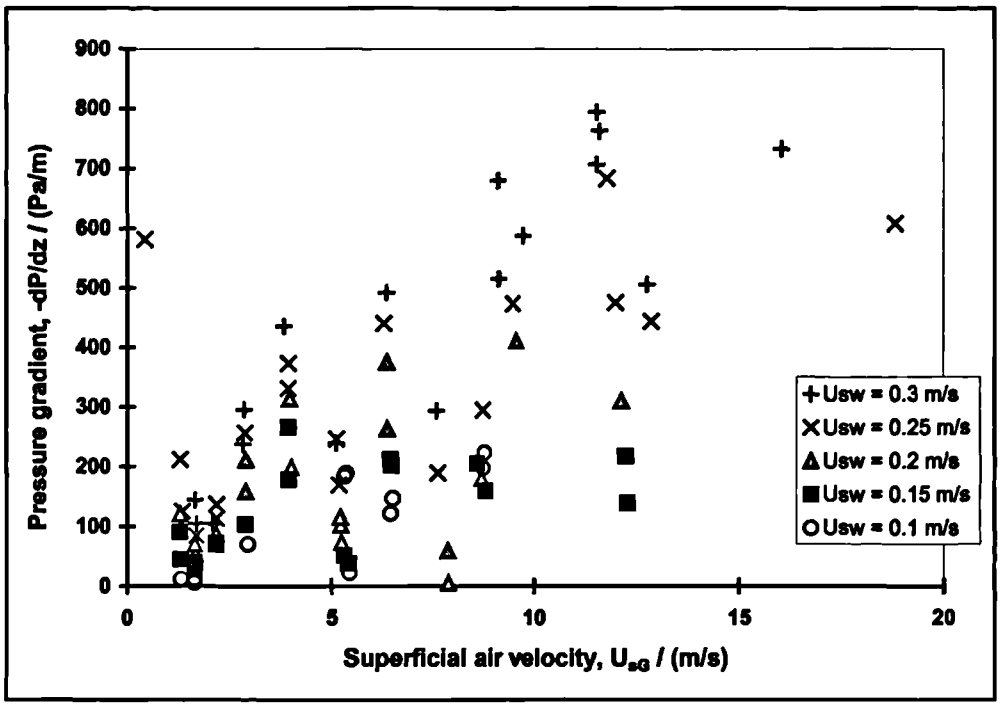

Figure 5.28: Pressure gradient data measured in the uphill leg of the "V"-section; 0 bar(g) runs, 0.1 m/s < U_{sL} < 0.3 m/s

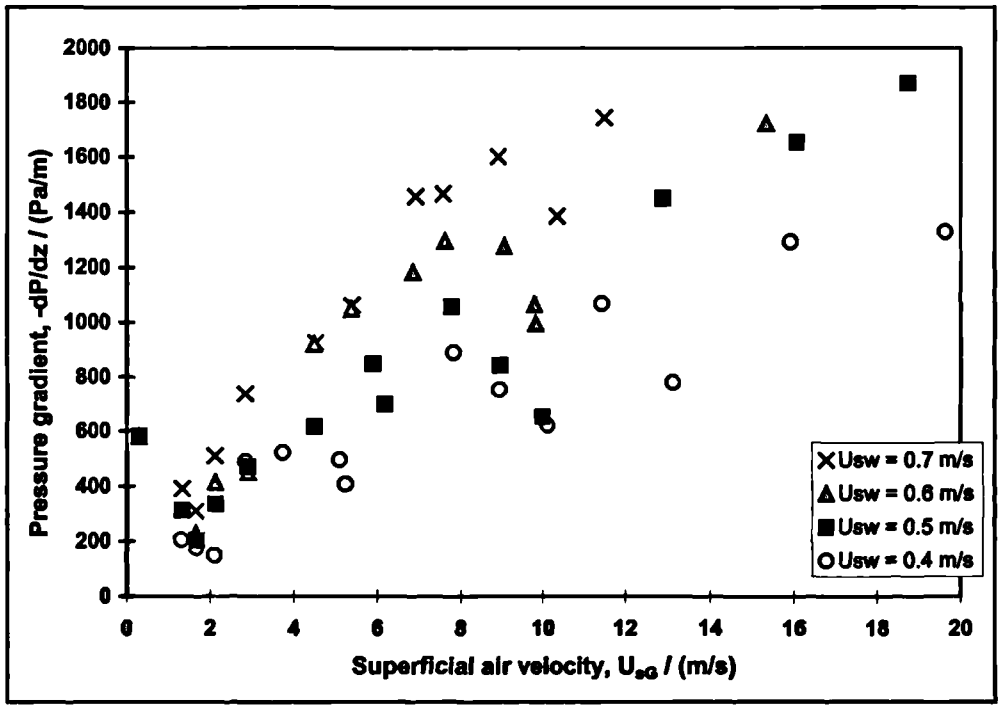

Figure 5.29: Pressure gradient data measured in the uphill leg of the "V"-section; 0 bar(g) runs, 0.4 m/s < U_{sL} < 0.7 m/s

Figure 5.30 and Figure 5.31 show the same information obtained from the experiments at 5 bar(g). The data are more scattered for the 5 bar(g) data than those measured at atmospheric pressure, with less clearly apparent trends.

Overall, the data show reasonably consistent increases in pressure gradient with both superficial air and water velocities and a significant increase with system pressure.

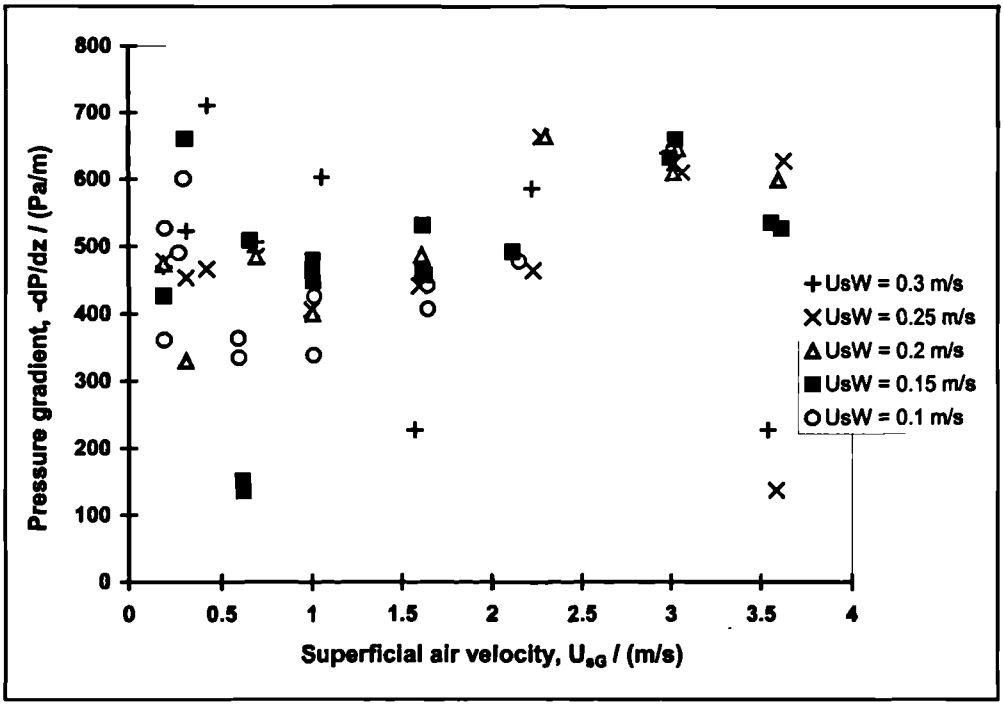

Figure 5.30: Pressure gradient data measured in the uphill leg of the "V"-section; 5 bar(g) runs, 0.1 m/s < U_{sL} < 0.3 m/s

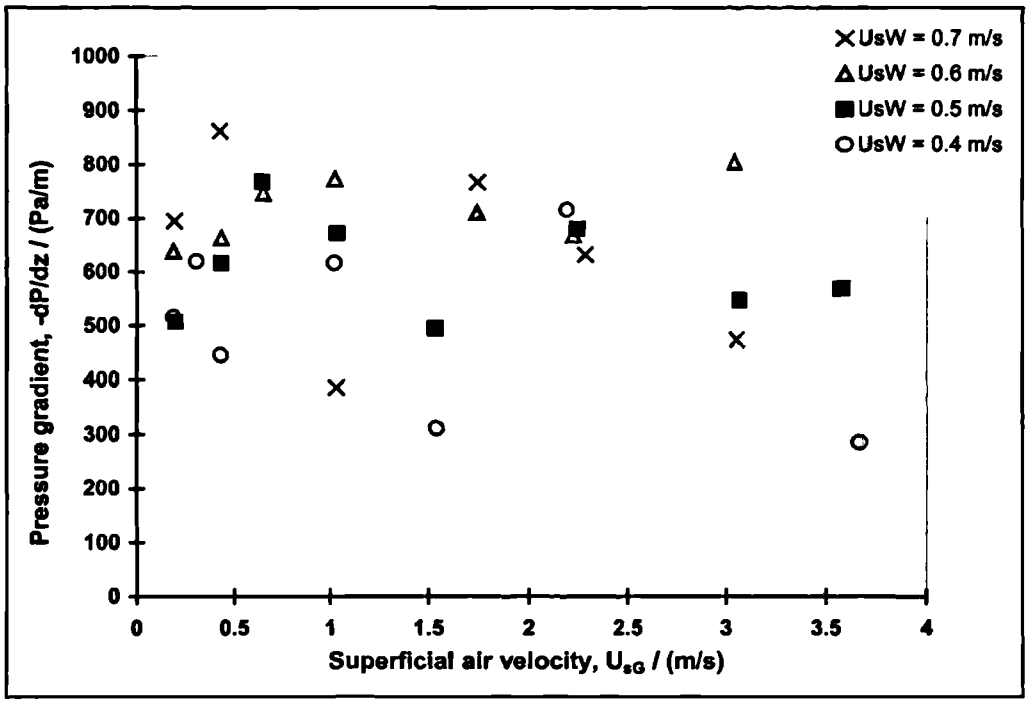

Figure 5.31: Pressure gradient data measured in the uphill leg of the "V"-section; 5 bar(g) runs, 0.4 m/s < U_{sL} < 0.7 m/s

5.2. Comparison of experimental data with predictive methods

In this section, comparison is made between the experimental data measured in this Campaign, and several predictive correlations and/or phenomenological models from the published literature. Details of the methods used in this section are presented in Chapter 2.

5.2.1. Flow reversal in upwardly-inclined slug flow

In Section 5.1.1 it is reported that flow reversal was observed in the film region between liquid slugs for a large range of the fluid velocities studied. Wood (1991) reported that, at atmospheric pressure, this would occur for gas velocities lower than 7.7 m/s for an upward pipe inclination of +1.5°. This is in close agreement with these experiments, for which a "critical gas velocity" of approximately 8 m/s was observed.

In Chapter 2, the solution of the one-dimensional mass and momentum balances in the slug tail (Taitel & Barnea, 1990) was described. The solution for upwardly-inclined flow indicates that film reversal occurs some way downstream of a slug body. Results are presented in Figure 5.32.

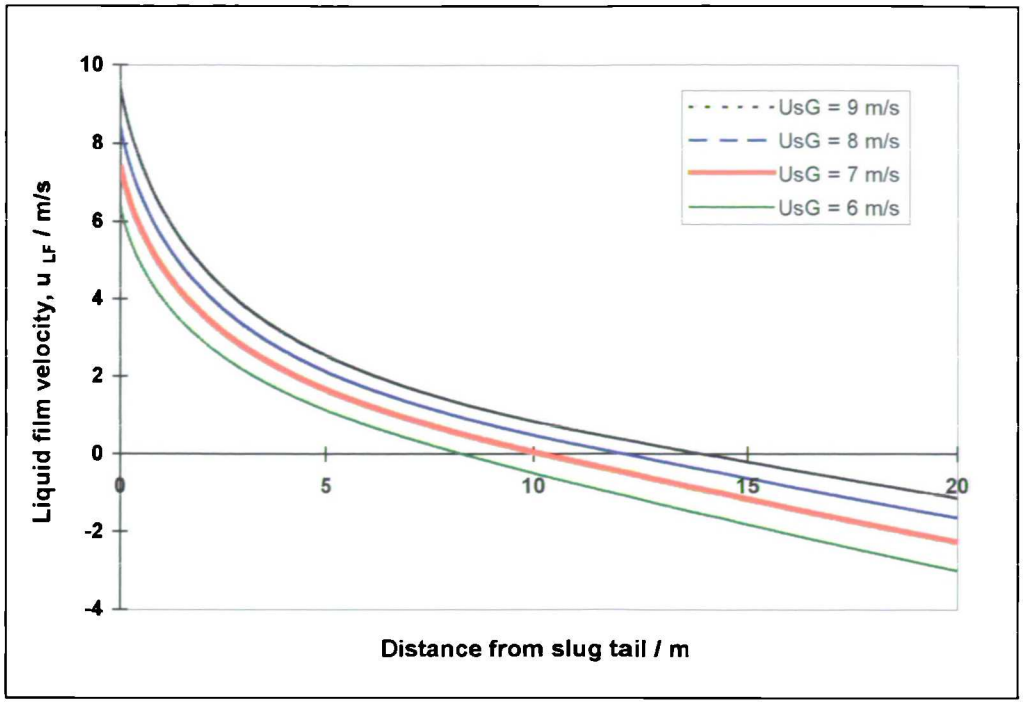

Figure 5.32: Velocity variation in the film region of slug flow calculated using the Taitel & Barnea (1990) model; +1.5° upwardly-inclined flow, U_{sL} = 0.4 m/s, air/water, atmospheric pressure

Figure 5.32 shows the liquid film velocity solution for several gas superficial velocities, at a constant liquid superficial velocity of 0.4 m/s. The solution requires information about the slug liquid holdup (calculated in this case by the correlation of Gregory *et al.*, 1978), the gas and liquid wall shear stresses (calculated from the classical Blasius friction factor relationship) and the interfacial shear stress (found using the Andritsos & Hanratty (1991) friction factor correlation). For higher gas velocities at atmospheric pressure (*e.g.*, as shown in Figure 5.15), a typical slug frequency for a liquid superficial velocity of 0.4 m/s is 0.25 Hz. With the estimate $U_T - 1.2U_{mix}$, neglecting the length of the slug itself and the contribution of U_{sL} to U_{Mix}, the average lengths of the slug tails would be 29 m at U_{sG} − 6 m/s, rising to 43 m at U_{sG} 9 m/s.

It is apparent that reversal of the liquid film is predicted for all the gas velocities tested, up to a value of 9 m/s. This does not agree with the experimental observations. It is clear that the simple Taitel & Barnea model is not able to capture the physics of the tail profile exactly. The liquid velocity decays too rapidly to zero, indicating that the true interfacial stress may be greater than predicted by the Andritsos & Hanratty (1991) correlation. Nevertheless, the trend is that the length of the tail required to achieve reverse flow increases more than linearly with the superficial gas velocity. Since the actual tail length is approximately proportional to

the superficial gas velocity, these trends are consistent with there being a critical velocity above which reverse flow does not occur. However, in the experiments, it is not possible to study the motion of a single slug and the film behaviour behind it. At any given time, several slugs are present in the test-section, so that the distance between slugs may be less than that required for reverse film flow (*e.g.* 13.9 m for a gas superficial velocity of 9 m/s, as illustrated in Figure 5.32). It was observed during the experiments that the reversal of the liquid film was not observed for high superficial velocities, due in part to the short time interval between slugs giving insufficient time for the deceleration of the liquid film before it was overridden by the next slug.

5.2.2. Liquid holdup

Analysis of data from the first experimental campaign (presented in Chapter 4) showed that the correlation of Chisholm (1972) gives fairly good predictions for average liquid holdup in near-horizontal flows across a wide range of flow patterns.

Figures 5.33 and 5.34 show the liquid holdup data measured in these experiments plotted against the predictions from the correlations of Chisholm (1972) and Premoli *et al.* (1970) respectively, described in Section 2.1.1. It is clear that the Chisholm (1972) correlation performs better, with the Premoli *et al.* (1970) expression tending to consistently over-predict liquid holdup. However, at high liquid holdups, the Premoli *et al.* correlation performs well.

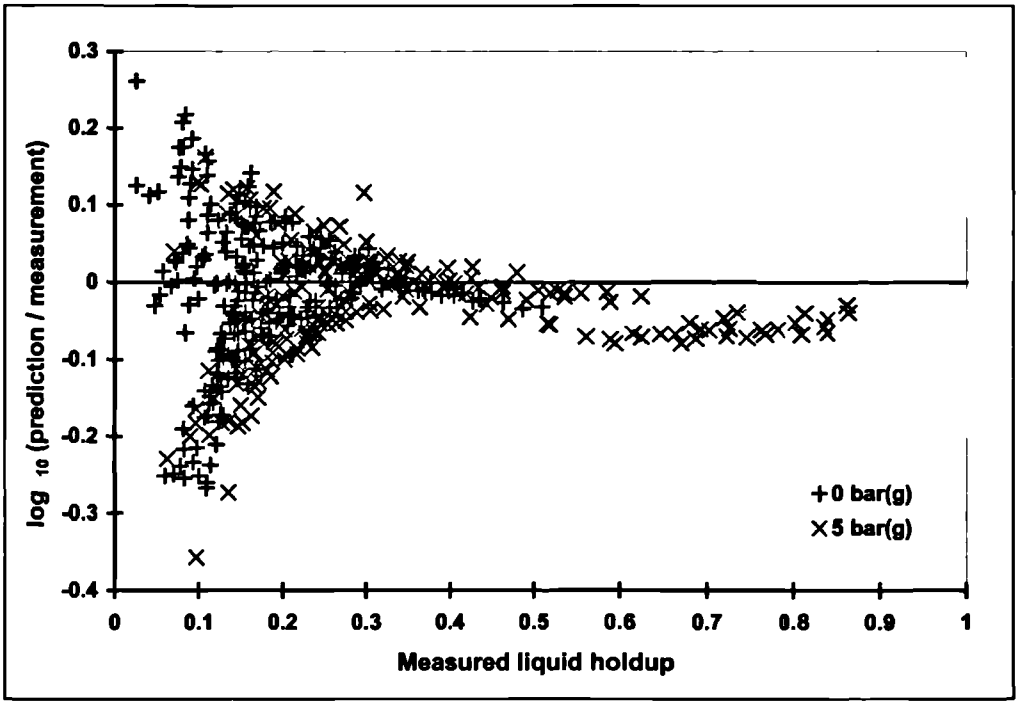

Figure 5.33: Measured liquid holdup data compared with predictions by the Chisholm (1972) correlation; 0 and 5 bar(g), +1.5° upwardly-inclined flow

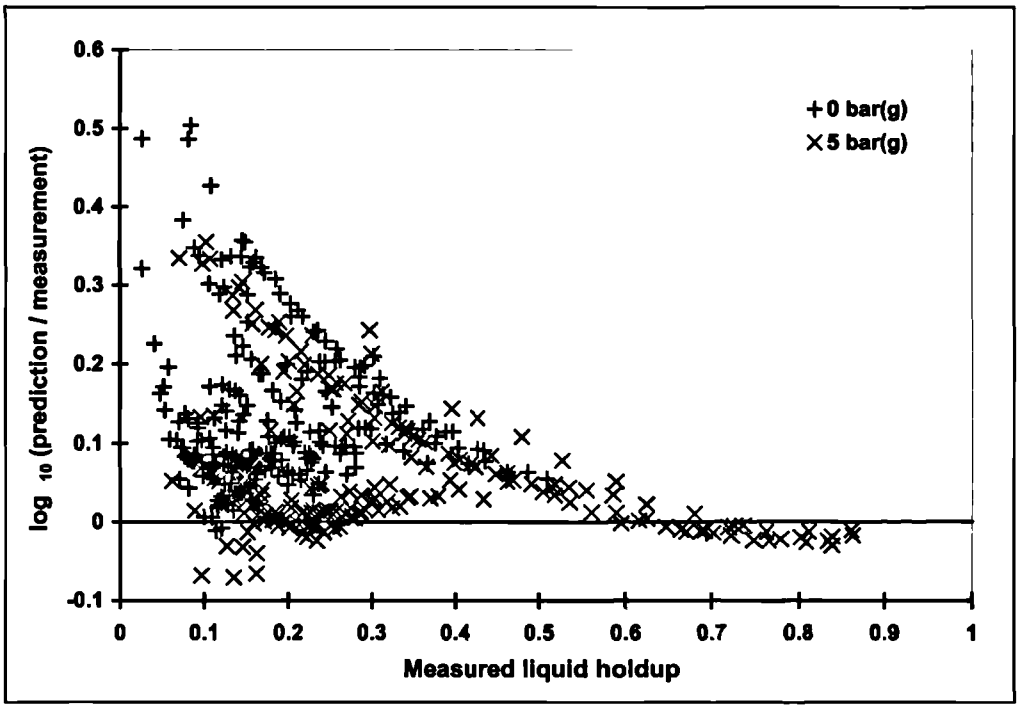

Figure 5.34: Measured liquid holdup data compared with predictions by the Premoli *et al.* (1970) correlation; 0 and 5 bar(g), +1.5° upwardly-inclined flow

The relative performance of the correlations may be compared using the mean, standard deviation and root mean square relative errors, defined in Appendix 1, as shown in Table 5.3:

	Chisholm (1972)	Premoli et al. (1970)
Mean relative error	-0.031	0.287
Standard deviation	0.188	0.336
Root mean square relative error	0.190	0.442

Table 5.3: Relative error in liquid holdup correlations for 450 holdup measurements

Despite its simplicity, the Chisholm (1972) relationship performs well.

5.2.3. Slug length

The mean slug length obtained in these experiments is compared with other published values in Table 5.4.

	Slug length, (L_S/ D)
Experimental result	13.9
King (1998)	17
Manolis (1995)	20
Nicholson *et al.* (1978)	12-30
Dukler *et al.* (1985)	16
Norris (1982)	82.4
Scott *et al.* (1986)	118.3

Table 5.4: Comparison of slug length data

The experimental result from this series of experiments is somewhat lower than previous measurements using the WASP facility at Imperial College. However, in the cases of Manolis (1995) and King (1998) the WASP test-section was horizontal so that slug growth could occur along the entire 36 m length of pipe. In the present work, the distance between the bottom of the "dip" and the first of the conductivity probes used to calculate slug length was just 14 m. It is suggested that this is considerably less than the distance required for the formation of fully developed slug flow.

The correlations of Norris (1982) and Scott *et al.* (1986) (see Section 2.3.5) suggest slug lengths four to seven times greater than those observed in the WASP facility. It is likely that

this is because the correlations were regressed from data for long, large-diameter oil pipelines, where terrain effects may be present.

5.2.4. Slug translational velocity

In Figure 5.35, the tail velocity data measured for 235 slugs taken from 37 experiments are plotted against the Froude number, defined as

$$Fr = \frac{U_{Mix}}{\sqrt{gD}} \qquad [5.1]$$

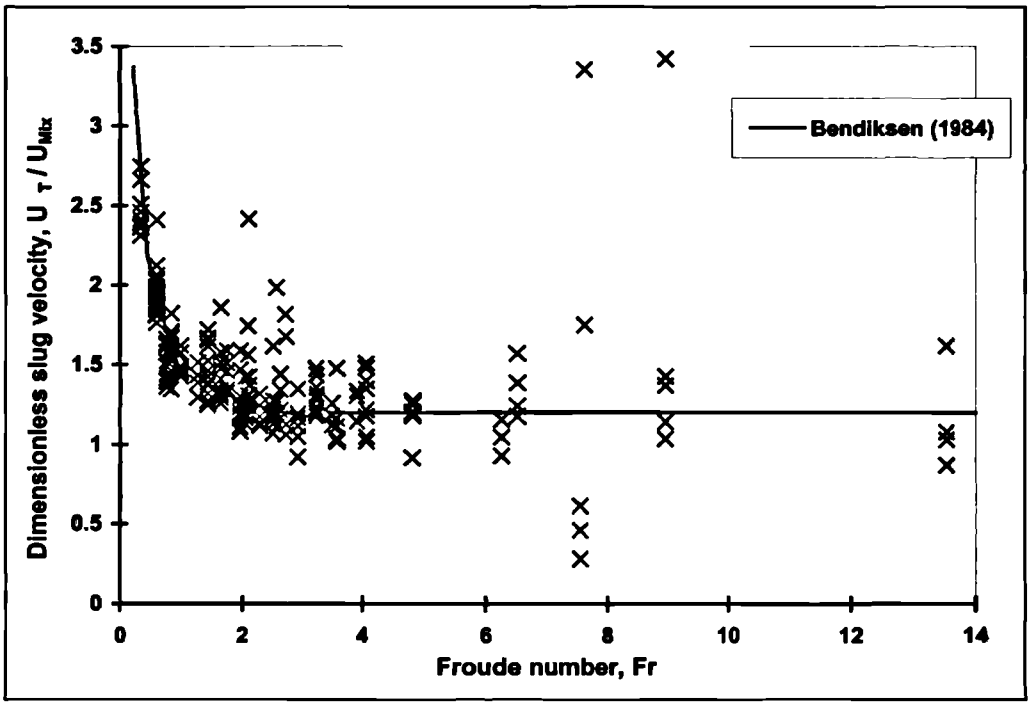

Figure 5.35: Variation of measured slug tail velocity with mixture velocity

Although the data are scattered, they exhibit the characteristic increase in slug translational velocity at low mixture velocities which was reported by Bendiksen (1984) and observed by Manolis (1995). A computational study of this effect is presented in Chapter 8 of the present work. It should be noted that the Bendiksen relationship, plotted Figure 5.35, was presented for the prediction of *horizontal* slug flow. The current data were measured in the rising leg of the "V"-section, inclined at 1.5° to the horizontal.

In Table 5.5, comparison is made between the experimental data and predictions using the correlations of Bendicksen (1984), and Manolis (1995). The statistical treatment of relative error is described in Appendix 1.

	Bendicksen (1984)	Manolis (1995)
Mean relative error	-0.031	-0.037
Std. deviation	0.231	0.227
Root mean square relative error	0.233	0.229

Table 5.5: Relative error in predictions from slug tail velocity correlations

The performance of both correlations is similar; both slightly underpredict tail velocity on average, and they have errors of similar magnitude.

5.2.5. Slug frequency

Frequency data from the gamma densitometer

The slug frequency data obtained from inspection of the liquid holdup-time traces from the gamma densitometer, reported in Section 5.1.5, are compared with several slug frequency correlations in Table 5.6.

	Relative error	Gregory & Scott (1969)	Heywood & Richardson (1979)	Tronconi (1990)	Manolis *et al.* (1995)
0 bar(g)	Mean	-0.294	-0.557	-0.908	-0.583
(184 points)	Std. deviation	0.599	0.458	0.0913	0.450
	Root mean square	0.666	0.720	0.913	0.735
5 bar(g)	Mean	-0.275	-0.135	-0.870	-0.377
(143 points)	Std. deviation	0.342	0.455	0.138	0.527
	Root mean square	0.438	0.473	0.881	0.646

Table 5.6: Relative error in some slug frequency correlations (measured slug frequencies from γ-densitometer traces, 0 and 5 bar(g))

The correlations perform better against the data measured at 5 bar(g) than they do against the atmospheric pressure data. This is the same trend as reported by King (1998) for horizontal slug flow. However, King found that most slug frequency correlations tend to overpredict slug frequency, whereas Table 5.6 indicates that all of the correlations *underpredict* the slug frequencies measured in the present work. It is likely that the slug frequencies produced by

the presence of a "dip" in the pipeline are higher than those from hydrodynamic slug growth in horizontal flow. It is also the case that the slug frequency tends to decrease with flow development and the rising limb of the test-section used in the current work was very short.

Of the correlations studied, the Gregory & Scott (1969) correlation performs best, with consistent results at both 0 and 5 bar(g) pressure. The correlation by Heywood & Richardson performs comparably at 5 bar(g), but gives a significantly worse fit to the atmospheric pressure data. As a general rule, the accuracy of the correlations was found to increase with their age.

Slug frequency data from PSD analysis of conductivity probe traces

For reasons of brevity, in this report only the best performing correlation (Gregory & Scott, 1969) is tested against the slug frequency data from PSD analysis of the conductivity probe data.

In the following charts (Figures 5.36 – 5.39) the slug frequencies measured at the 21.5 m and 28.7 m conductivity probes are plotted on the same axes as the results of the Gregory & Scott (1969) correlation. In each case the lines show the correlation for the values of U_{sG} in the legend, with the slug frequency increasing with U_{sG}.

Comparison of Figure 5.36 with Figure 5.37 shows that the correlation generally underpredicts the data, as discussed above. However, the results from the 28.7 m probe are less scattered, and lie closer to the correlation lines, than those from the 21.5 m probe. This suggests that as the flow moves away from the dip, many of the short, high frequency "dip slugs" collapse and/or merge to form a lower frequency, "random" slug flow. This is apparent from the traces such as those shown in Figure 5.6. This is also apparent for the 5 bar(g) data, plotted for the 21.5 m and 28.7 m probes in Figures 5.38 and 5.39 respectively. In this case, the spread of the data for the 28.7 m probe is actually very similar to the spread of the correlation.

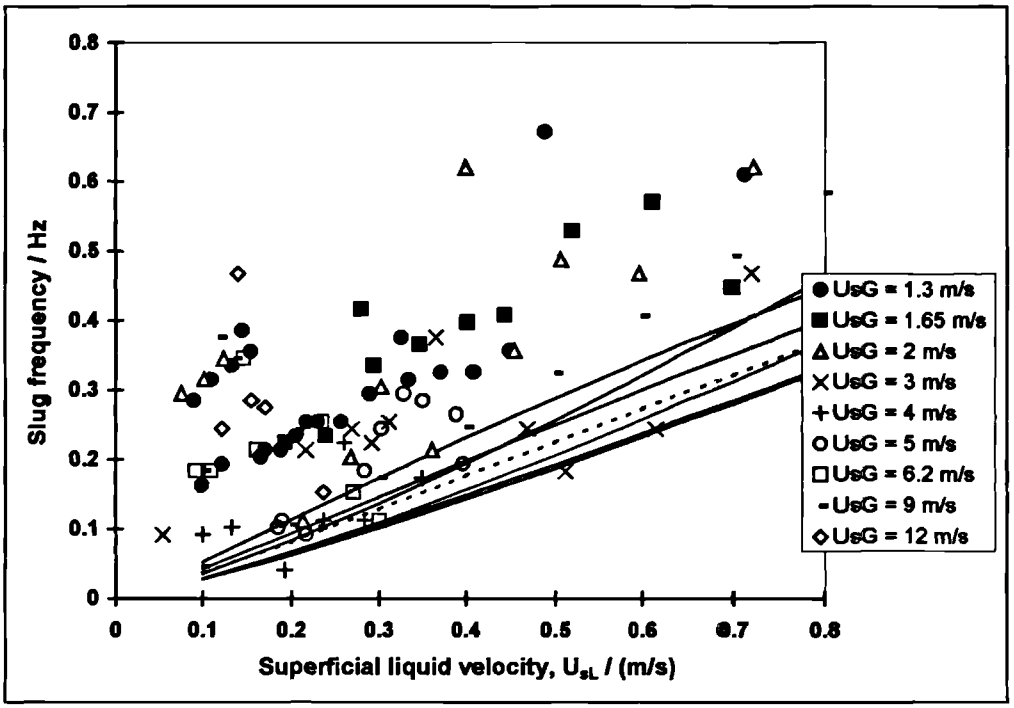

Figure 5.36: Slug frequencies for all runs with slug flow in the uphill leg of the "V"; 21.5 m probe, 0 bar(g) data, showing Gregory & Scott (1969) correlation

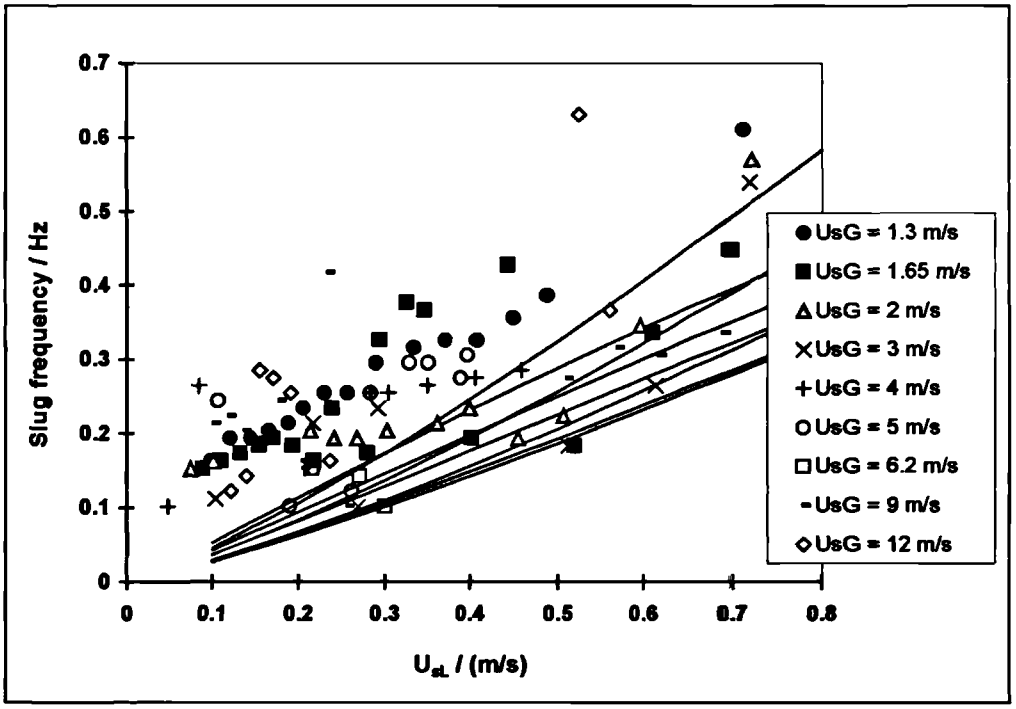

Figure 5.37: Slug frequencies for all runs with slug flow in the uphill leg of the "V"; 28.7 m probe, 0 bar(g) data, showing Gregory & Scott (1969) correlation

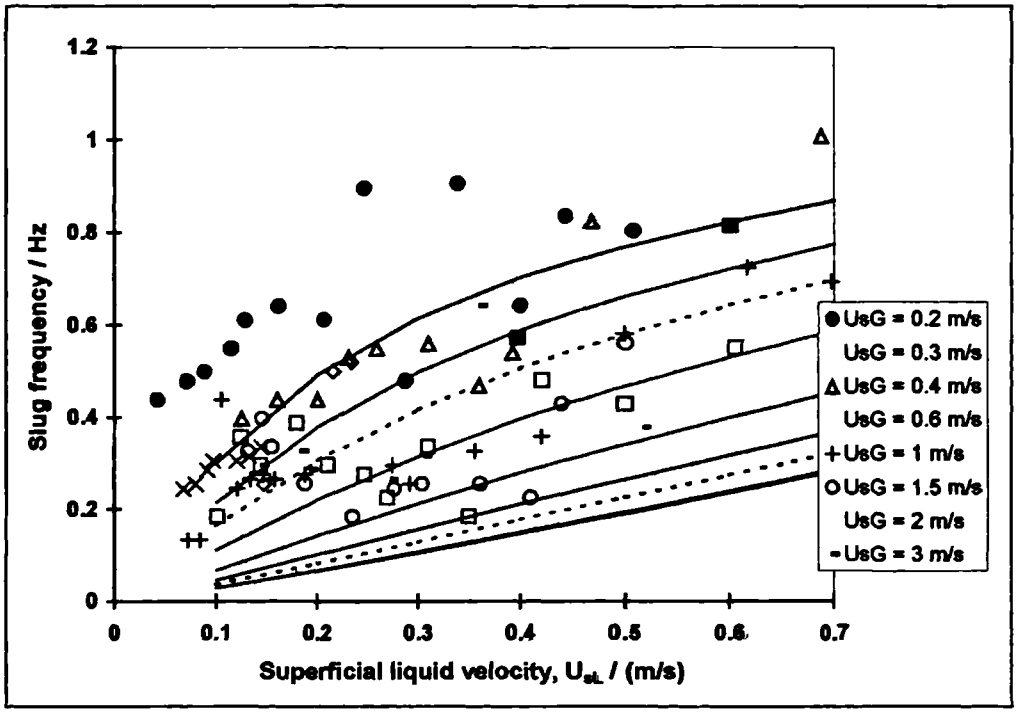

Figure 5.38: Slug frequencies for all runs with slug flow in the uphill leg of the "V"; 21.5 m probe, 5 bar(g) data, showing Gregory & Scott (1969) correlation

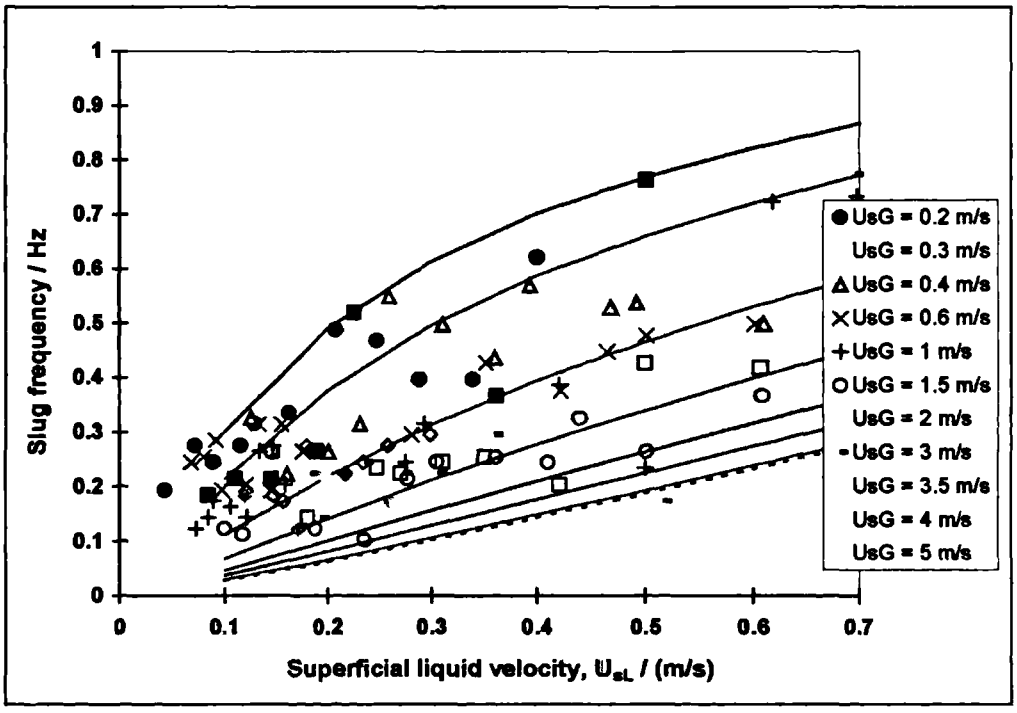

Figure 5.39: Slug frequencies for all runs with slug flow in the uphill leg of the "V"; 28.7 m probe, 5 bar(g) data, showing Gregory & Scott (1969) correlation

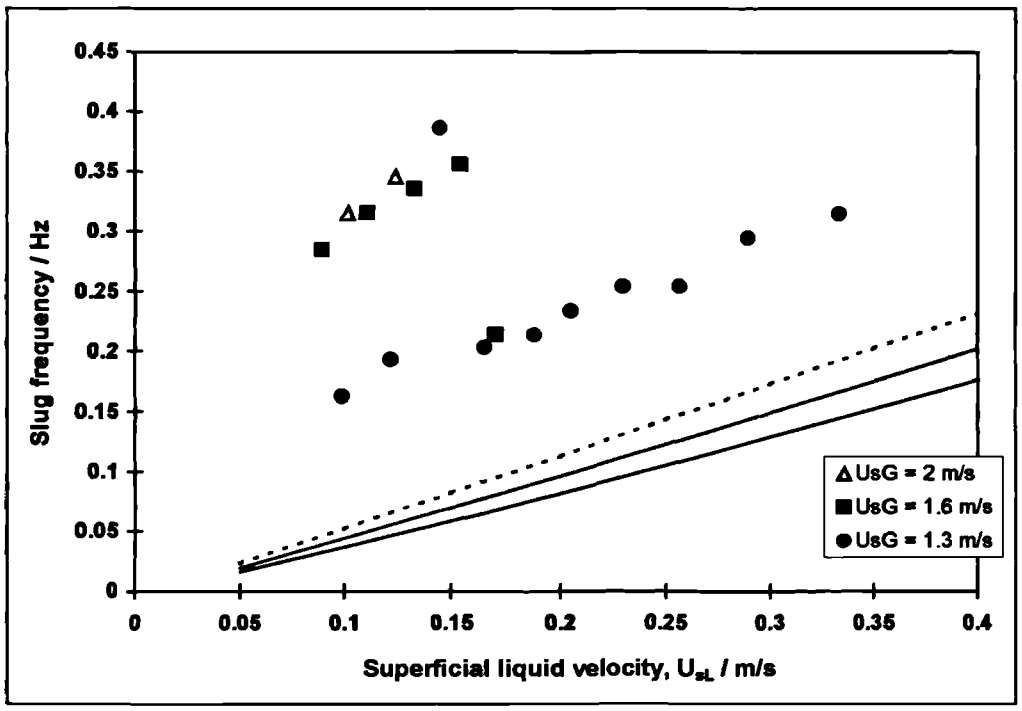

Figure 5.40: Slug frequencies for "steady-dip slugging" runs; 21.5 m probe, 0 bar(g) data, showing Gregory & Scott (1969) correlation

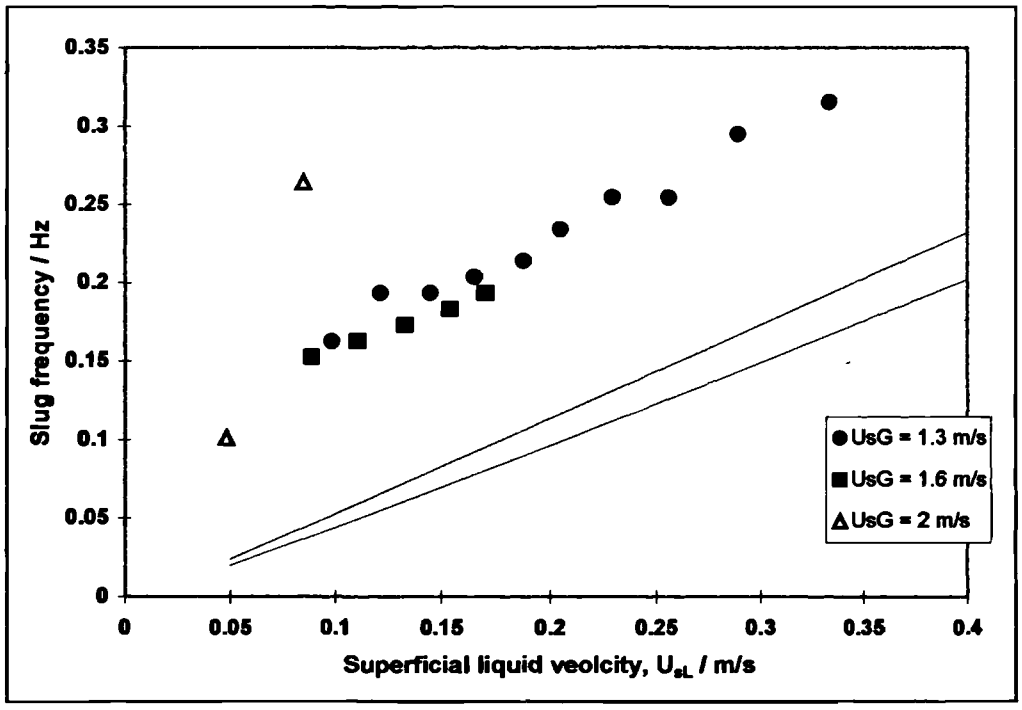

Figure 5.41: Slug frequencies for "steady-dip slugging" runs; 28.7 m probe, 0 bar(g) data, showing Gregory & Scott (1969) correlation

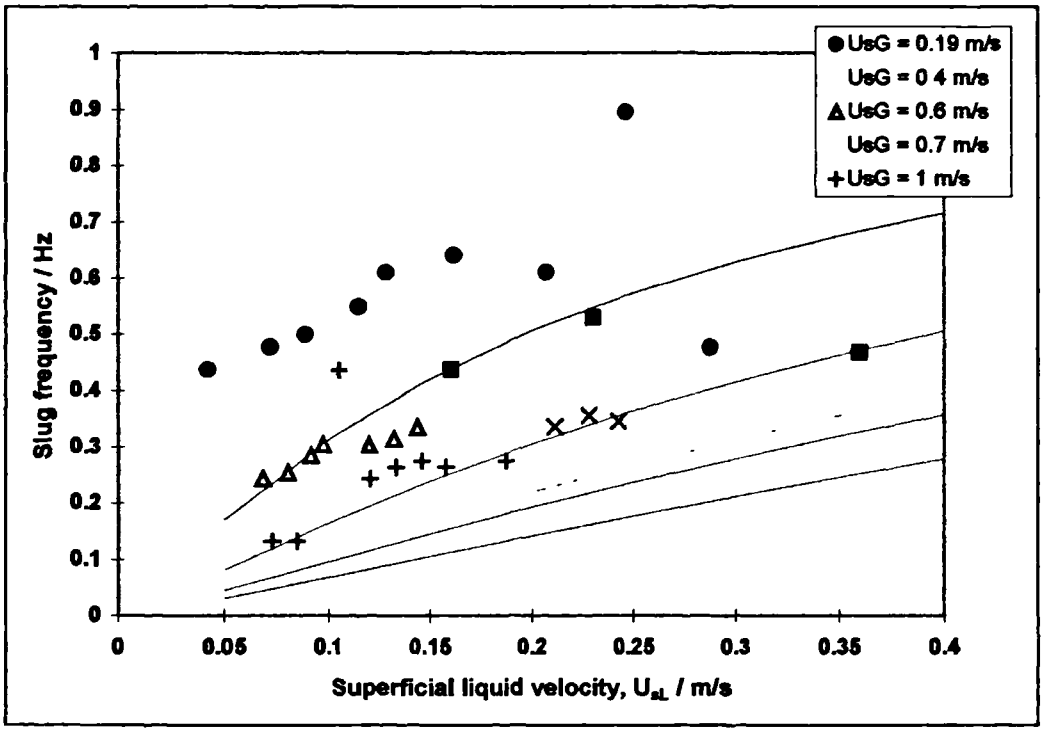

Figure 5.42: Slug frequencies for "steady-dip slugging" runs; 21.5 m probe, 5 bar(g) data, showing Gregory & Scott (1969) correlation

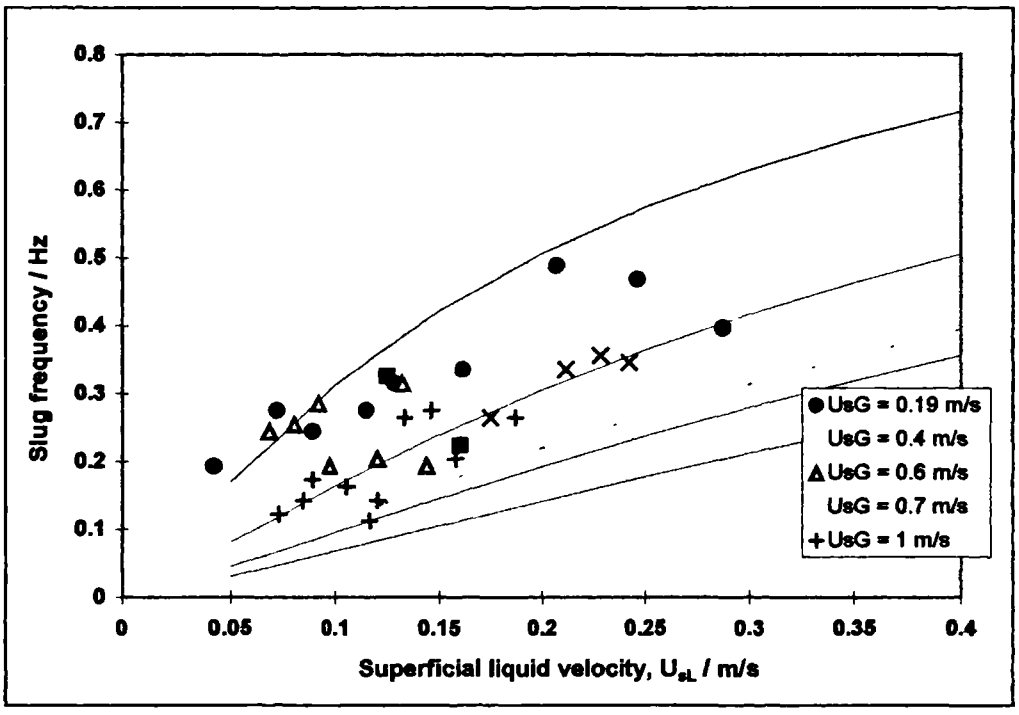

Figure 5.43: Slug frequencies for "steady-dip slugging" runs; 28.7 m probe, 5 bar(g) data, showing Gregory & Scott (1969) correlation

In Figures 5.40 – 5.43 only results from runs identified as "steady-dip slugging" are plotted. They show more clearly the trend discussed above: that, further from the dip, the measured slug frequencies tend to be lower. Therefore, whilst the Gregory & Scott (1969) correlation still tends to underpredict the slug frequency, the degree of underprediction is less severe.

5.2.6. Pressure gradient

Predictions of pressure gradient by several methods are compared with the experimental results in Table 5.7. In each case, N is the number of points considered. The statistical treatment of error is described in Appendix 1.

	P / bar(g)	N	Mean relative error	Root mean square relative error
Beggs & Brill (1973)		137	0.36	4.39
Friedel (1979)	0	137	0.42	4.84
Taitel & Barnea (1990)		137	-0.01	3.14
Beggs & Brill (1973)		218	-0.24	1.85
Friedel (1979)	5	218	-0.45	1.23
Taitel & Barnea (1990)		152	0.32	2.21

Table 5.7: Comparison of relative error in pressure gradient predictions

For the experiments at atmospheric pressure, the phenomenological model of Taitel & Barnea (1990) gives a marginally better prediction of the experimental data, although it does not perform as well as either the Beggs & Brill (1973) or the Friedel (1979) correlations at higher pressure. At 0 bar(g), both correlations tend to overpredict the experimental results, whilst the physical model approximately bisects the data. This trend is reversed for the experiments at 5 bar(g). Results of the Taitel & Barnea model are given for a smaller subset of the data than the other methods. This is because the solution of the equation for the slug tail film profile is not robust for all mixture velocities at all pipe inclinations. Only those mixture velocities which resulted in a converged solution are considered in the error results presented Table 5.7.

In Figures 5.44 – 5.49, the performance of these predictive methods is illustrated for a restricted range of liquid flow rates. For these flow rates, the agreement is very much better at atmospheric pressure than it is at 5 bar(g), which is counter to the data in Table 5.7. All of the methods perform very poorly at 5 bar(g).

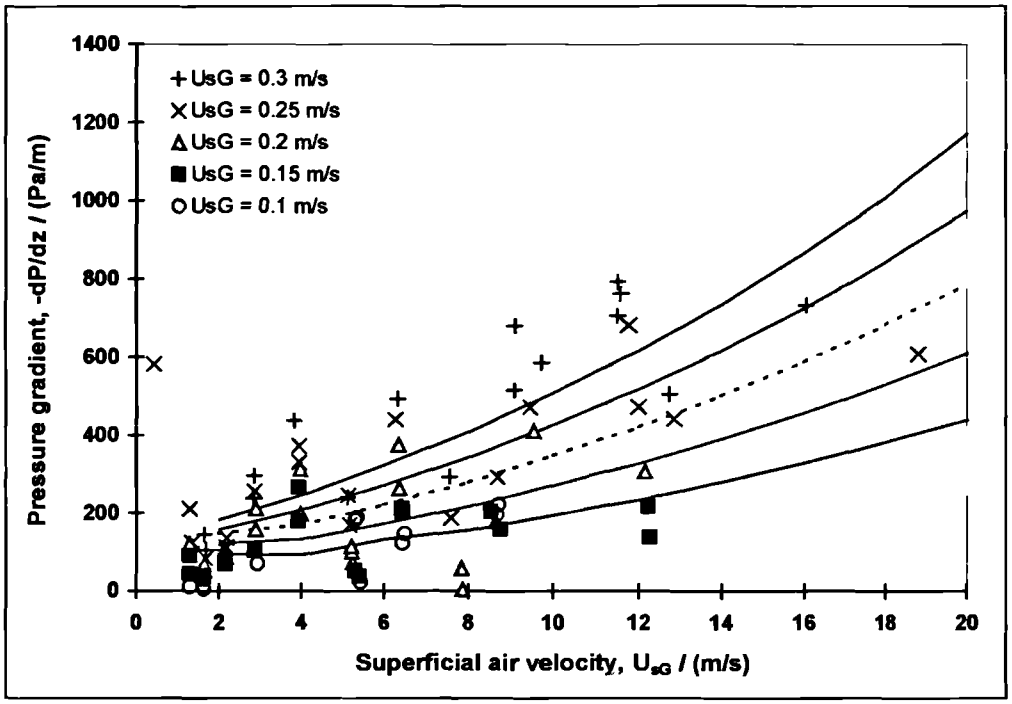

Figure 5.44: Pressure gradient measured at 0 bar(g) compared with prediction by Beggs & Brill (1973)

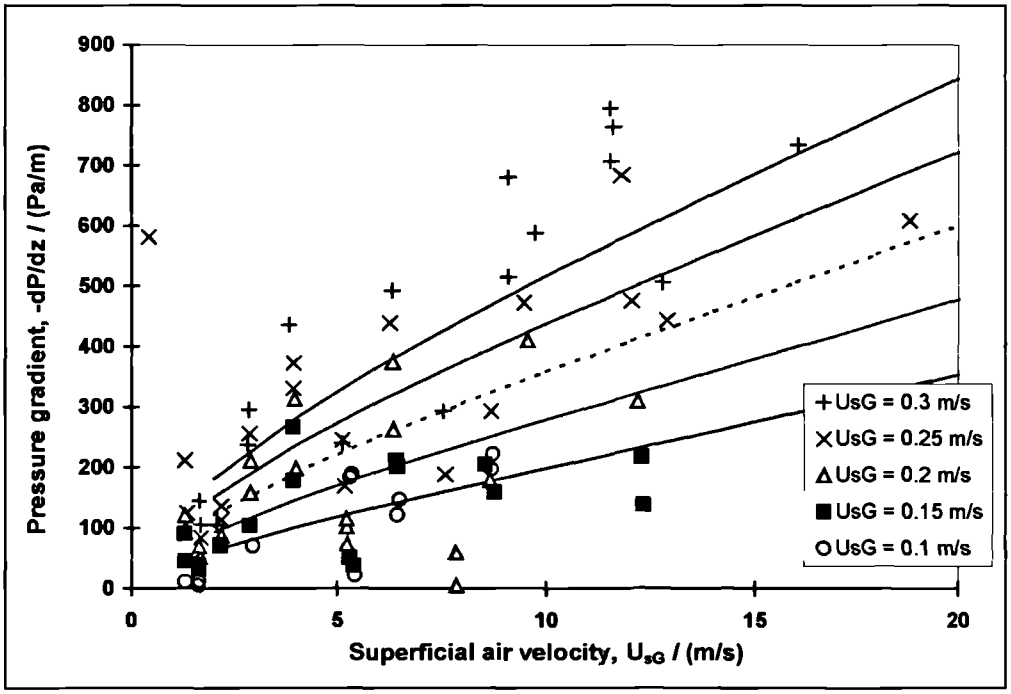

Figure 5.45: Pressure gradient measured at 0 bar(g) compared with prediction by Friedel (1979)

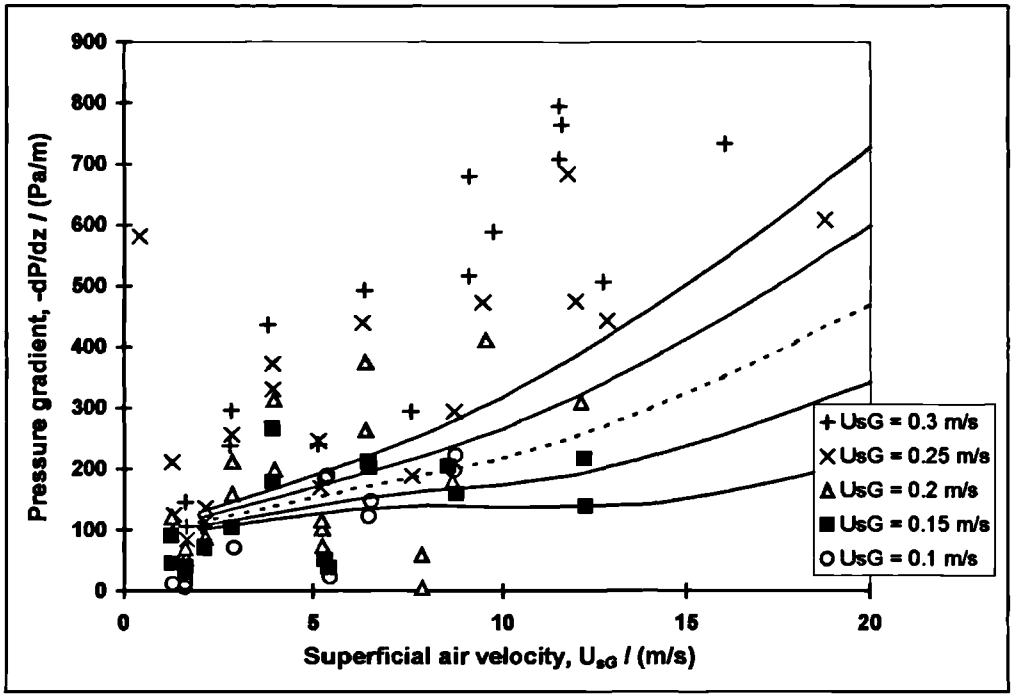

Figure 5.46: Pressure gradient measured at 0 bar(g) compared with prediction by Taitel & Barnea (1990)

The Beggs & Brill correlation (Figure 5.44) shows similar trends to the Taitel & Barnea model (Figure 5.46). However, the Friedel correlation (Figure 5.45) shows a different trend. It is not clear, due to the scatter of the data, which (if either) trend exists in the experimental results.

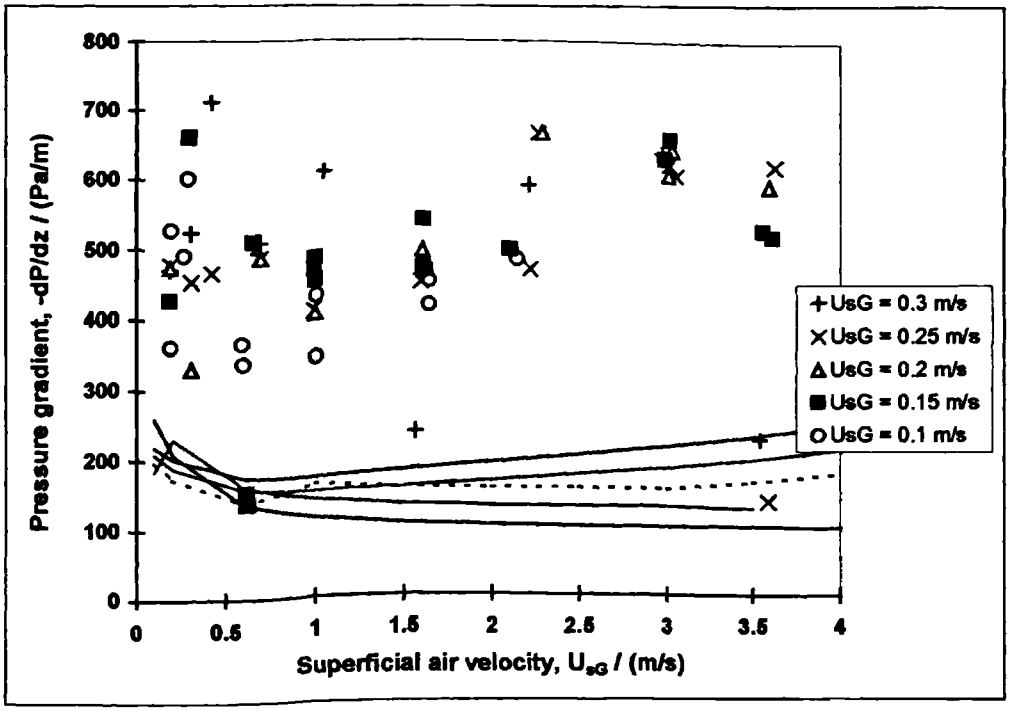

Figure 5.47: Pressure gradient measured at 5 bar(g) compared with prediction by Beggs & Brill (1973)

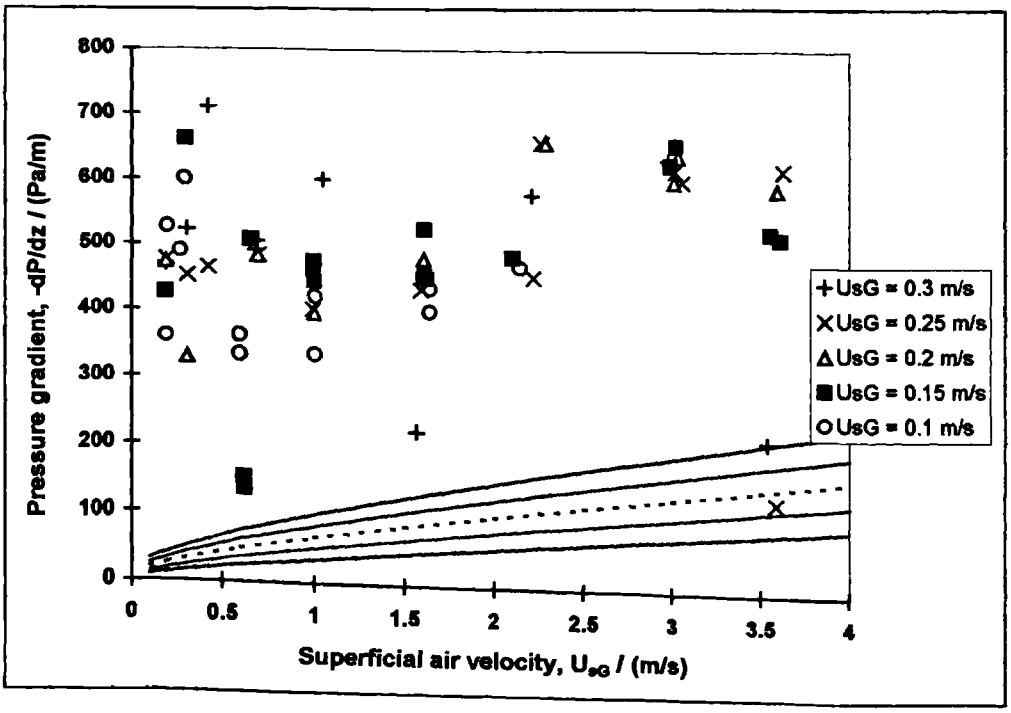

Figure 5.48: Pressure gradient measured at 5 bar(g) compared with prediction by Friedel (1979)

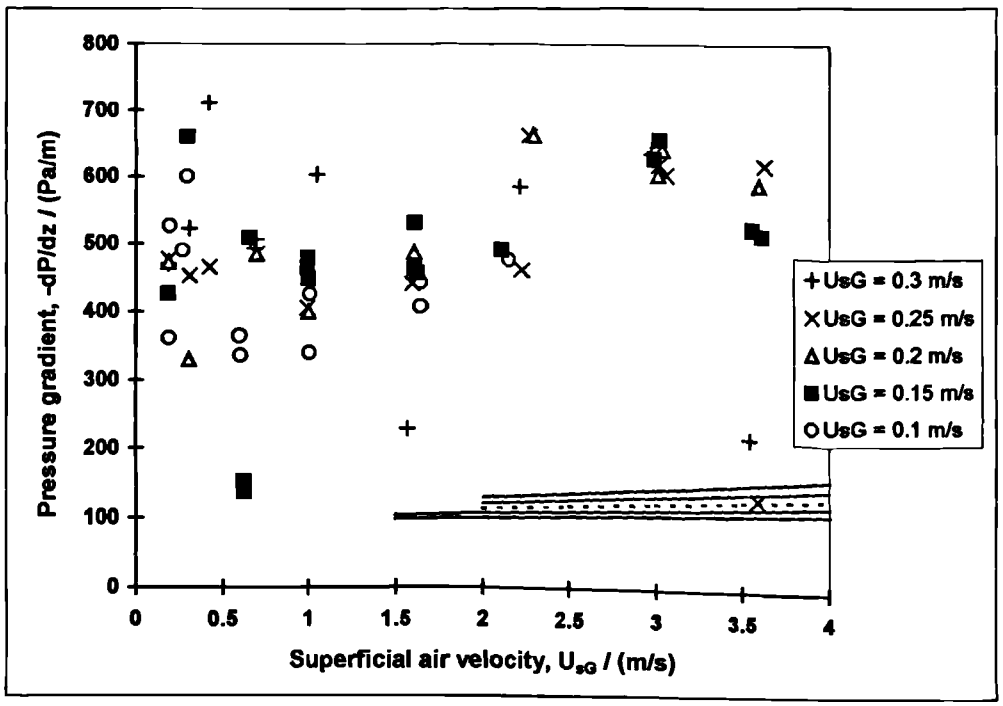

Figure 5.49: Pressure gradient measured at 5 bar(g) compared with prediction by Taitel & Barnea (1990)

5.3. Summary

A large set of data has been presented in this Chapter for two-phase flow in a ±1.5° "V"-section, for air-water flow at 0 and 5 bar(g). This adds to the significant body of data measured using the WASP facility at Imperial College.

Measurements were made of superficial gas and liquid velocities, liquid holdup at five points along the test-section and pressure gradient. The pressure gradient measurements were, unfortunately, affected by drift, which increased the scatter in the data considerably. The holdup measurements were analysed to obtain estimates of slug length, slug frequency and slug tail velocity. All of the data show considerable scatter but some general trends were observable.

Flow pattern maps measured at the pipe exit (Figures 5.2 and 5.3) are strongly influenced by the rising limb of the "V"-section. The presence of a "dip" in the pipeline causes a large increase in the size of the slug flow region of the flow pattern map, and introduces a significant region in which "dip slugging" occurs. This is characterised by short, high frequency slugs with very regular period and length, which are observed immediately

downstream of the dip. It was observed that the regular "dip-slugging" is not seen further from the dip: it appears that the short slugs quickly collapse and merge to form less regular slug flow as they propagate downstream.

Reverse flow was observed between slugs on the rising limb for cases when the superficial gas velocity fell below 8 m/s (for the experiments at atmospheric pressure), or 2.4 m/s (for flow at 5 bar(g)). This is in good agreement with Wood (1991) and not inconsistent with the Taitel & Barnea (1990) model (see Figure 5.32).

The measured data were compared against several correlations from the literature. Generally, correlations for slug parameters and pressure drop did not predict the experimental data particularly well. It is likely that this is due to the significant difference between horizontal two-phase flow, for which predictive correlations are usually derived, and the terrain effects studied in the present work. It was disappointing that the slug length and tail velocity data did not include very short slugs so that the change in slug translational velocity with slug length (as seen by Fagundes Netto *et al.*, 1998) could not be observed. However, the increase in the slug tail velocity at low values of the superficial mixture velocity was observed, and good agreement was seen between the experimental data and the correlations of Bendiksen (1984) and Manolis (1985). This has been explored further in a computational study, presented in Chapter 8 of the present work.

The measurements made near the dip accurately reflect the changes in the flow that occur due to the local change in slope. However, the measurements made near the end of the test-section were, in general, considerably affected by the short length (approximately 21 meters) of the rising limb. Thus the data were measured in developing, rather than fully developed flow. It was, nevertheless, possible to observe the evolution of the flow, in particular the fairly rapid transition from regular dip slugs to more random slugs, due to slug decay, death and growth. This is the subject of a phenomenological "slug tracking" model, presented in Chapter 7.

Chapter 6: Studies of terrain effects in slug flow II: Flow in a pipeline with a peak

In this Chapter, experimental data for two-phase air-water flow are presented for the in a "Λ"-section configuration of the WASP facility shown in Figure 6.1 (see Section 3.3.3 for further details).

Figure 6.1 shows the positions of the conductivity probes and other instrumentation in the WASP test-section for these tests.

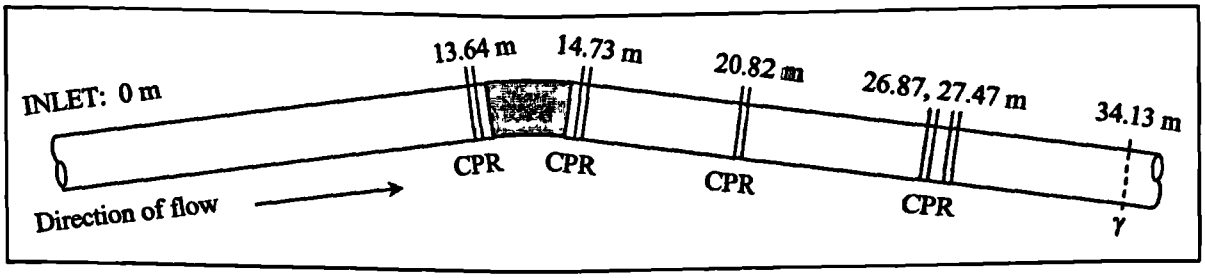

Figure 6.1. Relative positions of conductivity probes and gamma densitometer for Campaign 3 (*not to scale*)

In this work, data were collected for (nominally) steady-state experiments at (nominally) zero and five bar(g) exit pressure. As in the previous Campaigns (described in Chapters 4 and 5), observations were made of pressure drop, flow pattern, slug frequency, slug length and liquid holdup at different points along the test-section. The experimental results are presented in Section 6.1. A comparison of the data with some published predictive models and correlations (which were described previously in Chapter 2) is given in Section 6.2.

6.1. Experimental results

The detailed experimental matrix used for the campaign is included in Appendix 2, in which a unique run number is assigned to each experiment, and the experimental parameters are listed for each case. The original data files recorded for each experiment are included on CD-ROM number CD03, appended to this thesis.

6.1.1. Flow pattern

Flow pattern identification was carried out at the transparent visualisation section near the end of the downhill part of the test-section and the results were used to construct flow pattern maps.

The maps for 0 and 5 bar(g) are shown in Figure 6.2 and Figure 6.3 respectively. The abbreviations for flow patterns used in the legends are described in Table 6.1.

Abbreviation	Flow pattern
str.sm.(w.)	Stratified smooth flow with occasional "step changes" in the liquid film (see discussion below)
str.wa.	Stratified wavy flow
sw / slug	Transition between stratified wavy and slug flow; some interfacial waves completely block the pipe
slug	Slug flow
slug / ann.	Transition between slug and annular flow; the liquid film region between slugs is observed to form an annular layer around the pipe wall

Table 6.1: Explanation of abbreviations used in flow pattern maps

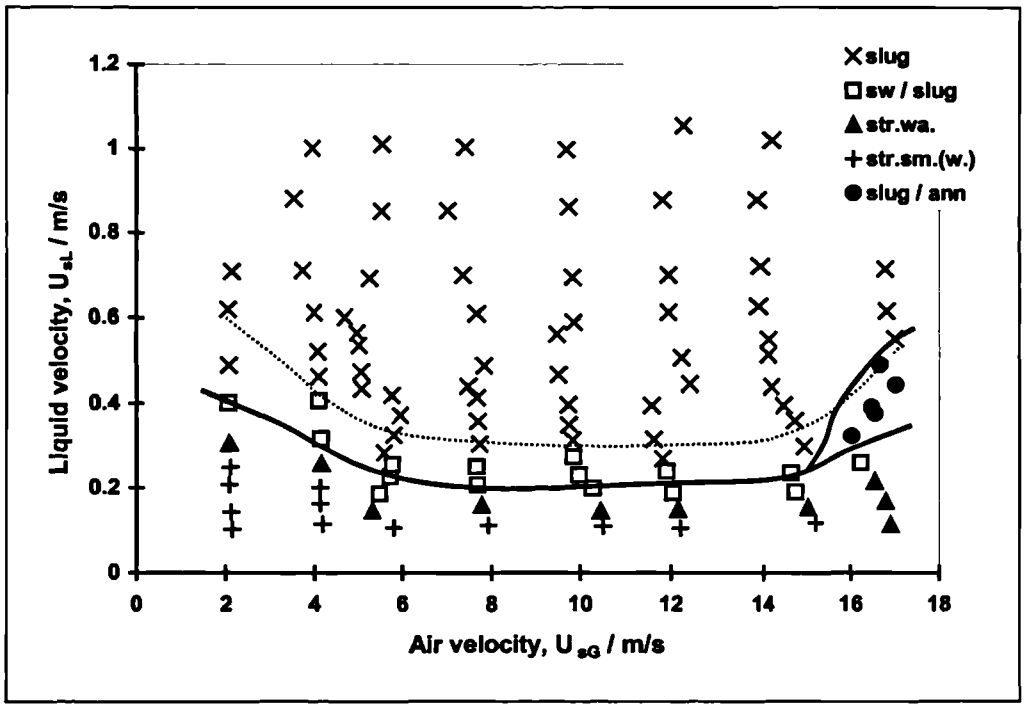

Figure 6.2: Flow patterns measured at 35 m from the test-section inlet, 0 bar(g)

In Figure 6.2 and Figure 6.3, the solid lines show the transition boundaries between the flow regimes. The dotted line shows the stratified wavy / slug flow transition boundary which was measured for –1.5° downhill flow, in Campaign 1 of the present work (see Chapter 4).

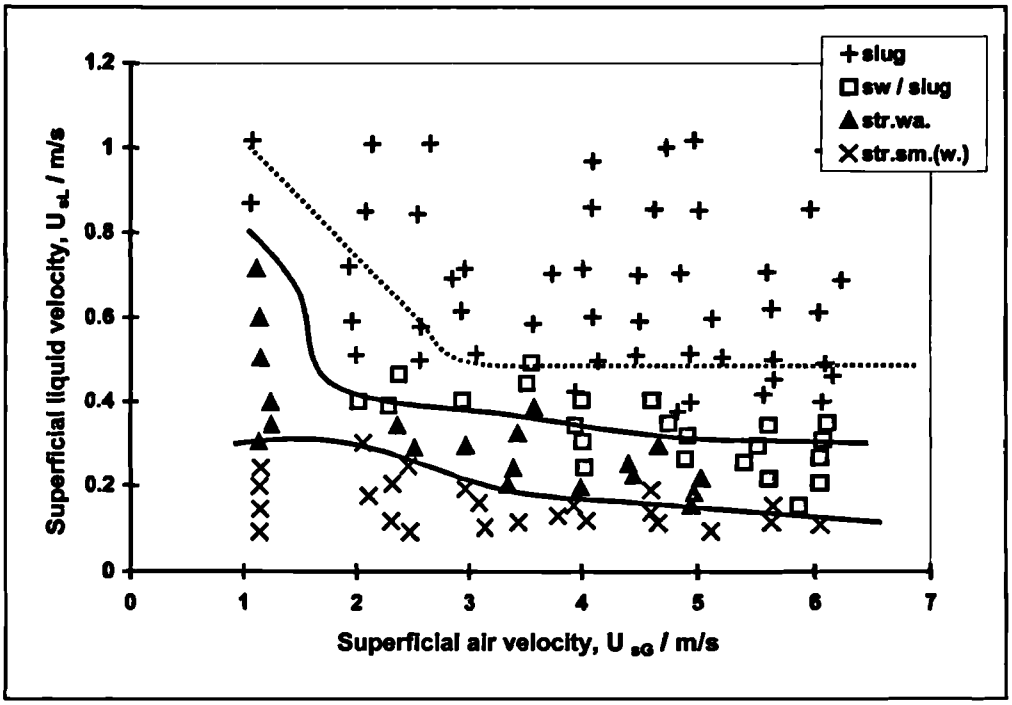

Figure 6.3: Flow patterns measured at 35 m from the test-section inlet, 5 bar(g)

An unusual feature of the flow pattern maps is the absence, at low superficial velocities, of the "stratified smooth" regime, which was observed in the experiments on the downwardly-inclined and "V-section" configurations described in Chapters 4 and 5. In place of the conventional stratified smooth region, a flow regime was identified at low flows, in which the interface of the stratified gas-liquid film was smooth and the film was not aerated. However, large periodic "waves" with very low frequency (as low as 0.1 Hz) were observed in the film. The waves caused periodic "step changes" in the thickness of the stratified liquid film. After each wave, the film thickness gradually decayed until the arrival of the next wave at the visualisation section. This flow pattern is illustrated in Figure 6.4.

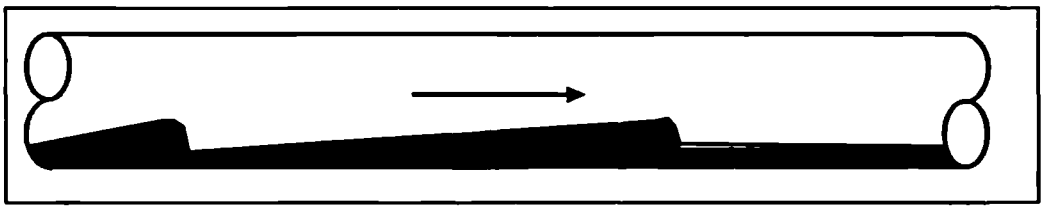

Figure 6.4: Illustration of "step changes" in the smooth stratified flow regime

A liquid holdup trace from the gamma densitometer (which was located 34.13m from the test-section inlet, and 19.95m downstream of the "peak" of the Λ-section), showing the low-frequency "surging" of the stratified smooth flow regime, is presented in Figure 6.5.

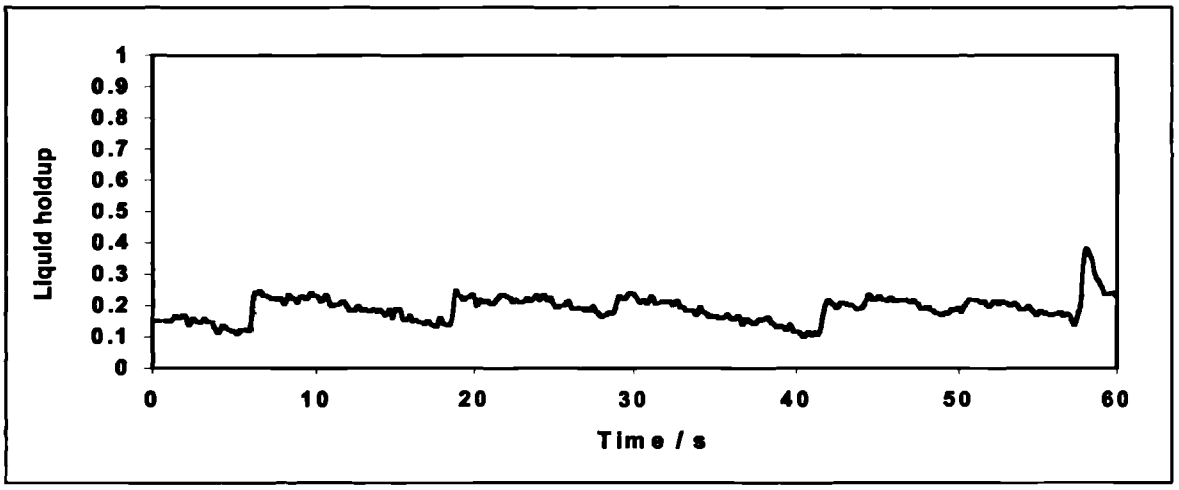

Figure 6.5: Liquid holdup-time trace from the gamma densitometer
U_{sL} = 0.10 m/s, U_{sG} = 5.81 m/s, P = 0 bar(g)

From inspection of the liquid holdup traces from the conductivity probes in the WASP facility test-section, it seems likely that the "surging" of the stratified liquid film, observed at the end of the test-section, is due to waves "lapping" over the top of the Λ-section and then collapsing as they propagate along the downhill limb of the test-section. The data from the probes suggest that for the very low flows at which this flow regime is observed, no *slugs* are present in the test-section at the top of the Λ-section.

In Figure 6.6, liquid holdup data are shown at several locations in the test-section for an experiment in which "surging" stratified smooth flow was observed at the visualisation section. The positions of the probes are shown in Figure 6.1. In the experiment, the superficial liquid and gas velocities were 0.13 m/s and 3.79 m/s respectively, and the pressure was 5.0 bar(g)

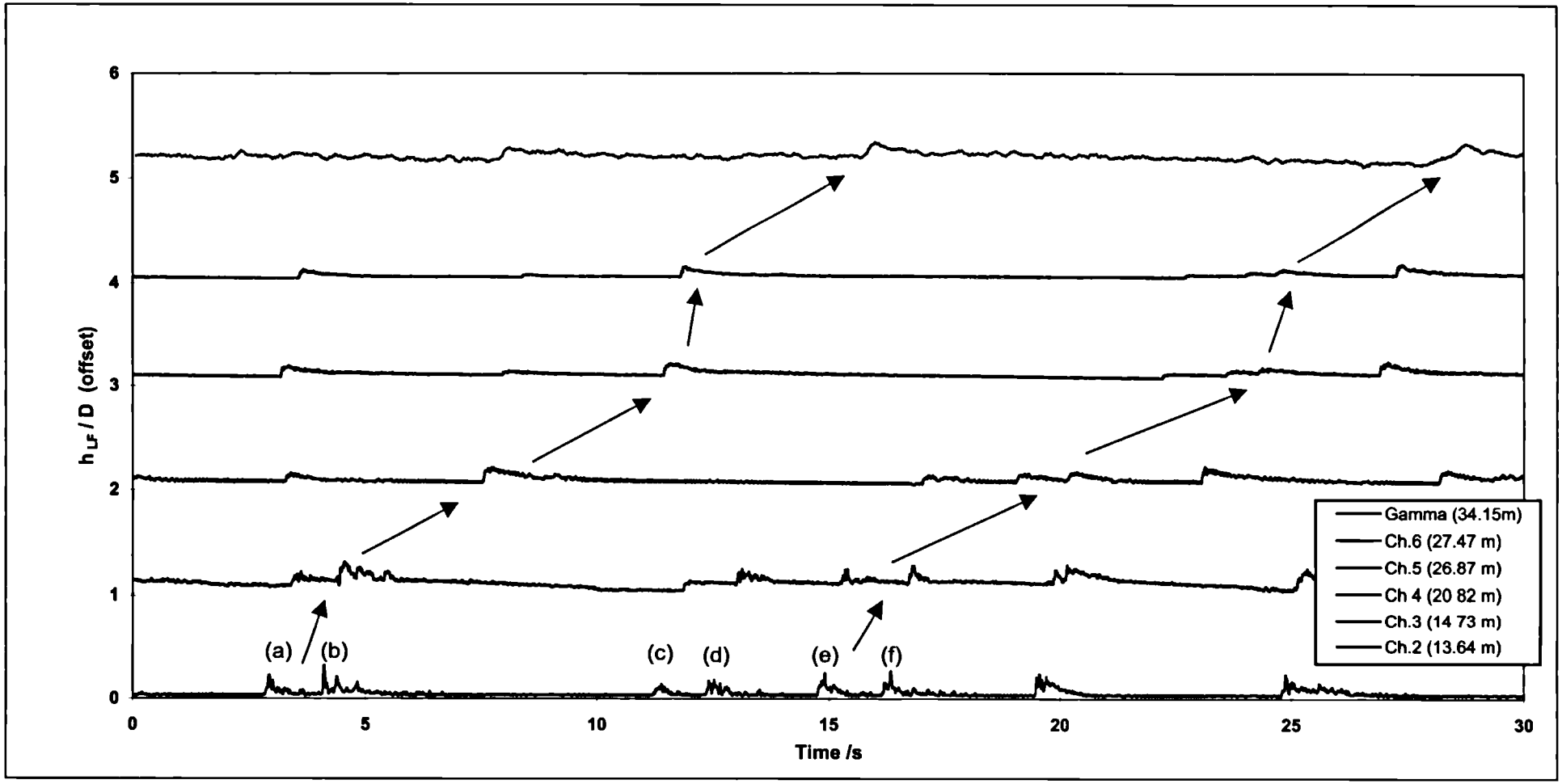

Figure 6.6: Liquid holdup traces from run PDM4128, showing propagation and merging of waves [U_{sG}=3.79 m/s, U_{sL} = 0.13 m/s, P=5 bar(g)]

In Figure 6.6 it is clear that frequency of the waves present in the pipe at the top of the Λ-section is considerably greater than that of the "surging" at the end of the test-section. There is considerable interaction between waves in the downhill leg of the Λ-section as waves dissipate and merge together to form the larger "surge" waves observed further downstream. In Figure 6.6, waves (a) and (b) have merged together by the time they reach the conductivity probe at 20.82 m. Similarly there appears to be interaction between waves (c) and (d), and (e) and (f). The pair of waves (c) and (d) merge to form a single wave by the 20.82 m probe. At this point, waves (e) and (f), a short distance upstream, are still distinct objects. At the 26.87m and 27.47m probes they are still observable as two separate waves, however the distance between them is now much less. At the gamma densitometer, waves (e) and (f) have merged, together with the slower wave resulting from the merging of (c) and (d) upsteram.

The slug flow regions shown in Figures 6.2 and 6.3 are slightly larger than were observed in downhill-only flow in Campaign 1 (see Chapter 4). It is likely that this is due to the formation of slug flow in the uphill leg of the Λ-section which then propagates over the "peak" and continues along the downhill leg of the test-section. Examples of experiments where this was observed are shown in Figure 6.7 and Figure 6.8. Although there is considerable interest in the calculation of the "slug dissipation rate" in hilly-terrain, where slugs formed in uphill pipe sections decay to form stratified flow in subsequent downhill sections, this was not regularly observed in the present experiments. It is likely that this is due in part to the relatively short length of the WASP facility test-section, so that the length of the downhill leg of the Λ-section was approximately 20m. It is likely that this is not sufficiently long for complete dissipation of slugs to occur, so that many of the slugs formed in the uphill leg persist right to the end of the test-section.

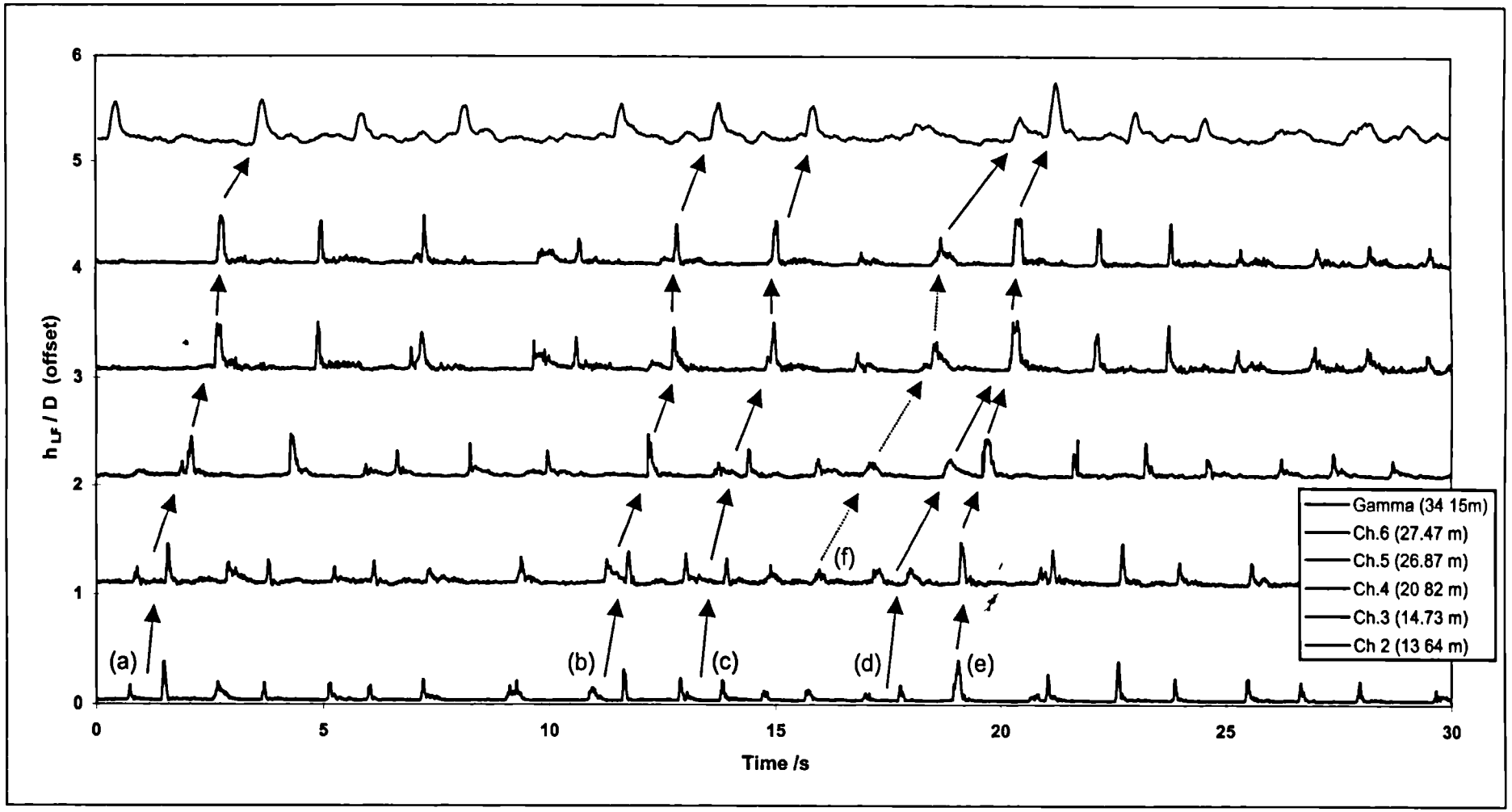

Figure 6.7: Liquid holdup traces from run PDM4056, showing propagation of slugs [U_{sG}=9.84 m/s, U_{sL} = 0.70 m/s, P=0 bar(g)]

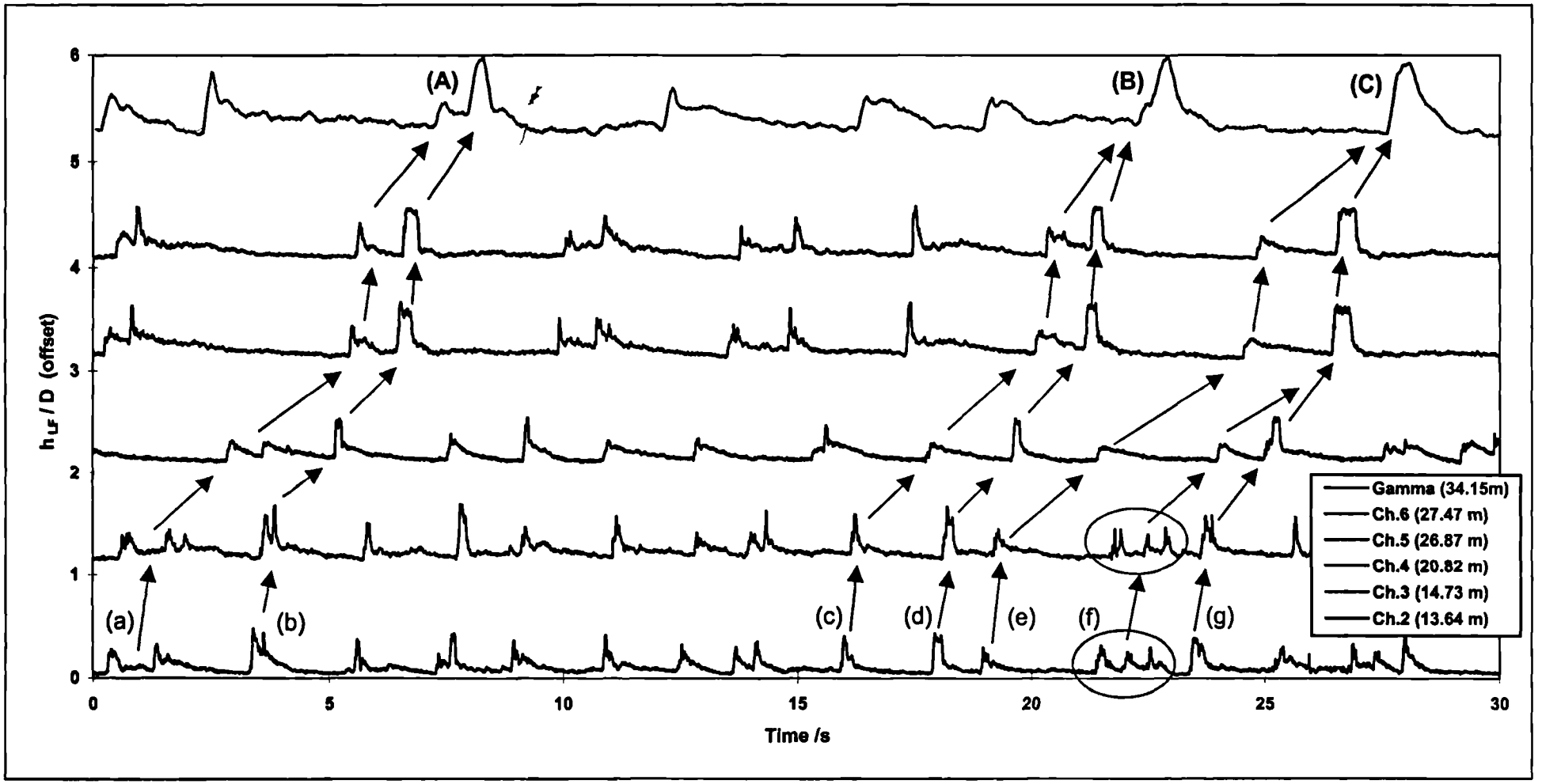

Figure 6.8: Liquid holdup traces from run PDM4125, showing propagation of slugs [U_{sG}=2.85 m/s, U_{sL} = 0.70 m/s, P=5 bar(g)]

Several wave/slug interactions are highlighted in Figure 6.7. The wave/slug pair marked as (a) have are just discernible as separate objects at the 20.82m probe, however they have merged to form a single slug by the 26.87m probe. The wave/slug pairs (b) and (c) behave similarly. The pair of waves denoted by (d) have merged by the 20.82m probe to form a single wave. Slug (e), immediately upstream, then merges with the wave formed from the pair (d). It is interesting to note that the enlarged slug formed from these interactions continues downstream and quickly catches up with wave (f) so that by the final probe in the test-section, slug (e) has almost caught wave (f).

These results suggest that slug flow may persist for some considerable distance after a "peak" due to the dissipation of short slugs to form slow-moving waves which are subsequently overtaken by faster-moving slugs. Although the longer slugs formed in this way will gradually dissipate, these will in turn form waves, which will be picked up by any remaining longer slugs in the pipeline. There may eventually be a maximum "survival distance" in the downhill leg of a Λ-section beyond which no slugs would be present in the pipe. The flow pattern map would then be similar to that measured in a "downhill only" pipe.

Figure 6.8 shows even more interaction between waves and slugs. In general, each of the large slugs or waves detected by the gamma densitometer at the end of the test-section is formed from the merging of two or more smaller waves further upstream. The pair of waves denoted by (a) merge to form a single wave, which is then "chased" by the faster-moving slug (b) which eventually forms slug (A).

Similarly, slug (B) is formed when slug (d) catches and assimilates the wave formed by the decay of slug (c). In the final example, slug (C) is formed by the merging of five distinct objects: wave (e) merges with another wave which is formed from the coalescence of the group of three waves, (f). This wave is then caught by slug (g), to form the large slug (C).

6.1.2. Liquid holdup

As in the first two Campaigns, liquid holdup was measured near to the end of the test-section, using a gamma densitometer. Time-averaged holdup data, calculated as the arithmetic mean of all the holdup samples recorded during each 180-second experimental run, are plotted in Figure 6.5. As in Chapters 4 and 5, the data are plotted against the inlet quality (defined as the mass fraction of gas at the pipe inlet).

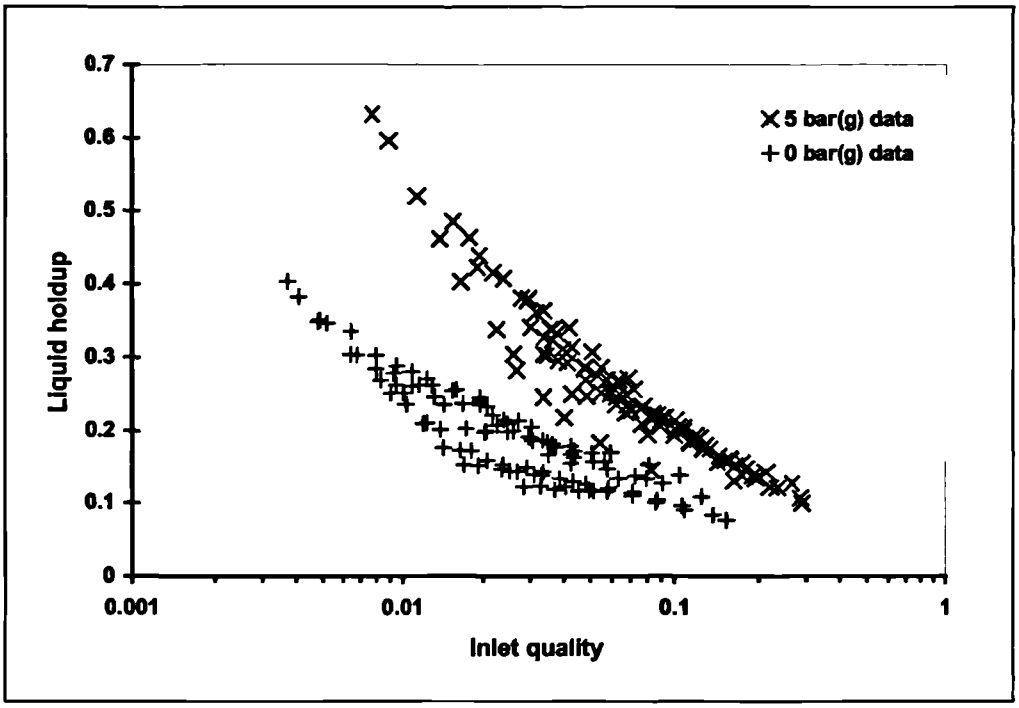

Figure 6.9: Liquid holdup data measured at 34.15 m from the pipe inlet

In Figures 6.10 and 6.11, the liquid holdup data measured at 0 and 5 bar(g) respectively are sorted according to flow pattern.

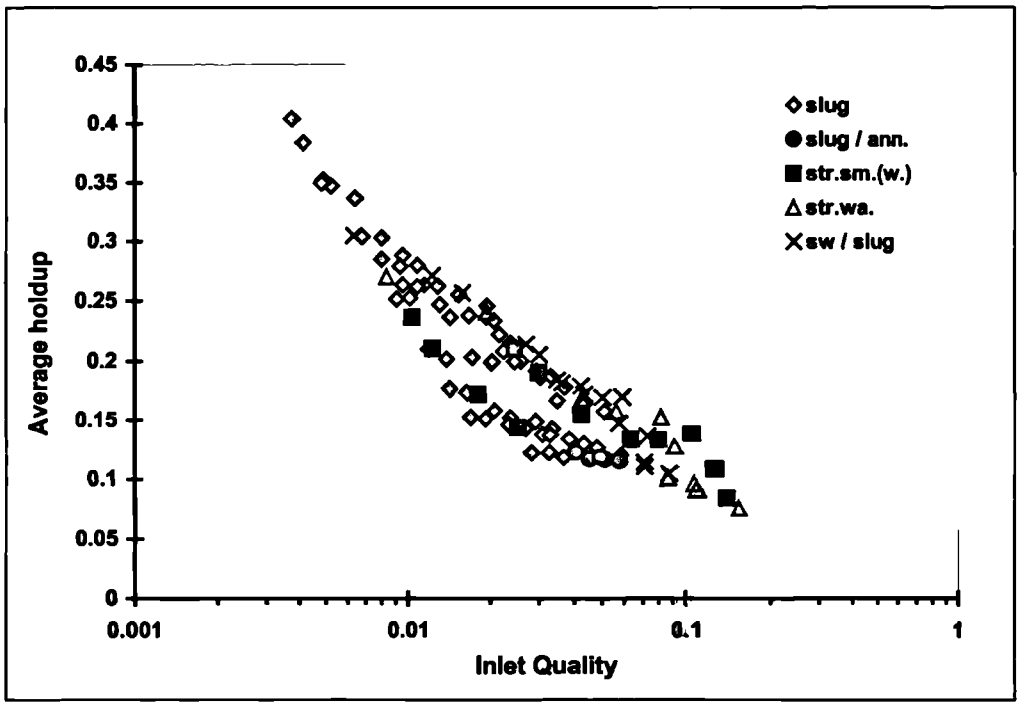

Figure 6.10: Time-averaged holdup data measured at 0 bar(g), showing flow pattern

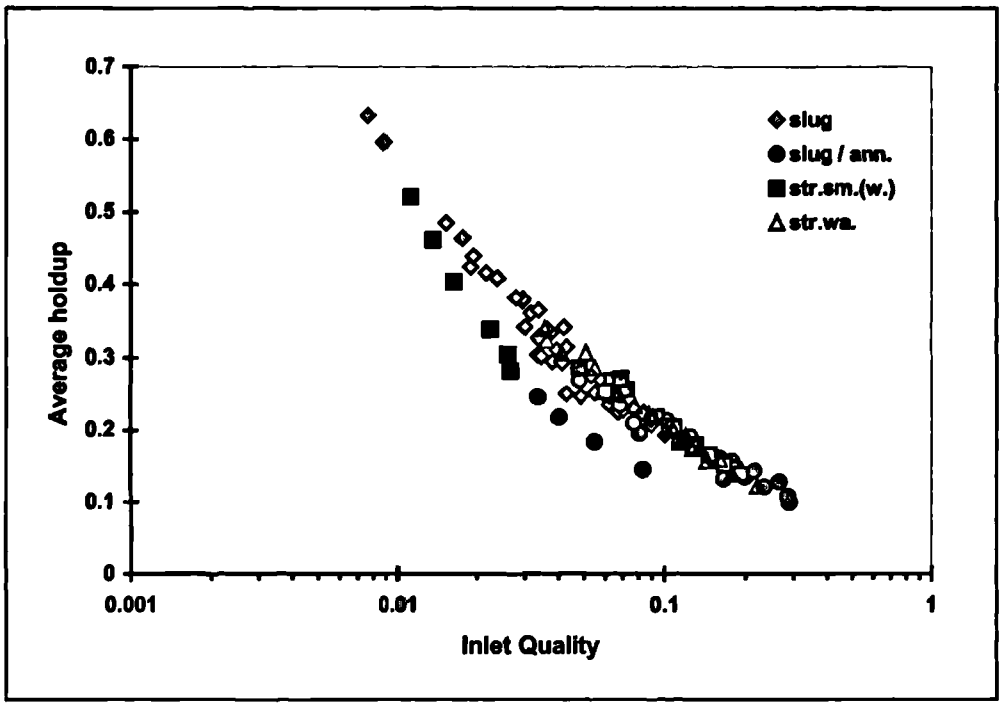

Figure 6.11: Time-averaged holdup data measured at 5 bar(g), showing flow pattern

Generally, there is no clear trend between flow pattern and liquid holdup. The holdup data show an approximate inverse-logarithmic dependence on the inlet quality, and as was seen in the results presented in Chapters 4 and 5, there is a strong effect of pressure.

The average liquid holdup data are compared with predictive correlations in Section 6.2.1.

6.1.3. Slug translational velocity

As in Campaigns 1 and 2, a subset of experimental runs was identified in which slug flow was observed near the end of the test-section. For a number of slugs in each of these runs, slug lengths and translational velocities were calculated from the liquid holdup traces measured using a pair of conductivity probes placed at 26.87 m and 27.47 m along the pipe. The calculation procedure was described in Section 4.1.3 in the Chapter 4.

The runs were chosen so that they were regularly spaced across the slug flow regions of the 0 and 5 bar(g) flow pattern maps, and so that the entire range of mixture velocities was represented at both pressures. The data set consists measurements on 144 slugs, taken from 29 experimental runs.

The data for the ratio of slug translational velocity to mixture velocity are plotted against slug length in Figure 6.12. The points are grouped in terms of mixture velocity as shown.

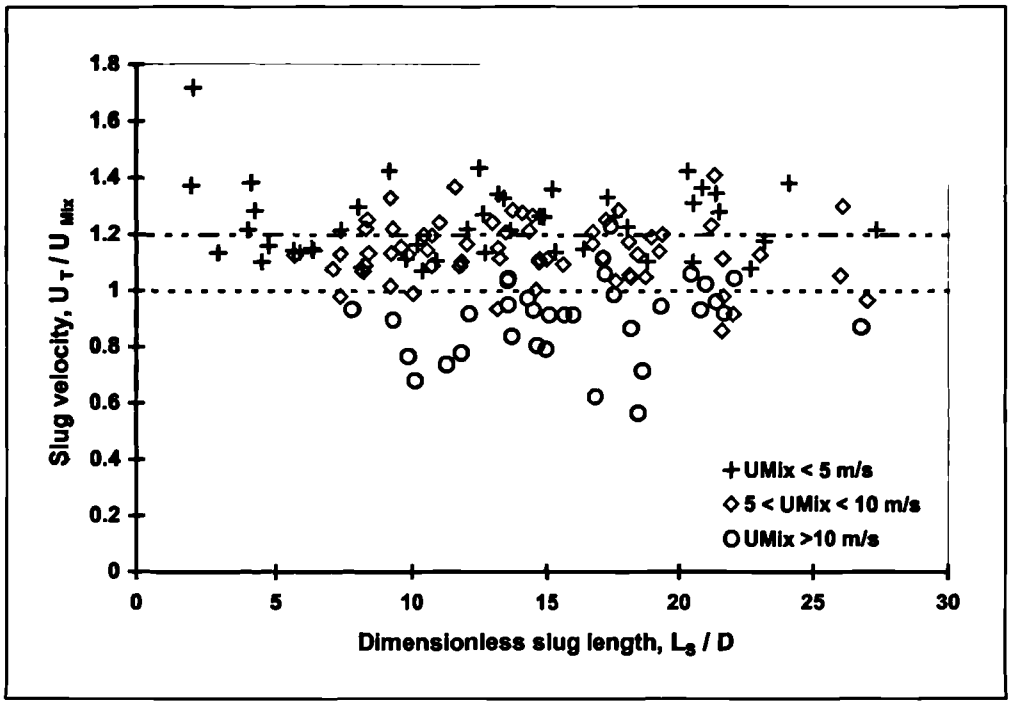

Figure 6.12: Dimensionless slug translational velocity *vs.* dimensionless slug length for a subset of 29 experimental runs

The slug translational velocity appears to be heavily influenced by the mixture velocity, as shown in Table 6.2, in which values of the mean slug translational velocity and the standard deviation are compared for three ranges of mixture velocity.

U_{Mix} / m/s	Mean U_T/U_{Mix}	Std.dev.
< 5	1.243	0.126
$5 \leq U_{Mix} < 10$	1.139	0.109
≥ 10	0.903	0.140

Table 6.2: Mean slug translational velocity measured in Campaign 3

In general, the dimensionless slug translational velocity *decreases* as the mixture velocity increases. This trend was also observed for the experiments conducted with a –1.5° downwardly-inclined test-section in Campaign 1, reported in Chapter 4 and also in the results for the "V"-section (see Figure 5.12). At low mixture velocities, gravitational motion of the

slug tail becomes significant and at high gas velocities, gas breakthrough may occur in the slug body.

Very few short slugs (with L_S/D less than about 8) were observed. However, the few data which were measured in this range suggest an upward trend in the slug translational velocity as L_S tends to zero. This agrees with the results of Fagundes Netto *et al.* (1998, 1999a) and Cook & Behnia (2000). However, in Figure 6.12 and Table 6.2, *mean* translational velocity data (*i.e.*, the average of the front and tail velocities) are presented. It is not possible to obtain the slug tail velocity explicitly unless the front velocity of the slug is assumed to be constant. Considerably more experimental work is needed to verify the trends suggested in Figure 6.12.

6.1.4. Slug length

The slug length data obtained from the analysis described in Section 6.1.3 are plotted as a slug length distribution in Figure 6.13.

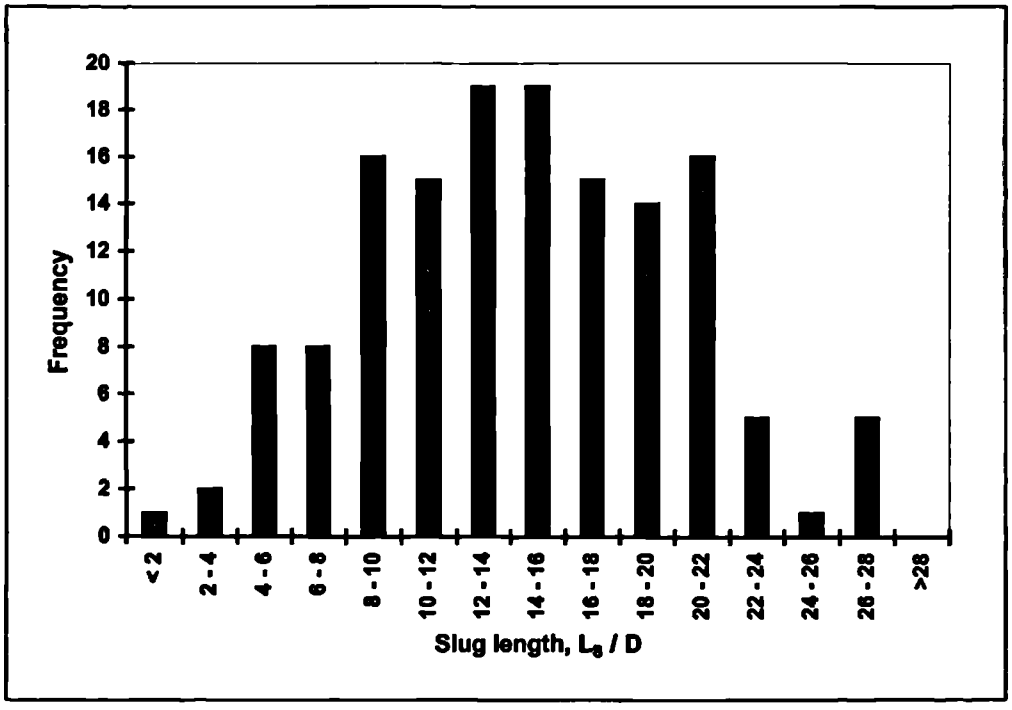

Figure 6.13: Distribution of dimensionless slug lengths for a subset of 29 experimental runs

The mean slug length is 14.35D and the standard deviation is 5.64D. The mean slug length is less than the value of 16.32D, obtained from the experiments in Campaign 1, when the test-section was inclined downwards at –1.5° for its entire length. The mean length is slightly

shorter in the downhill limb of the Λ-section, despite the same inclination angle, due to the presence of short "decaying" slugs in the pipe, which were formed in the uphill part of the pipe and which have not fully decayed before their arrival at the pair of conductivity probes about 14m after the "peak" of the Λ-section. Such slugs are not present in a downwardly-inclined straight pipe.

6.1.5. Slug frequency

As in the first two experimental Campaigns, slug frequency data were obtained from the liquid holdup/time traces from the gamma densitometer, measured near to the end of the test-section. The data, obtained simply by counting the number of slug peaks in a measured time period of 180 seconds, are expected to exhibit a maximum error of ± 2 counts in 180 seconds, or approximately 0.01 Hz. The results, grouped according to pressure and superficial liquid velocity, are plotted in Figures 6.14 – 6.16.

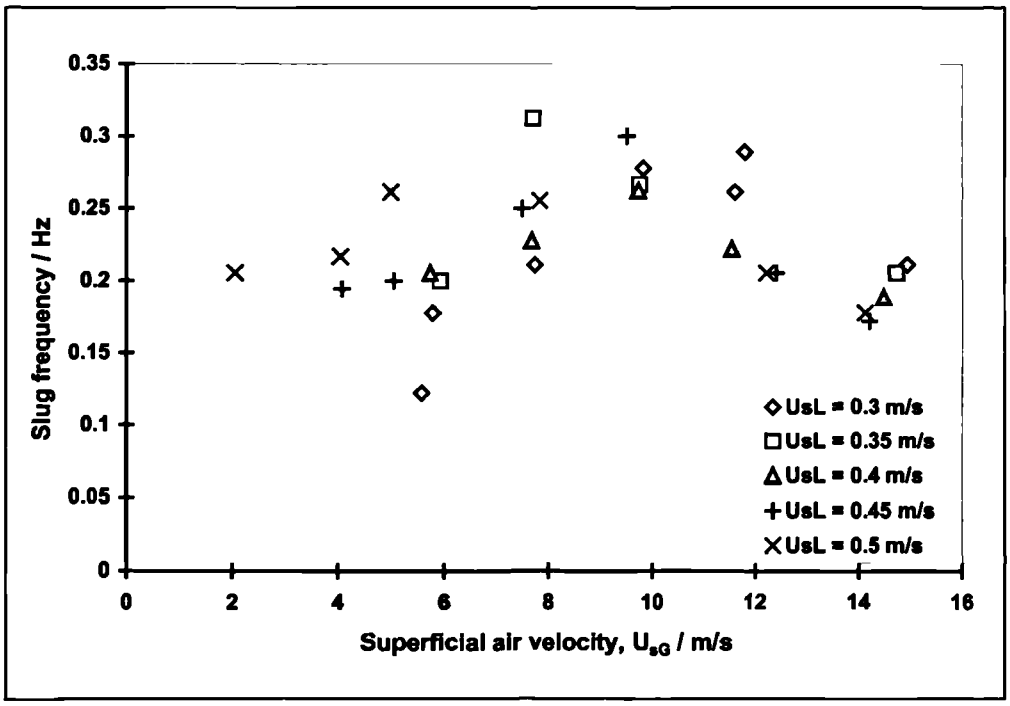

Figure 6.14: Slug frequencies (from inspection of the gamma densitometer traces) at 35.14 m from the inlet, 0 bar(g) runs, 0.3 m/s ≤ U_{sL} ≤ 0.5 m/s

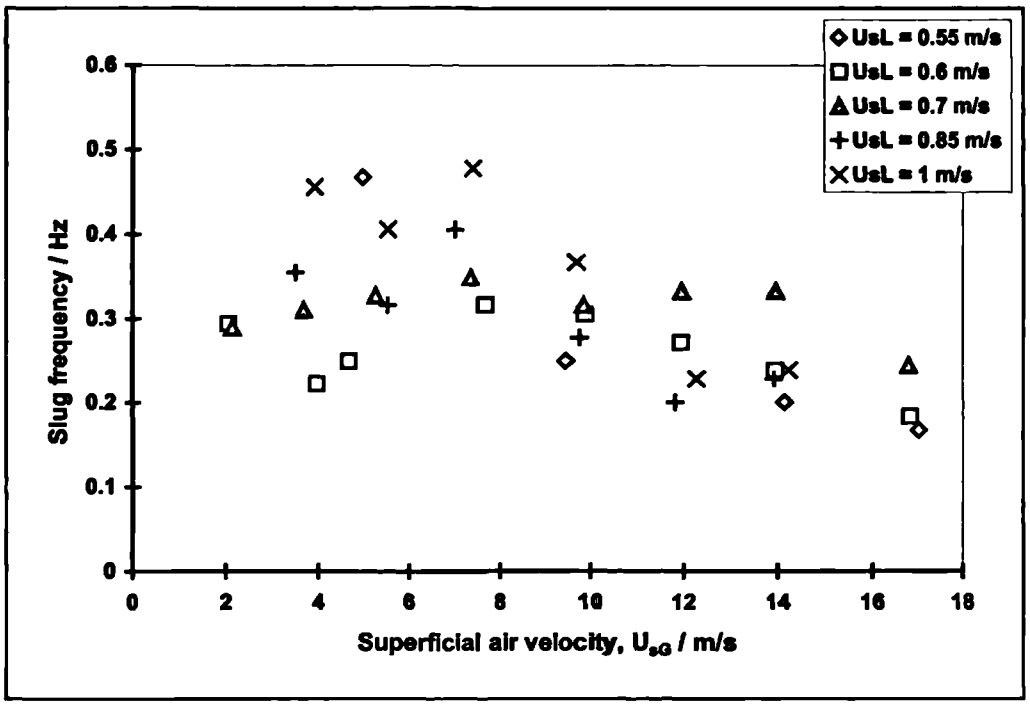

Figure 6.15: Slug frequencies (from inspection of the gamma densitometer traces) at 35.14 m from the inlet, 0 bar(g) runs, 0.55 m/s ≤ U_{sL} ≤ 1.0 m/s

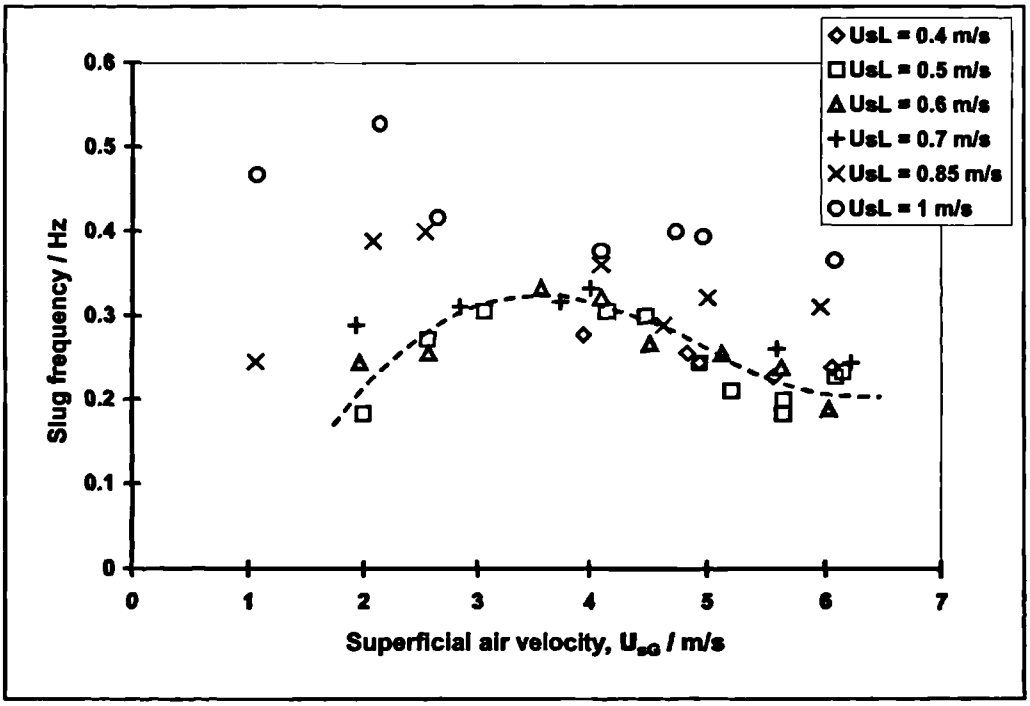

Figure 6.16: Slug frequencies (from inspection of the gamma densitometer traces) at 35.14 m from the inlet, 5 bar(g) runs, 0.4 m/s ≤ U_{sL} ≤ 1.0 m/s

Although the data in Figures 6.14 and 6.15 are scattered, in general the slug frequency increases with the superficial liquid velocity and, for all except the very lowest values of U_{sL}, is approximately independent of the superficial gas velocity.

The 5 bar(g) data in Figure 6.16 show a slightly more obvious trend than those measured at atmospheric pressure. This is shown in Figure 6.16 as a dashed line, which passes through a maximum slug frequency of 0.32 Hz at approximately U_{sG} = 3.5 m/s. However, this trend is not followed by the data measured at the highest superficial liquid velocities (0.85 m/s and 1.0 m/s).

The slug frequency data do not exhibit the conventional "tick" shape reported in the literature (see Section 2.3.4), in which the curve passes through a *minimum* frequency as U_{sG} increases. This is in contrast to the results from Campaigns 1 and 2 of the present work. It is likely that the slugs observed at the location of the gamma densitometer (where these frequency data were measured) result from the merging waves and slugs in the downhill limb of the Λ-section. The origin of the slugs may be different to that occurring in other geometries (*i.e*, hydrodynamic slugging in horizontal / downhill pipes; "dip-slugging" in a V-section) and so it would be surprising if the same trends were observed for the slug frequency.

Slug frequency data were also obtained by power spectral density (PSD) analysis of the liquid holdup/time traces from the conductivity probes (CPRs). This procedure, its advantages and its shortcomings are described in Section 5.1.5 in the previous Chapter. In the results measured in the "V"-section experiments, it was found that PSD analysis was most useful when the holdup/time data were truly periodic (*e.g.*, for "dip slugging" experiments) but that the technique was of more limited value in other cases.

In the present series of experiments, the data from the CPR traces show low periodicty, and thus PSD analysis is unlikely to produce meaningful results. This is demonstrated in Figure 6.17, in which slug frequency data from PSD analysis of the conductivity probe located at 27.47m from the test-section inlet are compared with the data obtained from inspection of the gamma densitometer data. This discrepancy is by more than a factor of ten in some cases.

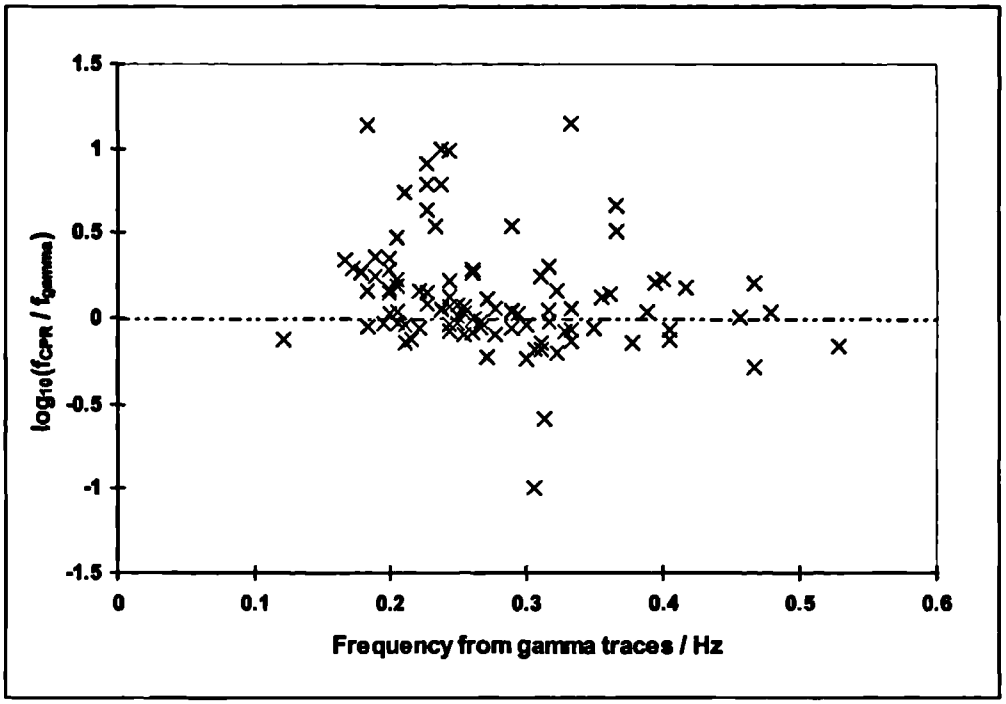

Figure 6.17: Comparison of frequency data from CPR and gamma traces

In the discussion of wave collapse and slug propagation presented in Section 6.1.1 above, it was noted that a great deal of wave/slug interaction occurred in the downhill portion of the Λ-section. In general, a continuous decrease in slug frequency is anticipated along the pipe, due to the progressive collapse and amalgamation of slugs. This would suggest that the slug frequency measured by PSD analysis of the 27.47m conductivity probe should generally be greater than, or at least equal to that observed at the gamma densitometer, some 6.66m further downstream. However, Figure 6.17 shows many data where a *lower* frequency is obtained from the PSD analysis. This suggests that the PSD slug frequency data have limited reliability in this case.

The dominant frequencies at each probe, obtained from the PSD analyses, are summarised in Table 6.3. A comparison is made with the data from inspection of the gamma densitometer traces.

	PSD analysis of CPR trace at...				Inspection of
	13.64m	14.74m	20.82m	27m	Gamma trace at 34.13 m
Dominant f / Hz	0.560	0.415	0.357	0.306	0.278
Std. deviation	0.388	0.314	0.216	0.264	0.077

Table 6.3: Dominant frequency data at points in the test-section (104 data points)

For the PSD analysis, CPR data were processed from all experimental runs. However, the gamma densitometer frequency data were obtained only from those runs which were previously identified as "slugging" at the visualisation section.

Despite the inherent ambiguity of the PSD frequency data, a clear trend is visible in the frequency data. The dominant slug/wave frequency tends to *decrease* further from the peak of the Λ-section. This is shown in Figure 6.18. The trend is consistent with the slug collapse/merging phenomena discussed in Section 6.1.1.

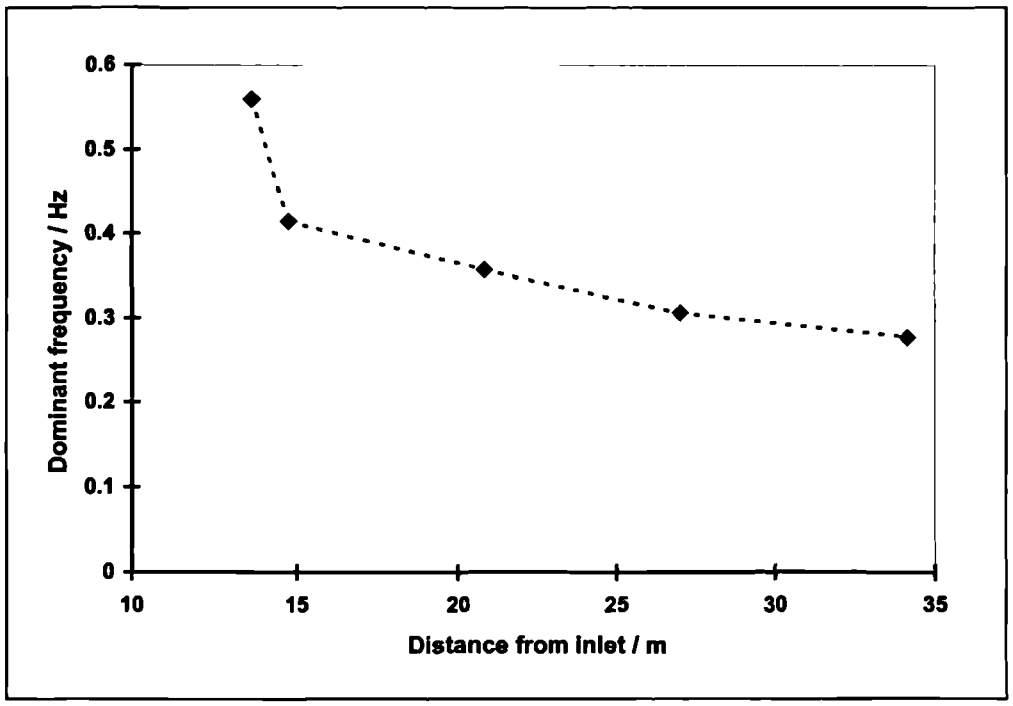

Figure 6.18: Variation of dominant PSD frequency along the test-section

6.1.6. Pressure gradient

As in the experiments described in Chapters 4 and 5, the pressure gradient was measured using a differential pressure transducer with tappings located close to the end of the test-section. The spacing between the tappings was 2.2 m. The averaging procedure and offset drift correction were applied as described in Chapter 4.

About half of the experiments were severely affected by offset drift in the measured pressure difference between the tappings. However, it was possible to identify a subset of "good" data, where the measured offset was approximately the same before and after a group of two or three experiments. Only the data with minimal offset are presented here.

The data for near-atmospheric outlet pressure are presented in Figures 6.19 and 6.20 and the data for 5 bar(g) outlet pressure are shown in Figures 6.21 and 6.22.

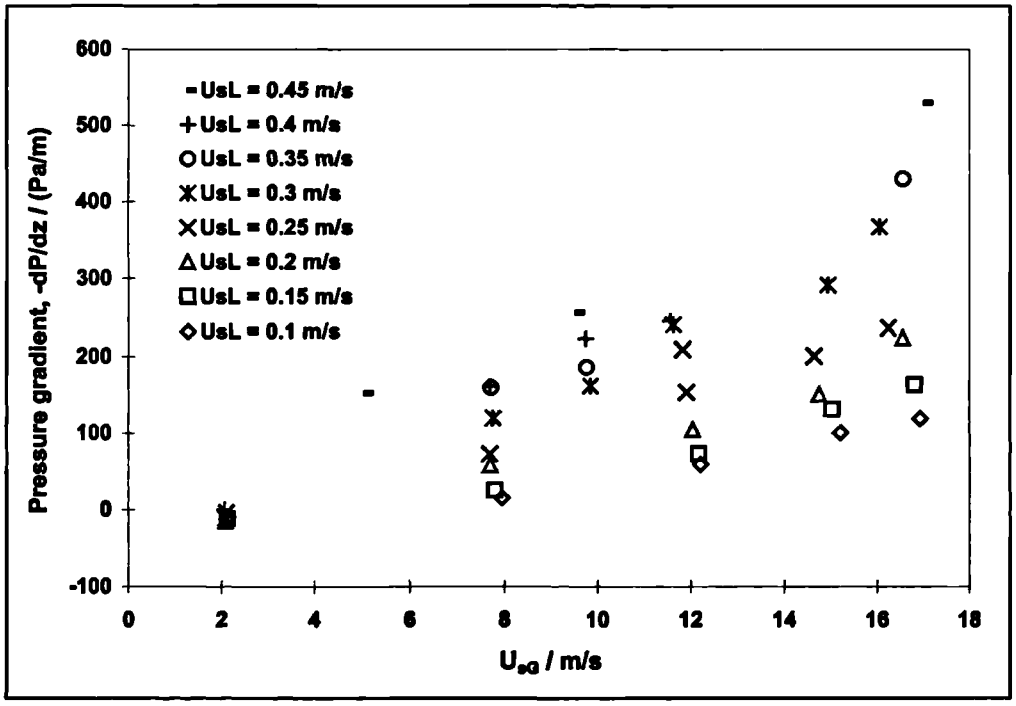

Figure 6.19: Pressure gradient data measured in the downhill leg of the "Λ"-section; 0 bar(g) runs, 0.1 m/s < U_{sL} < 0.45 m/s

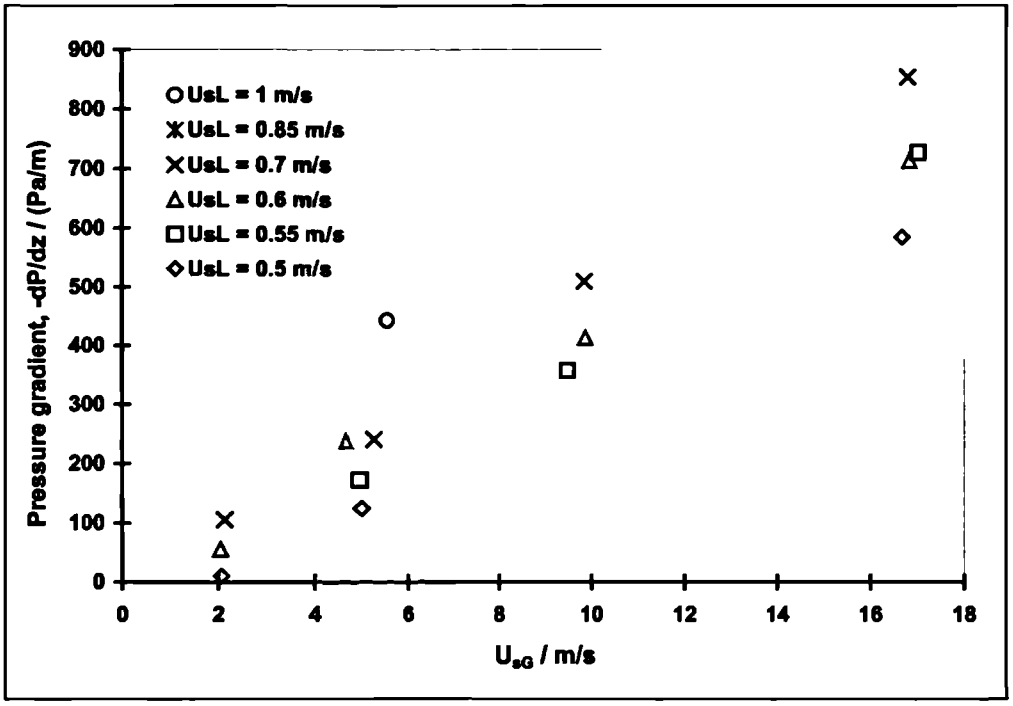

Figure 6.20: Pressure gradient data measured in the downhill leg of the "Λ"-section; 0 bar(g) runs, 0.5 m/s < U_{sL} < 1.0 m/s

Generally, the results show the expected trends with pressure gradient increasing with superficial phase velocities. A particularly interesting finding is that some of the data exhibit *positive* pressure gradients (*i.e.* an increase of pressure along the pipe). This would not be surprising in slug flow where some recovery of the gravitational pressure gradient would be expected (although this is usually offset by increased frictional pressure gradient). However, the positive pressure gradients observed here are in the "surging stratified flow" region (see Figure 6.4). Though the pressure gradients are rather low, and though measurements of pressure gradient in this region are subject to greater inaccuracy (Shaha, 1999), the positive gradient could be significant. One could hypothesise that the pressure increases due to a "pumping" action by the waves on the gas. This matter needs much further investigation.

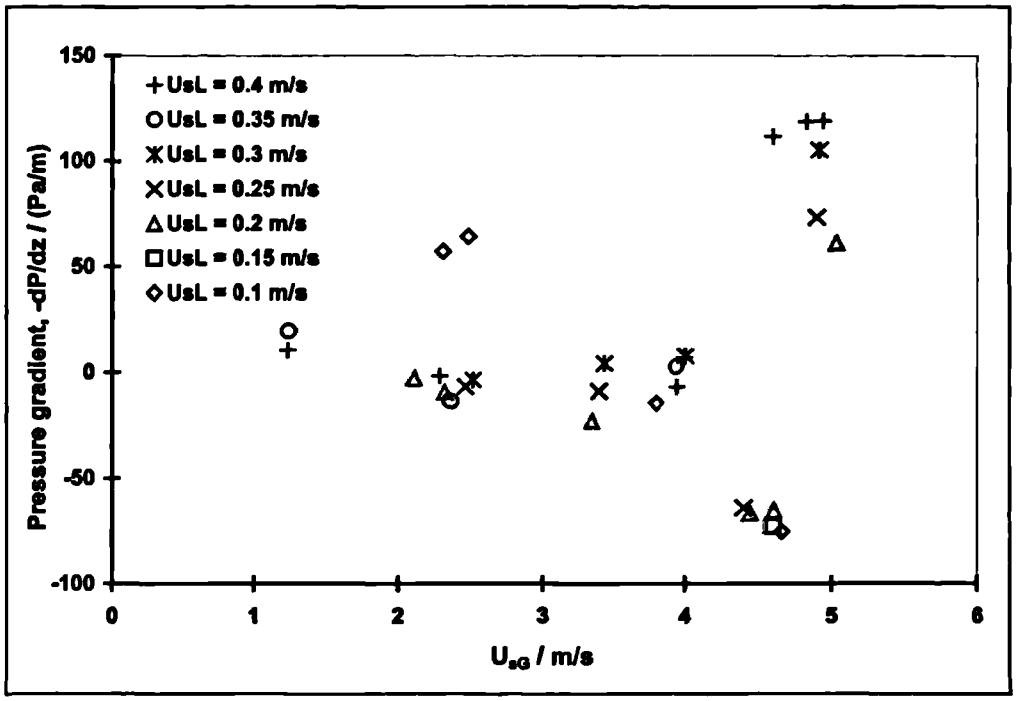

Figure 6.21: Pressure gradient data measured in the downhill leg of the "Λ"-section; 5 bar(g) runs, 0.1 m/s < U_{sL} < 0.4 m/s

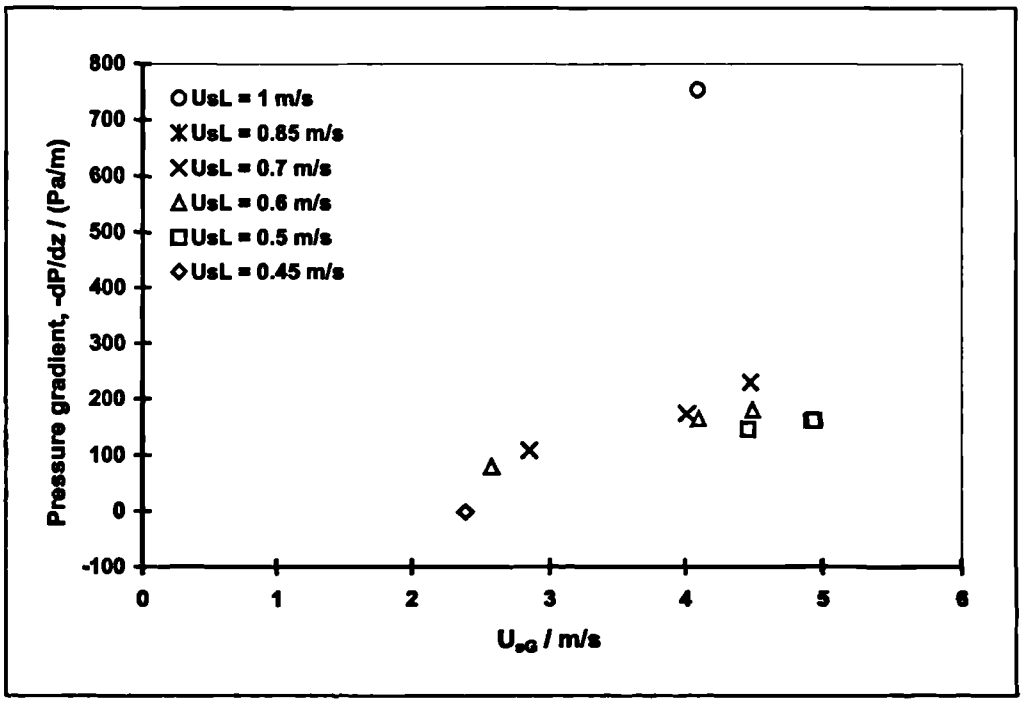

Figure 6.22: Pressure gradient data measured in the downhill leg of the "Λ"-section; 5 bar(g) runs, 0.45 m/s < U_{sL} < 1.0 m/s

6.2. *Comparison of results with predictive methods*

In this Section, comparison is made between the experimental data measured in this Campaign, and several predictive correlations and/or phenomenological models from the published literature. Details of the methods used in this section are presented in Chapter 2.

6.2.1. *Liquid holdup*

Analysis of data from the first two experimental campaigns (presented in Chapters 4 and 5) showed that the correlation of Chisholm (1972) gives fairly good predictions for average liquid holdup in near-horizontal flows across a wide range of flow patterns.

Figures 6.23 and 6.24 show the liquid holdup data measured in these experiments plotted against the predictions from the correlations of Chisholm (1972) and Premoli *et al.* (1970) respectively. At atmospheric pressure, the two correlations perform comparably and there is no consistent under- or over-prediction by either method. At 5 bar(g), both expressions tend to slightly over-predict liquid holdup.

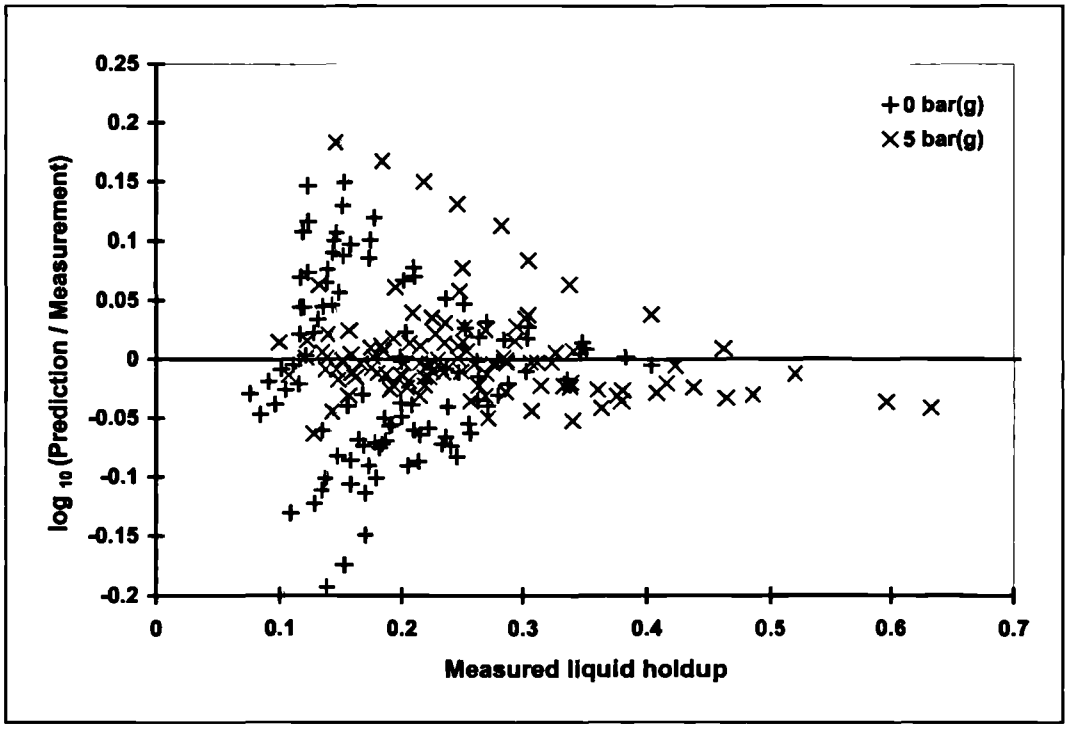

Figure 6.23: Measured liquid holdup data compared with predictions by the Chisholm (1972) correlation; 0 and 5 bar(g), -1.5° downhill limb of Λ-section

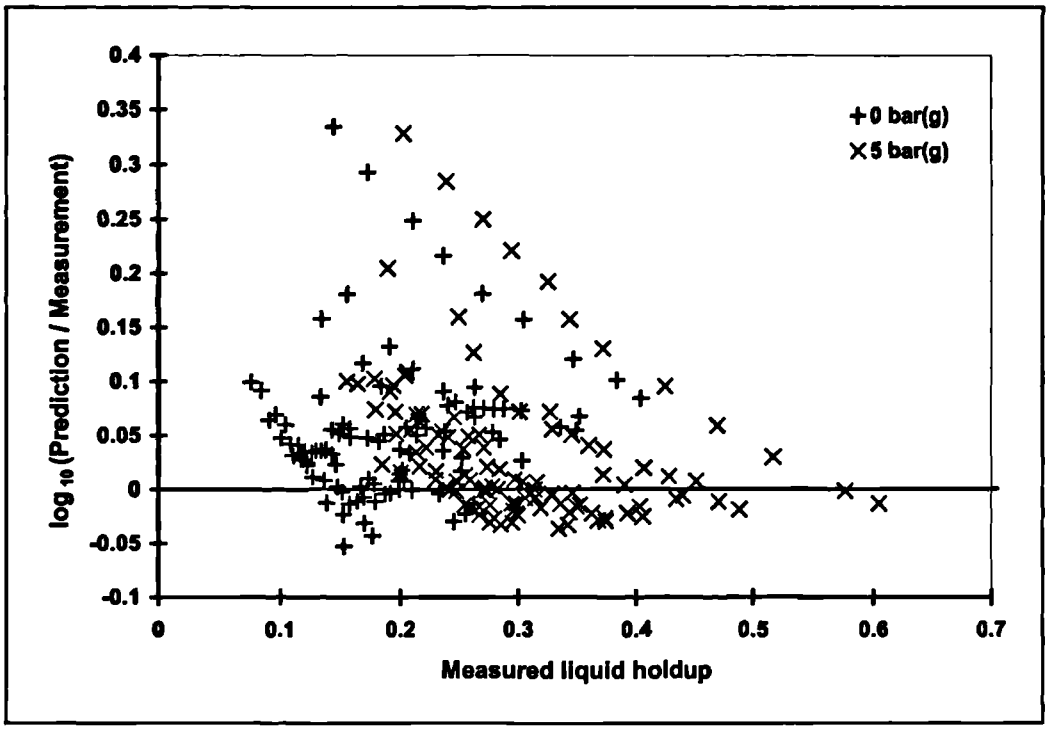

Figure 6.24: Measured liquid holdup data compared with predictions by the Premoli *et al.* (1970) correlation; 0 and 5 bar(g), -1.5° downhill limb of Λ-section

The relative performance of the correlations is compared using the mean, standard deviation and root mean square relative errors, defined in Appendix 1, and shown in Table 6.4.

	All data		0 bar(g)		5 bar(g)	
	Chisholm	Premoli	Chisholm	Premoli	Chisholm	Premoli
N	216	216	104	104	112	112
Mean	-0.015	0.084	-0.037	0.105	0.005	0.064
Std.dev	0.135	0.123	0.170	0.115	0.086	0.127
rms	0.136	0.149	0.173	0.156	0.086	0.142

Table 6.4: Relative error in liquid holdup correlations for 216 holdup measurements

Despite its simplicity, the Chisholm (1972) relationship performs well overall, and better for the data measured at elevated pressure. The Premoli *et al.* (1970) expression performs better than the Chisholm (1972) relationship at atmospheric pressure.

6.2.2. Slug length

The mean slug length obtained in these experiments is compared with other published values in Table 6.5.

	Slug length, (L_S / D)
Experimental result	14.35
Campaign 2: *V-section*	13.9
Campaign 1: *downflow*	16.3
King (1998): *horizontal*	17
Manolis (1995): *horizontal*	20
Nicholson et al. (1978)	12-30
Dukler et al. (1985)	16
Norris (1982)	82.4
Scott et al. (1986)	118.3

Table 6.5: Comparison of slug length data

As in Campaign 2 (with the "V"-section), the experimental result from this series of experiments is lower than earlier measurements using the WASP facility at Imperial College, when the WASP test-section was horizontal. Then, slug growth could occur along the entire 36 m length of pipe, however, in the present work, the distance between the top of the "peak" and the first of the conductivity probes used to calculate slug length was just 14 m. This is certainly less than the distance required for the formation of fully developed slug flow. This issue is considered further in the context of a slug tracking model, in Section 7.5 of the next Chapter.

6.2.3. Slug translational velocity

In Figure 6.25, the tail velocity data described in Section 6.1.3 is plotted against the Froude number, defined as

$$Fr = \frac{U_{Mix}}{\sqrt{gD}} \qquad [6.1]$$

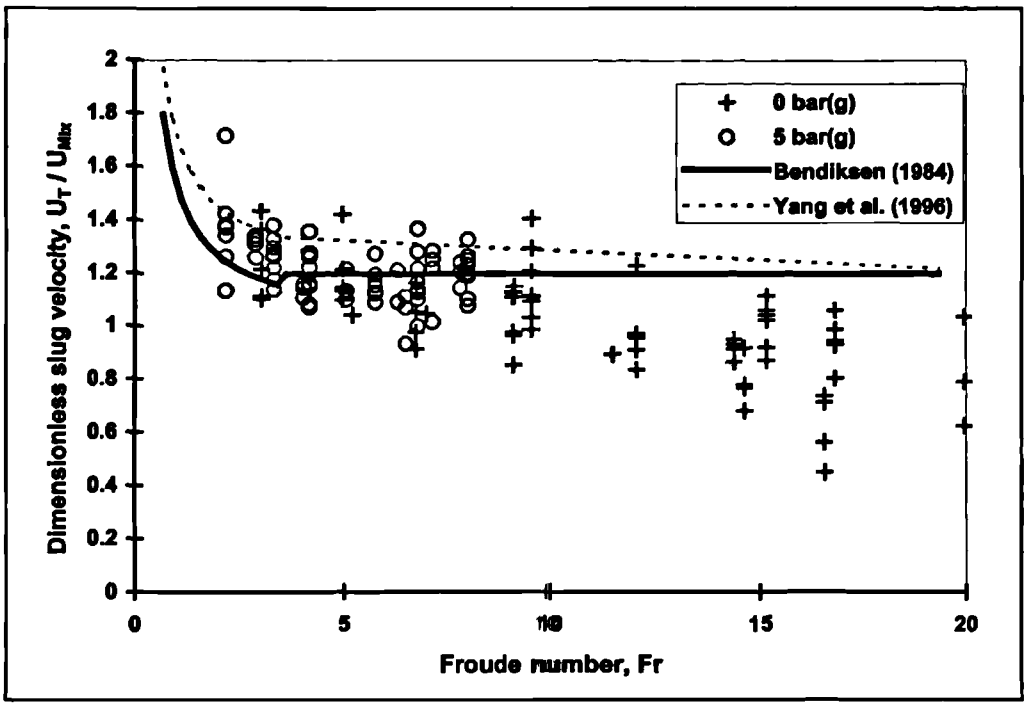

Figure 6.25: Variation of measured slug tail velociy with mixture velocity

In Figure 6.25, the 5 bar(g) data exhibit less scatter than the 0 bar(g) data. At the higher Froude numbers in the atmospheric pressure experiments, the slug translational velocity is considerably *less* than the mixture velocity, possibly due to gas breakthrough in the slug body. There is some evidence of an increase in slug translational velocity at low Froude number, particularly for the data measured at elevated pressure. The Bendiksen relationship, plotted in Figure 6.25, is intended for the prediction of *horizontal* slug flow. However, the correlation by Yang *et al.* (1996) is also shown, which includes the effect of pipe inclination. This gives a worse fit to the data than the Bendiksen correlation. The current data were measured in the downhill leg of the "Λ"-section, inclined at -1.5° to the horizontal.

In Table 6.6, comparison is made between the experimental data and predictions using the correlations of Bendicksen (1984), and Yang *et al.* (1996).

	Bendiksen (1984)	Yang et al. (1996)
Number of data points	144	144
Mean relative error in predictions	0.166	0.242
Std. deviation	0.574	0.605
Root mean square relative error	0.595	0.650

Table 6.6: Relative error in predictions from slug tail velocity correlations

The Bendiksen (1984) correlation marginally outperforms the Yang *et al.* (1996) relationship, despite the latter's inclusion of the pipe inclination. Both correlations significantly overpredict the slug translation velocity data measured in the experiments.

6.2.4. Slug frequency

The slug frequency data considered in this Section are those obtained from inspection of the liquid holdup-time traces from the gamma densitometer, reported in Section 6.1.5. The predictions from four correlations for slug frequency are compared in Table 6.7. The statistical treatment of relative error is summarised in Appendix 1.

		Gregory & Scott (1969)	Heywood & Richardson (1979)	Tronconi (1990)	Manolis *et al.* (1995a)
0 bar(g)	Mean relative error	0.352	-0.630	-0.928	0.027
	Std. deviation	0.825	0.225	0.052	0.885
(60 data points)	Root mean square relative error	0.890	0.669	0.930	0.878
5 bar(g)	Mean relative error	-0.024	-0.332	-0.884	-0.266
	Std. deviation	0.292	0.349	0.077	0.381
(44 data points)	Root mean square relative error	0.289	0.479	0.887	0.461

Table 6.7: Relative error in some slug frequency correlations (measured slug frequencies from γ-densitometer traces, 0 and 5 bar(g))

As in the results from the "V"-section experiments (see Chapter 5), the correlations perform better against the data measured at 5 bar(g) than they do against the atmospheric pressure data: this was also found by King (1998) for horizontal slug flow.

None of the correlations predicts the experimental data particularly successfully. At 5 bar(g), the Gregory & Scott (1969) expression performs best. In general, the correlations tend to *underpredict* the slug frequency.

Slug frequency data from the 5 bar(g) experiments are compared with the Gregory & Scott (1969) predictions in Figure 6.26.

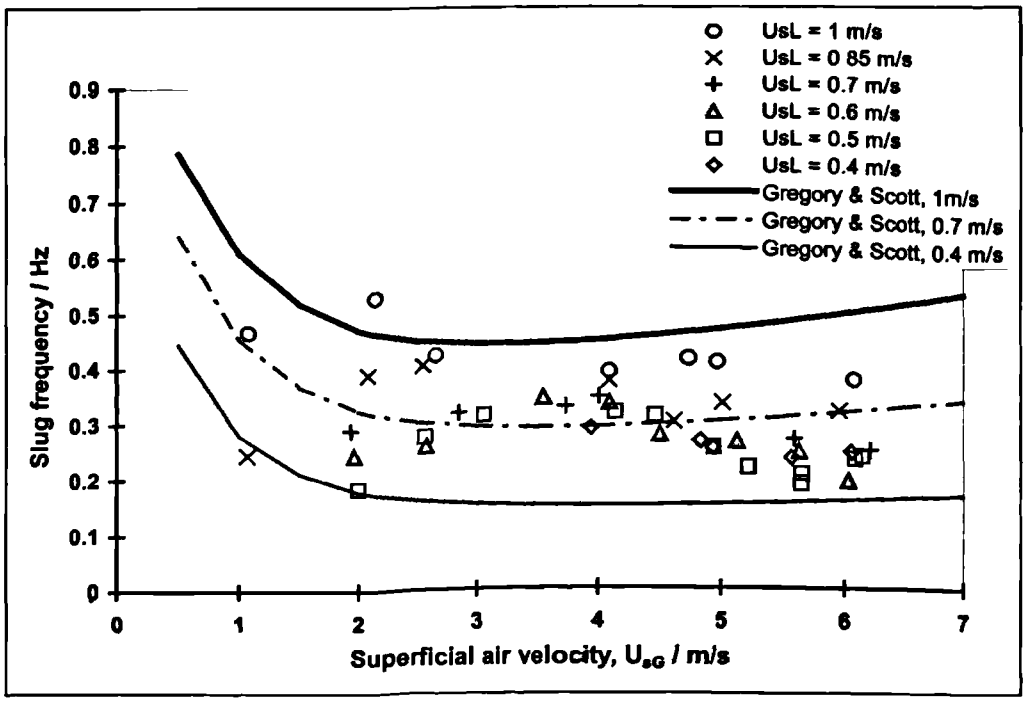

Figure 6.26: Comparison of 5 bar(g) slug frequency data with Gregory & Scott (1969) correlation

The trend shown by the data (ambiguously, a maximum) are not well-predicted by the correlation, which shows a concave shape.

6.2.5. Pressure gradient

Predictions of pressure gradient by several methods are compared with the experimental results in Table 6.8. Again, only data which were judged relatively free from drift (see Section 6.1.6) in the transducer were used. The relative error in a prediction is defined in Appendix 1. In each case, N is the number of points considered.

	Friedel (1979)		Beggs & Brill (1973)		Taitel & Barnea (1990)	
Pressure / bar(g)	0	5	0	5	0	5
N	52	39	52	39	52	39
Mean relative error	0.714	0.875	0.713	0.001	0.249	0.226
Std. deviation	0.171	0.342	0.681	3.645	0.209	0.358
Root mean square relative error	0.734	0.938	0.982	3.598	0.324	0.420

Table 6.8: Comparison of relative error in pressure gradient predictions

At both 0 and 5 bar(g), the phenomenological model of Taitel & Barnea (1990) gives a significantly better prediction of the experimental data than the two correlations.

All methods tend to overpredict the experimental results; the overprediction is considerably worse at elevated pressure.

The pressure gradient data are shown together with predictions by the Taitel & Barnea (1990) model in Figures 6.27 – 6.30

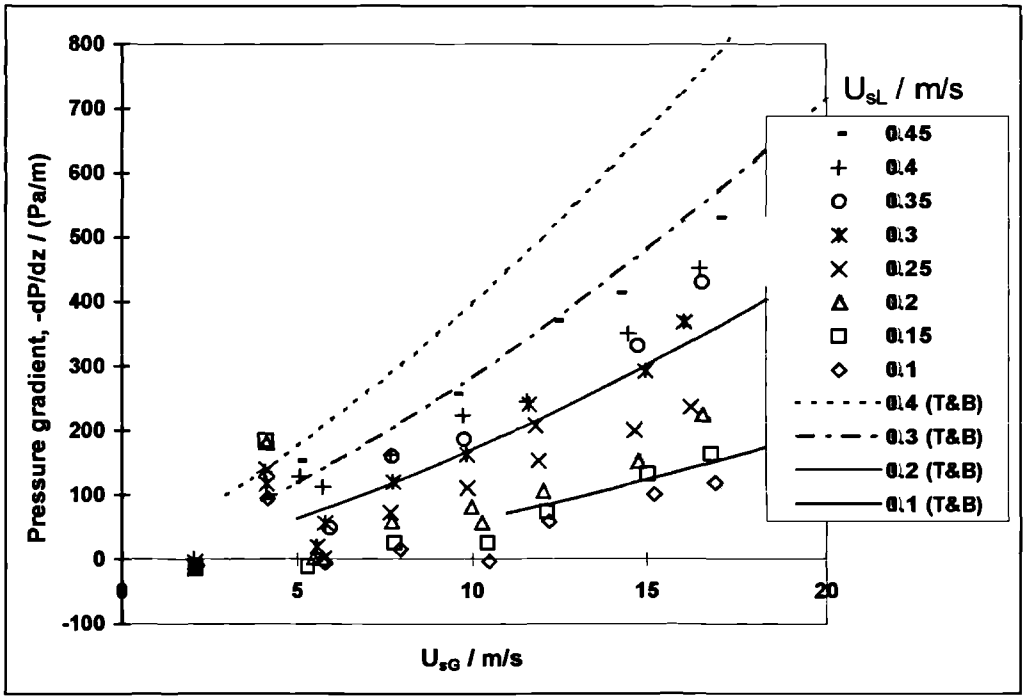

Figure 6.27: Pressure gradient data measured at 0 bar(g), showing predictions by Taitel & Barnea (1990) model ($0.1 < U_{sL} < 0.45$ m/s)

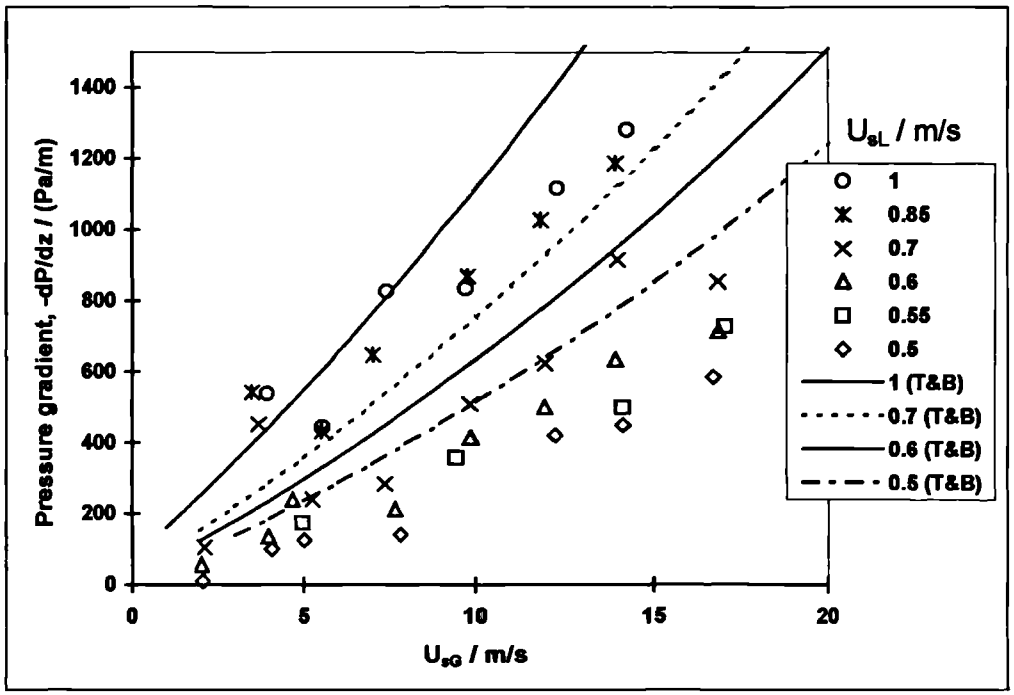

Figure 6.28: Pressure gradient data measured at 0 bar(g), showing predictions by Taitel & Barnea (1990) model ($0.5 < U_{sL} < 1.0$ m/s)

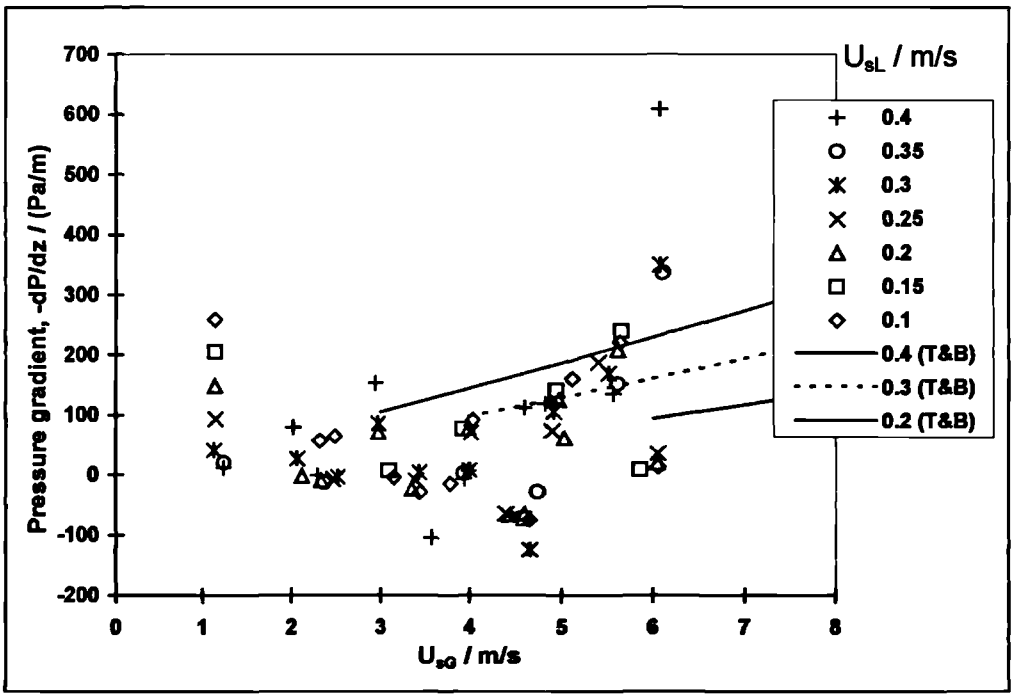

Figure 6.29: Pressure gradient data measured at 5 bar(g), showing predictions by Taitel & Barnea (1990) model ($0.1 < U_{sL} < 0.4$ m/s)

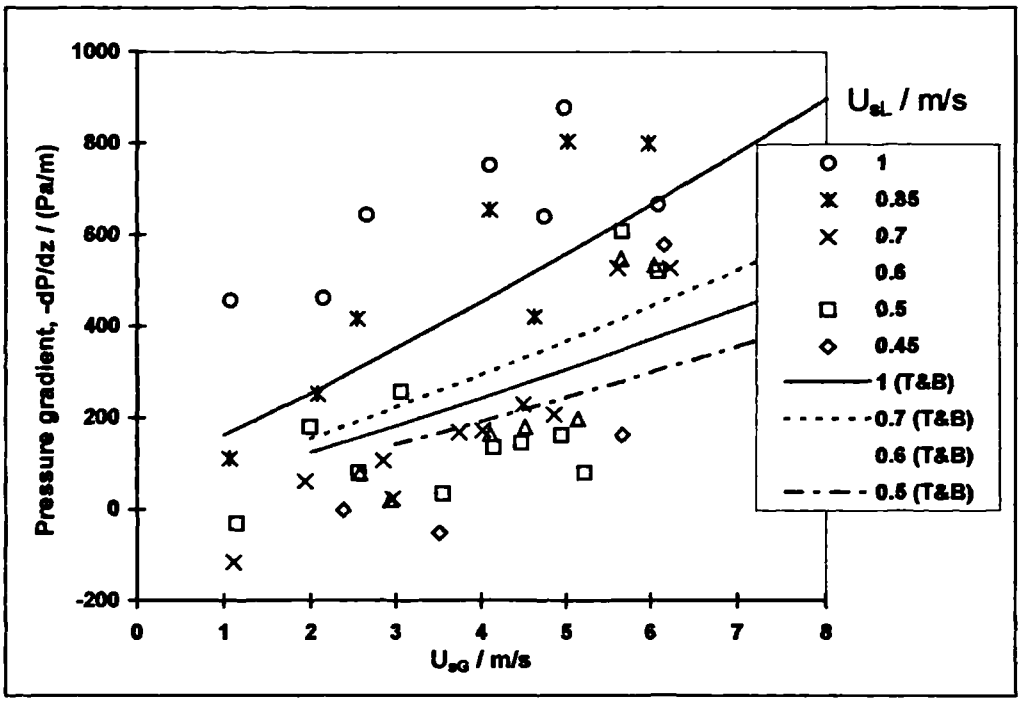

Figure 6.30: Pressure gradient data measured at 5 bar(g), showing predictions by Taitel & Barnea (1990) model ($0.45 < U_{sL} < 1.0$ m/s)

The pressure gradient data are compared with the Beggs & Brill (1979) correlation in Figure 6.31. When compared with Figure 6.28, it is clear that the trends predicted by the two methods are not the same; the Beggs & Brill trend is convex, whereas Taitel & Barnea's (1990) method predicts a concave shape. It is unclear from the experimental data which is the more accurate trend.

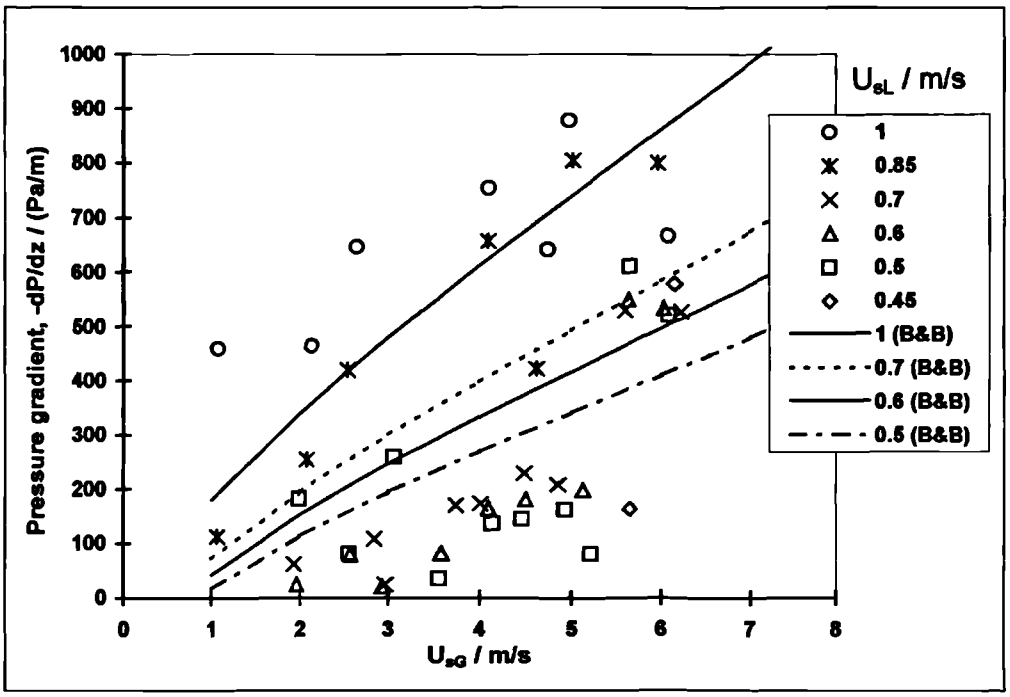

Figure 6.31: Pressure gradient data measured at 0 bar(g), showing predictions by Beggs & Brill (1979) correlation ($0.5 < U_{sL} < 1.0$ m/s)

6.3. Summary

In this Chapter, a large set of experimental data has been presented, for two-phase flow in a ±1.5° "Λ"-section. As in the first two experimental campaigns (reported in Chapters 4 and 5 of the present work), measurements of superficial gas and liquid velocities, liquid holdup at five points in the test-section and pressure gradient were obtained. The holdup measurements were analysed to yield values of slug length, slug frequency and slug tail velocity.

It was found that, in the downhill limb of the "Λ"-section, flow pattern maps measured at the pipe exit showed an increase in the size of the slug flow regime compared with purely downhill flow (described in Chapter 4). This was attributed to the formation of slugs in the rising limb of the "Λ"-section and their persistence into the downhill limb. The relatively short length of pipe between the apex of the Λ-section and the pipe exit was unlikely to provide sufficient distance for the collapse of these slugs and the establishment of a purely "downhill" flow pattern map. "Stratified smooth" flow was not observed at the end of the pipe. Instead, this regime was affected by low amplitude, low frequency "surges" in the thickness of the stratified film. This was caused by the collapse of short slugs and the coalescence of interfacial waves in the downward limb of the "Λ"-section.

The measured data were compared with several correlations and models from the literature. Generally, as has been found throughout the present work, correlations for slug parameters and pressure drop did not predict the experimental data with great accuracy. The slug translational velocity data (measured in the downhill limb of the "Λ"-section) exhibited particularly poor agreement with the correlations of Bendiksen (1984) and Manolis (1995) at high Froude numbers, with measured slug translational velocities rather *less* than the mixture velocity. This trend was also observed for purely downhill flow, at the same inclination as the current series of experiments, as described in Chapter 4 of the present work. The effect could be due to gas breakthrough in the slug body.

Chapter 7: A quasi-steady state model of slug flow

The development of a quasi-steady state, one-dimensional slug flow model is described in this Chapter. The underlying principles behind the model are presented, as are the closure relationships which are included. A summary is given of the different "events", *i.e.* interactions between slug and wave objects, which the model can currently handle. A description of the algorithm used to implement the model is presented. The assumptions made, and the resulting limitations and inaccuracies, are highlighted.

An important result is that realistic slug length distributions and frequencies are obtained as output from the model when very short, very high-frequency "precursor" slugs are introduced at the start of the pipe. However, this is not true in all cases, as is discussed further in Sections 7.4.4 and 7.4.5.

Slug tracking using a one-dimensional slug flow model is a useful tool which allows calculation of slug characteristics (length, velocity, frequency *etc.*) at a given point in a pipeline from the history of the flow conditions upstream. If sufficiently detailed phenomenological models are used to calculate the propagation of the slugs, and their interactions with each other and with interfacial waves in the region of the slug unit, then it can be shown (*e.g.* King, 1998) that a slug tracking model can reproduce experimental slug flow data with reasonable accuracy.

The disadvantage of the slug tracking approach is the computational effort required to calculate the progression of a large number of slugs and waves through a system. The simplest method of slug tracking uses the front and tail velocities of slugs and waves to propagate them along the pipe; this requires just two "nodes" for each slug or wave.

However, the situation is made more complex if a gas entrainment model is used to account for the pickup of gas at the front of a liquid slug, in which case the liquid holdup in a slug body may change with time. This causes variation in the shape of the liquid film profile to the rear of the slug, which in turn changes the conditions at the front of the next slug upstream. King (1998) took account of this by recalculating the liquid film profile for each slug at each time step. Taitel & Barnea (1998) used the approximation of a flat liquid film behind each slug, with a film holdup calculated from the equilibrium film height for the

equivalent stratified flow case. If the film region is very long, and the flow is nearly steady, the tail profile asymptotically approaches this equilibrium film height.

The work described in this Chapter uses the one-dimensional quasi-steady state slug tail profile methodology proposed by Taitel & Barnea (1990) as a basis for calculating the film parameters of each slug tail. These values are then used to obtain the propagation velocity of each slug, in a similar manner to the approach of King (1998). However, the quasi-steady state assumption is further used to avoid the need to calculate the film profile for each slug at each time step. Thus, film profiles for a range of slug liquid holdups and tail velocities are calculated once only and then stored in a lookup-table, from which the film parameters used in the slug propagation algorithm are then obtained. This considerably reduces computation time compared to the method of King (1998) whilst retaining exactly the same level of detail in the model.

In what follows, Sections 7.1 and 7.2 describe the physical principles and closure relationships incorporated in the model and the procedure for treating the allowed slug/wave interaction "events". In Section 7.3, a description is then given of the algorithm used to implement the model. Some results are presented in Section 7.4 for horizontal and near-horizontal flows for several different flow conditions. The results of a systematic study of the effects of inlet conditions are also presented.

7.1. Description of the model

Figure 7.1 shows a representation of two neighbouring slugs. The front and tail positions of slug i are denoted by X_i and Y_i, with $U_{Fi} = \dot{X}_i$ and $U_{Ti} = \dot{Y}_i$, the respective front and tail velocities. u_{LS} and u_{GS} are respectively the mean liquid and gas velocities in the slug body and ε_{LSi} is the liquid holdup within the body of slug i. The lengths of the slug body and film region of slug unit i are respectively L_{Si} and L_{Fi}.

The liquid film holdup and mean velocity at the end of the film behind slug i are denoted by ε_{LFi} and u_{LFi} respectively. These are the values which are "seen" by the front of the next slug immediately upstream.

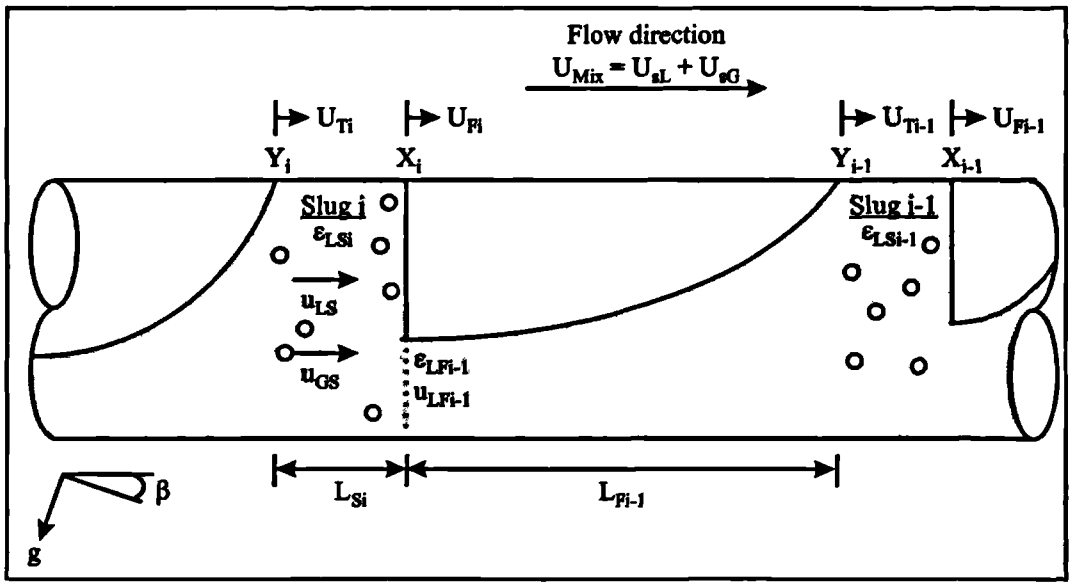

Figure 7.1: General notation for the slug flow model

The average superficial liquid and gas velocities in the pipe are U_{sL} and U_{sG} respectively and their sum, U_{Mix}, is the mixture velocity (also referred to as the total superficial velocity). We consider a long, straight section of circular pipe of constant diameter D and area A, inclined to the horizontal at angle β, so that positive β denotes upwardly-inclined flow. In the coordinate system used, the x-axis is directed along the centreline of the pipe in the downstream direction, with x = 0 at the pipe inlet.

7.1.1. Basic equations

The subscripts L and G denote liquid and gas respectively, with S and F similarly denoting the slug and film regions. The subscript i denotes the label of slug i. Thus, the phase holdups in the slug and film regions are related by

$$\varepsilon_{GSi} + \varepsilon_{LSi} = 1 \qquad [7.1]$$

and

$$\varepsilon_{GFi} + \varepsilon_{LFi} = 1 \qquad [7.2]$$

The mixture velocity, is constant throughout the system (incompressible flow is assumed). Thus,

$$U_{Mix} = u_{LS}\varepsilon_{LSi} + u_{GS}\varepsilon_{GSi} \qquad [7.3]$$

and

$$U_{Mix} = u_{LFi}\varepsilon_{LFi} + u_{GFi}\varepsilon_{GFi} \quad [7.4]$$

The front position of slug i is propagated along the pipe using the slug front velocity U_{Fi}. This is obtained from a local mass balance across the front region of slug i. If $\dot{M}_{LP_i}$ is defined as the rate of liquid mass pickup by slug i, then,

$$\dot{M}_{LPi} = \rho_L \varepsilon_{LSi} A(U_{Fi} - u_{LS}) \quad [7.5]$$

and

$$\dot{M}_{LPi} = \rho_L \varepsilon_{LFi-1} A(U_{Fi} - u_{LFi-1}) \quad [7.6]$$

where ρ_L is the liquid density, so that U_{Fi} may be obtained by solution of Equations [7.5] and [7.6]. Eliminating $\dot{M}_{LP_i}$ from Equations [7.5] and [7.6], we obtain:

$$U_{Fi} = \frac{u_{LS}\varepsilon_{LSi} - \varepsilon_{LFi-1}u_{LFi-1}}{(\varepsilon_{LSi} - \varepsilon_{LFi-1})} \quad [7.7]$$

Similarly, U_{Fi} may be eliminated from Equations [7.5] and [7.6] to obtain:

$$\frac{\dot{M}_{LPi}}{\rho_L} = \frac{A(u_{LS} - u_{LFi-1})}{(1/\varepsilon_{LFi-1} - 1/\varepsilon_{LSi})} \quad [7.8]$$

Thus, if the values of u_{LSi}, u_{LFi-1}, ε_{LFi-1} and ε_{LSi} are known then both the slug front velocity and the liquid pickup rate may be calculated. In the present model, it is assumed that gas and liquid are picked up simultaneously at the front of the slug and are shed together at its tail. The liquid holdup in the slug is assumed to correspond to that of a homogenous mixture of the gas and liquid picked up at the slug front. Thus, ε_{LSi} is given by

$$\varepsilon_{LSi} = \frac{(\dot{M}_{LPi}/\rho_L)}{(\dot{M}_{LPi}/\rho_L + \dot{V}_{GPi})} \quad [7.9]$$

where $\dot{V}_{GPi}$ is the volumetric gas pickup rate at the slug front. This is obtained from a closure relationship, discussed in Section 7.1.3 below. This homegenous mixture is continually added to the front of the slug and shed from its tail.

The values of ε_{LFi-1} and u_{LFi-1} depend on the distance from the previous slug (see Figure 7.1), and are calculated using the analysis of Taitel & Barnea (1990). The rate at which liquid is shed from the slug tail is given by

$$\dot{M}_{LSi} = \rho_L \varepsilon_{LSi} A (U_{Ti} - u_{LS}) \qquad [7.10]$$

where U_{Ti} is the tail velocity of slug i. The shed liquid slows down in the film region (and may even reverse in flow direction for the case of an upwardly-inclined pipe). The velocity of the liquid in the film region is given by:

$$u_{LF} = U_T - \frac{\dot{M}_{LSi}}{\varepsilon_{LF} \rho_L A} \qquad [7.11]$$

At the tail of slug i, (position Y_i in Figure 7.1), combination of Equations [7.10] and [7.11] gives $u_{LF} = u_{LSi}$ as expected.

The shedding rate is used to obtain the slug tail profile. In their 1990 work, Taitel & Barnea presented three models for gas-liquid slug flow. The most elaborate involves calculation of the liquid film profile extending upstream from the tail of the slug. The one-dimensional mass and momentum balances result in the following expression for the profile behind slug i:

$$\frac{-dh_{LF}}{dz} = \frac{\frac{\tau_L S_L}{A_L} - \frac{\tau_G S_G}{A_G} - \tau_I S_I \left(\frac{1}{A_L} + \frac{1}{A_G} \right) + (\rho_L - \rho_G) g \sin\beta}{(\rho_L - \rho_G) g \cos\beta - \rho_L (U_{Ti} - u_{LF}) \frac{(U_{Ti} - u_{LSi}) \varepsilon_{LSi}}{\varepsilon_{LF}^2} \frac{d\varepsilon_{LF}}{dh_{LF}} - \rho_G (U_{Ti} - u_{GF}) \frac{(U_{Ti} - u_{GSi})(1 - \varepsilon_{LSi})}{(1 - \varepsilon_{LF})^2} \frac{d\varepsilon_{LF}}{dh_{LF}}} \qquad [7.12]$$

where h_{LF} is the liquid film height and ε_{LF} is the liquid film holdup a distance z upstream from the slug tail, τ_L is the liquid wall shear stress, τ_G is the gas wall shear stress, τ_I is the interfacial shear stress, S_L is the length of the wetted perimeter of the liquid region, S_G is the length of the perimeter of the gas region, S_I is the length of the chordal gas-liquid interface, A_L and A_G are the cross-sectional areas of the liquid and gas regions respectively, ρ_G is the gas density and g is the acceleration due to gravity. In Equation [7.12], u_{LSi} and u_{GSi} are assumed equal to the mixture velocity (the "no-slip" assumption, see below). The gas velocity in the film region, u_{GF}, is given by:

$$u_{GF} = \frac{(U_{Mix} - \varepsilon_{LF} u_{LF})}{(1 - \varepsilon_{LF})} \qquad [7.13]$$

u_{LF} is related to ε_{LF} and U_T via Equations [7.10] and [7.11]. Thus, apart from U_T and the shear stresses τ_L, τ_G and τ_i (for which closure laws are required; see below), and the fluid densities, the acceleration due to gravity and the pipe inclination (which are known), all other variables in Equation [7.12] can be related uniquely to h_{LF}, the liquid film height. Thus, Equation [7.12] can be solved to give h_{LF} as a function of distance upstream from the slug tail.

The solution procedure for Equation [7.12] is described in detail in Chapter 2 of the present work. The geometric relationships required for the solution are given in the same Chapter. The necessary closure relationships are outlined in Sections 2.2 and 2.3 respectively.

7.1.2. Key simplifying approximations

A number of simplifying approximations are made in the model.

Separated flow

Gas-liquid slug flows are highly complex. Accurate modelling of these flows requires a description of the non-uniform interface shape, which has a great bearing on the interphase momentum transfer. Here, the assumption is made that the flow is largely separated: in the film region, the liquid and gas behave as a stratified flow, with no aeration of the liquid film and no entrained liquid droplets in the gas flow. This assumption has the corollary that instantaneous, perfect separation of gas and liquid must occur at the end of the slug body. More realistically, it is likely that the region where separation occurs is quite short. It is likely that Equation [7.12] is a very poor approximation in this region: the shape of the slug tail differs greatly in practice from that calculated from Equation [7.12]. The bubble nose moves towards the centre of the pipe as the fluid velocity is increased (see Section 8.4.1) and the shed liquid drains from the top of the tube into the liquid film in a complex manner. The detailed shape for the slug tail has been obtained (Pan, 1996; Manfield *et al.*, 1999) using a three-dimensional computational fluid dynamics model. This is discussed in Section 8.5.2 of the present work. However, this approach is not well suited to a one-dimensional slug tracking model.

No slip

The simplification is made that there is no "slip" in the slug body, *i.e.* the slip ratio is unity. Thus,

$$u_{LS} = u_{GS} = U_{Mix} \qquad [7.14]$$

The gas and liquid picked up at the slug front are assumed to be mixed into a homogeneous bubbly mixture which is continuously added to the slug front. This process of acretion causes the slug front to move at a velocity greater than the mixture velocity. However, the gas-liquid mixture (assumed uniform throughout the slug) is shed continuously at the tail. Thus, in a fully developed slug flow, the pickup and shedding rates are equal. In the scheme developed here, this is not necessarily true since the slug front and tail velocities are considered independently, so that slug growth and collapse effects are included.

Instantaneous propagation of information

It is assumed that the slug body holdup is constant throughout each slug. Since ε_{LSi} is determined by the rate of gas entrainment at the front of slug i, which is in turn a function of the film holdup and velocity immediately in front of slug i, then the holdup of slug i may vary with time. Changes are therefore passed instantaneously along the slug, and thus cause an immediate variation in the film behind slug i, which is instantaneously "seen" by the next slug upstream, and so on. It has been found that, as long as changes are gradual, the effect is small and diminishes as it propagates upstream.

Flat gas-liquid interface

The gas-liquid interface in the film region is assumed to be flat across the cross section of the pipe. This leads to several useful geometric relationships, which are shown in Figure 2.2 in Chapter 2.

7.1.3. Closure relationships

The mass and momentum balances used in the model require a number of external relationships to "close" the system of equations. Expressions are required for the gas and liquid wall shear stresses and the gas-liquid interfacial shear stress in the film region, to calculate the variation of liquid velocity and holdup along the film. An expression for the liquid wall shear stress in the slug is needed to calculate the pressure gradient within each slug and hence the pressure drop along the pipe. Additionally, an expression for slug tail velocity is required to obtain the liquid mass shedding rate, and a correlation is used to calculate the gas entrainment rate which determines the slug body holdup.

Shear stresses

Classical single-phase flow correlations are used to obtain the gas and liquid wall shear stresses in the film region. Here, the gas and liquid-phase friction factors are given by the Blasius relationships. The interfacial friction factor is calculated using the correlation of Andritsos & Hanratty (1987). These expressions are described in Section 2.3.1 of Chapter 2.

Slug tail velocity

The tail velocity of a slug, U_T varies in a complex was with mixture velocity (see, for example, Figure 6.25). At low mixture velocities, the ratio (U_T / U_{Mix}) falls with increasing mixture velocity but then, according to most relationships available in the literature (*e.g.* Bendiksen, 1984), the ratio attains a value of around 1.2 which is independent of mixture velocity. At higher velocity, gas may "break through" the slug body and (U_T / U_{Mix}) may become less than unity. In the present model, it is assumed that (U_T / U_{Mix}) = 1.2 *for slugs of sufficient length*. This covers the range of main practical application. The qualification "for slugs of sufficient length" is introduced since, in developing slug flow, slugs of much smaller length than found in fully developed slug flow are encountered. These slugs may have a higher velocity than those with the normal (fully developed) length range.

Recent work has shown that, for short slugs, U_T increases with decreasing slug length (Fagundes Netto *et al.*, 1998, 1999a, 1999b; Cook & Behnia, 2000). This effect has also been demonstrated using three-dimensional computational fluid dynamics (CFD) modelling of a single liquid slug, which is described in Chapter 8 of the present work. To describe developing slug flow it is necessary to take account of this effect.

Figure 7.2 shows data by Fagundes Netto *et al.* (1998) for (U_T / U_{Mix}) as a function of (L_S / D). The experimental data are bounded but fits used previously tend towards an infinite value of U_T as $L_S \rightarrow 0$. However, this is physically unreal and so in the current work the function for (U_T / U_{Mix}) has been bounded with the values of 1.2 and 1.4 at the upper and lower ends of the slug length range, respectively.

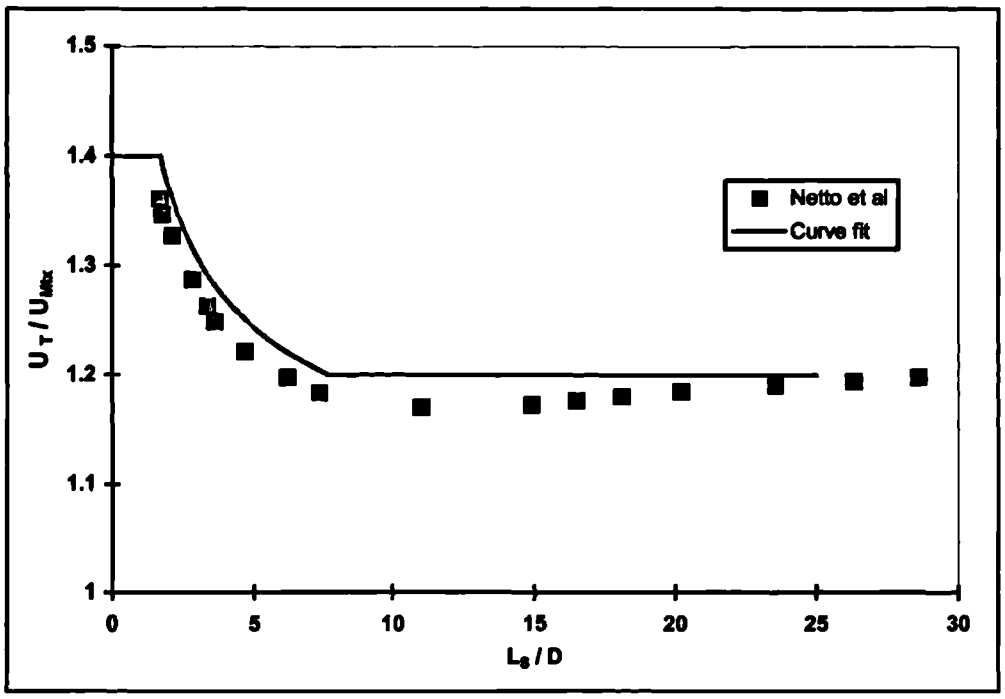

Figure 7.2: Variation of slug length *vs.* tail velocity plot, after Fagundes Netto *et al.* (1998)

The function fitted to the data is as follows:

$$\begin{aligned} U_T &= 1.4U_{Mix} && \left(\frac{L_S}{D}\right) \le 1.696 \\ U_T &= U_{Mix}\left(1+0.51\left(\frac{L_S}{D}\right)^{-0.46}\right) && 1.696 < \left(\frac{L_S}{D}\right) \le 7.575 \\ U_T &= 1.2U_{Mix} && \left(\frac{LS}{D}\right) > 7.575 \end{aligned} \qquad [7.15]$$

Gas entrainment and slug body holdup

The liquid holdup in the slug body, ε_{LSi}, is required for the calculation of the slug front velocity and also the liquid shedding rate at the slug tail. This may be specified using a slug holdup correlation, which gives the value as a function of U_{Mix}. In this case the slug body holdup is the same for all slugs and is constant in time. Alternatively, a gas entrainment model may be used to calculate the rate of gas pickup at the front of the slug as a function of the film parameters immediately ahead of the slug. In this case, the slug body holdup can be different for each slug, and furthermore may change with time due to any variation of the height and velocity of the film ahead of the slug.

In this work, the first method is used to specify the holdup of the first slug in the system (denoted as slug 0), to initialise the model and provide information for subsequent slugs. The correlation chosen is that by Gregory *et al.* (1978):

$$\varepsilon_{LS0} = \frac{1}{1+\left(\frac{U_{Mix}}{8.66}\right)^{1.39}} \qquad U_{Mix} < 9.17 ms^{-1}$$

$$\varepsilon_{LS0} = 0.48 \qquad U_{Mix} \geq 9.17 ms^{-1} \qquad [7.16]$$

For subsequent slug propagation, the gas entrainment correlation of Manolis (1995) is used. This relationship, similar in form to that of Nydal and Andreussi (1991) but regressed from data obtained from the Imperial College WASP facility, relates the slug body holdup (derived from a consideration of the rate of gas pickup at the slug front) to the relative velocity of the slug front and liquid film, and the length of the chordal gas-liquid interface in front of the slug, S_I (which is assumed to be flat):

$$\frac{\dot{V}_{GF}}{A} = 0.14576\frac{S_I}{D}((U_F - u_{LF}) - U_{Man}) \qquad [7.17]$$

The value U_{Man}=2.1265 m/s corresponds to the relative velocity ($U_F - u_{LF}$) below which no gas entrainment occurred. To obtain the slug front velocity and slug body holdup, Equation [7.17] is solved iteratively with Equations [7.5], [7.6] and [7.13].

7.2. Events that may occur in a simulation

As well as the continuous advancement of the positions of slugs and waves, and the recalculation of their holdups and velocities at each time step, a slug tracking model must additionally be able to handle certain discrete "events". In this work, the following events are allowed:

- Slug enters pipe
- Slug leaves pipe
- Slug becomes a wave
- Slug overtakes a wave
- Slug catches a slug

In what follows, a brief description of each event is given, along with an explanation of how the event is handled by the model.

Slug enters pipe

The work presented in this Chapter does not use a slug initiation model to describe the growth of slugs from perturbations on a stratified liquid film near the inlet region of the pipe, neither is a correlation used for slug frequency or slug length. Such methodologies are described in an exhaustive work by Hale (2000).

In this work, two alternative methods have been used. In the first, a mean time interval between the "injection" of slugs into the pipe is set, and a list of "injection times" is then calculated by the code, with a specified degree of random variation. In the results presented here, a time interval of Δt is specified, with successive slugs injected at intervals of $\Delta t + \Delta t_{Random}$, where Δt is the mean time interval and Δt_{Random} is uniformly distributed in the range $\pm 0.35\Delta t$. At each time step, a check is made of the injection time of the latest slug "awaiting" injection to see if it should be allowed to proceed. If so, then the front position of the slug is advanced at the calculated front velocity, and the tail position is "held back" until the front position has advanced to an "initial slug length", L_{In}, which is also specified in the model. Once the initial slug length is reached, the slug tail is advanced at speed U_{Ti} and checking starts for the injection time of slug i+1. With this method, all of the slugs have the same initial length L_{In}.

This method has led to the useful result that if a large number of very short slugs (length of order 2D) are injected at high frequency (of order 4 Hz) then a very high proportion of the slugs shrink to become slow-moving waves within a few meters of the pipe entrance region. These waves contain the necessary mass for the rapid growth of the few remaining slugs. Thus initiation of large slugs is allowed to occur by a Darwinian "survival of the fittest" process.

The disadvantage of this scheme is that the individual superficial phase velocities are not known *a priori* and must be calculated after the simulation has finished, from the slug body holdup (if a slug is present at the inlet), or from the film holdup and velocity, at the inlet. Only the mixture velocity is known with certainty when the simulation is started. This is clearly a major limitation, and so an alternative method was devised in order that the user could specify the true values of U_{sL} and U_{sG} which would be used by the simulation. In this,

the user specifies a mean and standard deviation for the lengths of the "inlet slugs" and a matrix of slug lengths is calculated by the code, using a normal distribution. After a slug is "launched", the true velocities are calculated by time-averaging the conditions at the pipe inlet from the instant when the slug front was introduced into the pipe. When the time-averaged velocities reach the specified values, the next slug is launched and the time-averaging process is restarted.

The time-averaging procedure is described below for the calculation of the liquid superficial velocity. If a slug body is present at the pipe inlet then the volumetric liquid flow rate is

$$\dot{V}_{LS} = u_{LS}\varepsilon_{LS}A \qquad [7.18]$$

otherwise, a film region is present at the inlet so that

$$\dot{V}_{LF} = u_{LF}\varepsilon_{LF}A \qquad [7.19]$$

Thus, if u_{LS} is set to zero unless a slug is present at the inlet, and u_{LF} is set to zero unless a film region is at the inlet, then the total volumetric liquid flow is

$$\dot{V}_{L} = (u_{LS}\varepsilon_{LS} + u_{LF}\varepsilon_{LF})A \qquad [7.20]$$

so that, in a period of t seconds, the total inlet liquid volume is

$$V_{L} = A\int_{t=0}^{t}(u_{LS}\varepsilon_{LS} + u_{LF}\varepsilon_{LF})dt \qquad [7.21]$$

and the time-averaged liquid superficial velocity is

$$U_{sL} = \frac{1}{t}\int_{t=0}^{t}(u_{LS}\varepsilon_{LS} + u_{LF}\varepsilon_{LF})dt \qquad [7.22]$$

Using the simplifying assumptions of no slip (Equation [7.14]) and constant mixture velocity ($U_{Mix} = U_{sL} + U_{sG}$) throughout the system, then

$$U_{sL} = \frac{1}{t}\int_{t=0}^{t}(U_{Mix}\varepsilon_{LS} + u_{LF}\varepsilon_{LF})dt \qquad [7.23]$$

For N discrete time steps of Δt seconds, [7.23] is approximated as

$$U_{sL} \approx \frac{1}{N\Delta t}\sum_{i=1}^{N}\left[(U_{Mix}\varepsilon_{LS} + u_{LF}\varepsilon_{LF})\Delta t\right]_{i} \qquad [7.24]$$

Slug leaves pipe

A slug is deemed to have left the pipe when its tail position is beyond the specified pipe length. At this instant, the film parameters (holdup and velocity) immediately in front of the next slug or wave upstream are recorded, and used to derive the front velocity of that object, and the shape of its film profile, until the next object reaches the end of the pipe.

Slug becomes a wave

In the case where a slug's tail velocity is greater than its front velocity, the slug length becomes smaller. This effect is enhanced by the use of a variable slug tail velocity (see Section 7.1.3) which causes the rate of slug shrinkage to become greater with decreasing slug length. When the slug tail position overtakes the slug front, the positions are set to be equal and the slug is then propagated as a wave, with an initial wave holdup equal to the slug body holdup at the instant of slug collapse.

The physics of wave propagation are not incorporated in the model described in the present work. Instead a very crude algorithm is used to propagate the waves and make sure that their mass is conserved. Waves are generally short-lived, since they propagate slowly and are rapidly overtaken by slugs, so this use of a crude wave model still gives reasonable results for the slugs themselves.

The wave velocity (i.e. the velocity at which the wave front and back positions are advanced) is set equal to the film velocity immediately in front of the wave. The liquid height is then varied along the wave profile, but there is no variation in liquid film velocity. Thus, at all points in the wave profile, the liquid film is assumed to be moving at the wave front velocity, *i.e.* the wave is effectively propagated as a rigid body (but see also Section 7.3.3). Thus there is a sudden (albeit small) change in the liquid film velocity at all points along the wave profile at the instant of wave formation, and momentum is no longer conserved between the wave front and the front of the next slug upstream.

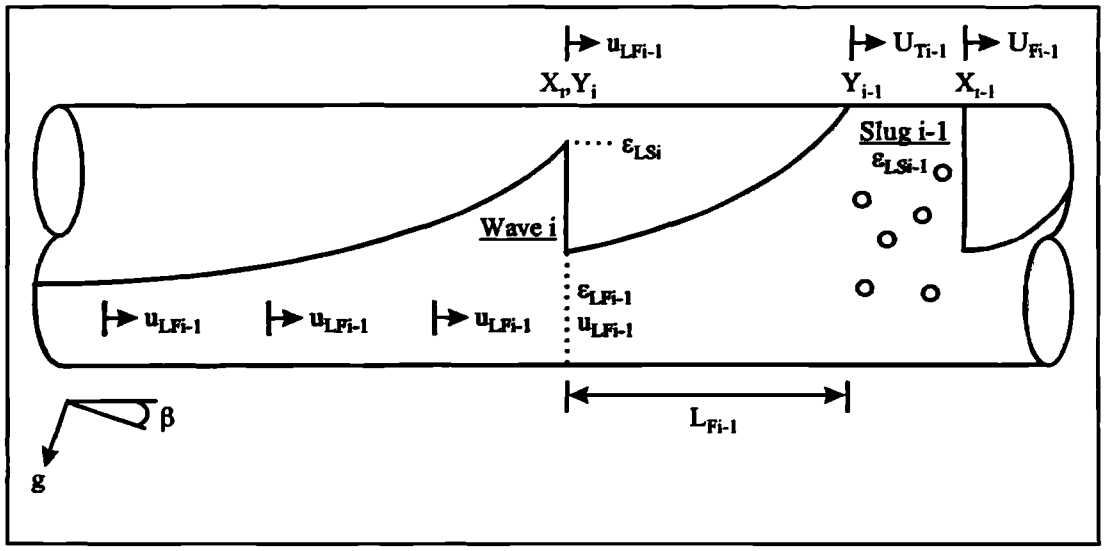

Figure 7.3: Wave formation at the instant when Y_i becomes equal to X_i

Figure 7.3 shows the situation where a slug (i) has just collapsed to become a wave. The wave i is assumed to be unaerated, and propagating at speed u_{LFi-1}. In the case where the next object upstream (i+1) is a slug, then wave i would be quickly overtaken by slug i+1. In the event of two or more waves following in succession, they are assumed to **all** propagate at the velocity of the liquid film immediately in front of the **leading wave** in the group.

Slug overtakes a wave

When a slug is propagating behind a wave (see Figure 7.4) it generally moves faster than the wave velocity. When the slug front reaches the position of the wave front then the model must account for the "merging" of the slug and wave. This is handled using an object-oriented approach, whereby the wave object is "killed" at the instant when a slug overtakes it, and removed from the list of "live" objects which are propagated by the model. This greatly simplifies the accounting process necessary to identify the location and state of each object during the simulation, and also avoids the need to renumber each object after an interaction event.

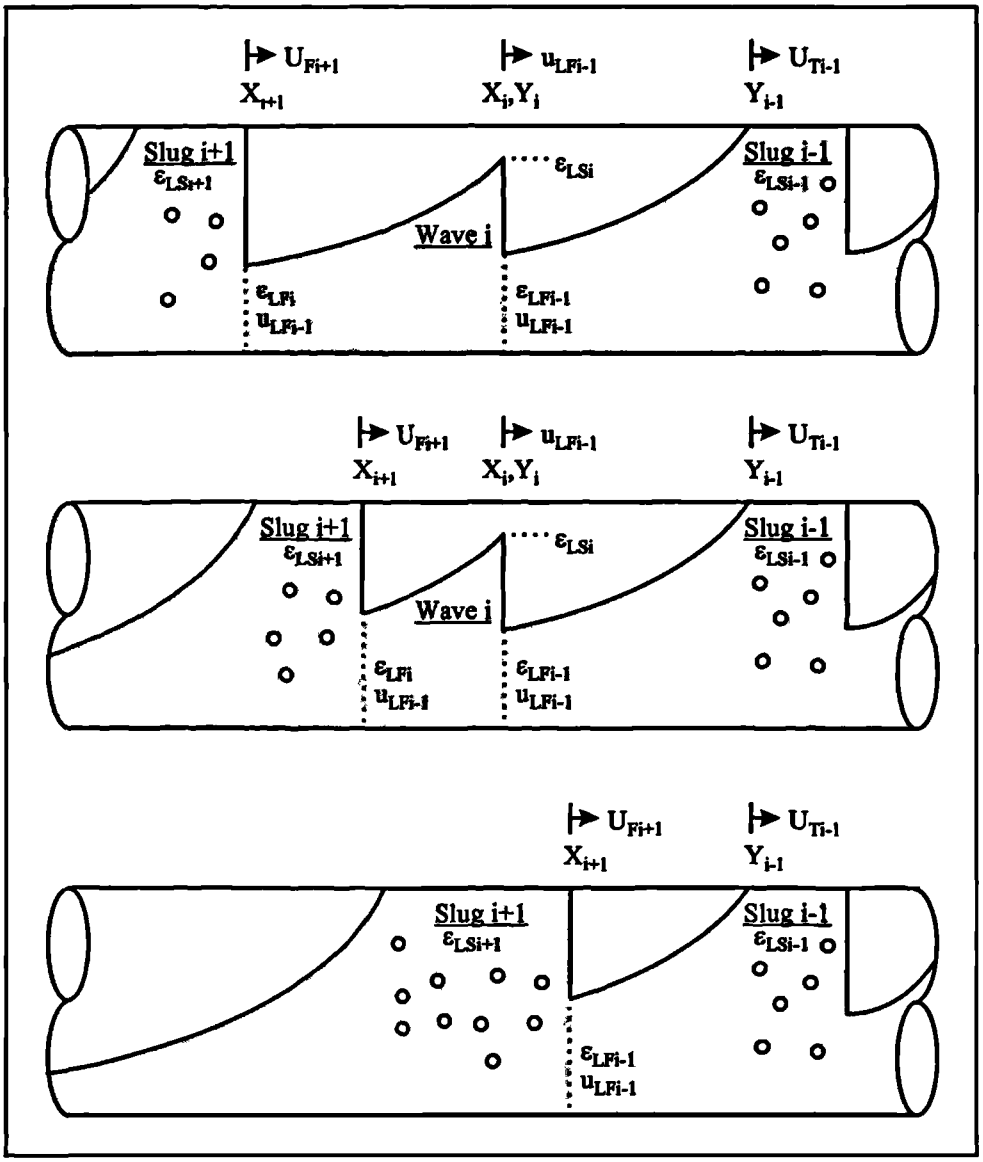

Figure 7.4: A slug overtaking a slow-moving wave

Slug catches a slug

The case of a fast slug catching up with a slower slug is permitted by the model and is handled in much the same way as a slug overtaking a wave, *i.e.* the slower moving object is "killed" and removed from the list of "live" objects. However, it is not anticipated that such an event will ever occur, due to the similarity of slug velocities. Furthermore, the use of a gas entrainment correlation based on chordal interface length leads to the result that as the distance between two slugs decreases and the liquid film height in front of the upstream slug rises, the chordal interface length is decreased. This causes a reduction in the rate of gas entrainment and thus in the front velocity of the upstream slug, so that it may no longer be travelling faster than the tail of the downstream slug.

This suggests that the actual mechanism for the "merging" of slugs observed in real flow is that the downstream slug collapses into a slow-moving wave, which is then overtaken by the upstream slug.

7.2.1. Wave propagation

Although not shown clearly in Figure 7.4, when a wave is following immediately upstream of a slug, special treatment is required to ensure conservation of mass. As the slug moves away from the wave, the film region becomes longer, and mass must be moved from the wave and transferred to the "new" section of film. In this model, this is achieved quite crudely by shifting the position of the wave front upstream, and consequently reducing the height of the wave.

Figure 7.3 shows a situation where a wave is following a slug. At time t the film length between slug (i-1) and wave i is given by

$$L_{Fi} = Y_{i-1} - X_i \qquad [7.25]$$

At time t+Δt,

$$L_{Fi} = (Y_{i-1} + U_{Ti-1}\Delta t) - (X_i + u_{LFi-1}\Delta t) \qquad [7.26]$$

so the change in film length is

$$\Delta L_{Fi} = (U_{Ti-1} - u_{LFi-1})\Delta t \qquad [7.27]$$

The negligible change in ε_{LSi-1} during the time interval is ignored, so there is no change in the tail profile of slug (i-1). Also, the tail region immediately in front of the wave i is approximated as a flat film with (constant) holdup ε_{LFi-1}, so the change in the mass of the film may be determined approximately as

$$\Delta m_{LFi-1} \approx \rho_L A(U_{Ti-1} - u_{LFi-1})\varepsilon_{LFi-1}\Delta t \qquad [7.28]$$

where m_{LFi-1} is the mass of liquid between the tail of slug (i-1) and the front of wave i.

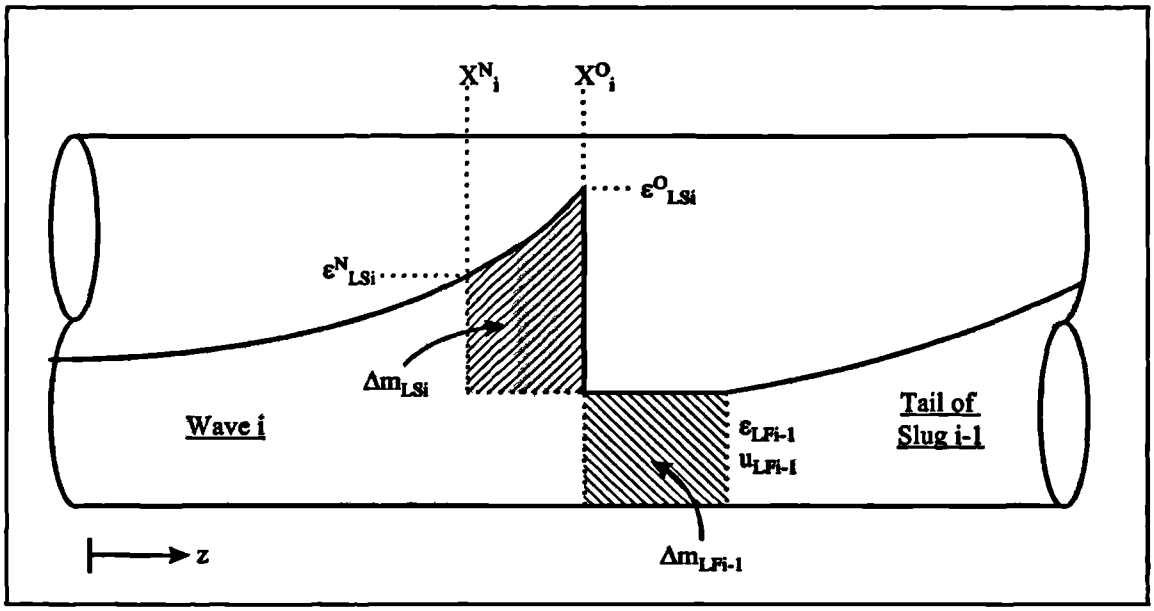

Figure 7.5: Close-up view of adjustments to wave front

In Figure 7.5, the region of "new film" is denoted by Δm_{LFi-1}. The corresponding region which must be removed from wave i to compensate is shown as Δm_{LSi}. X^O_i and ε^O_{LSi} are respectively the "old" wave front position and wave holdup prior to adjustment, and X^N_i and ε^N_{LSi} are corresponding ("new") values after the adjustment to conserve mass. Thus, the mass which must be "removed" from the wave (shown as the shaded area under the wave in Figure 7.5) is given by

$$\Delta m_{LS_i} = \rho_L A \int_{z=X_i^N}^{X_i^O} \left(\varepsilon_{LS_i} - \varepsilon_{LF_{i-1}}\right) dz \qquad [7.29]$$

This can be approximated as a trapezium, as shown in Figure 7.6:

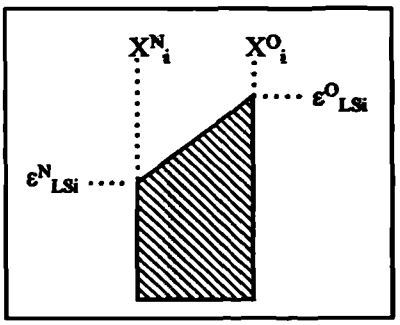

Figure 7.6: Approximate region which must be removed from wave

The change in mass of the wave is thus

$$\Delta m_{LS_i} \approx \frac{\rho_L A\left(X_i^O - X_i^N\right)\left(\varepsilon_{LS_i}^O + \varepsilon_{LS_i}^N - 2\varepsilon_{LF_{i-1}}\right)}{2} \qquad [7.30]$$

Determination of the point (X^N_i, ε^N_{LSi}) requires systematic stepping upstream along the tail profile from the point (X^O_i, ε^O_{LSi}) in small increments, which is computationally intensive. An approximation can be made using an approximate value of the gradient $\frac{d\varepsilon}{dz}$, close to the point (X^O_i, ε^O_{LSi}), by determining a value of the film holdup ε'_{LSi} at a short distance Δz upstream of the old wave front. Thus,

$$\frac{d\varepsilon}{dz} \approx \frac{\varepsilon_{LS_i}' - \varepsilon_{LS_i}^O}{\Delta z} \qquad [7.31]$$

and

$$\varepsilon_{LS_i}^N \approx \varepsilon_{LS_i}^O + \frac{d\varepsilon}{dz}\left(X_i^O - X_i^N\right) \qquad [7.32]$$

If Δm_{LFi-1} is balanced with Δm_{LSi} so as to conserve mass, then Equations [7.28] and [7.30] may be solved using the approximation [7.32], which results in a quadratic equation in X^N_i. This has only one positive real root, which is the required solution:

$$X_i^N = \frac{-b - \sqrt{b^2 - 4ac}}{2a} \qquad [7.33]$$

where

$$a = \frac{d\varepsilon}{dz}$$

$$b = 2\left(\varepsilon_{LF_{i-1}} - \varepsilon_{LS_i}^O - \left(X_i^O \frac{d\varepsilon}{dz}\right)\right) \qquad [7.34]$$

$$c = 2X_i^O \varepsilon_{LS_i}^O + \frac{d\varepsilon}{dz}\left(X_i^O\right)^2 - 2X_i^O \varepsilon_{LF_{i-1}} - 2\frac{\Delta m_{LF_{i-1}}}{\rho_L}$$

It is important to note that the *same* wave profile is used when this procedure is repeated during successive time steps. Since the wave profile is determined by the wave holdup at the front of the wave, the value ε^O_{LSi} is not used as this decreases with each application of the procedure. Instead, the original wave holdup ε_{LSi}, determined at the instant the wave was

formed from slug i, is used. Therefore, a record must be kept of the cumulative length of film which has been "removed", ΔL_{Fi}, since the formation of the wave. The film profile calculated for ε_{LSi} is then used, with the value ε^{O}_{LSi} obtained at a distance ΔL_{Fi} upstream along the profile.

This very simple procedure causes the wave front to propagate at a velocity much lower than u_{LFi-1} and, in certain cases, if the adjustment $\left|X_i^O - X_i^N\right|$ is greater than the distance ($u_{LFi-1}\Delta t$), then the wave front position may actually retreat upstream.

Furthermore, the decrease in wave holdup may cause the wave to dissipate completely. If ε^{N}_{LSi} becomes smaller than ε_{LFi-1} then the wave is assumed to have completely disappeared, and is removed for the list of "live" objects propagated by the model. As wave i "dies", a sudden (small) reduction in film velocity occurs between the point X^{N}_{i} and the front of the next slug object upstream, *i.e.* X_{i+1}. This is the second case where momentum is not conserved by the model.

7.3. Implementation of the model

Only the section of the algorithm which deals with slug and wave propagation is summarised here. A comprehensive treatment of the solution procedure for the film profile equations, as used in this work, is given in Chapter 2.

7.3.1. Object states

The slug propagation model is implemented using an object-oriented algorithm. This treats each wave or slug as a separate "object" which may be assigned one of several states. These are:

1. Object is a slug which has yet to be injected into the pipe
2. Object is a slug, propagating along the pipe
3. Object is a wave, propagating along the pipe
4. Object has reached the pipe exit
5. Object has been "killed"

An object is assigned state 5 when it is either overtaken by a following object or when it is a wave (State 3) which has dissipated completely. A "dead" object is no longer propagated by

the algorithm: its front and tail nodes are not written as output data and the algorithm searches upstream for the next object whose state is 2, 3 or 4.

The major advantage of an object-oriented approach is that no procedure is needed to renumber objects after a wave dissipates or is overridden by a faster-moving slug. Also, the size, number and complexity of the arrays used to store information about objects are all reduced. Finally, as future developments are made to the model, it will be straightforward to add new "states" without the need to re-write large sections of the algorithm.

7.3.2. Look-up tables

The slug (and wave) tail profile parameters are stored as look-up tables. For a given value of U_{Mix}, the film holdup and velocity at a distance L_F from the tail of a slug is a function of the slug body holdup, ε_{LS} and the tail velocity U_T. Thus, for the specified value of U_{Mix}, tail profile information is calculated for a range of values of these two variables and the data are stored as a three-dimensional array before the main slug tracking routine is started. To retrieve data from the array, values of L_F, ε_{LS} and U_T must be known.

The array contains values of the angle γ (see Figure 2.2 in Chapter 2) as a function of L_F, ε_{LS} and U_T. Certain constraints and approximations are used to simplify the look-up procedure and thus reduce the computation time required.

1. When the film profiles are calculated using Equation [7.12], the profile is discretised in increments of Δz. Since the gradient $\frac{dh_{LF}}{dz}$ is very steep immediately upstream of the slug body, the tail profile is not discretised evenly. The function used is:

$$\begin{array}{ll} \Delta z = 0.001\,\text{m} & z < 1\,\text{m} \\ \Delta z = 0.01\,\text{m} & 1\,\text{m} \le z < 15\,\text{m} \\ \Delta z = 0.1\,\text{m} & z \ge 15\,\text{m} \end{array} \qquad [7.35]$$

   Before interrogating the look-up table, the algorithm rounds the value of L_F to the smallest accuracy, *i.e.* to the nearest 0.001 m.

2. Solution of the film profile Equation [7.12] is not robust for all values of ε_{LS} at all values of U_T. Thus, upper and lower boundaries for the value of ε_{LS} are specified. The array is calculated only for slug body holdups in the range $0.4 \le \varepsilon_{LS} \le 0.96$, in

increments of 0.01. When a value of ε_{LS} is used to interrogate the array, if it lies outside of this range then it is explicitly set to be equal to the appropriate bounding value.

3. For each additional value of U_T used in the array, the size of the data file increases by approximately 5 MB. On computers without very large memory, this can cause a dramatic reduction in the speed of computation of the model. To maintain a manageable file-size, only three values of U_T are used to calculate the array, namely 1.2, 1.3, and 1.4 times the mixture velocity.

4. Due to the finite spacing of ε_{LS} and U_T described above, a linear interpolation scheme is used. This locates four values of γ in the array which correspond to the two ε_{LS} values either side of the calculated slug body holdup, at the two values of U_T which lie either side of the calculated tail velocity. Interpolation results in a single value of γ, which is then used to calculate values of u_{LF}, ε_{LF} and S_I. However, if the slug tail velocity calculated by Equation [7.15] is exactly 1.2 or 1.4 times U_{Mix} then there is no need of interpolation in the U_T dimension of the array.

This linear interpolation scheme introduces a degree of inaccuracy into the model, since in the range $1.2U_{Mix} \leq U_T \leq 1.4U_{Mix}$ the slug tail velocity function (Equation [7.15]) used to advance the slug tail positions is non-linear. This can be seen in Figure 7.7.

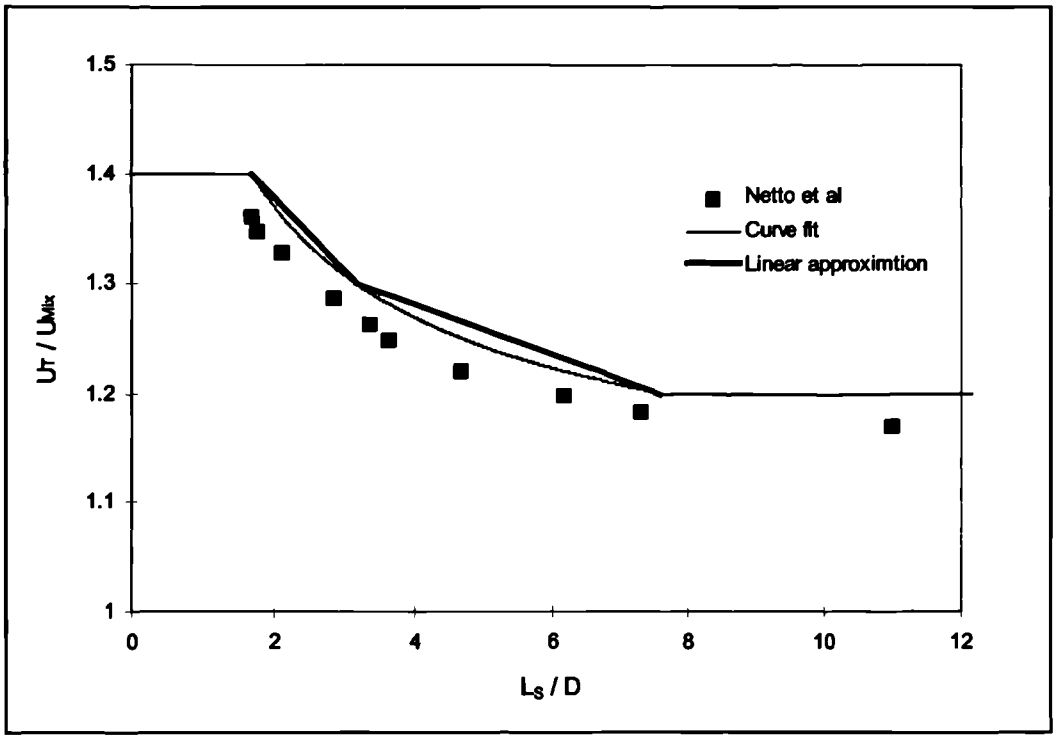

Figure 7.7: Linear approximation of slug tail velocity correlation used in array look-up procedure.

7.3.3. Slug and wave propagation scheme

At each time step the following operations are performed:

1. A check is made to see which is the leading (furthest downstream) "live" object in the pipe, so that time is not wasted looping through objects which have already reached the end of the pipe or been "killed".

2. For object i, the status of objects downstream is checked (*i.e.* i-1, i-2, i-3 *etc.*) until a "live" object is found whose status is 2, 3 or 4. This is denoted slug (i-j).

3. If slug (i-j) has already reached the end of the pipe, then the film values in front of object i are set equal to those values recorded at the instant slug (i-j) reached the end of the pipe (see Section 7.2).

4. If object (i-j) is a wave then the film holdup in front of object i is obtained from the wave film profile. However, the film velocity at the front of object i is set equal to that immediately in front of wave (i-j), unless object (i-j-1) is also a wave, in which case a

check is made downstream for the next object with state 2 or 4, and the film velocity at the end of this object's tail is used.

5. If object (i-j) is a slug, so the film parameters in front of object i are obtained from the slug tail profile, using Y_{i-j}-X_i as the film length, U_{Ti-j} as the tail velocity and ε_{LSi-j} as the slug holdup.

6. If object i has state 2, then the front velocity is obtained by iterative solution of the local mass balance and the gas pickup correlation. The position of the front of slug i is advanced by a distance $U_{Fi}\Delta t$. Checks are made for slug injection and the slug overriding the object downstream. The slug tail velocity is then calculated from the new slug length, and used to update the position of the slug tail. Finally, if the tail position has overtaken the front position, the slug is "collapsed" to become a wave, and assigned state 3.

7. If object i is a wave (state 3) then the mass conservation routine is invoked if object (i-j) is a slug. Then, the wave front position X_i is advanced by a distance $u_{LFi-1}\Delta t$ and the tail position is set equal to the new front position.

8. A check is performed to see if object i has reached the end of the pipe.

9. The counter i is increased by 1.

10. If i is not the final slug in the simulation then slug injection checks are made and the algorithm loops back to step 1.

11. On completion of the simulations for the given time step, the front and tail positions of all slugs are written to an output file, and the algorithm moves forward to the next time step, with increment Δt. When the last object has reached the end of the pipe, the simulation is stopped.

The scheme described above was found to give good results when the inlet slug length was large, and/or the mixture velocity was low. However, if very short slugs (*e.g.*, $L_{In} / D < 0.5$) were introduced at the inlet, it was found that very small time steps were require in order to accurately "capture" the slug whilst it was present at the inlet. If small time steps were *not* used, the entire slug could propagate beyond the inlet in a single time step, and the iterative

calculation of the slug body holdup (see Section 7.1.3) could not be performed before the slug was "launched".

A disadvantage of using a smaller value for the time step is that the computation time required for a simulation increases proportionately. Thus an adaptive timestepping routine was included in the algorithm, to ensure an adequate level of detail at the pipe inlet. In this sceme, *two* values for the time step are arbitrarily specified by the user, Δt_1 and Δt_2, so that $\Delta t_2 << \Delta t_1$. In general, the larger value, Δt_1 is used if a stratified film is present at the inlet, and the smaller value, Δt_2 is used if a slug body is present.

The implementation of this scheme is slightly different, depending on which of the two alternate modes is used to "launch" slugs at the inlet (see Section 7.2).

The first mode is the "injection times" mode, whereby the code initially computes a matrix of *times* $t_{In,i}$ for the injection of the front of each slug. Then, a check is made at the beginning of each time step (*i.e.* at time = t) to see whether a slug will be injected during the step (*i.e.*, whether $t_{In,i} < t + \Delta t$). If so, a shorter time step $\Delta t_1'$ is calculated so that now, $(t + \Delta t_1')$ is equal to $t_{In,i}$. Thus, the front of the slug will be "injected" at the *start* of the next time step. For subsequent time steps, the model uses the shorter value Δt_2 for the duration of the slug injection event. Once the tail of the slug has passed the inlet then the simulation reverts to the longer timestep.

In the alternate mode of operation, the user specifies the inlet superficial velocities and slug length distribution, and the injection time of each slug, $t_{In,i}$ is not known initially. Thus, a check cannot be made to verify in advance whether a slug front is about to be injected. Instead, the larger time step Δt_1 is used until the time step *after* a slug front is injected by the subroutine which computes the time-averaged superficial velocities. Thereafter, the smaller time step Δt_2 is used until the model detects that the slug tail has passed the inlet. This is anticipated to be *slightly* less accurate than the first method, however no effects have been observed.

7.3.4. Programming issues

The model is encoded using Visual Basic for Applications (VBA) (Microsoft, 1995) implemented within a spreadsheet program, Microsoft Excel version 7.0. This is a high-level

programming language, well-suited to this model in that it is based on object-oriented principles. The features of the spreadsheet program and its operating system, namely, storage and manipulation of large arrays, file handling, input and output using multiple spreadsheets and graphical presentation of results, are readily accessible from the code. However, VBA is not a compiled language and so code does not run as quickly as if it was written in, say, C++ or FORTRAN90. A further disadvantage is that a spreadsheet is not an efficient method of storing arrays of data, so that the data tables and output files used and produced by the model are often very large.

7.4. Results

In this section, results from simulations of several flow conditions are included. Firstly, a treatment of the calculation of the slug tail profile is given, then a comparison is made between results from the model and some experimental data. Results from idealised slug tracking simulations, developed using the two alternative slug injection schemes described in Section 7.2, are presented. The results of a study using a novel "slug initiation" method are shown.

7.4.1. Slug tail profile calculation

The variation of the film holdup ε_{LF} as several model parameters are adjusted is shown in Figures 7.8 to 7.11. The "base case" conditions for these results assumes air-water flow in a 78 mm diameter, smooth horizontal pipe, with mixture velocity 7.5 m/s, slug body holdup 0.75 and slug tail velocity of $1.3U_{Mix}$. In each case, integration of Equation [7.12] is performed between z = 0 m and z = 40 m (*i.e.*, $0 < (z / D) < 513$).

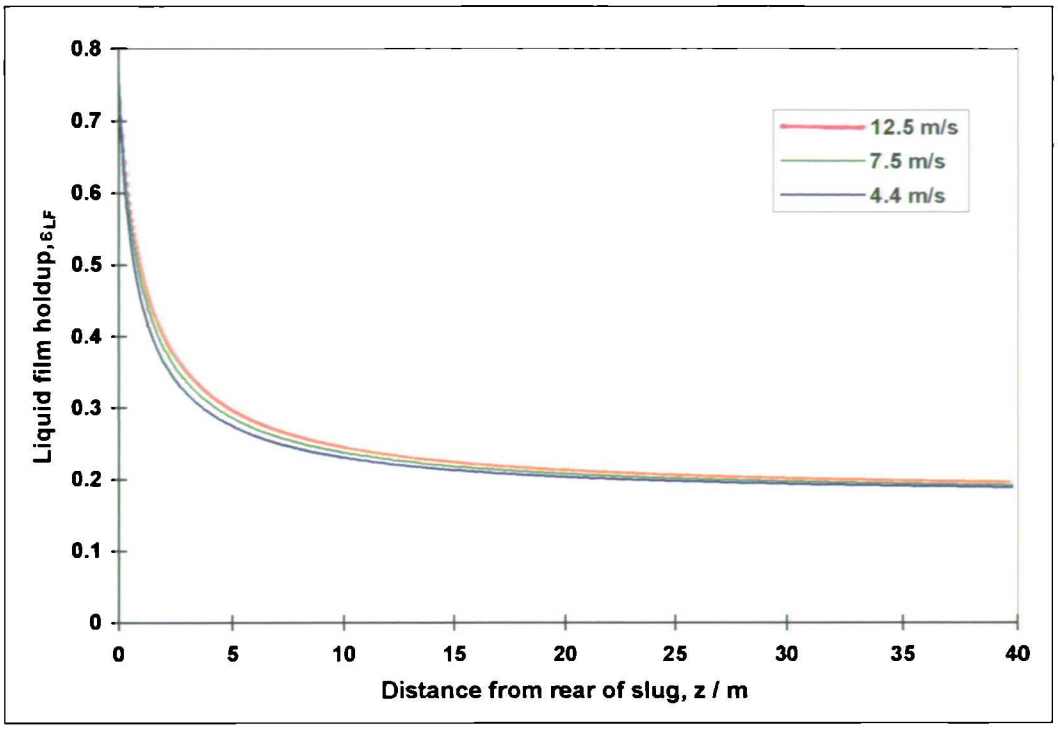

Figure 7.8: Variation of ε_{LF} with mixture velocity

($U_T = 1.3\ U_{Mix}$, $\varepsilon_{LS} = 0.75$, $\beta = 0°$)

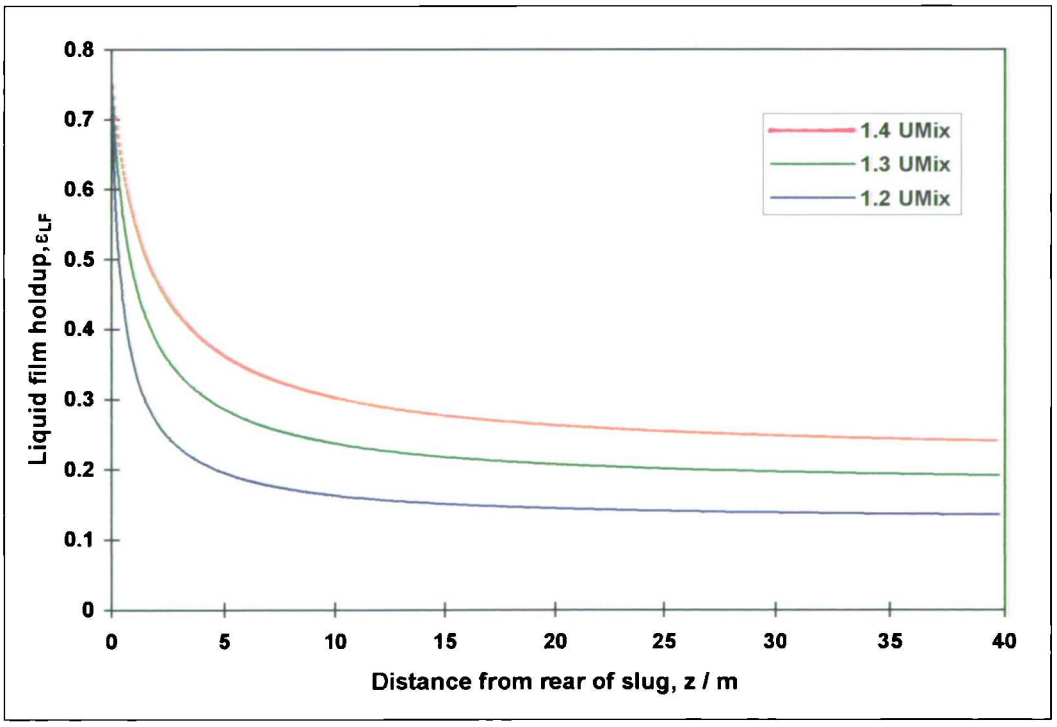

Figure 7.9: Variation of ε_{LF} with slug tail velocity

($U_{Mix} = 7.5$ m/s, $\varepsilon_{LS} = 0.75$, $\beta = 0°$)

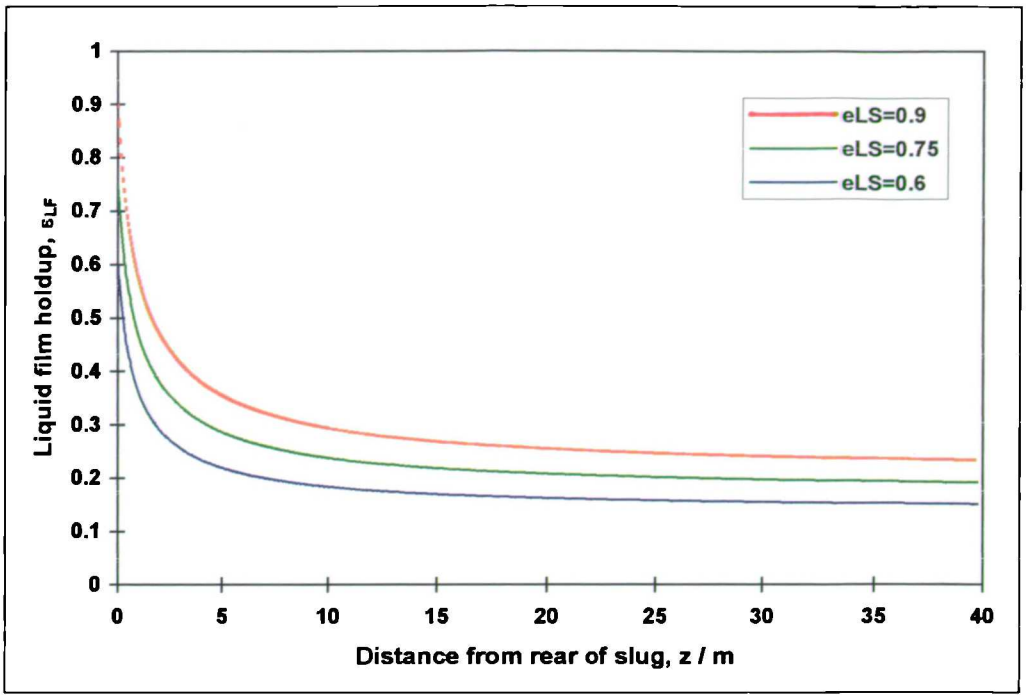

Figure 7.10: Variation of ε_{LF} with slug body holdup

(U_{Mix} = 7.5 m/s, U_T = 1.3 U_{Mix}, β = 0°)

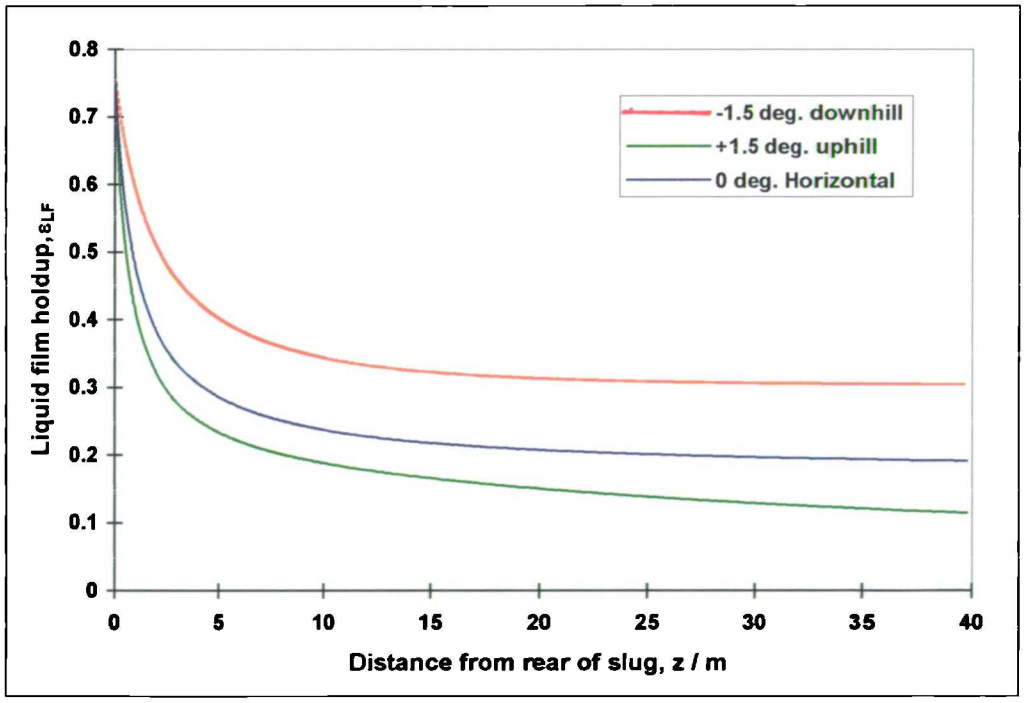

Figure 7.11: Variation of ε_{LF} with pipe inclination

(U_{Mix} = 7.5 m/s, U_T = 1.3 U_{Mix}, ε_{LS} = 0.75)

In general, the shape of the liquid film profile in the slug tail region is similar for the cases shown here. The film thickness is greatest immediately upstream of the slug decreases further from the slug (as does the film velocity). Figure 7.8 shows that the solution of Equation [7.12] results in a liquid film profile whose thickness is virtually independent of the mixture velocity. However, in Figure 7.9 it is clear that a change in liquid shedding rate and tail velocity can have a significant effect on the film profile upstream of a slug. An increase in slug tail velocity (observed for shorter slugs) causes a significant increase in the film thickness. Figure 7.10 demonstrates a similar thickening of the liquid film as the liquid holdup in the slug body increases. The effect of pipe inclination is shown in Figure 7.11, which demonstrates that Equation [7.12] predicts significantly different film profiles for upwardly-inclined, downwardly-inclined and horizontal pipes.

The appreciable change in the thickness of a film caused by changes in the tail velocity or the liquid holdup of its leading slug has important implications for the conservation of mass in a slug tracking model. As the film holdup changes over time, the total amount of mass in the system may vary significantly. To ensure that mass is conserved, some adjustment to either the film length or thickness is required. This has not been implemented in the model described in the present work, and thus mass is not conserved particularly well in the current execution of the modelling scheme.

The effects of the same variations in mixture velocity, slug tail velocity, slug body holdup and pipe inclination on the liquid film velocity profile are shown in Figure 7.12 to Figure 7.15, respectively.

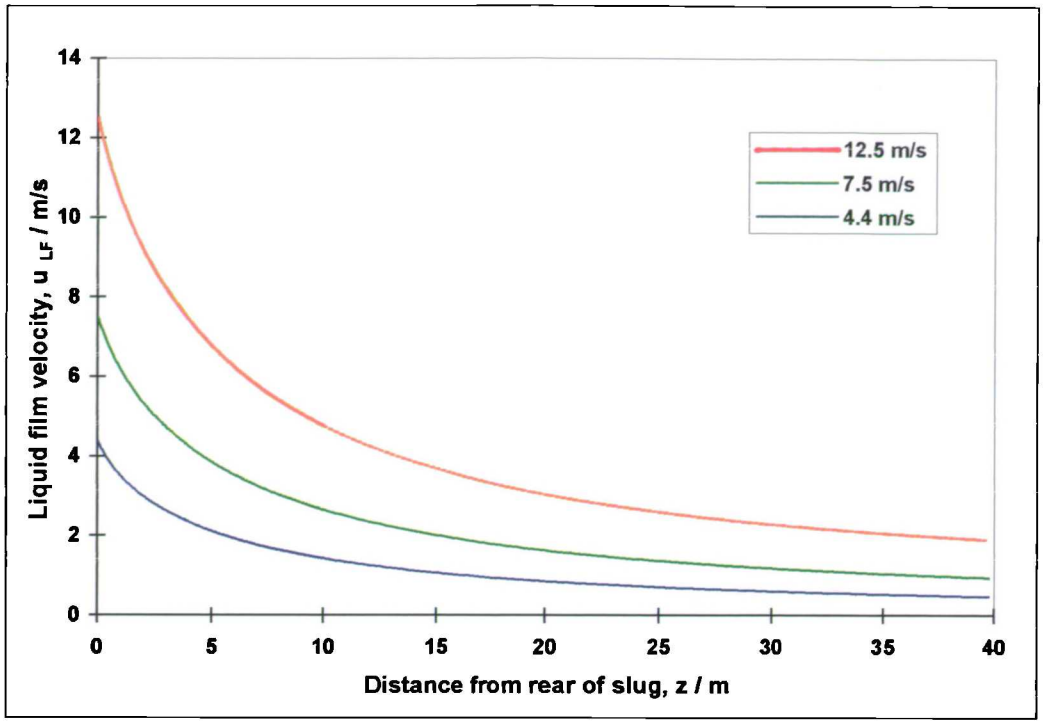

Figure 7.12: Variation of u_{LF} with mixture velocity

($U_T = 1.3\ U_{Mix}$, $\varepsilon_{LS} = 0.75$, $\beta = 0°$)

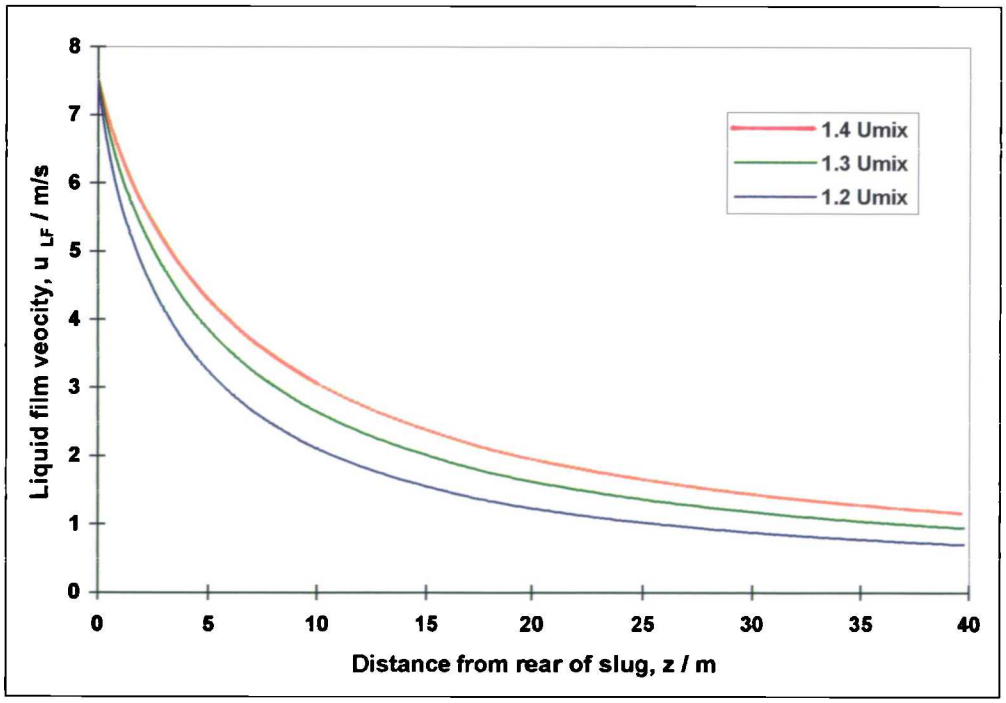

Figure 7.13: Variation of u_{LF} with slug tail velocity

($U_{Mix} = 7.5$ m/s, $\varepsilon_{LS} = 0.75$, $\beta = 0°$)

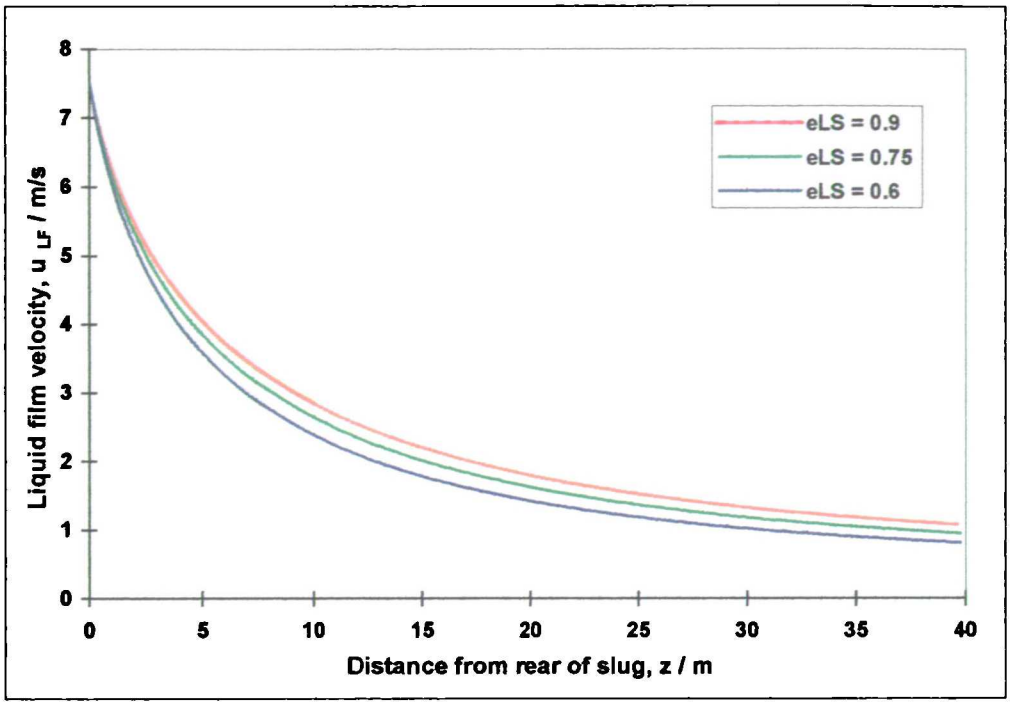

Figure 7.14: Variation of u_{LF} with slug body holdup

(U_{Mix} = 7.5 m/s, U_T = 1.3 U_{Mix}, $\beta = 0°$)

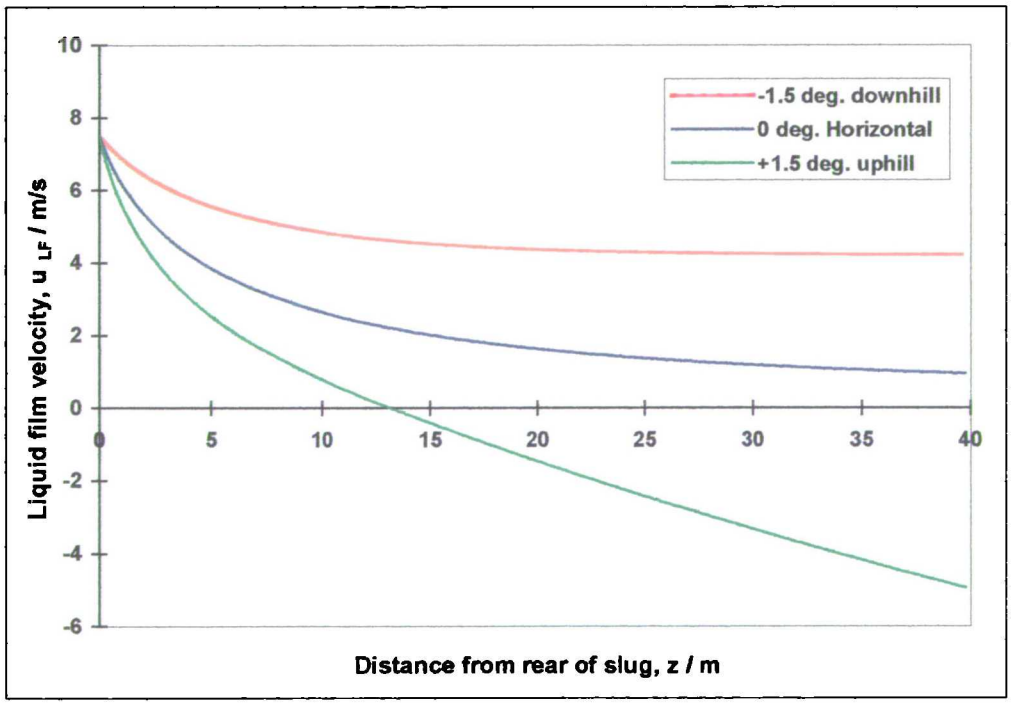

Figure 7.15: Variation of u_{LF} with pipe inclination

(U_{Mix} = 7.5 m/s, U_T = 1.3 U_{Mix}, ε_{LS} = 0.75)

The inclination of the pipe has the greatest effect on the film velocity profile upstream of the slug. For the upwardly-inclined case shown in Figure 7.15, reversal of the liquid film occurs

some 13 m upstream of the slug tail. The prediction of film profile reversal was discussed in detail, in the light of experimental observations of slug flow in the "rising limb" of a V-section, in Chapter 5 of this thesis.

Since the "no slip" assumption has been made for the slug body, and the slug tail profile is integrated from $u_{LF} = u_{LS}$ at the back of the slug, any variation in the mixture velocity (and hence u_{LS}) will cause a commensurate change in the film velocity profile in the slug tail. This is shown in Figure 7.12. Varying the slug tail velocity also leads to a significant change in the film velocity profile, due to the coupled effect on the liquid shedding rate from the slug: this is demonstrated in Figure 7.13. It appears that the value of the slug body holdup does not significantly affect the film velocity profile upstream of the slug, however. This is shown in Figure 7.14.

7.4.2. Horizontal flow prediction

To evaluate the performance of the slug tracking model, comparisons were made with experimental data. Initially, prediction of slug flow in a horizontal system was investigated. In the present work, no experimental data were measured using a horizontally-oriented test-section and so data obtained by King (1998) on the Imperial College WASP facility were used. King's (1998) data and the corresponding data from the 1-D simulation are shown in Figure 7.16. King (1998) reported that the experiment was performed at atmospheric pressure, with gas and liquid superficial velocities of 4 m/s and 1 m/s respectively.

As several liquid holdup probes are installed on the WASP facility it is possible to take the output from one probe and use this as the input condition for a simulation. The output from the simulation may then be compared with the experimental trace from a second probe, sited a known distance downstream. The liquid holdup trace obtained by King using a probe sited a distance of 20.5m from the WASP facility inlet is shown in Figure 7.16. The experimental and simulated data are then compared after a distance of 7.2 m, where the next probe downstream was located in King's experiments. This trace is offset by unity and thus plotted as the upper of the two traces.

Only the arrival and departure times of each slug or wave at the first probe are required as input: values of the liquid holdup and velocity are *not* required as they are calculated from the film conditions at the inlet at the time that each object is introduced into the pipe. This

represents a significant advantage over King's (1998) model, which required the holdup of each slug or wave, a value for the film holdup and an estimate of the liquid velocity as input. Thus, in Figure 7.16, the uppermost traces ("20.5 m") show the experimental data from the probe and also a simulated trace calculated *0.01m downstream* from the "injection point". This small step is necessary so that the slug body and film liquid holdup may be calculated by the model.

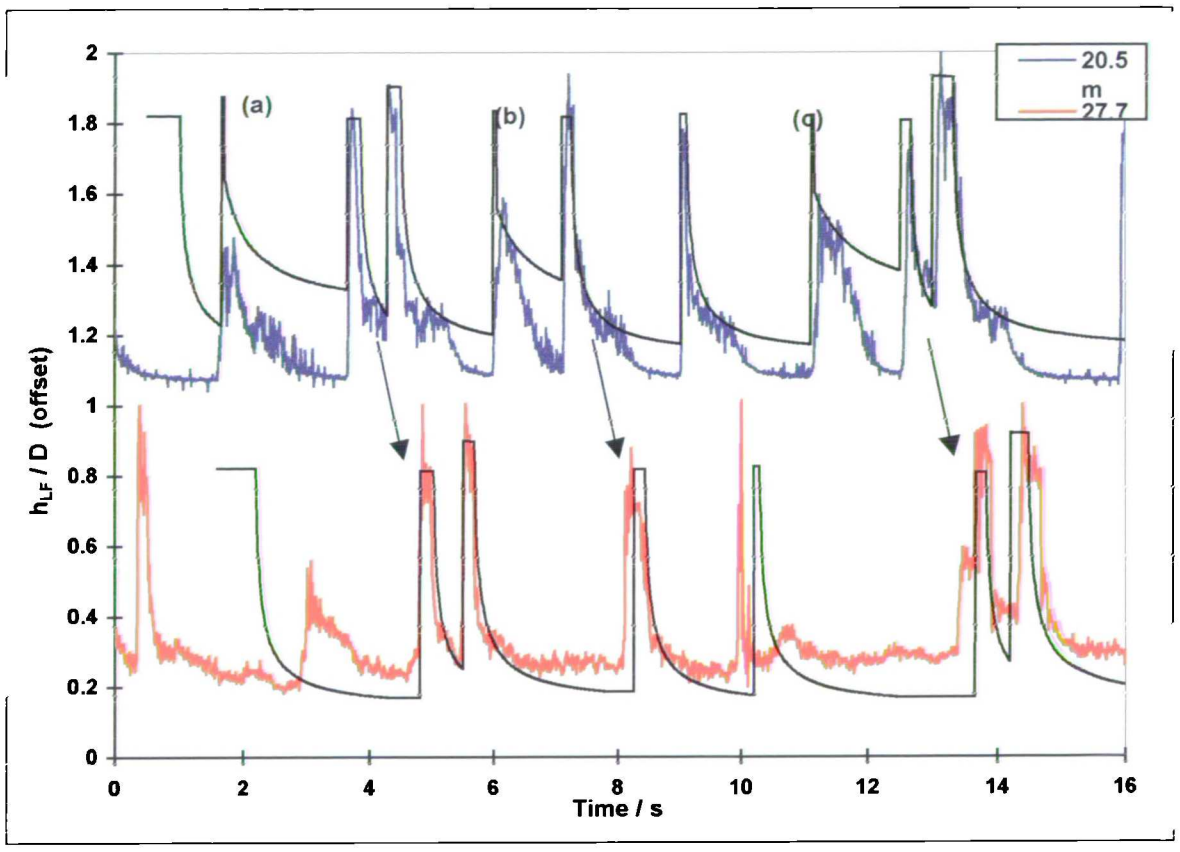

Figure 7.16: Horizontal slug flow data of King (1998) compared with model prediction (U_{sG} = 4 m/s, U_{sL} = 1 m/s, air/water, atmospheric pressure)

The simulation was run for 16 seconds, using a coarse time step (Δt_1) of 0.01 seconds. A fine time step (Δt_2) of 0.001 seconds was used for the slug injection events (see Section 7.3.3). The initial computation of the data matrices (the "lookup tables") took 189 seconds†, using a specified value of 31m for the maximum film length. Thereafter, the slug propagation algorithm took a further 161 seconds to compute the slugs' progress along a 30 m pipe. Note that the first slug on the simulated traces is used to initialise the simulation and is not intended

† Simulations were run on a personal computer with a single 450 MHz AMD® K6-III CPU, with 384 MB RAM (with a bus frequency of 100 MHz) The Microsoft® Windows98® operating system was used.

to represent a feature of the flow. The wave denoted as (a) in Figure 7.16 is the first object injected after the "initialisation" slug.

The experimental and simulated data show good agreement, particularly for the position of the slugs and their holdup. The model correctly predicts the collapse of waves (b) and (c). The only object not well modelled is object (a), which is predicted to dissipate completely but in reality propagates at a similar velocity to the other slugs in the system and reaches the probe at 27.7 m. This suggests that object (a) is not a decaying wave (as was stated by King, 1998) but is in fact a slug with an abnormally low liquid holdup, which decays into a wave just before reaching the 27.7 m probe.

7.4.3. Prediction of slug flow in a downwardly-inclined pipe

A comparison was made between the predictions of the model and slug flow data which were measured in a –1.5° downwardly-inclined pipe, during the first experimental Campaign conducted for the present work (see Chapter 4). Data from run number MTD1027 were used for the comparison. In this experiment, air and water at atmospheric pressure were used, with superficial velocities 10.05 m/s and 0.57 m/s, respectively. The experimental and simulated data are shown in Figure 7.17

It should be noted that the order of the traces in Figure 7.17 is the reverse of that in Figure 7.16, so that the upstream-most trace is plotted at the *bottom* of Figure 7.17 and the downstream-most trace at the top. The lower traces were obtained from electircal conductivity probes situated at 14.4m, 20.5m and 27.7m from the pipe inlet. Although these probes provide useful data for the arrival and departure times of each slug or wave, which is sufficient for comparison with a slug tracking model, it is not anticipated that the peak values of the liquid holdup accurately represent the flow conditions in the pipe. However, the true instantaneous liquid holdup is obtained using the gamma densitometer, which was situated 35.2 m from the test-section inlet, and which is shown as the top trace in Figure 7.17.

In this comparison, the data from the 14.4 m probe are taken as the starting point for the simulation. As in Section 7.4.2 above, only the arrival and departure times of the slug/wave objects are taken from the probe – values of the liquid holdup and velocity are not required as input to the simulation and are calculated immediately by the model. The first slug in the

simulation was used purely to initialise the model and does not represent an observed feature of the flow.

As in the comparison in Section 7.4.2, coarse and fine time steps were used of 0.01 and 0.001 seconds respectively. The simulation was run for a pipe of length 40m, for a duration of 25 seconds. The computational time required for calculation of the lookup tables was approximately 200 seconds, and the slug propagation algorithm ran for 194 seconds.

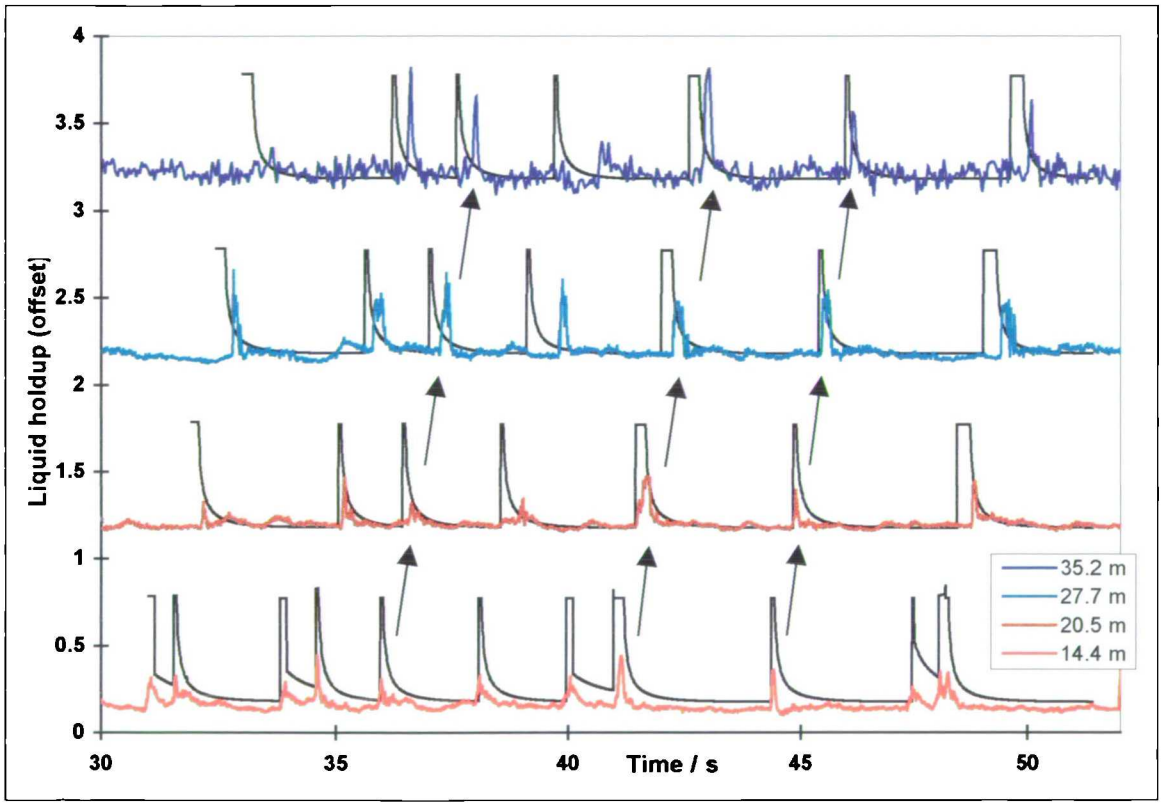

Figure 7.17: Experimental and simulated liquid holdup data for run MTD1027 (U_{sL} = 10.05 m/s, U_{sL} = 0.57 m/s, P = 0.0 bar(g), β = -1.5°)

The agreement between the first and last traces is fairly good, given the much longer pipe which is simulated (20.8 m) relative to the comparison with King's (1998) data in Section 7.4.2, where a distance of only 7.2 m was used. In particular, the collapse of several waves is correctly predicted. However, the arrival time of each slug at the final probe location (35.2m from the pipe inlet, *i.e.* 20.8 m downstream from the point at which the simulation was initiated) is generally predicted to occur earlier than was observed in the experiment. This is more clearly shown in Figure 7.18, in which the experimental and simulated data are compared at the first (*i.e.*, the "input") and the last probe locations.

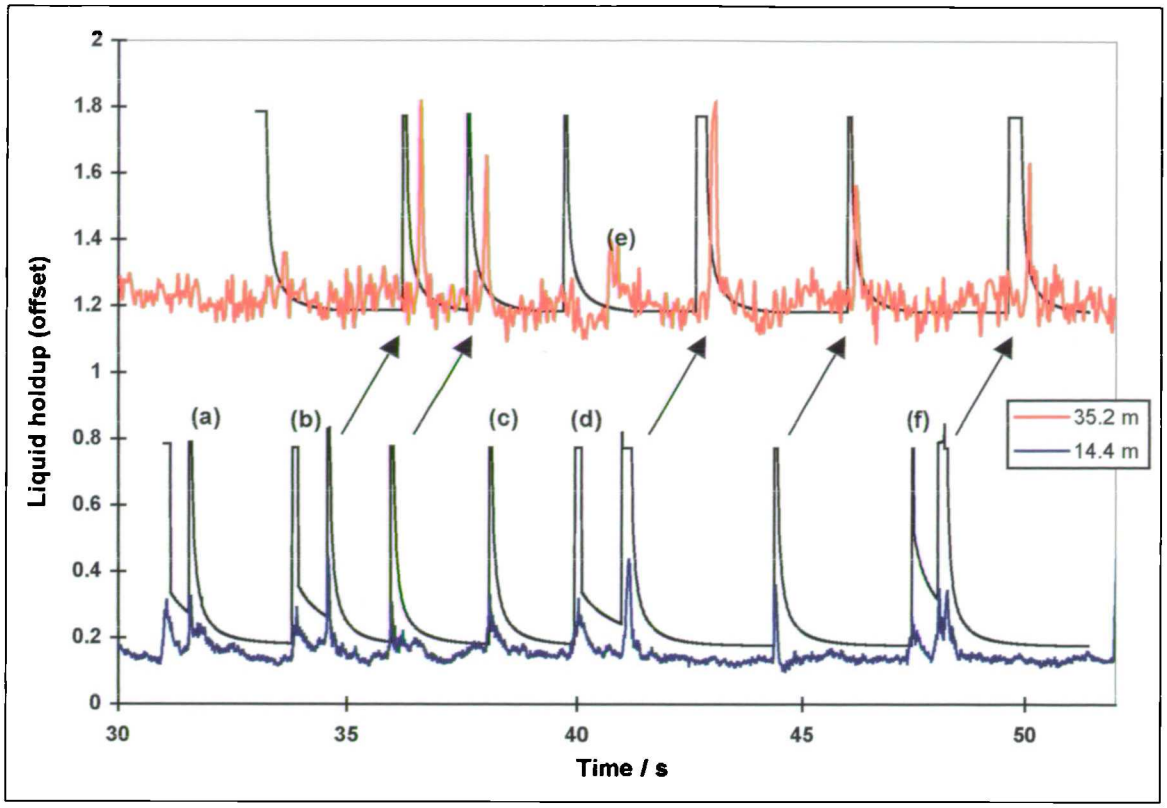

Figure 7.18: Liquid holdup traces at 14.4 m and 35.2 m from the inlet (run MTD1012)

The overprediction of the slug velocities which leads to the early predicted arrival of several of the slugs at the final probe may be due in part to the calculated film velocity profile, which is both faster and "flatter" for a downwardly-inclined pipe than for a horizontal system, as shown in Figure 7.15.

The model correctly simulates the collapse of the slugs denoted by (a), (b) and (d) in Figure 7.18. The model also predicts that wave (f) is picked up by a faster-moving slug upstream: this too agrees with the experimental data. However, the object shown as (c) is modelled incorrectly: the simulation predicts that it propagates as a slug, however the experimental data suggest that the wave moves more slowly and that object (e) has decayed to become a wave by the time it reaches the probe 20.8 m beyond the start of the simulation. This is confirmed by the video recording which was made of the experiment: the visualisation section was located approximately 1m upstream of the gamma densitometer in the test-section, *i.e.*, approximately 34 m from the pipe inlet.

That some objects (*i.e.*, waves or slugs) decay and collapse, but others do not, indicates that the model is sensitive to the exact conditions specified at the start of a simulation. The

growth or decay of a slug is determined primarily by the thickness of the leading film, which is quite sensitive to the tail velocity of the leading slug.

7.4.4. Tracking of short slugs

During the development of the slug tracking scheme in the present work, it was found that a novel approach could be used to "initiate" slug flow at the start of a simulation. Instead of reliance on a closure relationship for slug length or slug frequency (as has been used by Taitel & Barnea, 1998a), or a mechanistic model of slug development (Hale, 2000), it was found that if a large number of very short "sluglets" (length of order 2D) were injected at high frequency (of order 4 Hz) then a large proportion of the sluglets decayed to form slow-moving waves within a short distance from the pipe inlet. The remaining slugs would then pick up the mass from these waves and grow to form long, stable slugs from the high frequency "precursor" sluglets.

This approach has recently been pursued, independently of the author, by Cook & Behnia (2000) who used a less detailed model than has been developed in the present work. They simulated the propagation of a large number of short slugs and concluded that the average slug length (and thus the slug frequency) a large distance downstream of the initiation point was independent of the detailed conditions at the inlet.

In Table 7.1, a summary is given of six cases which have been simulated using the 1-D model. In each case, 2000 slugs were injected at the inlet of a 0.078m diameter, horizontal pipe; the physical properties used were those of air and water at atmospheric pressure. The "injection times" mode of operation (see Section 7.2) was used, so that a value of the total superficial velocity U_{Mix} was specified. The individual superficial velocities were then calculated at the *end* of the simulation, using the time-averaging method described in Section 7.2.

The values of the slug length, L_{In} and the nominal (± 35%) slug frequency, f_{in} which were specified at the pipe inlet are listed for each case. The model output which is summarised in Table 7.1 was calculated a distance of 25m from the pipe inlet and comprises the mean slug length $\overline{L_S}$ and the standard devation, the number of slugs passing the 25m monitoring point, N, and the gas and liquid superficial velocities.

Case	Input				Output (calculated 25 m from the pipe inlet)				
	U_{Mix} / m/s	L_{In} / D	f_{in} / Hz	N	U_{sG} / m/s	U_{sL} / m/s	N	$\overline{L_S}$ / D	Std. dev. L_S/D
1	7.5	1.5	5	2000	3.88	3.62	496	16.54	3.36
2	7.5	1.5	4	2000	4.27	3.23	491	16.96	4.19
3	7.5	2	4	2000	4.20	3.30	707	14.47	8.55
4	7.5	2	3	2000	4.71	2.79	656	16.46	8.55
5	7.5	1	5	2000	3.93	3.57	454	13.68	5.33
6	7.5	1	3	2000	4.80	2.70	620	10.71	4.06

Table 7.1: Summary of cases used in the development of the 1-D model

It is clear from Table 7.1 that the majority of the inlet "sluglets" do not survive to the 25m monitoring point. This is clearly seen in Figure 7.19, which shows simulated liquid holdup traces at several locations in the pipe, for the conditions simulated in Case 2 in Table 7.1, but for a shorter simulated period of approximately 30 seconds. As in earlier plots of experimental data, the traces for successive locations in the pipe are incremented by unity so that several traces may be plotted on the same axes.

The bottom trace in Figure 7.19 shows the passage of the high frequency sluglets at the pipe inlet. However, the trace 5m further downstream shows that a significant number of the slugs have already decayed to form waves, which are now visible. By 10m from the inlet, most of these waves have been overtaken by faster-moving slugs; by 25m almost all the wave/slug interactions have occurred and the simulated slug flow is effectively "fully developed". This is seen more clearly in Figure 7.20, which shows a shorter period of time during the simulation.

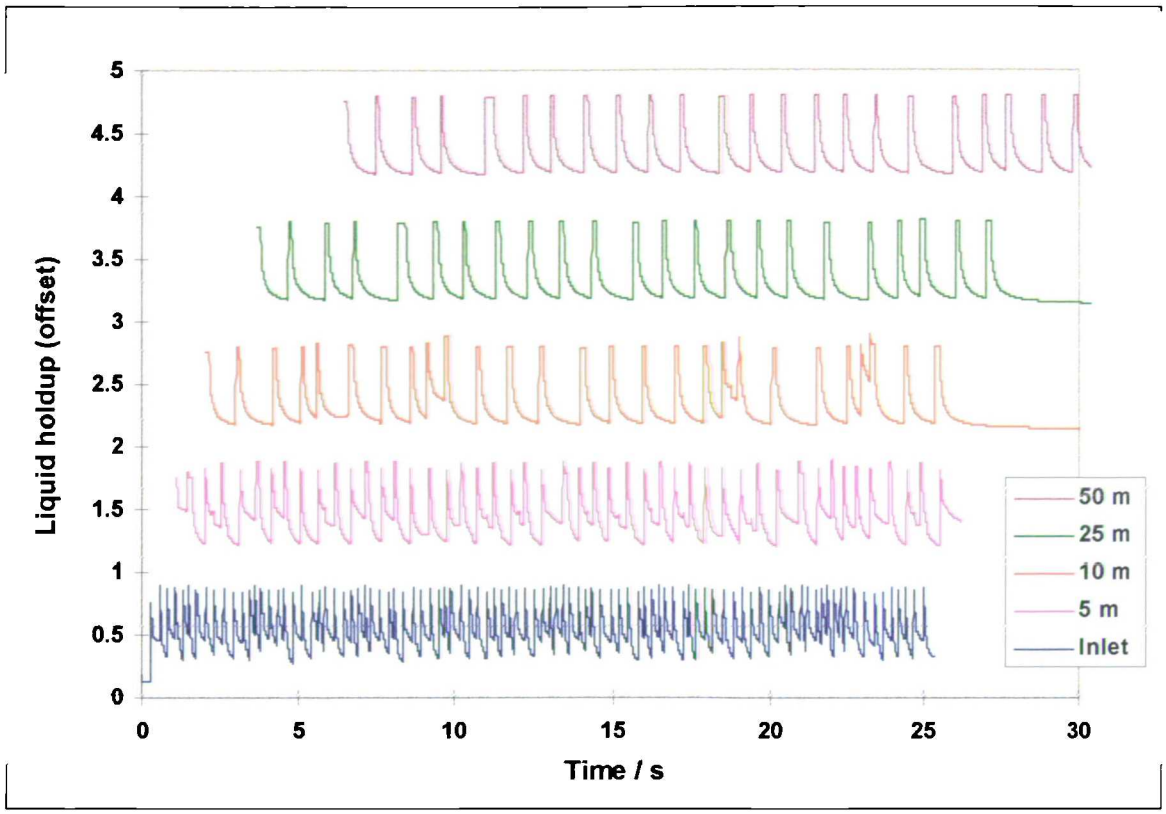

Figure 7.19: Case 2 - Liquid holdup traces at different locations along the pipe

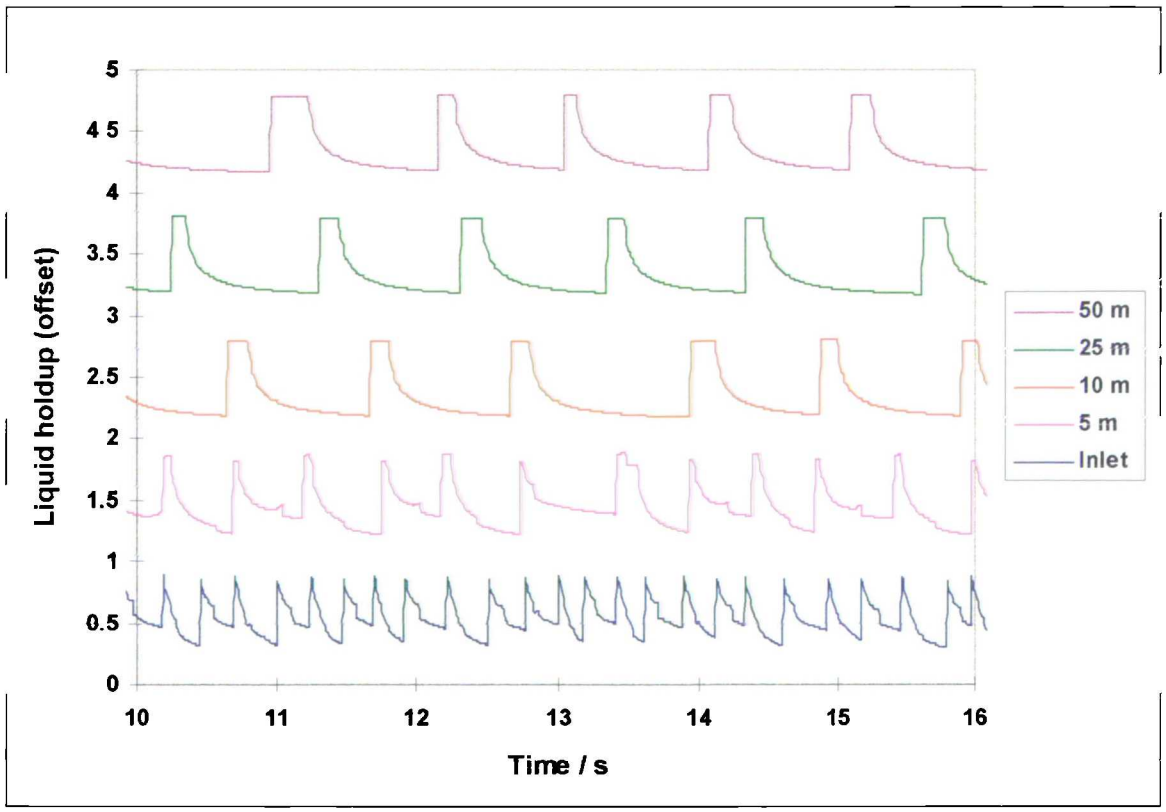

Figure 7.20: Case 2 - Liquid holdup traces at different locations along the pipe

Slug length distributions were calculated at 1m, 5m, 25m and 50m from the pipe inlet. These are shown in Figures 7.21 to 7.24.

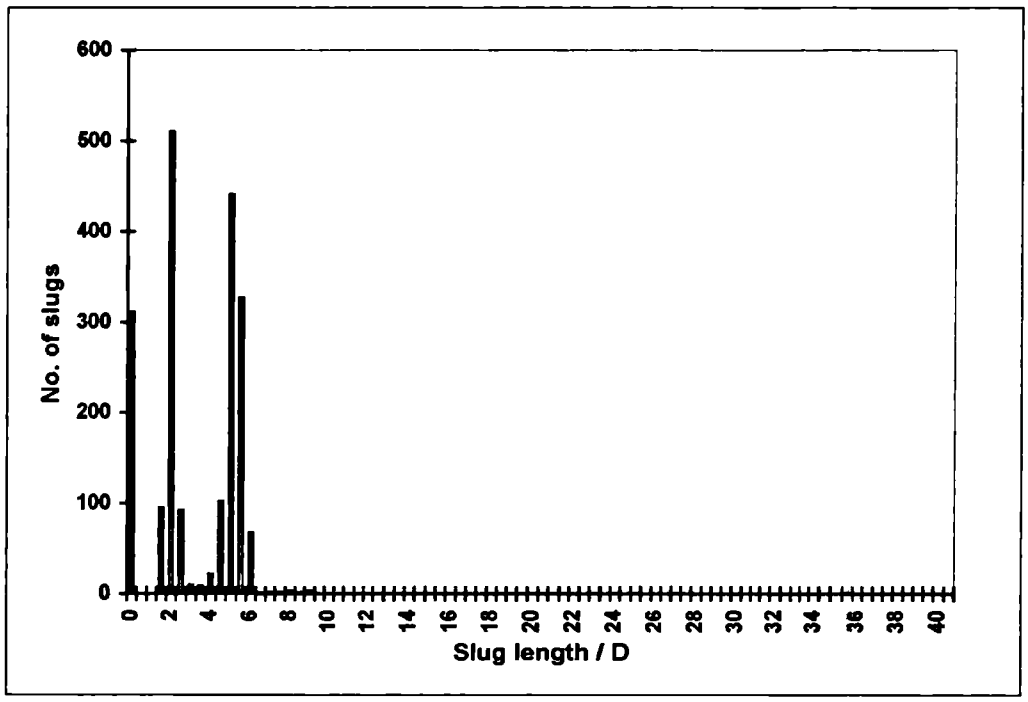

Figure 7.21: Case 2 - Slug length distribution, 1 m from pipe inlet

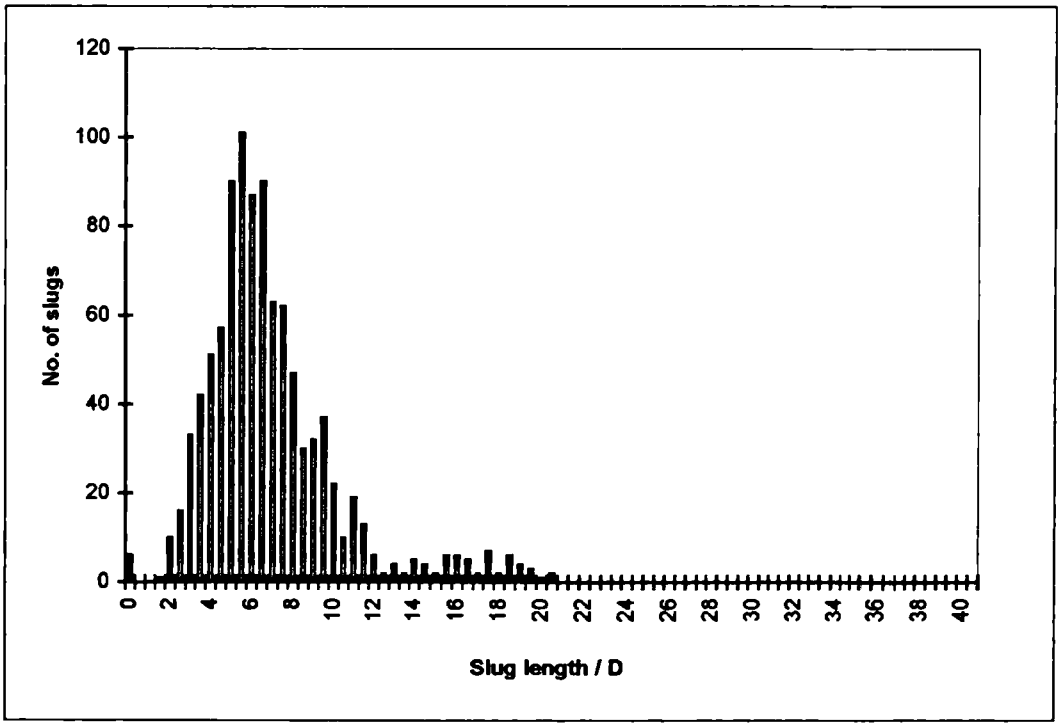

Figure 7.22: Case 2 - Slug length distribution, 5 m from pipe inlet

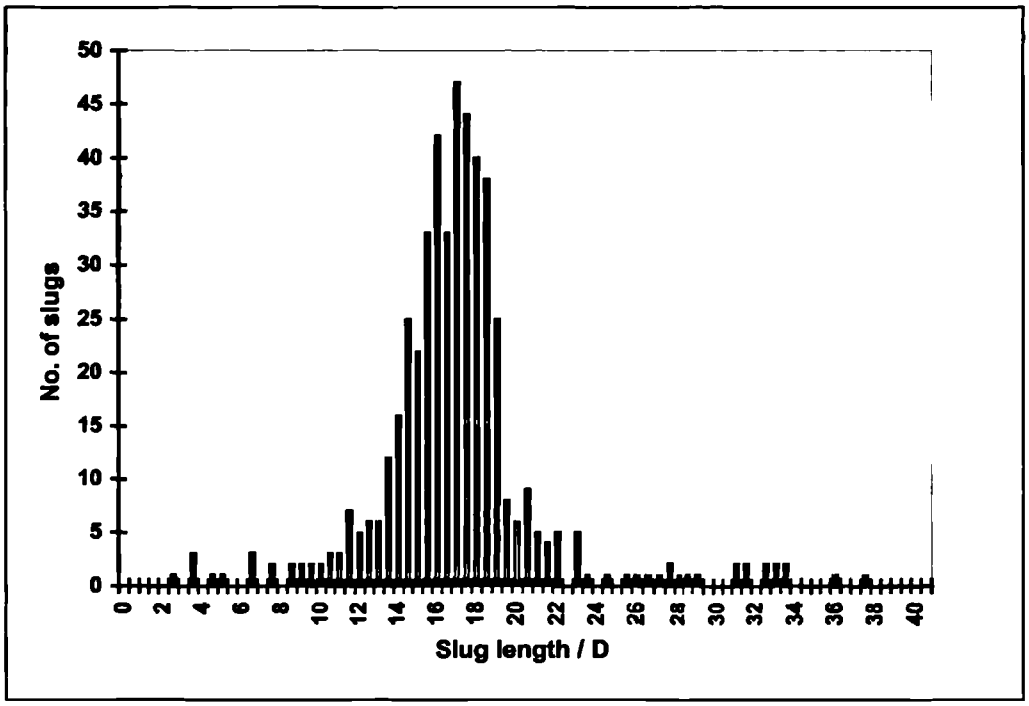

Figure 7.23: Case 2 - Slug length distribution, 25 m from pipe inlet

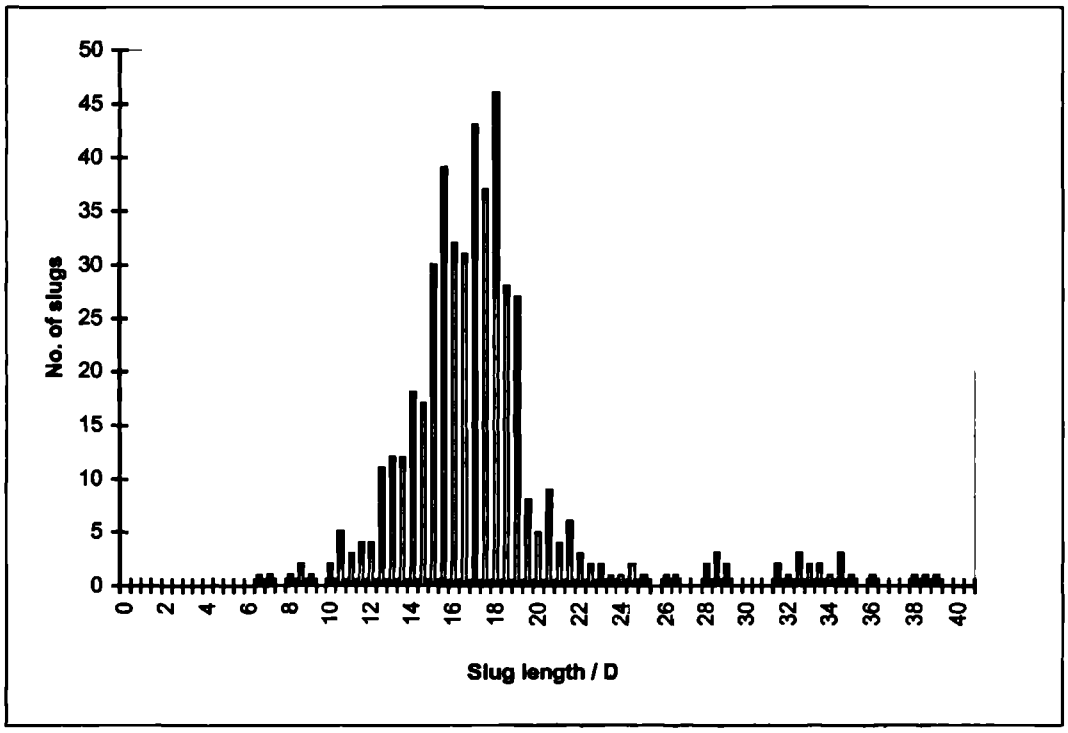

Figure 7.24: Case 2 - Slug length distribution, 50 m from pipe inlet

In the slug length distribution histograms, an object is considered to have zero length if it is propagating as a wave, so that the positions of its front and tail are equal.

In Figure 7.21, which shows the distribution of slug lengths 1m from the pipe inlet, a significant number of sluglets have already had sufficient time to more than double in size from their initial length of 1.5D. A correspondingly large number (approximately 300) of objects have decayed into slow-moving waves with zero length.

Further along the pipe, the slug length distribution quickly assumes the classical "log normal" shape. Figure 7.22 shows how the distribution has developed at a distance of 5m from the inlet. The mean slug length is around 6D at this point, although a small number of much larger slugs have already formed.

There is little difference between Figure 7.23 and Figure 7.24, which show the slug length distributions at 25m and 50m from the pipe inlet, repsectively. This suggests that once the slug flow has "developed" from the interaction of waves and short slugs close to the pipe inlet, the remaining slugs continue to propagate along the pipe with little or no interaction, nor significant change in length.

If similar slug length distributions are plotted for a different case, with a longer initial slug length L_{in} and a lower slug injection frequency f_{in}, it is found that the development of the slug length distribution along the pipe differs significantly from that shown in Figures 7.23 and 7.24. This is apparent in the results from Case 4, for which the values specified for L_{in} and f_{in} were 2D and 3 Hz (±35%), respectively.

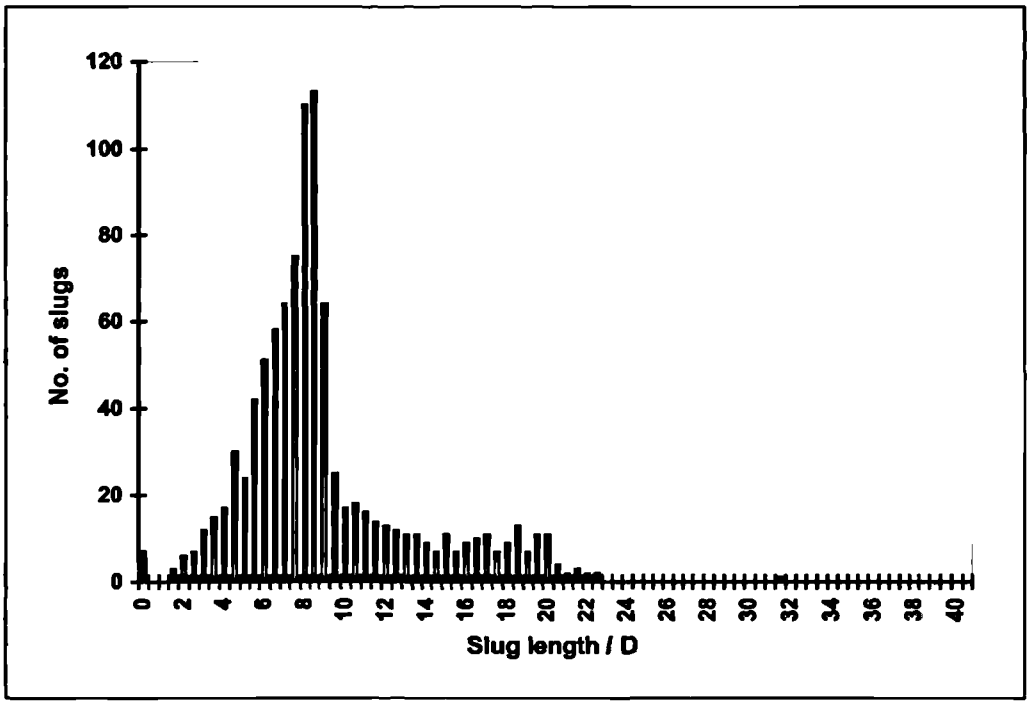

Figure 7.25: Case 4 - Slug length distribution, 10 m from inlet

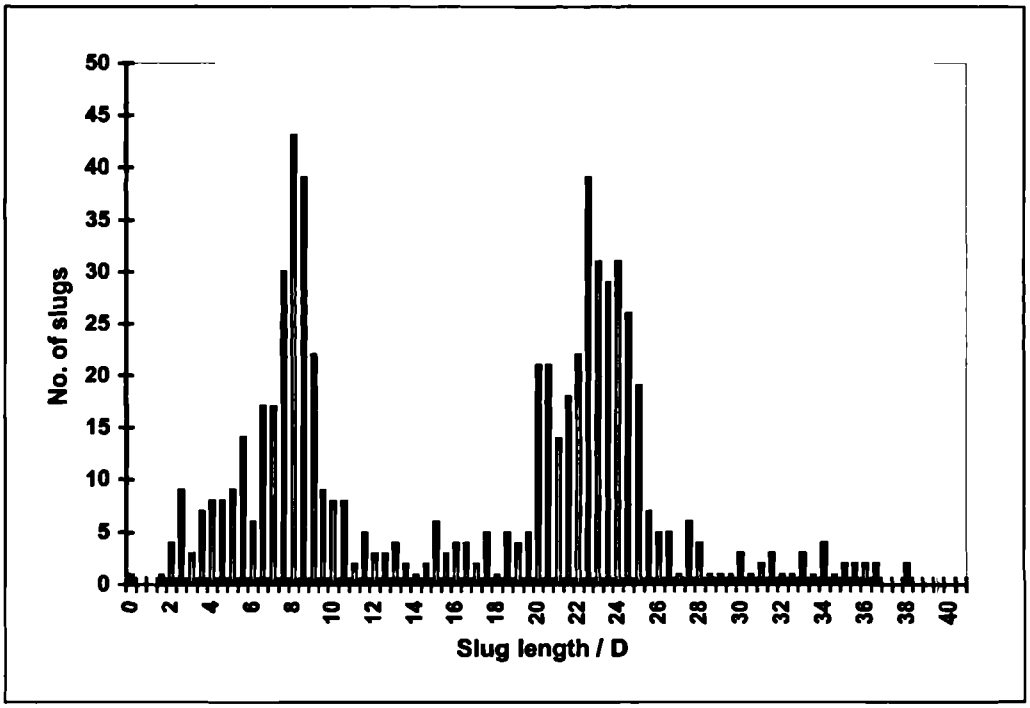

Figure 7.26: Case 4 - Slug length distribution, 25 m from inlet

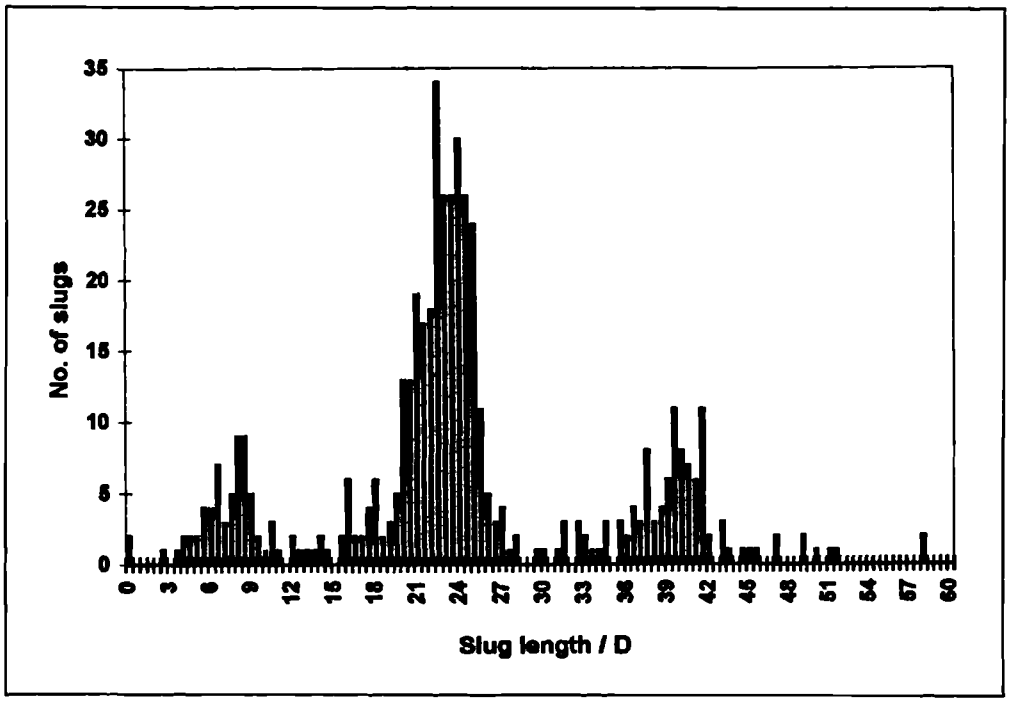

Figure 7.27: Case 4 - Slug length distribution, 50 m from inlet

In this case, the slug length distributions at 25m and 50m from the inlet (shown in Figures 7.26 and 7.27 respectively) have multiple peaks, indicating that the flow is still "developing" even after 50m.

It appears from these slug length distributions that small variations in the initial length and frequency of the slugs introduced at the start of a slug tracking simulation may significantly affect the development of the flow a large distance from the inlet. However, it is not possible to make direct comparisons between the cases shown in Table 7.1 as the gas and liquid superficial velocities are not the same for each case. This is a consequence of using the "injection times" mode of operation of the model.

One finding from this work was that, with the "injection times" mode of operation of the model, it was difficult to identify sets of inlet conditions (*i.e.*, values of L_{In} and f_{In}) which resulted in an acceptable value for the ratio (U_{sL} / U_{Mix}). In slug flow, this ratio is usually considerably below 0.2; at higher values, *plug* and *bubbly* flows are encountered. In the recent work by Cook & Behina (2000), the ratio of U_{sL} / U_{Mix} was 0.5.

7.4.5. Effect of small variation of inlet slug parameters

To investigate the effect of small variations in inlet conditions, a much larger number of cases were simulated and the results for superficial liquid and gas velocities were obtained. The inlet sluglet length, L_{In} was varied in the range $0.1 \leq (L_{In}/D) \leq 3$ and nominal inlet frequencies in the range $2\ Hz \leq f_{in} \leq 6\ Hz$ were simulated. In each case, 1000 sluglets were injected at the pipe inlet and their propagation was simulated for 40 meters. The conditions simulated were air/water flow at atmospheric pressure in a horizontal, 0.078 m diameter pipe. A mixture velocity of 10.5 m/s was specified for all cases.

Results for the liquid superficial velocity are shown in Figure 7.28.

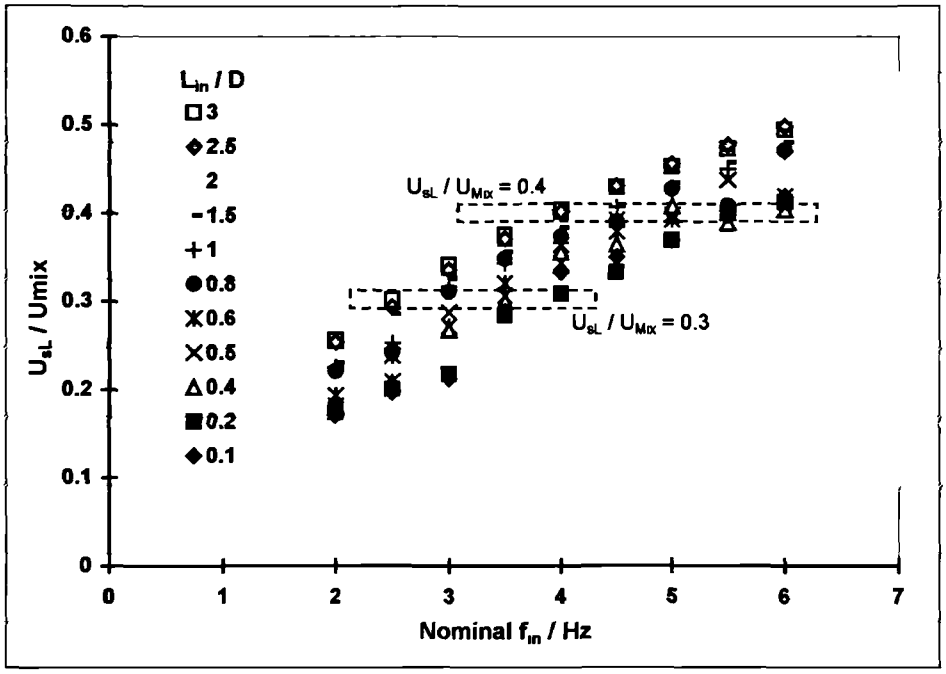

Figure 7.28: Effect of varying inlet sluglet length and frequency on calculated superficial liquid velocity (U_{Mix} = 10.5 m/s)

The liquid superficial velocity increases almost linearly with the sluglet inlet frequency. The initial sluglet length also has an effect, but a less significant one. This is because the length of the slug body is in general small with respect to the total length of the slug unit. Thus, the mass of liquid contained within the slug body is only a small proportion of that contained within the film region, so that a small increase in the length of the slug body does not significantly affect the total amount of liquid entering the system. However, this does not remain true for the case of very high injection frequencies, beyond the range investigated in

the present work, where the ratio of the slug body length to the film length becomes more significant.

The mean and standard deviation slug length were calculated for each case at a distance of 40m from the pipe inlet. These data are shown in Figure 7.29, plotted against liquid superficial velocity which was calculated at the inlet.

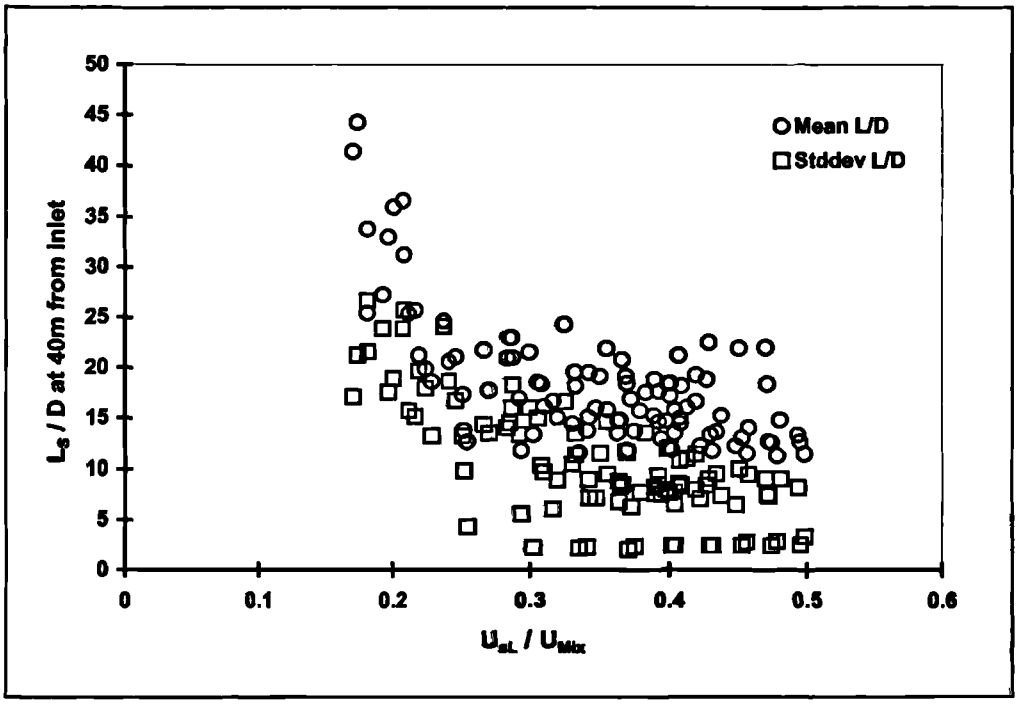

Figure 7.29: Slug length data calculated 40m from pipe inlet (U_{Mix} = 10.5 m/s)

Figure 7.29 shows that for a given mixture velocity, longer slugs are formed when the liquid superficial velocity is low. The standard deviation follows a similar trend to the mean slug length, with higher values corresponding to low liquid superficial velocities. Thus, the simulated flow exhibits long slugs if the superficial liquid velocity is low, and shorter slugs if the liquid velocity is higher.

The large number of runs shown in Figure 7.28 allows small subsets to be selected in which both superficial velocities are approximately the same. Two such subsets are indicated in Figure 7.28, for U_{sL}/U_{Mix} = 0.3 and 0.4. For these two sets of simulations, the mean slug length (measured at 40m from the pipe inlet) and the standard deviation are plotted in Figures 7.30 and 7.31, respectively.

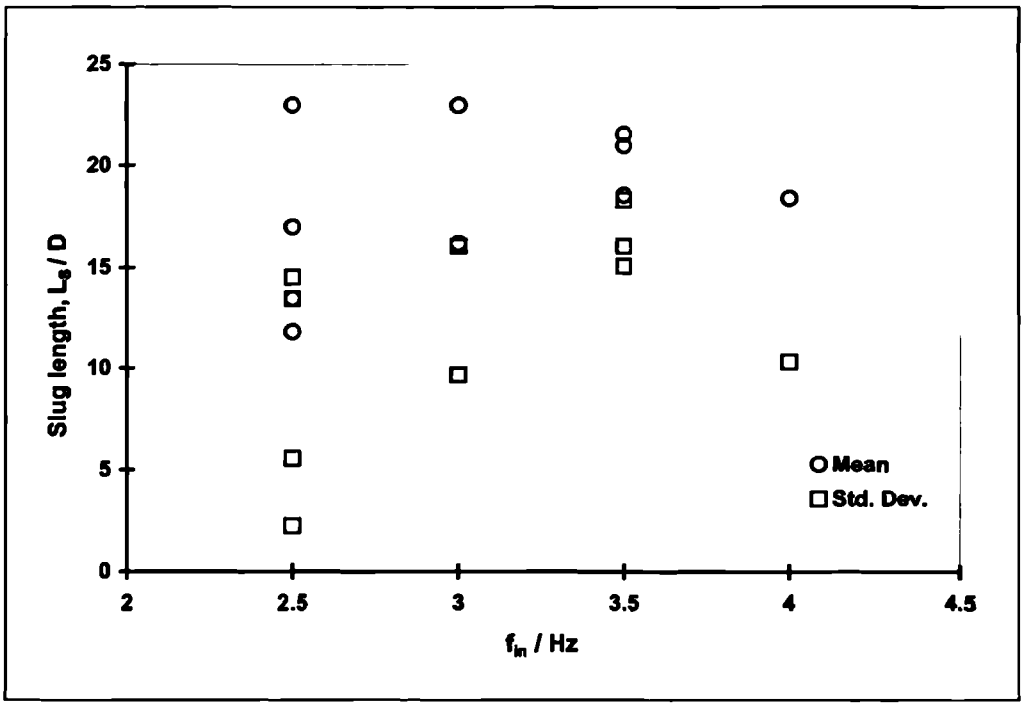

Figure 7.30: Mean slug length and standard deviation at 40m from pipe inlet (U_{Mix} = 10.5 m/s, U_{sL} / U_{Mix} ≈ 0.3)

The data in Figure 7.30 exhibit considerable scatter, which is probably due to the relatively small number of sluglets (1000) which were "launched" in the simulation. After propagating for 40m along the pipe, only a few hundred slugs remain. This may not be enough for an accurate statistical analysis. However, despite the scatter, it appears that there is little effect on the mean slug length as the input frequency is adjusted, and that the mean value of L_S/D is about 20.

The scatter is considerably smaller in the data for the simulations where U_{sL}/U_{Mix} = 0.4, which are plotted in Figure 7.31.

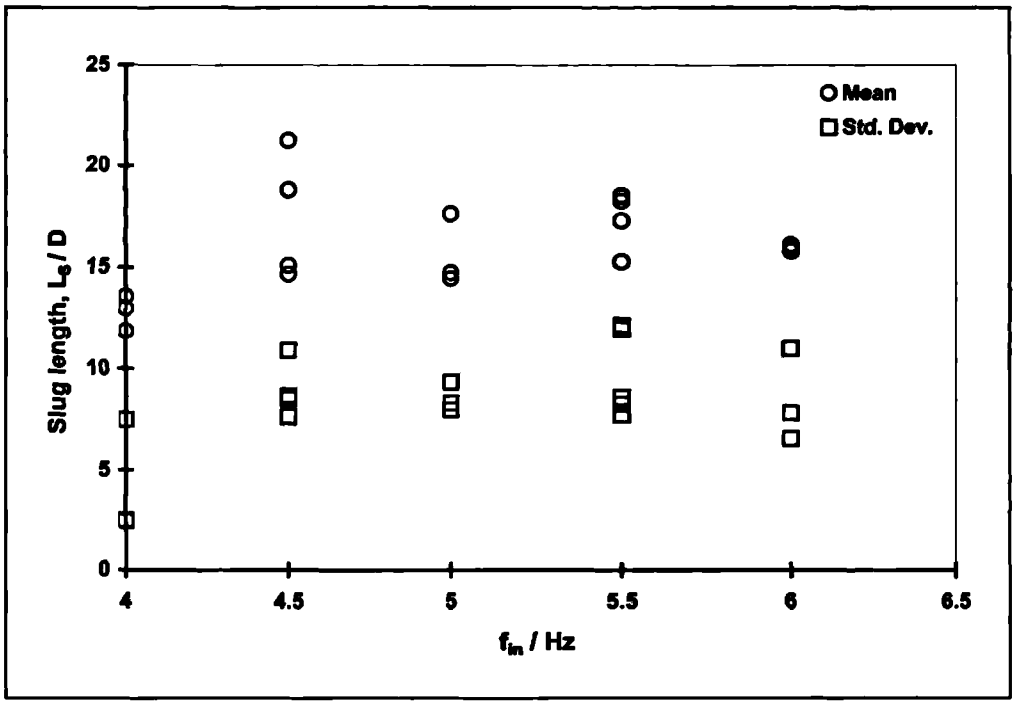

Figure 7.31: Mean slug length and standard deviation at 40m from pipe inlet (U_{Mix} = 10.5 m/s, U_{sL} / U_{Mix} ≈ 0.4)

It appears that for these simulations, the mean slug length is effectively *independent* of the detailed conditions at the inlet. This is in agreement with the results of Cook & Behnia (2000). However, it appears that this is the case only if the initial slug frequency is high (> 3Hz), so that there is a great deal of wave/slug interaction close to the pipe inlet. This results in high liquid superficial velocities, of the order $0.3U_{Mix}$ and higher, which are greater than the velocities generally encountered in hydrodynamic slug flow. As the ratio U_{sL}/U_{Mix} increases, the flow regime is more usually described as "plug flow". Here, plugs of unaerated liquid are separated by short film regions, and the plug frequency is generally high.

Cook & Behnia (2000) used their model to simulate flow with a mixture velocity of 1.2 m/s, with $U_{sL} = U_{sG} = 0.6$ m/s so that $U_{sL} / U_{Mix} = 0.5$. It is highly unlikely that such conditions would result in the formation of stable slug flow, instead it is more probable that plug flow would result.

Attempts were made to simulate low liquid superficial velocities using the 1-D model developed in the present work. It was intended to simulate flow with $U_{sL} / U_{Mix} < 0.1$, using the "injection times" mode of operation of the model with very short inlet sluglets ($L_{In} / D < 0.1$) and/or very low inlet frequencies ($f_{in} < 1$ Hz). However, it was found that at the low frequencies required to produce the low liquid flow rate, there was insufficient opportunity

for interaction between the waves and slugs close to the pipe inlet, and the simulation did not work.

Therefore, the second mode of operation was developed, whereby slugs are "launched" according to specified values of the liquid and gas superficial velocities, and the mean and standard deviation inlet slug length. The scheme which was developed to achieve this has already been described in Section 7.2, above. Ten cases were simulated, all with a specified mixture velocity of 10 m/s and a superficial liquid velocity of 2 m/s. As in earlier simulations, air/water flow in a horizontal, 0.078m pipe was modelled.

Initially, a normal slug length distribution of 2000 sluglets was calculated, with a mean L_{In}/D of 1 and an arbitrarily specified standard deviation of 0.2. For each case, a matrix of values of $L_{In,i}$ was then calculated by multiplying the original matrix by the required mean L_{In}/D.

A summary of the inlet conditions specified for the ten cases is shown in Table 7.2, together with the resulting slug parameters after slug propagation for 40m.

	Inlet					40 m		
Case	Mean L_{In}/D	$\left(\frac{\text{Std.dev.}}{\text{Mean}}\right)^{\dagger}$	Mean f_{in} / Hz	U_{sL} / m/s	U_{sG} / m/s	Mean L_S/D	Std.dev. L_S/D	Mean f / Hz
1	2.00	0.2	1.499	2	8	20.320	3.938	0.750
2	1.80	0.2	1.532	2	8	19.367	4.980	0.769
3	1.60	0.2	1.568	2	8	18.453	5.011	0.787
4	1.40	0.2	1.616	2	8	17.316	3.665	0.811
5	1.20	0.2	1.661	2	8	16.475	4.862	0.834
6	1.00	0.2	1.700	2	8	15.696	3.656	0.853
7	0.80	0.2	1.747	2	8	15.006	3.593	0.877
8	0.60	0.2	1.817	2	8	13.850	4.692	0.913
9	0.40	0.2	1.867	2	8	13.229	4.577	0.937
10	0.20	0.2	1.828	2	8	13.658	4.433	0.919

Table 7.2: Summary of cases with low liquid superficial velocities

† The standard deviation of 0.2 was used for the initial matrix calculated with L/D = 1, which was then multiplied by the required L_{in}/D value for each case.

As in earlier cases, the model was run with coarse and fine timesteps of 0.01s and 0.001 seconds respectively. A pipe length of 45 m was specified and lookup tables were computed using a specified maximum film length of 50m, to ensure that a slug present at the pipe inlet would always "see" a liquid film, even if the next object downstream was at the pipe exit. Computation of the lookup tables took approximately 3 minutes, and the slug propagation scheme then required roughly 1 hour of computation time for each case.

The results in Table 7.2 shows that when the superficial gas and liquid velocities are held constant and the mean inlet sluglet length is varied, the inlet slug frequency calculated by the time-averaging "slug launch" procedure varies correspondingly. This is plotted in Figure 7.32.

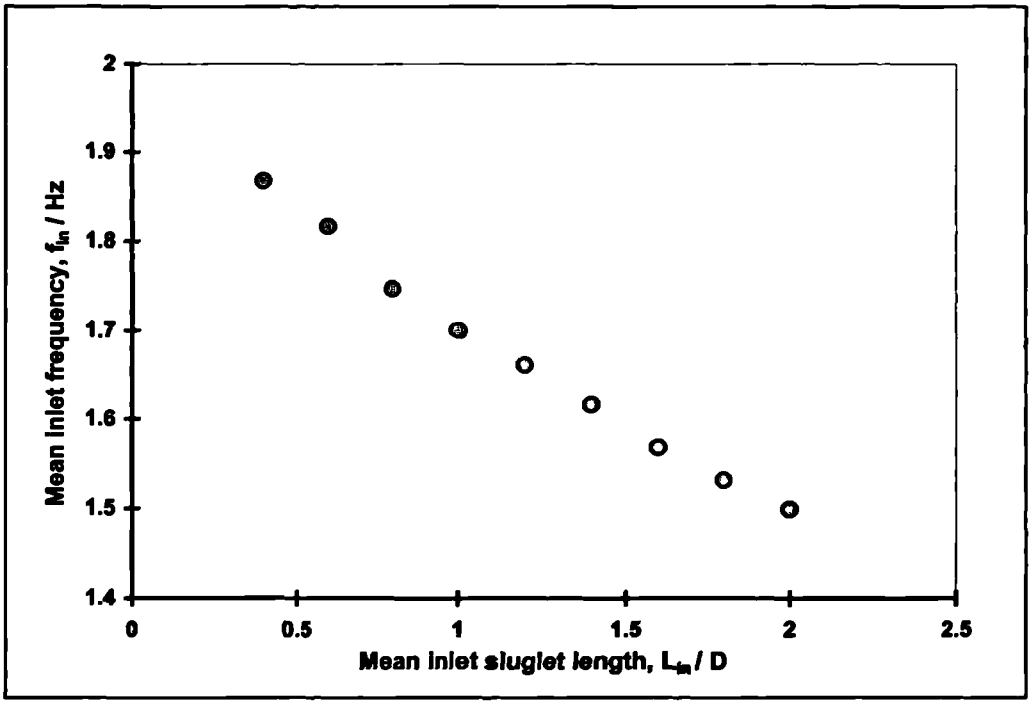

Figure 7.32: Inlet sluglet frequencies calculated by the "slug launch" routine (U_{sL} = 2 m/s, U_{sG} = 8 m/s)

It is found that the inlet slug frequency in turn affects the mean slug frequency and length which are calculated by the model after a propagation distance of 40m. These data are plotted in Figure 7.33.

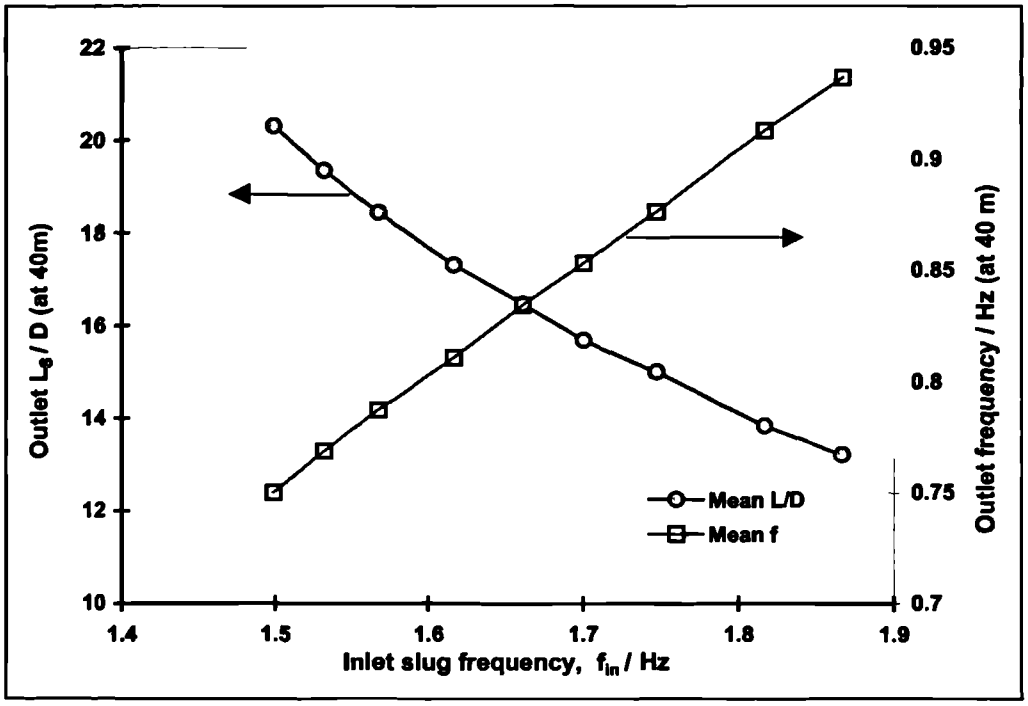

Figure 7.33: Effect of inlet slug frequency on slug parameters 40m downstream (U_{sL} = 2 m/s, U_{sG} = 8 m/s)

Note that the value of f_{in} may well be system dependent. Hence there is no *single* solution for slug flow in *short* pipes. These results show that the detailed slug parameters at the pipe inlet have a *significant* effect on the parameters calculated by the model a large distance downstream. The data contradict the results presented earlier for (unrealistically) high liquid flow rates by Cook & Behnia (2000), and suggest that slug initiation is an important area for further study.

7.5. Conclusions

In this Chapter, a quasi-steady state, one dimensional "slug tracking" model of slug flow has been developed. The underlying principles behind the model have been presented and the closure relationships have been described. The algorithm used to implement the model has been described in detail, together with the assumptions which have been made, and the resulting limitations.

Comparison of the model predictions with experimental slug flow data measured in horizontal and downwardly-inclined pipes has shown that it performs reasonably well, but is sensitive to the exact conditions which are specified to initiate the simulation. This is true particularly for the specification of very short slugs or waves at the pipe inlet: it is found that if these objects

are not specified very accurately at the simulated pipe inlet, their growth or decay along the pipe may not be modelled correctly.

It has been shown that if the liquid superficial velocity is high, so that the ratio of the liquid superficial velocity to the total mixture velocity is greater than about 0.3, realistic slug length distributions are obtained as output from the model at a large distance downstream when very short, high-frequency "precursor" slugs are injected at the pipe inlet. This is in agreement with the results of a model by Cook & Behnia (2000). However, it is likely that, for a given mixture velocity, such high liquid flow rates are more commonly encountered in the plug flow regime. In a systematic study during which low liquid flow rates were specified and the conditions at the pipe inlet were varied, it has been shown that, although the slug initiation process is a robust one, it is not independent of the detailed conditions at a pipe inlet. It is unfortunate, therefore, that a detailed model of slug initiation will be required, in which the physics describing the propagation of very short slugs and waves are incorporated. This is the subject of work in progress by Hale (2000).

Blank page.

Chapter 8: Computational modelling of gas-liquid slug flow

As has been discussed in previous chapters, the state of the art in two- and three-phase flow prediction is largely restricted to one-dimensional phenomenological models (such as that by Taitel & Barnea, 1990) which apply simplified physical models to idealised representations of multiphase systems. Extensions of such models have more recently been used in slug tracking schemes, such as that by Taitel & Barnea (1998) and the improved model presented in Chapter 7 of this thesis. These models rely heavily on empirical closure relationships to permit, for example, prediction of the wall and interfacial shear stresses, the translational velocity of the slug tail and the gas entrainment at the slug front. These closure relationships, which are often regressed from very limited data sets, are necessary to provide the required number of equations to balance the number of "unknown" variables.

The experiments described in Chapters 4, 5 and 6, and the model presented in Chapter 7, are predominantly concerned with two-phase gas-liquid slug flow. Whilst valuable insights into slug flow behaviour have been obtained from experimental techniques such as gamma-ray densitometry and high-speed videography, a better qualitative and quantitative understanding of slug flow phenomena is needed to improve the accuracy of slug flow prediction. The present chapter describes attempts to use three-dimensional Computational Fluid Dynamics (CFD) modelling as a means to this end.

In this chapter, the technique of CFD is introduced with particular reference to the commercial software suite CFX® v.4.3, produced by AEA Technology® plc, which was used in the present work. Issues relating to the generation of a CFD grid, or mesh, are described and the method used to simulate a moving liquid slug within the finite computational domain of a CFD grid is then discussed. Finally, results are presented from a number of "numerical experiments", which were conducted to study the behaviour of a single, isolated slug in varying degrees of detail.

8.1. Computational Fluid Dynamics (CFD)

Computational Fluid Dynamics (CFD) is concerned with the approximate numerical solution of the equations which govern the transport of mass and momentum in a fluid. For an incompressible Newtonian fluid, these are posed as the continuity and Navier-Stokes equations, which for a Cartesian system of coordinates are as follows:

Continuity equation (mass transport)

$$\frac{\partial u}{\partial x}+\frac{\partial v}{\partial y}+\frac{\partial w}{\partial z}=0 \qquad [8.1]$$

Navier Stokes Equations

$$\rho\left(\frac{\partial u}{\partial t}+u\frac{\partial u}{\partial x}+v\frac{\partial u}{\partial y}+w\frac{\partial u}{\partial z}\right)=-\frac{\partial p}{\partial x}+\mu\left(\frac{\partial^2 u}{\partial x^2}+\frac{\partial^2 u}{\partial y^2}+\frac{\partial^2 u}{\partial z^2}\right)+F_x \qquad [8.2]$$

$$\rho\left(\frac{\partial v}{\partial t}+u\frac{\partial v}{\partial x}+v\frac{\partial v}{\partial y}+w\frac{\partial v}{\partial z}\right)=-\frac{\partial p}{\partial y}+\mu\left(\frac{\partial^2 v}{\partial x^2}+\frac{\partial^2 v}{\partial y^2}+\frac{\partial^2 v}{\partial z^2}\right)+F_y \qquad [8.3]$$

$$\rho\left(\frac{\partial w}{\partial t}+u\frac{\partial w}{\partial x}+v\frac{\partial w}{\partial y}+w\frac{\partial w}{\partial z}\right)=-\frac{\partial p}{\partial z}+\mu\left(\frac{\partial^2 w}{\partial x^2}+\frac{\partial^2 w}{\partial y^2}+\frac{\partial^2 w}{\partial z^2}\right)+F_z \qquad [8.4]$$

where F_x, F_y and F_z are respectively the x, y and z components of body forces such as those caused by gravitational or electrical or magnetic fields. With judicious choice of initial and boundary conditions, these systems of equations may be solved simultaneously for the velocity and pressure throughout a system. However, analytical solution of the equations has been possible only for extremely simple systems, and it was not until the application of numerical solution using computers in the 1960s (Harlow & Fromm, 1965) that general progress became conceivable. This marked the advent of a new branch of fluid dynamics; computational fluid dynamics or CFD, in which discretised approximations to the Navier-Stokes equations are solved numerically over a "grid" of nodes representing the region in which the fluid flow occurs.

In this work, the Reynolds-averaged forms of the Navier-Stokes equations are solved. An ensemble average of the system of equations [8.1] to [8.4] is made, with $u=\bar{u}+u'$, *etc.* The ensemble is an hypothetical set of identical realisations of the same flow, which differ only in

the details of the turbulent flow. The average velocity is $\overline{u}$, and u' represents the deviation from $\overline{u}$ for a given realisation.

The Reynolds averaged equations have the same form as Equations [8.1] – [8.4] but with the addition of Reynolds stress terms on the right hand side of Equations [8.2] to [8.4]. These terms have the form $\left(-\rho\frac{\partial}{\partial x_j}\overline{u_i'u_j'}\right)$. Here, x_j stands for (x, y, z), u_i stands for (u, v, w) and the repeated suffix j indicates a summation of three terms. These Reynolds stress terms are approximated using a turbulence model as described below.

Anderson (1995) stated that CFD should be considered to be a third branch of fluid dynamics which supplements, rather than usurps, the two older branches of theoretical and experimental fluid dynamics. That said, CFD is essentially closer to the experimental branch than pure theoretical analysis, since the user performs "numerical experiments" by setting the initial conditions for a flow simulation and then making adjustments to the flow or geometry according to the simulation results. This approach is very similar to the iterative (... design → prototype → testing → redesign → prototype→ ...) procedure used in engineering design, and CFD has developed an important role in this process. For a wide range of applications in the automotive, aeronautical, marine, process and power generation industries, it is often possible to use CFD modelling to obtain design data which would previously have been measured from a preliminary prototype. This allows reductions in both the lead time and the cost for the design and development of a new product.

CFD also has several other advantages over the more traditional branch of experimental fluid dynamics (Fletcher, 1996). In particular, the application of CFD makes possible:

- The study of very large systems, where controlled experiments are difficult or prohibitively expensive to perform (*e.g.* air flow around buildings).
- The study of hazardous systems or systems outside their normal operating envelope (*e.g.* simulation of toxic gas releases from a chemical reactor)

CFD also allows the generation of detailed results for virtually all locations within a flow system, *e.g.*, shear stresses on turbine blades or temperature gradients in a coal burner, which would otherwise be practically impossible to measure without affecting the flow itself. These advantages have brought about the rapid development of CFD as a commercial design and

analysis "tool". However, most practical flows are turbulent and it should be remembered that CFD relies on empirical turbulence models whose generality should always be questioned.

8.2. Commercial CFD software packages

Several major software companies now market their distinct versions of CFD programs, such as CFX, FLUENT, STAR-CD and PHOENICS. All function in essentially the same way, and make extensive use of graphical user interfaces (GUIs) so that the various numerical schemes and physical models are, in general, readily accessible by the user. Commercial CFD software "suites" contain three distinct components: a pre-processor, a flow solver and a post-processor. In this section, a brief introduction of the software package used in the present work, CFX4.3, is given. A detailed discussion of the features of this software is considerably beyond the scope of this thesis, however, and the reader is directed to the CFX4.3 User Guide (AEA Technology, 1999) for further information.

8.2.1. Pre-processor

In the pre-processing stage of the CFD process, the user specifies the geometry of the region in which flow is to be simulated. This region is then subdivided into a "grid" (or "mesh") of small, adjacent "cells", over which the discretised Navier-Stokes equations will be solved. The numerical description of the grid thus produced is written to a file which is subsequently used as input to the flow solver program.

In CFX4.3, two pre-processors are available, MESHBUILD and BUILD. The simpler of these, MESHBUILD, was used for the present work. The region of interest, or "computational domain", is specified graphically by the user. Points, lines and arcs are specified which define internal and external boundaries of the geometry. This may be achieved either by explicitly defining the coordinates of the domain (which was the method used in the present work), or by importing geometry data from compatible Computer Aided Design (CAD) software.

Once the geometry of the system to be studied is specified, the user must define one or more non-overlapping orthogonal "blocks" whose edges will be subdivided to allow generation of the grid. A system with very simple geometry may be specified as a single block, however

more complex simulations may require several blocks. Single- and multi-block representations of a circular pipe are illustrated in Figure 8.1 and Figure 8.2 respectively.

The user may specify a number of two-dimensional "patches" at boundaries of the computational domain, where the boundary conditions to the problem are to be defined. For example, a patch might be defined as an inlet boundary, a pressure boundary or a symmetry plane.

The number and distribution of subdivisions to be applied to the faces of each block are then specified. Several CFD software packages allow subdivision of a surface into triangular elements so that a grid of tetrahedral cells may then be generated. However, CFX4.3 employs quadrilateral subdivisions for surface meshing in order to generate a grid of hexahedral (cuboidal) cells. This is because the solution of the discretised flow equations is simplified using an orthogonal structured grid (Pan, 1996).

Finally, the grid of cells is generated by projection of the surface subdivisions throughout the entire domain. A machine-readable "geometry file" is then written which contains information describing the geometry of the flow domain and the position and orientation of each block, cell and patch within the grid.

In an alternative mode of operation, the user may choose not to define the boundary patches or even create the grid using the pre-processor. In this case, the geometry file contains only the coordinates of the computational domain and the block information. The user must then specify the boundary "patches" and create the grid using instructions in the "command file", which is used to control the flow solver program. This option was not used in the present work.

The issues involved in efficient grid generation are complex and a large body of work is devoted to the subject (*e.g.*, Thompson *et al.*, 1985; Arcilla *et al.*, 1991). The number of cells, their size and their distribution within the mesh may significantly affect the solution of the flow equations (Wendt, 1996). In general, the larger the number of cells in a given domain, the higher the accuracy of the solution. However, a CFD simulation using a "fine mesh" (*i.e.*, a large number of small cells) requires increased computational time and computer memory, and hence is more costly. A compromise must be achieved between the cost and the accuracy required. To achieve this, a grid may be non-uniform, *i.e.* finer in regions where large

variations in flow are anticipated, and coarser in regions where the flow is more uniform. Care must be taken to avoid sudden changes in cell distribution within a grid: geometric progressions may be used to specify the sizes of adjacent cells in order to create a gradual transition between coarse and fine regions of the mesh.

In the present work, grids were created to represent straight pipes of circular cross-section. A circle may be "meshed" in a single block, using a cylindrical or body-fitted grid, as shown in Figure 8.1.

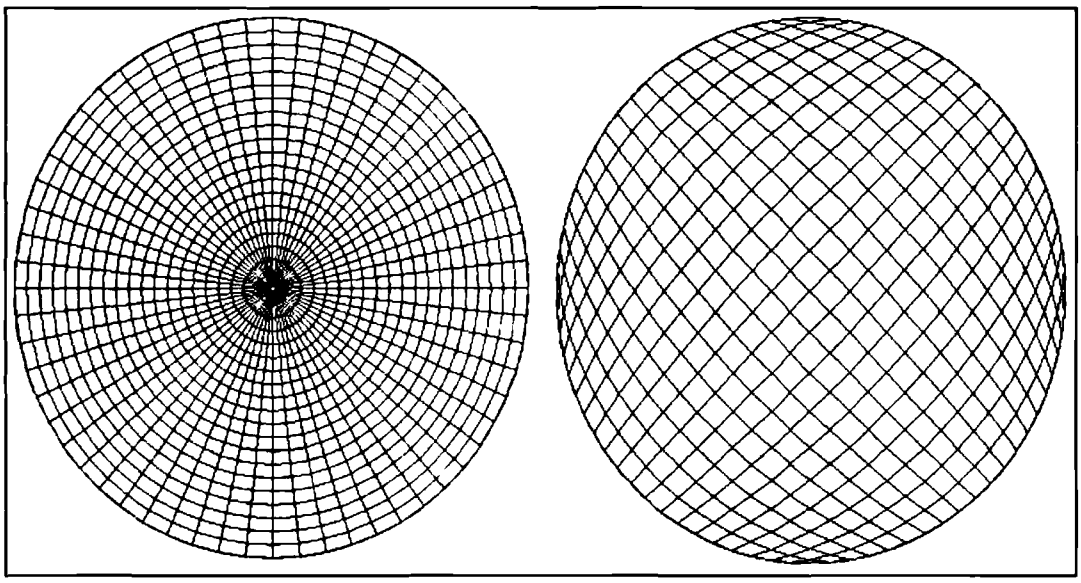

Figure 8.1: Cylindrical and body-fitted single-block grids for a circle

Both of the schemes shown in Figure 8.1 have shortcomings. The cells of the cylindrical mesh converge on a central point and thus the orthogonal grid is highly deformed in this region. In the single-block body-fitted grid, cells are "stretched" near to the circumference of the circle so that their approximation to orthogonal, hexahedral elements is poor. An alternative method for fitting an orthogonal grid to a circle, commonly known as a "butterfly" or "focussed" mesh (AEA Technology, 1999), uses a body-fitted scheme with five blocks and is shown in Figure 8.2. This is characterised by a square or rectangular block in the centre of the circle, with four other blocks surrounding it. The problems associated with both single-block grids are thus avoided: this leads to fewer convergence problems during the solution of the discretised equations.

In the present work, "butterfly" grids were employed wherever possible. However, for one series of simulations, a single-block body-fitted grid as shown in Figure 8.1 was used. This work is discussed further in Section 8.5.

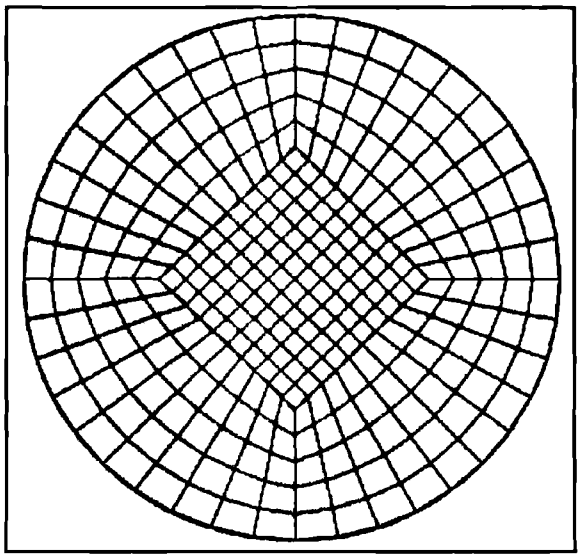

Figure 8.2: Five-block "butterfly grid"

If a flow is symmetric about an axis or a plane, it is frequently possible to model a small portion of the complete flow domain and then reflect the results in the appropriate direction. For example, a pipe flow may be axi-symmetric (*e.g.*, in vertical flow) so that it is possible to model a thin "wedge" of a pipe as a sector of a cylindrical grid, using symmetry boundaries in the appropriate places. This may result in extensive savings in computing resources, or allow the use of a much finer mesh than could be used if the entire flow domain was modelled. In the present work, the flow was always assumed to be symmetrical about the vertical bisecting plane of the horizontal pipe being modelled. Thus, "half-pipe" grids were used, as shown in Figure 8.3.

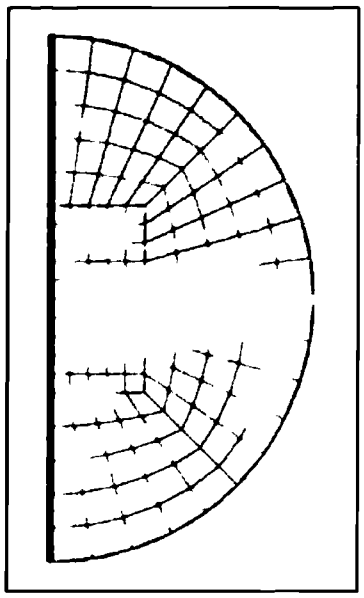

Figure 8.3: "Half-pipe" four-block grid, showing line of symmetry

Once generated, a geometry file may be further optimised using a secondary pre-processor, which identifies blocks within the grid which may be merged to improve the structure of the mesh and reduce the complexity of the solution. A second, smaller geometry file is produced in which the features of the grid are described more efficiently. The secondary pre-processor in CFX4.3 is called CFX-MESHIMPORT and was used in the present work.

8.2.2. Flow solver

The flow solver makes approximations to the partial differential equations for mass and momentum using discretised forms of the derivatives. The resulting equations are no longer continuous and can thus be applied to the discrete mesh of cells.

Transformation

If a body-fitted grid is used, the equations must be transformed into an alternative coordinate system than that used by the pre-processor, so that all cells in the grid are identical in computational space, before the equations are discretised. This is a purely internal operation within the CFD code, performed in CFX4.3 using the algorithm by Rhie & Chow (1983). The user has no control over this process: a reverse transformation is performed before the final results are accessed by the user. The transformation operation is discussed by Pan (1996), and in considerable detail by Ferziger & Perić (1997). The particular transformation algorithms employed within CFX4.3 are described in the software documentation (AEA Technology, 1999).

Discretisation

Three distinct approaches to the numerical solution of the Navier Stokes equations are commonly used by CFD software: finite difference methods (FDMs), finite element methods (FEMs) and spectral methods. Each uses a different method of approximating the unknown variables in the partial differential equations. FDMs use truncated Taylor series for the approximation of the derivatives, FEMs describe the local variation of unknown variables using simple linear or quadratic functions, and spectral methods use truncated Fourier series for the approximation. The different methods are discussed by, amongst many others, Ferziger & Perić (1997) and Fletcher (1996).

The basis of CFX4.3 is a "conservative finite-difference method", (also called a "vertex-centred finite-volume method" by Wendt, 1996) which uses truncated Taylor series expansions for the discretisations. Variables are defined at the centre of each cell in the mesh, and the equation for each variable is integrated over each control volume to obtain a discrete equation which connects the variable at the centre of the control volume with its neighbours. This procedure is described fully in the CFX4.3 documentation (AEA Technology, 1999).

Solution

The discretised Navier-Stokes equations form a large system of non-linear equations which is then solved using iterative matrix techniques, which are preferred to more computationally-intensive direct techniques such as Gaussian elimination (Pan, 1996).

Iteration is used to progressively adjust an initial guess in order to systematically approach a solution. Two "nested" iterations are used. During the "inner" iteration, the discrete spatial transport equation for each variable is solved in turn, using fixed values of all other variables. The "outer" iteration then solves for the coupling between the variables.

For incompressible flows, pressure does not obey a transport equation, so an alternative treatment must be used. At each outer iteration, a pressure-velocity coupling algorithm is used to simultaneously calculate the pressure in each cell and estimate corrections to the velocity components, so that mass is conserved. CFX4.3 uses a variation of Patankar & Spalding's (1972) SIMPLE (Semi-Implicit Method for Pressure Linked Equations) algorithm, known as the SIMPLEC (SIMPLE Corrected) algorithm (Van Doormaal & Raithby, 1984).

The CFX4.3 flow solver is controlled using a "command file" to specify parameters used by the solver. These parameters include the physical properties of the fluid(s), boundary conditions, physical models (*e.g.* turbulence) used in the simulation, the differencing and pressure-velocity coupling schemes to be used, the number of iterations and timesteps, output options (the level of detail and interval at which it is to be produced), *etc.*

In the present work, only a very small subset of the available features in CFX4.3 was used. Though the software is capable of simulating a practically infinite range of physical systems, most users (the present author included) are familiar only with those features which they use in their own applications. Cheo (1995) noted that this often leads to embarrassment when a novice CFD user approaches a CFD "expert" for help: even very experienced CFD users are often completely unfamiliar with features of the software other than the small number which they themselves use.

8.2.3. Physical models

To simulate any system other than the most idealised cases, physical models must be used in conjunction with the basic mass and momentum conservation equations, to account for (*e.g.*) turbulence, non-Newtonian fluid behaviour, heat and mass transfer, multiphase flow, *etc.* CFX4.3, in common with all commercial CFD software packages, incorporates a range of models for different types of flow and several physical processes.

A detailed description of all the available features is given in the CFX4.3 documentation (AEA Technology, 1999), however three aspects of the model developed in the present work are discussed in this Section.

Turbulence modelling

A number of turbulence models are available for turbulent flow calculations, of which the k-ε model is perhaps the best known. This model is used in the present work (and by default in CFX4.3). A detailed description of the model is given by Jones & Launder (1972). In effect, the k-ε model uses an eddy-viscosity hypothesis for the turbulence, so that the Reynolds stresses $\left(-\rho\overline{u_i'u_j'}\right)$ are modelled as

$$-\rho\overline{u_i'u_j'} \approx \mu_T \frac{\partial \overline{u}_i}{\partial x_j} \qquad [8.5]$$

This has the effect of replacing the viscosity term in the momentum equations [8.2] – [8.4] with an "effective viscocity", μ_{eff}, defined as

$$\mu_{eff} = \mu + \mu_T \qquad [8.6]$$

Here, μ_T is the turbulent viscosity, which is assumed to be

$$\mu_T = C_\mu \rho \frac{k^2}{\varepsilon} \qquad [8.7]$$

where C_μ is an empirical constant whose value is approximately 0.09 (Young, 1989) and k is the mean turbulent kinetic energy per unit mass,

$$k = \frac{1}{2}\left(\overline{u'^2} + \overline{v'^2} + \overline{w'^2}\right) \qquad [8.8]$$

where u′, v′ and w′ are the fluctuating velocity components in the x, y and z-directions respectively. The turbulence dissipation rate (*i.e.*, the rate at which turbulent kinetic energy is destroyed by viscous action) ε is related to a characteristic length scale of the turbulence, L_ε,

$$\varepsilon = \frac{k^{3/2}}{L_\varepsilon} \qquad [8.9]$$

Transport equations are then written for the scalars k and ε, which are solved as discussed in Section 8.2.2. These are

$$\frac{\partial}{\partial t}(\rho k) + \frac{\partial}{\partial x_i}\left(\rho \overline{u_i}\right) - \frac{\partial}{\partial x_i}\left[\left(\mu + \frac{\mu_T}{\sigma_k}\right)\frac{\partial k}{\partial x_i}\right] = P - \rho\varepsilon \qquad [8.10]$$

and

$$\frac{\partial}{\partial t}(\rho\varepsilon) + \frac{\partial}{\partial x_i}\left(\rho \overline{u_i}\,\varepsilon\right) - \frac{\partial}{\partial x_i}\left[\left(\mu + \frac{\mu_T}{\sigma_\varepsilon}\right)\frac{\partial \varepsilon}{\partial x_i}\right] = C_1 P\left(\frac{\varepsilon}{k}\right) - C_2\rho\left(\frac{\varepsilon^2}{k}\right) \qquad [8.11]$$

where U is the mean fluid velocity and P is the shear production rate, which for incompressible flow is defined as

$$P = \mu_{eff}\frac{\partial u_i}{\partial x_j}\left(\frac{\partial u_i}{\partial x_j} + \left(\frac{\partial u_j}{\partial x_i}\right)\right) \qquad [8.12]$$

The values of the constants are given in Table 8.1.

Constant in k-ε model	Value
C_μ	0.09
σ_k	1.00
σ_ε	1.30
C_1	1.44
C_2	1.92

Table 8.1: Constants used in the k-ε turbulence model (Abbot & Basco, 1989)

A modification to the transport equations for k and ε is available in CFX4.3 in the form of the "deferred correction" option. This may be invoked by the user to reduce or eliminate difficulties caused by non-convergence of the equations to a unique solution. This option effectively "switches off" the higher-order terms in the transport equations for k and ε, resulting in a more robust but less accurate solution. Most commonly, the user may specify that the truncated equations are used for a certain number of iterations during the calculation, and the complete equations are used thereafter.

A wall boundary condition for velocity must be provided, which defaults in CFX4.3 to zero velocity ("no slip") at the wall. This was adopted for the present work. However, the k-ε model is not used in the near-wall region as it cannot describe the turbulent velocity profile. Close to the wall ($y^+ \leq 5$) it can be shown (Young, 1989) that:

$$u^+ = y^+ \qquad [8.13]$$

where u^+ and y^+ are the dimensionless fluid velocity and the dimensionless distance from the wall, respectively:

$$u^+ = \frac{u}{u^*} \qquad [8.14]$$

$$y^+ = \frac{y\rho u^*}{\mu} \qquad [8.15]$$

Here, u^* is the "friction velocity",

$$u^* = \sqrt{\frac{\tau_w}{\rho}} \qquad [8.16]$$

Further from the wall, for Newtonian fluids the flow is represented by:

$$u^+ = \frac{1}{\kappa} \ln y^+ + B \qquad [8.17]$$

where κ, the von Karman constant, is equal to 0.4 and B has a value of 5.5 for smooth walls. Equations [8.13] and [8.14] are used to describe the velocity profile near to the wall. The k-ε model is used from a distance of about $y^+ = 30$ outwards.

Free surface modelling in multiphase flows

The present work is principally concerned with the modelling of the gas-liquid interfaces in two-phase slug flow. Two alternative methods are used to model interfaces, or *free surfaces*, in CFD simulations (Ferziger & Perić, 1997). In an *interface tracking method*, as illustrated in Figure 8.4, the free surface is made up of cell boundaries. This produces a sharp interface and the grid is readjusted at each time step in a transient simulation.

Alternatively, *interface capture methods* may be used, where the interfacial shape is determined by cells which are partially filled, illustrated in Figure 8.5. This is achieved either by the solution of a transport equation for the liquid-phase holdup, as in the "volume of fluid", or VOF method, or by tracking the motion of zero-mass particles which are initially positioned at the original location of the interface.

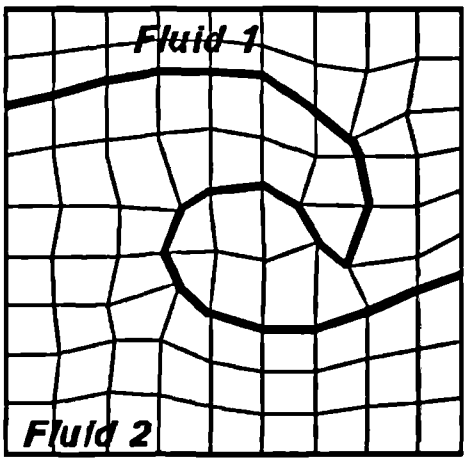

Figure 8.4: Interface tracking by grid deformation (after Ubbink, 1997)

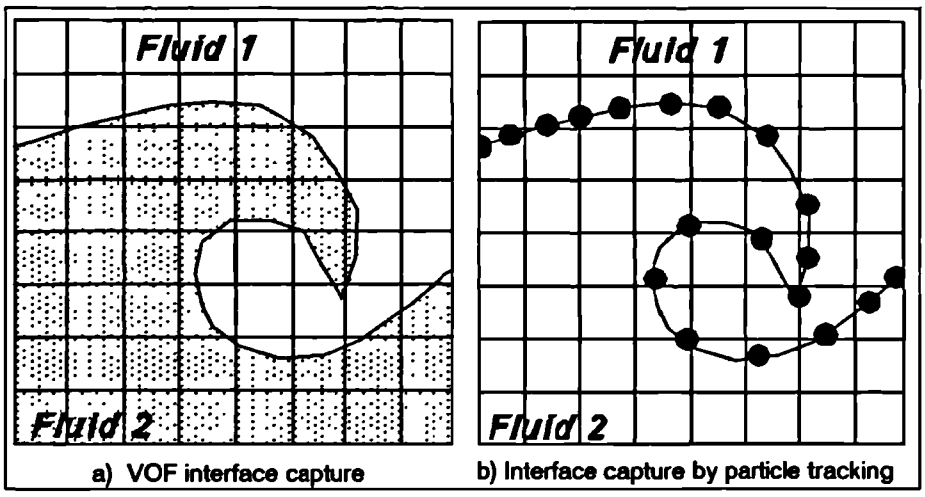

Figure 8.5: Interface capture methods (after Ubbink, 1997)

CFX4.3 incorporates two basic models for multiphase flows, namely a multi-fluid model and a VOF model. The multi-fluid model has one solution field for each phase. These interact via inter-phase transfer of transported variables (*e.g.*, momentum, heat and mass). An inter-phase slip algorithm is then used to solve the coupled equations.

The VOF model (referred to, confusingly, as the "homogeneous model" in CFX4.3) is used in the present work. In this method, the solution fields for each phase are approximated to a single flow field for one "fluid" whose physical properties vary between the extremes of the individual phases, depending on the value of a volume fraction scalar. This is illustrated in Figure 8.6. The volume fraction of the liquid phase, ε_L, is assumed to obey a transport equation and is convected with the fluid.

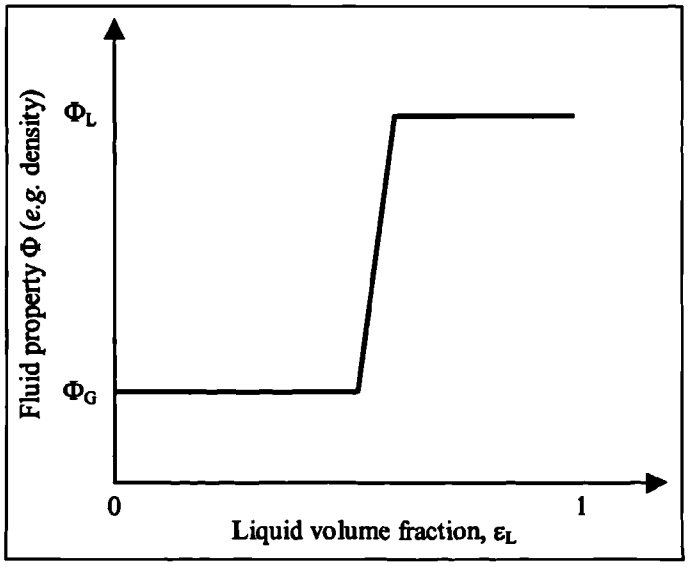

Figure 8.6: Variation of "homogeneous fluid" property with volume fraction

The position of the interface is assumed to be where the value of the volume fraction scalar is equal to 0.5. The curvature of the interface is also calculated, using the method of Hirt & Nichols (1981).

An inherent problem with the VOF method is "smearing" of the interface due to numerical diffusion. In CFX4.3 a "surface sharpening algorithm" is available, which attempts to overcome this by correction of the volume fraction scalar at the end of each timestep.

Firstly, the cells which lie on the interface are identified by determining whether (ε_L - 0.5) for each cell is different in sign from any of the surrounding control volumes. Then, fluid located on the "wrong" side of the interface is identified and moved to the correct side, ensuring that volume is conserved. This negative diffusion method effectively prevents simulation of cases where there is dispersion of gas in the liquid phase, or *vice versa*. Despite this limitation, interface sharpening was used in the present work. One of three options, or "levels", may be selected for the algorithm, levels 1, 2 or 3. This specifies respectively whether all, some or none of the cells on the interface remain fixed during the sharpening operation. The default level of sharpening is level 2, and this option was used throughout the present work.

Surface tension model

In his CFD study of the fluid flow in a slug tail, Pan (1996) was unable to incorporate the effects of surface tension as a reliable surface tension model was not, at that time, available for use with CFX. This resulted in difficulties in the simulation of the slug tail shape and effectively prevented modelling of the slug front.

Recent releases of the software, CFX4.2 and CFX4.3 (used here) include a model for surface tension at the interface between two fluids, which can be used with the VOF model. The model used in CFX-4 is based on the Continuum Surface Force model of Brackbill *et al.* (1992), and leads to an extra body force in the momentum equation, F_s,

$$F_s = \sigma \kappa \mathbf{n} \qquad [8.18]$$

where σ is the surface tension coefficient (equal to 0.0725 Nm^{-2} for air/water), κ is the surface curvature defined as

$$\kappa = \nabla \bullet \mathbf{n} \qquad [8.19]$$

and **n** is the normal to the surface, given by

$$\mathbf{n} = \frac{\nabla \varepsilon_L}{|\nabla \varepsilon_L|} \qquad [8.20]$$

where ε_L is the volume fraction of the liquid phase.

The "wall adhesion force" which occurs where the interface between the two fluids intersects a wall can also be included in this treatment, if the surface normal and the curvature are modified in the vicinity of the walls. An additional boundary condition for volume fraction at the wall must be set so that the normal vector **n**, defined as the volume fraction gradient, is at the required contact angle to the wall. The default wall contact angle of 90° was used in the present work.

8.2.4. Post-processing

The main output from the flow solver is in the form of large sets of values for the velocity components, pressure, viscosity, volume fraction, *etc.*, for each point in the grid and at user-specified intervals during the iterative and/or transient calculation. These data are displayed and analysed using a graphical post-processor program which incorporates data visualisation tools including mesh display, vector plotting, contour plotting, 3D surface plots and particle tracking. The graphical images are easily manipulated (by translation, rotation, zooming *etc.*) for presentation.

A second, smaller output file is also produced by CFX4.3 which contains a summary of the iteration procedure (to allow the user to check for errors during convergence) and also a user-specified data set in the form of a large list of numbers. The user may thus obtain quantitative results by direct evaluation of these data.

Two graphical post-processors were used in the present work: CFX-VIEW (which was used almost exclusively) and CFX-ANALYSE, a newer package which was used to obtain a few three-dimensional images. In many cases (see Section 8.5) the solution results were viewed using a post-processor and then a series of high resolution "screen capture" images was produced. Measurements (*e.g.*, of slug length) were then made directly from the images, by studying each image at high magnification using third-party graphics software (Paintshop Pro® v.5.0).

8.3. CFD modelling of slug flow

To the present author's knowledge, only limited application of CFD has been made to the study of slug flow. Hope (1990) identified the feasibility of modelling a single Taylor bubble using a moving-wall boundary condition and performed a qualitative investigation of this using the PHOENICS software. Subsequently Pan (1996) extended this work using a predecessor of CFX4.3, CFDS-FLOW3D, and conducted a detailed investigation of the behaviour of the nose of a single Taylor bubble at different pipe inclinations. In particular, Pan's CFD calculations of the translational velocity of the Taylor bubble in a horizontal pipe as a function of the total superficial velocity were very similar to the experimental results obtained by Manolis (1996) in the WASP facility at Imperial College. This is discussed further in Section 8.4.

Pan's work has recently been extended to three-phase gas-liquid-liquid slug flow by Odozi (2000) although CFD modelling of three-phase flow using the VOF model in CFX4.3 has been found to be problematic.

A short study by Ejedawe and Hughes (1999), under the supervision of the present author, used CFX4.2 to develop a method for simulation of the front and tail of a Taylor bubble. This preliminary work is extended and discussed in Sections 8.5 and 8.6.

Other groups of workers have also reported studies of slug flow using CFD. Mao & Dukler (1991) wrote a dedicated CFD program to simulate the liquid flow around a Taylor bubble in vertical flow: Pan (1996) reported that this was "limited in ability and flexibility". Issa & Tang (1990) used a similar approach, also for vertical flow. Moe (1993) simulated the motion of a single bubble in a pipe containing stagnant liquid, but did not extend this to flowing systems. Recently, Ubbink (1997) included a case study of the shape and rise velocity of Taylor bubbles in vertical flow as part of a more general investigation into modelling of gas-liquid interfaces. He used a moving-wall boundary condition and simulated a "wedge" of the axi-symmetric vertical flow. The initial position of the interface was taken from experimental observations and Ubbink simulated the development of the interface shape with time.

Lun *et al.* (1996) used the commercial CFD program FIDAP to simulate the growth of a wave on the interface of "two immiscible fluids with different properties" (although the authors did not report which fluids) in a horizontal stratified gas-liquid flow. The method used to

simulate the free surface was not described. Lun *et al.* (1996) developed a coarse two-dimensional grid to represent the flow domain. Significant numerical instabilities during the solution, leading to convergence difficulties, were reported. These were ascribed to the coarse mesh. The authors reported results showing the growth of a wave until it completely broached the pipe and thus initiated slug flow. However, it seems unlikely that the simulated wave growth was completely unrelated to the numerical instabilities; this calls into question the results' credence.

8.3.1. Simulating slug flow in a CFD grid

To "capture" a moving slug within the finite flow domain of a CFD grid, a moving-wall boundary condition is employed in the present work, as proposed by Hope (1990). This is illustrated in Figure 8.7. The wall boundaries of the grid are moved at a velocity U_{Wall}, equal and opposite to the translational velocity of the slug tail. Liquid is admitted to the "downstream" boundary plane of the grid at velocity ($U_{Wall} - u_{LS}$), where u_{LS} is the superficial velocity of the liquid inside the slug body. In the present work, a uniform velocity profile was used at the liquid inlet boundary and entrainment of gas in the liquid was not modelled. Thus, u_{LS} is equal to the total superficial velocity, U_{Mix}.

The initial position of the gas-liquid interface at the slug tail is specified according to the desired length of the slug to be studied. At the start of the simulation, the interface is flat and vertical as if supported by an imaginary "dam". When this "dam" is instantaneously removed (*i.e.*, when the transient simulation is started) the liquid flows along the pipe under the action of gravity and wall shear stress, and a phase distribution develops over a period of about 2 seconds (Pan, 1996) which is equivalent to a slug tail. After this period, the shape of the interface remains roughly constant, however its axial position in the grid may slowly change.

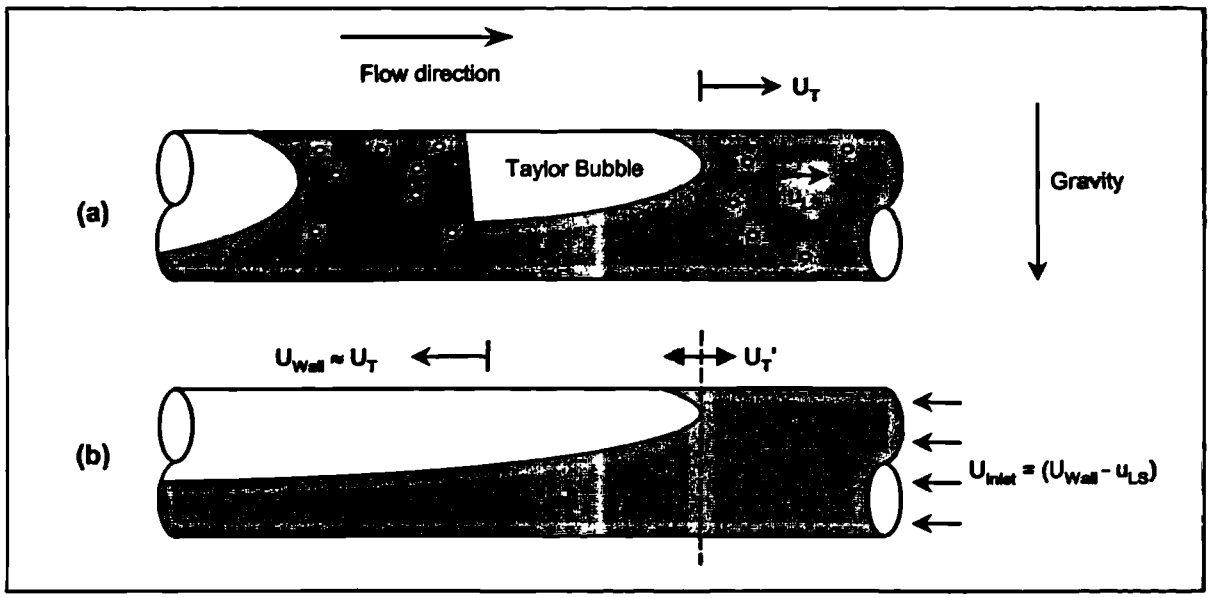

Figure 8.7: Slug flow in (a) fixed and (b) moving coordinate systems

If the specified wall velocity is exactly equal to $-U_T$ then a "steady-state" is eventually reached in which the slug tail position within the grid does not change with time. However, if the velocities are not quite equal, a slug tail develops whose shape is almost indistinguishable from the "steady-state" case but whose position in the grid moves at velocity U_T'. Thus, the translational velocity of the slug tail can now be calculated as

$$U_T = \left(-U_{Wall} + U_T'\right) \qquad [8.21]$$

Features of the half-pipe, moving-wall grid are illustrated in Figure 8.8, which also shows the initial position of the interface for a slug tail simulation, discussed in Section 8.4 below.

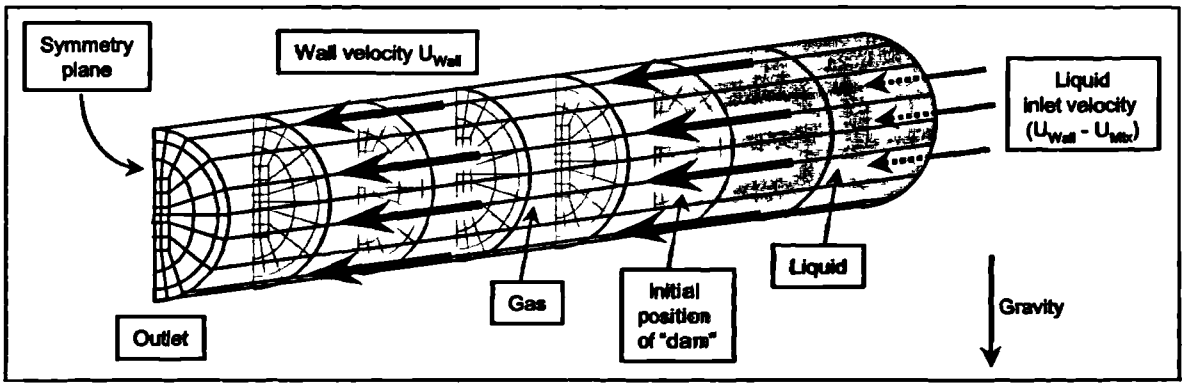

Figure 8.8: Moving-wall grid for a slug tail simulation

The outlet plane of the grid is modelled as a pressure boundary. In CFX4.3, the pressure at the boundary plane is user-specified. Neumann boundary conditions, *i.e.*, zero normal gradients, are imposed on velocity and also on all other transported variables, *i.e.*, k, ε, temperature, volume fractions *etc.* A value of 0.0 bar(g) (*i.e.*, atmospheric pressure) was used for the outlet pressure throughout the present work.

For all cases simulated in the present work, air and water were used for the "test fluids". Values of the fluids' physical properties (density, viscosity, *etc.*) were obtained from the database in CFX4.3, at an arbitrarily selected reference temperature of 288 K.

The "ambient values" of the density and viscosity of the fluid *outside* the pressure boundary default in CFX4.3 to those of the denser phase in a multiphase simulation. This creates a vertical pressure gradient across the pressure boundary, so that outflow of fluid from the grid may be affected. To reduce these effects, the "ambient phase" beyond the pressure boundary was specified to be air at atmospheric pressure and 288 K.

8.4. A model of the slug tail

Pan (1996) conducted simulations to investigate the effect of the total superficial velocity (U_{Mix}) and also the liquid viscosity on the slug tail translational velocity. His calculations were performed on a single-block body-fitted grid, in the absence of a surface tension model. A similar set of simulations has been performed for the present work, using a "butterfly" grid and including surface tension effects.

A semi-cylindrical, four-block, "butterfly" grid was constructed to represent a section of pipe of diameter 80 mm and length 2.4 m. In the axial direction, the pipe was divided into 100 cells, using a symmetrical geometric progression to give a finer mesh at the middle of the pipe, where the slug tail was situated. The grid is illustrated in Figure 8.9. The vertical scale in Figure 8.9(b), showing the axial cell distribution, is exaggerated by a factor of 3.8.

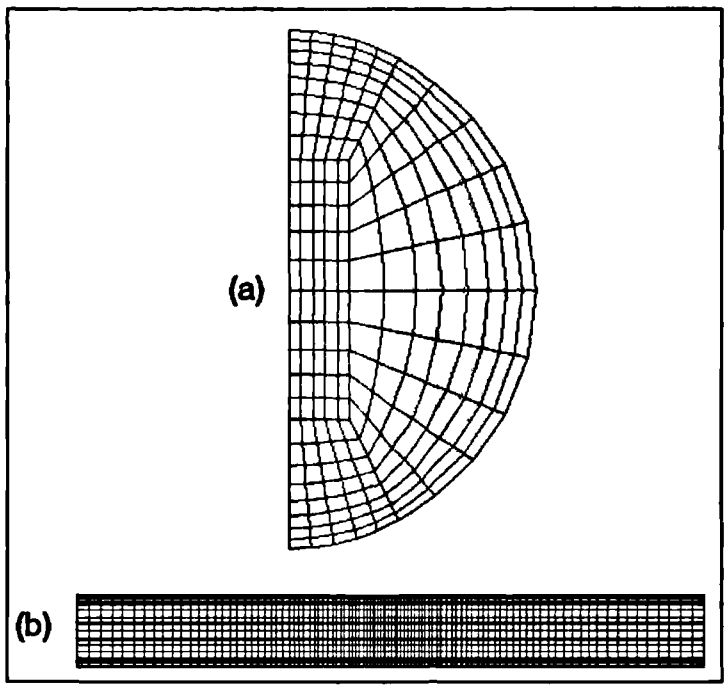

Figure 8.9: (a) Radial and (b) axial cross-sections of the grid used for the slug tail simulations

The initial position of the "dam-break" interface was half-way along the grid, *i.e.*, 1.2 m from the inlet boundary, and simulations of 5 seconds duration were conducted using timesteps of 0.01 seconds (Pan, 1996, found no difference between the results of simulations using 0.005 and 0.02 seconds). Each timestep was solved using twenty outer iterations, as it was found that this gave a similar "residual error sum" (a measure of the degree of convergence of the solution) to simulations using thirty iterations, but with less computational expense. If ten iterations were used per timestep, it was found that the residual error sum was approximately 50% greater than for the twenty-iteration case.

The "mass source residual sum", reported by the solver program at the end of each iteration, was monitored in order to gauge the degree of convergence. This value has dimensions of mass per unit time. It has been suggested (Lo, 1998) that an acceptable criterion for convergence of each timestep of a transient simulation, might be when the ratio of the mass source residual sum to the mass flow through the flow domain's inlet boundaries falls below a value of 10^{-3}. In the present work, this was used as a rough guide, but generally a more stringent criterion of 10^{-4} was used.

8.4.1. Results and discussion

Sample results showing the development of the interface after a dam break are shown in Figure 8.10. Air is shown as white and water is shown as grey. In this case, the wall velocity is 8 m/s from right to left, with a liquid inlet velocity of 1.2 m/s from the right hand side. The plots show the distribution of the phases *at the central symmetry plane of the pipe.* The vertical scale has been exaggerated (vertical : horizontal ratio = 3.8 : 1) to show the interface shape in greater detail. Only the central 1.4 m of the simulated region is shown. The simulation extends approximately 0.5 m in each direction beyond the edges of the Figures shown.

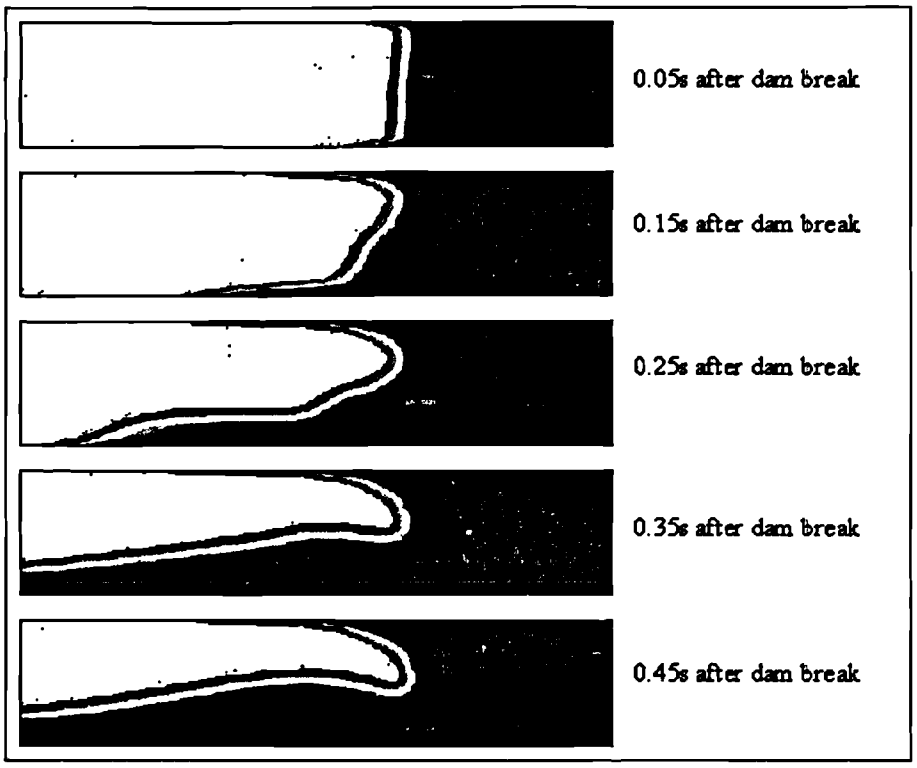

Figure 8.10: Development of the slug tail shape after a dam-break

Numerical experiments were conducted using this model with the values of the wall velocity used by Pan (1996). For each case, the liquid inlet velocity was adjusted in steps of 0.01 m/s until the axial position of the slug tail, once developed from the initial "dam-break", remained constant in the grid between 3.0 seconds and the end of the simulation at 5.0 seconds. Pan's data were used as a starting point and then a trial-and-error procedure was adopted to identify the value of the liquid inlet velocity (to the nearest 0.01 m/s) which gave a steady-state solution. The results are shown in Table 8.2.

Case	U_{Wall} / m/s	Mixture velocity, U_{Mix} / m/s	Inlet velocity, (U_{Wall} - U_{Mix}) / m/s	U_{Mix} / m/s (Pan, 1996)
1	0.94	0.50	0.44	0.5
2	1.44	1.00	0.44	1
3	2.47	2.01	0.46	2
4	3.49	3.05	0.44	3
5	4.60	4.07	0.53	4
6	6.86	6.06	0.80	6
7	9.14	8.04	1.10	8

Table 8.2: Results from slug tail velocity simulations

It was found that Pan's values of the liquid inlet velocity were slightly too high for the current simulations, so that the slug was not stationary within the mesh and the slug tail moved "upstream" towards the pressure boundary. In all cases, very little correction (a few percent) was needed to produce a steady-state result. It is suggested that this correction is due to the additional surface tension effects, and the more sophisticated four-block mesh incorporated in the present work.

From the results in Table 8.2, the ratio (U_T / U_{Mix}) is readily obtained for each "steady-state" slug tail calculation. The data are plotted in Figure 8.11 and compared with experimental data measured at Imperial College by Manolis (1995), in the WASP and Low Pressure Rig (LPR) facilities. Also plotted are the CFD results by Pan (1996). The Froude number, plotted as abscissa, is defined as

$$Fr = \frac{U_{Mix}}{\sqrt{gD}} \qquad [8.22]$$

where g is the acceleration due to gravity and D is the pipe diameter.

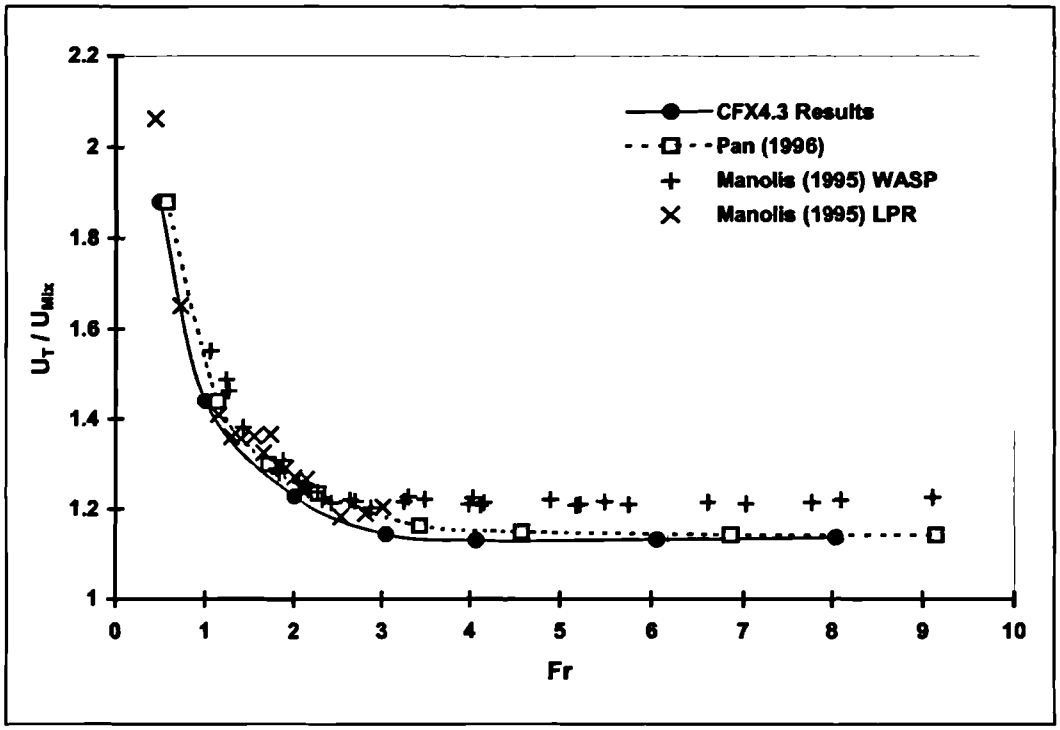

Figure 8.11: Slug tail velocity results

Both the results by Pan (1996) and the present work slightly underpredict the experimental data. Indeed, the underprediction is slightly more significant when surface tension effects are included. At higher Froude numbers, both CFD simulations tend towards the same result, $(U_T/U_{Mix}) \approx 1.14$. This is significantly lower than the widely-accepted value of 1.2, recommended by Bendiksen (1984) for $Fr \geq 3.5$, which is much closer to the experimental data.

The slug tail shapes (seen 5.0 seconds after the start of the simulation) are plotted in Figure 8.12 for the 7 cases listed in Table 8.2. As in Figure 8.10, the vertical scale in each diagram has been exaggerated by a factor of 3.8 and only the central section of the simulated result is shown.

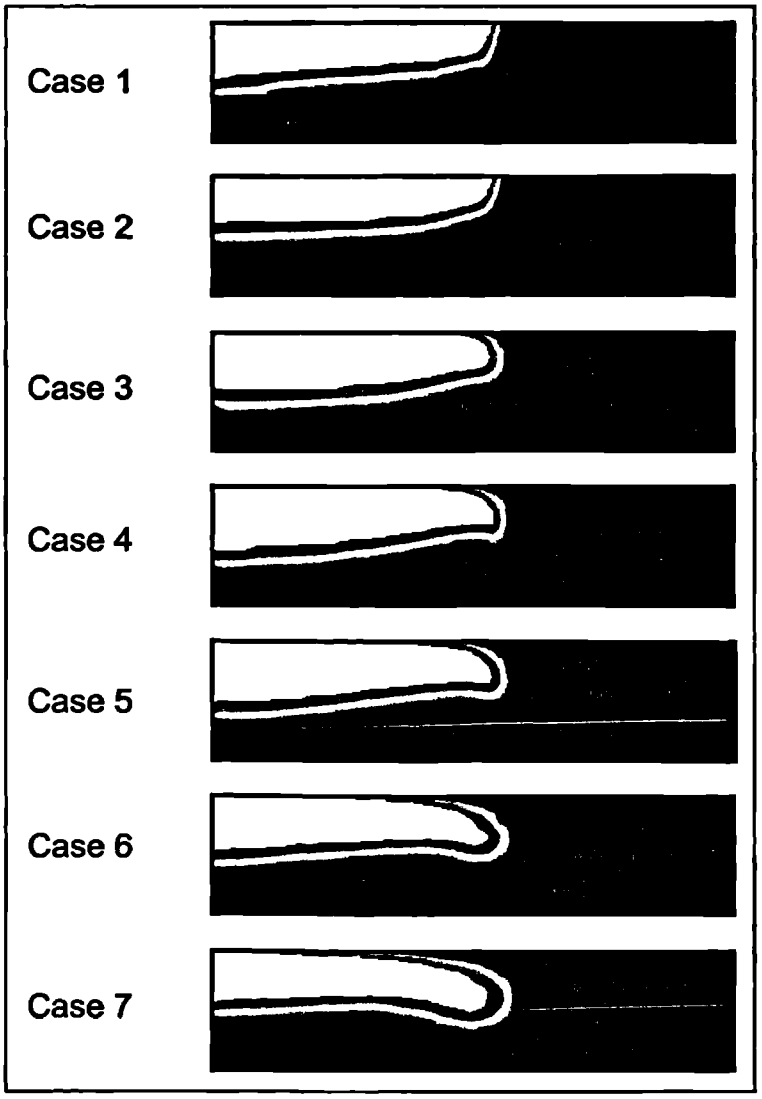

Figure 8.12: Interface shapes for the slug tail simulations listed in Table 8.2.

The process of liquid drainage from the tail of the slug is highly three-dimensional at elevated Froude numbers. This is discussed in Section 8.5.1 below. It is found that at low velocities, the Taylor bubble does not protrude into the body of the slug, but as the translational velocity is increased, the nose of the bubble protrudes further into the slug and moves closer to the axial centreline of the pipe, as shown in Figure 8.13 below.

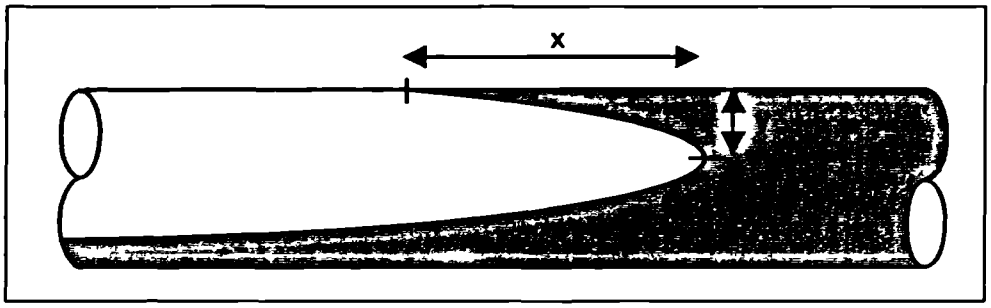

Figure 8.13: Diagram showing bubble penetration into the slug

The axial and radial distances by which the bubble nose penetrates into the slug body are shown in Figure 8.14 and Figure 8.15 respectively. These effects are consistent with experimental observations such as those by Bendiksen (1984).

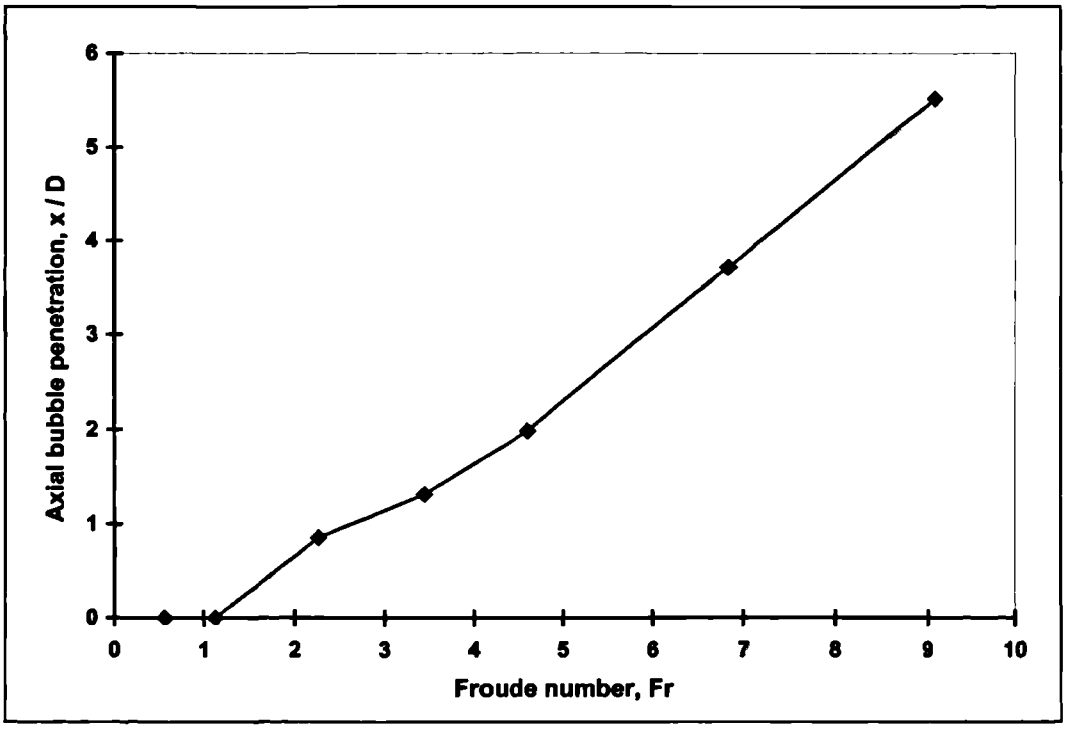

Figure 8.14: Bubble penetration in the axial direction

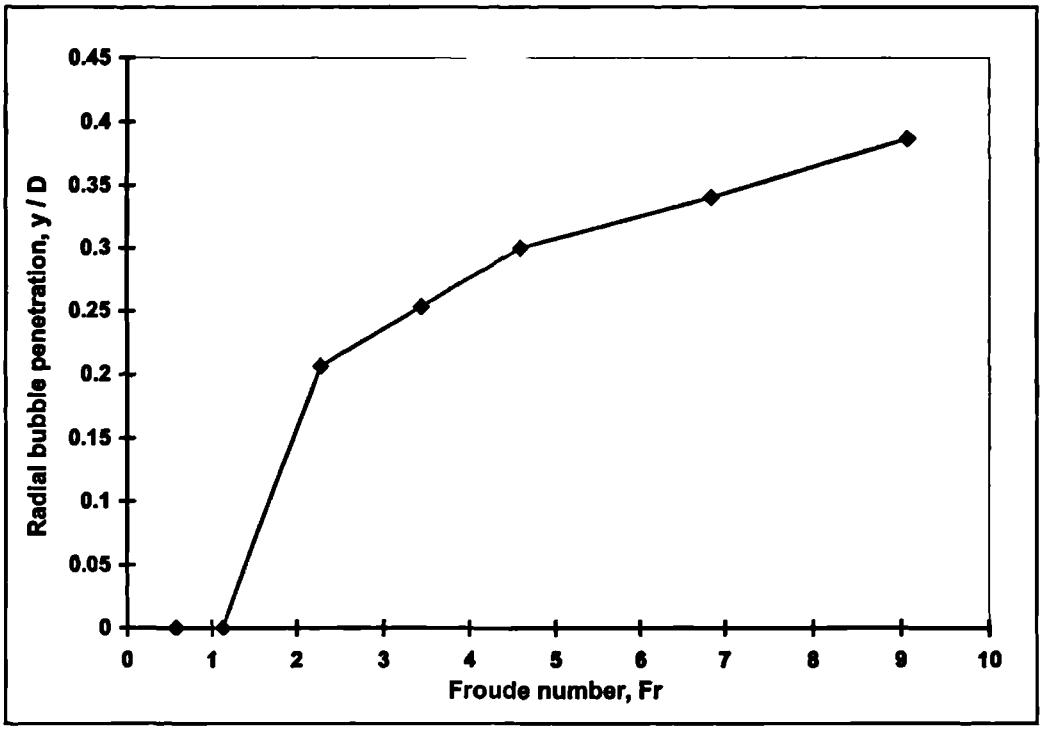

Figure 8.15: Bubble penetration in the radial direction

Ejedawe & Hughes (1999) showed that when surface tension effects are included in the simulation, the nose of the Taylor bubble is predicted to lie closer to the central axis of the pipe, for a given Froude number, than was suggested by the results of Pan (1996).

To investigate the grid-dependence of the solution, the cases summarised in Table 8.2 were run again using a coarser grid, shown in Figure 8.16. The dimensions of the flow domain are identical to those in Figure 8.9 above, however the cell distribution is considerably more coarse. The grid contains 60 cells in the axial direction, arranged as before using a geometric progression to describe the cell distribution.

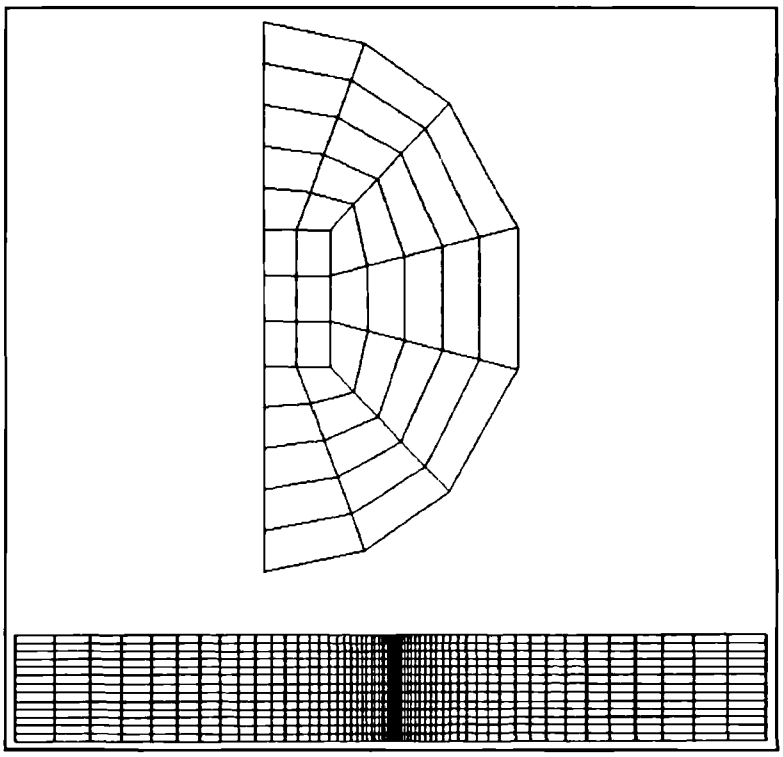

Figure 8.16: Coarse grid for slug tail simulations

For each case, the value of the liquid inlet velocity required to produce a steady-state solution was found to be the same as for the fine-grid results shown in Table 8.2, to within 0.002 m/s.

8.5. The "solid slug front" (SSF) model

The results discussed in Section 8.4 were produced in the absence of any effects resulting from the presence of the slug front, and assume a fully-developed turbulent velocity profile within the slug body. In each case, the inlet velocity profile was taken to be uniform and a distance of 1.2 m (L/D = 15) was allowed for the flow to develop. This is clearly not an accurate representation of the entire flow field within the slug.

The mixing of the liquid film after it is "picked up" by a faster-moving slug has a significant effect on the fluid flow within the slug and the development of the velocity profile along the slug body. Photographic studies (Davies, 1992) have shown the presence of a "recirculation zone" at the slug front which strongly affects the entrainment and dispersion of gas bubbles, and the wall shear stress within the slug. The recent experimental results of Fagundes Netto *et al.* (1998) and Cook & Behnia (2000) have demonstrated a variation in slug translational velocity as a function of slug length. It is thought that this is due in part to the interaction of the slug tail with the recirculation zone for shorter slugs.

In the present work, a number of CFD simulations have been performed using a solid barrier to approximate the effects of the gas-liquid interface at the slug front. This allows the pickup of liquid at the slug front to be modelled, so that the recirculation zone is simulated. The moving-wall model of the slug tail (Section 8.4) is now extended to include the solid boundary at the slug front. An illustration of this is shown in Figure 8.17.

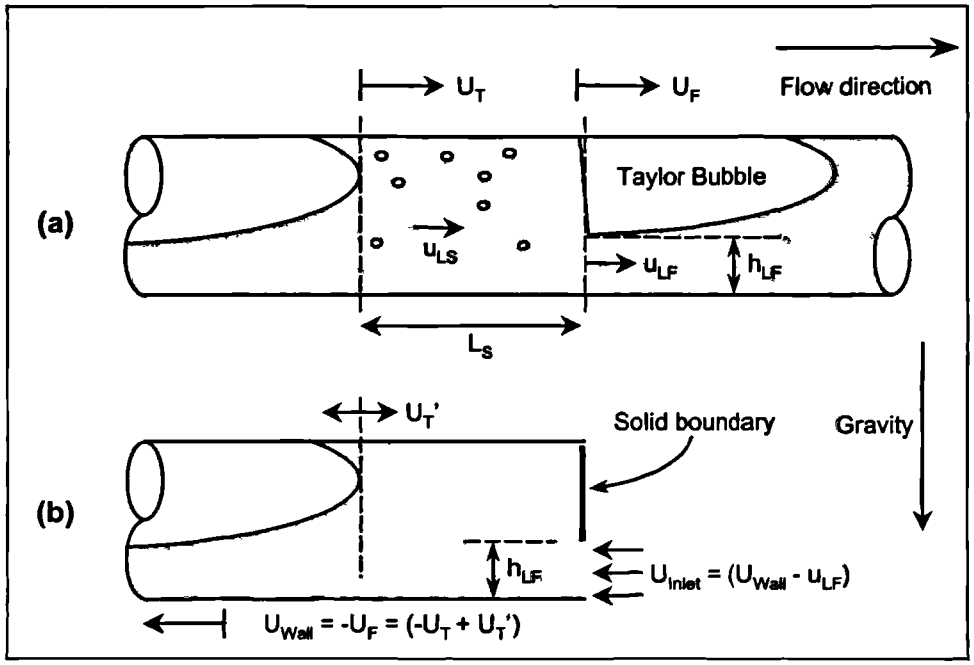

Figure 8.17: The SSF model in a moving coordinate system

As described in Section 8.3.1, the wall of the CFD grid is moved at a velocity approximately equal to the slug tail translational velocity. Thus, the liquid film in front of the slug, with velocity u_{LF} and height h_{LF}, is modelled in the moving coordinate system by introducing liquid to the grid under the solid barrier, through an inlet region with height h_{LF}, at velocity $(U_{Wall} - u_{LF})$. For the case with no gas bubble entrainment, studied here, where $u_{LS} = U_{Mix}$, the mass balance at the slug front requires that

$$U_{Wall} - u_{LF} = \frac{U_{Wall} - U_{Mix}}{\varepsilon_{LF}} \qquad [8.23]$$

where ε_{LF} is the holdup of the liquid film.

As in the simulation of the tail of an "infinitely long" slug, if the value of the inlet velocity is not specified to exactly maintain the slug tail at a constant position, the slug tail moves within the grid at velocity U_T'. The translational velocity of the tail is thus $(-U_{Wall} + U_T')$. It is found

that, for given values of the inlet and wall velocities, U_T' varies according to the length of the slug body. Several simulations were performed to investigate this effect.

Development of a CFD grid for this method is considerably more complicated than for the "infinitely long slug" case discussed in Section 8.4. Separate boundary surfaces must be defined for the "solid slug front" boundary and for the liquid inlet region, and these must be located within separate "blocks" (or groups of blocks) or cells. Two alternate schemes to achieve this are illustrated in Figure 8.18. The interblock boundaries are identified as heavy black lines and the liquid inlet "patch" is shaded.

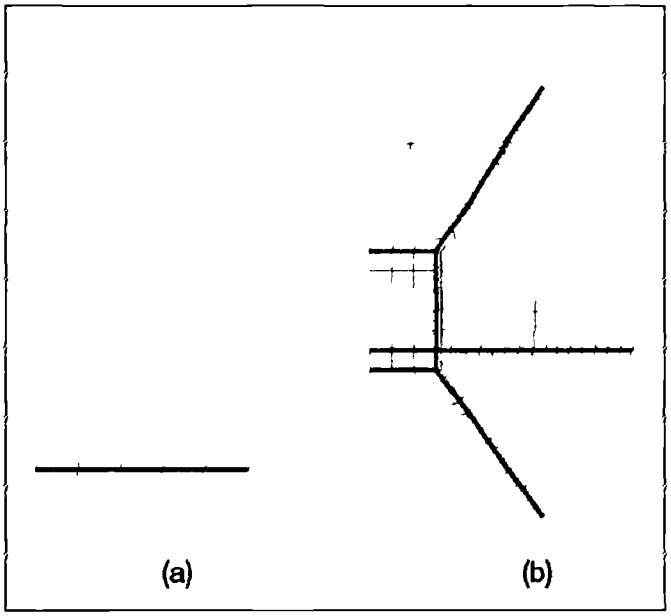

Figure 8.18: (a)Two-block and (b)six-block meshes for a SSF model

The six-block scheme illustrated in Figure 8.18(b) is preferred, since it obviates the two regions of distorted cells in the two-block scheme which may lead to convergence problems. However, generation of the six-block grid is considerably more complicated. Thus, the simpler mesh was used initially, in order to demonstrate the feasibility of the SSF technique. Six-block meshes were used for subsequent work.

The flow domain investigated using the SSF model was a horizontal, semi-cylindrical "half pipe" of length 4.8 m and diameter 80 mm. The same distribution of cells in the axial direction was used for all cases simulated, although different cell arrangements in the radial direction of the grid had to be developed for each case due to the different heights of the liquid inlet region underneath the "solid slug front".

In the axial direction, a total of 227 cells were arranged in four axial blocks. A finer mesh was specified in the "downstream" half of the pipe since this was the region of greatest interest, where the slug body was to be located. In the upstream half of the grid, a much coarser cell distribution was used. The two regions of different cell density were connected with a region in which the ratio of successive cell lengths was described using a geometric progression. Close to the outlet pressure boundary of the grid, a very coarse mesh was specified as this was found to aid convergence of the simulation by "damping" errors due to gas inflow at the outlet pressure boundary . A schematic diagram of the grid is shown in Figure 8.19.

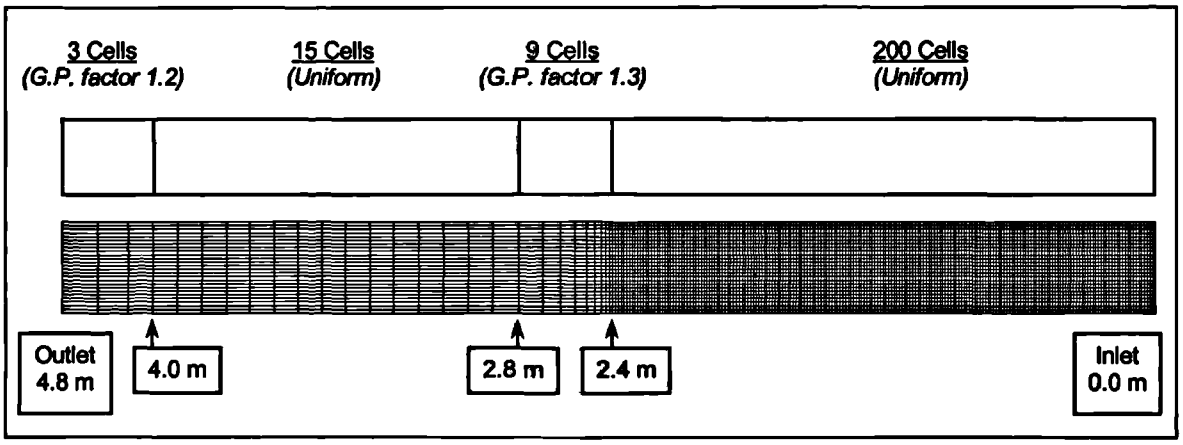

Figure 8.19: Axial cell arrangement in the SSF model grid (*not to scale*).

The initial position of the "dam-break" interface was half-way along the grid, *i.e.*, 2.4 m from the inlet boundary.

The velocity of liquid entering the grid was specified so that the slug body would shrink slowly with time, after the shape of the slug tail had developed from the initial "dam-break". The transient simulation was then run, using timesteps of 0.0025 seconds, until the nose of the Taylor bubble reached the solid wall above the inlet boundary, *i.e.*, until the slug body had shrunk to zero length. For the cases simulated in the present work, this was found to take approximately 8-15 seconds. The calculation required about 80-150 hours of computing time[2].

[2] In the present work, CFX4.3 was run under the Microsoft® WindowsNT® operating system, on a personal computer with a single 700 MHz Athlon® CPU, 512 MB RAM (with a bus frequency of 100 MHz) and a 7200 rpm UDMA-66 IDE disk drive.

Figure 8.20 shows the change in the length of the slug body with time for case SSF01 (see Table 8.3). Only the downstream part of the grid, of length 2.7m (L/D = 34), is shown. As in previous Figures, the vertical scale has been exaggerated by a factor of 3.8 relative to the horizontal scale.

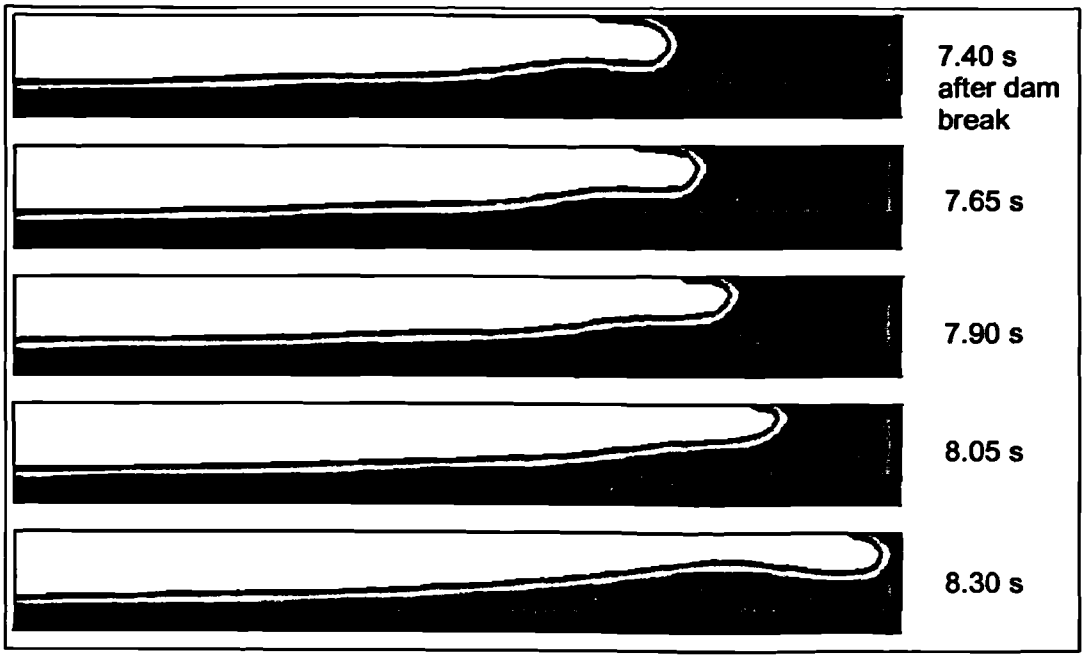

Figure 8.20: Progression of the nose of the Taylor bubble towards the solid wall at the front of the slug *(Case SSF01)*

Output files were produced at intervals of twenty timesteps. Each timestep was solved using up to thirty outer iterations. The smaller timestep and larger number of iterations compared with the earlier work on the slug tail (Section 8.4) were chosen to reduce the likelihood of convergence errors due to the considerably finer mesh used with the SSF model. Despite this, frequent convergence errors were still encountered. Two means of circumventing this problem were identified: running the simulation using a coarse grid, or using "deferred correction" in the iterative solution of the k-ε turbulence model (see Section 8.2.3). The latter option was preferred since it was felt that as fine a mesh as possible should be used in order to accurately obtain the position of the Taylor bubble nose at each timestep. For all simulations using the SSF model, deferred correction was used for the first 15 iterations in each timestep.

8.5.1. Summary of cases used with the solid slug front model

Results from five cases simulated using the SSF model are included in this thesis. These are summarised in Table 8.3. For case SSF01, arbitrary values were used for the wall and inlet velocities (8 m/s and 6 m/s respectively) and the liquid film height (0.2 times the pipe diameter). This translates to a slug moving with a *front velocity* of 8 m/s over a film with velocity 2 m/s and height 0.2D.

For subsequent cases, a value of 1.6 was used for the product ($\varepsilon_{LF}U_{Inlet}$), so that the same volumetric "pickup rate" of liquid at the front of the slug was used for each case. Thus, cases SSF02-05 simulate the effect of varying the length of the liquid film *downstream* of the slug.

Case	U_{Wall} / m s^{-1}	h_{LF} / D	ε_{LF}	U_{Inlet} (= $U_{Wall}-u_{LF}$) / m s^{-1}	u_{LF} / m s^{-1}	$\varepsilon_{LF} \times U_{Inlet}$ / m s^{-1}	Duration of simulation / s
SSF01	8	0.2000	0.1424	6.00	2.00	0.85	8.40
SSF02	12.6	0.2035	0.1459	11.00	1.60	1.60	13.15
SSF03	12.6	0.2690	0.2167	7.40	5.20	1.60	12.20
SSF04	12.6	0.4116	0.3880	4.10	8.50	1.59	13.25
SSF05	12.6	0.3400	0.2998	5.34	7.26	1.60	14.80

Table 8.3: Summary of cases used with the SSF model

From the mass balance in Equation [8.23], the mixture velocity may be calculated as

$$U_{Mix} = U_{Wall} - \varepsilon_{LF}U_{Inlet} \qquad [8.24]$$

Thus, for cases SSF02 – SSF05 the same mixture velocity, 11 m/s, was used. Thus the Froude number, calculated from Equation (8.22), is 12.42 and the value of U_{Mix} is less than the moving wall velocity in every case. The results from cases SSF02 – SSF05 are discussed further in Section 8.5.4.

8.5.2. Liquid film drainage in the slug tail

As discussed in Section 8.4.1, the shape of the slug tail is highly three-dimensional, especially in the region immediately behind the slug body where the nose of the Taylor bubble protrudes into the slug body, and the liquid "drains" around the outside of the bubble

in a film region close to the pipe wall. This effect was observed in all simulations conducted for the present work, and is illustrated in this Section using results from case SSF04.

The mesh used for this case is depicted in Figure 8.21. A six-block "butterfly" grid was used to eliminate convergence difficulties which were encountered using a two-block grid.

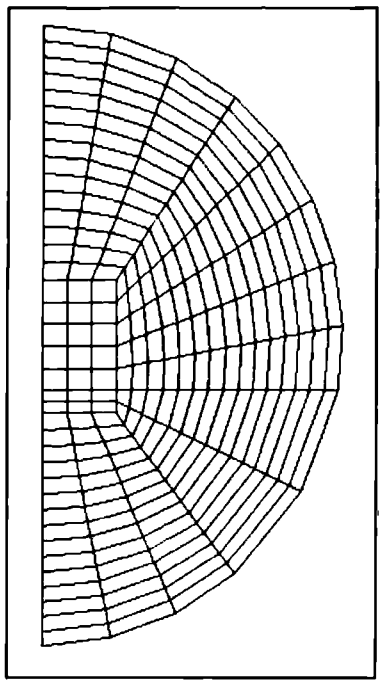

Figure 8.21: Grid cross-section for case SSF04.

The results presented in this Section are taken from case SSF04, 9.0 seconds after the start of the "dam break" simulation. At this time, the distance between the solid wall at the front of the slug body and the nose of the Taylor bubble at its tail is 1.043 m (*i.e.*, 13.041 pipe diameters).

Views of the three-dimensional surface of the bubble nose are shown in Figure 8.22 and Figure 8.23. The "isosurface" plots, generated using the CFX-ANALYSE postprocessor, show where the liquid holdup is equal to 0.50.

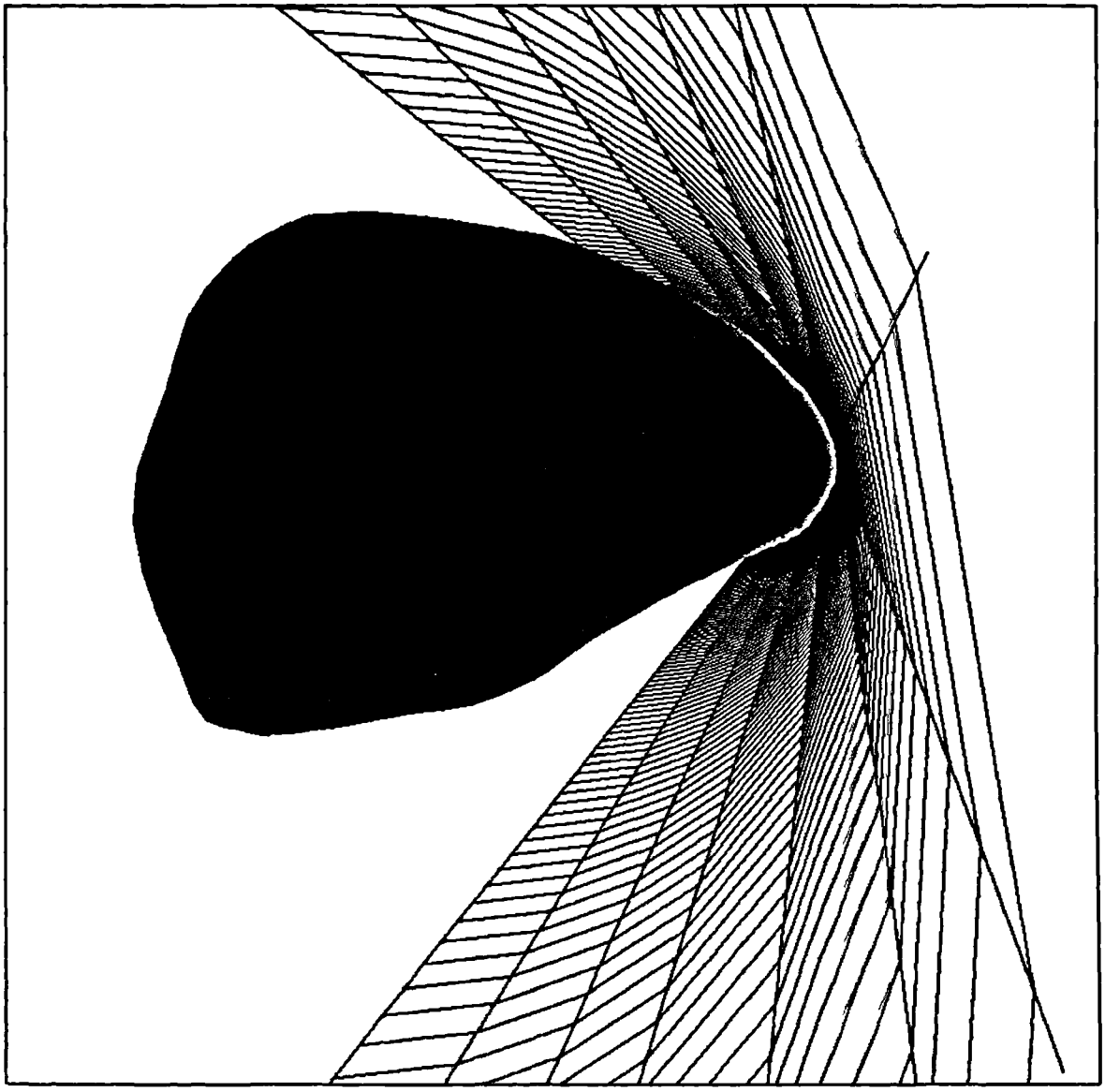

Figure 8.22: 3-D isosurface plot of slug tail interface, showing film drainage region (Case SSF04, 9.0 seconds after dam-break)

The point of view is from within the slug body, looking upstream. In Figure 8.22 the shape and position of the gas-liquid interface relative to the pipe wall (shown as a mesh outline) are clearly seen. Drainage of liquid from the slug body into the stratified film behind the slug occurs in the region between the bubble and the pipe wall. The bubble rises gradually in the pipe and expands laterally until it meets the pipe wall in the upstream region.

In Figure 8.23, a slightly different point of view is shown so that the inner surface of the Taylor bubble is visible. The intersection of the interface with the pipe wall is shown.

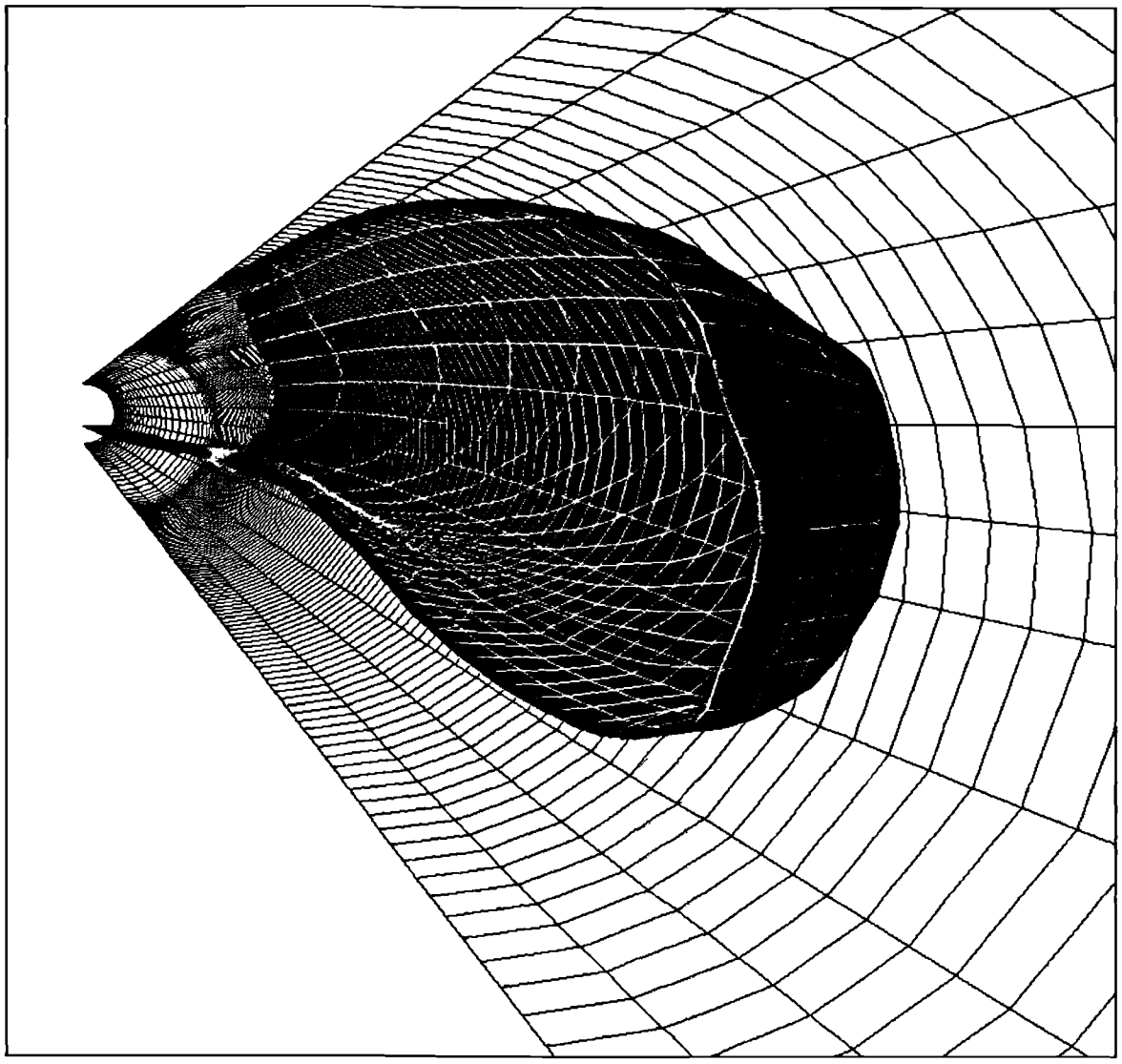

Figure 8.23: 3-D isosurface plot of slug tail interface, showing inside of bubble nose (Case SSF04, 9.0 seconds after dam-break)

It is clear from the 3-D plots that the approximation of a flat interface, used in many 1-D models of slug-flow, including that presented in Chapter 7 of the present work, is not valid close to the nose of the Taylor bubble. A longitudinal ridge of liquid is apparent, positioned about the central bisecting plane of the pipe. Contours showing the position of the gas-liquid interface (*i.e.*, where the liquid holdup has a value of 0.50) are shown in Figure 8.24 for pipe cross-sections at several locations upstream of the Taylor bubble nose. The pattern of liquid drainage around the pipe wall is also shown, as velocity vectors. The locations of the cross-sections in Figure 8.24 are listed in Table 8.4.

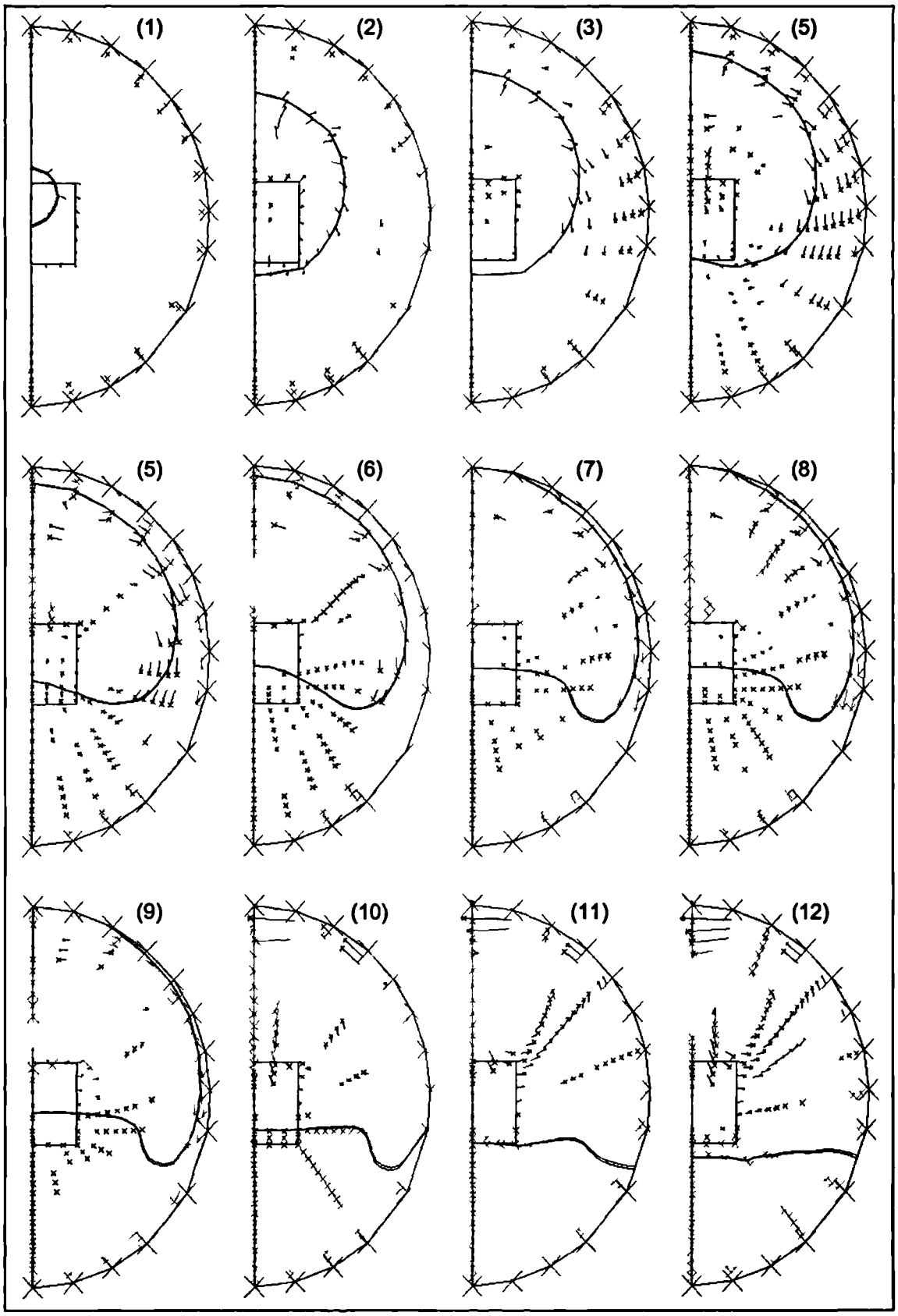

Figure 8.24: Interface positions and velocity vectors showing liquid drainage around the nose of the Taylor bubble at locations along the slug tail (Case SSF04, 9.0 seconds after dam-break)

Cross-section in Figure 8.24	Distance from outlet plane / m	Distance from bubble nose / D
1	3.675	0.00
2	3.625	0.62
3	3.575	1.25
4	3.5	2.19
5	3.4	3.44
6	3.3	4.69
7	3.2	5.94
8	3.1	7.19
9	3	8.44
10	2.6	13.44
11	2.2	18.44
12	1.8	23.44

Table 8.4: Positions of cross-sections plotted in Figure 8.24

The draining liquid film is still present in cross-section (9), a distance of 8.44 pipe diameters from the slug body. The "ridge" of liquid persists in the stratified liquid layer for some distance upstream of this point; its remnant is still apparent in cross-section (11), situated 18.44D from the slug body. The interface is still not perfectly flat in the final cross-section, image (12), although the "ridge" has disappeared by this point.

It is not clear what maintains the interface shape in equilibrium in the region where the "ridge" is present. For the cross-section denoted as (8) in Figure 8.24, the pressure and turbulence intensity are plotted in Figure 8.25 and Figure 8.26 respectively. Apart from a region of slightly *lower* pressure situated where the draining film enters the stratified liquid layer, no hint is provided by the examination of these parameters as to the mechanism which sustains the interface shape.

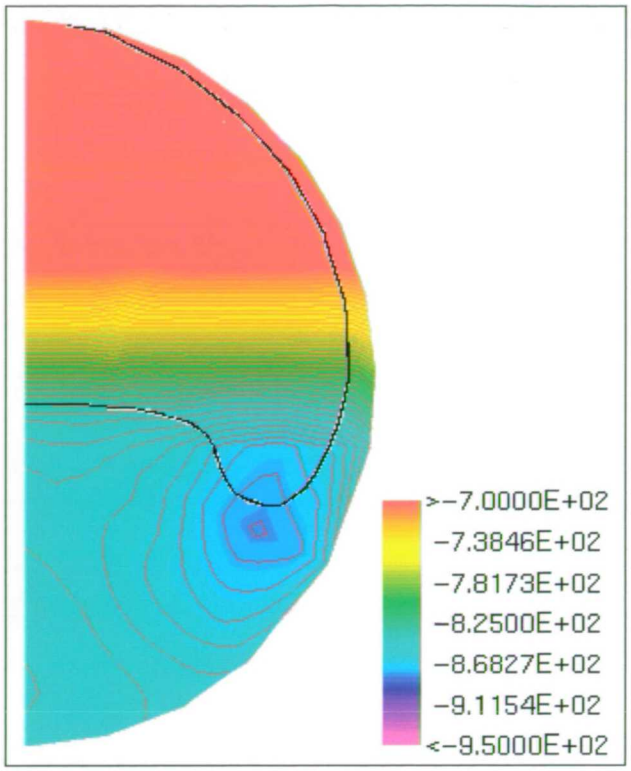

Figure 8.25: Pressure contours (in Pa(g)) at cross-section (8) in Figure 8.24

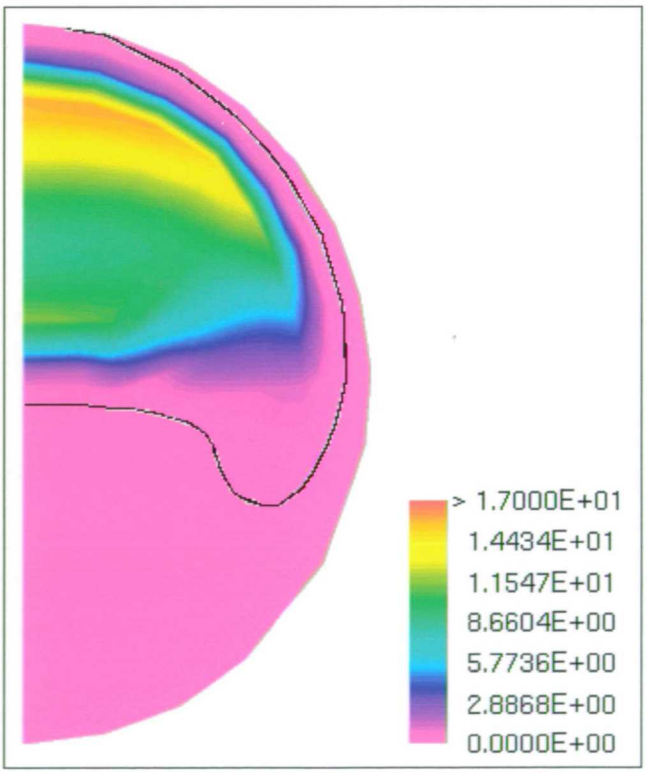

Figure 8.26: Mean turbulent kinetic energy per unit mass, k (J/kg) at cross-section (8) in Figure 8.24

8.5.3. Variation of tail velocity with slug length: Case SSF01

The principal objective in the development of the SSF model was to study the influence of slug body length, L_S, on the translational velocity of the slug tail in horizontal flow. Specifically, the aim was to reproduce the increase in U_T which has been observed for short slugs by Fagundes Netto *et al.* (1999b) and Cook & Behnia (2000), described earlier in Chapter 2 of this thesis. This was done using case SSF01 where the values for U_{Wall}, U_{Inlet} and h_{LF} were specified arbitrarily.

The conditions used initially with the SSF model are summarised in Table 8.3 above. In this case, the mixture velocity is 7.25 m/s and the Froude number is 8.07.

A two-block grid was constructed, as shown in Figure 8.27.

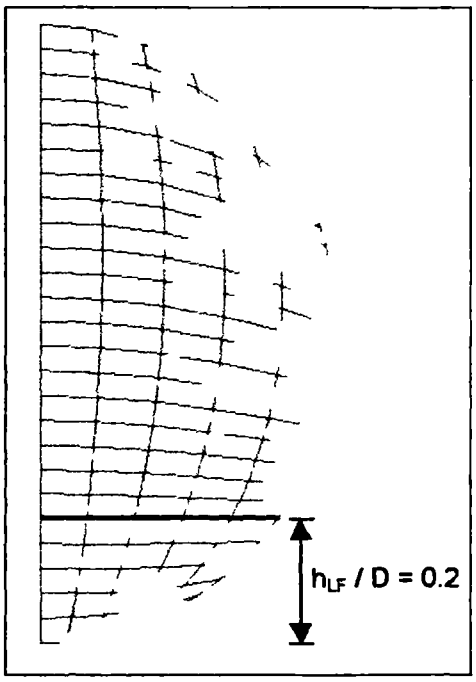

Figure 8.27: Cross-section of grid used for case SSF01

The simulation was run for 8.40 seconds until the nose of the Taylor bubble reached the solid wall at the downstream end of the grid (as shown in Figure 8.20 above). Dump files were generated every 0.05 seconds and from these a series of high-resolution images of the Taylor bubble nose was made. By scrutinising these images at high magnification, using graphics software, the position of the nose of the bubble was ascertained for every dump file. The results are plotted in Figure 8.28.

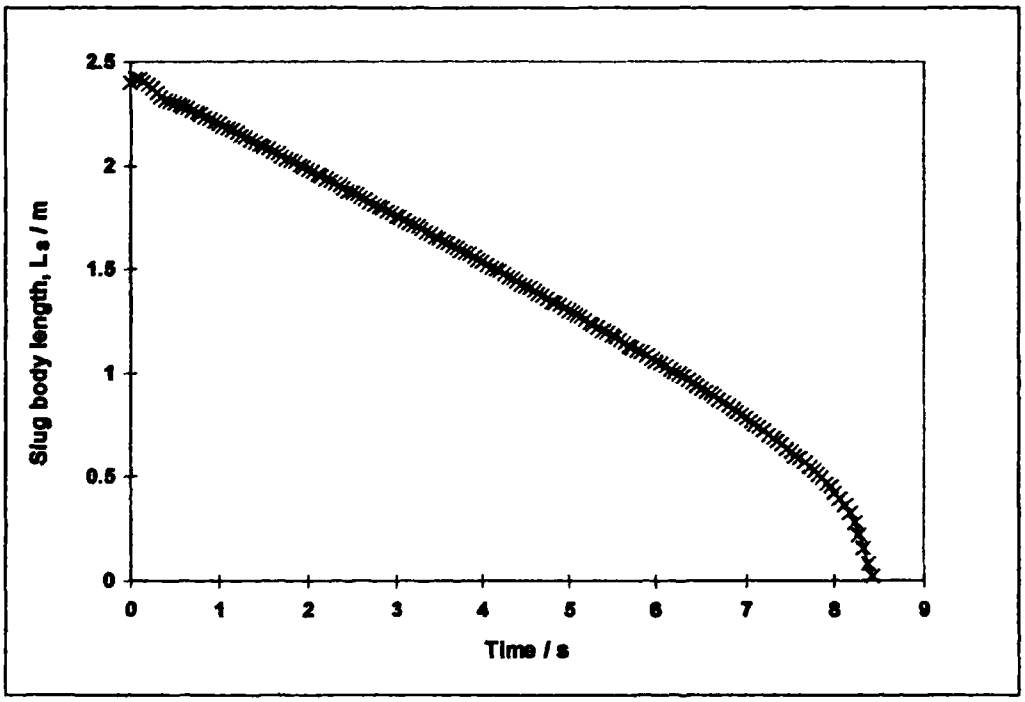

Figure 8.28: Variation of slug body length during simulation of case SSF01

From these data, values of U_T may be obtained for each time interval: if the change in slug body length between two successive dump files is Δx m, and the interval between dump files is Δt s, then

$$U_T = \frac{\Delta x}{\Delta t} \qquad [8.25]$$

Thus, the data plotted in Figure 8.28 can be presented as a graph of the instantaneous value of U_T as a function of the slug body length, as shown in Figure 8.29. The scatter around L_S = 2.4 m is caused by the initial acceleration of the interface from rest, during the formation of the "slug tail" shape after the dam break. At lower values of L_S, the scatter is caused by the resolution of the images used to obtain the length of the slug body. However, a clear trend is visible: the slug tail velocity tends towards an asymptote at large values of the slug body length. For case SSF01, the asymptotic value is 8.221 m/s: for this case, this is taken to be the value of the translational velocity of an "infinitely long slug", $U_{T,\infty}$. The data can thus be presented in the dimensionless form used by Fagundes Netto *et al.* (1999b) and Cook & Behnia (2000), as shown below in Figure 8.30, which also shows the correlations and the original data presented by Fagundes Netto *et al.* (1998).

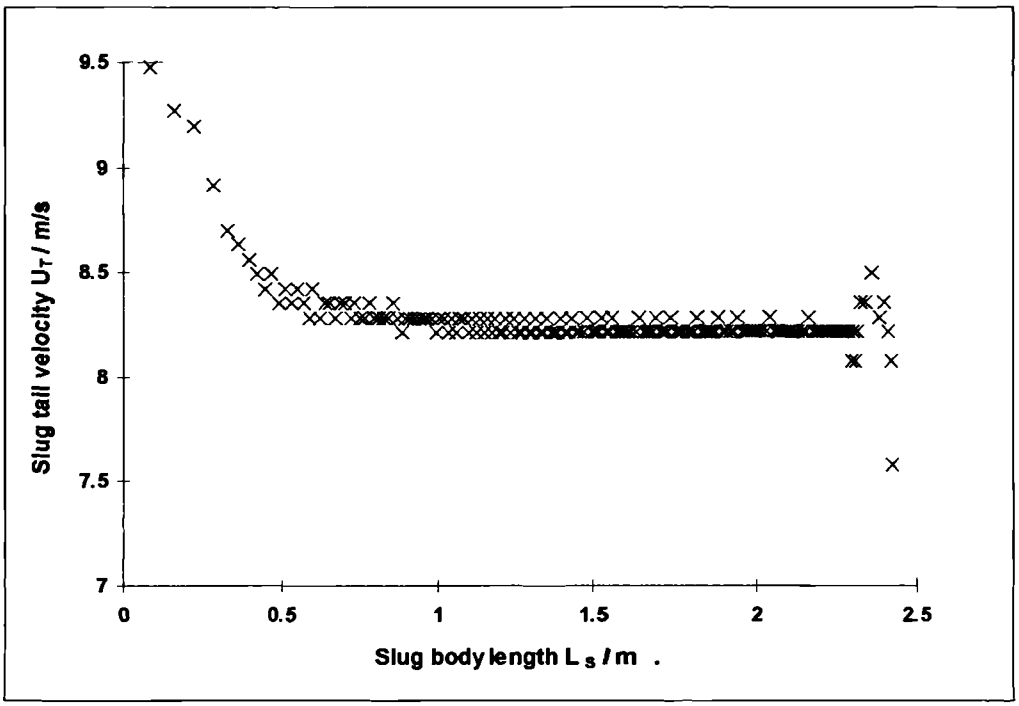

Figure 8.29: Calculated slug tail velocity for case SSF01

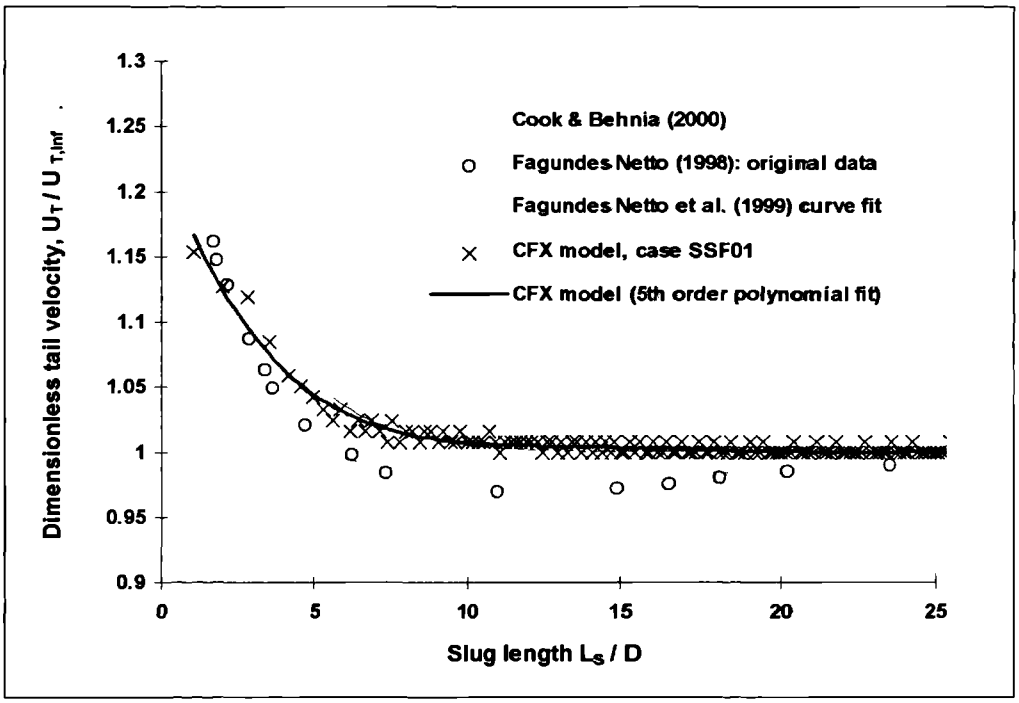

Figure 8.30: Comparison of results from case SSF01 with experimental results

In Figure 8.30, the correlation by Cook & Behnia (2000) intercepts the ordinate axis at a value of 1.6. The intercept for the expression by Fagundes Netto *et al.* (1999b) is much lower, with a value of 1.12. The results from the CFX simulation do not extend to zero slug length, since it is not possible to calculate a value of the tail velocity once the nose of the

Taylor bubble reaches the solid wall at the slug front. In any event, the concept of tail velocity is probably worthless for slugs with L/D less than about 2, which are *always* far from steady-state.

The data measured by Fagundes Netto *et al.* (1999b) suggested that there is a region of slug lengths for which the dimensionless slug tail velocity is less than unity; their correlation includes this effect. However, the results of Cook & Behnia (2000) show no evidence of this effect, and the phenomenon was not observed in the present work.

Liquid velocity vectors inside the front of the slug body are plotted in Figure 8.31, at 6.0s after the dam break. At this instant, the distance between the nose of the Taylor bubble and the solid slug front is 13.2D. The plane shown is the central bisecting plane of the grid, and the vertical scale has been exaggerated by a factor of 3.8.

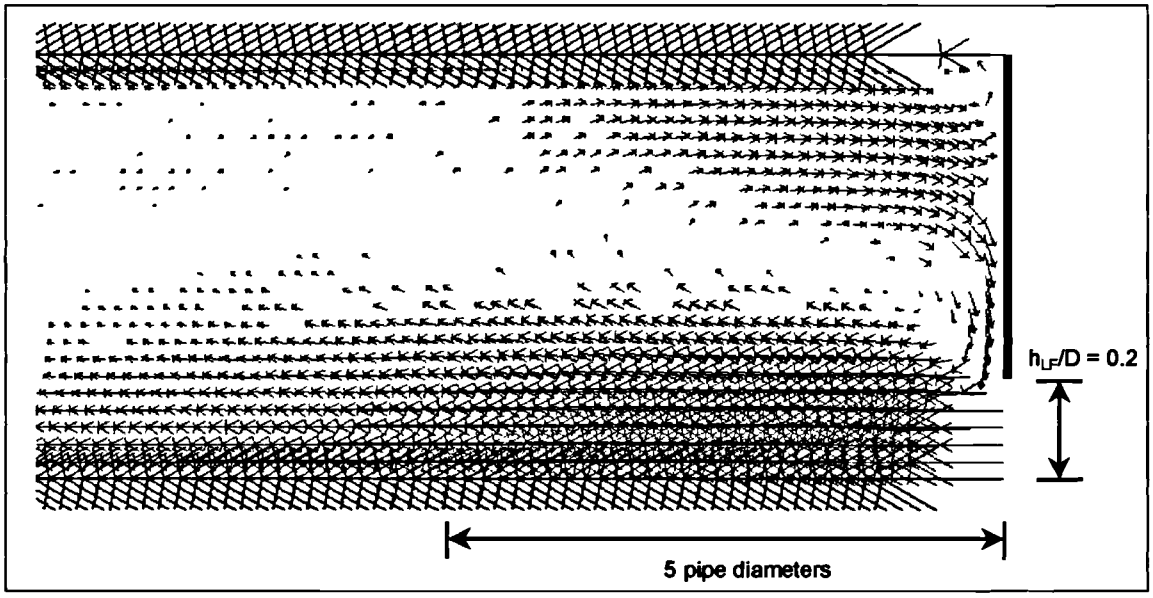

Figure 8.31: Velocity vectors at the front of the slug body (Case SSF01, 6.0 seconds after dam break)

The moving-wall velocity vectors are clearly visible at the top and bottom of the Figure. The "recirculation zone", caused by the entry of liquid into the grid, extends well into the slug body. This is shown more clearly by a contour plot showing where the axial component of the fluid velocity is equal to zero, as in Figure 8.32. The ratio of vertical to horizontal scales is the same as in Figure 8.31.

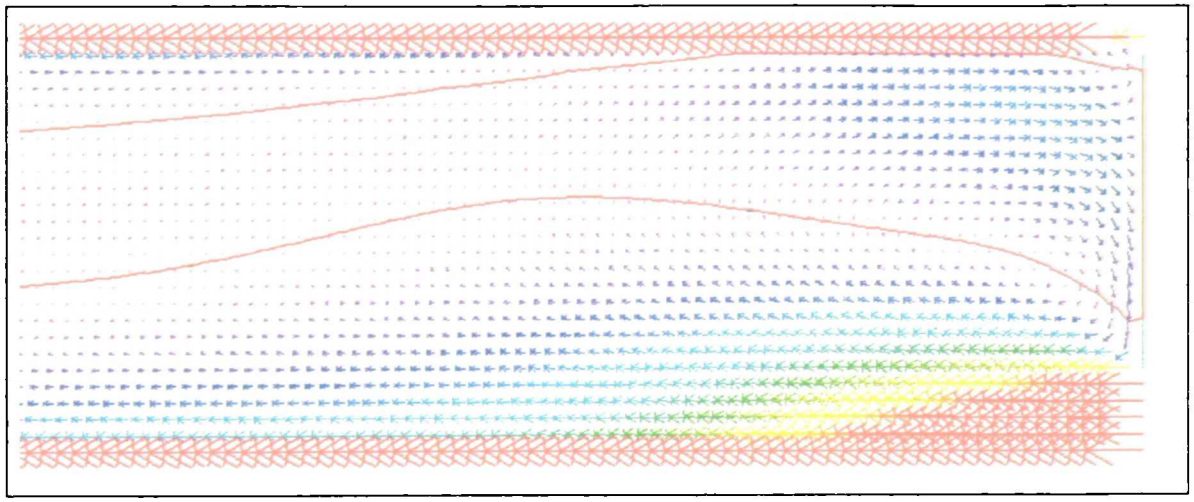

Figure 8.32: Contour showing where the axial velocity component is equal to 0 m/s (Case SSF01, 6.0s after dam-break)

The change in velocity profile along the slug body, due to the recirculation zone, causes a large variation in the wall shear stress along the grid. This is shown in Figure 8.33.

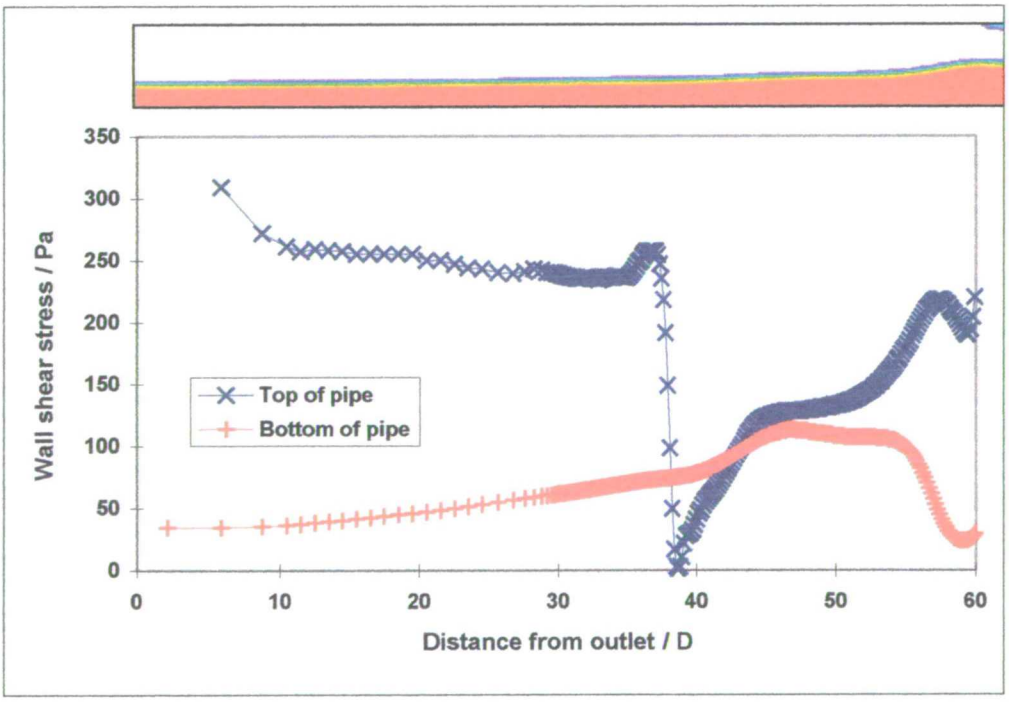

Figure 8.33: Liquid-phase wall shear stress for case SSF01 (6.0s after dam-break)

Since the "homogeneous" multiphase model is used, CFX calculates a value for the liquid-phase wall shear stress even where there is no liquid present near the wall, for example at the top of the pipe in the Taylor bubble region. These data are shown in Figure 8.33 but are obviously not physically applicable. An alternative plot of these data is shown in Figure 8.34.

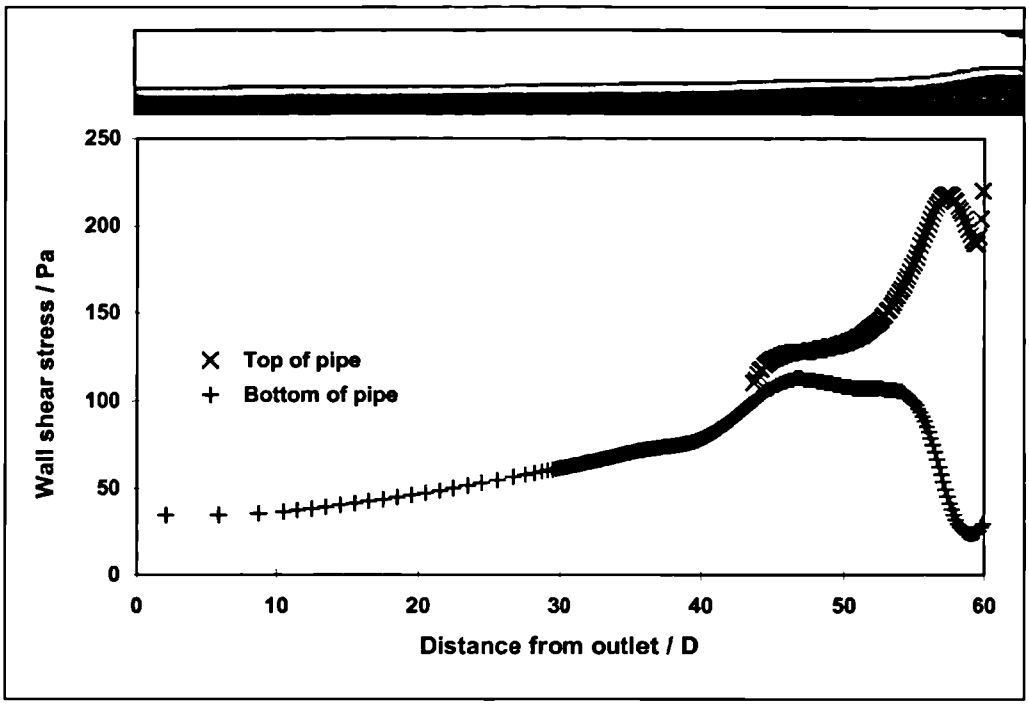

Figure 8.34: Liquid-phase wall shear stress for case SSF01 (6.0 s after dam-break)

At the slug front, the shear stress is high at the top of the pipe due to the high velocity of the liquid relative to the wall, and correspondingly lower at the bottom of the pipe. Within the upstream section of the slug, the flow becomes progressively well mixed and the stress becomes more uniformly distributed around the pipe wall. At the tail of the slug the stress gradually decreases, reflecting the gradual deceleration of the liquid film.

It is clear that the use of a constant value of the wall shear stress to calculate the frictional pressure drop across the slug body (as in, *e.g.*, the model of Taitel & Barnea, 1990) is a major simplification. This is explored further in Section 8.5.4, below.

8.5.4. The effect of film length

The results of Fagundes Netto *et al.* (1998, 1999a, 1999b) and Cook & Behnia (2000) suggest no influence on the slug tail behaviour of the film properties at the slug front. The film height and velocity vary along a slug tail, so that if the distance between two slugs is short, the upstream slug "sees" a thick, fast film at its front. However, if the two slugs are separated by a longer distance, the film ahead of the upstream slug is thinner, and moves more slowly. A series of CFD simulations were performed to investigate whether this has a significant effect on the behaviour of the tail of the upstream slug. These are listed as cases SSF02-SSF05 in Table 8.3.

Four consistent pairs of values for ε_{LF} and u_{LF} were obtained at several locations along a slug tail, based on a solution of the 1-D film profile equation used in the model discussed previously in Chapter 7. The solution used a value of 10.5 m/s for the mixture velocity, 0.8 for the liquid holdup in the slug body and $1.2U_{Mix}$ (*i.e.*, 12.6 m/s) for the translational velocity of the slug tail. Thus, the "shedding velocity" from the slug body, $\varepsilon_{LS}(U_T - U_{Mix})$, is equal to 1.68 m/s. Since mass is conserved in the tail profile calculation, the product $\varepsilon_{LF}(U_T - u_{LF})$ also has this value at all points in the slug tail.

The results are shown in Table 8.5 and are plotted in Figure 8.35.

Film length		Film height		Film velocity			Film holdup
L_F / m	L_F / D	h_{LF} / mm	h_{LF} / D	u_{LF} / m/s	u_{LF} / U_{Mix}	$(U_T - u_{LF})$ / m/s	ε_{LF}
0.5	6.25	39.3	0.4916	9.1666	0.8730	3.4334	0.4893
1	12.5	32.9	0.4116	8.2701	0.7876	4.3299	0.3880
5	62.5	21.5	0.2690	4.8468	0.4616	7.7532	0.2167
45	562.5	16.3	0.2035	1.0891	0.1037	11.5109	0.1459

Table 8.5: Results from the 1-D model

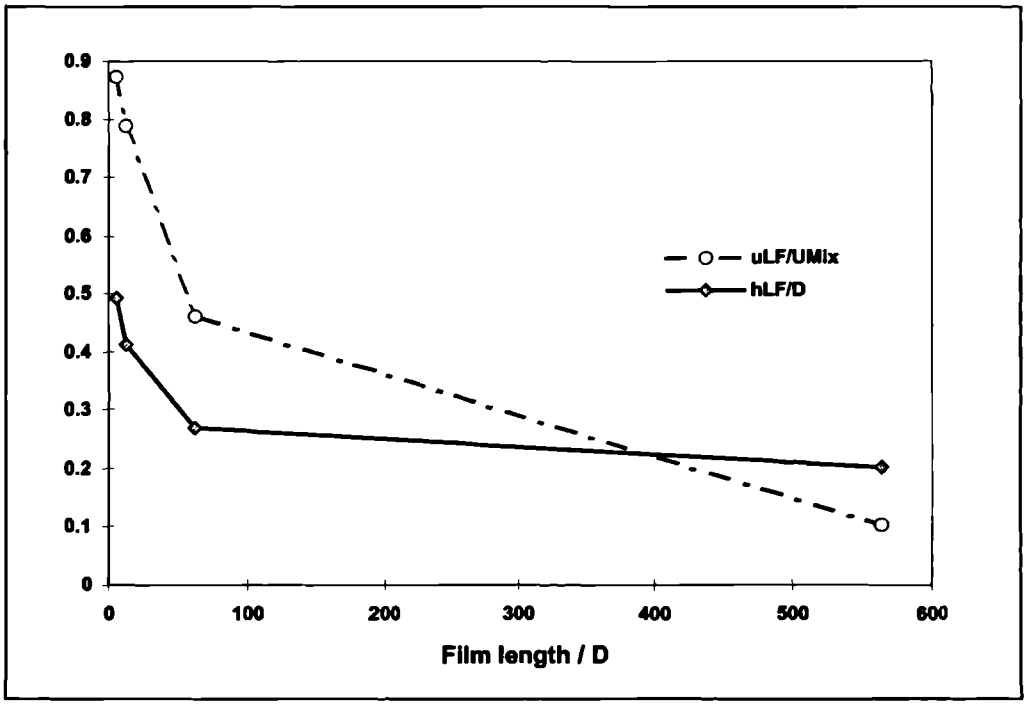

Figure 8.35: Film properties calculated from the 1-D model

Several CFD simulations were performed to evaluate the feasibility of using these data to specify the inlet boundary conditions for the SSF model. It was found that the values of the velocity of the liquid entering the CFD grid were too high, so that the slug body did not shrink slowly with time, but instead grew steadily. Thus, lower values of the inlet velocity were used in order to produce the "shrinking slug" result. These are shown in Table 8.3 above. The values used for the film height are taken from the 1-D model results (Table 8.5) but the slightly higher film velocities result in a value of 1.60 for the product $\varepsilon_{LF}(U_T - u_{LF})$. A revised mixture velocity of 11 m/s is thus calculated from Equation [8.24].

Due to the different size of the liquid inlet boundary for each case, a different 6-block CFD grid was required for each case. These are shown in Figure 8.36.

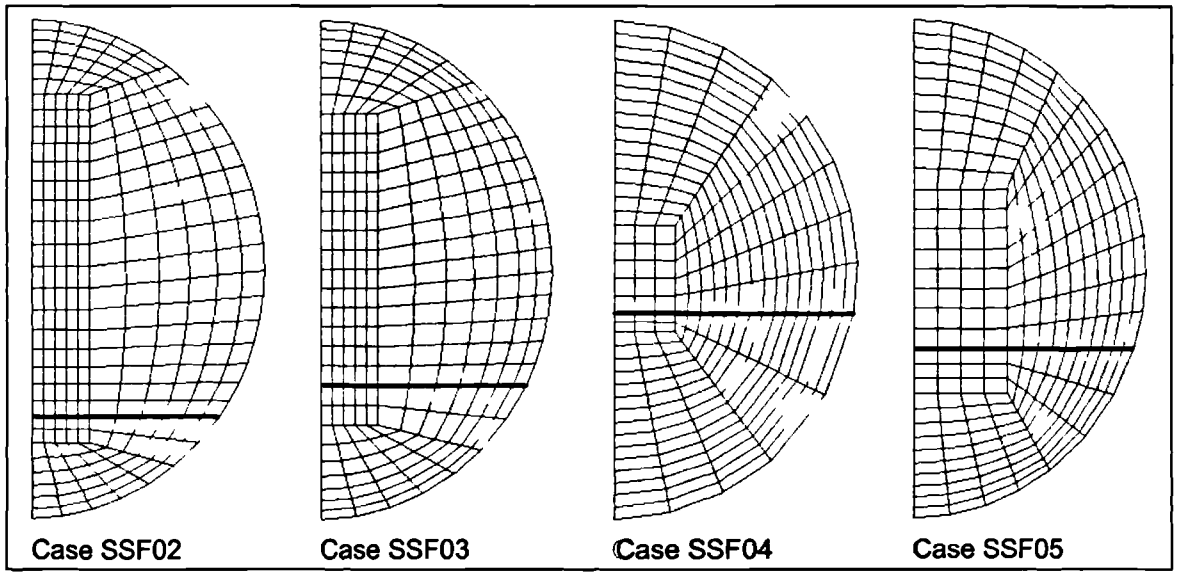

Figure 8.36: 6-block grids with different sizes for the liquid inlet boundary

For each case, the translational velocity of the slug tail was calculated, as described in Section 8.5.3. The results are presented in Figure 8.37.

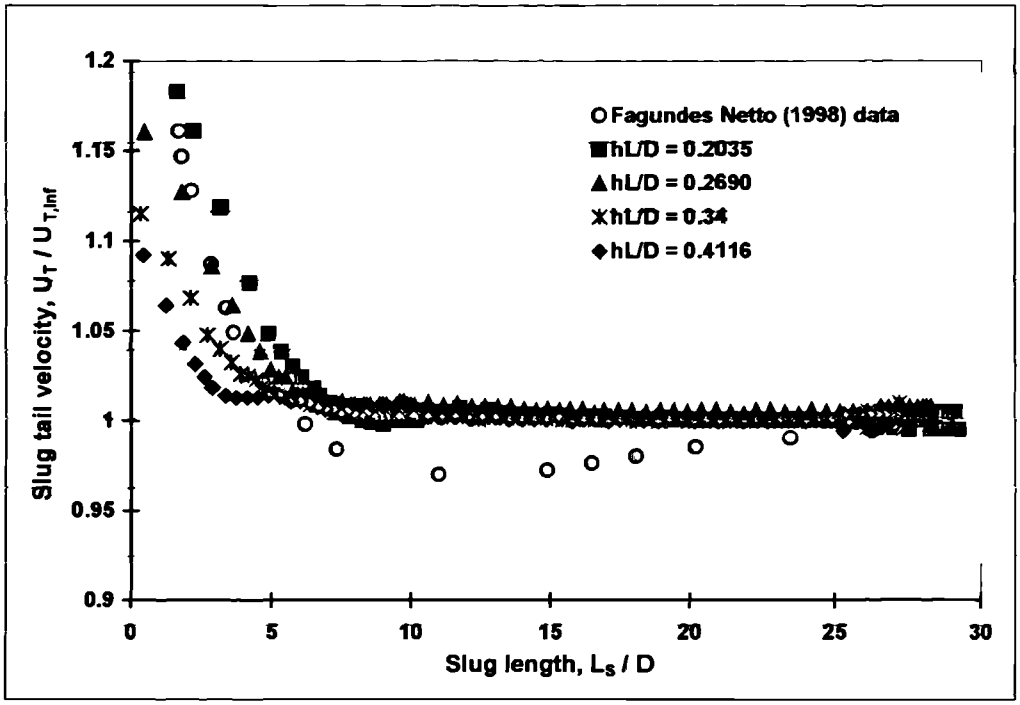

Figure 8.37: Results from cases SSF02 – SSF05

The results for short slug lengths are more clearly seen in Figure 8.38.

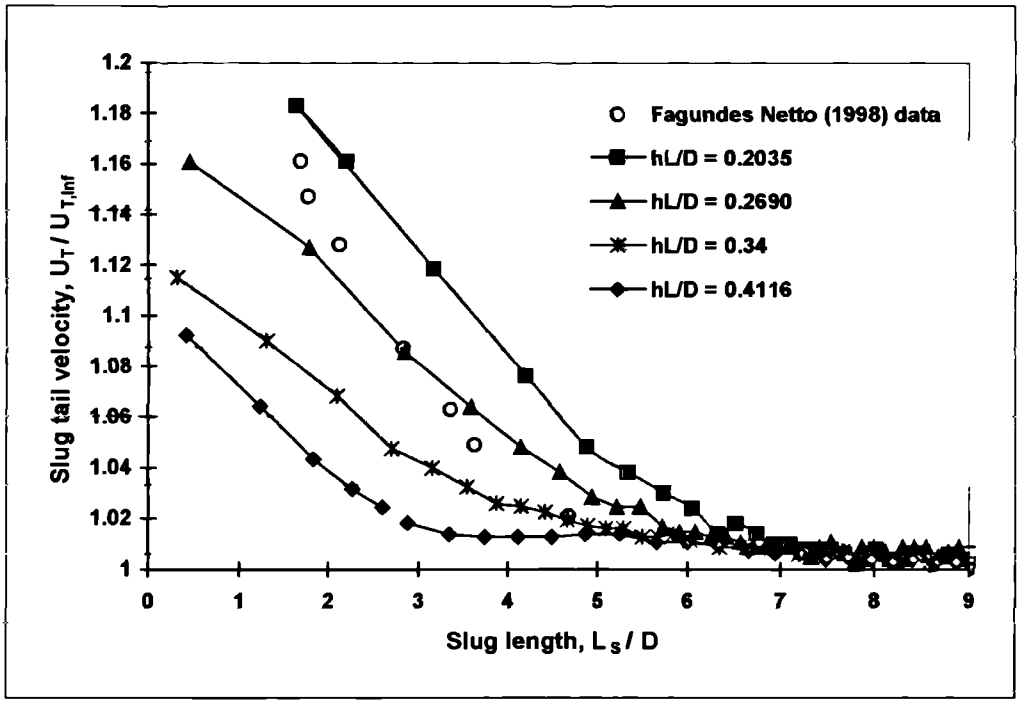

Figure 8.38: Calculated increase in slug tail velocity for short slugs

These results suggest that the film length ahead of a short slug has a significant influence on its tail velocity. It appears that this is due to the size of the recirculation zone inside the slug

body, which changes according to the thickness of the film entering the slug, and the relative velocity of the slug front and the liquid film.

The extent of the recirculation zone for the different cases is most clearly demonstrated using particle tracking plots. These show the calculated paths which would be followed by imaginary particles of zero-mass and neutral buoyancy if they were mixed with the fluid at a specified point in the flow domain. In Figure 8.39, particle tracking plots are shown for cases SSF02-SSF05. In each case, the particles are introduced with the fluid at the inlet boundary region, underneath the solid slug front. The data in each plot are shown at the instant where the slug body length is approximately 13D. It should be noted that, unlike most other plots in this Chapter, *the horizontal and vertical scales in Figure 8.39 are equal.*

Figure 8.39 shows that the recirculation of liquid within the slug body is most intense, and extends furthest upstream into the slug body, when the liquid film in front of the slug is thin. This occurs when the film ahead of a slug is long, *i.e.*, when the spacing between two slugs is large. As the film length becomes shorter, the film gets thicker and its velocity increases. Hence, the relative velocity ($U_F - u_{LF}$) is smaller, so that the recirculation zone in the slug body is shorter, and the recirculation is less fierce.

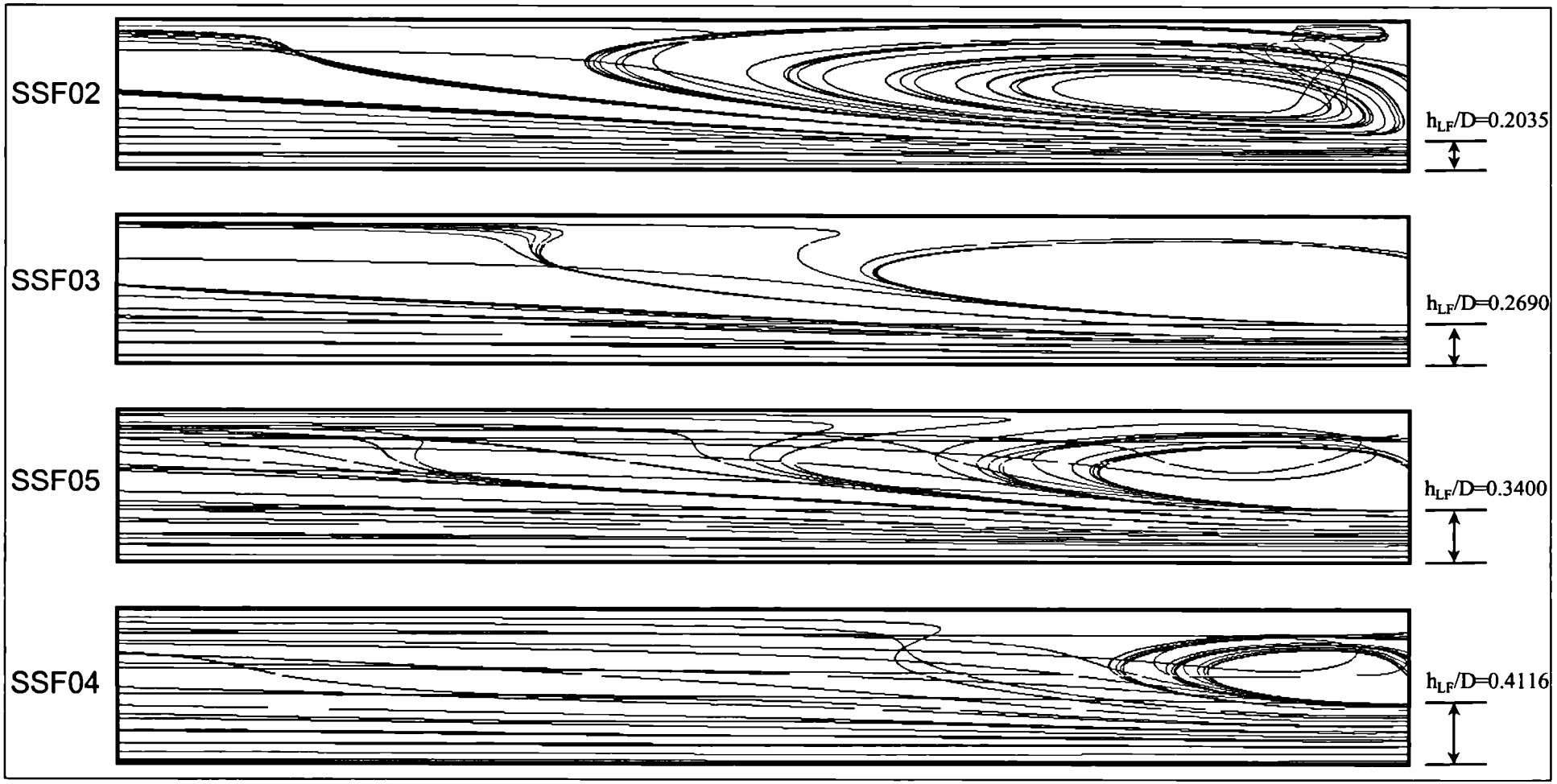

Figure 8.39: Particle tracking plots showing the recirculation zones at the slug front for cases SSF02-SSF05 (liquid inlet is from right of page)

Wall shear stress effects

The wall shear stress in the slug body is strongly affected by the change in the recirculation zone. Plots of the wall shear stress are shown in Figures 8.40 – 8.43.

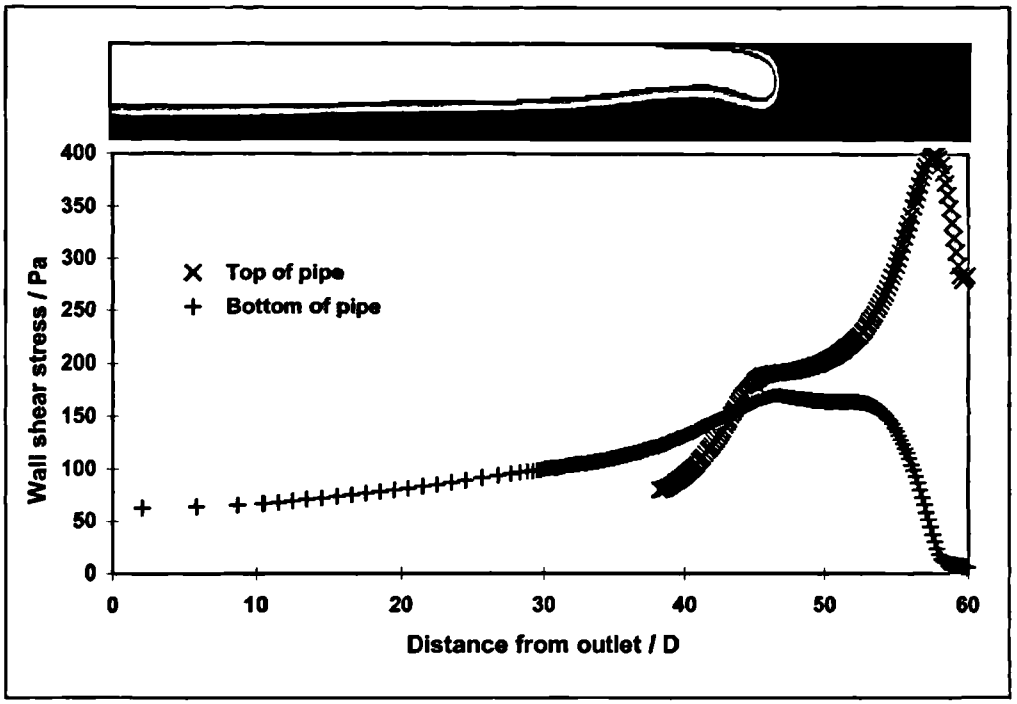

Figure 8.40: Liquid-phase wall shear stresses for case SSF02 (10.0 s after dam-break)

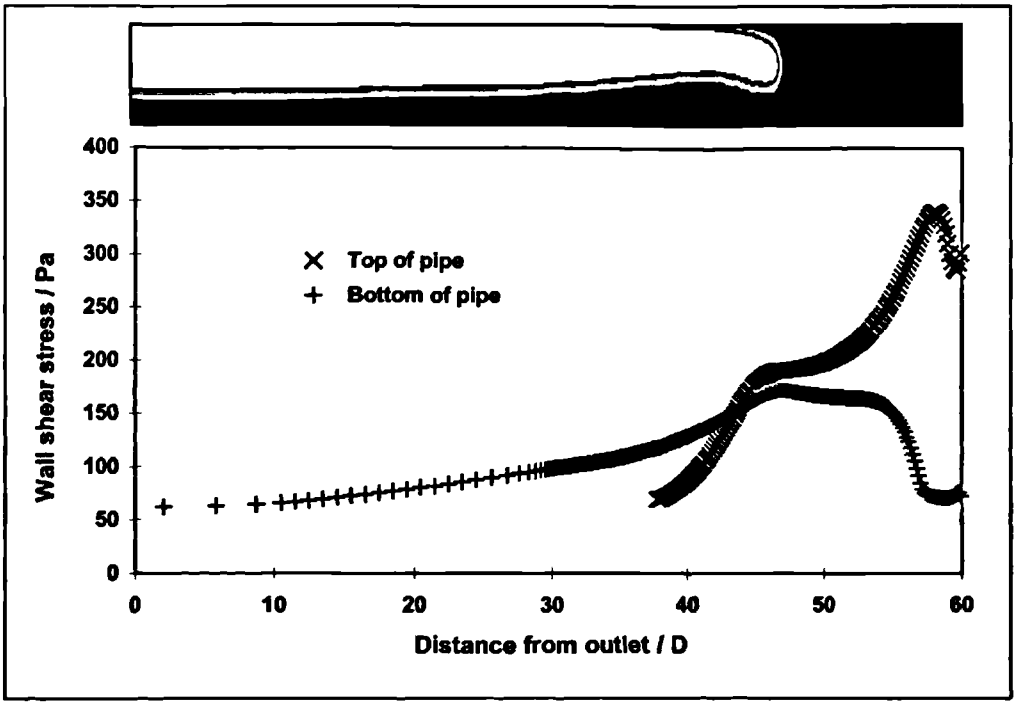

Figure 8.41: Liquid-phase wall shear stresses for case SSF03 (9.0 s after dam-break)

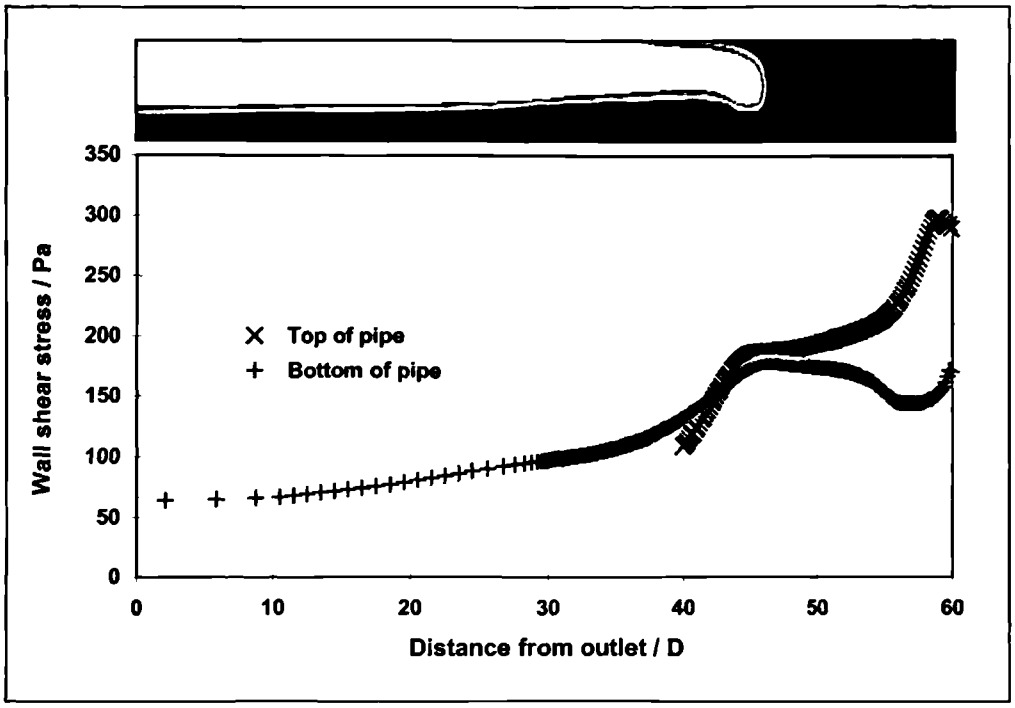

Figure 8.42: Liquid-phase wall shear stresses for case SSF04 (9.0 s after dam-break)

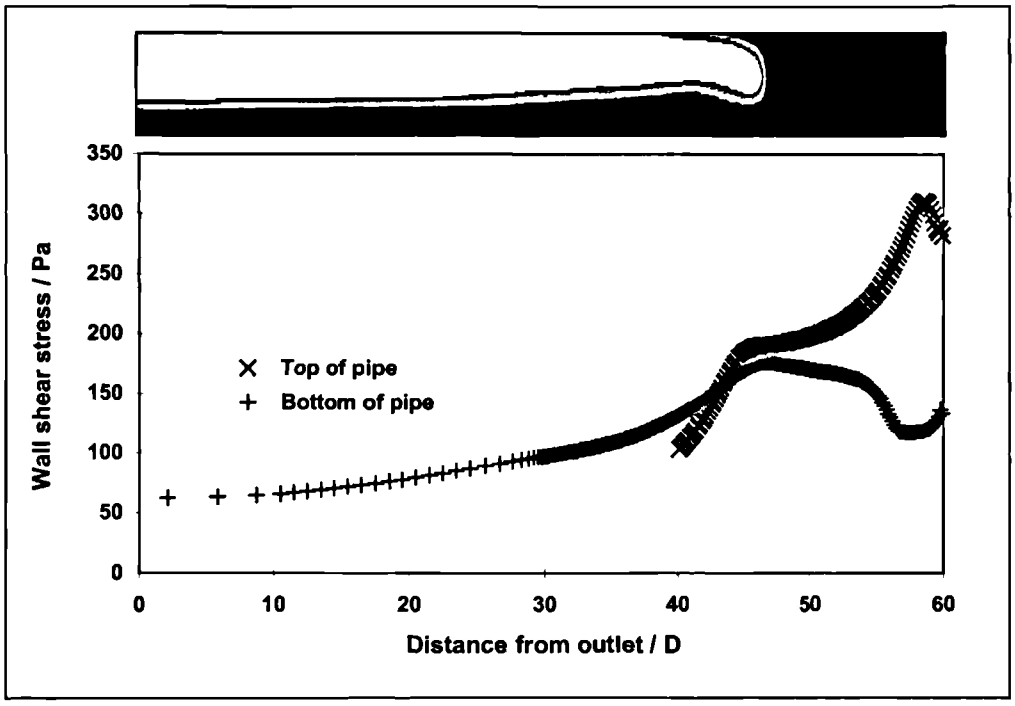

Figure 8.43: Liquid-phase wall shear stresses for case SSF05 (11.0 s after dam-break)

From these calculations, it is apparent that the height and velocity of the liquid film at the front of the slug has a significant influence on the calculated wall shear stress at the front of the slug body. In the film region, however, there is very little difference between the results

from the four cases. In Figure 8.44, the wall shear stress at the top of the pipe for each of the four cases is plotted on the same axes.

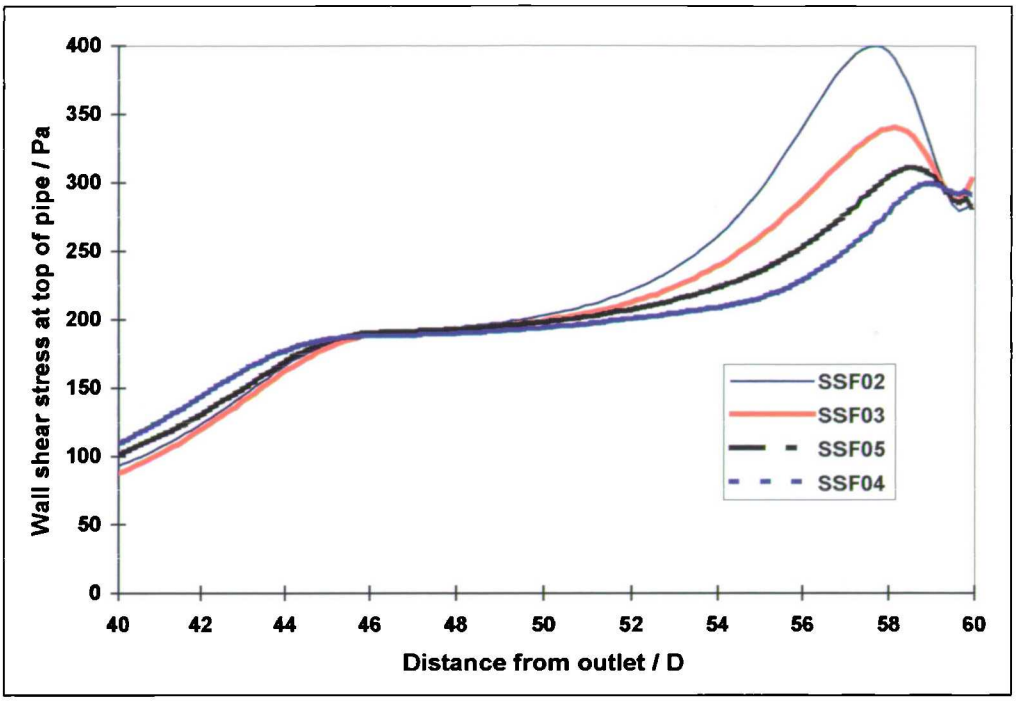

Figure 8.44: Predicted wall shear stress at the top of the pipe for the four cases

There is considerable circumferential variation in the calculated shear stress in the slug body. This is plotted at several locations around the pipe wall, for case SSF04, in Figure 8.45.

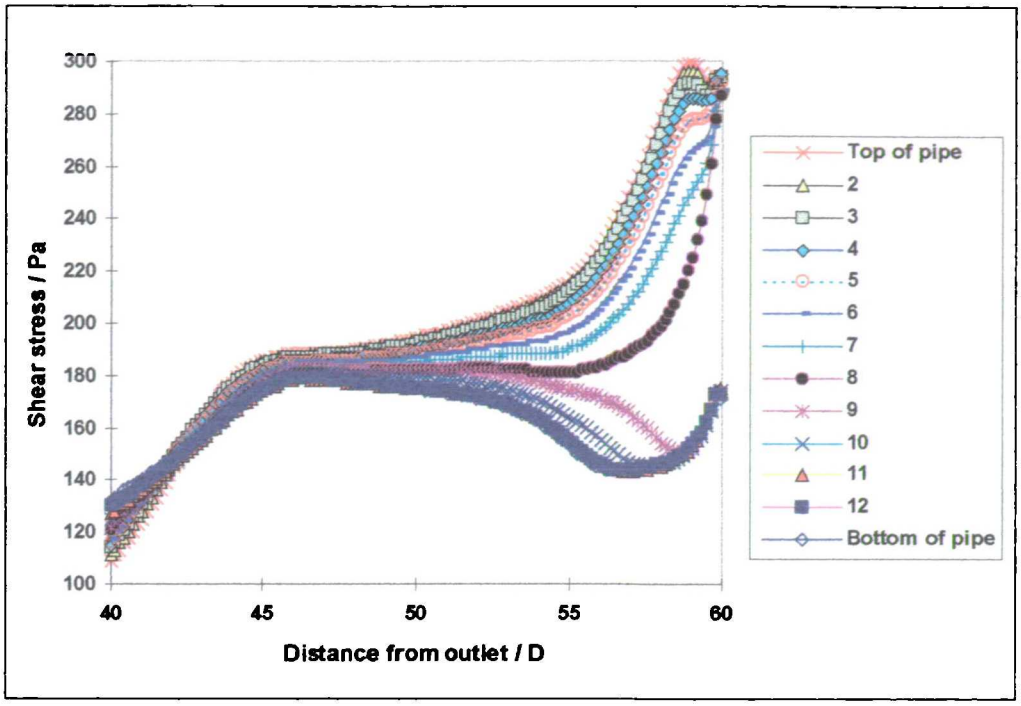

Figure 8.45: Distribution of wall shear stress around the pipe wall (Case SSF04, 9.0 s after dam-break)

In Figure 8.46, the calculated shear stress data are shown for the bottom of the pipe:

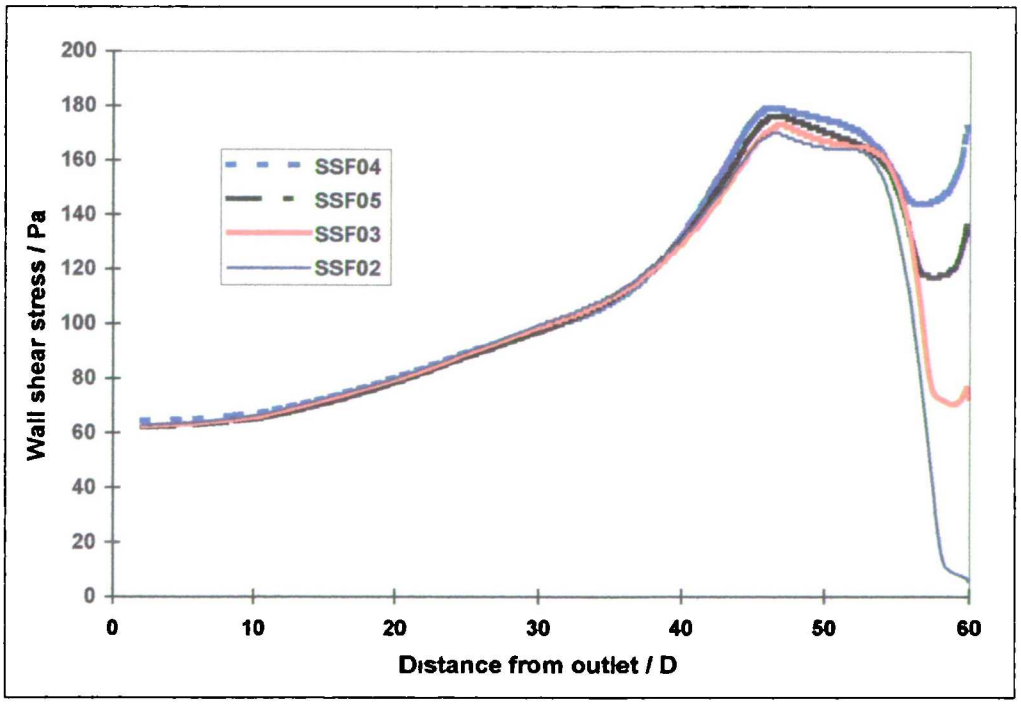

Figure 8.46: Predicted wall shear stress at the bottom of the pipe for the four cases

These results indicate that the use of a modified single-phase friction factor to calculate the wall shear stress (and hence the frictional pressure drop) in the slug body does not accurately represent the variation in shear stress within the slug body. The shear stress at the top of the pipe is considerably greater than at the bottom of the pipe, and exhibits a peak close to the front of the slug body. At the bottom of the pipe, however, the shear stress is at a minimum at the very front of the slug. These effects are most pronounced when the film height ahead of the slug is low.

The friction-factor approach is, however, currently used in 1-D models for the calculation of the pressure drop in slug flow.

The discrepancy between the results shown in Figure 8.44 and Figure 8.45, and the friction-factor approach, is easily demonstrated. The flow in the slug body is assumed to be single-phase liquid (as in these CFD calculations) and the mixture velocity, calculated by a mass balance, for cases SSF02 – SSF05 is equal to 11.0 m/s. Thus, the Reynolds number,

$$\mathrm{Re} = \frac{\rho D u_{LS}}{\mu} \qquad [8.26]$$

is equal to 8.8×10^5 for a pipe diameter of 0.08 m.

The Fanning friction factor, f is obtained in this case by the Nikuradse equation,

$$\frac{1}{\sqrt{f}} = 4\log_{10}\left(\mathrm{Re}\sqrt{f}\right) - 0.4 \qquad [8.27]$$

and has a value of 2.98×10^{-3}. Hence, the wall shear stress,

$$\tau_w = \frac{\rho u_{LS}^2 f}{2} \qquad [8.28]$$

is found to be 180.1 Pa for the slug body. Figure 8.45 suggests that the wall shear stress towards the rear of the slug body is calculated by CFX to be close to 180 Pa for case SSF04, so the friction factor method works extremely well in this region. However, at the front of the slug body the peak wall shear stress is nearly twice this value, with the highest shear stress values calculated at the top of the pipe where the effect of the recirculation zone is most significant.

In the film region, solution of the 1-D tail profile equations (as described in Chapter 2) yields the results shown in Figure 8.47, for $U_{Mix} = 11$ m/s and $U_T = 1.2 \times U_{Mix}$. It should be noted that no solution exists for the case where the liquid holdup in the slug body, ε_{LS}, is equal to unity. However, the two results shown in the plot suggest that the value of ε_{LS} has little effect on the shear stress in the film region.

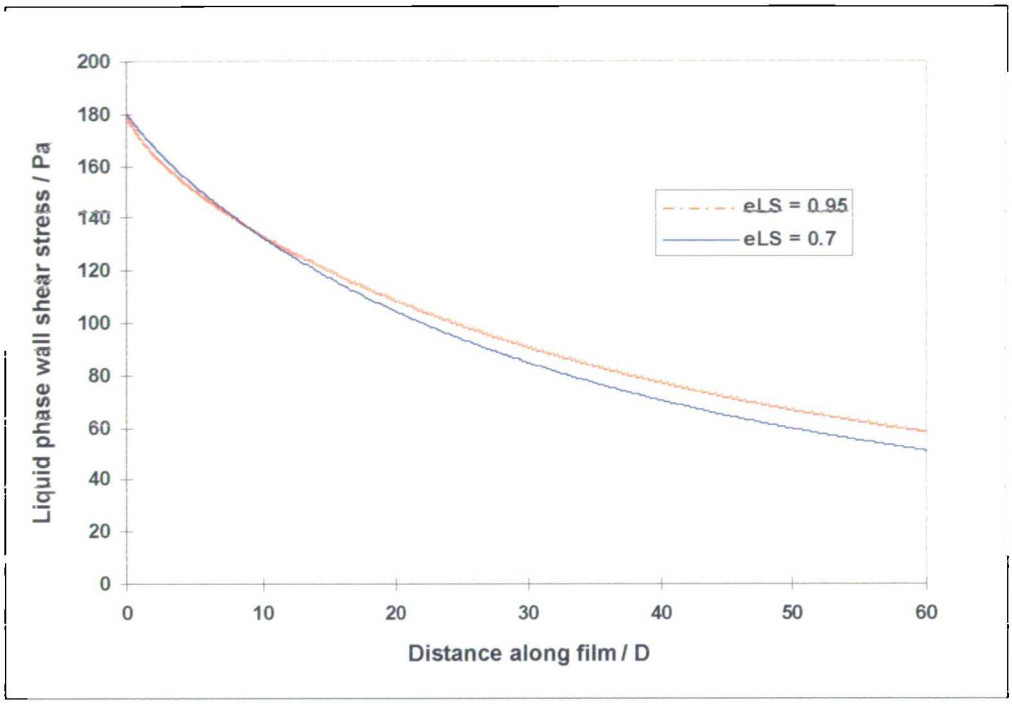

Figure 8.47: Liquid-phase wall shear stress predictions by the 1-D tail profile equation (U_{Mix} = 11 m/s, $U_T = 1.2 \times U_{Mix}$)

In Figure 8.48, these data are compared with the values predicted for the bottom of the pipe by the SSF model.

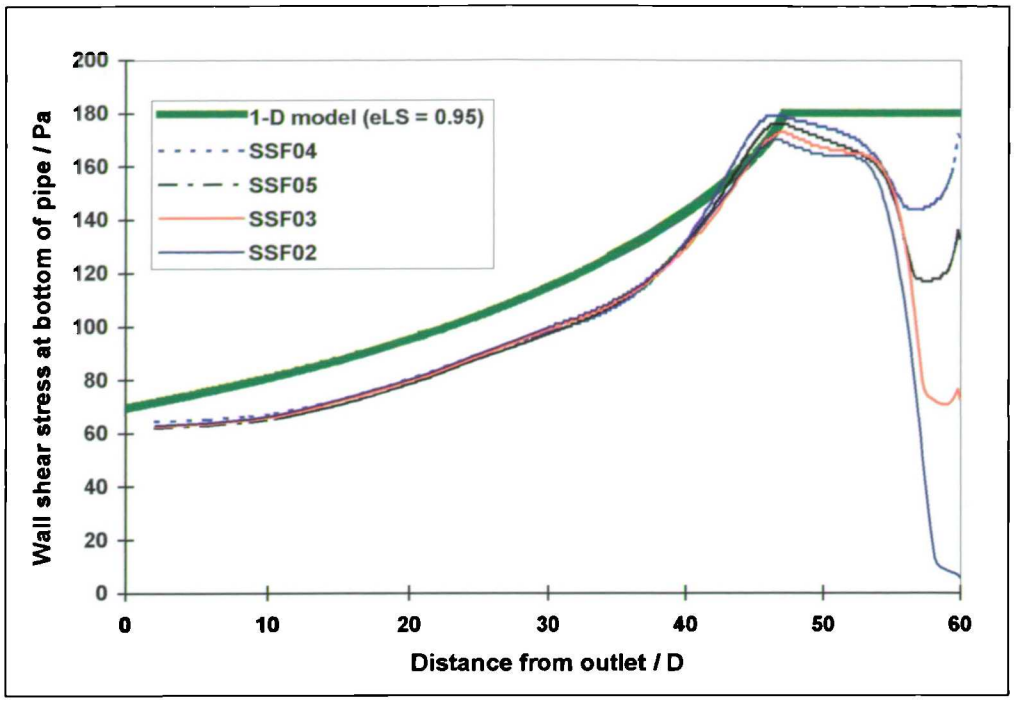

Figure 8.48: Comparison of CFX and 1-D shear stress predictions

In the tail region, the shear stress is predicted slightly higher by the 1-D model than by the CFX simulations. At the very back of the slug body, the two methods agree almost exactly. However, within the slug body itself, the 3-D model predicts considerably lower wall shear stress than does the Nikuradse equation for friction factor.

Effect of the film length on the shape of the Taylor bubble nose

It was found that, although the wall velocity and Froude number were not varied for the four cases SSF02 – SSF05, the calculated position of the nose of the Taylor bubble was not the same for each case. The data showing axial and radial penetration of the Taylor bubble into the slug body (as indicated by Figure 8.13), at the instant when the slug body length is ≈13D, are plotted in Figure 8.49. These show a systematic trend of lesser penetration for lower inlet film height, reflecting the increased extent of recirculation.

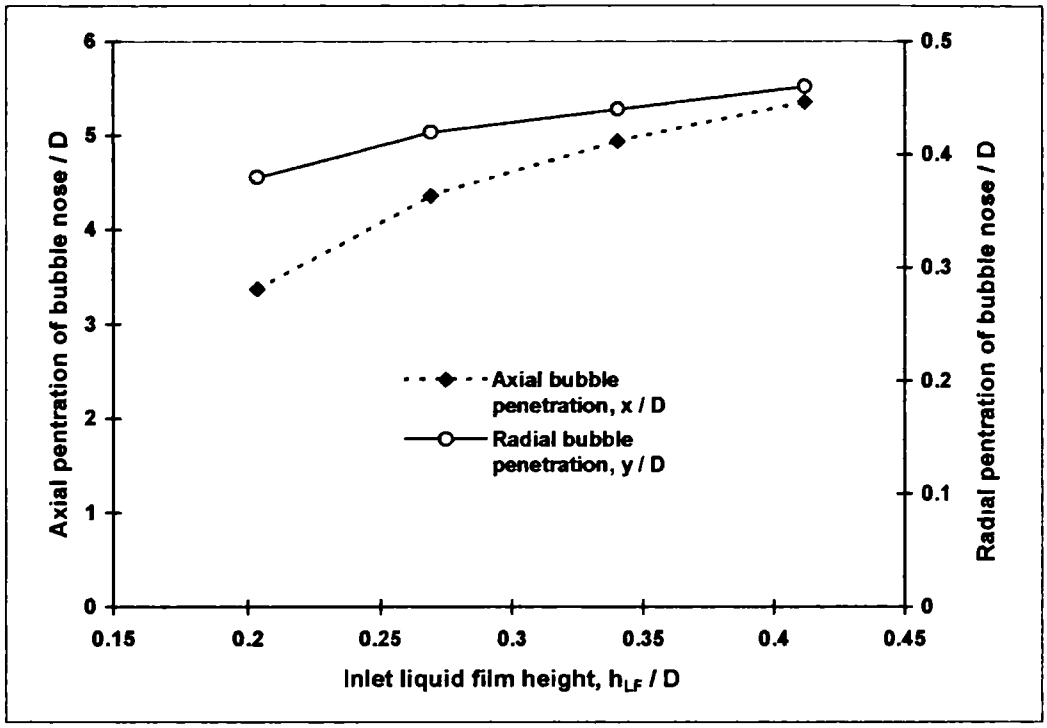

Figure 8.49: Position of the Taylor bubble nose for cases SSF02 – SSF05 at the instant when $L_S/D = 13$

8.6. Simulating a slug front as a gas-liquid interface

As well as modelling the slug tail, a "dam break" approach may also be used to simulate the gas-liquid interface at a slug front. The feasibility of this approach was first demonstrated by Ejedawe & Hughes (1999).

A complication arises from the need to simulate the slower-moving liquid film at the front of the slug. In the present work, this is achieved by introducing a long slug tail into the grid, some distance downstream of the slug front interface, from which the liquid film develops and then flows into the slug front. The initial conditions used to achieve this are shown in Figure 8.50.

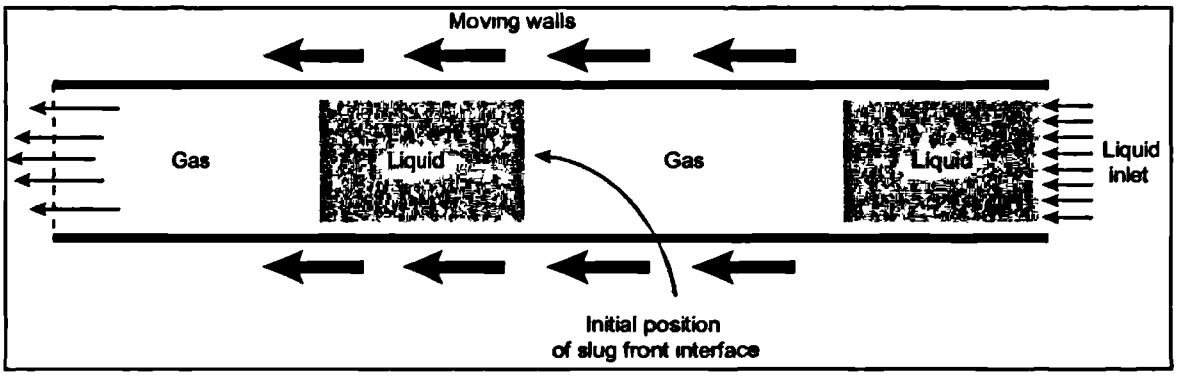

Figure 8.50: Initial conditions for slug front model

In this way, an entire "slug unit" consisting of a slug and its downstream Taylor bubble may be modelled. In the present work, results are reported from a single simulation performed using this technique, as a basis for future work.

The dimensions of the flow domain used for the "slug unit" simulation were the same as for the Solid Slug Front (SSF) model: a section of pipe of diameter 80 mm and length 4.8 m. A four-block "butterfly grid" was used, with 205 cells in the axial direction, illustrated in Figure 8.51. The downstream portion of the grid contained 200 cells, spaced uniformly, in a distance of 4.0 m. The upstream 0.8 m section of the grid contained 5 cells, spaced using a geometric progression so that the ratio of successive cell lengths was 0.47.

The wall velocity, U_{Wall} was specified as 8.0 m/s, with a uniform inlet velocity (*c.f.* the slug tail simulation described in Section 8.4) of 1.2 m/s at the downstream end of the grid. The mixture velocity is thus 6.8 m/s, so that the wall velocity is equal to $1.176 \times U_{Mix}$.

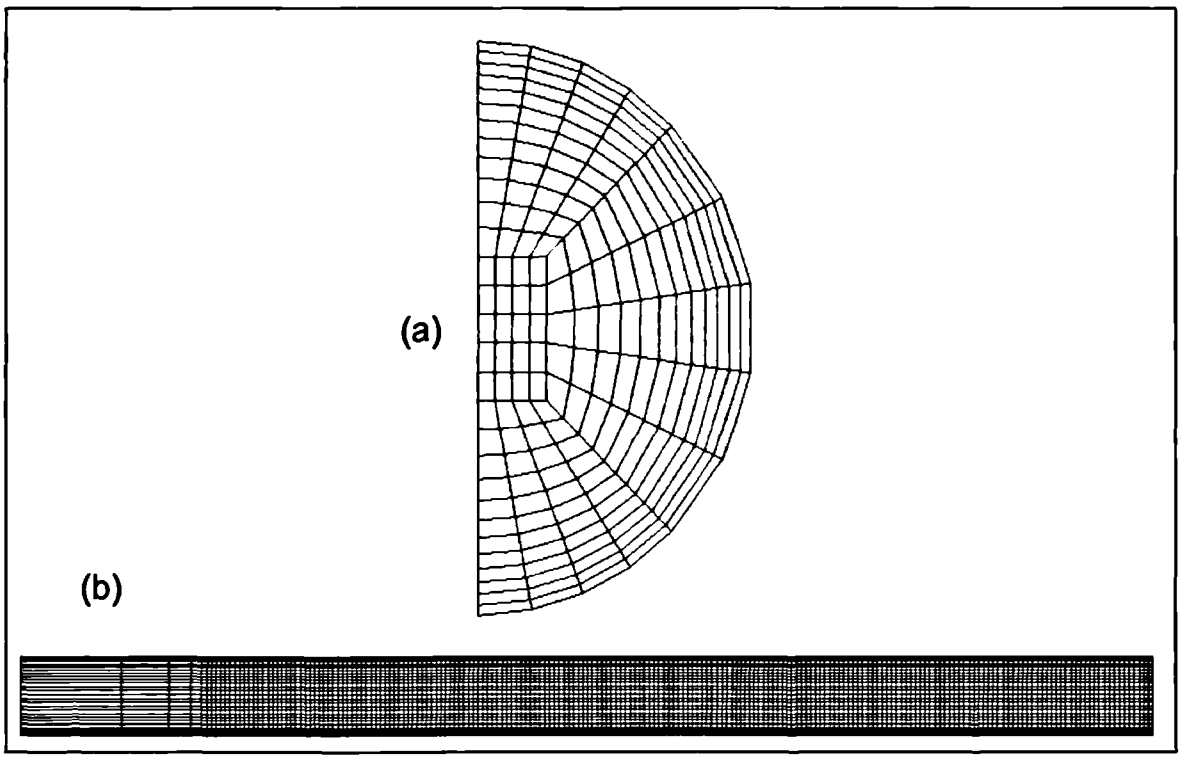

Figure 8.51: (a) Radial and (b) axial cross-sections of the grid used for the "slug unit" simulation (*not to scale*)

The initial distribution of gas and liquid in the grid is summarised in Table 8.6.

Cell range	Distance from inlet / m	Initial contents
$k < 35$	$z < 0.70$	Liquid
$35 \leq k < 75$	$0.70 \leq z < 1.50$	Gas
$75 \leq k < 135$	$1.50 \leq z < 2.70$	Liquid
$k \geq 135$	$z \geq 2.70$	Gas

Table 8.6: Initial distribution of phases for the "slug unit" simulation

The simulation was run using timesteps of 0.005 seconds, with 20 inner iterations each. "Deferred correction" of the k-ε equations was used for the first 10 iterations in each timestep.

The development of the gas-liquid interfaces after the start of the simulation is shown below in Figure 8.52. As in previous plots, the vertical scale has been exaggerated by a factor of 3.8.

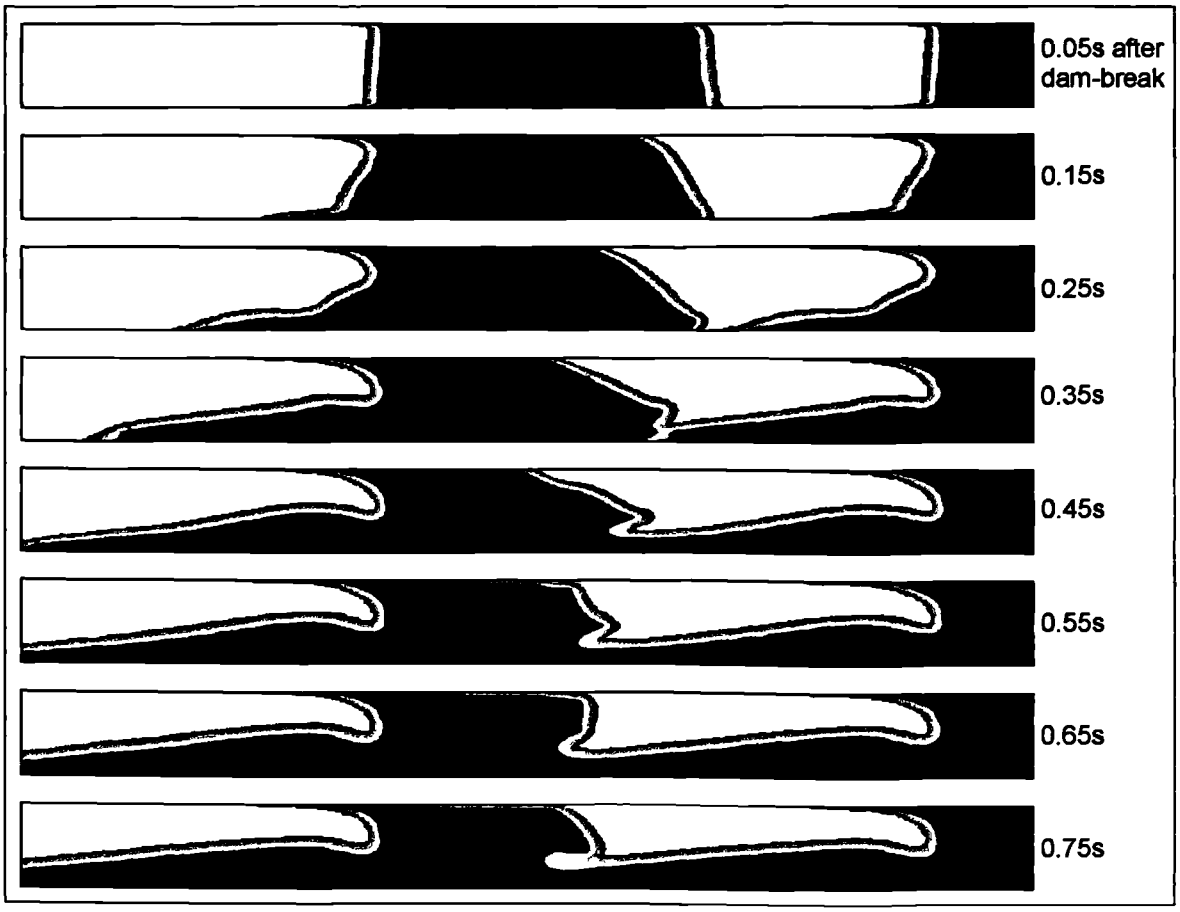

Figure 8.52: Development of the slug front and tail shapes in a "slug unit" simulation

It was found that the shape of the simulated slug front interface agrees closely with the author's own experimental observations and also with published work (*e.g.*, Fagundes Netto *et al.*, 1999a). A promising result was the simulation of "rolling" of the slug front over the liquid film during the course of the transient simulation, in a manner similar to a wave breaking on a beach. It was anticipated that this would result in the entrainment of gas into the slug body. However, it was found that the use of the surface sharpening algorithm caused the entrainment effect to be damped. Instead of being assimilated by the slug body, gas was conveyed around the outside of the slug, in a thin layer close to the pipe wall. In the last plot in Figure 8.52, the interface is visible as a yellow region along the top of the pipe, stretching upstream from the slug front. This is more clearly seen in Figure 8.53, in which the interface is plotted (at the central bisecting plane of the flow domain) as a series of contours. The velocity vectors in the slug body are also shown.

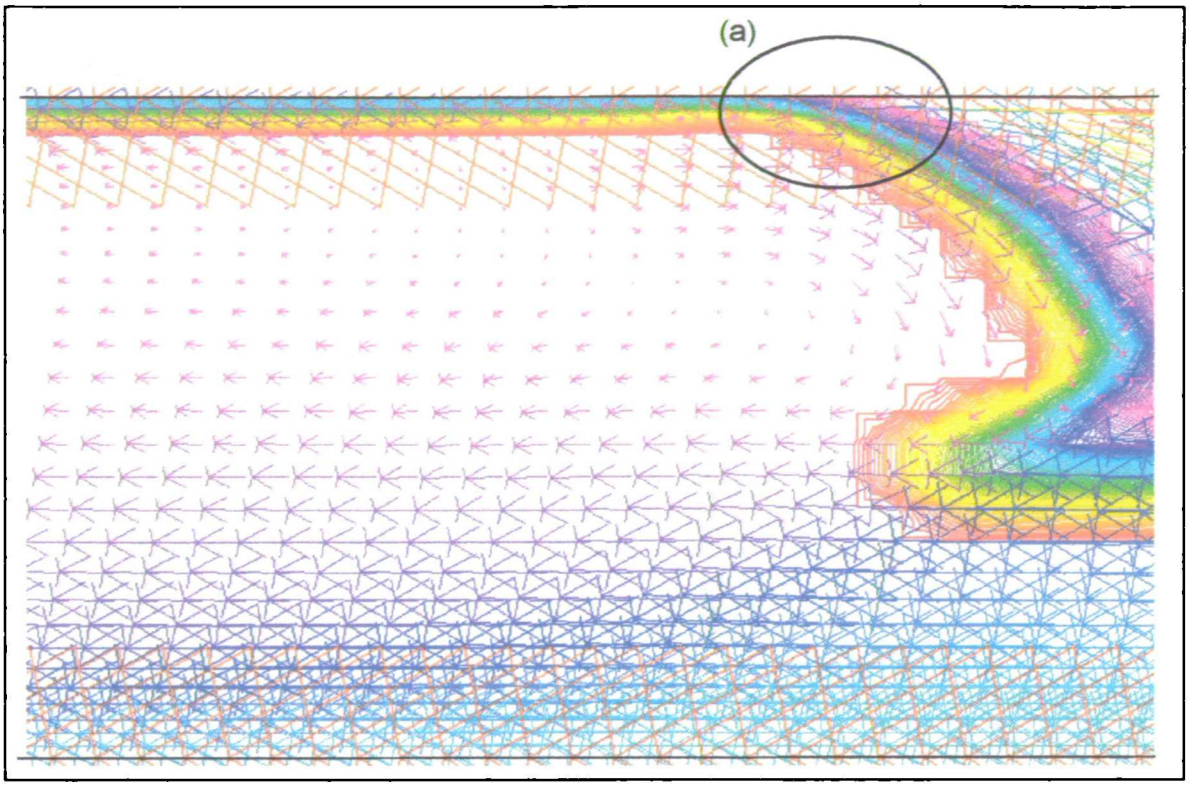

Figure 8.53: Velocity vectors and gas-liquid interface contours at the front of a slug

The recirculation zone at the front of the slug body is clearly visible. However, if the interface behaviour was represented correctly by the simulation, the interface would intersect the pipe wall in the region denoted as (a) in Figure 8.53. Unfortunately it does not: instead, gas "leaks" around the outside of the slug body, causing the Taylor bubble ahead of the slug to "shrink" steadily as the transient simulation progresses. It is suggested that this simulation method may be improved by means of an alternative method of modelling the interface (*e.g.* a multi-fluid or interface-tracking model) or by a reduction in the 90° wall contact angle used in the surface tension model.

The presence of the recirculation zone results in a large value of the wall shear stress at the top of the pipe, at the front of the slug body. At the bottom of the pipe, there is also an increase in wall shear stress in the slug body, but this occurs towards the *rear* of the slug. These results are shown, 5.0 seconds after the start of the transient simulation, in Figure 8.54.

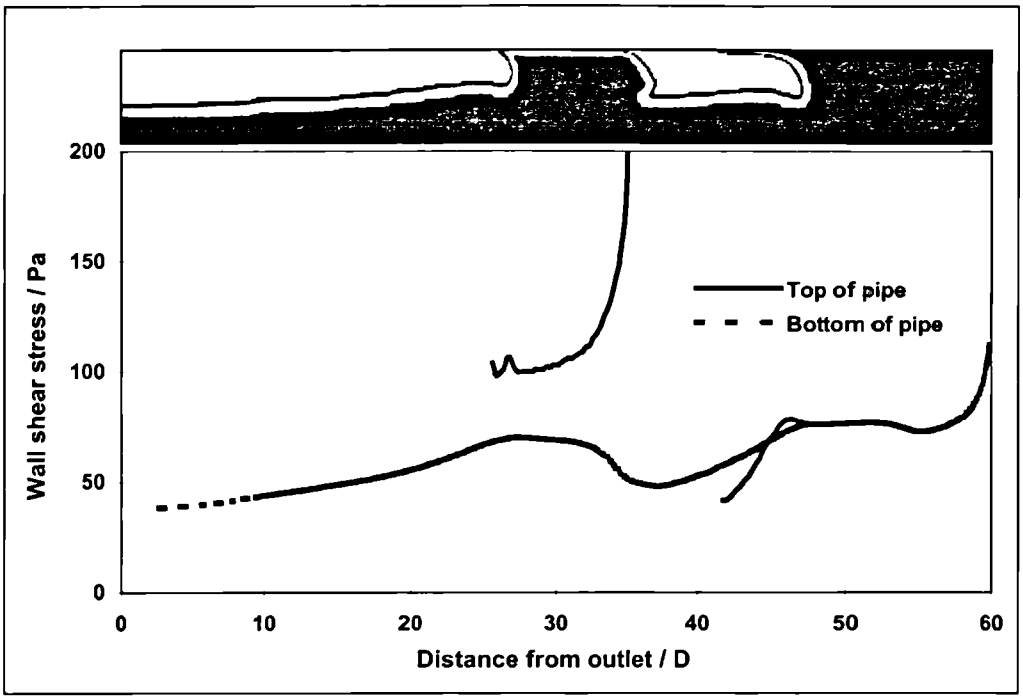

Figure 8.54: Liquid-phase wall shear stresses from the "slug unit" simulation (5.0s after dam-break)

The shear stress at the pipe roof is approximately 100 Pa at the rear of the slug body, *i.e.*, about 30% greater than the corresponding value at the bottom of the pipe. The shear stress at the top of the pipe increases along the slug body and tends sharply to infinity at the very front of the slug. This is likely to be an erroneous effect due to the incorrect prediction of the intersection of the pipe wall and the interface at the slug front.

However, this is significantly different from the predictions of the SSF model, which suggested that the peak shear stress at the slug front was approximately twice the value at the back of the slug. Until the issue of "gas leakage" around the slug body is resolved, the prediction of shear stress in the region where the interface meets the wall is likely to be highly inaccurate.

For the case presented here, the calculation of the single-phase slug body wall shear stress is summarised in Table 8.7. The calculation procedure is the same as in Section 8.5.4, above.

u_{LS} m/s	Re_{LS}	f	τ_w / Pa
6.8	544000	0.00324159	74.95

Table 8.7: Wall shear stress calculation for the slug body

In Figure 8.55, the calculated shear stress data from the 1-D tail profile model (as described in Chapter 2) are compared with the predictions *for the bottom of the pipe* taken from the CFX "slug unit" model. The shear stress in the slug body region is assumed to be the single-phase value calculated in Table 8.7.

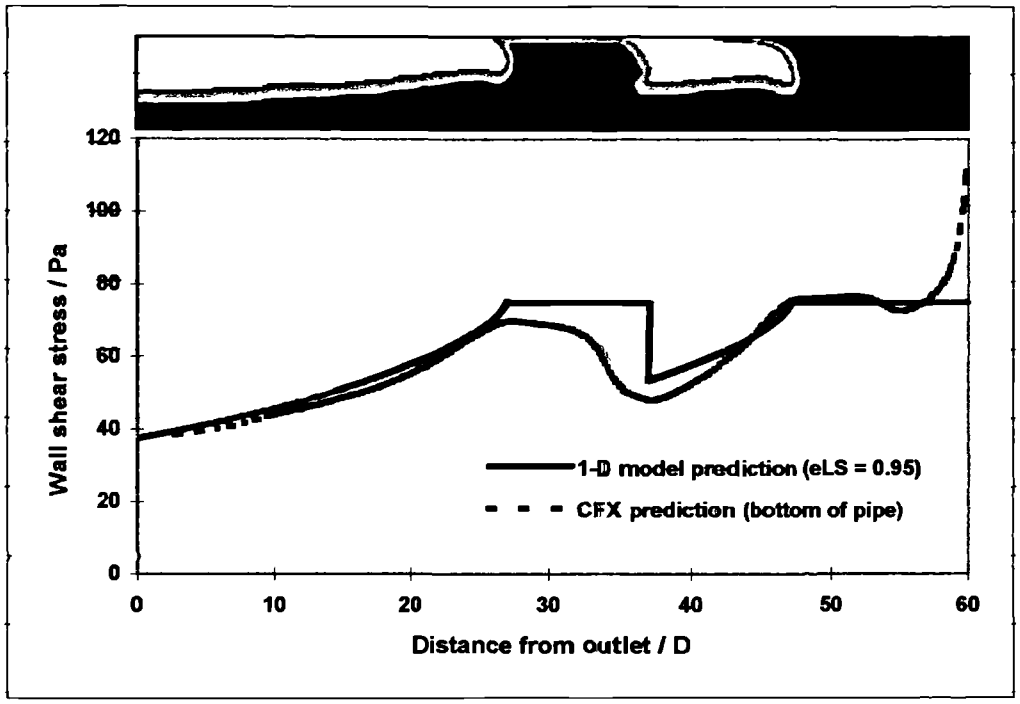

Figure 8.55: Comparison of shear stress predictions at the pipe bottom, from 1-D model and CFX simulation (5.0s after dam-break)

The agreement between the 1-D and 3-D calculations of the tail region is very good indeed. In the slug body, the 3-D results show that the shear stress at the bottom of the pipe is at a minimum at the front of the slug body, with the peak at the very back of the slug.

8.7. Summary

In this chapter, basic computational methods used in Computational Fluid Dynamics (CFD) have been introduced, with particular reference to the commercial software suite CFX4.3, used in the present work. Development of a CFD method to study the motion of Taylor bubbles in horizontal flow has been discussed.

A novel technique to represent the front of a liquid slug using a solid boundary has been developed. This has allowed the simulation of the "recirculation zone" at the front of the slug. The recirculation zone has a significant effect on U_T, the translational velocity of the

slug tail, particularly for short slugs. This has been systematically investigated. The results have shown good agreement with the experimental observations of Fagundes Netto *et al.* (1999) and Cook & Behnia (2000). Furthermore, additional effects have been identified due to the length of the leading liquid film, ahead of the slug, which were not detected in the experimental work.

Calculations for the wall shear stress, both in the slug body and the liquid film region, have been presented. The recirculation of fluid inside the slug body causes a large increase in the calculated wall shear stress at the front of the slug body at the top of the pipe, with an off-setting decrease at the bottom of the pipe. Overall, there may be a slight increase in the mean shear stress in the slug body due to the recirculation zone, which is not currently taken into consideration by the simple modified single-phase approach commonly used in 1-D slug flow models. The variation of shear stress in the film region calculated using the CFD methods have been shown to agree more closely with the predictions from the 1-D tail profile solution.

Limitations of the Volume of Fluid (VOF) model used to simulate "free surfaces" have been highlighted. In particular, the inability of the method to adequately describe the entrainment of one phase into another (*i.e.*, the entrainment of gas bubbles into the slug body) is a major shortcoming. The development of a detailed, 3-D model of slug flow which includes entrainment of gas at the front of the slug, its transport along the slug body and disentrainment at the tail, and also transport of gas within the liquid film, will require a different approach.

Blank page.

Chapter 9: Conclusions and recommendations for future work

This Chapter is organised into two parts. In Section 9.1 the conclusions from the present work are presented. Then, in Section 9.2 some recommendations are suggested for future development of the experimental and modelling studies which have formed the basis of this thesis.

9.1. Summary and conclusions

9.1.1. Experimental work

The main conclusions from the experimental work relate to the occurrence of slug flow in inclined pipes. Three extended Campaigns of experiments were performed, with flow in 77.92 mm internal diameter pipes, with the following configurations:

1. A 36 m long straight pipe run, inclined downwards (in the direction of flow) by 1.5° to the horizontal.

2. A "V-section pipe" with the first 14 m length inclined downwards at 1.5° and the remaining 21 m inclined upwards at 1.5°. The two lengths were connected by a smooth-bore, flexible connector.

3. A "Λ-section pipe" with the first 14 m inclined upwards at 1.5° and the remaining 21m inclined downwards at 1.5°. Again, the two lengths were joined with a smooth, flexible connector.

Experiments were conducted with pipe exit pressures close to atmospheric pressure and at 5 bar(g).

Large data sets were obtained during each of the Campaigns, over a wide range of gas and liquid superficial velocities. Pressure gradient and average liquid holdup were measured near the exit of the pipe using a pressure transducer and a gamma densitometer respectively. Flow patterns were observed near the end of the pipe using a transparent visualisation section and were deduced at other locations from the outputs of twin-wire conductance probes which

measured instantaneous chordal mean holdups at a number of positions along the pipe. The outputs from the twin-wire conductance probes were also used to obtain estimates of slug length, slug frequency and slug tail velocity. The data show the normal scatter associated with two-phase flow measurements but some general trends were observable. The experimental data were found, in general, to be poorly predicted by the correlations and models available in the literature.

In downhill flow, it was found that the region of occurrence of slug flow was smaller, in terms of the phase superficial velocities, than for horizontal flow, with the stratified/slug transition occurring at significantly higher liquid superficial velocity.

In the experiments conducted on the "V"-section, flow pattern maps measured at the pipe exit were found to be strongly influenced by the rising limb of the "V"-section. The presence of a "dip" in the pipeline caused a large increase in the size of the slug flow region of the flow pattern map, and introduced a significant region in which "dip slugging" occurred. This was characterised by short, high frequency slugs with very regular period and length, which were observed immediately downstream of the dip. However, regular "dip-slugging" was not seen further from the dip: the short slugs quickly collapsed and merged to form less regular slug flow as they propagated downstream. Reverse flow was observed between slugs in the rising limb for cases when the superficial gas velocity fell below 8 m/s (for the experiments at atmospheric pressure), or 2.4 m/s (for flow at 5 bar(g)). This agrees well with published data.

In the experiments conducted on the "Λ"-section, flow pattern maps measured at the pipe exit showed an increase in the size of the slug flow regime compared with purely downhill flow. This was attributed to the formation of slugs in the rising limb of the "Λ"-section and their persistence into the downhill limb. The relatively short length of pipe between the apex of the Λ-section and the pipe exit was unlikely to provide sufficient distance for the collapse of these slugs and the establishment of a flow pattern map characteristic of purely downwards flow. "Stratified smooth" flow was not observed at the end of the pipe. Instead, this regime was affected by low amplitude, low frequency "surges" in the thickness of the stratified film. This was caused by the collapse of short slugs and the coalescence of interfacial waves in the downward limb of the "Λ"-section.

9.1.2. One-dimensional slug flow modelling

A one-dimensional, quasi-steady state kinematic model of slug flow was developed. Whereas earlier models have used a constant liquid film thickness between slugs, the present scheme was based on the solution of the 1-D film profile in the slug tail region, with slug liquid holdup calculated from a gas entrainment correlation. Key features of the model were its use of object-oriented programming and "lookup tables" to considerably increase the efficiency of the algorithm compared with earlier schemes. This was achieved by interpolating data from a large array rather than continually solving the 1-D film profile equations in the slug tracking algorithm. A crude treatment was used for wave propagation, and no attempt was made to damp the "instantaneous information propagation" in the model. Due to these simplifications, rigorous continuity of mass and momentum are not assured.

The model was found to accurately predict the collapse of interfacial waves and the propagation of slugs when compared with experimental data. An important result was that realistic slug length distributions and frequencies were obtained as output from the model when very short, very high-frequency "precursor" slugs were introduced at the start of the pipe. However, it was found that the slug parameters (average length and frequency) predicted at a large distance downstream were affected by small variations in the length and frequency of the short slugs introduced at the inlet. This suggests that a detailed mechanistic model of slug initiation is required for the pipe inlet. Some previous slug tracking studies had suggested that a fully developed slug flow would occur which was *independent* of the characteristics of a random distribution of short slugs at the pipe entrance which was used to initialise the model. The more rigorous model presented here suggests that this is incorrect; the characteristics of the developed slug flow are *dependent* on the initial conditions.

9.1.3. Three-dimensional slug flow modelling

Simulation of a single, isolated slug and its associated film region has been conducted using a three-dimensional Computational Fluid Dynamics (CFD) model. A novel technique has been developed to represent the front of a liquid slug using a solid boundary. This has allowed the simulation of the "recirculation zone" at the front of the slug. It has been shown that the recirculation zone has a significant effect on the translational velocity of the slug tail, particularly for short slugs. The simulated results have shown good agreement with the experimental observations of the "wake effect" by Fagundes Netto *et al.* (1999) and Cook &

Behnia (2000). Furthermore, additional effects have been identified due to the length of the leading liquid film, ahead of the slug, which were not detected in the experimental work.

The "dam break" method used to simulate the development of the gas-liquid interface in the slug tail region has been extended to the slug front, and has been shown to correctly simulate the shape of the slug front interface and the liquid recirculation zone within the slug body. However, prediction of the slug front interface in the region where it intersects the pipe wall is poor.

Calculations for the wall shear stress, both in the slug body and the liquid film region, have been presented. The recirculation of fluid inside the slug body causes a large increase in the calculated wall shear stress at the front of the slug body at the top of the pipe, with an off-setting decrease at the bottom of the pipe. Overall, there may be a slight increase in the mean shear stress in the slug body due to the recirculation zone. The wall shear stress in the film region calculated using the CFD methods have been shown to agree closely with the predictions from the 1-D tail profile solution.

9.2. Recommendations for future work

9.2.1. Experimental work

It is recommended that future experimental work should address the following aims:

1. More detailed closure relationships should be obtained for the slug flow parameters used in the models; in particular slug translational velocity, the gas entrainment rate at the slug front and the rate of gas transport through the slug body.

2. A detailed study of interfacial wave propagation should be conducted to elucidate closure relationships and modelling procedures for wave tracking.

3. Flow should be studied over a much wider range of pressures. This would require modification to the experimental facilities used in the present work. Alternatively, a gas with a significantly greater density than air (*e.g.*, sulphur hexafluoride, SF_6) could be used as the gas phase in a closed-loop multiphase flow facility.

4. "Slug tracking" data should be obtained for air-oil flow. Electrical conductivity probes would not be suitable for such work – the installation of other instrumentation at multiple points along a test-pipe, for example a succession of gamma densitometers, would be required.

5. A large array of probes could be placed close to the inlet of the test-section, to study the initiation of slug flow from interfacial waves created at the pipe inlet.

6. A series of experiments could be conducted to study the "wake effect" for short slugs of $L_S/D \leq 8$. An experimental facility would allow the "injection" of slugs and/or gas bubbles of known volume and thus length. Studies should be conducted in the *slug* flow regime, with appropriate ranges of gas and liquid superficial velocity (*i.e.*, $U_{sL}/U_{Mix} \leq 0.2$) rather than the *plug* flow regime, occurring at higher liquid flow rates, which have been reported in the literature.

9.2.2. One-dimensional modelling

It is recommended that future development of the 1-D modelling aspects of the present work may include the following:

1. A physical model of wave propagation should be developed. The slug tracking scheme currently uses a robust, but highly simplified treatment for wave propagation, which (approximately) conserves mass but does not correctly conserve momentum. An improved wave model should simulate the formation of a wave from a collapsing slug and its subsequent deceleration from the slug translational velocity to a slower "wave velocity". The propagation, growth and decay of waves could then be simulated correctly.

2. A mass conservation routine should be added to the slug propagation algorithm which takes into account the variation in the liquid holdup of a slug, ε_{LSi} over time. As ε_{LSi} changes, the shape (and thus the liquid content) of the associated film region also varies: currently this results in a small discrepancy in the liquid "book keeping" in the model. Mass conservation could be ensured by slightly adjusting the film length by changing the position of the next slug front upstream, X_{i+1}, at each time step.

Accurate mass conservation requires that a rigorous physical model is used for wave propagation, and *vice versa*.

3. Currently, when film profile data are obtained from the lookup tables, a rounded value of the film length is used, rather than the exact value ($Y_{i-1} - X_i$). The lookup algorithm should be improved to interpolate the exact value, to eliminate rounding errors.

4. "Convection" of void fraction through the slug body could be modelled so that the assumption of instantaneous, perfect mixing of gas and liquid within the slug body is no longer used. This would eliminate the undesirable effects of instantaneous upwind propagation of information through the simulation, whereby a change in the conditions at a slug front results in an immediate change to the conditions at its tail, and thus at the front of the next slug upstream, *etc.* "Convection" could be achieved using an information "buffer" consisting of several nodes along each slug body, with a discrete transport equation to describe how the slug body holdup scalar is passed between the nodes.

5. The "wake effect" relationship used by the model should be extended to include the additional effect of the film length ahead of a slug, which was revealed using the Solid Slug Front (SSF) model in the CFD study in the present work.

6. The phenomenological model of slug initiation developed by Hale (2000) could be coupled directly to the slug tracking algorithm.

7. Dynamic effects could be included in the model so that gas compressibility is modelled and the effect of gas expansion on slug propagation is simulated.

8. The model should be extended to include the "source/sink" effects at the change of inclination occurring in a V- or Λ-section.

9. The model could be extended to the case of transient and/or three-phase slug flow.

9.2.3. Three-dimensional CFD modelling

The following recommendations are made for future 3-dimensional CFD modelling studies of slug flow:

1. The CFD models reported in the present work have been developed for a single geometry (a horizontal pipe with a diameter of 80 mm) and a limited range of flow conditions. The study of the translational velocity of the slug tail using the Solid Slug Front (SSF) model could be extended to include the effects of pipe diameter and inclination. In particular, closure relationships for slug propagation in downwardly-inclined pipes could be obtained.

2. The effects of fluid density and viscosity on the slug tail velocity have not been studied in the present work. These could be investigated using the SSF model in its current form.

3. The VOF ("homogenous") multiphase model in CFX4.3 does not simulate entrainment of one phase into another other due to negative diffusion imposed by the surface sharpening algorithm. This limits the simulation of slug flow to the case where the liquid holdup in the slug body is unity, *i.e.*, no gas entrainment in the slug. A more sophisticated multiphase model should be used instead of the VOF model, to simulate gas entrainment at the slug front and the transport of gas along the slug body. Although not included in the present work, a preliminary study by the author has shown that the "particle drag model" model incorporated in CFX4.3 could be used to simulate these effects. This requires the specification of a "continuous" and a "dispersed" phase (*i.e.*, liquid and gas, respectively) and a mean "particle diameter" for the dispersed phase (*i.e.*, the diameter of the dispersed bubbles in the slug body). The shape of the gas-liquid interface at the slug front and tail may be developed from initial "dam-breaks", as in the present work. However, a surface sharpening algorithm is not used with the particle drag model: instead, a high-order differencing scheme (for example, the van Leer scheme) must be specified to prevent smearing of the interface due to numerical diffusion.

4. The incorrect prediction of the gas-liquid interface at the slug front, in the region where it meets the pipe wall, may be eliminated using a more sophisticated multiphase model. This would allow further insight into the variation of wall shear stress in the slug body, and the detailed mixing effects in the recirculation zone at the slug front. However, it is likely that *extremely* fine meshes will be required for the correct simulation of these effects, with cell sizes several orders of magnitude smaller than used in the present work.

5. Considerable computer run-times (>150 hours in many cases) were required for each simulation in the present work. More modern, high-performance computer hardware is required to reduce the computation time for future work, so that more complex simulations may be performed.

6. Recently, solution algorithms used in commercial CFD software have been adapted to make use of advances in parallel computing. In the latest release of CFX4.3, it is possible to parallelise a simulation to run on 2 or more CPUs simultaneously, with a corresponding decrease in run-time. As the cost/performance ratio of CPUs falls exponentially (Moore, 1965; Mann, 2000) and the use of multi-CPU hardware and operating systems becomes widespread, parallel processing is now a realistic strategy for the implementation of CFD models. If CFD modelling of slug flow is to be progressed significantly, the author advises that parallelisation is the only practical option for future work which incorporates the detailed physics suggested above, with the necessary fine meshes and short time steps.

Nomenclature

Roman Symbols

Symbol	Denotes	Dimensions
A	Pipe cross-sectional area	m^2
A_G	Cross-sectional area of gas bubble	m^2
A_L	Cross-sectional area of liquid film	m^2
B	Relative surface roughness	-
Bo	Bond number	-
C	"C-ratio" parameter defined in Equation [2.74]	-
C_1	Constant in Equations [2.67], [xx8.11]	-
C_2	Constant in Equations [2.67], [xx8.11]	-
C_E	Electrical capacitance	F
C_μ	Viscosity constant	-
D	Pipe diameter	m
d	Separation of conductivity probe wires	m
E	Parameter in Equation [2.12]	-
E_1	Parameter in Equation [2.6]	-
E_2	Parameter in Equation [2.6]	-
F	Parameter in Equation [2.12]	-
f_G	Gas friction factor	-
f_{GO}	Friction factor calculated from Re_{GO}	-
f_I	Interfacial friction factor	-
f_{in}	Inlet slug frequency	s^{-1}
f_L	Liquid friction factor	-
f_{LO}	Friction factor calculated from Re_{LO}	-
f_{NS}	No slip friction factor	-
Fr	Froude number	-
Fr_{Mod}	Modified Froude number	-
f_{TP}	Two-phase friction factor	-
F_x	x-component of body force	N
F_s	Surface tension body force	N
F_y	y-component of body force	N
F_z	z-component of body force	N
g	Acceleration due to gravity	$kg\ m\ s^{-2}$
G_E	Electrical conductivity	Ω^{-1}
H	Parameter in Equation [2.12]	-
$\tilde{h}$	Dimensionless thickness of aerated film	-

Symbol	Denotes	Dimensions
h_L	Liquid depth	m
h_{LF}	Thickness of stratified liquid film	m
h_{LS}	Equivalent liquid height in slug body	m
i	Slug number	-
I	Gamma photon intensity	$m^{-2}\ s^{-1}$
J	Parameter in Equation [2.6]	-
J_G	Gas mass flux	$kg\ m^{-2}\ s^{-1}$
J_G^{**}	Modified Wallis flooding parameter	-
k	Constant in Equation [2.84]	-
k	Mean turbulent kinetic energy per unit mass	$J\ kg^{-1}$
K_c	Controller gain	-
Δl	Distance between conductivity probes	m
L_1	Parameter in Equation [2.26]	-
L_2	Parameter in Equation [2.27]	-
L_C	Critical slug length	-
L_F	Length of stratified film region	m
L_{Fi}	Length of film region behind slug i	m
$L_{in,i}$	Length of injected slug i	m
L_S	Length of slug body	m
L_{Si}	Length of slug body i	m
L_U	Length of slug unit	m
L_ε	Characteristic turbulent length scale	m
$\dot{m}_G$	Gas mass flux	$kg\ m^2\ s^{-1}$
$\dot{m}_L$	Liquid mass flux	$kg\ m^2\ s^{-1}$
m_{LFi}	Total mass contained in the film behind slug i	kg
$\dot{M}_{LPi}$	Rate of liquid mass pickup by front of slug i	$kg\ s^{-1}$
m_{LSi}	Mass of wave i	kg
$\dot{M}_{LSi}$	Rate of liquid shed from tail of slug i	$kg\ s^{-1}$
n	Parameter in Equation [2.77]	-
N_{LV}	Liquid velocity number	-
p	Instantaneous, localised pressure	Pa
P	System pressure	Pa
P	Shear production rate	Pa
Q_L	Static liquid volume accumulated in "V"-section	m^3
r	Radius of conductivity probe wires	m
Re	Reynolds number	-
Re_G	Gas-phase Reynolds number	-
Re_{GO}	Gas Reynolds number defined by Eqn. [2.16]	-

Symbol	Denotes	Dimensions
Re_L	Liquid-phase Reynolds number	-
Re_{LO}	Liquid Reynolds number defined by Eqn. [2.16]	-
Re_{NS}	"No slip" Reynolds number	-
Re_S	Slug Reynolds number	-
S	Slip ratio	-
S	Parameter in Equation [2.30]	-
S_G	Length of perimeter of gas region	m
S_I	Gas-liquid interface length	m
S_L	Length of wetted liquid perimeter	m
t	Time	s
$t_{in,i}$	Injection time of slug i	s
Δt	Discrete time step	s
Δt_{Random}	Random variation in slug injection interval	s
u	Fluid velocity in x-co-ordinate direction	$m\ s^{-1}$
u^+	Dimensionless fluid velocity	-
u^*	Friction velocity	$m\ s^{-1}$
u'_{MF}	Minimum velocity for gas entrainment in Eqn [	$m\ s^{-1}$
U_{AH}	Critical wave velocity of interfacial waves	$m\ s^{-1}$
u_D	Drift velocity	$m\ s^{-1}$
U_F	Slug front velocity	$m\ s^{-1}$
U_{Fi}	Velocity of front of slug i	$m\ s^{-1}$
u_G	Gas velocity	$m\ s^{-1}$
u_{G0}	Gas bubble rise velocity in stagnant liquid	$m\ s^{-1}$
u_{GFF}	Velocity of gas bubbles in liquid film	$m\ s^{-1}$
u_{GFi}	Gas velocity at end of film i	$m\ s^{-1}$
u_{GS}	Gas velocity in slug body	$m\ s^{-1}$
U_{Inlet}	Liquid velocity at CFD inlet boundary	$m\ s^{-1}$
u_L	Liquid velocity	$m\ s^{-1}$
u_{LF}	Liquid film velocity in stratified film region	$m\ s^{-1}$
u_{LFi}	Liquid film velocity at end of film i	$m\ s^{-1}$
u_{LS}	Liquid velocity in slug body	$m\ s^{-1}$
U_{Man}	Critical velocity for gas entrainment in Eqn. [2.75]	$m\ s^{-1}$
U_{Mix}	Total superficial velocity (Mixture velocity)	$m\ s^{-1}$
$U_{Mix,min}$	Value of U_{Mix} resulting in minimum slug frequency	$m\ s^{-1}$
U_{NA}	Critical velocity for gas entrainment in Eqn. [2.72]	$m\ s^{-1}$
U_{sG}	Average superficial gas velocity	$m\ s^{-1}$
U_{sL}	Average superficial liquid velocity	$m\ s^{-1}$
U_{sW}	Average superficial water velocity	$m\ s^{-1}$
U_T	Slug tail (or translational) velocity	$m\ s^{-1}$

Symbol	Denotes	Dimensions
U_T'	Velocity of tail position within CFD grid	$m\ s^{-1}$
$U_{T,\infty}$	Translational velocity of a long, stable slug	$m\ s^{-1}$
U_{Ti}	Velocity of tail of slug i	$m\ s^{-1}$
U_{Wall}	Moving wall velocity of CFD grid	$m\ s^{-1}$
v	Fluid velocity in y-co-ordinate direction	$m\ s^{-1}$
v	Output voltage from conductivity probe	V
$\dot{V}_{GF}$	Volumetric gas entrainment rate at slug front	$m^3\ s^{-1}$
V_L	Liquid volume	m^3
$\dot{V}_L$	Volumetric liquid flow rate	$m^3\ s^{-1}$
$\dot{V}_{LF}$	Volumetric liquid flow rate in film region	$m^3\ s^{-1}$
$\dot{V}_{LS}$	Volumetric liquid flow rate in slug body	$m^3\ s^{-1}$
$\dot{V}_{LT}$	Volumetric liquid shedding rate at slug tail	$m^3\ s^{-1}$
w	Fluid velocity in z-co-ordinate direction	$m\ s^{-1}$
We	Weber number	-
We_{Mix}	Mixture Weber number	-
x	Axial penetration distance of Taylor bubble nose	m
Δx	Change in slug body length	m
X	Parameter in Equation [2.25]	-
x_G	Inlet quality (gas phase mass fraction)	-
X_i	Distance of slug front i from beginning of pipe	m
$\dot{X}_i$	Rate of change of position of slug front i	$m\ s^{-1}$
y	Parameter in Equation [2.32]	-
y	Radial penetration distance of Taylor bubble nose	m
y^+	Dimensionless distance from the pipe wall	-
Y_i	Distance of slug tail i from beginning of pipe	m
$\dot{Y}_i$	Rate of change of position of slug tail i	$m\ s^{-1}$
z	Axial distance along the pipe centre line	m
Δz	Discrete length interval	m

Greek Symbols

Symbol	Denotes	Dimensions
β	Angle of pipe inclination from horizontal	Radians
β	Constant in Equation [2.83]	-
γ	Electrical conductivity	Ω^{-1} m
γ	Angle subtended by gas-liquid interface	Radians
γ	Linear γ-ray absorption coefficient	m^{-1}
ε	Dielectric constant	J s^{-1} m^{-1} xx
ε	Turbulence dissipation rate	J kg^{-1} s^{-1}
ε_{GFi}	Gas holdup at end of film region behind slug i	-
ε_{GSi}	Gas holdup in slug i	-
ε_{L}	Liquid holdup	-
ε_{L0}	Liquid holdup in a horizontal pipe	-
ε_{LF}	Liquid holdup in stratified film region	-
ε_{LFi}	Liquid holdup at end of film behind slug i	-
ε_{LH}	Homogeneous liquid holdup	-
ε_{LS}	Liquid holdup in slug body	-
ε_{LSi}	Liquid holdup in slug i	-
$\varepsilon_{L\beta}$	Liquid holdup in an inclined pipe	-
κ	Surface curvature	m^{-1}
κ	von Karman constant	-
μ	Mass γ-ray absorption coefficient	kg^{-1} m^{2}
μ	Parameter in Equations [2.95] & [2.96]	ft s^{-1}
μ_{eff}	Effective viscosity	Pa s
μ_{G}	Gas dynamic viscosity	Pa s
μ_{L}	Liquid dynamic viscosity	Pa s
μ_{T}	Turbulent viscosity	Pa s
ρ_{G}	Gas density	kg m^{-3}
ρ_{L}	Liquid density	kg m^{-3}
ρ_{M}	Mixture density	kg m^{-3}
ρ_{TP}	Two-phase density defined in Eqn. [2.29]	kg m^{-3}
σ	Surface tension	N m^{-1}
σ	Parameter in Equations [2.95] & [2.96]	ft s^{-1}
ϕ	Two-phase modifier for pressure gradient	-
ϕ	Holdup in aerated liquid film	-
φ	Slug frequency	s^{-1}
σ_{k}	Constant in Equation [xx8.10]	-

Symbol	Denotes	Dimensions
σ_ε	Constant in Equation [xx8.11]	-
τ_D	Control-loop derivative time constant	s^{-1}
τ_G	Gas wall shear stress	Pa
τ_I	Control-loop integral time constant	s
τ_I	Interfacial shear stress	Pa
τ_L	Liquid wall shear stress	Pa
ψ	Constant in Equation [2.83]	-

References

- **Abbot, M. B. & Basco, D. R. (1989)** "Computational fluid dynamics" *Longman, U.K.*
- **Adams, D. N. (1978)** "The hitchhiker's guide to the galaxy" *Heinemann, London, U.K.. (originally broadcast by BBC Radio 4, U.K., 8 March).*
- **AEA Technology PLC (1999)** "CFX-4 documentation" *On-line reference guide, supplied on CD with CFX-4.3 software.*
- **Anderson Jr., J. D. (1995)** "Computational fluid dynamics: the basics with applications" *McGraw-Hill, U.S.A.*
- **Andreussi, P. & Bendiksen, K. H. (1989)** "An investigation of void fraction in liquid slugs for horizontal and inclined gas-liquid pipe flow" *Int. J. Multiphase Flow*, **15**, pp 937-946.
- **Andritsos, N. & Hanratty, T. J. (1987)** "Influence of interfacial waves in stratified gas-liquid flows" *A.I.Ch.E.J.*, **33** (3), pp 444-454.
- **Arcilla, A. S., Häuser, J., Eiseman, P. R. & Thompson, J. F. (eds.)** "Numerical grid generation in computational fluid dynamics and related fields" *North Holland,* Amsterdam.
- **Badie, S. (2000) "Horizontal stratifying / annular gas-liquid flow"** *PhD Thesis, University of London.*
- **Bannerjee, S. (1980)** "Separated flow models II - High order dispersion effects in the averaged formulation" *Int. J. Multiphase Flow*, **6**, pp 241-248.
- **Barnea, D. (1990)** "The effect of bubble shape on pressure drop calculations in vertical slug flow" *Int. J. Multiphase Flow*, **16**, pp 79-89.
- **Barnea, D. & Brauner, N. (1985)** "Holdup of the liquid slug in two-phase intermittent flow" *Int. J. Multiphase Flow,* **11**, pp 43-49.
- **Barrett, N., Hill, T. J. & King, M. J. S. (1998)** "Understanding and development of a slug hysteresis model for hilly terrain pipelines" *1st North American Conf. Multiphase Technology,* Banff, Canada, June.

- **Bendiksen, K. H. (1984)** "An experimental investigation of the motion of long bubbles in inclined tubes" *Int. J. Multiphase Flow,* **10**, pp 467-483.

- **Bendiksen, K. H. & Espedal, M. (1992)** "Onset of slugging in horizontal gas-liquid pipe flow" *Int. J. Multiphase Flow.*, **18**, pp 237-247.

- **Bendiksen, K. H., Malnes, D., Moe, R. & Nuland, S. (1991)** "The dynamic two-fluid model OLGA: theory and application" *Soc. Petr. Engrs. Production Engineering*, **6**, pp 171-180.

- **Bendiksen, K. H., Malnes, D. & Nydal, O. J. (1996)** "On the modelling of slug flow" *Chem. Eng. Comm.*, **141**, pp 71-102.

- **Benjamin, T. B. (1968)** "Gravity currents and related phenomena" *J. Fluid Mech.*, **31**, pp 209-248.

- **Brackbill, Kothe & Zemach (1992)** "A continuum method for modelling surface tension" *J. Comp. Phys.*, **100**, p. 335-357.

- **Brill, J. P., Schmidt, Z., Coberly, W. A., Herring, J. D. & Moore, D. W. (1981)** "Analysis of two-phase tests in large-diameter flow lines in Prudhoe Bay field" *S.P.E.J.*, June 1981, pp 363-378.

- **Brown, R. C., Andreussi, P. & Zanelli, S. (1978)** "The use of wire probes for the measurement of liquid film thickness in annular gas-liquid flows" *Can. J. Chem. Eng.*, **56**, pp 754-757.

- **Burke, N. E. & Kashou, S. F. (1995)** "Slug sizing / slug volume prediction, state of the art review and simulation" *Proc. 27th Offshore Tech. Conf.*, Houston, Texas, 1-4 May, SPE Paper OTC7744

- **Chapman, G., Cleese, J,. Gilliam, T., Idle, E., Jones, T. & Palin, M. (1974)** "Monty Python and the holy grail" *Python (Monty) Pictures Ltd, London, UK.*

- **Cheo, M. (1995)** "Simulation of flow around bends using CFDS-FLOW3D" *Third year undergraduate link project report, Department of Chemical Engineering and Chemical Technology, Imperial College of Science, Technology and Medicine, University of London.*

- **Chisholm, D. (1967)** "A theoretical basis for the Lockhart-Martinelli correlation for two-phase flow" *Int. J. Heat & Mass Transfer*, **10**, p 1767.

- **Chisholm, D. (1972)** "An equation for velocity ratio in two-phase flow" *N.E.L. Report No. 535.*

- **Cook, M. & Behnia, M. (1997)** "Film profiles behind liquid slugs in gas-liquid pipe flow" *A.I.Ch.E.J.*, 43(9), pp 2180-2181.

- **Cook, M. & Behnia, M. (2000)** "Slug length prediction in near horizontal gas liquid intermittent flow" *Chem. Eng. Sci.*, **55**, pp 2009-2018.

- **Davies, S. R. (1992)** "Studies of two-phase intermittent flow in pipelines" *PhD Thesis, University of London.*

- **Dukler, A. E. & Hubbard, M. G. (1975)** "A model for gas-liquid slug flow in horizontal and near-horizontal tubes" *Ind. Eng. Chem. Fundam.*, **14**, pp 337-347.

- **Dukler, A. E., Moalem Maron, D. & Brauner, N. (1985)** "A physical model for predicting the minimum stable slug length" *Chem. Eng. Sci.*, **40**, p 1379-1385.

- **Ejedawe, U. & Hughes, D. (1999)** "Computational fluid dynamics (CFD) prediction of slug flow" *Final year undergraduate research project report, Department of Chemical Engineering and Chemical Technology, Imperial College of Science, Technology and Medicine, University of London.*

- **Fagundes Netto, J. R., Fabre, J. Grenier, P. & Péresson, L. (1998)** "An experimental study of an isolated long bubble in an horizontal liquid flow" *3rd Int. Conf. Multiphase Flow, ICMF'98*, Lyon, France, June 8-12.

- **Fagundes Netto, J. R., Fabre & Péresson, L. (1999a)** "Shape of long bubbles in horizontal slug flow" *Int. J. Multiphase Flow*, **25**, pp 1129-1160.

- **Fagundes Netto, J. R., Fabre, J., Péresson, L. & Duhet-Suchaux, P. (1999b)** "Evolution of the flow structure in a horizontal two-phase slug flow" *Two-Phase Modelling & Experimentation 1999*, Celata, G. P., Di Marco, P. & Shah, R. K. (eds.), Edizoni ETS, Piza.

- **Fairhurst, C. P. & Barrett, N. (1997)** "Oil/Water/Gas transport in undulating pipelines - field observations, experimental data and hydraulic model comparisons" *Proc. SPE Ann. Tech. Conf,* San Antonio, Texas, 5-8 October.

- **Fernandes, R. C., Semiat, R. & Dukler, A. E. (1983)** "Hydrodynamic model for gas-liquid slug flow in vertical tubes" *A.I.Ch.E.J.*, **29**, pp 981-989.

- **Ferziger, J. H. & Perić, M. (1997)** "Computational methods for fluid dynamics" *Springer-Verlag, Berlin.*

- **Ferschneider, G. (1983)** "Écoulements diphasiques gaz-liquide à poches et à bouchons en conduits" *Rev. Inst. Fr. Petr.*, **38**, pp 153-182.

- **Fletcher, C. A. J. (1996)** "Computational techniques for fluid dynamics. Volume 1: fundamental and general techniques" *2nd Edn., Springer-Verlag, Berlin.*

- **Gilchrist, A. & Wong, T. N. (1991)** "Modelling of slug flow accounting for slug growth and acceleration effects" *5th Int. Conf. on Multiphase Production,* Cannes, France, June 19-21.

- **Gomez, L. E., Shoham, O. & Taitel, Y. (2000)** "Prediction of slug liquid holdup: horizontal to upward vertical flow" *Int. J. Multiphase Flow*, **26**, pp 517 - 521

- **Gregory, G. A. & Scott, D. S. (1969)** "Correlation of liquid slug velocity and frequency in horizontal cocurrent gas-liquid slug flow" *A.I.Ch.E.J.*, **15** (6), pp 933-935.

- **Gregory, G. A., Nicholson, M. K. & Aziz, K. (1978)** "Correlation of the liquid volume fraction in the slug for horizontal gas-liquid slug flow" *Int. J. Multiphase Flow,* **4**, pp 33-39.

- **Grenier, P., Fabre, J. & Fagundes Netto, J. R. (1997)** "Slug flow in pipelines: recent advances and future developments" *Proc. 8th Int. Conf. Multiphase Production*, Cannes, France, June 18-20.

- **Hale, C. P. (2000)** "Slug formation, growth and decay in gas-liquid flows" *PhD Thesis, University of London.*

- **Hall, A. R. W. (1992)** "Multiphase flow of oil, water and gas in horizontal pipes" *PhD Thesis, University of London.*

- **Harlow, F. H. & Fromm, J. E. (1965)** "Computer experiments in fluid dynamics" *Scientific American*, **212** (3), p 104.

- **Hetsroni, G. (ed.) (1982)** "Handbook of Multiphase Systems", *Hemisphere Publishing, London.*

- **Hewitt, G. F. (1978)** "Measurement of two-phase flow parameters" *Academic Press, London.*

- Hewitt, G.F. (1997) "Two phase gas-liquid slug flow in the transient & steady states" FED. 224, Proc. ASME.

- **Hewitt, G. F., Shires, G. L., Harrison, P. S. & Parry, S. J. (1997)** "The MIXMETER flowmeter – another step towards routine multiphase flow measurement?" *8th Int. Conf. Multiphase Production,* Cannes, France, 18-20 June, *BHR group, Cranfield, UK.*

- **Heywood, N. I. & Richardson, D. N. (1979)** "Slug flow of air-water mixtures in a horizontal pipe: Determination of liquid holdup by γ-ray absorption" *Chem. Eng. Sci.,* **34**, pp 17-30.

- **Hill, T. J., Fairhurst, C. P. & Nelson, C. J. (1996)** "Multiphase production through hilly terrain pipelines in Cusiana oilfield, Colombia" *Soc. Petr. Engrs. Ann. Tech. Conf. & Exhib.,* Denver, Colorado, October 6-9, SPE 36606, pp 319-334.

- **Hill, T., Fairhurst, C. P. & Sugarman, P. (1998)** "Multiphase flow course - a presentation of design and operational issues concerning multiphase production systems" *Multiphase Production Training Course,* June 24-25, BP Exploration, Dyce, Aberdeenshire.

- **Hirt, C. W. & Nichols, B. D. (1981)** "Volume of fluid (VOF) method for dynamics of free boundaries" *J. Comput. Phys.,* **14**, p. 227.

- **Hope, C. B. (1990)** "The development of a water soluble photochromic dye tracing technique and its application to two-phase flow" *PhD Thesis, University of London.*

- **Hustvedt, E. (1993)** "Determination of slug length distributions by use of the OLGA slug tracking model" *6th Int. Conf. Multiphase Production,* Cannes, France, June 16-18.

- **Issa, R. I. & Tang, I. F. (1990)** "Modelling of vertical gas-liquid slug flow in pipes" *Proc. Symp. on Advances in Gas-Liquid flows,* Dallas, Nov. 1990.

- Issa, R.I. & Woodburn, P.J. (1998) "Numerical prediction of instabilities & slug formation in two-phase flow" *

- **Jones, W. P. & Launder, B. E. (1972)** "The prediction of laminarisation with a two-equation model of turbulence" *Int. J. Heat & Mass Trans.,* **15**, p. 301-319.

* Proc. 3rd Int. Conf. Multiphase Flow, ICMF '98, Lyon, France, 8-12 June

- **Khor, S. H. (1997)** "Three-phase liquid-liquid-gas stratified flow in pipelines", *PhD Thesis, University of London.*

- **Khor, S. H., Mendes-Tatsis, M. A. & Hewitt, G. F. (1997)** "One-dimensional modelling of phase holdups in a three-phase stratified flow" *Int. J. Multiphase Flow*, **23** (5), pp 885-897.

- **King, M. J. S. (1998)** "Experimental and modelling studies of transient slug flow" *PhD Thesis, University of London.*

- **King, M. J. S. (1999)** *Private communication, BP Amoco plc.*

- **King, M. J. S., Hale, C. P., Lawrence, C. J. & Hewitt, G. F. (1997)** "A kinematic model for slug flow accounting for aeration effects" *Multiphase Flow Systems Programme Report, WASP/34, MPS/93, Department of Chemical Engineering and Chemical Technology, Imperial College of Science, Technology and Medicine, University of London.*

- **Kokal, S. L. & Stanislav, J. F. (1989a)** "An experimental study of two-phase flow in slightly inclined pipes - I. Flow patterns" *Chem. Eng. Sci.*, **44**, pp 665-679.

- **Kokal, S. L. & Stanislav, J. F. (1989b)** "An experimental study of two-phase flow in slightly inclined pipes - II. Liquid holdup and pressure drop" *Chem. Eng. Sci.*, **44**, pp 681-693.

- **Kurban, A. P. A. (1997)** "Stratified liquid-liquid flow" *PhD Thesis, University of London.*

- **Lo, S. (1998)** *Private communication, CFX International, AEA Technology plc.*

- **Lockhart, R. W. & Martinelli, R. C. (1949)** "Proposed correlation of data for isothermal, two-phase, two-component flow in pipes", *Chem, Eng. Prog.*, **45**, pp 39-48.

- **Lun, I., Calay, R. K. & Holdo, A. E. (1996)** "Modelling two-phase flows using CFD" *Applied Energy*, **53**, pp 299-314.

- **McAdams, W. H., Woods, W. K. & Heroman, L. C. (1942)** "Vaporisation inside horizontal tubes. II - Benzene-oil mixtures" *Trans. A.S.M.E.*, **64**, p 93-100.

- **Machado, R. T. H. (1997)** "Multiphase flow in venturi: an experimental and theoretical study" *PhD Thesis, University of London.*

- **Manabe, R., Tomiyama, A., Hosokawa, S., Torii, T. & Hasegawa, M. (1999)** "Onset of slugging of a residual stagnant liquid at a V-shaped portion of a pipeline" *Energy Sources Tech. Conf. & Exhib.*, A.S.M.E. paper ETCE99-6664.

- **Mandhane, J. M., Gregory, G. A. & Aziz, K. (1974)** "A flow pattern map for gas-liquid flow in horizontal pipes", *Int. J. Multiphase Flow*, **1**, pp 537-553.

- **Manfield, P. D., Lawrence, C. J. & Hewitt, G. F. (1999)** "Drag reduction with additives in multiphase flow", *Multiphase Sci. & Tech.*, **11**, pp 197-221.

- **Manfield, P. D., Lawrence, C. J. & Hewitt, G. F. (2000)** "Towards a 3-D model of slug flow", *Proc. 1st Academic Users' Conf., CFX International,* Reading, UK, March 15.

- **Mann, C. C. (2000)** "The end of Moore's Law?" *Massachusets Inst. Tech. Rev.,* May/June, *http://www.techreview.com/articles/may00/mann.htm*

- **Manolis, I. G. (1995)** "High pressure gas-liquid slug flow" *PhD Thesis, University of London.*

- **Manolis, I. G., Mendes-Tatsis, M. A. & Hewitt, G. F. (1995a)** "The effect of pressure on slug frequency in two-phase horizontal flow" *2nd International Conference on Multiphase Flow,* Kyoto, Japan, April 3-7.

- **Manolis, I. G., Mendes-Tatsis, M. A. & Hewitt, G. F. (1995b)** "The shedding rate in horizontal and inclined pipes / 'Push-out' experiments" *Multiphase Fluid Systems Programme Report, WASP/14, MPS/60, Department of Chemical Engineering and Chemical Technology, Imperial College of Science, Technology and Medicine, University of London.*

- **Mao, Z. & Dukler, A. E. (1991)** "The motion of Taylor bubbles in vertical tubes. II. Experimental data and simulations for laminar and turbulent flow" *Chem. Eng. Sci.*, **46**, p. 2055-2075.

- **Mareuge, I. (2000)** "Determination of phase distribution in three-phase air-oil-water flow using a three-beam gamma densitometer" *Multiphase Flow Systems Programme Report (in preparation), Department of Chemical Engineering and Chemical Technology, Imperial College of Science, Technology and Medicine, University of London*

- **Microsoft (1995)** "Microsoft Excel/Visual Basic for Windows 95 programmer's guide" *Microsoft Press, U.S.A.*

- **Minami, K. & Shoham, O. (1993)** "Pigging dynamics in two-phase flow pipelines: experiment and modelling" *68th Ann. Tech. Conf. & Exhibition of the Soc. Petr. Engrs.*, Houston, TX, October 3-6, SPE Paper 26568.

- **Moalem Maron, D., Yacoub, N. & Brauner, N. (1982)** "New thoughts on the mechanism of gas-liquid slug flow" *Letters in Heat & Mass Trans.*, **9**, pp 333-342.

- **Moe, R. (1993)** "Transient simulation of 2-3D stratified and intermittent two-phase flows. Part II. Applications" *Int. J. Numer. Methods in Fluids*, **16**, p. 967-983.

- **Moissis, R. & Griffith, P. (1962)** "Entrance effects in slug flow" *J. Heat Transf., Trans. A. S. M. E.*, **84**, pp 29-39.

- **Molyneux, P. D. & Tait, A. R. (1997)** "The measurement and prediction of multiphase flow phenomena in a pipeline dip" *Proc. 8th Int. Conf., Multiphase '97,* pub. BHR group, 18-20 June, Cannes, France, pp 57-73.

- **Moore, G. (1965)** *Cited in http://www.intel.com/intel/museum/25anniv/hof/moore.htm*

- **Nicholson, M. K., Aziz, K. & Gregory, G. A. (1978)** "Intermittent two-phase flow in horizontal pipes: predictive models" *Can. J. Chem. Eng.*, **56**, pp 653-663.

- **Norris, L. (1982)** "Correlation of Prudhoe Bay liquid slug lengths and holdups during 1981 large diameter flowline tests" *Exxon Internal Report, October* (cited in Scott *et al.*, 1986)

- **Nydal, O. J. & Andreussi, P. (1991)** "Gas entrainment in a long liquid slug advancing in a near horizontal pipe" *Int. J. Multiphase Flow,* **17**, 179-189.

- **Nydal, O. J. & Banerjee, S. (1995)** "Object oriented dynamic simulation of slug flow" *2nd Int. Conf. Multiphase Flow*, Kyoto, Japan, April 3-7.

- **Nydal, O. J. & Banerjee, S. (1996)** "Dynamic slug tracking simulations for gas-liquid flow in pipelines" *Chem. Eng. Commun.*, **141**, pp 13-39.

- **Odozi, U. A. (2000) "Three-phase gas/liquid/liquid slug flow"** *PhD Thesis, University of London.*

- **Orell, A. & Rembrand, R. (1986)** "A model for gas-liquid slug flow in a vertical tube" *Ind. Eng. Chem. Fundam.* **25**, pp 196-206.

- **Paglianti, A., Andreussi, P. & Nydal, O. J. (1993)** "The effect of fluid properties and geometry on void distribution in slug flow" *6th Int. Conf. Multiphase Production,* Cannes, France, June 16-18.

- **Pan, L. (1996)** "High pressure three-phase (gas/liquid/liquid) flow" *PhD Thesis, University of London.*

- **Pan, L. & Hewitt, G.F. (1996)** "Precise measurement of cross sectional phase fractions in three-phase flow using a dual-energy gamma densitometer" *American Nuclear Society, Proc. National Heat Trans. Conf.*, Portland, OR, August 5-9.

- **Pan, L., Mendes-Tatsis, M. A. & Hewitt, G. F. (1994)** "Dual-energy gamma-ray densitometer for the measurement of multiphase flow - experiments with two-phase flow" *Multiphase Flow Systems Programme Report, WASP/7, MPS/37, Department of Chemical Engineering and Chemical Technology, Imperial College of Science, Technology and Medicine, University of London.*

- **Patankar, S. V. & Spalding, D. B. (1972)** "A calculation procedure for heat, mass and momentum transfer in three-dimensional parabolic flows" *Int. J. Heat & Mass Transfer,* **15,** p 1787-17xx.

- **Pauchon, C., Dhulesia, H., Lopez, D. & Fabre, J. (1993)** "TACITE: a comprehensive mechanistic model for two-phase flow" *6th Int. Conf. Multiphase Production,* Cannes, France, June 16-18.

- **Pauchon, C., Ferschneider, G. & Ferre, D. (1996)** "Method for modelling multiphase flows in pipelines" *US Patent no. 5550761,* August 27.

- **Petritsch, G. & Mewes, D. (1998)** "Experimental investigation of the flow pattern in a horizontal pipe with a large diameter" *Proc. 3rd Int. Conf. Multiphase Flow,* Lyon, France, June 8-12.

- **Premoli, A., Francesco, D. & Prina, A. (1970)** "An empirical correlation for evaluating two-phase mixture density under adiabatic conditions" *European Two-Phase Flow Group Meeting.*

- **Rhie, C. M. & Chow W. L. (1983)** "Numerical study of the turbulent flow past an airfoil with trailing edge separation" *A.I.A.E.J.*, **21,** pp 1527-1532.

- **Roberts, I. F. (1996)** "Modelling and experimental studies of transient stratified multiphase flows" *PhD Thesis, University of London.*

- **Rothe, P. H. & Crowley, C. J. (1986)** "Insignificant terrain effects in multiphase pipelines" *Creare/AGA Report,* AGA Report Number L51526.

- **Ruder, Z., Hanratty, P. J. & Hanratty, T. J. (1989)** "Necessary conditions for the existence of stable slugs" *Int. J. Multiphase Flow,* **15**, pp 209-226.

- **Schlichting, H. (1969)** "Boundary layer theory" *6th Edition, McGraw-Hill, New York.*

- **Scott, S. L., Shoham, O. & Brill, J. P. (1986)** "Prediction of slug length in horizontal large-diameter pipes" *56th Regional Meeting of Soc. Petr. Engrs.,* Oakland, CA, April 2-4, SPE Paper 15103.

- **Scott, S. L., Shoham, O. & Brill, J. P. (1987)** "Modelling slug growth in large diameter pipes" *3rd Int. Conf. on Multiphase Flow,* den Haag, Netherlands, May 18-20.

- **Shaha, J. (1997)** "Phase interactions in transient stratified flow" *MPhil/PhD Transfer Report, MPS/96, Department of Chemical Engineering & Chemical Technology, Imperial College, University of London, UK.*

- **Shaha, J. (1999)** "Phase interactions in transient stratified flow" *PhD Thesis, University of London.*

- **Srichai, S. (1994)** "High pressure separated two-phase flow" *PhD Thesis, University of London.*

- **Stanislav, J. F., Kokal, S. & Nicholson, M. K. (1986)** "Intermittent gas-liquid flow in upward inclined pipes" *Int. J. Multiphase Flow,* **12**, pp 325-335.

- **Sylvester, N. D. (1987)** "A mechanistic model for two phase vertical slug flow in pipes" *J. Energy Res. Technol.* **109**, pp 206-213.

- **Taitel, Y. & Barnea, D. (1990a)** "A consistent approach for calculating pressure drop in inclined slug flow" *Chem. Eng. Sci.,* **45**, pp 1199-1206.

- **Taitel, Y. & Barnea, D. (1990b)** "Two-phase slug flow" *Adv. Heat Transf.,* **20**, 83-132.

- **Taitel, Y. & Barnea, D. (1998a)** "Effect of gas compressibility on a slug tracking model" *Chem. Eng. Sci.* **53** (11), pp 2089-2097.

- **Taitel, Y. & Barnea, D. (1998b)** "Slug behaviour in top and low elbows" *Proc. 11th Int. Conf. Heat Transf.*, August 23-28, Kyongiu, Korea.

- **Taitel, Y. & Barnea, D. (1999)** "Slug tracking in hilly terrain pipelines" *Soc. Petr. Engrs. Ann. Tech. Conf. & Exhibition,* Houston, Texas, October 3-6, SPE Paper 56521.

- **Taitel, Y. & Dukler, A. E. (1976)** "A model for predicting flow regime transitions in horizontal and near horizontal gas-liquid flow" *A.I.Ch.E.J.*, **22**, pp 47-55.

- **Thompson, J. F., Warsi, Z. U. A. & Mastin, C. W. (1985)** "Numerical grid generation – foundations and applications" *Elsevier, New York.*

- **Thwaites, G. R., Kulov, N. N. & Nedderman, R. M. (1976)** "Liquid film properties in two-phase annular flow." *Chem. Eng. Sci.*, **31**, pp 481-486.

- **Tronconi, E. (1990)** "Prediction of slug frequency in horizontal two-phase flow" *A.I.Ch.E.J.*, **36**, pp 701-709.

- **Ubbink, O. (1997)** "Numerical prediction of two-fluid systems with sharp interfaces" *PhD Thesis, University of London.*

- **Ujang, P. (2000)** "Terrain effects in slug flow" *MPhil/PhD Transfer Report, MPS/1xx, Department of Chemical Engineering & Chemical Technology, Imperial College, University of London, UK.*

- **Van Doormal, J. P. & Raithby, G. D. (1984)** "Enhancements of the SIMPLE method for predicting incompressible fluid flows" *Numer. Heat Transf.*, **7**, pp. 147-163.

- **Wallis, G. B. (1969)** "One-dimensional two-phase flow" *McGraw-Hill, New York.*

- **Wendt, J. F. (ed.) (1996)** "Computational fluid dynamics: an introduction" *2nd Edn., Springer-Verlag, Berlin.*

- **Wood, D. G. (1991)** "Mechanistic modelling of terrain-induced slugs in gas-condensate lines" *5th Int. Conf. Multiphase Production,* June, Cannes, France (Reproduced in "A compendium of publications by the BP group on multiphase flow production technology", 2nd Edn., Mackley, I. G. (ed.) (1992), BP Exploration, UK)

- **Woods, B. D., Hurlburt, E. T. & Hanraty, T. J. (2000)** "Mechanism of slug formation in downwardly inclined pipes" *Int. J. Multiphase Flow*, **26**, pp 977-998.

- **Wong, T. N. & Gilchrist, A. (1993)** "A model for transient analysis of gas-liquid slug flow in pipelines of an offshore well head" *3rd Int. Offshore & Polar Eng. Conf.*, Singapore, June 6-11.

- **Woods, B. D. & Hanratty, T. J. (1996)** "Relation of slug stability to shedding rate" *Int. J. Multiphase Flow*, **22**, pp 809-828.

- **Yang, J., Sarica, C., Chen, X. & Brill, J. P. (1996)** "A study of intermittent flow in downward inclined pipes" *Int. Mech. Eng. Congress & Exposition (I.M.E.C.E.)*, Atlanta, USA, November 17-22.

- **Young, A. D. (1989)** "Boundary Layers" *BSP Professional Books, Oxford.*

- **Zheng, G. H. (1991)** "Two-phase slug flow in hilly terrain pipelines" *PhD Thesis*, University of Tulsa, USA.

- **Zheng, G. H., Brill, J. P. & Shoham, O. U. (1992)** "An experimental study of two-phase slug flow in hilly terrain pipelines" *Soc. Petr. Engrs. 67th Ann. Tech. Conf. & Review*, Washington DC, October 4-7, SPE Paper 24788.

- **Zheng, G. H., Brill, J. P. & Taitel, Y. (1993)** "Slug flow behaviour in a hilly terrain pipeline" *Int. J. Multiphase Flow*, **20**(1), pp 63-79.

- **Zuber, N. & Findlay, J. A. (1965)** "Average volumetric concentration in two-phase flow systems" *J. Heat Transf.*, **87**, pp 453-46.

Appendix 1: Formulae for statistical error calculation

Throughout the present work, the relative error, E, between an experimental measurement and the value predicted using a model or correlation is given by

$$E = \frac{P - M}{M} \qquad [A1.1]$$

where P and M are the predicted and measured values, respectively.

The mean, or average, error, $\overline{E}$ is given by

$$\overline{E} = \frac{\sum_{i=1}^{N} E_i}{N} \qquad [A1.2]$$

where N is the number of data points in the sample.

The standard deviation, σ, is obtained from

$$\sigma = \sqrt{\frac{\sum_{i=1}^{N} (E_i - \overline{E})^2}{(N-1)}} \qquad [A1.3]$$

The root mean square error, E_{rms} is defined as

$$E_{rms} = \sqrt{\frac{\sum_{i=1}^{N} E_i^{\,2}}{N}} \qquad [A1.4]$$

which is equivalent to

$$E_{rms} = \sqrt{\overline{E}^2 + \frac{\sigma^2 (N-1)}{N}} \qquad [A1.5]$$

Appendix 2: Matrix of experimental runs

A2.1. Campaign 1: -1.5° downflow

Campaign 1: -1.5° downflow					
Run	U_{sG} / m/s	U_{sL} / m/s	Exit pressure / bar(a)	Pressure gradient / (Pa/m)	Flow Pattern at end of test-section
mtd1002	4.50	0.40	1.07	-43.4	Str.Sm.
mtd1003	5.92	0.40	1.09	230.6	Slug
mtd1004	5.88	0.40	1.05	64.8	Str.Wa.
mtd1005	8.09	0.38	1.12	333.6	Slug
mtd1006	10.18	0.36	1.14	346.0	Slug
mtd1007	12.08	0.38	1.18	504.5	Slug
mtd1008	4.26	0.61	1.11	260.0	Slug
mtd1010	5.86	0.60	1.14	330.1	Slug
mtd1011	7.99	0.57	1.20	526.2	Slug
mtd1012	10.05	0.57	1.24	665.3	Slug
mtd1014	12.19	0.59	1.48	1643.6	Slug
mtd1015	4.65	0.58	1.09	243.4	Slug
mtd1016	4.80	0.41	1.04	-54.4	Str.Sm.
mtd1017	6.36	0.40	1.02	2.3	Slug
mtd1018	7.79	0.43	1.12	320.5	Slug
mtd1019	10.54	0.38	1.16	319.9	Slug
mtd1020	12.57	0.38	1.17	510.0	Slug
mtd1021	4.39	0.71	1.14	384.6	Slug
mtd1022	5.87	0.80	1.20	552.5	Slug
mtd1024	7.47	0.78	1.26	1032.3	Slug
mtd1025	10.06	0.79	1.36	1484.5	Slug
mtd1026	11.67	0.75	1.38	1351.1	Slug
mtd1027	4.27	0.98	1.19	656.1	Slug
mtd1028	5.87	0.90	1.23	801.1	Slug
mtd1031	8.13	0.99	1.34	1268.3	Slug
mtd1032	10.04	0.99	1.43	1777.8	Slug
mtd1034	11.58	0.98	1.48	1984.2	Slug
mtd1035	10.11	0.79	1.35	1679.8	Slug
mtd1038	3.65	0.30	1.04	4.6	Str.Sm.
mtd1039	1.82	0.30	1.05	5.0	Str.Sm.
mtd1040	5.75	0.29	1.05	3.1	Str.Sm.
mtd1041	7.27	0.29	1.05	6.2	Str.Wa.
mtd1042	8.76	0.28	1.07	427.2	Str.Wa./Slug
mtd1043	10.18	0.29	1.09	434.1	Str.Wa./Slug
mtd1045	10.12	0.27	1.10	278.1	Str.Wa./Slug
mtd1046	11.59	0.29	1.11	365.0	Str.Wa./Slug
mtd1047	12.21	0.29	1.11	449.9	Str.Wa./Slug
mtd1048	13.74	0.29	1.14	512.5	Str.Wa./Slug
mtd1049	15.14	0.28	1.15	569.4	Slug/Ann.
mtd1051	1.70	0.21	1.04	-128.7	Str.Sm.
mtd1052	3.60	0.21	1.05	-113.1	Str.Sm.
mtd1053	5.48	0.20	1.04	-86.0	Str.Sm.

Campaign 1: -1.5° downflow					
Run	U_{sG} / m/s	U_{sL} / m/s	Exit pressure / bar(a)	Pressure gradient / (Pa/m)	Flow Pattern at end of test-section
mtd1054	7.05	0.19	1.05	-55.1	Str.Sm.
mtd1055	8.47	0.19	1.05	-11.7	Str.Sm.
mtd1056	9.89	0.20	1.06	66.5	Str.Wa.
mtd1057	11.33	0.20	1.06	130.9	Str.Wa.
mtd1058	13.45	0.19	1.08	167.7	Str.Wa.
mtd1059	14.59	0.20	1.10	259.2	Str.Wa.
mtd1060	16.03	0.20	1.11	438.5	Str.Wa./Ann.
mtd1061	1.50	0.10	1.03	25.3	Str.Sm.
mtd1062	3.38	0.09	1.03	34.6	Str.Sm.
mtd1063	5.22	0.11	1.04	43.6	Str.Sm.
mtd1065	6.93	0.10	1.04	-37.9	Str.Sm.
mtd1066	10.02	0.09	1.05	9.6	Str.Wa.
mtd1067	8.29	0.11	1.04	-16.3	Str.Sm.
mtd1068	12.15	0.10	1.06	93.5	Str.Wa.
mtd1069	13.31	0.11	1.07	154.1	Str.Wa.
mtd1070	14.66	0.10	1.07	204.8	Str.Wa.
mtd1071	16.02	0.10	1.08	253.3	Str.Wa.
mtd1101	1.05	0.09	5.68	439.0	Str.Sm.
mtd1102	1.91	0.10	5.52	450.5	Str.Sm.
mtd1103	2.98	0.10	5.58	471.0	Str.Sm.
mtd1104	3.96	0.10	5.46	401.0	Str.Sm.
mtd1105	4.97	0.12	5.34	445.8	Str.Wa.
mtd1106	5.94	0.11	5.18	493.3	Str.Wa.
mtd1107	1.00	0.20	5.77	377.2	Str.Sm.
mtd1108	2.03	0.19	5.73	358.8	Str.Sm.
mtd1109	3.04	0.19	5.62	418.7	Str.Wa.
mtd1110	3.95	0.20	5.60	456.2	Str.Wa.
mtd1111	4.97	0.20	5.40	503.0	Str.Wa.
mtd1113	5.88	0.19	5.15	119.2	Str.Wa.
mtd1114	1.00	0.29	5.85	395.6	Str.Sm.
mtd1115	5.99	0.30	5.16	440.7	Str.Wa./Slug
mtd1116	4.92	0.29	5.39	432.5	Str.Wa.
mtd1117	3.95	0.30	5.51	388.7	Str.Wa.
mtd1118	2.95	0.30	5.57	358.9	Str.Sm.
mtd1119	2.07	0.30	5.70	506.9	Str.Sm.
mtd1140	6.00	0.39	5.09	776.0	Str.Wa./Slug
mtd1141	4.95	0.40	5.29	499.8	Str.Wa./Slug
mtd1142	4.09	0.41	5.44	456.4	Str.Wa.
mtd1143	2.99	0.39	5.56	330.8	Str.Sm.
mtd1145	2.01	0.37	5.61	74.1	Str.Sm.
mtd1146	1.00	0.40	5.69	168.4	Str.Sm.
mtd1147	1.07	0.59	5.81	205.4	Str.Sm.
mtd1148	2.08	0.59	5.62	226.0	Str.Wa.
mtd1149	3.01	0.60	5.59	361.1	Slug
mtd1150	3.96	0.59	5.51	443.9	Slug
mtd1151	4.92	0.60	5.38	583.0	Slug
mtd1152	6.05	0.59	5.17	697.1	Slug
mtd1192	1.09	0.79	5.80	279.8	Str.Sm.
mtd1193	1.99	0.80	5.67	579.3	Slug
mtd1194	3.09	0.80	5.38	829.9	Slug
mtd1195	3.97	0.78	5.45	610.0	Slug

Campaign 1: -1.5° downflow					
Run	U_{sG} / m/s	U_{sL} / m/s	Exit pressure / bar(a)	Pressure gradient / (Pa/m)	Flow Pattern at end of test-section
mtd1196	4 97	0.79	5.31	1090.6	Slug
mtd1198	5 99	0.79	5.20	894.0	Slug
mtd1199	1.06	1.00	5.71	232.4	Slug
mtd1201	2.12	0.99	5.63	666 6	Slug
mtd1202	3 20	0 99	5.43	807.4	Slug
mtd1203	4 05	1.01	5.38	957.9	Slug
mtd1206	6 03	0.99	5.22	1283.1	Slug
mtd1207	5 01	1.02	5.38	1101.5	Slug
mtd1293	2.01	0.49	1.02	88.8	Str.Sm.
mtd1294	4.18	0.50	1.09	612.0	Slug
mtd1295	5.70	0.40	1.12	540.6	Slug
mtd1304	5.76	0.50	1.15	666.9	Slug
mtd1305	7.94	0.50	1.20	1053.7	Slug
mtd1306	9.94	0.50	1.26	1363.8	Slug
mtd1308	11.92	0.50	1.32	1264.0	Slug
mtd1309	13.79	0.50	1.35	1708.6	Slug
mtd1336	17.64	0.18	1.19	795.0	Str.Wa./Ann.
mtd1337	19.92	0.20	1.23	992.4	Str.Wa./Ann.
mtd1338	23.64	0.18	1.28	1289.4	Str.Wa./Ann.
mtd1339	27.34	0.20	1.36	1714.8	Ann.
mtd1340	31.91	0.19	1.45	1931.3	Ann.
mtd1343	18.45	0.28	1.27	1255.1	Slug/Ann.
mtd1344	20.31	0.28	1.30	1516.5	Str.Wa./Ann.
mtd1345	23.64	0.30	1.37	1889.0	Ann.
mtd1346	17.86	0.41	1.38	1799.6	Slug
mtd1347	20.13	0.41	1.42	2020.0	Slug/Ann.
mtd1348	24.79	0.38	1.45	2290.3	Ann.
mtd1350	17.62	0.51	1.43	2075.4	Slug
mtd1351	19.76	0.49	1.47	2291.6	Slug
mtd1353	23.07	0.51	1.55	2323.7	Slug/Ann.
mtd1354	17.72	0.60	1.52	2056.9	Slug
mtd1356	20.24	0.59	1.57	2060.4	Slug
mtd1359	24.05	0.59	1.69	2834.7	Slug/Ann.
mtd1360	18.01	0.79	1.70	2717.7	Slug
mtd1362	20.70	0 82	1.80	2994.4	Slug/Ann.
mtd1363	18.17	1.00	1.85	3162.0	Slug/Ann.
mtd1365	7.39	0.20	5.62	780.2	Str.Wa.
mtd1366	7.41	0.30	5.64	941.5	Str.Wa./Slug
mtd1367	7.43	0.40	5.60	1021.4	Slug
mtd1368	7.39	0.52	5.63	1138.9	Slug
mtd1370	7.39	0.80	5.67	1788.5	Slug
mtd1371	7.39	0.63	5.61	1440.5	Slug
mtd1374	8 81	0.19	5.52	815.4	Str.Wa.
mtd1375	8.48	0.41	5.50	1206.5	Slug
mtd1376	8.81	0.61	5.54	1627.9	Slug
mtd1378	8.85	0.79	5.63	1775.9	Slug
pdm1002	1.46	0.02	1.03	-73.7	Str.Sm.
pdm1003	3.34	0.02	1.04	-74.0	Str.Sm.
pdm1004	5.41	0.02	1.04	-74.3	Str.Sm.
pdm1005	6.91	0.02	1.04	-80.8	Str.Sm.
pdm1006	8.42	0.02	1.04	-84.3	Str.Sm.

Campaign 1: -1.5° downflow					
Run	U_{sG} / m/s	U_{sL} / m/s	Exit pressure / bar(a)	Pressure gradient / (Pa/m)	Flow Pattern at end of test-section
pdm1007	9.86	0.02	1.04	-79.8	Str Sm.
pdm1008	11.31	0.02	1.03	-60.5	Str.Wa.
pdm1009	13.51	0.02	1.05	-32.7	Str.Wa.
pdm1010	14.84	0 02	1.05	-15.6	Str.Wa.
pdm1011	16.31	0.02	1.06	3.6	Str.Wa.

A2.2. Campaign 2: ∓1.5° "V"-section

Campaign 2. ∓ 1.5° "V"-section						
Run	U_{sG} / m/s	U_{sL} / m/s	Exit pressure / bar(a)	dP/dz/ (Pa/m)	Flow Pattern (35m)	Reverse flow?
pdm2006	10.32	0.05	1.08	181.5	Str.Wa.	n
pdm2007	10.17	0.05	1.08	195.4	Str.Wa.	n
pdm2008	10.28	0.08	1.07	257.5	Str.Wa.	n
pdm2009	10.03	0.10	1.08	257.7	Str.Wa./Slug	n
pdm2010	9.98	0.14	1.08	316.0	Str.Wa./Slug	n
pdm2011	9.80	0.17	1.09	405.4	Slug	n
pdm2012	9.55	0.20	1.11	410.7	Slug	n
pdm2013	9.46	0.23	1.12	472.9	Slug	n
pdm2014	9.92	0.27	1.13	557.7	Slug	n
pdm2015	9.74	0.29	1.14	587.7	Slug	n
pdm2016	10.20	0.36	1.18	682.9	Slug	n
pdm2018	10.11	0.39	1.18	622.2	Slug	n
pdm2019	9.96	0.46	1.22	869.4	Slug	n
pdm2020	12.95	0.05	1.07	-54.4	Str.Wa.	n
pdm2021	12.75	0.08	1.07	-14.9	Str.Wa.	n
pdm2022	12.72	0.12	1.09	62.4	Str.Wa.	n
pdm2023	12.63	0.16	1.09	193.0	Str.Wa./Slug	n
pdm2024	13.08	0.21	1.12	314.3	Str.Wa./Slug	n
pdm2025	12.85	0.25	1.14	443.3	Str.Wa./Slug	n
pdm2026	12.74	0.30	1.16	505.8	Slug	n
pdm2027	13.11	0.38	1.22	780.9	Slug	n
pdm2028	13.01	0.43	1.24	1034.7	Slug	n
pdm2029	12.88	0.52	1.30	1450.2	Slug	n
pdm2032	15.99	0.05	1.07	40.4	Str.Sm.	n
pdm2033	15.76	0.08	1.07	95.1	Str.Wa.	n
pdm2034	15.50	0.11	1.08	153.5	Str.Wa.	n
pdm2035	16.03	0.15	1.10	262.4	Str.Wa.	n
pdm2036	15.76	0.19	1.12	394.0	Str.Wa./Slug	n
pdm2037	16.06	0.22	1.14	531.7	Str.Wa./Slug	n
pdm2038	15.89	0.27	1.16	849.8	Slug	n
pdm2039	16.05	0 30	1.16	732 6	Slug	n
pdm2040	15.73	0.35	1.22	987.5	Slug	n
pdm2041	15.92	0.40	1.25	1291.9	Slug	n
pdm2042	15.59	0.45	1.29	1420.7	Slug	n
pdm2044	16.07	0.51	1.34	1653 9	Slug	n
pdm2046	19.16	0.06	1.11	98.0	Str.Wa.	n

Campaign 2: ∓ 1.5° "V"-section						
Run	U_{sG} / m/s	U_{sL} / m/s	Exit pressure / bar(a)	dP/dz/ (Pa/m)	Flow Pattern (35m)	Reverse flow?
pdm2047	19 58	0.08	1.11	151.1	Str.Wa.	n
pdm2048	19.18	0.12	1.13	244 0	Str Wa.	n
pdm2049	19 63	0.16	1.15	401.3	Str Wa.	n
pdm2050	19.25	0.20	1.16	527.4	Str.Wa./Slug	n
pdm2051	18.81	0.23	1.18	608.5	Str.Wa./Slug	n
pdm2052	19.12	0.28	1.23	835.4	Slug	n
pdm2053	19 30	0.34	1.26	1036.7	Slug	n
pdm2054	19 63	0.39	1.29	1328.7	Slug	n
pdm2055	19 27	0.44	1.34	1527.8	Slug	n
pdm2058	22.59	0.05	1.03	531.9	Str.Wa.	n
pdm2059	22.81	0.09	1.06	634.5	Str.Wa.	n
pdm2060	23.20	0.15	1.10	820.3	Str.Wa.	n
pdm2061	23.29	0.18	1.13	944.5	Str.Wa./Ann.	n
pdm2062	22.03	0.27	1.20	1143.2	Str.Wa./Ann.	n
pdm2063	22.30	0.32	1.28	1452.8	Str.Wa./Ann.	n
pdm2064	22.39	0.37	1.32	1726.4	Slug/Ann.	n
pdm2065	23.35	0.42	1.37	1950.3	Slug/Ann.	n
pdm2066	22.68	0.52	1.46	2398.5	Slug/Ann.	n
pdm2068	9.98	0.51	1.21	653.5	Slug	n
pdm2069	9.82	0.57	1.24	996.3	Slug	n
pdm2070	9.79	0.62	1.27	1065.7	Slug	n
pdm2071	10.36	0.69	1.32	1385.8	Slug	n
pdm2073	15.70	0.56	1.37	1593.3	Slug	n
pdm2074	15.34	0.59	1.38	1721.2	Slug	n
pdm2075	18.73	0.52	1.39	1870.3	Slug	n
pdm2078	3.75	0.05	1.06	1.7	Slug	y
pdm2079	3.87	0.07	0.06	547.7	Slug	y
pdm2080	3.93	0.09	0.08	547.6	Slug	y
pdm2081	3.93	0.10	0.10	547.6	Slug	y
pdm2082	3.93	0.12	0.11	547.7	Slug	y
pdm2083	3.93	0.13	0.13	547.7	Slug	y
pdm2084	3.93	0.14	1.07	178.6	Slug	y
pdm2085	3.93	0.16	1.07	266.2	Slug	y
pdm2086	3.93	0.17	1.06	330.4	Slug	y
pdm2087	3.99	0.19	1.08	198.6	Slug	y
pdm2088	3.97	0.21	1.07	313.7	Slug	y
pdm2089	3.94	0.24	1.07	372.9	Slug	y
pdm2090	3.94	0.26	1.09	331.1	Slug	y
pdm2091	3.92	0.28	1.08	369.2	Slug	y
pdm2093	3.82	0.30	1.08	435 8	Slug	y
pdm2094	3.85	0.35	1.09	477.3	Slug	y
pdm2095	3.68	0.36	1.09	432.1	Slug	y
pdm2096	3.74	0.41	1 09	524.5	Slug	y
pdm2097	3.69	0.46	1.10	569.6	Slug	y
pdm2098	5.35	0.04	1.05	207.3	Slug	y
pdm2099	5.38	0.06	1.05	155.9	Slug	y
pdm2100	5.37	0.07	1.06	172.3	Slug	y
pdm2101	5.35	0.09	1.06	188.9	Slug	y
pdm2102	5.31	0.10	1.06	183.7	Slug	y
pdm2105	5.43	0.11	1.06	22.5	Slug	y
pdm2106	5.45	0.12	1.04	25.5	Slug	y

Campaign 2: ∓ 1.5° "V"-section						
Run	U_{sG} / m/s	U_{sL} / m/s	Exit pressure / bar(a)	dP/dz/ (Pa/m)	Flow Pattern (35m)	Reverse flow?
pdm2107	5.40	0.13	1.05	38.5	Slug	y
pdm2108	5.30	0.17	1.06	51.6	Slug	y
pdm2109	5.23	0.19	1.06	73.6	Slug	y
pdm2110	5.22	0.19	1.06	102.5	Slug	y
pdm2111	5.21	0.22	1.07	115.4	Slug	y
pdm2112	5.17	0.24	1.07	169.8	Slug	y
pdm2113	5.13	0.26	1.08	246.3	Slug	y
pdm2114	5.14	0.28	1.09	246.3	Slug	y
pdm2115	5.12	0.30	1.09	239.7	Slug	y
pdm2116	5.10	0.33	1.08	277.9	Slug	y
pdm2117	5.09	0.35	1.09	298.9	Slug	y
pdm2119	5.25	0.39	1.09	408.8	Slug	y
pdm2120	5.10	0.40	1.10	497.4	Slug	n
pdm2121	6.53	0.03	1.04	63.7	Str.Wa.	y
pdm2122	6.52	0.06	1.05	73.2	Str.Wa.	y
pdm2123	6.45	0.07	1.04	98.5	Str.Wa./Slug	y
pdm2124	6.43	0.09	1.06	121.9	Slug	y
pdm2125	6.49	0.11	1.06	146.9	Slug	y
pdm2126	6.46	0.13	1.07	146.9	Slug	y
pdm2127	6.42	0.15	1.07	212.2	Slug	y
pdm2128	6.45	0.16	1.08	202.0	Slug	y
pdm2129	6.35	0.20	1.08	263.2	Slug	y
pdm2130	6.34	0.22	1.07	375.0	Slug	y
pdm2131	6.26	0.23	1.08	439.9	Slug	y
pdm2132	6.29	0.27	1.09	432.4	Slug	y
pdm2134	6.32	0.30	1.10	492.3	Slug	y
pdm2135	6.25	0.34	1.11	583.9	Slug	y
pdm2136	6.22	0.43	1.14	579.9	Slug	y
pdm2137	6.18	0.52	1.15	698.7	Slug	n
pdm2138	7.58	0.02	1.05	69.9	Str.Wa.	y
pdm2139	7.62	0.04	1.05	42.2	Str.Wa.	y
pdm2140	7.60	0.05	1.05	69.7	Str.Wa.	y
pdm2141	7.63	0.07	1.06	62.5	Str.Wa.	y
pdm2142	7.56	0.08	1.06	81.5	Str.Wa.	y
pdm2143	7.56	0.10	1.06	100.6	Str.Wa.	y
pdm2144	7.55	0.12	1.05	147.4	Str.Wa.	y
pdm2147	7.98	0.13	1.05	-77.2	Slug	y
pdm2148	7.85	0.15	1.05	-52.0	Slug	y
pdm2149	7.85	0.18	1.07	5.0	Slug	y
pdm2150	7.83	0.20	1.08	59.1	Slug	y
pdm2151	7.58	0.24	1.08	189.0	Slug	y
pdm2152	7.55	0.30	1.09	293.3	Slug	y
pdm2153	7.59	0.36	1.12	465.9	Slug	y
pdm2154	8.89	0.02	1.05	113.0	Str.Wa.	n
pdm2155	8.81	0.04	1.05	122.4	Str.Wa.	n
pdm2156	8.81	0.05	1.06	130.7	Str.Wa.	n
pdm2157	8.85	0.07	1.04	134.8	Str.Wa.	n
pdm2159	8.72	0.10	1.05	222.5	Slug	n
pdm2160	8.69	0.12	1.05	197.3	Slug	n
pdm2161	8.76	0.14	1.05	159.4	Slug	n
pdm2162	8.54	0.16	1.05	205.1	Slug	n

Campaign 2: ∓ 1.5° "V"-section						
Run	U_{sG} / m/s	U_{sL} / m/s	Exit pressure / bar(a)	dP/dz/ (Pa/m)	Flow Pattern (35m)	Reverse flow?
pdm2164	8 76	0.18	1.06	186 1	Slug	n
pdm2165	8 65	0.21	1.07	179 9	Slug	n
pdm2166	8.69	0.26	1.09	293.8	Slug	n
pdm2167	9.17	0.29	1.10	518.0	Slug	n
pdm2168	9.09	0.31	1.11	515.1	Slug	n
pdm2169	9.09	0.32	1.13	679 8	Slug	n
pdm2170	9.07	0.37	1.14	639.8	Slug	n
pdm2171	8 91	0.42	1.16	754.4	Slug	n
pdm2173	8 93	0.52	1.19	843.9	Slug	n
pdm2174	11.83	0.02	1.03	60.6	Str.Wa.	n
pdm2175	11.69	0.04	1.05	78.6	Str.Wa.	n
pdm2176	11.64	0.05	1.03	98.2	Str.Wa.	n
pdm2177	11.55	0.07	1.04	120.4	Str.Wa.	n
pdm2178	11.47	0.09	1.04	160.2	Str.Wa.	n
pdm2179	11.39	0.10	1.04	182.0	Str.Wa./Slug	n
pdm2182	12.44	0.12	1.07	82.5	Str.Wa./Slug	n
pdm2183	12.27	0.14	1.07	138.9	Slug	n
pdm2184	12.23	0.16	1.07	217.1	Slug	n
pdm2185	12.16	0.17	1.07	255.3	Slug	n
pdm2186	12.13	0.19	1.08	309.2	Slug	n
pdm2187	11.99	0.24	1.09	475.0	Slug	n
pdm2188	11.78	0.26	1.10	683.6	Slug	n
pdm2189	11.70	0.28	1.11	635.7	Slug	n
pdm2190	11.60	0.30	1.11	763.1	Slug	n
pdm2191	11.53	0.33	1.13	793.9	Slug	n
pdm2194	11.54	0.32	1.14	706.9	Slug	n
pdm2195	11.43	0.39	1.16	1068.6	Slug	n
pdm2196	11.23	0.47	1.21	1247.4	Slug	n
pdm2197	11.15	0.55	1.24	1349.3	Slug	n
pdm2199	4.36	0.53	1.09	775.1	E.B.F.	y
pdm2201	4.51	0.51	1.09	617.1	E.B.F.	y
pdm2202	4.49	0.62	1.14	920.7	E.B.F.	y
pdm2203	4.52	0.71	1.15	925.0	E.B.F.	y
pdm2204	5.89	0.51	1.14	848.0	E.B F.	n
pdm2207	5.38	0.62	1.16	1048.4	E.B.F.	y
pdm2208	5.40	0.71	1.18	1061.6	E.B.F.	n
pdm2209	6.86	0.60	1.18	1182.5	Slug	y
pdm2211	6.92	0.70	1.19	1455.8	Slug	n
pdm2212	7.83	0.40	1.11	890.1	Slug	y
pdm2213	7.78	0.50	1.15	1057.9	Slug	y
pdm2214	7.62	0.61	1.18	1295.8	Slug	n
pdm2216	7.57	0.72	1.20	1466.9	E.B.F.	n
pdm2217	9.03	0.60	1.21	1277.7	Slug	n
pdm2218	8.88	0.70	1.24	1600.5	Slug	n
pdm2219	11.51	0.71	1.31	1743.6	Slug	n
pdm2408	1.29	0.06	1.04	99.1	Str.Wa./Slug	y
pdm2409	1.30	0.08	1.05	53.0	Str.Wa./Slug	y
pdm2410	1.30	0.10	1.06	11.9	Str.Wa./Slug	y
pdm2411	1.29	0.12	1.05	20.9	Slug	y
pdm2412	1.29	0.14	1.06	44.9	Slug	y
pdm2413	1.27	0.17	1.06	90.5	Slug	y

Campaign 2: ∓ 1.5° "V"-section						
Run	U_{sG} / m/s	U_{sL} / m/s	Exit pressure / bar(a)	dP/dz/ (Pa/m)	Flow Pattern (35m)	Reverse flow?
pdm2414	1.27	0.19	1.06	94.0	Slug	y
pdm2415	1.27	0.21	1.05	120.8	Slug	y
pdm2416	1.28	0.23	1.06	171.3	Slug	y
pdm2417	1.28	0.26	1.07	211.7	Slug	y
pdm2419	1.33	0.26	1.06	125.2	Slug	y
pdm2420	1.33	0.29	1.07	114.0	Slug	y
pdm2421	1.31	0.33	1.07	172.5	Slug	y
pdm2422	1.31	0.37	1.07	180.4	Slug	y
pdm2423	1.31	0.41	1.07	205.6	Slug	y
pdm2424	1.31	0.45	1.07	248.3	Slug	y
pdm2425	1.33	0.49	1.08	313.5	Slug	y
pdm2430	1.33	0.71	1.11	390.4	Slug	n
pdm2431	1.61	0.03	1.07	2.3	Str.Wa./Slug	y
pdm2432	1.63	0.05	1.06	6.8	Str.Wa./Slug	y
pdm2433	1.62	0.09	1.06	5.5	Slug	y
pdm2434	1.63	0.11	1.07	12.7	Slug	y
pdm2435	1.63	0.13	1.07	31.6	Slug	y
pdm2436	1.64	0.15	1.08	39.8	Slug	y
pdm2437	1.64	0.17	1.08	42.5	Slug	y
pdm2438	1.65	0.19	1.08	53.6	Slug	y
pdm2439	1.64	0.22	1.08	70.2	Slug	y
pdm2440	1.67	0.24	1.08	84.4	Slug	y
pdm2441	1.68	0.28	1.07	102.3	Slug	y
pdm2442	1.67	0.29	1.09	105.2	Slug	y
pdm2443	1.64	0.32	1.09	144.8	Slug	y
pdm2444	1.65	0.35	1.09	150.5	Slug	y
pdm2445	1.67	0.40	1.09	176.9	Slug	y
pdm2446	1.67	0.44	1.10	139.0	Slug	y
pdm2447	1.67	0.52	1.10	203.6	Slug	n
pdm2449	1.65	0.61	1.10	231.0	Slug	n
pdm2450	1.65	0.70	1.09	310.9	Slug	n
pdm2451	2.14	0.04	1.05	-31.1	Str.Wa./Slug	y
pdm2452	2.12	0.06	1.06	-25.4	Str.Wa./Slug	y
pdm2453	2.12	0.08	1.05	-11.9	Slug	y
pdm2454	2.08	0.10	1.06	-7.5	Slug	y
pdm2455	2.14	0.12	1.06	29.5	Slug	y
pdm2456	2.15	0.15	1.07	72.9	Slug	y
pdm2457	2.15	0.17	1.06	69.8	Slug	y
pdm2458	2.16	0.21	1.07	87.7	Slug	y
pdm2459	2.17	0.24	1.09	136.8	Slug	y
pdm2460	2.17	0.27	1.08	113.9	Slug	y
pdm2461	2.06	0.30	1.07	105.0	Slug	y
pdm2462	2.09	0 36	1.08	190.6	Slug	y
pdm2463	2.10	0.40	1.08	150.3	Slug	y
pdm2464	2.10	0.45	1.09	332.7	Slug	y
pdm2465	2.12	0 51	1.10	336.7	Slug	y
pdm2466	2.11	0.60	1.10	415.8	Slug	n
pdm2467	2.10	0 72	1.12	512.9	Slug	n
pdm2470	2.93	0.02	1.06	4.8	Str.Wa.	y
pdm2471	2.95	0.04	1.06	23.6	Str.Wa.	y
pdm2472	2.94	0.05	1.07	14.8	Str.Wa./Slug	y

Campaign 2: ∓ 1.5° "V"-section						
Run	U_{sG} / m/s	U_{sL} / m/s	Exit pressure / bar(a)	dP/dz/ (Pa/m)	Flow Pattern (35m)	Reverse flow?
pdm2473	2.93	0 07	1.07	40.9	Slug	y
pdm2474	2.93	0.10	1.07	70.6	Slug	y
pdm2475	2 87	0 14	1.07	103.9	Slug	y
pdm2476	2.88	0.18	1.08	211.7	Slug	y
pdm2477	2.87	0.22	1.07	158.5	Slug	y
pdm2478	2.86	0.27	1.08	256.6	Slug	y
pdm2479	2.85	0.29	1.08	295.2	Slug	y
pdm2480	2.82	0.31	1.08	238.0	Slug	y
pdm2481	2.82	0.36	1.09	322.9	Slug	y
pdm2482	2.84	0.42	1.10	492.2	Slug	y
pdm2484	2.88	0.47	1.09	458.0	Slug	n
pdm2485	2.91	0.51	1.10	471.9	Slug	n
pdm2486	2.90	0.61	1.12	451.8	Slug	n
pdm2487	2.83	0.72	1.13	738.2	Slug	n
pdm2220	0.62	0.03	5.96	330.5	Str.Wa.	y
pdm2221	0.61	0.04	6.00	366.2	Str.Wa.	y
pdm2222	0.61	0.06	6.02	323.4	Str.Wa./Slug	y
pdm2223	0.60	0.07	6.04	334.0	Str.Wa./Slug	y
pdm2224	0.60	0.08	6.06	324.0	Slug	y
pdm2225	0.60	0.09	6.04	335.0	Slug	y
pdm2226	0.59	0.10	6.07	363.6	Slug	y
pdm2227	0.62	0.12	6.06	145.5	Slug	y
pdm2228	0.62	0.13	6.07	152.3	Slug	y
pdm2229	0.62	0.14	6.05	136.5	Slug	y
pdm2232	0.65	0.15	6.08	508.7	Slug	y
pdm2233	0.70	0.17	6.05	501.5	Slug	y
pdm2234	0.69	0.21	6.08	484.9	Slug	y
pdm2235	0.70	0.23	6.04	469.9	Slug	y
pdm2236	0.69	0.24	6.04	485.8	Slug	y
pdm2237	0.69	0.28	6.04	506.4	Slug	y
pdm2238	0.68	0.32	6.08	491.9	Slug	y
pdm2239	0.68	0.35	6.07	519.7	Slug	y
pdm2241	0.66	0.42	6.15	352.3	Slug	y
pdm2242	0.67	0.47	6.16	471.8	Slug	y
pdm2243	0.65	0.50	6.15	767.6	Slug	n
pdm2244	0.65	0.60	6.13	747.1	Slug	n
pdm2245	0.65	0.71	6.12	802.6	Slug	n
pdm2247	1.04	0.03	6.08	-14.2	Str.Wa.	y
pdm2248	1.04	0.04	6.06	-82.0	Str.Wa.	y
pdm2249	1.04	0.06	6.06	-104.6	Str.Wa.	y
pdm2250	1.04	0.07	6.08	-81.3	Str.Wa./Slug	y
pdm2251	1.04	0.08	6.06	-46.0	Slug	y
pdm2252	1.00	0.09	6.12	338.8	Slug	y
pdm2253	1.01	0.11	6.09	425.6	Slug	y
pdm2254	1.00	0.12	6.11	475.5	Slug	y
pdm2255	1.00	0.13	6.10	479.2	Slug	y
pdm2256	0.99	0.15	6.11	464.7	Slug	y
pdm2257	1.00	0.16	6.10	448.5	Slug	y
pdm2258	1.00	0.19	6.11	400.2	Slug	y
pdm2258	1.00	0.19	6.11	400.2	Slug	y
pdm2260	0.99	0.24	6.10	406.1	Slug	y

Campaign 2: ∓ 1.5° "V"-section						
Run	U_{sG} / m/s	U_{sL} / m/s	Exit pressure / bar(a)	dP/dz/ (Pa/m)	Flow Pattern (35m)	Reverse flow?
pdm2263	1.05	0.27	6.08	626.0	Slug	y
pdm2264	1.05	0.29	6.05	603.2	Slug	y
pdm2265	1.04	0.36	6.09	582.5	Slug	y
pdm2266	1.02	0.42	6.17	616.9	Slug	y
pdm2267	1.03	0.50	6.10	672.8	Slug	n
pdm2268	1.02	0.62	6.13	773.9	Slug	n
pdm2270	1.03	0.70	6.05	385.7	Slug	n
pdm2271	1.72	0.02	6.03	80.4	Str.Wa.	y
pdm2272	1.70	0.03	6.03	197.6	Str.Wa.	y
pdm2273	1.69	0.05	6.02	259.0	Str.Wa.	y
pdm2274	1.67	0.07	6.05	352.9	Str.Wa./Slug	y
pdm2275	1.66	0.08	6.01	341.0	Str.Wa./Slug	y
pdm2276	1.64	0.10	6.04	407.4	Str.Wa./Slug	y
pdm2277	1.64	0.12	6.02	442.3	Slug	y
pdm2278	1.62	0.13	6.01	457.3	Slug	y
pdm2279	1.61	0.14	6.01	462.6	Slug	y
pdm2280	1.61	0.15	5.97	531.1	Slug	y
pdm2281	1.61	0.19	5.96	486.6	Slug	y
pdm2282	1.59	0.23	5.96	441.1	Slug	y
pdm2284	1.61	0.28	5.85	145.7	Slug	y
pdm2285	1.57	0.30	6.00	228.2	Slug	y
pdm2286	1.56	0.36	6.00	289.1	Slug	y
pdm2287	1.54	0.41	6.08	311.5	Slug	y
pdm2288	1.53	0.44	6.05	384.8	Slug	y
pdm2289	1.53	0.50	6.06	495.6	Slug	n
pdm2292	1.74	0.61	6.10	710.9	Slug	n
pdm2293	1.74	0.71	5.99	767.3	Slug	n
pdm2294	2.27	0.02	6.07	428.4	Str.Wa.	y
pdm2295	2.25	0.03	6.07	417.7	Str.Wa.	y
pdm2296	2.22	0.04	6.07	415.8	Str.Wa.	y
pdm2297	2.21	0.05	6.04	437.9	Str.Wa.	y
pdm2298	2.19	0.07	6.03	471.9	Str.Wa./Slug	y
pdm2300	2.15	0.10	6.01	477.2	Slug	y
pdm2301	2.12	0.12	6.02	507.3	Slug	y
pdm2302	2.11	0.14	6.00	491.5	Slug	y
pdm2304	2.32	0.18	6.05	640.0	Slug	y
pdm2305	2.29	0.21	6.05	663.4	Slug	y
pdm2306	2.27	0.25	6.04	663.0	Slug	y
pdm2307	2.22	0.27	6.03	463.3	Slug	y
pdm2308	2.22	0.31	6.01	585.2	Slug	y
pdm2309	2.20	0.35	6.01	619.3	Slug	y
pdm2310	2.19	0.42	6.02	716.0	Slug	y
pdm2311	2.16	0.45	6.03	712.9	Slug	n
pdm2313	2.24	0.50	6.14	680.7	Slug	n
pdm2314	2.23	0.61	6.14	669.0	Slug	n
pdm2315	2.28	0.71	6.15	632.5	Slug	n
pdm2318	2.94	0.03	5.99	371.5	Str.Wa.	y
pdm2319	3.01	0.04	6.03	378.8	Str.Wa.	y
pdm2320	2.98	0.06	6.00	386.7	Str.Wa.	y
pdm2321	2.95	0.07	5.98	390.0	Str.Wa.	y
pdm2322	3.02	0.08	6.02	426.8	Str.Wa.	y

Campaign 2: ∓ 1.5° "V"-section						
Run	U_{sG} / m/s	U_{sL} / m/s	Exit pressure / bar(a)	dP/dz/ (Pa/m)	Flow Pattern (35m)	Reverse flow?
pdm2323	2.98	0 09	5 98	421.5	Str Wa./Slug	y
pdm2324	2.95	0.13	6 03	674.8	Slug	y
pdm2325	3.02	0.14	6 05	660.6	Slug	y
pdm2326	2.99	0.15	6 02	633.0	Slug	y
pdm2327	3.03	0.18	6.05	646.4	Slug	y
pdm2328	3.01	0.19	6.02	609.6	Slug	y
pdm2329	3.06	0.24	6.04	610.2	Slug	y
pdm2330	3.01	0.27	6.03	624.9	Slug	y
pdm2331	2.97	0.31	6 01	640.0	Slug	y
pdm2334	3.08	0.36	5.86	645.9	Slug	n
pdm2335	3.08	0 52	6 02	547.9	Slug	n
pdm2336	3.05	0.61	6 00	805.2	Slug	n
pdm2340	3.06	0.70	6.02	474.6	Slug	n
pdm2341	3.54	0 03	6.02	-4.7	Str.Wa.	n
pdm2342	3.54	0.05	5.98	413.8	Str.Wa.	n
pdm2343	3.59	0.06	5.98	441.7	Str.Wa.	n
pdm2344	3.53	0.08	5.96	435.5	Str Wa./Slug	n
pdm2345	3.58	0.09	5.98	469.1	Str.Wa./Slug	n
pdm2346	3.54	0.11	5.96	480.8	Str Wa./Slug	n
pdm2347	3.58	0.12	5.99	512.6	Str.Wa./Slug	n
pdm2348	3.62	0.13	5.99	506.5	Str.Wa./Slug	n
pdm2349	3.56	0.15	5.98	534.8	Str Wa./Slug	n
pdm2350	3.61	0.16	6.00	526.3	Str.Wa./Slug	n
pdm2351	3.63	0.18	6.03	571.8	Slug	n
pdm2352	3.59	0.22	5.99	599.1	Slug	n
pdm2353	3.63	0.23	6.01	627.0	Slug	n
pdm2355	3.59	0.26	5.97	137.8	Slug	n
pdm2356	3.54	0.30	5.96	228.4	Slug	n
pdm2357	3.62	0.35	5.96	305.4	Slug	n
pdm2358	3.66	0.41	5.99	285.4	Slug	n
pdm2359	3.61	0.47	5.98	468.4	Slug	n
pdm2360	3.58	0.52	5.96	569.8	Slug	n
pdm2361	3.63	0.55	5.98	688.2	Slug	n
pdm2364	3.62	0.59	5 99	1004.8	Slug	n
pdm2365	3.57	0 69	6.02	1150.5	Slug	n
pdm2366	4.28	0.02	6.04	568.7	Str.Sm.	n
pdm2367	4.22	0.04	6.00	582.4	Str.Sm.	n
pdm2368	4.24	0.07	6.02	611.4	Str.Wa.	n
pdm2369	4.34	0.10	5 94	598.1	Str.Wa./Slug	n
pdm2370	4.22	0.12	5.98	615.1	Str.Wa./Slug	n
pdm2371	4.31	0.15	5 99	671.8	Slug	n
pdm2372	4.27	0.17	6.00	635.6	Slug	n
pdm2374	4.35	0.21	6.01	668.0	Slug	n
pdm2375	4.27	0.26	5.98	701.7	Slug	n
pdm2376	4.31	0.30	5.97	781.5	Slug	n
pdm2377	4.34	0.37	5.98	837.2	Slug	n
pdm2380	4.36	0.40	5.96	789.5	Slug	n
pdm2381	4.29	0.45	6 05	862.0	Slug	n
pdm2382	4.33	0.51	6.05	783.6	Slug	n
pdm2383	4.25	0.60	6.05	1072.3	Slug	n
pdm2384	4.36	0.70	5.99	1126.3	Slug	n

Campaign 2: ∓ 1.5° "V"-section						
Run	U_{sG} / m/s	U_{sL} / m/s	Exit pressure / bar(a)	dP/dz/ (Pa/m)	Flow Pattern (35m)	Reverse flow?
pdm2385	5.05	0.02	6.03	337.0	Str.Sm.	n
pdm2386	5.04	0.04	6 04	484.3	Str.Sm.	n
pdm2390	4.99	0.06	6.03	552.1	Str.Sm.	n
pdm2392	5.02	0.12	6.02	576.9	Str.Wa.	n
pdm2393	4.93	0.14	5.99	582.0	Str.Wa./Slug	n
pdm2394	5.00	0.16	6.03	379.2	Str.Wa./Slug	n
pdm2395	5.00	0.20	6.03	445.9	Str.Wa./Slug	n
pdm2396	5.00	0.23	6.04	479.2	Slug	n
pdm2397	5.00	0.27	6.04	554.6	Slug	n
pdm2398	4.99	0.29	6.04	565.6	Slug	n
pdm2399	4.99	0.35	6.02	653.9	Slug	n
pdm2400	5.01	0.40	6.08	636.9	Slug	n
pdm2401	5.01	0.46	6.07	822.7	Slug	n
pdm2402	5.01	0.50	6.07	857.3	Slug	n
pdm2405	5.03	0.60	5.97	732.5	Slug	n
pdm2406	4.99	0.70	6.08	1115.1	Slug	n
pdm2488	0.19	0.04	6.04	242.7	Slug	y
pdm2489	0.19	0.07	6.04	461.7	Slug	y
pdm2490	0.19	0.09	6.02	526.6	Slug	y
pdm2491	0.19	0.11	6.06	361.1	Slug	y
pdm2492	0.19	0.13	6.07	383.6	Slug	y
pdm2493	0.19	0.16	6.13	426.6	Slug	y
pdm2494	0.19	0.21	6.14	473.4	Slug	y
pdm2495	0.19	0.25	6.10	477.4	Slug	y
pdm2496	0.19	0.29	6.16	469.8	Slug	y
pdm2497	0.19	0.34	6.20	535.3	Slug	y
pdm2498	0.19	0.40	6.26	516.8	Slug	y
pdm2501	0.19	0.44	6.13	450.6	Slug	y
pdm2502	0.20	0.51	6.14	507.5	Slug	y
pdm2503	0.19	0.61	6.16	638.9	Bubbly	n
pdm2504	0.19	0.70	6.05	695.0	Bubbly	n
pdm2506	0.29	0.03	6.03	273.0	Str.Wa.	y
pdm2507	0.29	0.06	6.05	437.7	Str.Wa.	y
pdm2508	0.27	0.08	6.05	490.1	Slug	y
pdm2509	0.29	0.11	6.11	600.5	Slug	y
pdm2510	0.30	0.14	6.04	660.4	Slug	y
pdm2511	0.30	0.19	6 01	329.8	Slug	y
pdm2512	0.30	0.22	6.02	375.3	Slug	y
pdm2513	0.31	0.27	5 99	453.1	Slug	y
pdm2515	0.31	0.30	6.03	522.5	Slug	n
pdm2516	0.31	0.36	6.00	584.1	Slug	n
pdm2517	0.31	0.40	5.98	620.1	Bubbly	n
pdm2518	0.30	0.45	6 01	646.7	Bubbly	n
pdm2520	0.30	0.50	0.50	581.7	Bubbly	n
pdm2521	0.30	0 60	0 60	581.7	Bubbly	n
pdm2522	0.29	0.70	0.70	581.8	Bubbly	n
pdm2523	0.41	0.03	0.03	581.9	Str Wa.	y
pdm2524	0.41	0.06	0 06	581.9	Str.Wa./Slug	y
pdm2525	0.41	0.09	0.09	581.9	Str.Wa./Slug	y
pdm2526	0.41	0.13	0.12	581.9	Slug	y
pdm2527	0.41	0.16	0.16	581.9	Slug	y

Campaign 2: ∓ 1.5° "V"-section						
Run	U_{sG} / m/s	U_{sL} / m/s	Exit pressure / bar(a)	dP/dz/ (Pa/m)	Flow Pattern (35m)	Reverse flow?
pdm2528	0.41	0.20	0.19	581.9	Slug	y
pdm2529	0 42	0.23	0.23	581.8	Slug	y
pdm2562	0 42	0.26	6.15	465.8	Slug	y
pdm2563	0 42	0.31	6 18	710.8	Slug	y
pdm2564	0.43	0.36	6.09	712.9	Slug	y
pdm2565	0.43	0.39	6.04	446.6	Slug	n
pdm2566	0.43	0.47	6.05	539.6	Slug	n
pdm2567	0.43	0.49	6 06	616.9	Slug	n
pdm2568	0.43	0 61	6.06	663.4	Slug	n
pdm2569	0 43	0.69	6 00	862.1	Bubbly	n

A2.3. Campaign 3: ±1.5° "Λ"-section

Campaign 3: ±1.5° "Λ"-section					
Run	U_{sG} / m/s	U_{sL} / m/s	Exit pressure / bar(a)	dP/dz / (Pa/m)	Flow Pattern (35m)
PDM4002	5.81	0.11	1.05	-5.8	Str.Sm.(Wa.)
PDM4003	5.32	0.15	1.05	-11.2	Str.Wa.
PDM4004	5.48	0.19	1.06	1.5	Str.Wa./Slug
PDM4005	5.72	0.23	1.06	1.2	Str.Wa./Slug
PDM4006	5.78	0.26	1.06	1.5	Str.Wa./Slug
PDM4007	5.58	0.28	1.07	19.4	Slug
PDM4008	5.81	0.33	1.08	55.9	Slug
PDM4009	5.95	0.37	1.09	48.1	Slug
PDM4010	5.75	0.42	1.11	111.8	Slug
PDM4013	5.07	0.43	1.10	127.9	Slug
PDM4015	5.06	0.47	1.11	152.5	Slug
PDM4016	5.00	0.53	1.13	125.4	Slug
PDM4017	4.97	0.56	1.14	173.5	Slug
PDM4018	4.67	0.60	1.15	239.0	Slug
PDM4021	5.26	0.69	1.16	240 8	Slug
PDM4023	7.95	0.11	1.05	15.1	Str.Sm.(Wa.)
PDM4024	7.79	0.16	1.07	25.0	Str.Wa.
PDM4025	7.69	0.21	1.07	57.7	Str.Wa./Slug
PDM4026	7.67	0.25	1.08	72.3	Str.Wa./Slug
PDM4027	7.74	0.30	1.11	119.2	Slug
PDM4028	7.70	0.36	1.12	159.2	Slug
PDM4029	7.69	0.41	1.14	160.9	Slug
PDM4034	7.84	0.49	1.16	141.2	Slug
PDM4035	7.68	0.61	1.20	212.0	Slug
PDM4036	7.37	0.70	1.23	283.9	Slug
PDM4037	10.49	0.11	1.07	-3.5	Str Sm.(Wa.)
PDM4038	10.44	0.15	1.08	25.0	Str.Wa.
PDM4039	10.27	0.20	1.10	55.8	Str.Wa./Slug
PDM4042	9.97	0.23	1.11	79.7	Str.Wa./Slug
PDM4043	9.85	0.27	1.12	110.5	Str.Wa./Slug
PDM4046	9.84	0.31	1.14	161.6	Slug

Campaign 3: ±1.5° "Λ"-section					
Run	U_{sG} / m/s	U_{sL} / m/s	Exit pressure / bar(a)	dP/dz / (Pa/m)	Flow Pattern (35m)
PDM4047	9.76	0.35	1.15	185.8	Slug
PDM4048	9.74	0.40	1.16	222.4	Slug
PDM4049	9.52	0 47	1.19	255.9	Slug
PDM4050	9.48	0.56	1.24	357.3	Slug
PDM4053	9.86	0.59	1.26	413.1	Slug
PDM4056	9.84	0.69	1.30	509.2	Slug
PDM4057	12.20	0.11	1.08	59.1	Str.Sm.(Wa.)
PDM4058	12.16	0.15	1.09	73.1	Str.Wa.
PDM4059	12.03	0.19	1.11	104.7	Str.Wa./Slug
PDM4060	11.90	0.24	1.12	153.3	Str.Wa./Slug
PDM4061	11.82	0.27	1.15	208.6	Slug
PDM4062	11.62	0.31	1.17	240.7	Slug
PDM4063	11.56	0.39	1.19	245.3	Slug
PDM4066	12.42	0.44	1.24	370.2	Slug
PDM4069	12.23	0.50	1.28	420.1	Slug
PDM4070	11.94	0.61	1.33	499.0	Slug
PDM4071	11.94	0.70	1.38	623.3	Slug
PDM4073	15.20	0.12	1.11	100.6	Str.Sm.(Wa.)
PDM4074	15.02	0.16	1.12	131.9	Str.Wa.
PDM4075	14.74	0.19	1.13	151.1	Str.Wa./Slug
PDM4076	14.65	0.24	1.15	200.5	Str.Wa./Slug
PDM4079	14.95	0.30	1.19	292.0	Slug
PDM4082	14.74	0.36	1.22	331.8	Slug
PDM4083	14.48	0.40	1.23	350.6	Slug
PDM4084	14.21	0.44	1.26	413.9	Slug
PDM4085	14.12	0.51	1.30	449.0	Slug
PDM4086	14.13	0.55	1.31	498.7	Slug
PDM4087	13.92	0.63	1.35	633.7	Slug
PDM4090	13.95	0.72	1.51	915.0	Slug
PDM4093	16.92	0.12	1.10	118.8	Str.Wa.
PDM4094	16.81	0.17	1.13	163.2	Str.Wa.
PDM4095	16.55	0.22	1.15	224.0	Str.Wa.
PDM4096	16.24	0.26	1.17	236.2	Str.Wa./Slug
PDM4097	16.04	0.32	1.20	367.8	Slug/Ann.
PDM4098	16.56	0.38	1.25	430.5	Slug/Ann.
PDM4101	16.49	0.39	1.26	452.0	Slug/Ann.
PDM4104	17.03	0.44	1.31	529.8	Slug/Ann.
PDM4105	16.66	0.49	1.33	584.0	Slug/Ann.
PDM4106	17.01	0.55	1.39	726.4	Slug
PDM4107	16.83	0.61	1.41	713.3	Slug
PDM4108	16.79	0.71	1.48	853.1	Slug
PDM4111	2.48	0.09	5.75	64.4	Str.Sm.(Wa.)
PDM4112	2.31	0 12	5.77	57.1	Str.Sm.(Wa.)
PDM4113	2.11	0.18	5.61	-3.0	Str.Sm.(Wa.)
PDM4114	2.32	0.20	5.76	-9.6	Str.Sm.(Wa.)
PDM4115	2.46	0.25	5.79	-6.8	Str.Sm.(Wa.)
PDM4116	2.51	0.29	5.56	-3.8	Str.Wa.
PDM4117	2.36	0.34	5.85	-13.6	Str.Wa.
PDM4118	2.29	0.39	5.69	-2.0	Str.Wa./Slug
PDM4119	2.38	0 47	5.87	-1.2	Str.Wa./Slug
PDM4122	2.56	0.50	5.69	81.1	Slug

Campaign 3: ±1.5° "Λ"-section					
Run	U_{sG} / m/s	U_{sL} / m/s	Exit pressure / bar(a)	dP/dz / (Pa/m)	Flow Pattern (35m)
PDM4124	2.57	0.58	5.65	79.1	Slug
PDM4125	2.85	0.69	5.38	109.0	Slug
PDM4127	3.44	0.11	5.80	-28.7	Str.Sm.(Wa.)
PDM4128	3.79	0.13	5.44	-14.5	Str.Sm.(Wa.)
PDM4129	3.35	0.20	5.77	-23.2	Str.Wa.
PDM4130	3.40	0.24	5.61	-9.3	Str.Wa.
PDM4131	3.43	0.33	5.57	3.9	Str.Wa.
PDM4134	3.58	0.39	5.57	-104.4	Str Wa.
PDM4135	3.51	0.44	5.59	-50.1	Str.Wa./Slug
PDM4136	3.55	0.49	5.60	35.1	Str.Wa./Slug
PDM4137	3.57	0.59	5.81	81.2	Slug
PDM4138	3.74	0.70	5.51	170.5	Slug
PDM4141	4.04	0.12	5.57	92.4	Str.Sm.(Wa.)
PDM4142	3.94	0.15	5.63	77.3	Str.Sm.(Wa.)
PDM4143	3.99	0.20	5.57	78.1	Str.Wa.
PDM4144	4.02	0.24	5.66	71.4	Str.Wa./Slug
PDM4146	4.01	0.31	5.68	7.6	Str.Wa./Slug
PDM4147	3.94	0.34	5.66	2.5	Str.Wa./Slug
PDM4148	4.00	0.40	5.62	6.8	Str.Wa./Slug
PDM4149	3.95	0.42	5.74	-7.1	Slug
PDM4152	4.14	0.50	5.55	136.8	Slug
PDM4154	4.10	0.60	5.61	164.9	Slug
PDM4155	4.01	0.71	5.69	174.4	Slug
PDM4157	4.66	0.11	5.57	-75.2	Str.Sm.(Wa.)
PDM4158	4.60	0.14	5.54	-72.9	Str.Sm.(Wa.)
PDM4159	4.61	0.19	5.52	-65.3	Str.Sm.(Wa.)
PDM4160	4.45	0.22	5.70	-66.6	Str.Wa.
PDM4161	4.41	0.25	5.71	-64.1	Str.Wa.
PDM4164	4.66	0.30	5.64	-125.1	Str.Wa.
PDM4165	4.75	0.35	5.42	-29.0	Str.Wa./Slug
PDM4167	4.60	0.40	5.66	111.6	Str.Wa./Slug
PDM4168	4.47	0.51	5.73	146.1	Slug
PDM4169	4.51	0.59	5.80	181.2	Slug
PDM4170	4.49	0.70	5.76	230.5	Slug
PDM4173	5.12	0.09	5.69	160.3	Str.Sm.(Wa.)
PDM4174	4.95	0.15	5.71	140.4	Str.Wa.
PDM4175	4.97	0.18	5.73	124.0	Str.Wa.
PDM4177	5.03	0.22	5.67	60.9	Str.Wa.
PDM4178	4.90	0.27	5.66	73.2	Str.Wa./Slug
PDM4179	4.92	0.32	5.80	105.0	Str.Wa./Slug
PDM4180	4.83	0.38	5.78	118.5	Slug
PDM4181	4.94	0.40	5.81	118.8	Slug
PDM4182	4.94	0.51	5.78	162.2	Slug
PDM4185	5.21	0.51	5.69	80.6	Slug
PDM4187	5.13	0.60	5.78	197.9	Slug
PDM4188	4.85	0.71	5.95	208.9	Str.Sm.(Wa.)
PDM4189	6.05	0.11	5.63	13.5	Str.Sm.(Wa.)
PDM4190	5.86	0.15	5.66	8.7	Str.Wa./Slug
PDM4191	6.04	0.21	5.66	19.6	Str.Wa./Slug
PDM4192	6.04	0.27	5.74	36.4	Str.Wa./Slug
PDM4195	6.06	0.31	5.62	349.1	Str.Wa./Slug

Campaign 3: ±1.5° "Λ"-section					
Run	U_{sG} / m/s	U_{sL} / m/s	Exit pressure / bar(a)	dP/dz / (Pa/m)	Flow Pattern (35m)
PDM4196	6.10	0.35	5.62	336.0	Str.Wa./Slug
PDM4199	6.06	0 40	5.65	607.7	Slug
PDM4200	6.15	0.46	5.57	578 6	Slug
PDM4201	6 09	0.49	5 63	521.2	Slug
PDM4202	6 03	0.61	5.70	533 6	Slug
PDM4205	6 22	0.69	5.65	527 9	Slug
PDM4208	5 63	0.11	5.52	220 3	Str.Sm.(Wa.)
PDM4209	5.65	0.15	5.62	238.7	Str.Sm.(Wa.)
PDM4210	5.61	0.22	5.60	207.6	Str.Wa./Slug
PDM4211	5.40	0.26	5.75	187.1	Str.Wa./Slug
PDM4212	5.51	0.29	5.68	168.4	Str.Wa./Slug
PDM4213	5.61	0.34	5.64	150.9	Str.Wa./Slug
PDM4214	5.56	0.42	5.74	134.1	Slug
PDM4216	5 65	0.45	5.57	163.5	Slug
PDM4219	5.65	0.50	5.69	609.5	Slug
PDM4220	5.63	0.62	5.63	548.2	Slug
PDM4221	5.59	0.71	5.71	529.5	Slug
PDM4224	2.54	0.84	5.50	418.6	Slug
PDM4226	2.65	1.01	5.56	646.0	Slug
PDM4227	4.09	0.86	5.73	656.4	Slug
PDM4230	4.09	0.97	5.67	753.8	Slug
PDM4231	5.01	0.85	5.81	804.6	Slug
PDM4232	4.97	1.02	5.82	878.0	Slug
PDM4235	7.03	0.85	1.25	647.3	Slug
PDM4238	7.42	1.00	1.30	826.1	Slug
PDM4239	9.75	0.86	1.33	867.3	Slug
PDM4242	9.70	1.00	1.39	833.6	Slug
PDM4245	13.90	0.88	1.48	1186.3	Slug
PDM4246	14.21	1.02	1.58	1281.4	Slug
PDM4249	11.81	0.88	1.41	1025.4	Slug
PDM4250	12.28	1.05	1.52	1114.9	Slug
PDM4253	6.08	0.99	5.88	667.4	Slug
PDM4254	5.96	0.85	5.83	800.2	Slug
PDM4257	4.73	1.00	5.66	640.8	Slug
PDM4259	4.62	0.86	5.69	422.1	Slug
PDM4262	2.08	0.85	5.52	253.9	Slug
PDM4265	2.14	1.01	5.64	464.1	Slug
PDM4266	1.06	0.87	5.66	112.5	Slug
PDM4269	1 07	1.02	5.56	458.0	Slug
PDM4272	3.50	0.88	1.17	541.5	Slug
PDM4273	5 53	0.85	1.21	432.0	Slug
PDM4276	3.92	1.00	1.19	538.4	Slug
PDM4279	5.54	1.01	1.25	442.3	Slug
PDM4282	2.15	0.10	1.03	-9.4	Str.Sm.(Wa.)
PDM4283	2.12	0.14	1.04	-11.4	Str.Sm.(Wa.)
PDM4284	2.09	0.21	1.04	-14.6	Str.Sm.(Wa.)
PDM4287	2.10	0.25	1.04	-3.3	Str.Sm.(Wa.)
PDM4288	2.08	0.31	1.04	-11 4	Str.Wa.
PDM4289	2.06	0 40	1.05	0.6	Str.Wa./Slug
PDM4290	2.07	0.49	1.06	10 5	Slug
PDM4291	2.05	0.62	1.07	55.7	Slug

Campaign 3: ±1.5° "Λ"-section					
Run	U_{sG} / m/s	U_{sL} / m/s	Exit pressure / bar(a)	dP/dz / (Pa/m)	Flow Pattern (35m)
PDM4294	2.13	0.71	1.09	105 9	Slug
PDM4297	4.16	0.12	1.03	94.1	Str.Sm.(Wa.)
PDM4298	4.12	0.16	1.04	185 0	Str.Sm.(Wa.)
PDM4299	4 12	0 20	1.04	180.8	Str.Sm.(Wa.)
PDM4300	4.14	0.26	1.05	139.7	Str.Wa.
PDM4301	4.13	0.32	1.06	116.6	Str.Wa./Slug
PDM4302	4.08	0.41	1.07	135 8	Str.Wa./Slug
PDM4303	4 08	0 46	1.08	95.1	Slug
PDM4304	4 06	0.52	1.09	100.5	Slug
PDM4307	3.97	0.61	1.09	134.0	Slug
PDM4310	3.68	0.71	1.12	452.8	Slug
PDM4311	1.14	0.09	5.58	258.0	Str.Sm.(Wa.)
PDM4312	1.14	0.15	5.59	204.4	Str.Sm.(Wa.)
PDM4313	1.14	0.20	5.59	147.7	Str.Sm.(Wa.)
PDM4314	1.15	0.24	5.60	93.0	Str.Sm.(Wa.)
PDM4315	1.13	0.30	5.60	39.7	Str.Wa.
PDM4317	1.24	0.34	5.60	19.8	Str.Wa.
PDM4318	1.24	0.40	5.60	10.5	Str.Wa.
PDM4321	1.15	0.50	5.59	-30.2	Str.Wa.
PDM4322	1.14	0.60	5.55	-72.8	Str.Wa.
PDM4323	1.11	0.72	5.53	-114.9	Str.Wa.
PDM4326	2.06	0.30	5.56	26.3	Str.Sm.(Wa.)
PDM4327	2.01	0.40	5.68	79.5	Str.Wa./Slug
PDM4328	1.99	0.51	5.72	181.8	Slug
PDM4331	1.96	0.59	5.61	23.6	Slug
PDM4332	1.93	0.72	5.68	62.5	Slug
PDM4333	3.14	0.10	5.59	-4.4	Str.Sm.(Wa.)
PDM4334	3.09	0.16	5.60	7.0	Str.Sm.(Wa.)
PDM4337	2.97	0.19	5.73	70.6	Str.Sm.(Wa.)
PDM4338	2.97	0.30	5.69	85.7	Str.Wa.
PDM4339	2.94	0.40	5.70	152.8	Str.Wa./Slug
PDM4340	3.06	0.51	5.44	258.6	Slug
PDM4343	2.93	0.62	5.73	19.8	Slug
PDM4344	2.96	0.71	5.61	25.2	Slug

The files from the three experimental campaigns are archived on CD-ROM numbers CD01 – CD03, appended to this thesis. The data are compressed using the PKzip® (WinZip®) format, compatible with the MS-DOS®, Microsoft® Windows® 95/98/2000/*etc.* and Windows NT® operating systems.

The data files are in the following formats:

*.cpr High-speed data acquisition output file, containing conductivity probe data sampled at 500 Hz. The data files are in binary format, whereby the data from the ten sampled channels are stored as a sequence of two-byte records. The first

41 bytes of each file contains header information; thus bytes 42 and 43 contain the output from Channel 1 at the first time step, bytes 44 and 45 are from Channel 2, *etc.* Bytes 62 and 63 then contain data from Channel 1 at the second time interval, *ad nauseum.*

*.gam Gamma densitometer output file, in ASCII text format, consisting of two columns of data describing the liquid holdup measured by each of the two gamma photon energies at time intervals of 0.04 seconds.

*.rig Low-speed data acquisition output file, containing pressure / flow *etc* data at approximately 1.2 second intervals in ASCII text format. The header information in each file explains the layout of the data in the file.

Additionally, a number of files containing processed and summarised data from the experiments in Microsoft® Excel® v.7.0 format are included on each CD-ROM. The spreadsheet file "CPR Processing.xls" contains a Visual Basic application to extract the data from the binary *.cpr files.

Appendix 3: Matrix of CFD simulations

Model	Run	U_{Wall} / m/s	U_{Inlet} / m/s	Duration / s
Slug Tail	ST01	0.94	0.44	5
	ST02	1.44	0.44	5
	ST03	2.47	0.46	5
	ST04	3.49	0.44	5
	ST05	4.6	0.53	5
	ST06	6.86	0.8	5
	ST07	9.14	1.1	5
Solid Slug Front	SSF01	8.0	6.0	9
	SSF02	12.6	11.0	14
	SSF03	12.6	7.4	13
	SSF04	12.6	4.1	14
	SSF05	12.6	5.34	15
Whole Slug	WS01	8.0	1.2	10

The data files are archived on CD-ROM number CD04, appended to this thesis. The files are compressed using the PKzip® (WinZip®) format, compatible with the MS-DOS®, Microsoft® Windows® 95/98/2000/*etc.* and Windows NT® operating systems.

The files included on the CD-ROM are in the following formats:

*.dmp	CFX4 dump file (machine-readable output file)
*.f	User FORTRAN file (used to set initial conditions)
*.fc	CFX4.3 command file
*.geo	CFX4 geometry file (machine-readable mesh file)
*.log	CFX-MESHBUILD log file (from which the mesh can be reconstructed)
*.out	CFX4 text output file (iteration summary, wall shear stress etc)

Appendix 4: Study of slug motion near a pipe exit

A brief series of experiments was conducted in which the front and tail velocities of a slug were measured as it left the WASP facility test-section and entered the slug catcher. The results are reported in this Appendix.The motivation for the study was a prediction by the commercial slug tracking scheme OLGA (King, 1999) that the slug tail accelerated rapidly as the slug body passed out of the test section. The aim was to measure tail velocities near the outlet to check this prediction.

The WASP facility test-section was positioned horizontally for the tests. Air and water at atmospheric pressure were used as test fluids, with flow measurement performed at the test-section inlet. The design and operation of the WASP facility is described in Chapter 3 of this thesis.

A Kodak® Ekta-Pro2000^{TM} high-speed digital video camera was used to produce a sequence of images of each slug as it passed the transparent visualisation section. The camera was operated at a frequency of 1000 Hz, with a shutter speed of 0.2 ms. The front and tail velocities of each slug were then obtained by inspection of the digital images, aided by a graduated scale fixed to the visualisation section, which showed axial and vertical distance in the photographs, measured in centimeters. The digital images are archived on CD-ROM number CD03, appended to this thesis.

Several slugs were photographed over a range of gas and liquid superficial velocities. The experiments are summarised in Table A4.1.

A sample image showing the passage of the slug front (with flow from right to left) is given below:

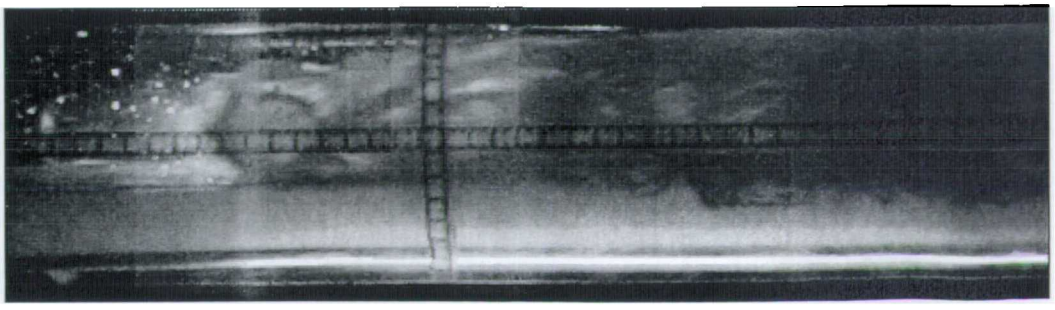

Figure A4.1: High speed video image of slug front (Run PDM3003, Image 636)

The left-hand side of the image shown in Figure A4.1 was 0.49 m from the pipe exit (*i.e.*, 6.3D). The image shows a region 0.41m × 0.08 m in size.

By comparing consecutive images, obtained at 0.001 second intervals, and measuring the change in the position of the slug front or tail as appropriate, it was possible to obtain averaged values for the slug front and tail velocity (U_F and U_T respectively) as the slug passed through the visualisation section. A mean slug length, L_S, was also calculated, from the average of the front and tail velocities and the time interval between the arrival of the slug front and tail in the visualisation section. These results are shown in Table A4.1. The error in the velocity measurements, calculated from the estimated error in the distance measurement from each photograph, is expected to be in the region of ±5%.

Run	U_{sG} / m/s	U_{sL} / m/s	U_{Mix} / m/s	U_F / m/s	U_T / m/s	L_S / D
3002	2	0.4	2.4	2.67	2.84	24.4
3003	4	0.6	4.6	5.63	5.25	28.4
3004	6	0.7	6.7	7.21	5.22	43.9
3005	8	0.5	8.5	9.40	9.27	37.5

Table A4.1: Results from slug exit study

The length of each slug was considerably greater than the distance of the pipe exit from the visualisation section. Thus, the slug tail velocity U_T was obtained in each case after most of the slug body had left the test-section and entered the slug catcher.

In the results of these experiments, the acceleration effect predicted by King (1999) using the OLGA slug tracking code would be shown by the measured slug tail velocity greatly exceeding that of the slug front. However, this was not observed. Indeed, in three of the four experiments, the slug tail was observed to be travelling *slower* than the slug front: this may be due in part to the design of the slugcatcher, which contains internal baffles to assist with phase separation and which may restrict the passage of the slug as it enters the vessel.

Whilst interesting, the results from these experiments did not shed light on any detailed aspects of slug flow phenomena and so the study was not pursued further.